# UNIVERSITÉ DE TOURS

***ÉCOLE DOCTORALE : SSBCV***

**Centre d'Etude des Pathologies Respiratoires**
**INSERM UMR-1100**

# THÈSE présentée par :

**Roxane DOMAIN**

soutenue le : **11 janvier 2024**

pour obtenir le grade de : **Docteur de l'université de Tours**
Discipline / Spécialité : Sciences de la Vie et de la Santé / Biochimie

# Mécanismes protéolytiques impliqués dans la maturation de la cathepsine C et de ses protéases à serine cibles dans les cellules immunitaires

**THÈSE dirigée par :**

| | |
|---|---|
| **M Brice KORKMAZ** | Chargé de Recherche, INSERM UMR-1100, Tours |

**RAPPORTEURS :**

| | |
|---|---|
| **Mme Rita VANBEVER** | Professeure, Université Catholique de Louvain |
| **M Charaf BENARAFA** | Professeur, Université de Bern |

**PRESIDENTE :**

| | |
|---|---|
| **Mme Marie-Claude VIAUD-MASSUARD** | Professeure, Université de Tours |

---

**JURY :**

| | |
|---|---|
| **M Charaf BENARAFA** | Professeur, Université de Bern |
| **Mme Isabelle COUILLIN** | Directrice de Recherche, CNRS UMR-7355, Orléans |
| **Mme Sevil KORKMAZ-ICÖZ** | Docteure, Université de Heidelberg |
| **M Brice KORKMAZ** | Chargé de Recherche, INSERM UMR-1100, Tours |
| **M Christophe PAGET** | Directeur de Recherche, INSERM UMR-1100, Tours |
| **M Moez RHIMI** | Directeur de Recherche, INRAE UMR-1319, Jouy-en-Josas |
| **Mme Rita VANBEVER** | Professeure, Université Catholique de Louvain |
| **Mme Marie-Claude VIAUD-MASSUARD** | Professeure, Université de Tours |

*Je dédie cette thèse à mes grand-mères.*
*Josette Benzoni, mamie yoyo, dont la carrière scientifique*
*m'a inspiré à réaliser cette profession.*
*Mamie Jacqueline qui m'a appris à poursuivre*
*chaque jour de ma vie avec un sourire.*

# Remerciements :

Ce travail a été effectué au sein de l'unité INSERM UMR-1100 (Centre d'Étude des Pathologies Respiratoires, CEPR, Tours) dirigée par le Dr Mustapha Si-Tahar, au sein de l'équipe 2 « Mécanismes protéolytiques dans l'inflammation » (Directeur d'équipe : Pr Gilles Lalmanach). Cette étude a bénéficié du soutien financier du Ministère de l'Enseignement Supérieur, de la Recherche et de l'Innovation.

Je tiens à exprimer mes remerciements à :

Monsieur **Brice Korkmaz**, Chargé de Recherche INSERM, pour m'avoir accueillie comme doctorante sous sa tutelle. J'ai bénéficié, durant ces 3 années à vos côtés, de vos connaissances, de votre expérience et de votre grande gentillesse. Je vous remercie de m'avoir guidée, encouragée et soutenue pendant les moments difficiles. Merci infiniment, pour la confiance que vous m'avez donnée dans la réalisation de nos projets, c'est pour moi une grande fierté. Merci de m'avoir permis de réaliser un congrès en Italie et un aux USA, je n'oublierai jamais les moments joyeux que nous avons passés ensemble. Un très grand merci pour l'attention toute particulière que vous accordez à la poursuite de ma carrière. Toutes vos qualités me motivent à poursuivre l'aventure avec vous, je vous remercie de m'en avoir donné l'opportunité, c'est avec excitation que j'envisage le futur.

Madame **Rita Vanbever**, Professeure à l'Université Catholique de Louvain et **Monsieur Charaf Benarafa**, Professeur à l'Université de Berne pour me faire l'honneur d'évaluer ce travail en tant que rapporteurs. Merci de votre intérêt pour cette étude.

Madame **Isabelle Couillin**, Directrice de Recherche CNRS à Orléans, Madame **Sevil Korkmaz-Icöz**, Docteure à l'Université de Heidelberg, Monsieur **Christophe Paget**, Directeur de Recherche INSERM à Tours, Monsieur **Moez Rhimi**, Directeur de Recherche INRAE à Jouy-en-Josas et Madame **Marie-Claude Viaud-Massuard**, Professeure à l'université de Tours, pour avoir accepté d'être examinatrices et examinateurs de cette thèse.

Monsieur **Mustapha Si-Tahar**, Directeur de l'unité INSERM UMR-1100, pour m'avoir accueillie au sein du CEPR, mais également pour vos encouragements lors de communications orales et votre soutien dans les projets scientifiques, mais aussi dans les activités du laboratoire comme la Fête de la Science, les Olympiades et les 10 Km de Tours.

Monsieur **Gilles Lalmanach**, Professeur à l'université de Tours, pour m'avoir acceptée au sein de votre équipe depuis déjà cinq années. Merci pour votre disponibilité, vos conseils de grande qualité et votre écoute. Je tiens aussi à vous remercier pour votre pédagogie exceptionnelle, tous vos cours auxquels j'ai pu participer pendant mes études de la Licence au Master, ont renforcé mon intérêt pour les matières que vous enseignez. Je pense qu'un sujet intéressant ne l'est qu'avec le bon professeur, merci d'avoir exacerbé mon intérêt qui m'a poussé à intégrer le CEPR.

Monsieur **Fabien Lecaille**, Professeur à l'Université de Tours, pour m'avoir acceptée en tant que stagiaire de première et de deuxième année de Master. Merci pour la confiance que vous m'avez accordée durant ces stages. Mon stage de M1 a pour moi été le moment clé qui a révélé mon envie de faire du métier de chercheur ma profession. Merci donc de m'avoir fait partager votre passion. Je vous remercie également pour le soutien que vous m'avez apporté tout au long de mes cinq années au laboratoire, ainsi que pour vos conseils et votre qualité d'écoute.

Cette thèse, qui approche de sa fin, est aussi l'occasion pour moi de remercier l'ensemble des personnes qui ont participé à la réalisation de ce travail :

Monsieur **Rich Williams** pour la synthèse des inhibiteurs utilisés lors de ce travail.

Monsieur **Jérôme Zoidakis**, pour la réalisation des études protéomiques passées et futures. Merci pour votre incroyable joie de vivre, vos conseils scientifiques et vos recommandations en littérature. J'espère avoir la chance de collaborer avec vous dans le futur et de vous croiser en congrès.

Madame **Kuan-Ju Chen**, pour la participation au projet sur les HL-60. Mais aussi pour vos nombreux conseils scientifiques et sur les possibilités de carrières. Merci pour votre gentillesse et les bons moments passés en congrès.

Monsieur **Patrick P. McDonald**, pour vos participations et conseils sur les articles de cette thèse. Merci également pour votre bonne humeur et votre humour qui l'accompagne. Je reste éblouie par vos compétences linguistiques exceptionnelles !

Madame **Nathalie Heuzé-Vourc'h** et Monsieur **Thomas Sécher** pour la confiance qu'ils m'ont accordée lors de notre collaboration. Mais aussi pour leurs conseils avisés et leur culture scientifique impressionnante.

**Seda Seren**, pour l'initiation du projet sur les cellules HL-60. Merci pour les nombreux conseils tant scientifiques qu'en couture. Un grand merci pour ton soutien lors de ma candidature de thèse et pour la confiance que tu m'as accordée. Merci également pour ta grande gentillesse et pour les excellents moments que j'ai passés à tes côtés, j'espère qu'il y en aura plein d'autres !

**Loic Gonzalez**, pour ta participation aux différents projets et pour m'avoir montré comment *flusher* des pattes de souris et utiliser le FACS. Merci aussi pour les excellents moments passés à mes côtés en tant que colloc' et pour les soirées inoubliables que nous avons passées ensemble !

**Quentin Guilbert**, pour le travail formidable que tu as réalisé sur les cellules THP-1 et U-937. Merci de m'avoir fait confiance lors de ton recrutement, sans doute une des meilleures propositions que j'ai pu faire à Baris ! Merci pour tous ces bons moments que nous avons passés ensemble au laboratoire et pour m'avoir montré toutes les surprises possibles et inimaginables qu'un Western-Blot peut avoir (HAHA). Merci très sincèrement pour ton amitié depuis la L2, et pour toutes ces répliques de Kaamelott qui éclairent mes journées. Merci pour ta gentillesse, ton humour et ta grande force de travail, j'espère pouvoir retravailler avec toi bientôt. Si ce n'est pas le cas, on ira se mettre des piverts dans la tête au bar !

**Thibault Chazeirat**, que je commence par remercier pour son travail sur les différents projets. Mais mes remerciements sont loin d'être finis, merci pour m'avoir conseillé en L3 de faire le Master que tu avais réalisé et de m'avoir écouté dès ce moment-là, ignorant à l'époque que tu n'étais pas près de te débarrasser de moi ! Merci de m'avoir guidée et tout appris à la paillasse pendant mes deux stages de Master, non seulement tu as fait confiance à l'idée d'une stagiaire mais tu m'as poussé à la présenter et à la réaliser. Merci donc d'avoir été « mon doctorant » (HAHA quelle insolence) lors de ces stages. Merci pour tous tes conseils scientifiques et pour le côté paternaliste dont tu fais preuve. Merci pour ton humour, ton écoute incroyable, ton soutien et tous les excellents moments que nous avons passés ensemble. Il me tarde de continuer l'aventure à tes côtés !

Je tiens à remercier également tous les membres du laboratoire que j'ai eu la chance de rencontrer :

**Paul Bigot**, peu de mots peuvent décrire la reconnaissance que j'éprouve à ton égard. Merci pour ton soutien incommensurable lors de notre présence à des heures indécentes au laboratoire, et lors des moments difficiles tant professionnels que personnels. Merci pour toutes ces discussions autour d'une cigarette (L'ironie de la recherche sur la BPCO : ça fait fumer !) sources de joies de mes journées. Merci pour ton humour intarissable, ta générosité, ta bienveillance, ta grande culture et ton esprit perspicace et critique que j'affectionne particulièrement. La peine qu'a engendrée ton départ, égalera la joie que je ressentirai à chacune de nos retrouvailles.

**Aubin Pitiot**, pour ton amitié et la bienveillance dont tu fais preuve. Mon cher Binôme de bureau, les yeux de mon dos, merci pour les excellents moments passés à papoter. Tu as la capacité de rendre les moments passés à tes côtés légers et agréables. Merci pour ton soutien, et l'acceptation de mes nombreux travers telle que la maniaquerie avec laquelle j'organise mon bureau…(ou même le tiens parfois !).

**Alexis David**, pour ta discrétion initiale qui a exacerbé tes incroyables « *punchs lines* ». Merci pour la joie que tu apportes à notre bureau ! Merci aussi à **Baptiste** pour ajouter une touche supplémentaire à cette bonne ambiance.

**Christelle Parent**, pour ta grande gentillesse et ton écoute. Merci pour les bons moments que j'ai pu passer à tes côtés, autour d'une clope, d'un verre et d'une manip' (quand même). Merci aussi pour la grande disponibilité dont tu fais preuve et ton professionnalisme.

**Catherine Douteau**, pour tes qualités de secrétaire exceptionnelle. Merci pour les moments que nous avons partagé ainsi que pour ton écoute et ton soutien. Merci pour la gentillesse que tu m'as accordée, je respecte profondément la dévotion dont tu fais preuve à l'égard de tes amis (et de tes ennemis !).

**Anne-Sophie Venet-Charles**, pour avoir organisé nos congrès en Italie et aux USA. Merci pour ta bonne humeur et ta tolérance pour les commandes ou demandes de dernière minute !

**Catherine Neau**, pour ton aide dans mes projets mais aussi pour l'intérêt que tu portes à mon sujet de thèse et pour l'écoute dont tu fais preuve lors de mes explications. Merci aussi pour ta grande gentillesse et bienveillance, qui rendent la vie au labo si charmante.

**Lise Vanderlynden**, pour ta gentillesse et la réalisation des plus beaux Western Blot du laboratoire !

**Lydie Nadal Desbarats**, **Thomas Baranek**, **Fabien Lecaille**, **Sandrine Dallet-Choisy et Agnès Petit-Courty** pour m'avoir permis de réaliser des enseignements qui furent un vrai plaisir et une expérience particulièrement gratifiante.

**Julien Burlaud-Gaillard** pour m'avoir appris à prendre de belles photos de mes cellules. Merci aussi pour ta grande gentillesse.

Merci aux anciens doctorants **Adeline**, **Coco**, **Woodys** et **Mylène** pour leurs accueils bienveillants. Un grand merci aux doctorants dont j'ai eu l'honneur d'être la présidente ! **Camille**, **Emilie**, **Adélaïde**, **Alexis**, **Aubin**, **Sandra** et **Mike**, merci pour les excellents moments que nous avons passés ensemble et pour l'atmosphère que nous avons créée.

Enfin merci à tous les membres du laboratoire pour leur gentillesse et leur accueil : **Ahlame Saïdi, Delphine Fouquenet, Déborah Bréa**, **Maria Cabrera**, **Virginie Hervé**, **Sophie Iochmann**, **Déborah Le Pennec**, **Jeoffrey Pardessus Pascale Reverdiau**, **Alan Wacquier**, **Virginie Vasseur, Benoit Briard, Elise Biquand, Guy Ilango, Lilou, Gabrielle** et les Marion : **Marion Lavergne, Marion Ferreira, Marion Pronost**. En espérant n'avoir oublié personne, j'espère que vous pardonnerez une doctorante fatiguée.

Je remercie tous les membres de ma famille pour leur soutien, et plus en détail :

**Papa**, pour l'énorme soutien que tu m'as accordé et la patience dont tu as fait preuve dans la réalisation de mon choix de carrière. Merci d'être toujours là dans les bons moments comme dans les mauvais, j'ai toujours soutenu avoir le meilleur papa du monde et j'en demeure convaincue. Je ne le dis pas souvent, alors je profite de cette thèse pour te dire que je t'aime. **Catherine**, pour ton soutien et la grande joie de vivre dont tu fais profiter toute la famille. Merci de m'avoir accepté et considéré comme ta fille, nous avons eu des moments difficiles mais qui ne sont rien comparé aux merveilleux moments que nous passons ensemble à présent.

**Mouty**, pour tous les encouragements que tu m'apportes. Merci pour la fierté dont tu fais preuve quand tu parles de moi et pour l'inquiétude que tu m'accordes quand je suis trop occupée pour te répondre. Bien que je sois vraiment occupée, j'apprécie quand même cette preuve d'amour, malgré cela je ferai en sorte, à l'avenir, de moins t'inquiéter.

Mes frères, **Nany**, **Floppy** et **Antoine**, pour votre soutien au quotidien et parce que vous êtes toujours là. En tant que petite dernière, je suis parfaitement consciente de la chance que j'ai d'avoir 3 grands frères aussi exceptionnels. Merci pour la protection que vous m'avez apportée, votre sens de l'humour inépuisable, votre générosité (au cas où vous n'auriez pas compris, je paierai…pas) tout ce que vous m'apportez depuis toujours et même toutes les tortures que vous m'avez fait subir ! Je vous remercie aussi de vous être liés à des femmes exceptionnelles **Morgane**, **Melina** et **Michèle** qui m'ont offert (avec votre participation) les plus beaux cadeaux qu'il m'ait été donné de recevoir **Noémie**, **Abel**, **Margaux** et **Mara**. Si vous lisez ces mots en grandissant, je vous remercie pour l'incroyable bonheur que vous m'apportez tous les quatre, merci de m'avoir montré qu'il n'y a pas de plus beau rôle que celui d'être votre Tata Roro. **Melina**, merci pour ta grande joie de vivre, ton côté diva, ton soutien, ta générosité et pour avoir choisi mon frangin ! **Morgane**, merci pour ton soutien depuis maintenant presque 20 ans. Ta gentillesse, ta patience sans limite, ton écoute, ton sens de l'humour, ton côté artistique et toutes tes nombreuses qualités qui m'éblouissent, merci d'être toujours là et d'avoir intégré notre famille et ajouté la tienne par la même occasion. Merci à **Océane** et à **Jérôme** pour leur sympathie et leurs bonnes humeurs, merci de m'avoir choisie comme marraine de **Victoire**. Si tu lis ces mots **Victoire**, j'espère pouvoir t'apprendre toutes les choses que j'ai apprises durant ma courte vie et que j'apprendrai. Merci à toi et à **Louis** de m'apporter tant de joie de vivre uniquement par votre présence.

Pour finir ces longs remerciements, je tiens à remercier mes amis :

**Samy**, *my love*, mon âme-sœur, merci d'être mon meilleur ami depuis maintenant presque 15 ans (aïe). Merci pour tout le soutien que tu m'apportes au quotidien et pour tes mots qui résonnent comme des mantras en moi. Merci de m'encourager par ta motivation, ton courage, ton éthique, ta générosité qui ne sont que quelques-unes de tes nombreuses qualités. Merci de me comprendre et de m'aider, dans le passé, le présent et les nombreuses années dont notre amitié sera constituée.

**Clara**, merci d'être ma meilleure amie malgré nos longues périodes de silence. En tant que future psychiatre, je pense que tu devrais analyser notre amitié, qui ressemble aux montées et descentes d'un esprit bipolaire ! Malgré cela, chaque retrouvaille n'est que pur bonheur, comme si le temps de notre relation s'arrête pendant nos absences de contact. Alors merci pour m'avoir encouragée, supportée et soutenue depuis toutes ces années.

**Fanny** et **Léa**, merci à toutes les deux pour votre soutien et pour tous les bons moments que nous avons passés ensemble. **Fanny**, merci pour tous nos déjeuners ensemble, ils éclaircissent systématiquement mes journées. **Léa**, merci pour tous les lendemains de cuites à squatter chez toi (Haha). Plus sérieusement, vous êtes toutes deux exceptionnelles, merci d'être mes amies tout simplement.

*Last but not least*, **Julien**, merci de m'avoir encouragé depuis le début, dans mes études. Merci de me dire que je suis « super Roro ». Merci de croire que presque tout ce que j'entreprends, je vais le réussir. Merci pour les moments merveilleux que nous avons partagés ensemble. Merci à la générosité de ta famille **Rosa**, **Christian** et **Alex**. Merci pour votre accueil incroyable.

# Résumé en français :

La cathepsine C (CatC) est une protéase à cystéine qui catalyse la maturation des protéases à sérine pro-inflammatoires du neutrophile (PSN), telles que l'élastase, la protéinase 3 et la cathepsine G, et des granzymes (Gzms) des lymphocytes cytotoxiques (LC) impliquées dans l'activation des voies de signalisation qui déclenchent la mort cellulaire programmée des cellules cancéreuses ou infectées par un virus. La CatC représente ainsi une cible thérapeutique potentielle dans toutes les pathologies inflammatoires et/ou auto-immunes impliquant les PSN. Les inhibiteurs chimiques de la CatC sont actuellement évalués dans les essais précliniques et cliniques. Une inactivation génétique de la CatC est observée chez les patients atteints du syndrome de Papillon-Lefèvre (SPL). Dans les neutrophiles de ces patients, seules de faibles quantités de PSN actives sont détectées (<10% par rapport aux individus sains) ce qui suggère l'implication d'une protéase alternative à la CatC, que nous avons nommé la NSPs-AAP-1 (*NSPs-Alternative Activating Protease-1)* impliquée dans l'activation des zymogènes de PSN. La caractérisation enzymatique des Gzms dans les LC de patients atteints du SPL a également révélé une voie d'activation indépendante de la CatC impliquée dans l'activation des Gzms (~50% par rapport aux individus sains). Au cours de ce travail de thèse, nous avons étudié les processus protéolytiques non-dépendants de la CatC impliqués dans l'activation des PSN et des Gzms en bloquant la maturation de la CatC dans des modèles cellulaires. Nos résultats ont démontré l'existence de la NSPs-AAP-1 impliquée dans l'activation des PSN qui est une protéase à cystéine inhibée par les inhibiteurs de type nitrile de la CatC. La voie non-dépendante de la CatC de l'activation des Gzms dans les LC est médiée par une protéase alternative différente de la NSPs-AAP-1. Cette protéase est résistante aux inhibiteurs de protéase à cystéine. Cette étude suggère que le ciblage pharmacologique de la CatC pour bloquer les PSN dans les maladies inflammatoires ou auto-immunes ne devrait pas altérer l'activité cytotoxique des LC.

**Mots clés** : neutrophile, lymphocyte, cathepsine C, protéase à sérine du neutrophile, granzyme, inhibiteur de protéase

# Résumé en anglais :

The cysteine protease cathepsin C (CatC) activates immune cells serine proteases including pro-inflammatory neutrophil serine proteases (NSPs) (elastase, proteinase 3 and cathepsin G) and cytotoxic lymphocyte (CL) granzymes (Gzms) involved in the activation of signaling pathways that trigger programmed cell death in virus-infected or cancerous cells. CatC represents a potential therapeutic target in all inflammatory and/or autoimmune diseases involving NSPs. Chemical inhibitors of CatC are currently being evaluated in preclinical and clinical trials. Genetic inactivation of CatC has been observed in patients with Papillon-Lefèvre syndrome (PLS). In neutrophils from these patients, only small amounts of active NSPs are detected (<10% compared to healthy individuals), suggesting the involvement of an alternative protease to CatC, which we have named NSPs-AAP-1 (NSPs-Alternative Activating Protease-1) involved in the activation of NSP zymogens. Enzymatic characterization of Gzms in CLs from PLS patients also revealed a CatC-independent activation pathway involved in Gzms activation (~50% compared to healthy individuals). In this thesis work, we investigated CatC-independent proteolytic processes involved in the activation of NSPs and Gzms by blocking CatC maturation in cellular models. Our results clearly demonstrated the existence of NSPs-AAP-1 involved in the activation of NSPs, which is a cysteine protease inhibited by nitrile-type CatC inhibitors. The CatC-independent pathway of Gzms activation in CLs is mediated by an alternative protease different from NSPs-AAP-1. This protease is resistant to cysteine protease inhibitors, suggesting that pharmacological targeting of CatC to block NSPs in inflammatory or autoimmune diseases would not alter the cytotoxic activity of CLs.

**Keywords** : neutrophil, lymphocyte, cathepsin C, neutrophil serine protease, granzymes, protease inhibitor

# Table des matières :

Remerciements……4
Résumé en français……..……..……...….12
Résumé en anglais…….……14
Table des matières…….……16
Liste des publications……..…..20
Liste des communications…….....22
Liste des tableaux……..24
Liste des figures……...……..26
Liste des abréviations……...….28
Préambule……..30

**I. Revue bibliographique……..**32

**1. Les cellules immunitaires**……34

1.1. Le polymorphonucléaire neutrophile…….36

1.1.1. La maturation du neutrophile……..37

1.1.2. Les granules du neutrophile……37

1.1.3. Le rôle du neutrophile dans la lutte contre les pathogènes……39

1.2. Le monocyte et le macrophage……..41

1.2.1. La différentiation des monocytes……..……...……....42

1.2.1.1. *La différentiation en cellules dendritiques*……..44

1.2.1.2. *La différentiation en macrophages*……...……...44

1.2.2. Les rôles pathologiques des monocytes-macrophages……..…...…45

1.3. Les lymphocytes……46

1.3.1. Les lymphocytes T…….……..…47

1.3.2. Les lymphocytes B…….……49

1.3.3. Les natural killers……...……...….50

1.4. Les lignées de cultures cellulaires immunitaires……50

**2. La cathepsine C**……...…….....51

2.1. Les généralités sur les protéases……....52

2.1.1. La nomenclature EC……...…….53

2.1.2. La classification en famille et en clan……..……54

2.2. Les différentes classes de protéases……...…55

2.2.1. Les protéases à cystéine (EC 3.4.14)……55
2.2.2. Les protéases à sérine (EC 3.4.21)……..…….56
2.2.3. Les protéases acides (EC 3.4.23)……..……...57
2.2.4. Les métalloprotéases matricielles (EC 3.4.24)…….……58
2.2.5. Les protéases à thréonine (EC 3.4.24)……..59
2.3. Les mécanismes de régulation des protéases…….59
2.4. Les cathepsines à cystéine…….60
2.4.1. Les cathepsine L-like……...……65
2.4.1.1. *La cathepsine L*……65
2.4.1.2. *La cathepsine S*……....66
2.4.1.3. *La cathepsine K*……...……68
2.4.1.4. *La cathepsine V*……...69
2.4.1.5. *La cathepsine F*……...……69
2.4.2. La cathepsine C……..….70
2.4.2.1. *La biosynthèse et la maturation de la cathepsine C*……..…70
2.4.2.2. *La localisation intracellulaire et la sécrétion de la cathepsine C*…….……..…72
2.4.2.3. *La structure du site catalytique et la spécificité de la cathepsine C*……...……..…73
2.4.2.4. *Les inhibiteurs de type nitrile de la cathepsine C*…….74
2.4.2.5. *Les fonctions biologiques de la cathepsine C*…….…….76
2.4.2.6. *Les fonctions pathologiques de la cathepsine C*……...…78
**3. Les protéases à serine maturées par la cathepsine C**……81
3.1. Les protéases à serine du neutrophile..……...…81
3.1.1. La biosynthèse des protéases à sérine du neutrophile…..……....81
3.1.2. Les caractéristiques structurales des protéases à sérine du neutrophile.……82
3.1.3. Les inhibiteurs physiologiques des protéases à sérine du neutrophile…….……82
3.1.4. Les fonctions physiologiques des protéases à sérine du neutrophile……..……83
3.1.5. Les fonctions pathologiques des protéases à sérine du neutrophile…….….84

3.2. Les granzymes……...86
3.2.1. La biosynthèse des granzymes……..……...…86
3.2.2. Les caractéristiques structurales des granzymes……..……86
3.2.3. Les fonctions physiologiques des granzymes……...……...87
**4.** Ciblages pharmacologiques de la cathepsine C thérapeutique……..89
4.1. Icat$C_{XPZ-01}$……...……..89
4.2. BI-9740 et BI-1291583……..91
4.3. Brensocatib……92
4.4. HSK31858…….93
4.5. GSK27936600……...……93
4.6. Composé 22……..…….……93
**II. Travaux personnels……...……**96
**Objectif de la thèse**……..…98

**Manuscrit 1** : Pharmacological inhibition of cathepsin S and of NSPs-AAP-1 (a novel, alternative protease driving the activation of neutrophil serine proteases)……102

**Manuscrit 2** : Activation of neutrophil elastase-related serine proteases in myelomonocytic cells…….……128

**Manuscrit 3** : Activation of granzymes in cytotoxic lymphocytes……..152

**III. Discussion, conclusion et perspective……...**172

**Références bibliographiques**……...…….184

**Annexes**……..198
**Annexe 1** : Cathepsin C inhibition as a potential treatment strategy in cancer……200
**Annexe 2** : Modulation of the expression and activity of cathepsin S in reconstructed human skin by neohesperidin dihydrochalcone……...218
**Annexe 3** : Neutrophils play a major role in the destruction of the olfactory epithelium during SARS-CoV-2 infection in hamsters ……..…….....236
**Annexe 4** : Alpha-1-antitrypsin protects vascular grafts of brain-dead rats against ischemia/reperfusion injury ……..…..254
**Annexe 5** : Pharmacological inhibition of the cysteine protease cathepsin C improves graft function after heart transplantation in rats ……...268

# Liste des publications :

## Publication en premier auteur

1. **Pharmacological inhibition of cathepsin S and of NSPs-AAP-1 (a novel, alternative protease driving the activation of neutrophil serine proteases)**

**Roxane Domain*,** Seda Seren*, Uwe Jerke, Manousos Makridakis, Kuan-Ju Chen, Jérôme Zoidakis, Moez Rhimi, Xian Zhang, Tillia Bonvent, Cécile Croix, Loïc Gonzalez, Dedong Li, Jessica Basso, Christophe Paget, Marie-Claude Viaud-Massuard, Gilles Lalmanach, Guo-Ping Shi, Ali Aghdassi, Antonia Vlahou, Patrick P. McDonald, Isabelle Couillin, Rich Williams, Ralph Kettritz, Brice Korkmaz

**: Equal contribution*

***Accepted in Biochem Pharmacol (March 5th, 2024), will be published September 5th, 2024***

## Manuscrits en préparation

1. **Activation of neutrophil elastase-related serine proteases in myelomonocytic cells**

**Roxane Domain**, Thibault Chazeirat*, Quentin Guilbert*, Lise Vanderlynden, Patrick P. McDonald, Rich Williams and Brice Korkmaz

**: Equal contribution*

2. **Activation of granzymes in cytotoxic lymphocytes**

**Roxane Domain**, Loïc Gonzalez, Jérôme Zoidakis, Antonia Vlahou, Peter Eickholz, Patrick P. McDonald, Rich Williams, Christophe Paget and Brice Korkmaz

## Publication de collaboration

1. **The proteolytic airway environment associated to pneumonia acts as a biological barrier for anti-infective antibody treatment**

Blin Timothée*, Parent Christelle*, Pichon Gabrielle, Guillon Antoine, Youenn Jouan, Hassan Allouchi, Aubrey Nicolas, **Domain Roxane**, Korkmaz Brice, Sécher Thomas[$], Heuzé-Vourc'h Nathalie[$]

***Eur J Pharm Biopharm. 2024**, DOI: 10.1016/j.ejpb.2023.12.003.*

** : equally contributed to experiment implementation*

*$ : equally contributed to the study design*

2. **Pharmacological inhibition of the cysteine protease cathepsin C improves graft function after heart transplantation in rats**

Baoer Liu, Brice Korkmaz, Patricia Kraft, Tobias Mayer, Alex A. Sayour, Marc A. Grundl, **Roxane Domain**, Matthias Karck, Gábor Szabó1, Sevil Korkmaz-Icöz

***J Transl Med, 2023**, DOI: 10.1186/s12967-023-04659-6*

3. **Alpha-1-Antitrypsin Protects Vascular Grafts of Brain-Dead Rats Against Ischemia/Reperfusion Injury**

JuQingwei Ding, Sivakkanan Loganathan, Pengyu Zhou, Alex Ali Sayour, Paige Brlecic, Tamás Radovits, **Roxane Domain**, Brice Korkmaz, Matthias Karck, Gábor Szabó, Sevil Korkmaz-Icöz

***J Surg Res, 2022**, DOI: 10.1016/j.jss.2022.11.047*

4. **Neutrophils play a major role in the destruction of the olfactory epithelium during SARS-CoV-2 infection in hamsters**

Clara Bourgon, Audrey St Albin, Ophélie Ando-Grard, Bruno Da Costa, **Roxane Domain**, Brice Korkmaz, Bernard Klonjkowski, Sophie Le Poder, Nicolas Meunier

***Cell Mol Life Sci, 2022**, DOI: 10.1007/s00018-022-04643-1*

5. **Modulation of the expression and activity of cathepsin S in reconstructed human skin by neohesperidin dihydrochalcone**

Juliette Sage*, Justine Renault*, **Roxane Domain**, Krzysztof K Bojarski, Thibault Chazeirat, Alhame Saidi, Emmanuelle Leblanc, Carine Nizard, Sergey A Samsonov, Robin Kurfurst, Gilles Lalmanach, Fabien Lecaille

***Matrix Biol, 2022**, DOI: 10.1016/j.matbio.2022.02.003*

*: *Equal contribution*

6. **Cathepsin C inhibition as a potential treatment strategy in cancer**

Brice Korkmaz, Anne-Sophie Lamort, **Roxane Domain**, Céline Beauvillain, Artur Gieldon, Ali Önder Yildirim, Georgios T Stathopoulos, Moez Rhimi, Dieter E Jenne, Ralph Kettritz

***Biochem Pharmacol, 2021**, DOI: 10.1016/j.bcp.2021.11480*

# Liste des communications :

## *Communications orales*

1. **40th Winter School on proteinases and inhibitors, Tiers, Italie (2023)**

Proteolytic pathways involved in the activation of pro-inflammatory neutrophil serine proteases
**Roxane Domain**, Seda Seren and Brice Korkmaz

2. **Courte présentation des travaux de thèse non confidentiels à l'attention du Professeure Christine Pham** Washington University of St Louis, USA (2023)

3. **International Symposium on Cathepsin C: ISyCatC III (2022**)

Proteolytic processes involved in the maturation of neutrophil serine proteases and granzymes.
**Roxane Domain**, Seda Seren, Uwe Jerke, Gilles Lalmanach, Ralph Kettritz and Brice Korkmaz

## *Communications par poster*

1. **The 47th FEBS Congress, Tours, France (2023)**

Cathepsin C-independent activation of pro-inflammatory neutrophil serine proteases
**Roxane Domain**, Moez Rhimi and Brice Korkmaz

2. **ASPET 2023 Annual Meeting in St. Louis, Missouri, USA, (2023)**

Consequences of pharmacological inhibition of cathepsin C using IcatCXPZ-01 on maturation of granzyme zymogens in cytotoxic lymphocytes
**Roxane Domain** and Brice Korkmaz

3. **39th Winter School on proteinases and inhibitors, web meeting (2022)**

Cathepsin C-independent maturation of granzyme zymogens in cytotoxic lymphocytes.
**Roxane Domain**, Thomas Baranek, Christophe Paget, Brice Korkmaz

4. **33th Biotechnocentre Symposium, Domaine des Hauts de Bruyères, France (2021)**

Cathepsin C-independent maturation of granzyme zymogens in cytotoxic lymphocytes.
**Roxane Domain**, Thomas Baranek, Christophe Paget, Brice Korkmaz

5. **Biomedical research day Anger-Tours, Anger, France (2021)**

Proteolytic pathway involved in the maturation of granzyme zymogens in cytotoxic lymphocytes.
**Roxane Domain**, Thomas Baranek, Christophe Paget, Brice Korkmaz

# Liste des tableaux :

**Tableau 1 :** Exemples de lignées cellulaires immunitaire immortalisées et leurs caractéristiques……..……51

**Tableau 2 :** Identité et similarité de la séquence protéique de la forme mature des cathepsines à cystéine humaine et la papaïne……...61

**Tableau 3 :** Caractéristiques des cathepsines à cystéine humaines……..63

**Tableau 4 :** Inhibiteurs de la cathepsine S en cours d'essais cliniques….……68

**Tableau 5 :** Inhibiteurs de la cathepsine C en cours d'essais cliniques…….……...76

**Tableau 6 :** Localisation chromosomique des gènes des granzymes chez la souris et chez l'Homme……...86

# Liste des figures :

**Figure 1 :** Leucocytes du sang périphérique humain……..34
**Figure 2 :** Différentiation des cellules souches hématopoïétiques……...35
**Figure 3 :** Neutrophile quiescent et neutrophile activé ayant sécrété des « Neutrophil Extracellular Traps » (NETs)……...…….36
**Figure 4 :** Maturation du polynucléaire neutrophile……...….37
**Figure 5 :** Granulopoïèse du polynucléaire neutrophile……...38
**Figure 6 :** Systèmes antimicrobiens du neutrophile…….40
**Figure 7 :** Diapédèse des leucocytes……....42
**Figure 8 :** Stades cellulaires de la différentiation monocytaire……43
**Figure 9 :** Différenciation des monocytes en macrophage M1 ou M2……...…….45
**Figure 10 :** Stades cellulaires de la différentiation lymphocytaire……...……...…47
**Figure 11 :** Différents types de lymphocytes……..…….....49
**Figure 12 :** Nomenclature de Schechter et Berger……...52
**Figure 13 :** Illustration structurale des endo- et exopeptidases……....53
**Figure 14 :** Nomenclature EC…….…….54
**Figure 15 :** Illustration du site actif d'une protéase…….....55
**Figure 16 :** Mécanismes catalytiques des protéases à cystéine et des protéases à sérine…...56
**Figure 17 :** Mécanismes catalytiques des protéases acides et des métalloprotéases matricielles……....58
**Figure 18 :** Illustration des mécanismes de régulation des protéases……60
**Figure 19 :** Arbre phylogénétique des cathepsines à cystéine……61
**Figure 20 :** Structure tridimensionnelle des cathepsines à cystéine……...……..62
**Figure 21 :** Mécanisme catalytique des cathepsines à cystéine……...64
**Figure 22 :** Illustration schématiques des zymogènes des protéases CatL-Like…….…….65
**Figure 23 :** Pro-cathepsine L et formes matures……..…….……...66
**Figure 24 :** Pro-cathepsine S et auto-maturation…….……..…..……67
**Figure 25 :** Présence de la cathepsine C dans divers tissus sains…….70
**Figure 26 :** Maturation protéolytique de la pro-cathepsine C et structure cristallisée du monomère de la cathepsine C mature……...71
**Figure 27 :** Structures de la pro- et mature cathepsine C humaine……...……...72

**Figure 28 :** Schéma de la liaison d'un substrat peptidique avec le site actif de la cathepsine C……..…..73
**Figure 29 :** Structures chimiques des inhibiteurs de type nitrile de la cathepsine C……...…75
**Figure 30 :** Structure cristallisée de l'IcatC$_{XPZ-01}$ complexé au site actif la cathepsine C humaine……75
**Figure 31 :** Activation de la pro-chymase par la cathepsine C……...…….....77
**Figure 32 :** Illustration de la maturation des protéases à serine du neutrophile par la cathepsine C dans le promyéolocyte……...……..77
**Figure 33 :** Manifestations cliniques des patients atteints du syndrome de Papillon-Lefèvre.78
**Figure 34 :** Conséquences de l'inactivation génétique de la cathepsine C sur la stabilité des protéases à sérine neutrophilique humaines……...……...79
**Figure 35 :** Conséquences de l'inactivation génétique de la cathepsine C sur l'activation des granzymes…….....80
**Figure 36 :** Conséquences de l'inactivation génétique chez l'homme ou d'une déplétion chez la souris de la cathepsine C sur l'activation de ses protéases à serine cibles……80
**Figure 37 :** Activation des protéases à serine du neutrophile…...……...81
**Figure 38 :** Structure tridimensionnelle de l'élastase complexée à l'inhibiteur OMTKYIII...82
**Figure 39 :** Structure et mécanisme d'action des serpines illustrés par l'alpha-1 antitrypsin (AAT)……...…….83
**Figure 40 :** Cercle vicieux de l'infection et de l'inflammation dans les pathologies inflammatoires pulmonaires chroniques……...84
**Figure 41 :** Physiopathologie de la granulomatose avec polyangéite…….….85
**Figure 42 :** Structure de la granzyme A……...87
**Figure 43 :** Voies de mort cellulaires activées par les granzymes A et B……..…..88
**Figure 44 :** Illustration du ciblage pharmacologique des protéases à serine du neutrophile par l'inhibition de cathepsine C dans le promyélocyte à l'aide des inhibiteurs chimiques……...89
**Figure 45 :** Elimination de l'élastase dans les neutrophiles en culture traités avec l'IcatC$_{XPZ-01.}$ …….....90
**Figure 46 :** Conséquences de l'inactivation génétique ou pharmacologique de cathepsine C……...…….91
**Figure 47 :** Illustration des cascades protéolytiques impliquées dans l'activation des protéases à serine du neutrophile et des granzymes dans des cellules saines ou issues de patients déficitaires en cathepsine C…….……..99

# Liste des abréviations :

| | |
|---|---|
| $\alpha$1-PI | $\alpha$1-proteinase inhibitor |
| aa | Acides aminés |
| AAT | Alpha-1 antitrypsine |
| ANCA | Anti-neutrophil cytoplasmic antibodies |
| ATCC | American type culture collection |
| ATRA | All-trans retinoic acid |
| BPCO | Broncho-pneumopathie chronique obstructive |
| Cat | Cathepsine |
| CEPR | Centre d'Etude des Pathologies Respiratoires |
| CD | Cellules dendritiques |
| DFF45 | DNA fragmentation factor 45 kDa subunit |
| DMSO | Dimethyl sulfoxide |
| DPPI | Dipeptidyl peptidase I |
| ERO | Espèces réactives de l'oxygène |
| Flt3L | FMS-related tyrosine kinase 3 ligand |
| G-CSF | Granulocyte-colony stimulating factor |
| GM-CSF | Granulocyte-macrophage colony-stimulating factor |
| GPA | Granulomatose avec polyangéite |
| Gzms | Granzymes |
| ICAD | Caspase-activated DNase inhibitor |
| ICAM1 | Intercellular adhesion molecule 1 |
| IFN-$\gamma$ | Interferon-$\gamma$ |
| IL | Interleukine |
| IUBMB | International Union of Biochemistry and Molecular Biology |
| LHVS | Leucine-homophenylalanine-vinyl sulfone |
| LPS | Lipopolysaccharide |
| LB | Lymphocytes B |
| LT | Lymphocytes T |
| LTh | Lymphocyte T helper |
| LTreg | Lymphocyte T regulateur |
| LTfh | Lymphocyte T follicular helper |

| | |
|---|---|
| LAMP | Lysosomal-associated membrane protein |
| MEC | Matrice extracellulaire |
| MHC | Major Histocompatibility Complex |
| MPO | Myéloperoxidase |
| MMP | Métalloprotéase matricielle |
| NADPH | Nicotinamide adénine dinucléotide phosphate hydrogéné |
| NE | Elastase neutrophilique |
| NK | Natural killer |
| NET | Neutrophil extracellular traps |
| NGAL | Neutrophil gelatinase associates lipocalin |
| NSP | Neutrophil serine protease |
| NSPs-AAP | NSPs alternative activating protease |
| OMS | Organisation Mondiale de la Santé |
| PBMC | Peripheral blood mononuclear cells |
| PMA | Phorbol myristate acetate |
| PNN | Polynucléaire neutrophile |
| PSN | Protéases à serine du neutrophile |
| PSN4 | Protéase à serine du neutrophile 4 |
| PSN-AAP | PSN-Protéase Activatrice Alternative |
| PR3 | Protéinase 3 |
| SLPI | Secretory leukocyte protease inhibitor |
| SCF | Stem-cell factor |
| SPL | Syndrome de Papillon-Lefèvre |
| TCR | T cell receptor |
| TPO | Thrombopoïétine |
| TNF-$\alpha$ | Tumor necrosis factor-$\alpha$ |
| TRAIL-R | TNF-related apoptosis-inducing ligand-receptor |

# Préambule

Les pathologies infectieuses et inflammatoires pulmonaires comptent parmi les dix principales causes de mortalité dans le monde en 2019 selon l'Organisation Mondiale de la Santé (OMS), et ont donc des conséquences médicales et socio-économiques importantes. De ce fait, l'étude de celles-ci constitue un sujet de recherche majeur répondant à des questions sanitaires d'ordre mondial.

L'unité de recherche INSERM UMR-1100, « ***Centre d'Étude des Pathologies Respiratoires (CEPR)*** », dirigée par le Docteur Mustapha Si-Tahar, a pour objectif d'étudier la physiopathologie des maladies respiratoires et de proposer de nouvelles stratégies thérapeutiques au travers de thématiques convergentes entre trois équipes constitutives. Pour développer des thématiques de recherche fondamentale, translationnelle et clinique, l'unité UMR-1100 dispose d'un environnement approprié tant sur le plan humain que matériel avec des structures d'appui efficaces. L'Unité est actuellement composée de trois équipes de recherche : l'équipe 1 « ***Infection respiratoire et immunité*** » dirigée par le Docteur Mustapha Si-Tahar, l'équipe 2 « ***Mécanismes protéolytiques dans l'inflammation*** » dirigée par le Professeur Gilles Lalmanach et l'équipe 3 « ***Aérosolthérapies et biothérapies à visée respiratoire*** » dirigée par le Docteure Nathalie Heuze-Vourc'h.

L'équipe 2 s'intéresse aux protéases impliquées dans les inflammations pulmonaires dans le but de proposer de nouvelles approches thérapeutiques. Le groupe thématique du Docteur Brice Korkmaz se penche sur le ciblage pharmacologique d'une protéase synthétisée dans la moelle osseuse, la cathepsine C. Cette protéase active les enzymes de dégradation des cellules immunitaires impliquées dans les maladies inflammatoires respiratoires. La cathepsine C représente donc une cible thérapeutique potentielle dans toutes les pathologies inflammatoires associant une dégradation tissulaire enzymatique. Au cours de cette thèse, nous avons étudié les « ***Mécanismes protéolytiques impliqués dans la maturation de la cathepsine C et de ses protéases à serine cibles dans les cellules immunitaires*** » et collaboré avec certaines équipes du « ***Consortium International de la Cathepsine C*** » mis en place par le Docteur Brice Korkmaz en 2016.



# I. Revue bibliographique

## 1. Les cellules immunitaires

Le système immunitaire est présent dans tout le corps dans un état de vigilance. Les organes du système immunitaire sont nommés organes lymphoïdes et comprennent la moelle osseuse, les ganglions, la rate, les amygdales et le thymus. Les organes du système immunitaire protègent ensemble l'organisme des pathogènes, par la détection de signaux de danger et la coordination d'une réponse appropriée à ceux-ci. Bien que différents, ces organes ont pour caractéristique commune d'abriter les cellules immunitaires, celles-ci sont très importantes pour défendre l'organisme contre les agents pathogènes. Les cellules immunitaires sont appelées globules blancs ou leucocytes. Il existe plusieurs types différents de leucocytes qui jouent chacun un rôle dans le système immunitaire. Ces cellules comprennent les granulocytes neutrophiles, les monocytes, les lymphocytes, tels que des lymphocytes T, B et NK (pour Natural Killer), ainsi que les polynucléaires basophiles et éosinophiles.

Les cellules mononuclées du sang périphérique (PBMC) sont toutes les cellules du sang périphérique ayant un noyau rond. Ces cellules sont constituées des lymphocytes (cellules T, cellules B, cellules NK) et des monocytes qui ont un noyau rond, ainsi que des granulocytes (neutrophiles, basophiles et éosinophiles) qui ont des noyaux multi-lobés. Dans un échantillon type de leucocytes sanguins humains, environ 60% seront des neutrophiles, 30% seront des lymphocytes, 6% seront des monocytes, 3% seront des éosinophiles et 1% seront des basophiles (Kouzehkanan et al., 2022) (**Figure 1**). Au sein de la population de lymphocytes elle-même, 70-85% seront des lymphocytes T, 5-10% des lymphocytes B et 5-20% des NK.

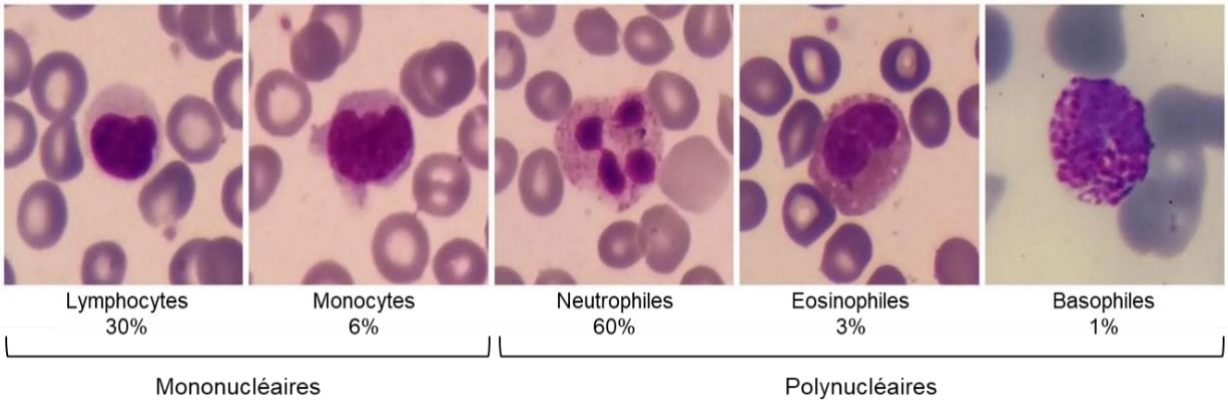


**Figure 1 : Leucocytes du sang périphérique humain.** Images microscopiques (objectif x100) de leucocytes issus de sang de volontaires sain colorés à la coloration Giemsa. Les pourcentages correspondent aux pourcentages de cellules dans le sang. D'après (Kouzehkanan et al., 2022).

L'hématopoïèse est le processus qui permet à partir des cellules souches hématopoïétiques pluripotentes d'obtenir toutes les cellules du sang périphérique. Chaque jour, un adulte sain produit environ 100 milliards de leucocytes. En cas de nécessité, notre corps est capable de multiplier la production de cellules par 10 (Borregaard, 2010). La cellule souche hématopoïétique est capable soit de s'auto-renouveler soit de se différencier en une cellule progénitrice. La cellule progénitrice peut devenir un progéniteur de cellule myéloïde grâce à l'action du SCF (pour « Stem-Cell Factor ») et de la thrombopoïétine (TPO) ou un progéniteur de cellule lymphoïde grâce à l'action de l'interleukine-7 (IL-7). Le progéniteur de cellule myéloïde peut se transformer en granulocyte neutrophile, éosinophile ou basophile ou en monocyte. Le monocyte peut ensuite se différencier en plusieurs types de cellules, dont l'une est le macrophage. Les progéniteurs de cellule lymphoïde vont devenir des lymphocytes T (LT), des lymphocytes B (LB) ou des cellules « Natural Killer » (NK) (**Figure 2**) (Kaushansky, 2006).

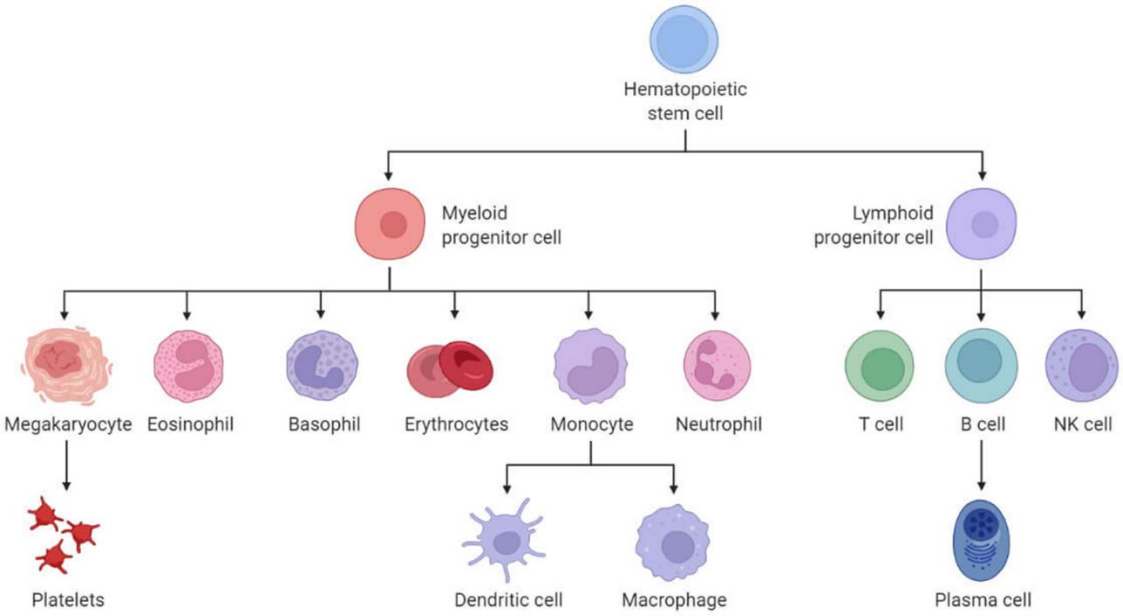


**Figure 2 : Différentiation des cellules souches hématopoïétiques.** D'après (Raza et al., 2021).

Les granulocytes neutrophiles, éosinophiles, basophiles et les macrophages sont des cellules capables d'internaliser des agents pathogènes étrangers ou d'attaquer des parasites trop gros pour être absorbés par dégranulation dans le cas des basophiles. Les lymphocytes B, également appelés cellules B, sont maturés dans la moelle osseuse, par opposition aux cellules T qui sont maturés dans le thymus. Les lymphocytes B fabriquent des anticorps, qui sont des protéines globulaires qui ont la capacité de se fixer et de participer à la destruction des pathogènes. Les lymphocytes NK (Natural Killer) sont également appelés cellules tueuses naturelles. Ils

attaquent les tumeurs et tuent les cellules cancéreuses. Les lymphocytes T, parfois appelés simplement cellules T, sont des lymphocytes qui se différencient en trois types de cellules : les lymphocytes T auxiliaires, cytotoxiques et régulateurs. Les lymphocytes T cytotoxiques sont des lymphocytes qui tuent les cellules infectées ou anormales pouvant entraîner la formation d'un cancer. Ils peuvent être la cause de rejet, car ils sont responsables de l'attaque d'un organe transplanté. Les lymphocytes T cytotoxiques se distinguent par la présence du récepteur CD8 à leur surface cellulaire. Les lymphocytes T régulateurs sont des cellules qui suppriment ou régulent la fonction des autres types de cellules immunitaires. Ils empêchent l'attaque du « soi », une dérégulation peut donc entraîner des maladies auto-immunes. Ils régulent l'activité des cellules immunitaire en diminuant leur activité à la suite de l'élimination d'un pathogène. Les lymphocytes T régulateurs présentent le récepteur CD4 à leur surface cellulaire.

## 1.1 Le polymorphonucléaire neutrophile

Le polynucléaire neutrophile (PNN) est une cellule de l'immunité innée produite lors de l'hématopoïèse dans la moelle osseuse. Le PNN est en première ligne de défense pour combattre les agents pathogènes qui ont franchi la barrière cutanéomuqueuse. C'est également la première cellule immunitaire à migrer du sang jusqu'au site inflammatoire ou infectieux afin de limiter la propagation de l'agent pathogène dans le corps, mais aussi de limiter les dégâts causés par le processus inflammatoire (**Figure 3**). Il a un rôle dans l'immunité innée et adaptative mais aussi dans l'homéostasie tissulaire. Le rôle du PNN est souvent bénéfique, mais lorsqu'il est activé de manière excessive et prolongée ou alors est déficitaire, des pathologies surviennent (Kolaczkowska and Kubes, 2013).

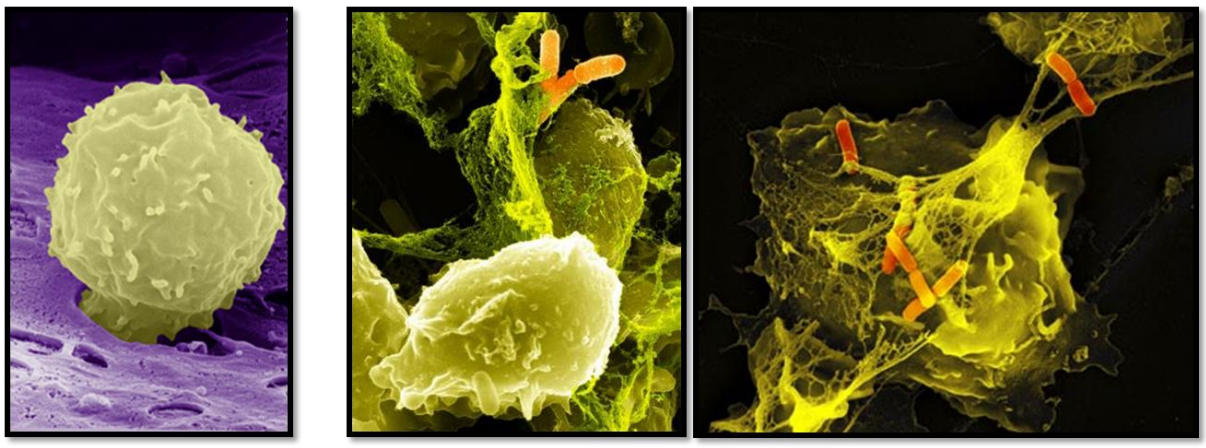

**Figure 3 : Neutrophile quiescent et neutrophile activé ayant sécrété des « Neutrophil Extracellular Traps » (NETs).** Image de microscopie électronique de PNN ayant libéré des NET, en orange des bactéries emprisonnées par les filets de chromatine. D'après (Brinkmann et al., 2004).

### 1.1.1 La maturation du neutrophile

Lors de l'hématopoïèse du PNN, le GM-CSF (pour « Granulocyte-Macrophage Colony-Stimulating Factor ») transforme les cellules progénitrices myéloïdes en précurseur de granulocyte. Ensuite l'action du G-CSF (pour « Granulocyte-Colony Stimulating Factor »), de l'interleukine-5 (IL-5) et du SCF permet le passage du stade de cellule progénitrice au PNN. Ainsi, le PNN, pour devenir mature, passe du stade myéloblaste à promyélocyte puis du stade myélocyte à métamyélocyte (Ley et al., 2007). La maturation médullaire du PNN dure environ 14 jours avant libération dans le sang où sa demi-vie est d'environ 8 heures (Pillay et al., 2010). La production de PNN représente 50 à 70 % de l'hématopoïèse, ainsi un adulte sain produit environ 50 milliards de PNN par jour (**Figure 4**).

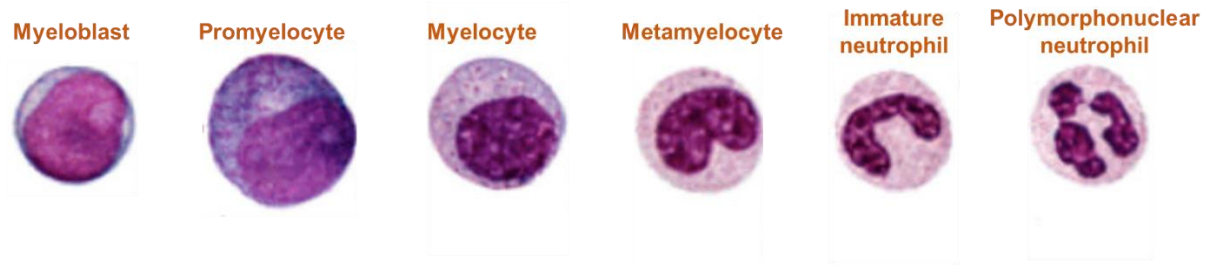


**Figure 4 : Maturation du polynucléaire neutrophile.** D'après (Cowland and Borregaard, 2016).

### 1.1.2 Les granules du neutrophile

Des études sur les PNN et sur leur formation dans la moelle osseuse ont mis en évidence la présence de trois types distincts de granules dans le PNN mature. Leur formation séquentielle dans la moelle osseuse a donné lieu à la description des granules primaire, secondaire et tertiaire (Bainton and Farquhar, 1966). La granulopoïèse commence lors de la différentiation des myéloblastes en promyélocytes. Les granules azurophiles, également appelés granules primaires, apparaissent dans les promyélocytes. La granulopoïèse continue avec la formation des granules spécifiques, aussi appelés granules secondaires, qui sont formés dans les myélocytes et les métamyélocytes. Ensuite les granules gélatinases, aussi appelés granules tertiaires, sont formées dans les PNN à noyau peu segmenté (« band cell »). Pour finir, les vésicules sécrétoires sont formées dans les PNN juste avant la libération des cellules dans le sang (**Figure 5**) (Cowland and Borregaard, 2016).

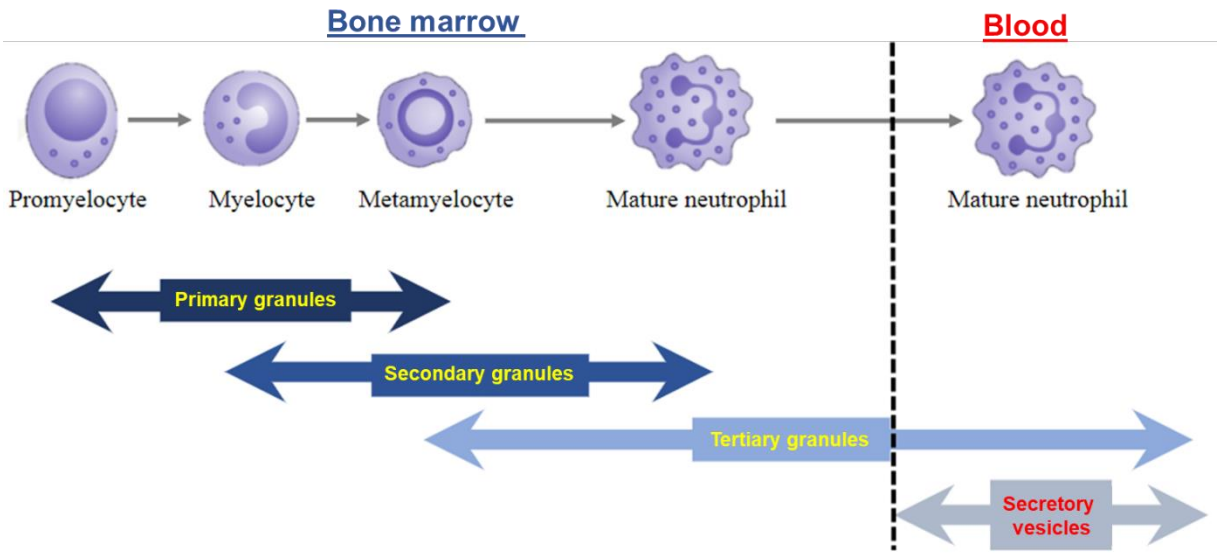


**Figure 5 : Granulopoïèse du polynucléaire neutrophile.** D'après (Cowland and Borregaard, 2016).

Les granules azurophiles sont majoritairement produits dans les promyélocytes et représentent 20% des granules des PNN matures. Le nom de ces granules provient du colorant azur de méthylène qui les colore lors d'un marquage de May-Gründwald Giemsa couramment utilisé en hématologie. Le granule azurophile contient des hydrolases acides et des protéines antimicrobiennes, c'est pourquoi ce granule a longtemps été considéré comme le lysosome des PNN (Cham et al., 1994). Les protéines membranaires des granules primaires ont permis d'exclure cette supposition car contrairement aux lysosomes, les granules azurophiles n'expriment pas les protéines LAMP I (pour « Lysosomal-associated membrane protein I **»)** et LAMP II (pour « Lysosomal-associated membrane protein II **»)** à leurs surfaces (Cieutat et al., 1998). Le granule azurophile étant peu sensible aux signaux de sécrétion, leur rôle majeur est la dégradation des pathogènes contenus dans les phagolysosomes. Cette granulation primaire contient la myéloperoxydase (MPO) qui permet la production d'HOCl ayant un fort pouvoir bactéricide. De plus, elle contient le lysozyme avec son action d'hydrolyse de la liaison entre l'acide N-acétyl-muraminique et la N-acétyl-D-glucosamine, qui va dégrader les parois de certaines bactéries et ainsi les détruire. On retrouve également des protéines antimicrobiennes comme les défensines dans ce granule (Ganz et al., 1985). Pour finir, ce granule azurophile contient des protéases à sérine du neutrophile (PSN) telles que l'élastase de neutrophile (NE), la protéinase 3 (PR3), la cathepsine G (CatG) et la PSN-4) (Egesten et al., 1994; Perera et al., 2013). Les granules spécifiques et tertiaires sont produits dans les PNN pendant la phase de différenciation terminale dans la moelle osseuse. La découverte qui a permis de différencier le

granule spécifique du granule tertiaire chez l'homme a été la découverte du NGAL (pour « Neutrophil Gelatinase Associates Lipocalin ». Cette lipocaline est présente dans les granules spécifiques mais pas dans les granules tertiaires donc en la ciblant il a été possible de discriminer les deux types de granules (Kjeldsen et al., 1993). Les granules spécifiques contiennent de nombreuses molécules impliquées dans la destruction des pathogènes et la modulation de l'inflammation. Ces substances jouent un rôle dans l'élimination des pathogènes dans le phagolysosome mais également dans le milieu extracellulaire (Borregaard, 2010). Les granules tertiaires ou gélatinases contiennent les métalloprotéases 9 (MMP9 aussi appelée gélatinase B) et 25 (MMP25), ainsi que la protéine antibactérienne cathélicidine (CAP-18) (Othman et al., 2022). Ceux-ci sont plus petits que les granules spécifiques, et sont plus facilement sujet à l'exocytose. Cette particularité reflète leur contenu riche en protéase, permettant de dégrader la matrice extracellulaire, importantes pour la diapédèse, tandis que les granules spécifiques sont plutôt mobilisés pour leur arsenal antibactérien (Faurschou and Borregaard, 2003).

### 1.1.3 Le rôle du neutrophile dans la lutte contre les pathogènes

Les PNN sont des acteurs du système immunitaire inné. Il intervient en première ligne lors d'une infection ou d'une inflammation. Les PNN prennent en charge les bactéries, les virus, les champignons et les parasites ayant franchi les barrières cutanées ou les muqueuses du corps. De plus, les PNN reconnaissent les cellules du soi ayant était altérées et les éliminent (Nauseef, 2007).

Les PNN phagocytent les pathogènes qui vont ensuite être dégradés. Le contenu des granules est déversé dans le phagolysosome, ce qui contribue à la dégradation des microorganismes. L'action des hydrolases acides est favorisée par la diminution du pH dans le phagolysosome suite à sa fusion avec les granules (Levy, 2004). Les protéines cationiques telles que les défensines ont une activité microbicide sur les bactéries Gram négatives, Gram positives, les champignons et les virus. Les défensines perturbent la perméabilité des membranes des pathogènes pour les tuer. Les PSN contenues dans les granules participent à l'action antibactérienne dans les phagosomes (**Figure 6**). Le contenu des différents granules est déversé dans le phagosome pour former le phagolysosome dans lequel la cathélicidine (hCAP-18) est clivée par la NE pour former le LL-37 qui est un bactéricide puissant contre les bactéries Gram positives et Gram négatives (Borregaard and Cowland, 1997; Borregaard et al., 2007).

Les PNN activés produisent rapidement et massivement des espèces réactives de l'oxygène (ERO) (**Figure 6)** qui sont toxiques, ce processus est appelé l'explosion oxydative (Babior, 1984) . La production des ERO se fait dans la membrane interne du phagosome. L'oxygène du PNN est transformé en anion superoxyde sous l'action de la NADPH oxydase. Suite à la formation de l'anion superoxyde, d'autres enzymes entrent en jeu pour former d'autres ERO comme le peroxyde d'hydrogène ou encore le radical hydroxyle. La NADPH oxydase est un complexe multimoléculaire formé par des sous-unités présentes à différents endroits du PNN (cytosol, membranes des granules) quand il est au repos, afin d'assurer l'innocuité de cette enzyme (Lambeth, 2007). L'activation du complexe NADPH oxydase nécessite une étape de « priming » médiée par les cytokines pro-inflammatoires. À la suite de l'activation de l'enzyme, la production d'ERO aura lieu en réponse à un stimulus qui peut être d'origine bactérienne par exemple (Lambeth, 2007).

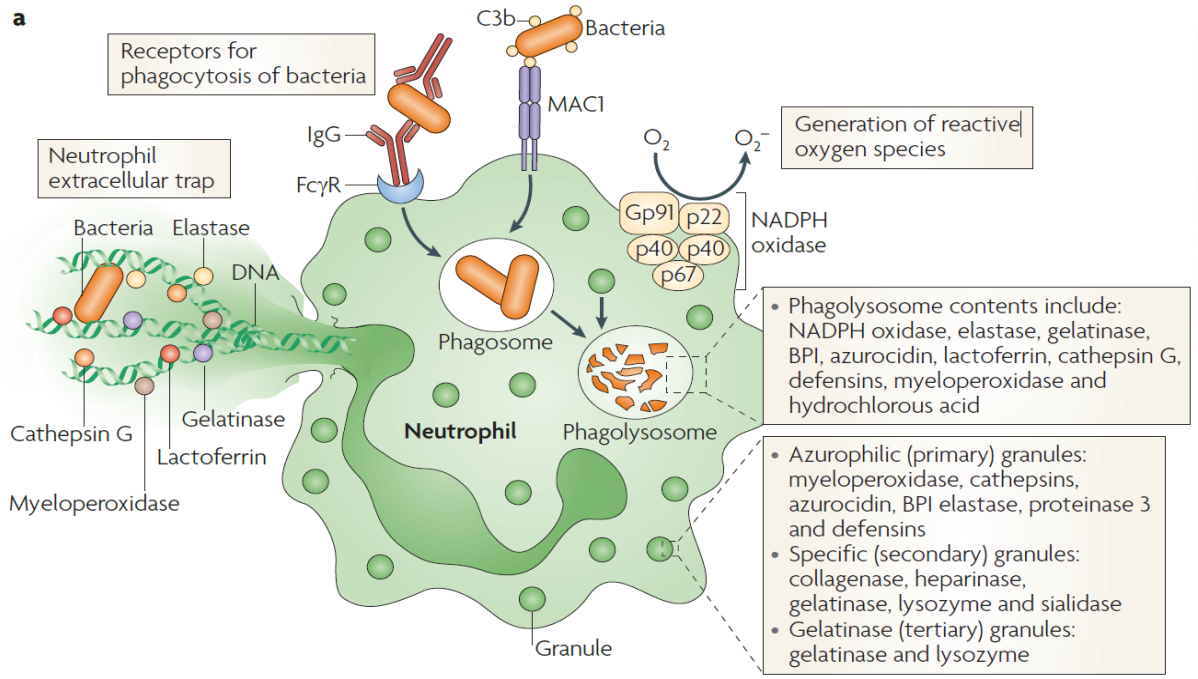


**Figure 6 : Systèmes antimicrobiens du neutrophile.** D'après (Hickey et Kubes, 2009).

Les PNN possèdent un système de défense supplémentaire qui est la libération de filet de chromatine décondensée dans le milieu extracellulaire : la nétose (Brinkmann et al., 2004) (**Figure 6 et 3**). Les « Neutrophil Extracellular Traps » (NET) sont recouverts de protéines provenant des granules. Les NET sont libérés suite à l'activation des PNN par du PMA (pour « Phorbol Myristate Acetate »), de l'IL-8 ou des lipopolysaccharides (LPS) et créent une barrière physique pour éviter la dispersion des bactéries ou des virus (Parker et al., 2012;

Pilsczek et al., 2010). La production de NET est réalisée selon deux mécanismes : le premier mécanisme est la décondensation et la libération de la chromatine du PNN engendrant la mort de la cellule ; le deuxième mécanisme est le relargage des filets de chromatines dans une vésicule de sécrétion ainsi le PNN ne meurt pas mais perd son noyau.

La nétose commence avec l'activation des PNN qui vont produire des ERO grâce à la NADPH oxydase. La NADPH permet la translocation de la NE et la MPO, qui sont des protéines des granules azurophiles, dans le noyau. Ces protéases clivent les histones et permettent la décondensation de la chromatine. Durant la formation des NET, une citrullination de l'histone H3 à lieu, cette conversion des résidus d'arginine en citrulline est réalisée par la peptidyl-arginine-deiminase 4 et augmente la décondensation de la chromatine. Après 120 minutes de nétose, les filets de chromatine chargés de protéines issues des granules sont libérés dans le milieu extracellulaire (Brinkmann et al., 2004).

## 1.2 Le monocyte et le macrophage

Les monocytes sont des cellules de l'immunité innée, elles font partie des cellules recrutées en réponse à un danger pour l'organisme (bactéries, virus, ou blessure). Les monocytes sont produits lors de l'hématopoïèse dans la moelle osseuse, une fois sur le site de l'infection, ils sont convertis en cellules dendritiques ou en macrophages. Leur migration dans les tissus est un phénomène appelé la diapédèse. La diapédèse est réalisée par les leucocytes afin d'arriver sur le site de l'inflammation, celle-ci comporte différentes étapes (**Figure 7**). Lors d'une infection, des cytokines pro-inflammatoires et des peptides bactériens stimulent les molécules d'adhésion des cellules endothéliales des vaisseaux sanguins. Cela permet une interaction de faible affinité avec les leucocytes, c'est l'étape de roulement ou « *rolling* ». Les chimiokines à la surface des cellules endothéliales entraînent l'activation des intégrines à la surface des leucocytes, qui vont se lier aux ligands présents sur les cellules endothéliales, c'est l'étape d'adhésion. Les leucocytes changent de forme et migrent en rampant à la surface des cellules endothéliales afin de trouver le site le plus proche pour passer à travers le vaisseau sanguin, c'est l'étape de « *crawling* » ou rampante. Le passage du leucocyte entre les cellules endothéliales (paracellulaire) ou à travers celle-ci (transcellulaire) est la diapédèse (Filippi, 2016).

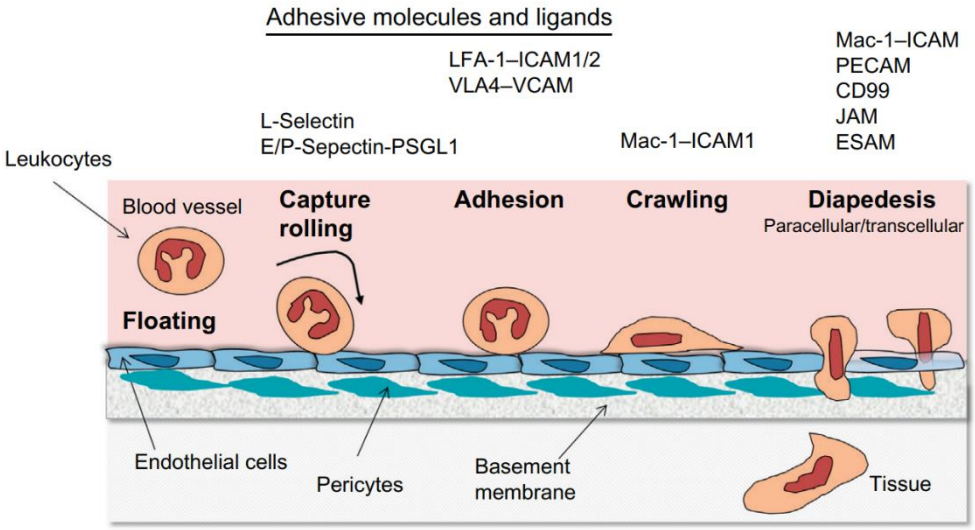


**Figure 7 : Diapédèse des leucocytes.** D'après (Filippi, 2016).

Une fois sur le site de l'infection les monocytes sont convertis en cellules dendritiques ou en macrophages. Ils peuvent dériver en différents types de macrophages, pro- ou anti-inflammatoire en fonction du type de chimiokines auxquelles ils ont été exposés, pouvant à la fois exacerber l'inflammation ou faciliter la réparation tissulaire. Leurs rôles variés tant dans l'homéostasie tissulaire que dans la réaction de l'immunité innée, font de ces cellules des cibles thérapeutiques intéressantes. Leurs rôles variés tant dans l'homéostasie tissulaire que dans la réaction de l'immunité innée, font de ces cellules des cibles thérapeutiques intéressantes, d'autant plus qu'elles sont impliquées dans de nombreuses pathologies (Kratofil et al., 2017).

### 1.2.1 La différentiation des monocytes

Comme précisé précédemment, les monocytes sont issus des cellules souches hématopoïétiques multipotentes, qui peuvent se différencier en progéniteur myéloïde. Les progéniteurs myéloïdes se différencient ensuite en progéniteur granulocyte-monocyte. Ceux-ci pourront se différencier en monoblaste puis en pro-monocyte. Enfin, ils dérivent en monocyte et migrent dans le sang (**Figure 8**).

Les monocytes sont classifiés en trois sous-catégories en fonction de l'expression des marqueurs de surface CD14 et CD16 : les monocytes « classiques » CD14 élevé ($CD14^+/CD16^-$) qui représentent 85% des monocytes circulants ; les monocytes « intermédiaires » ($CD14^+/CD16^+$) qui représentent 5-10% des monocytes circulants ; et les monocytes « non-classiques » CD16 élevé ($CD14^-/CD16^+$) qui représentent 5-10% des monocytes circulants. La stimulation par des endotoxines sur des volontaires sains a montré que les monocytes sanguins quittent la circulation en 2 heures et réapparaissaient

séquentiellement avec les $CD14^+$ en premier (après 4 heures), puis les $CD14^+/CD16^+$ et enfin les $CD16^+$ après 24 heures d'infection (Thaler et al., 2016 ; Patel et al., 2017). Un modèle mathématique indique que les monocytes $CD14^+$ ont une durée de vie courte dans le sang (1-2 jours) avant de se différencier en $CD14^+/CD16^+$ ou de disparaître de la circulation (Tak et al.,2017). Les différentes observations suggèrent que les monocytes $CD14^+$ sont les précurseurs des monocytes $CD16^+$ dans le sang et des macrophages ou cellules dendritiques dans les tissus (Coillard and Segura, 2019). Les monocytes $CD14^+$ et intermédiaires présentent des propriétés inflammatoires et sont référencés comme les monocytes inflammatoires, les monocytes $CD16^+$ présentent un comportement de patrouille dans les vaisseaux sanguins. La plasticité des monocytes inflammatoires leur permet d'altérer leur phénotype en fonction de l'environnement ou de la réponse immunitaire entraînée par des pathogènes (Mitchell et al., 2014).

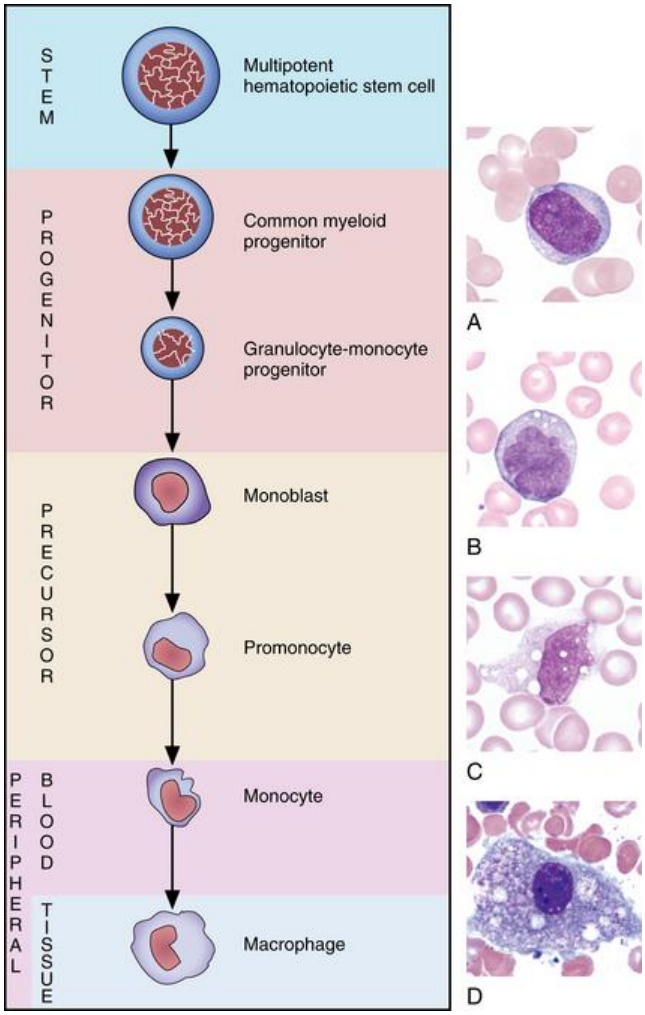


**Figure 8 : Stades cellulaires de la différentiation monocytaire.** D'après (Clinical gate : monocyte-maturation).

#### 1.2.1.1 La différentiation en cellules dendritiques

La différentiation des monocytes en cellules dendritiques (CD) est dépendante du *FMS-related tyrosine kinase 3 ligand* (Flt3L). Les CD sont des médiateurs importants aussi bien dans la réponse immunitaire innée qu'adaptative. En effet, elles font le lien entre deux phases de la réponse immunitaire : reconnaissance initiale des pathogènes et clairance de cellules spécifiques ou médiée par la reconnaissance d'anticorps. Il existe différents sous-types de CD : les classiques et les plasmacytoïdes. Les CD classiques sont des cellules hautement phagocytaires, spécialisées dans la présentation d'antigène. Elles ont une courte demi-vie (3-5 jours) et existent sous deux stades fonctionnels. Les CD classiques nouvellement différenciées et immatures ont une forte activité endocytaire avec des faibles taux de protéine majeur du complexe d'histocompatibilité I et II (MHC I et II). Après la rencontre avec des pathogènes ou des stimuli inflammatoires, elles présentent les MHC à leurs surfaces. Ces caractéristiques leur permettent de réaliser leur fonction soit la reconnaissance et capture d'antigène dans les tissus périphériques, puis leur migration vers les organes lymphoïdes secondaires et les cellules T afin d'initier la réponse immunitaire adaptative. Les plasmacytoïdes ne sont pas des cellules phagocytaires, mais présentent de haut taux de MCH II à leur surface cellulaire. Contrairement au CD classiques, elles ont une morphologie sphérique (Satpathy et al., 2012).

#### 1.2.1.2 La différentiation en macrophages

Les monocytes sanguins sont les précurseurs des macrophages, après la diapédèse sur le site de l'inflammation, le monocyte se différencie en macrophage. Ce n'est cependant pas l'unique précurseur des macrophages, en effet dans les tissus, il existe des macrophages résidentiels qui dérive du foie ou de la rate fœtale. C'est notamment le cas des macrophages alvéolaires, qui résident dans les alvéoles pulmonaires et sont dérivés de monocytes issus du foie fœtal puis sont capable d'auto-prolifération, mais en cas d'inflammation importante les monocytes de sang périphérique peuvent se différencier en macrophage alvéolaire (Woo et al., 2021). Les macrophages sont des cellules qui interviennent dans la réponse immunitaire innée et adaptative. Ce sont des cellules phagocytaires qui ont une activité antimicrobienne mais sont aussi impliquées dans la réparation tissulaire. Les macrophages sont capables d'efférocytose, c'est-à-dire la phagocytose de cellules apoptotiques notamment de leucocytes polynucléaires apoptotiques, ce qui permet la résolution de l'inflammation. Une dérégulation de cette fonction peut entraîner des pathologies inflammatoires chroniques ou auto-immunes (Das et al., 2015).

Les macrophages sont caractérisés par leur plasticité. En effet en fonction des stimuli de l'environnement, ils sont capables d'un large spectre d'activité, notamment dans la médiation de la réponse immunitaire innée. En fonction de leur activation, leurs rôles peuvent être totalement opposés, soit pro-inflammatoire, soit anti-inflammatoire. Ces deux phénotypes majeurs sont basés sur la polarisation des cellules T « helper » de type 1 (Th1) et des cellules T « helper » de type 2 (Th2). Les cytokines telles que l'interféron gamma (IFN-γ) et le « tumor necrosis factor-α » (TNF-α) sécrétées par les Th1 vont activer les macrophages en M1, c'est-à-dire pro-inflammatoire. Les interleukines 4 et 10 (IL-4 et IL-10) sécrétées par les Th2 vont au contraire activer le phénotype M2, soit anti-inflammatoire (Das et al., 2015). En fonction de leur sous-type, les monocytes peuvent se différencier en différents sous-types de macrophage. Dans le cas de l'arthrite rhumatoïde, une pathologie inflammatoire, les monocytes $CD14^+$ se différencient en M1 et en ostéoclaste, contribuant à l'inflammation synoviale et à l'érosion osseuse. De la même façon, les monocytes intermédiaires $CD14^+/CD16^+$ se différencient en M1 contribuant à l'inflammation tissulaire. En revanche, les monocytes $CD16^+$ se différencient en M2, soit anti-inflammatoire, contribuant à la phagocytose et à la résolution de l'inflammation (**Figure 9**) (Cutolo et al., 2022).

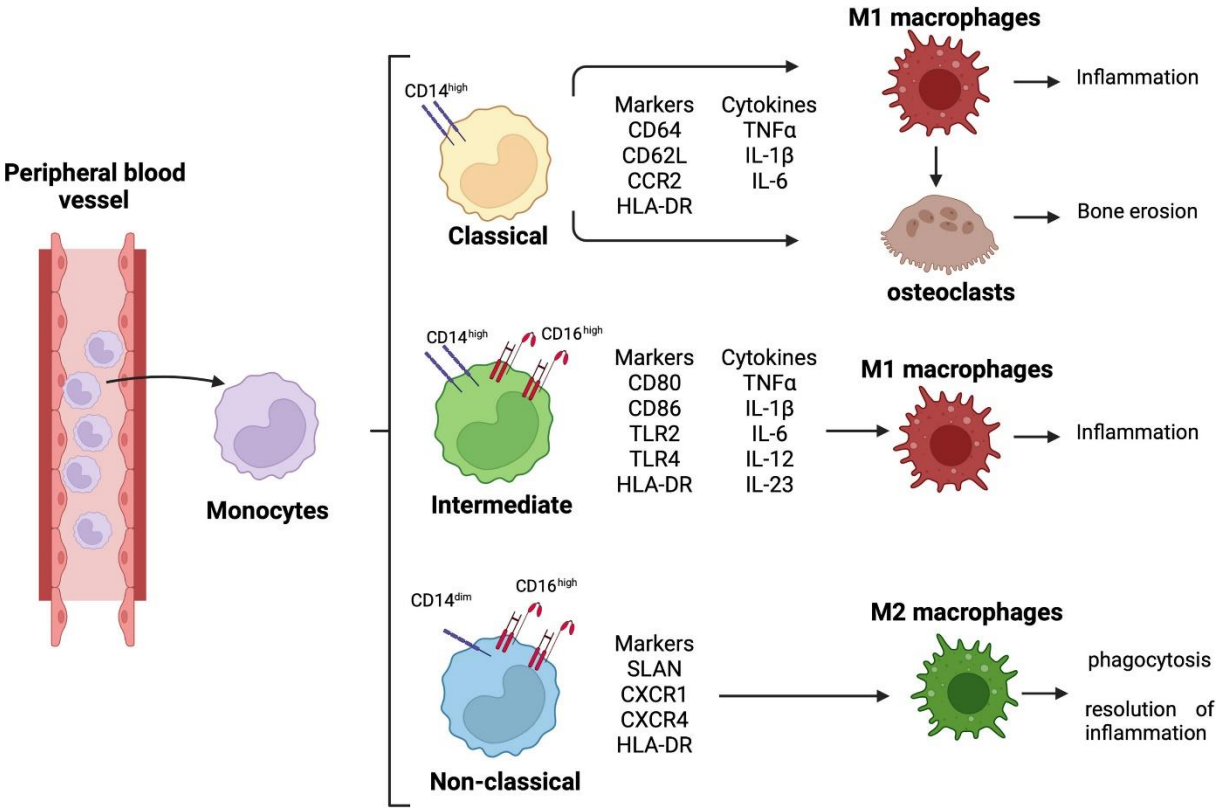


**Figure 9 : Différenciation des monocytes en macrophage M1 ou M2.** D'après (Cutolo et al., 2022).

### 1.2.2 Les rôles pathologiques des monocytes-macrophages

Les monocytes-macrophages sont impliqués dans de nombreuses pathologies, notamment lorsque la balance M1 (inflammatoire) / M2 (anti-inflammatoire) est perturbée. Le maintien de cette balance est spécialement important lors de la grossesse, en effet, les cellules du fœtus sont en contact avec le système immunitaire maternelle *via* le placenta. Cela entraîne l'activation des monocytes, les M1 vont avoir tendance à lutter contre le « non-soi » représenté par les cellules fœtales, et les M2 permettent de réguler l'inflammation afin que la grossesse soit poursuivie. La perturbation de cette balance vers une activation importante en macrophage M1, entraîne une pathologie : la pré-éclampsie.

La tuberculose est une pathologie causée par une bactérie, *Mycobacterium tuberculosis*. Cette bactérie a la caractéristique de repolariser les macrophages M1, qui défendent l'organisme contre cette infection, en macrophages M2, qui permettent de diminuer l'inflammation, de cette façon la bactérie arrive à éviter la réponse immunitaire. Avec leurs fonctions pro- et anti-inflammatoires, les macrophages sont impliqués dans de nombreuses pathologies telles que le cancer, la fibrose, l'asthme, l'artériosclérose, l'obésité, le diabète de type 2, arthrite rhumatoïde, la sclérose en plaques, la maladie de Crohn et les maladies inflammatoires de l'intestin (Shapouri-Moghaddam et al., 2018).

## 1.3 Les lymphocytes

Les lymphocytes représentent 20-40% des leucocytes sanguins humains. Il en existe 3 types : les lymphocytes T (LT), les lymphocytes B (LB) et les natural killer (NK). Les LT et LB sont de petites cellules alors que les NK ont une taille plus importante et contiennent des granules azurophiles. Comme les neutrophiles et les monocytes, les lymphocytes proviennent des cellules souches hématopoïétiques, cependant ceux-ci proviennent des précurseurs lymphoïdes et non des précurseurs myéloïdes. Les précurseurs lymphoïdes se différencient ensuite en progéniteurs B ou T puis en lymphoblastes, puis en pré-LT ou en pré-LB ou en NK, c'est la lymphopoïèse (**Figure 10**) (Wu et al., 2023).

Les pré-LT migrent vers le thymus où ils pourront se différencier et maturer en différents sous-types de LT, ils sont ensuite distribués vers les organes immunitaires comme la rate et les ganglions lymphatiques (Thome et al., 2014). Le « T » des LT a d'ailleurs pour origine le « T » de thymus, en revanche le « B » de LB a pour origine le « B » de *bone marrow* qui signifie moelle osseuse. En effet, les LB se différencient dans la moelle osseuse, une maturation

fonctionnelle a ensuite lieu après leur migration dans les organes lymphoïdes comme la rate et les ganglions lymphatiques (LeBien and Tedder, 2008). Initialement, on pensait que les NK se développaient exclusivement dans la moelle osseuse, mais il semblerait que ceux-ci, à l'image des LB et LT, se développent en forme mature dans les organes lymphoïdes secondaires (Abel et al., 2018).

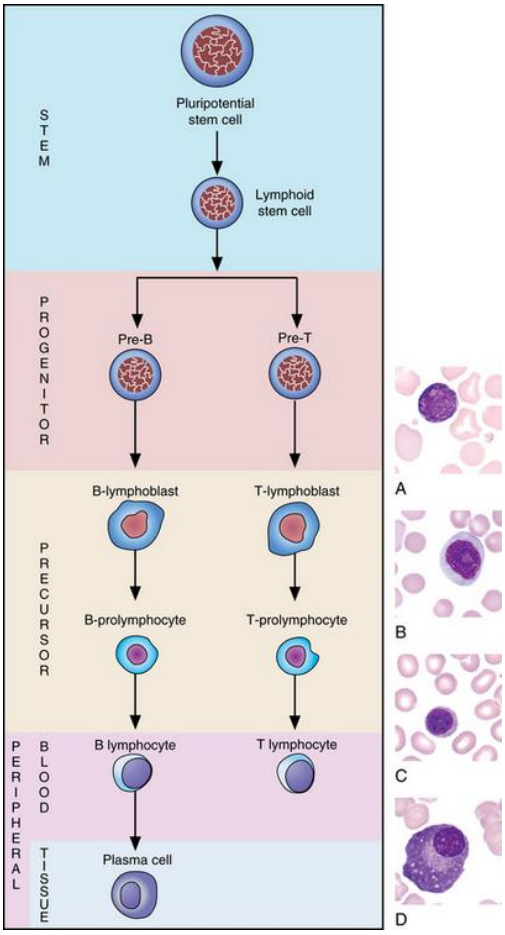


**Figure 10 : Stades cellulaires de la différentiation lymphocytaire.** D'après (Clinical gate : lymphocyte-maturation).

### 1.3.1 Les lymphocytes T

Les lymphocytes T sont les acteurs majeurs de l'immunité adaptative, il en existe de nombreux sous-types (**Figure 11**) ayant des fonctions différentes. Les deux principaux sous types sont les $CD8^+$ et les $CD4^+$. Les $CD4^+$ et $CD8^+$ sont des marqueurs cellulaires de surface et corécepteurs du TCR (T cell receptor), les LT commencent à se différencier en LT double positif $CD4^+/CD8^+$, puis se différencient en simple positif $CD4^+$ ou $CD8^+$ (Kumar et al., 2018). Les LT reconnaissent les antigènes présentés par les MHC sur les cellules présentatrices d'antigène. Cette reconnaissance par le TCR et la présence de cytokines permet l'activation des LT afin d'effectuer leurs fonctions. Les LT $CD8^+$ sont les LT cytotoxiques, ils participent à

l'élimination des cellules infectées et des cellules cancéreuses. Ils entraînent la mort cellulaire *via* l'interaction Fas/ligand et la sécrétion de perforine qui permet la création de pores dans la membrane de la cellule cible permettant aux granzymes (Gzms) d'entrer dans la cellule et d'ainsi déclencher l'apoptose (Sun et al., 2023). Les LT $CD8^+$ ne sont pas que des cellules cytotoxiques, elles se différencient aussi en cellule mémoire. Les LT $CD8^+$ mémoire procurent une protection à long terme contre l'antigène, notamment en cas de réexposition à celui-ci. Les LT $CD4^+$ sont les LT helper (Th), c'est-à-dire assistant, et jouent un rôle dans presque tous les aspects de la réponse immunitaire. Ils sont comme les LT cytotoxiques, activés par la reconnaissance avec l'antigène présenté par les MHC sur les cellules présentatrices, par la stimulation par des cofacteurs et par les cytokines. Ils se différencient en différents sous-types comme notamment les Th1, Th2, Th17, Treg (regulateur) et Tfh (follicular helper) qui ont des rôles très différents (Sun et al., 2023).

Les Th1 protègent l'hôte contre les bactéries et les virus via la sécrétion d'interféron-γ, une cytokine pro-inflammatoire (Meitei et al., 2023). Les Th2 protègent l'hôte contre les infections helminthiques, ils facilitent la réparation tissulaire, mais sont aussi impliqués dans l'asthme et les allergies *via* leur contribution à l'inflammation chronique (Walker et Mckenzie, 2018). Les Th17 contribuent aussi à la protection contre les pathogènes, surtout dans les muqueuses (Guglani et Khader, 2010), et participent aussi à l'inflammation chronique et aux maladies auto-immunes (Han et al., 2015). Les Tfh sont importants dans la réponse humorale en promouvant la prolifération et la maturation des LB (Zhu, 2018). Enfin, les Treg sont spécialisés pour maintenir la tolérance immunitaire *via* la suppression de la réponse immunitaire (Plitas et Rudensky, 2016). Du fait de leurs rôles variés, les LT peuvent être impliqués dans de nombreuses pathologies, c'est notamment le cas de la fibrose. La fibrose est caractérisée par l'accumulation de collagène et d'autres composants de la matrice extracellulaire dans le tissu. Elle est impliquée dans de nombreuses pathologies parmi lesquelles la cirrhose, la mucoviscidose, l'infarctus. La dérégulation des LT peut conduire en fonction de leurs sous-types à des phénomènes pro- ou anti-fibrotiques (Zhang and Zhang, 2020).

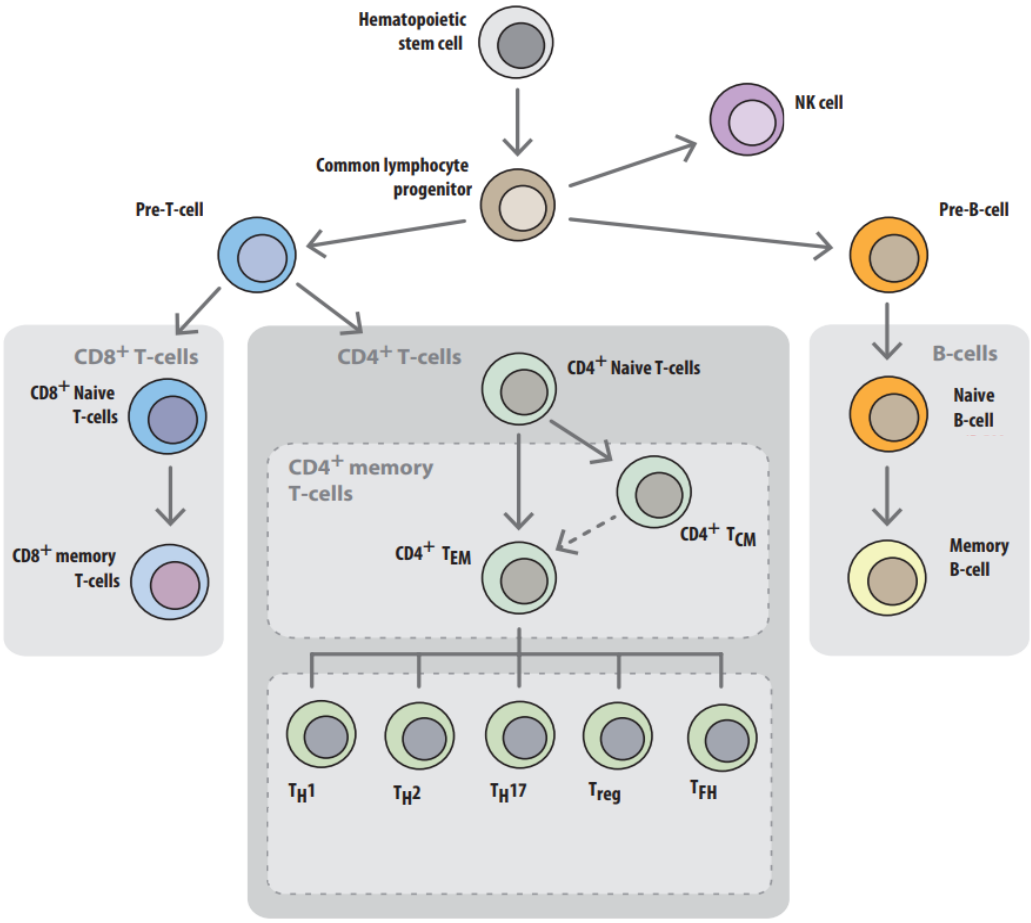


**Figure 11 : Différents types de lymphocytes.** Adaptée de (Pagani et al., 2007).

### 1.3.2 Les lymphocytes B

Les LB sont les acteurs centraux de la réponse immunitaire humorale du fait de leur production d'anticorps, ils protègent l'organisme *via* leur participation à la réponse immunitaire adaptative. De ce fait, une dérégulation dans le développement, la sélection ou la fonction des LB entraîne des maladies auto-immunes, des immunodéficiences ou encore des allergies (Pieper et al., 2013). Les LB ont cependant d'autres rôles que la production d'anticorps, comme la présentation d'antigène, la production de cytokines et la suppression de la réponse inflammatoire notamment via la production d'interleukine-10 (Mauri and Bosma, 2012). Les LB sont donc des cibles intéressantes pour le traitement des maladies auto-immunes, une stratégie thérapeutique consiste en la déplétion des LB. Cette stratégie s'est révélée efficace notamment pour le traitement des pathologies comme la neuromyélite, la sclérose en plaque ou l'arthrite rhumatoïde (Barnas et al., 2019).

### 1.3.3 Les natural killers

Les NK sont les lymphocytes prédominants dans la lutte contre les cellules cancéreuses et les cellules infectées par des virus. Le nom « *natural killer* », c'est-à-dire naturellement cytotoxique, souligne le fait que ces cellules n'ont pas besoin d'être activées par l'exposition antigénique contrairement aux LT cytotoxiques. On retrouve ces cellules dans le sang et de nombreux organes lymphoïdes ou non, comme la moelle osseuse, les ganglions, la peau, les intestins, le foie ou encore les poumons. Leur premier mécanisme cytotoxique implique la reconnaissance de récepteur de mort cellulaire présents à la surface de la cellule cible. Ces récepteurs comprennent les TNF-*related apoptosis-inducing ligand-receptor* (TRAIL-R) et Fas qui sont activés par les ligands TRAIL et Fas présents à la surface des NK. L'expression de ces récepteurs de mort cellulaire peut être induite par la sécrétion d'interféron-γ, et leur activation entraîne des signaux pro-apoptotiques (Zamai et al., 1998). Le second mécanisme est le même que celui des LT cytotoxiques, *via* la sécrétion de perforine et de granzyme (Akula et al., 2022). Les NK peuvent aussi avoir des rôles régulateurs notamment *via* la sécrétion de cytokines, et contribuent à la réponse des LT soit en la stimulant soir en l'inhibant. Étant donné leurs rôles multiples, la dérégulation des NK peut induire de nombreuses pathologies inflammatoires chroniques et ont un rôle dans l'obésité ou les cancers (O'Brien and Finlay, 2019).

## 1.4 Les lignées de cultures cellulaires immunitaires

Une lignée cellulaire est constituée de cellules issues d'une cellule originelle par mitose successive, présentant les mêmes caractéristiques fonctionnelles et structurelles et dont le devenir est identique pour un nombre limité de division. Une lignée est dite immortalisée lorsqu'elle a échappé à la sénescence cellulaire et peut se diviser indéfiniment. Les lignées immortalisées sont très souvent utilisées comme modèle cellulaire, grâce à leur capacité de division permettant une simplification de la culture cellulaire *in vitro*. Les lignées cellulaires immortalisées sont en général des cellules cancéreuses prélevées chez un patient, transformées artificiellement par un oncogène ou encore mutées pour des gènes impliqués dans la régulation du cycle cellulaire. Ainsi, il existe des lignées immortalisées pour les cellules immunitaires avec des origines propres et des possibilités de différenciation.

**Tableau 1 : Exemples de lignées cellulaires immunitaire immortalisées et leurs caractéristiques.** D'après (American Type Culture Collection (ATCC)).

| Lignée | Type cellulaire | Origine | Pathologie du patient d'origine | Différenciation |
|---|---|---|---|---|
| **HL-60** | Pro-myéloblaste | Sang humain | Leucémie promyélocytaire aiguë | Neutrophile (avec du DMSO ou ATRA) |
| **NB-4** | Pro-myélocyte | Moelle osseuse humaine | Leucémie promyélocytaire aiguë | Neutrophile (avec de l' ATRA) |
| **U-937** | Monocyte | Epanchement pleural humain | Lymphome histiocytaire | Macrophage (avec du PMA) |
| **THP-1** | Monocyte | Sang humain | Leucémie monocytaire aiguë | Macrophage (avec du PMA) |
| **JURKAT** | Lymphoblaste T | Sang humain | Leucémie des cellules T aiguë | Elles sont $CD4^+/CD8^+$ et peuvent différencier en $CD4^+$ ou en $CD8^+$ |
| **NK-92** | Natural Killer | Sang humain | Lymphome malin non hodgkinien | |

## 2. La cathepsine C

La cathepsine C (CatC) (EC 3.4.14.1) (également appelée dipeptidyl peptidase 1 (DPP1)), une cathepsine à cystéine maturée par d'autres cathepsines à cystéine (CatL-like protéases), est la protéase activatrice majeure des protéases à sérine des cellules immunitaire telle que les PSN, les protéases pro-inflammatoires du neutrophile, et les granzymes. Son inactivation génétique naturelle chez l'homme (provoquant le syndrome de Papillon-Lefèvre (SPL)) diminue sévèrement l'activation des PSN au stade promyélocytaire du développement des neutrophiles. De ce fait, la CatC a été décrite comme une cible thérapeutique potentielle dans toutes les pathologies inflammatoires neutrophiliques associées à une dégradation tissulaire enzymatique. Mais aussi dans le cancer, en effet l'inflammation chronique est un facteur de risque de cancer. De plus, la surexpression de la CatC a été observée dans différents tissus lors de la carcinogenèse et corrélée à des phénomènes métastasiques (Korkmaz et al., 2021) (**Annexe 1**). Des inhibiteurs chimiques non-toxiques de la CatC ont été développés à des fins thérapeutiques et ont été capables d'inhiber la CatC au niveau de la moelle osseuse dans des modèles précliniques et chez l'Homme. (Korkmaz et al., 2018a)

## 2.1. Les généralités sur les protéases

Les protéases sont des enzymes protéolytiques ayant la capacité d'hydrolyser les liaisons peptidiques *via* leur site actif. Dans les années 60, Schechter et Berger ont proposé une nomenclature visant à caractériser les surfaces d'interaction entre les substrats et les protéases. C'est dans le cadre de l'investigation du site actif de la papaïne que cette nomenclature a été proposée, ils ont montré que la papaïne a un site actif pouvant être subdivisé en sept sous-sites interagissant chacun avec les acides aminés des substrats (Schechter and Berger, 1967). Dans cette nomenclature, ces acides aminés sont désignés à partir du site de clivage, du côté N-terminale l'acide aminé le plus proche du site de clivage correspond à la position P1, puis P2, P3…Pn à mesure ou on se rapproche de l'extrémité N-terminale du substrat. À l'inverse du côté C-terminale l'acide aminé le plus proche du site de clivage correspond à la position P1', puis P2', P3'…Pn' à mesure ou on se rapproche de l'extrémité C-terminale du substrat. Chacune de ces positions interagit en miroir avec les résidus du site actif de la protéase, formant des poches appelées sous-sites et désignées selon le même principe mais par la lettre S, ainsi l'acide aminé en position P1 du substrat est en interaction avec les acides aminés du sous-site S1 de la protéase (**Figure 12**).

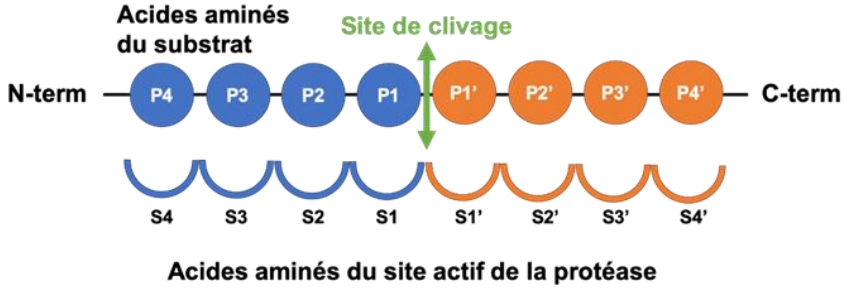


**Figure 12 : Nomenclature de Schechter et Berger.** Adaptée de (Schechter and Berger, 1967).

Le mécanisme catalytique du site actif fait partie des critères permettant de classer les protéases, aussi nommées peptidases ou protéinases. Elles représentent environ 2% du génome humain (Lopez-Otin and Bond, 2008). D'après la base de données MEROPS, il existe 703 peptidases humaines référencées, elles sont classées selon le mécanisme catalytique de leur site actif et souvent nommées par les acides aminés essentielles qui composent celui-ci. Les protéases peuvent être soit endopeptidasiques ou exopeptidasiques. Les endopeptidases clivent la chaîne peptidique de leur substrat et génèrent des fragments peptidiques de différentes tailles. Les exopeptidases clivent les protéines aux extrémités des chaînes peptidiques en N-terminale (aminopeptidase) ou en C-terminale (carboxypeptidase) (Kramer et al., 2017) (**Figure 13**). Il existe 8 familles référencées dans la base de données MEROPS : Aspartique (A), Cystéine (C),

Glutamique (G), Métallo (M), Asparagine (N), Mixed (P), Serine (S), Thréonine (T), Unknown (U). (https://www.ebi.ac.uk/merops/) (Rawlings et al., 2016).

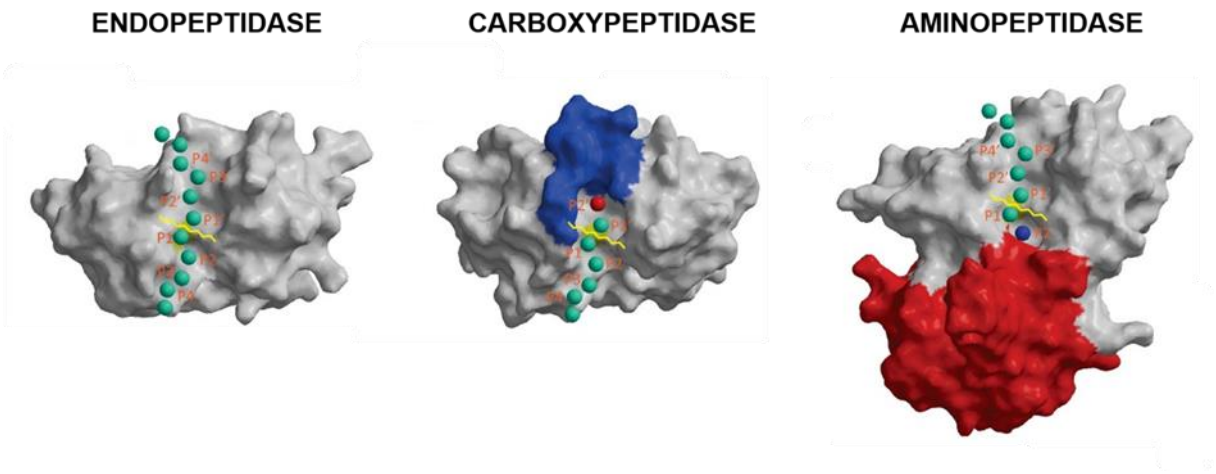


**Figure 13 : Illustration structurale des endo- et exopeptidases.** Les structures cristallisées de la CatL (endopeptidase) (Guncar et al., 1999), la CatB (carboxypeptidase) (Musil et al., 1991) et la CatC (aminopeptidase) (Turk et al., 2001a) sont représentées en gris. Les acides aminés du substrat sont représentés en vert et les sites de clivage sont représentés en jaune. D'après (Kramer et al., 2017).

Les protéases sont indispensables au maintien de l'organisme, en effet elles sont impliquées dans de nombreux mécanismes comme la biosynthèse, la maturation, la modulation des fonctions biologiques et le recyclage des protéines. Elles jouent un rôle déterminant dans la reproduction, le remodelage tissulaire, la coagulation et l'immunité. Si leur expression, structure ou activité est altérée cela peut engendrer différentes pathologies comme le cancer, l'ostéoporose, les désordres neurodégénératifs ou encore les maladies respiratoires ou auto-immunes. De ce fait, les protéases sont des cibles thérapeutiques particulièrement intéressantes (Kramer et al., 2017).

### 2.1.1. La nomenclature EC

La nomenclature EC a été mise en place par l'Union Internationale de Biochimie et de Biologie Moléculaire (IUBMB), celle-ci à été publiée en 1961 et agrandie 1964 par le comité de nomenclature de l'IUBMB. Cette classification classe les enzymes en 6 groupes selon le type de réaction qu'elles catalysent, et sont nommée par « l'Enzyme Comission (EC) number ». Le premier chiffre indique donc la classe de l'enzyme parmi les 6 groupes soit les enzymes EC.1 correspondent aux oxydo-réductases, EC.2 aux transférases, EC.3 aux hydrolases, EC.4 aux lyases, EC.5 aux isomérases, EC.6 aux ligases et EC.7 aux translocases (**Figure 14**). Les

sous-classes sont représentées par un second nombre indiquant le type de composé ou le groupe impliqué dans la réaction catalysée. Le troisième nombre indique la sous-sous-classe, qui précise un peu plus la réaction, et enfin le quatrième nombre permet d'identifier l'enzyme de façon individuelle (McDonald and Tipton, 2014). La classification complète en ligne est accessible gratuitement à l'adresse suivante : https://www.qmul.ac.uk/sbcs/iubmb/enzyme/

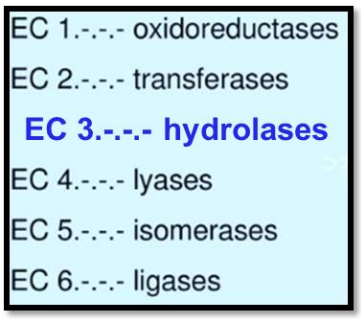


**Figure 14 : Nomenclature EC.** Les hydrolases sont une classe d'enzyme (lipases, phosphatases, glycosidases, peptidases and nucléosidases) qui utilisent l'eau pour rompre une liaison chimique, ce qui entraîne généralement la division d'une molécule plus grosse en molécules plus petites.

### 2.1.2. La classification en famille et en clan

Une autre classification que celle de l'IUBMB existe, celle-ci permet de suivre l'évolution phylogénétique des protéases, c'est la classification en famille et en clan. Cette classification repose sur l'homologie de séquence pour les familles et sur la comparaison de structure tridimensionnelle pour les clans. Les clans sont aussi définis en fonction de l'ordre des résidus du site catalytique. Les protéases d'une même famille ont des homologies de séquence statistiquement significatives. Les familles sont identifiées par une lettre qui représente leur type catalytique, ainsi Aspartique (A), Cystéine (C), Glutamique (G), Métallo (M), Asparagine (N), Mixed (P), Serine (S), Thréonine (T) et inconnue ou « *Unknown* » (U). L'analyse de l'homologie des séquences est limitée à la partie responsable de l'activité catalytique de l'enzyme pour définir les familles. Les clans regroupent des familles ayant un ancêtre commun pouvant être démontré avec une comparaison de séquences. La base de données MEROPS est disponible en ligne à l'adresse suivante : https://www.ebi.ac.uk/merops/ (Rawlings et al., 2016).

## 2.2 Les différentes classes de protéases

Le site actif d'une protéase est la région de la surface dans laquelle un substrat spécifique va se fixer et subir une réaction chimique. Le site actif est relativement petit par rapport au volume total de la protéase (n'occupe que 10 à 20 % du volume total). Le substrat est la molécule, ou une combinaison de molécules, qui sont de forme spécifique et complémentaire au site actif. La forme complémentaire du site actif à une molécule de substrat spécifique signifie que seul ce substrat sera capable de s'emboîter dans la protéase de sorte qu'elle ne catalyse qu'une réaction spécifique (**Figure 15**).

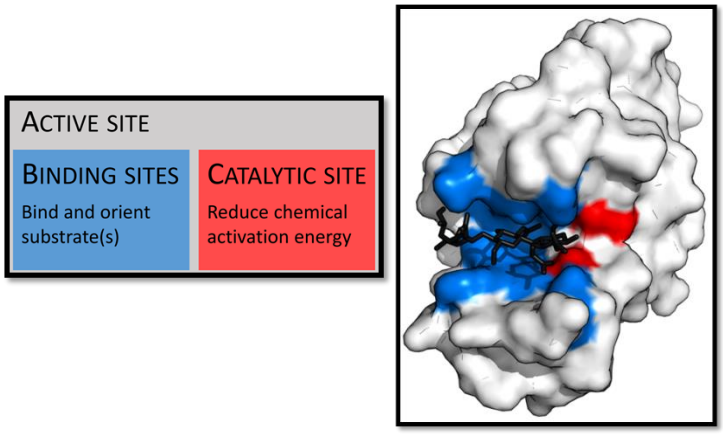


**Figure 15 : Illustration du site actif d'une protéase.** Le site d'interaction et le site catalytique du lysozyme sont représentés, respectivement, en bleu et en rouge. D'après (Wikipédia-active site).

### 2.2.1 Les protéases à cystéine (EC 3.4.14)

Les protéases à cystéine (EC 3.4.14), aussi nommées protéases à thiol, sont des peptidases dont le résidu d'acide aminé nucléophile de la triade (ou diade) catalytique est une cystéine (Erez et al., 2009) (**Figure 16**). Les protéases à cystéines doivent leurs noms au résidu cystéine présent dans leur site catalytique. La première étape du mécanisme réactionnel catalysé par les protéases à cystéine est la déprotonation du groupement thiol, de la cystéine du site actif, par la chaîne latérale basique d'un acide aminé voisin, généralement un résidu histidine. L'étape suivante est l'attaque nucléophile de l'atome de carbone constituant le carbonyle du substrat par l'anion sulfure de la cystéine déprotonée. Le fragment N-terminal du substrat est alors libéré, tandis que le résidu d'histidine revient à son état déprotoné et qu'un intermédiaire entre la protéase et le reste du substrat est formé par covalence à travers une liaison thioester.

Les protéases à cystéine sont largement présentes dans les organismes vivants. Celles-ci sont retrouvées dans les bactéries, les virus, les végétaux et les animaux. La famille des papaïnes (famille C1 clan CA) est la plus grande famille de protéase à cystéine. Cette famille est largement représentée par les protéases lysosomales dont l'activité est optimale dans un environnement réducteur légèrement acide. Dans le lysosome, les protéases à cystéine sont impliquées dans la dégradation et le recyclage des protéines, mais ce n'est pas leur unique fonction. En effet la découverte des processus biologiques spécifiques à chaque enzyme ainsi que leur identification comme biomarqueur dans les pathologies a mis en évidence d'autres rôles pour les protéases à cystéine. (Turk et al., 2012).

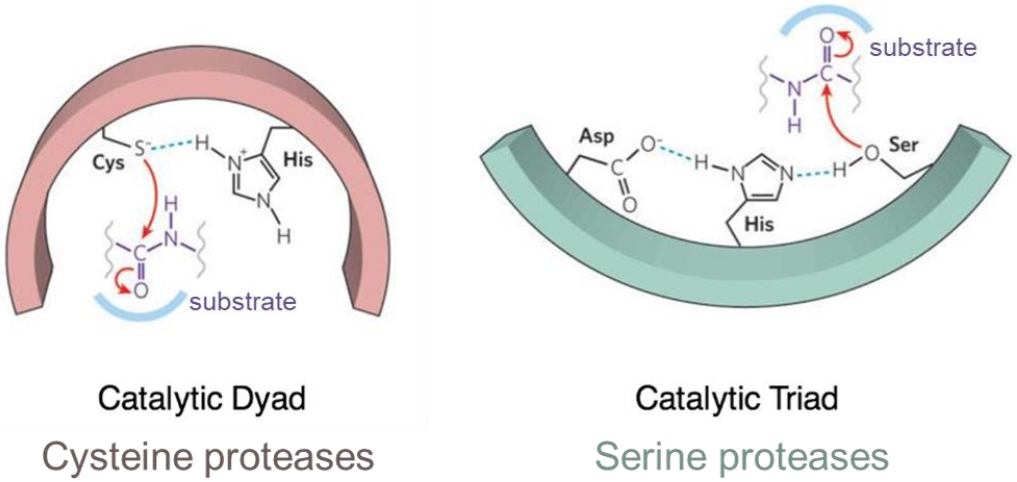


**Figure 16 : Mécanismes catalytiques des protéases à cystéine et des protéases à sérine.** On désigne généralement par triade catalytique les trois résidus d'acides aminés (diade catalytique désigne les deux résidus) qui interviennent ensemble dans le site actif d'une hydrolase. Ces résidus forment un réseau de transfert de charges qui polarise et active le résidu nucléophile, lequel attaque le substrat en formant un intermédiaire covalent hydrolysé ensuite pour libérer à nouveau l'hydrolase. Le nucléophile d'une telle triade est généralement la sérine ou la cystéine. D'après (Erez et al., 2009).

### 2.2.2 Les protéases à sérine (EC 3.4.21)

Les protéases à sérine représentent environ un tiers des protéases actuellement identifiées et sont présentes chez les eucaryotes, les procaryotes, les bactéries et les archées (Hedstrom, 2002). Le résidu serine présent dans leur site, jouant un rôle essentiel dans la catalyse, leur vaut le nom de protéases à sérine (**Figure 16**). Leur site actif présente une triade catalytique composée des chaînes latérales de trois acides aminés : His57, Asp102 et Ser195. Ces résidus sont en interaction et forment un relais de charge ce qui permet à la Ser195 d'hydrolyser la liaison peptidique *via* une attaque nucléophile de son groupe carbonyle. La trypsine est l'une des protéases à sérine les plus étudiées, son mécanisme a été particulièrement bien analysé. Les

protéases à sérine exercent différentes fonctions biologiques. Elles peuvent être des enzymes de digestion dans les glandes exocrines, des facteurs de coagulation ou encore des protéases leucocytaires associées aux granules (les PSN et les granzymes). Elles possèdent de nombreux inhibiteurs physiologiques.

### 2.2.3 Les protéases acides (EC 3.4.23)

*Les protéases aspartiques* : Les protéases acides ont été découvertes dans les sucs gastriques et sont connues et utilisées depuis des milliers d'années pour produire du fromage ou de la sauce soja (Schwann, 1836). Les techniques de biochimie modernes ont permis de découvrir d'autres protéases acides qui ont été renommées pepsine et chymosine (pour les enzymes digestives), cathepsine D (CatD), cathepsine E (CatE) et rénine. Le pH optimal pour l'action de ces protéases est entre 3.5 et 5.0. Le site catalytique des protéases aspartiques est composé de deux résidus aspartate, ils fonctionnent selon une réaction acido-basique. La polarisation d'une molécule d'eau par l'un des acides aspartiques déprotonés permet une attaque nucléophile sur la liaison peptidique du substrat (**Figure 17**). Les protéases aspartiques sont en cause dans plusieurs pathologies humaines comme le cancer du sein ou encore les maladies neurodégénératives (Szecsi, 1992).

*Les protéases à acide glutamique* : classées dans un premier temps avec les protéases aspartiques, elles ont été séparées par une analyse structurelle, moléculaire et mécanistique, ce qui a conduit à l'émergence de cette nouvelle classe de protéase. Le site actif de ces protéases est composé d'une dyade catalytique d'acide glutamique et de glutamine. Dans le règne vivant les protéases à acide glutamique ne sont retrouvées que chez les champignons (Sims et al., 2004).

### 2.2.4 Les métalloprotéases matricielles (EC 3.4.24)

Les métalloprotéases matricielles (MMP) sont des endopeptidases caractérisées par un atome de zinc au niveau du site catalytique. Le site actif fait intervenir 2 à 3 histidines et un acide aminé acide (glutamate/aspartate). Le zinc est en interaction avec les histidines, il permet aussi de lier une molécule d'eau, celle-ci fait une liaison hydrogène avec l'acide aminé acide. La molécule d'eau est alors polarisée et réalise une attaque nucléophile sur le carbone de la fonction carbonyle de la liaison peptidique ciblée. Le zinc permet de stabiliser l'oxyanion (Erez et al., 2009) (**Figure 17**). Ces protéases ont été identifiées grâce à leur activité protéolytique sur les composants de la matrice extracellulaire (MEC) tels que le collagène. Chez l'homme, il existe 23 MMP différentes et des études ont montré l'existence de MMP chez différentes espèces telles que les invertébrés, les plantes, les champignons, les virus, les protistes, les archées et les bactéries (Marino-Puertas et al., 2017). L'activité collagénolytique des MMP est impliquée dans le remodelage osseux, dans le développement embryonnaire mais également dans les phénomènes pathologiques (Amar et al., 2017). Les MMP jouent également un rôle dans l'inflammation. La MMP-2 et la MMP-3 augmentent la perméabilité vasculaire lors de la diapédèse (Vanlaere et Libert, 2009). La MMP-9 régule la capacité des macrophages à phagocyter les PNN (Butler et Overall, 2013). Les MMP-10, MMP-19 et MMP-28 régulent la production de macrophages anti-inflammatoires (Medzhitov, 2008). Alors que la MMP-12 régule la production des NET (Fingleton, 2017).

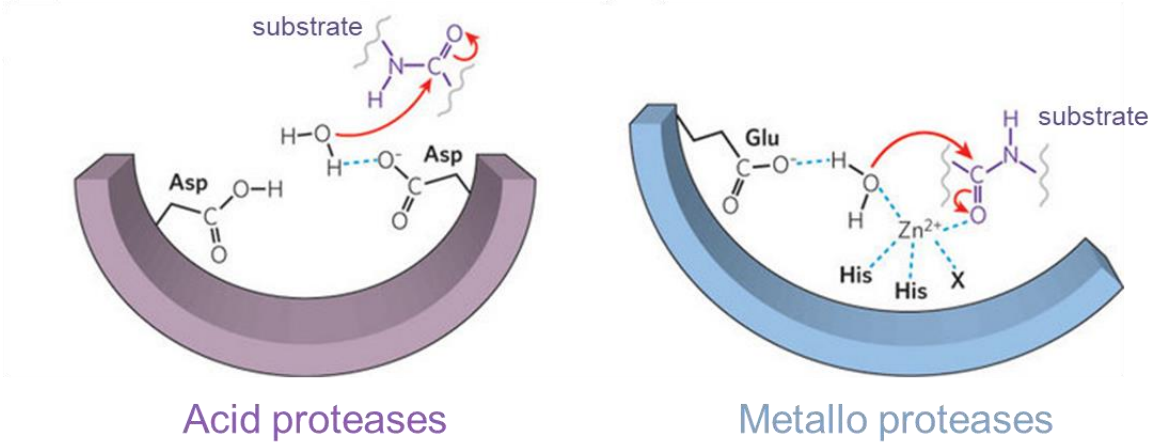


**Figure 17 : Mécanismes catalytiques des protéases acides et des métalloprotéases matricielles.** À gauche, le mécanisme catalytique des protéases acides est illustré. Brièvement, une molécule d'eau est coordonnée entre les aspartates, et activée par la déprotonation d'un de ces acides aminés acides. Cela permet la polarisation de $H_2O$ qui réalise une attaque nucléophile sur la liaison peptidique. Contrairement aux protéases à serine et cystéine, l'intermédiaire tétraédrique formé est non chargé. À droite, le mécanisme catalytique des métalloprotéases est illustré. De la même façon que pour les protéases acides, une $H_2O$ réalise l'attaque nucléophile. Celle-ci est en revanche coordonnée entre le zinc des histidines et un acide aminée acides. Cette fois, l'intermédiaire est un oxyanion stabilisé par l'ion zinc. D'après (Erez et al., 2009).

### 2.2.5 Les protéases à thréonine (EC 3.4.24)

Les protéases à thréonines ont été décrites pour la première fois en 1995 à la suite de la cristallographie du protéasome de *Thermoplasma acidophylum* (Löwe et al., 1995). Le résidu thréonine du site actif de cette classe de protéase se trouve en position N-terminal. Les protéases à thréonines sont retrouvées chez les archées, les bactéries, les levures et les hommes. (https://www.ebi.ac.uk/merops/).

## 2.3 Les mécanismes de régulation des protéases

Les protéases sont impliquées dans de nombreux processus physiologiques, leur capacité à hydrolyser d'autres protéines rend cruciale la régulation de leur activité. Celle-ci peut se faire à différents niveaux (**Figure 18**). Tout d'abord, une régulation transcriptionnelle, des facteurs de transcription participent à la régulation des protéases. La régulation peut également se faire *via* la pro-région qui inhibe les cathepsines à cystéine, celles-ci nécessitant la maturation de leur zymogène pour être actives. Les protéases peuvent aussi être régulées par l'environnement. En effet des paramètres comme le pH, les forces ioniques participent à la régulation de leur activité. Par exemple, les cathepsines à cystéine sont actives à pH acide, ce sont des protéases lysosomales, elles sont pour la plupart, à l'exception de la CatS, instables et non actives à pH neutre (Deu et al., 2012). Enfin, les protéases peuvent être régulées par des inhibiteurs endogènes, ils sont nombreux et peuvent être de différents types : réversible, irréversible, compétitif, incompétitif et non-compétitif. Les inhibiteurs réversibles se lient de façon transitoire à la protéase, à l'inverse des inhibiteurs irréversibles. Les termes compétitif, incompétitif et non-compétitif correspondent aux mécanismes d'action des inhibiteurs. Un inhibiteur compétitif agit en compétition avec le substrat pour le site actif de la protéase, et présente de ce fait des homologies structurelles avec le substrat. À l'inverse, un inhibiteur non-compétitif se fixe sur un autre site que le site actif de la protéase, il peut se lier à la forme libre de l'enzyme, ou au complexe enzyme-substrat. Les inhibiteurs incompétitifs ne peuvent se lier qu'au complexe enzyme-substrat (Deu et al., 2012).

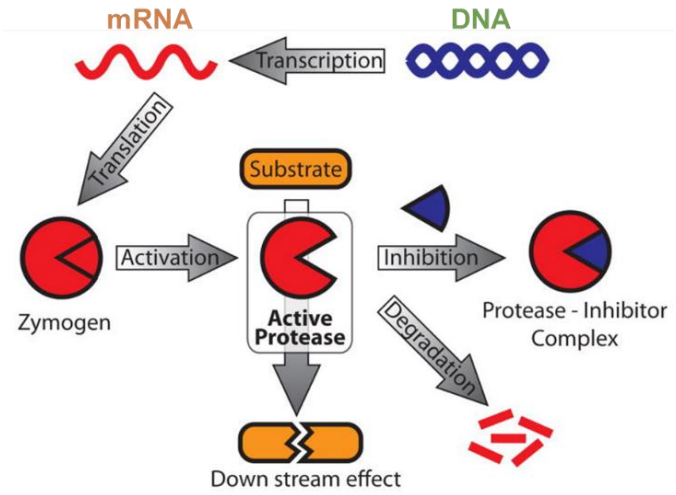


**Figure 18 : Illustration des mécanismes de régulation des protéases.** D'après (Deu et al., 2012).

## 2.4 Les cathepsines à cystéine

L'étymologie du mot cathepsine provient du grecque « kathepsein » qui signifie « digérer », et a été utilisé premièrement pour décrire les protéases da la muqueuse gastrique (Biasizzo *et al.*, 2022). Les cathepsines à cystéine appartiennent à la grande famille des papaïnes et sont formées de 11 membres : les cathepsines B, C, F, H, K, L, O, S, V, W et X (Turk et al., 2012). Elles peuvent être classées en fonction de l'homologie de séquence de la pro-région. De cette façon, on classe les cathepsines L, K, S, H et V parmi cathepsines L-*like* celle-ci possédant un motif ERW/FNIN conservé dans leur pro-région, les cathepsines B, C et O parmi les cathepsines B-*like*, et enfin les cathepsines F et W parmi les cathepsines F-*like* possédant un motif ERFNAQ conservé dans leur pro-région (Wex et al., 1999). En plus de l'homologie de leur pro-région, l'analyse de la phylogénie des cathepsines à cystéine permet de les catégoriser en cathepsines L-*like*, B-*like* et F-*like* (**Figure 19**). La forme mature est le domaine le plus conservé des cathepsines à cystéine, l'homologie de la séquence d'acides aminés de ce domaine est particulièrement importante chez les cathepsines L-*like*, ce qui donne une raison supplémentaire de les placer dans un seul et même groupe. En effet les cathepsines L, K, S et V présentent des pourcentages d'identité (pourcentage d'acides aminés identiques) supérieurs à 50% et de similarité (pourcentage d'acides aminés identiques ou similaires : ex : Arg-Lys) supérieure à 70% dans leur séquence protéique de la forme maure. En revanche, elles présentent des pourcentages d'identité inférieurs à 50% et de similarité inférieure à 60% avec les autres

cathepsines à cystéine, sauf la cathepsine H qui présentent des pourcentages de similarité avec les autres cathepsines L-like supérieurs ou égaux à 60% (**Tableau 2**) (Bromme, 2001).

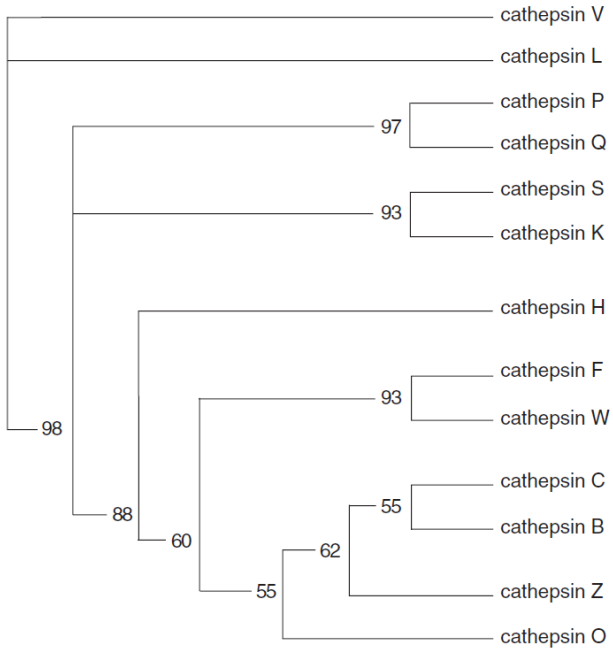


**Figure 19 : Arbre phylogénétique des cathepsines à cystéine.** D'après (Bromme, 2001). Arbre phylogénétique des cathepsines de mammifère basé sur la séquence d'acide aminés de la forme mature. La topologie est indiquée en pourcentage.

**Tableau 2** : **Identité et similarité de la séquence protéique de la forme mature des cathepsines à cystéine humaine et la papaïne.** La similarité est entre parenthèse. D'après (Brömme, 2001).

| Cathepsin | L | V | S | K | H | F | W | O | B | Z | C | Papain |
|---|---|---|---|---|---|---|---|---|---|---|---|---|
| L | 100 | 80 (88) | 55 (73) | 58 (74) | 45 (63) | 41 (57) | 31 (49) | 37 (52) | 29 (43) | 32 (48) | 36 (50) | 40 (54) |
| V | | 100 | 56 (73) | 57 (72) | 46 (61) | 42 (57) | 33 (49) | 37 (51) | 29 (43) | 32 (49) | 35 (50) | 43 (56) |
| S | | | 100 | 58 (71) | 44 (60) | 36 (54) | 31 (49) | 37 (53) | 31 (47) | 32 (47) | 33 (51) | 43 (57) |
| K | | | | 100 | 47 (61) | 41 (56) | 32 (50) | 36 (50) | 27 (44) | 30 (47) | 32 (46) | 44 (57) |
| H | | | | | 100 | 40 (54) | 32 (49) | 35 (52) | 29 (47) | 30 (42) | 39 (54) | 41 (55) |
| F | | | | | | 100 | 37 (53) | 34 (51) | 24 (42) | 28 (42) | 32 (49) | 41 (51) |
| W | | | | | | | 100 | 26 (41) | 25 (41) | 23 (36) | 28 (42) | 31 (46) |
| O | | | | | | | | 100 | 26 (39) | 31 (44) | 29 (45) | 31 (47) |
| B | | | | | | | | | 100 | 28 (41) | 34 (48) | 29 (41) |
| Z | | | | | | | | | | 100 | 33 (45) | 26 (40) |
| C | | | | | | | | | | | 100 | 33 (48) |
| Papain | | | | | | | | | | | | 100 |

Les cathepsines à cystéine sont des monomères de petit poids moléculaire (22 à 28 kDa) à l'exception de la CatC qui est un homo-tétramère de 200 kDa (Turk et al., 2001b). Les monomères de cathepsine à cystéine sont formés d'un domaine L (« Left domain ») en N-terminal constitué de trois hélices $\alpha$ qui sont liées entre elles par des ponts disulfures et d'un domaine R (« Right domain ») en C-terminal constitué d'un tonneau $\beta$. Le domaine L possède 3 hélices α, de plus de 30 acides aminés pour la plus longue. Le domaine R est composé de feuillets β qui forment une structure enroulée ressemblant à un baril avec un cœur hydrophobique, dont le bas est fermé par une hélice α. L'interface entre les deux domaines (en haut) forme la fente du site actif avec en son centre la triade catalytique, dont la cystéine et l'histidine proviennent de domaine différent. La cystéine est localisée sur la partie N-terminale de l'hélice centrale du domaine L, en revanche l'histidine est localisée dans le baril de feuillet β du domaine R. La surface de la fente du site actif est composée de deux courtes boucles du domaine L et de deux longues boucles du domaine R, qui ferment le haut du baril hydrophobique. Ainsi, le domaine L procure la surface d'interaction des résidus P3, P1 et P2' du substrat et le domaine R la surface d'interaction des résidus P2 et P1' (**Figure 20**) (Turk et al., 2012).

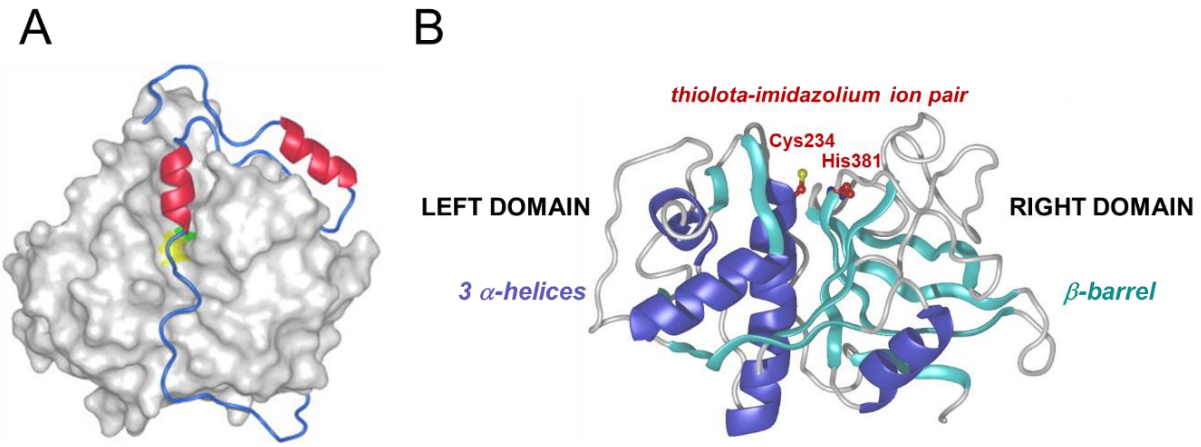


**Figure 20 : Structure tridimensionnelle des cathepsines à cystéine. (A)** La pro-CatB est représentée en gris avec son propeptide, en bleu, bloquant l'accès au site actif. Les hélices $\alpha$ du propeptide sont en rouge. La cystéine du site actif est colorée en jaune (PDB ID 2pbh). D'après (Turk et al., 2012). **(B)** Représentation de la CatV active composée de son domaine L (Left) et de son domaine R (Right), les hélices $\alpha$ sont représentées en bleu et les feuillets $\beta$ en turquoise, la dyade catalytique est en rouge (PDB ID 3H6S). D'après (Fonovic and Turk, 2014).

Les cathepsines à cystéine sont pour la plupart des endopeptidases, mais certaines possèdent des activités exopeptidasiques comme la CatC (**Tableau 3**) (Fonovic and Turk, 2014). Elles ont une activité optimale à pH acide (5.5-6.0) et sont inactivées à pH neutre sauf la cathepsine S (CatS) qui reste protéolytiquement active (Bromme et al., 1993).

**Tableau 3 : Caractéristiques des cathepsines à cystéine humaines.** D'après (Fonovic and Turk, 2014).

Localization and specificity of cysteine cathepsins.

| Name | Gene symbol | Substrate cleavage mode | Extracellular localization | Tissue and cell specificity |
|---|---|---|---|---|
| Cathepsin B | CTSB | Carboxydipeptidase endopeptidase | Secreted membrane bound | Ubiquitous |
| Cathepsin C | CTSC | Aminodipeptidase | n.d. | Ubiquitous |
| Cathepsin F | CTSF | Endopeptidase | Secreted | Ubiquitous |
| Cathepsin H | CTSH | Aminomonopeptidase endopeptidase | Secreted | Ubiquitous |
| Cathepsin L | CTSL | Endopeptidase | Secreted | Ubiquitous |
| Cathepsin K | CTSK | Endopeptidase | Secreted | Predominant in osteoclasts and synovial fibroblasts |
| Cathepsin O | CTSO | n.d. | n.d. | ubiquitous |
| Cathepsin S | CTSS | Endopeptidase | Secreted | Predominant in antigen presenting cells |
| Cathepsin V | CTSL2 | Endopeptidase | n.d. | Thymus, testis |
| Cathepsin W | CTSW | n.d. | n.d. | Cytotoxic lymphocytes |
| Cathepsin X | CTSZ | Carboxymonopeptidase | Secreted membrane bound | Ubiquitous |

Les cathepsines à cystéines sont synthétisées sous forme de pré-proenzyme inactive. Le propeptide, constitué généralement d'une vingtaine de résidus, permet le bon repliement des protéases et les stabilise. Le propeptide agit comme un inhibiteur de la protéase, via l'obstruction du site actif, c'est pour cela qu'il doit être clivé via une étape de maturation afin que la protéase soit active (Cygler and Mort, 1997). Le clivage et le relargage du propeptide activent les cathepsines à cystéine (Fonovic and Turk, 2014; Turk et al., 2012). La maturation des cathepsines est réalisée soit par un mécanisme intermoléculaire aussi appelé trans-activation (une cathepsine active hydrolyse le propeptide) soit par un mécanisme intramoléculaire aussi appelé auto-activation (la cathepsine hydrolyse son propre propeptide). Seules les endopeptidases sont capables d'auto-maturation. En effet, la position de leur propeptide, inversée dans le site catalytique comparé à la position naturelle d'un substrat, lui confère une résistance à la protéolyse. Cependant, un pH acide permet le relâchement des interactions faibles liant le propeptide au site catalytique ce qui rend ce dernier accessible. L'endopeptidase peut ainsi cliver son propre propeptide et déclencher une auto-maturation intermoléculaire (Fonovic and Turk, 2014; Turk et al., 2012).

Les cathepsines à cystéine de la famille des papaïnes, sont caractérisées par la présence dans le site actif d'une triade catalytique composée d'une cystéine (Cys25), d'une histidine (His159) et d'une asparagine (Asn175) (numérotation de la papaïne). Dans un premier temps, il est nécessaire que la fonction thiol de la Cys25 soit sous la forme réactive thiolate ($S^-$) et que

la fonction imidazole de His159 soit sous la forme imidazolium ($Im^+$), cette diade catalytique est formée par un transfert de proton entre Cys25 et His159. C'est l'Asn175 qui permet la bonne orientation de l'imidazole de l'His159 dans cette étape cruciale, d'où le nom de triade catalytique de la catalyse, la fonction carboxylique (C=O) de la liaison peptidique du substrat, subit une attaque nucléophile par la fonction thiolate. Cela entraîne une charge négative sur l'oxygène de la fonction ($C\text{-}O^-$) (**Figure 21A**), cette fonction est stabilisée par la fonction amine (NH) de la glutamine (Gln19) et de la Cys25 par liaison hydrogène, formant ainsi le premier état de transition tétraédrique, appelé oxyanion (**Figure 21B**). Le résidu imidazolium de l'His159 permet un transfert de proton avec la fonction amine de la liaison peptique du substrat, celui-ci est hydrolysé, c'est le clivage. De cette façon, la fonction amine du substrat est liée à l'His159 et la fonction carboxylique à la Cys25 (formant une fonction thioester), on appelle cet intermédiaire l'acyl enzyme (**Figure 21C**). L'étape suivante implique la dissociation de la fonction amine du substrat et son remplacement par une molécule d'eau, polarisée par la fonction imidazole celle-ci attaque la fonction carboxylique de l'acyl enzyme (**Figure 21D**). Cela entraîne la formation d'un deuxième état intermédiaire tétraédrique (**Figure 21E**). Enfin la dernière étape, la déacylation du groupement thioester entraîne la reconstruction de la fonction carboxylique du substrat hydrolysé et le retour à l'état actif de l'enzyme (**Figure 21 F**) (Rzychon et al., 2004). Bien que leur mécanisme catalytique soit similaire, il existe différents types de cathepsine à cystéine.

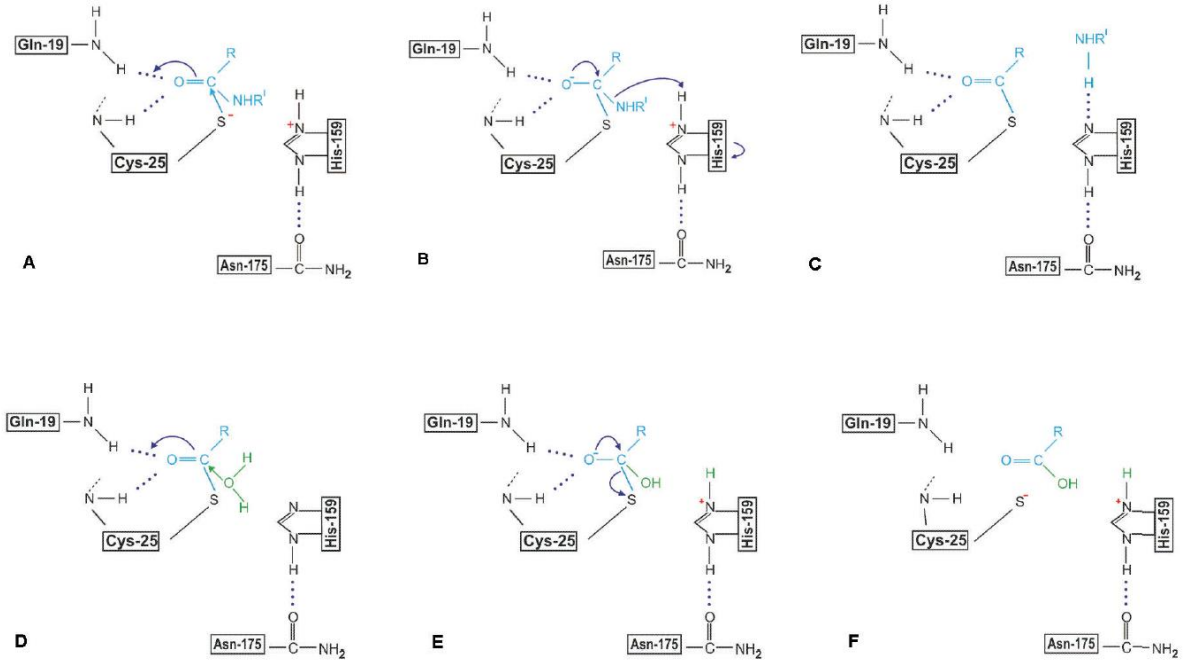


**Figure 21 : Mécanisme catalytique des cathepsines à cystéine.** D'après (Rzychon et al., 2004).

### 2.4.1 Les cathepsines L-like

#### 2.4.1.1 La cathepsine L

La cathepsine L (CatL) (EC 3.4.22.15) est une protéase ubiquitaire. Bien qu'elle ait été découverte dans les lysosomes, elle est aussi présente dans le milieu extracellulaire, le cytoplasme et le noyau. La CatL est codée par le gène *CTSL1* situé sur le chromosome 9q21-q22. Elle est synthétisée sous forme de pré-proprotéase de 333 acides aminés (aa) composée d'un propeptide de 96 aa et d'un domaine catalytique de 220 aa (Lecaille et al., 2002) (**Figure 22**). Bien que la CatL soit capable de s'auto-maturer (Menard et al., 1998), la CatD (Wiederanders and Kirschke, 1989) et les MMP (Hara et al., 1988) sont capables de maturer et d'activer la pro-CatL *in vitro*.

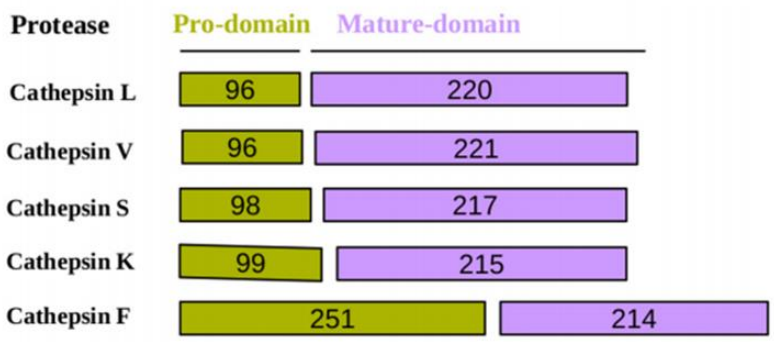


**Figure 22 : Illustration schématique des zymogènes des CatL-Like.** Les prodomaines sont représentés en vert et les domaines catalytiques en violet. D'après (Verma et al., 2016).

En fonction du type cellulaire, la CatL peut avoir deux différentes formes matures. La première est constituée de 220 résidus, formant une chaîne peptidique appelée « *single chain* ». La deuxième forme mature est obtenue suite à un clivage protéolytique, pour générer deux chaînes peptidiques : la première est la chaîne lourde, dite « *heavy chain* » et la deuxième est la chaîne légère dite « *light chain* » (**Figure 23**) (Gal et al., 1985). La CatL mature a principalement une activité endopeptidasique et coupe préférentiellement les liaisons peptidiques avec un résidu aromatique en position P2 et un résidu hydrophobe en position P3 (Portaro et al., 2000).

Comme précisé précédemment, la CatL est présente dans tous les compartiments cellulaires, mais également dans le milieu extracellulaire. Ce qui lui permet d'avoir diverses fonctions physiologiques telles que le recyclage des protéines, l'homéostasie cellulaire et la régulation immunitaire (Turk et al., 2012). De ce fait, un dysfonctionnement ou une dérégulation de cette protéase peut engendrer des pathologies, c'est notamment le cas de l'athérosclérose (Kitamoto

et al., 2007). La CatL a aussi un rôle de suppresseur de tumeur, en effet, elle est capable de réguler le cycle cellulaire, ce qui lui permet d'inhiber la prolifération et l'invasion des cellules tumorales, accélérant ainsi leur apoptose (Chwieralski et al., 2006). Paradoxalement, la CatL serait capable de participer au développement de résistance aux agents chimio-thérapeutiques *via* un rôle anti-apoptotique (Guicciardi et al., 2004).

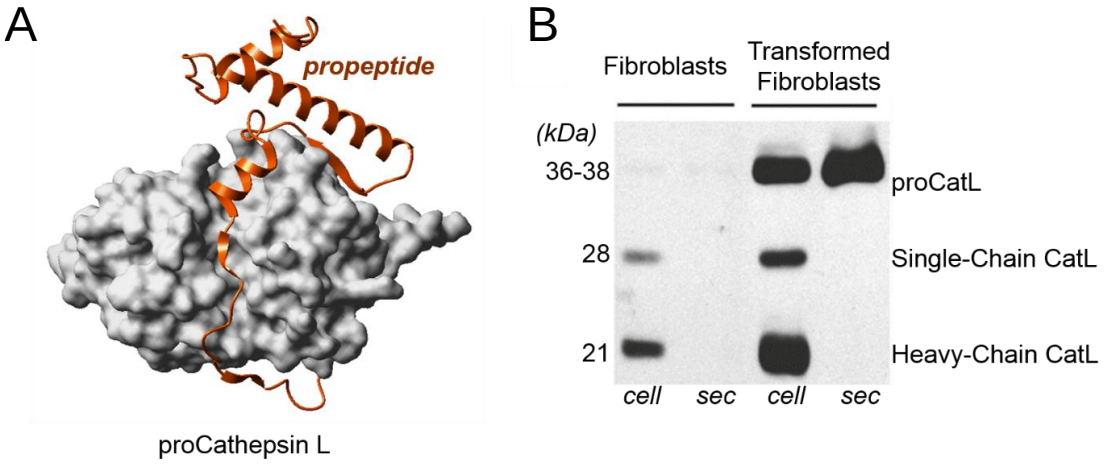


**Figure 23 : Pro-cathepsine L et formes matures. (A)** La pro-CatL est représentée en gris et son propeptide en orange (PDB ID: 1CS8). D'après (Coulombe et al., 1996). **(B)** Western-blot réalisé avec un anticorps anti-chaîne lourde de la CatL avec les lysats et les surnageants de fibroblastes en culture. D'après (Erickson et al., 2013). La pro-CatL est sécrétée par la voie constitutive pendant la transformation des fibroblastes et est retrouvée dans le surnageant de culture.

2.4.1.2 La cathepsine S

Contrairement à la CatL, la CatS (EC 3.4.22.27) n'est pas ubiquitaire, elle est exprimée préférentiellement dans les cellules présentatrices d'antigène comme les lymphocytes B, les cellules dendritiques, les monocytes, les PNN, les macrophages et les cellules présentatrices non-professionnelles d'antigène comme les cellules épithéliales et les cellules intestinales (Wilkinson et al., 2015). La CatS est codée par le gène *CTSS* qui est localisé sur le chromosome 1q21. Elle est synthétisée sous forme de pré-proenzyme de 331 aa composée, d'un propeptide de 16 aa, d'une chaîne légère de 98 aa et d'une chaîne lourde de 217 aa (Lecaille et al., 2002). En tant qu'endopeptidase, la CatS est capable de maturation inter- et intra-moléculaire (**Figure 24**) (Sage et al., 2013). La CatS mature est une endopeptidase lysosomale qui est une exception dans les protéases à cystéine car elle reste active à pH neutre. Elle affiche une préférence de substrats synthétiques pour les protéines avec des résidus hydrophobes ramifiés (Oliveira et al., 2010).

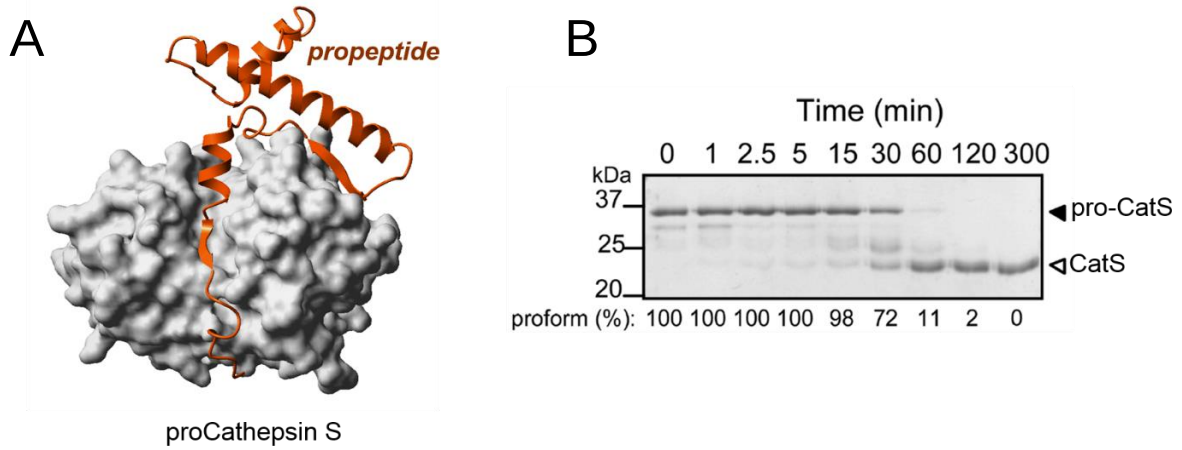


**Figure 24 : Pro-cathepsine S et auto-maturation. (A)** La pro-CatS est représentée en gris et son propeptide en orange (PDB ID: 2C0Y). D'après (Kaulmann et al., 2006). **(B)** L'analyse par Western-Blot de l'auto-maturation de la pro-CatS à 37°C pendant 300 minutes est réalisée avec un anticorps anti-CatS. D'après (Sage et al., 2013).

La CatS présente une fonction essentielle dans l'immunité car elle permet la maturation des molécules du complexe majeur d'histocompatibilité de classe II (MHC II) ainsi que la motilité des cellules dendritiques (Lukacs-Kornek and Turley, 2008). L'augmentation de son expression est associée à de nombreuses pathologies telles que le cancer, la fibrose kystique, l'asthme, l'emphysème et les douleurs neuropathiques (Flannery et al., 2006). Cette augmentation s'est aussi révélée comme biomarqueur de certaines pathologies (Lindahl et al., 2009) mais la contribution exacte dans la pathogénie reste encore floue. L'expression limitée à certains organes de la CatS en fait une cible thérapeutique intéressante. La CatS possède une activité élastinolytique importante, d'où son implication dans des pathologies comme la bronchopneumopathie chronique obstructive (BPCO) (Andrault et al., 2019). De plus, son rôle dans cette pathologie est exacerbé par sa capacité à hydrolyser les protéines de jonction cellulaire, rendant alors perméable le poumon, aux leucocytes comme les PNN aggravant la composante inflammatoire chronique de cette pathologie (Bigot et al., 2022). La CatS est impliquée dans la dégradation de nombreux composant de la MEC, elle agit aussi dans le vieillissement de la peau, *via* la catalyse du nidogène, un composant clé de la jonction dermo-épidermique (Sage et al., 2022) (**Annexe 2**). Son rôle pathologique explique le développement d'inhibiteurs synthétiques de la CatS actuellement en cours d'essais cliniques (**Tableau 4**).

Dans une étude réalisée au sein du laboratoire d'accueil, il a été démontré que l'inhibition pharmacologique de la CatS dans la lignée promyélocytaire HL-60 diminuait l'activité catalytique de la CatC de 80% (Hamon et al., 2016b). Cela indique le rôle de la CatS comme protéase capable de maturer la CatC dans ces cellules. La CatC permettant de maturer les PSN,

l'inhibition indirecte de la CatC, *via* l'inhibition de la CatS, pourrait inhiber les PSN et ainsi réduire l'inflammation.

**Tableau 4 : Inhibiteurs de la cathepsine S en cours d'essais cliniques.** D'après (Wilkinson et al., 2015).

| Drug | Cathepsin | Company | Stage | Disease | References |
|---|---|---|---|---|---|
| RWJ-445380 | S | Johnson & Johnson | Phase II | Rheumatoid arthritis | http://clinicaltrials.gov/ct2/show/study/NCT00425321 |
| VBY-036 | S | Virobay Inc. | Phase I | Neuropathic pain | http://clinicaltrials.gov/ct2/show/NCT01892891 |
| VBY-891 | S | Virobay Inc., LEO Pharma | Phase I | Psoriasis | http://clinicaltrials.gov/ct2/show/NCT01947738 |
| CRA-028129 | S | Celera | Phase I | Psoriasis | https://www.celera.com/celera/pr_1127168705 |

2.4.1.3 La cathepsine K

La cathepsine K (CatK) (EC 3.4.22.38) est codée par le gène *CTSK* qui se situe sur le chromosome 1q21. Elle est synthétisée sous forme de pré-proenzyme de 329 aa composée d'un propeptide de 15 aa, d'une chaîne légère de 99 aa et d'une chaîne lourde de 215 aa (Lecaille et al., 2002). La CatK est une endopeptidase puissante avec un S2 qui a une préférence pour les résidus hydrophobes non-aromatiques comme la leucine, l'isoleucine, la méthionine et la valine en P2. Les autres sous-sites acceptent une large gamme d'aa avec une préférence pour ceux chargés positivement tels que la lysine et l'arginine. Les petits résidus comme la glycine, l'alanine et la serine sont bien accommodés dans les sous-sites S4 et S3 (Bossard et al., 1996; Lecaille et al., 2003).

La CatK est l'unique protéase humaine connue capable de cliver le collagène de type I et II. Son activité collagénolytique est dépendante des glycosaminoglycanes (chondroïtine sulfate), contrairement à son activité peptidasique. Les glycosaminoglycanes forment un complexe avec la CatK, et agissent comme des activateurs (Li et al., 2002). La CatK est exprimée à des taux élevés dans les ostéoclastomes, les ovaires, l'intestin grêle et le colon. Des faibles taux de CatK ont été détectés dans le cœur, les muscles squelettiques, le placenta, les poumons, la prostate, les testicules, la rate, le thymus, les reins, le pancréas et le foie. La CatK n'a pas été détectée dans les leucocytes (Ketterer et al., 2017). Elle représente 98% des cathepsines exprimées dans les ostéoclastes, soulignant son rôle important dans la résorption osseuse, dû à son activité collagénolytique car le collagène I constitue 90% de la matrice osseuse (Drake et al., 1996). La mutation du gène codant pour la CatK engendre un déficit en CatK qui aboutit à la pycnodysostose.(Ketterer et al., 2017). De plus, il a été démontré que

l'œstrogène diminue l'expression de la CatK c'est pourquoi à la ménopause les femmes souffrent d'ostéoporose causée par la CatK (Bone et al., 2010). De ce fait, la CatK est une cible thérapeutique pour l'ostéoporose.

#### 2.4.1.4 La cathepsine V

La cathepsine V (CatV) (EC 3.4.22.43), également appelée la CatL2 est codée par le gène *CTSV* qui est sur le chromosome 9q22.2. La CatV est synthétisée sous forme de pré-proenzyme de 334 aa composée d'un propeptide de 17 aa, d'une chaîne légère de 96 aa et d'une chaîne lourde de 221 aa (Lecaille et al., 2002 ; Itoh et al., 1999). La séquence protéique de la CatV mature partage 79,5% d'identité avec la CatL, elle est donc étroitement apparentée d'où son nom de CatL2. Mais contrairement à la CatL qui est ubiquitaire, la CatV est exprimée de manière sélective dans le thymus, le testicule et la cornée. Son activité élastinolytique la différencie de la CatL (Puzer et al., 2004). La CatV accepte préférentiellement les résidus hydrophobes tels que le tryptophane, la phénylalanine, la leucine et la valine dans son sous-site S2. Le sous-site S3 de la CatV accepte préférentiellement la proline (Choe et al., 2006). La CatV a l'activité élastinolytique la plus élevée parmi les protéases humaines. Le taux de la CatV est augmenté dans certaines pathologies comme l'athérosclérose (Helske et al., 2006). C'est aussi un marqueur diagnostique des cancers du côlon, du sein et du col de l'utérus (Santamaria et al., 1998; Sioud and Hansen, 2001).

#### 2.4.1.5 La cathepsine F

La cathepsine F (CatF) (EC 3.4.22.41) est codée par le gène *CTSF* qui se situe sur le locus 11q13. La pro-CatF possède un très long propeptide de 251 acides aminés (**Figure 22**). Cette caractéristique est unique parmi les CatL-like. Il est composé d'un domaine C-terminal similaire au CatL-like, d'un peptide qui fait la liaison « *linker* » de 50 aa et d'un domaine N-terminal qui présente des caractéristiques structurelles similaires aux cystatines (inhibiteur endogène des cathepsines à cystéine) (Nagler et al., 1999). La structure de la CatF a été déterminée en complexe avec l'inhibiteur vinyl sulfone V. Ses sous-sites S2 et S3 possèdent des caractéristiques uniques. Contrairement à la CatS, sa poche S2 est définie par une leucine et une méthionine (Leu67 et Met205). La poche S3 qui contient généralement une glycine, alanine ou asparagine, est dans le cas de la CatF composée d'une aspartate, ce qui lui confère

une caractéristique électrostatique unique pouvant être exploitée dans la recherche d'inhibiteurs spécifiques (Schmitz et al., 2015).

Outre son activité de protéase lysosomale, la CatF à un rôle dans la régulation du MHC de classe II, notamment au niveau de la chaîne invariante du MHC II. Dans les macrophages, l'inhibition de la CatF bloque l'activation du MHC II, expliquant l'implication de cette protéase dans des pathologies inflammatoires (Somoza et al., 2002). La CatF est capable de réaliser des modifications sur la lipoprotéine LDL (Low density lipoprotéine), engendrant son accumulation dans l'artériosclérose (Oorni et al., 2004).

### 2.4.2 La cathepsine C

#### 2.4.2.1 La biosynthèse et la maturation de la cathepsine C

La CatC (EC 3.4.14.1), est une aminopeptidase à cystéine très conservée qui libère des dipeptides à partir de l'extrémité N-terminale des protéines et des peptides, d'où son autre dénomination de dipeptidyl peptidase I (DPPI) (McGuire et al., 1993; Turk et al., 2001a). Le gène qui code la CatC, CTSC, est situé sur le chromosome 11q14.1-q14.3 (Rao et al., 1997). La CatC est une protéase ubiquitaire, elle et son ARNm ont été détectés dans les extraits de différents tissus et à des niveaux particulièrement élevés dans la rate, le foie, les reins et les poumons (Korkmaz et al., 2021; Pham et al., 1997) (**Figure 25**). La CatC est aussi présente dans les cellules d'origine hématopoïétique (Rao et al., 1997). Dans les lysats de ces cellules, l'activité de la CatC a été mesurée en utilisant des substrats synthétiques (McGuire et al., 1993).

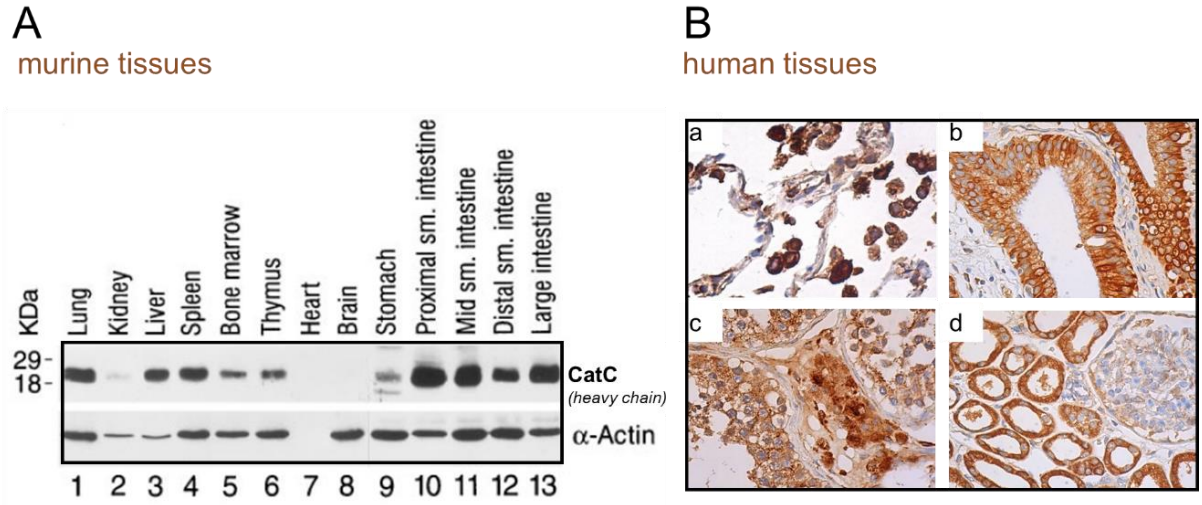


**Figure 25 : Présence of cathepsine C dans divers tissus sains. (A)** Expression de la cathepsine C dans différents tissus murins. D'après (Pham et al., 1997) et **(B)** humains (a-poumon, b-vésicule biliaire, c-testicules, d-rein). D'après (Korkmaz et al., 2021).

La CatC est synthétisée sous forme de pro-enzyme de ~60 kDa. Cette pro-enzyme est composée d'un domaine d'exclusion (Asp1-Gly119), d'un pro-peptide (Thr120-His206), d'une chaîne lourde (Leu207-Arg370) et d'une chaîne légère (Asp371-Leu439) (**Figure 26**) (Dahl et al., 2001; Turk et al., 2001a). Le propeptide agit comme une protéine chaperonne lors de la biosynthèse de la pro-CatC, lui assurant un bon repliement et une bonne stabilisation de la pro-CatC. Celle-ci va ensuite former un dimère. La maturation de la pro-CatC implique le triple clivage du dimère en monomères et son assemblage en homo-tétramère (Molgaard et al., 2007). Ces trois clivages libèrent un fragment N-terminal appelé domaine d'exclusion de 16 kDa, un peptide d'activation et une chaîne lourde de 23 kDa et une chaîne légère de 7 kDa (Molgaard et al, 2007; Turk et al., 2001). La CatC est une glycoprotéine avec quatre sites de glycosylation, dont trois sont sur le domaine d'exclusion et un sur la chaîne lourde (Turk et al., 2001a). (**Figure 27**)

Contrairement aux autres cathepsines à cystéine la CatC ne s'automature pas. Les CatL-like K, L, S, V et F sont capables de cliver le propeptide de la CatC *in vitro* (Dahl et al., 2001; Lamort et al., 2019). La maturation de la pro-CatC se fait en 2 étapes, la première étape permet de libérer le domaine d'exclusion et le propeptide et la deuxième étape permet d'obtenir la CatC mature tétramérique suite au clivage entre les chaînes lourde et légère (Lamort et al., 2019). Le domaine d'exclusion et la chaîne lourde sont stabilisés respectivement par deux et trois ponts disulfures intra-chaînes.

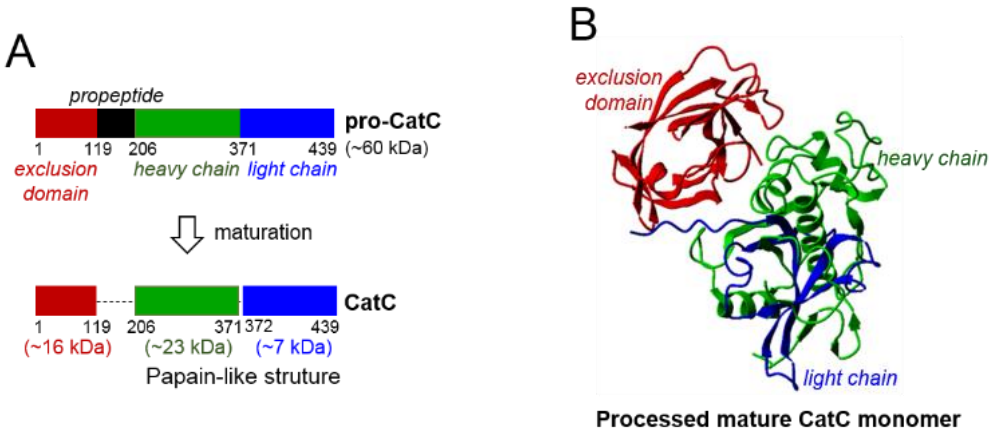


**Figure 26 : Maturation protéolytique de la pro-cathepsine C et structure cristallisée du monomère de la cathepsine C mature. (A)** Schéma du monomère de la pro-CatC d'environ 60 kDa et celui de sa forme mature obtenue suite aux clivages protéolytiques. Le domaine d'exclusion, le propeptide, la chaîne lourde et la chaîne légère sont représentés en rouge, noir, vert et bleu, respectivement. **(B)** Représentation en ruban du monomère de la CatC. Chaque monomère est composé d'un domaine d'exclusion (en rouge), d'une chaîne lourde (en vert) et d'une chaîne légère (en bleu) qui restent associés entres eux par des interactions hydrophobes (PDB ID 2DJF. D'après (Turk et al., 2001).

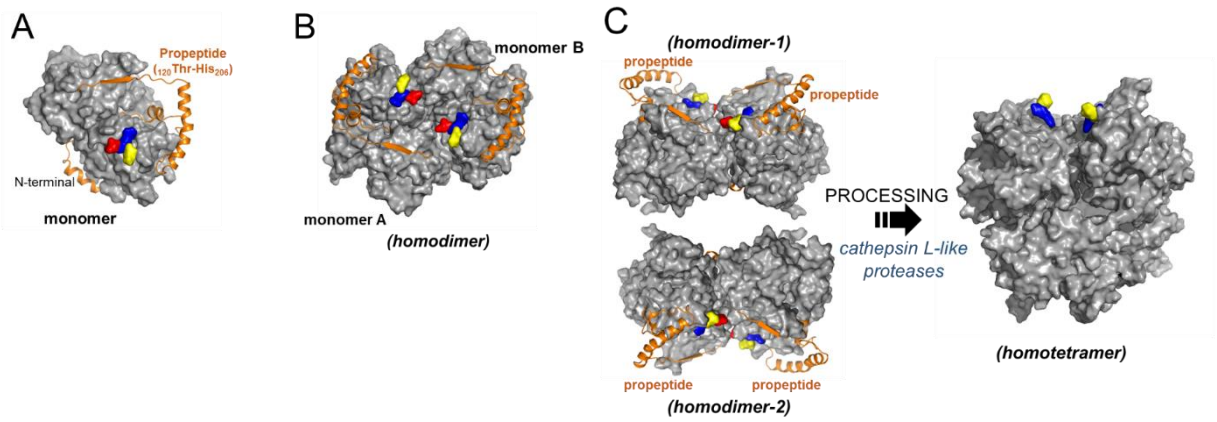


**Figure 27 : Structures de la pro- et mature cathepsine C humaine**. **(A)** Structure modélisée de la pro-CatC monomérique. La représentation de la surface du domaine d'exclusion et du domaine catalytique de type papaïne (en gris). La représentation en ruban du propeptide (résidus 120Thr-His206) (en orange). Les résidus Leu, Arg et Asp (369Leu-Arg/Asp371, la séquence entre les chaînes lourdes et légères contenant les sites de clivage des protéases maturant la pro-CatC) sont colorés, respectivement, en jaune, bleu et rouge. **(B)** L'homodimère de la pro-CatC constitué de monomères A et B en représentation de surface avec le même code couleur que précédemment. **(C)** Clivage et association des homodimères pour former la CatC tétramérique mature. D'après (Korkmaz et al., 2021).

### 2.4.2.2 La localisation intracellulaire et la sécrétion de la cathepsine C

La localisation intracellulaire de la CatC dans des PNN différenciés *in vitro* a été montrée par des techniques d'immunochimie (Hamon et al., 2016c). La CatC active a été détectée dans des granules cytoplasmiques, mais des stimuli chimiques ou physiologiques peuvent entraîner sa sécrétion dans le milieu extracellulaire. La CatC mature a été identifiée comme biomarqueur d'inflammation pulmonaire neutrophilique (Hamon et al., 2016c). La CatC est sécrétée dans le milieu extracellulaire par les mastocytes et les LT cytotoxiques ce qui indique sa présence leurs granules intracellulaires (Brown et al., 1993; Wolters et al., 1998). Une possible sécrétion de la CatC par les macrophages a été proposée sans être expérimentalement démontrée (Wolters et al., 1998). La CatC extracellulaire active a également été retrouvée dans les carcinomes épidermoïdes (Ruffell et al., 2013) et dans l'inflammation du système nerveux centrale (Koike et al., 2013).

La pro-CatC est secrétée par les cellules bronchiques et est présente dans les sécrétions pulmonaires de manière constitutive chez les sujets sains (Hamon et al., 2016c). La pro-CatC et la CatC mature sont présentes de manière constitutive dans l'urine de sujets normaux. Bien que la source de CatC urinaire reste à élucider, elle pourrait être sécrétée de manière constitutive par les cellules épithéliales rénales ou de la vessie (Hamon et al., 2016a).

2.4.2.3 La structure du site catalytique et la spécificité de la cathepsine C

La CatC mature est un tétramère composé de 4 monomères identiques possédant chacun un site catalytique accessible. Les monomères de la CatC active ont la structure classique « *papain-like* » des cathepsines à cystéine. Ils sont composés donc d'une chaîne lourde et d'une chaîne légère, le site catalytique étant composé de la diade catalytique formée par la cystéine 234 (Cys234) et l'histidine 381 (His381). La Cys234, de la diade catalytique, est localisée sur l'extrémité N-terminale de l'hélice $\alpha$ centrale de la chaîne lourde. Malgré la similitude structurelle de son site actif avec les « *papain-like* », c'est le domaine d'exclusion qui détermine son activité dipeptidasique (Turk et al., 2001a). En effet, le positionnement de ce domaine bloque le site actif au niveau du sous-site S2 (Turk et al., 2001a). Le groupement carboxyle porté par le résidu acide aspartique 1 (Asp1), conservé dans toutes les séquences connues de la CatC, stabilise le groupement $NH_3^+$ des substrats (**Figure 28**). De ce fait, les substrats et les peptides clivés par la CatC contiennent un $NH_3^+$ N-terminal libre non-protégé. Le sous-site S2 est en forme de poche et contient un ion chlorure et deux molécules de solvants (Turk et al., 2001a). Le site S1 est situé en surface et est de grande taille ce qui permet de contenir des résidus encombrants et hydrophobes (Poreba et al., 2014). Au-delà du site S2, le sillon du site actif est ouvert donc il n'y a pas de spécificité d'aa nécessaire pour la liaison du substrat (Legowska et al., 2016).

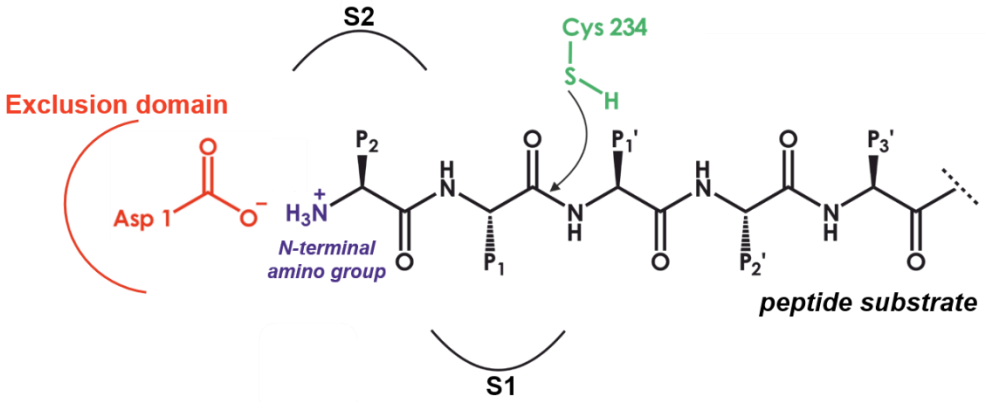


**Figure 28 : Schéma de la liaison d'un substrat peptidique avec le site actif de la cathepsine C.** D'après (Korkmaz et al., 2018a).

L'utilisation de substrat synthétique et peptidique a permis d'étudier la spécificité protéolytique de la CatC. La CatC ne peut pas accommoder une proline en P1 ou P'1, une isoleucine en P1 et une lysine, arginine ou ornithine en P2 (Tran et al., 2002). Elle conserve son activité protéolytique avec un environnement au pH entre 3 et 8, mais son pH optimal d'activité se situe autour de 5.5 (Dolenc et al., 1995). Elle se distingue par son activation pH dépendante

réalisée par les ions $Cl^-$ (Cigic and Pain, 1999). La structure cristallisée de la CatC a révélé la présence d'un ion $Cl^-$ au fond de la poche S2 et interagissant avec le groupement hydroxyle de la tyrosine 323 (Tyr323) afin de stabiliser la poche S2 (Turk et al., 2001a). Les substrats Gly-Phe-AMC (Korkmaz et al., 2018b) et Gly-Arg- AMC sont couramment utilisés pour mesurer l'activité de la CatC dans un tampon de pH 5.5 complémenté en ion $Cl^-$. La CatC est inhibée par des inhibiteurs synthétiques comme Gly-Phe-diazomethyl cétone, E-64, E-64c, dipeptide vinyl-sulfone LHVS (leucine-homophenylalanine-vinyl sulfone) mais aussi par les inhibiteurs protéiques comme les stéfines A et B et les cystatines C et F (Korkmaz et al., 2018b).

#### 2.4.2.4 Les inhibiteurs de type nitrile de la cathepsine C

Les inhibiteurs réversibles de type nitrile qui ont été récemment développés sont des inhibiteurs dipeptidyliques puissants et sélectifs de la CatC (**Tableau 5**). Ces inhibiteurs sont capables de traverser les membranes cellulaires pour aller inhiber la CatC intracellulaire et sont moins toxiques que d'autres inhibiteurs synthétiques apparentés (Korkmaz et al., 2018b). La première étude sur les inhibiteurs de CatC, publiée en 2006 par Bondebjerg et al (Bondebjerg et al., 2006), a débuté avec un inhibiteur modéré de la CatC, le glycyl-L-phénylalanine nitrile (Gly-Phe-CN). L'activité inhibitrice de la CatC a été améliorée par l'introduction de l'acide aminobutanoïque (Abu) en position P2 (Abu-Bip-CN), tandis que divers résidus d'acides aminés hydrophobes et aromatiques, tels que la phénylalanine (Phe) et le biphényle (Bip), ont été évalués en position P1. Abu-Bip-CN a été identifié comme l'inhibiteur le plus puissant de la série, mais s'est révélé peu puissant en raison de son hydrolyse rapide dans les milieux biologiques.

La stabilisation de la liaison peptidique peut être obtenue en remplaçant l'acide aminé N-terminal par un autre aa présentant un cycle pipéridine ou cyclohexyle comme chaîne latérale ou en insérant 1,1-cyclopropylaminonitrile en position P1. Grâce à ces stratégies, les inhibiteurs **brensocatib** (INS1007/AZD7986, (*S*)-N -((*S*)-1-cyano-2-(4-(3-méthyl-2-oxo-2,3-dihydrobenzo[d]-oxazol-5-yl)phényl)éthyl)-1,4-oxazépane- 2-carboxamide, IC50-CatC = 22 nM), **BI-9740 (**$IC_{50}$-CatC= 1.8 nM) et **IcatC$_{XPZ-01}$** ((*S*)-2-amino-N-((1*R*,2*R*)-1-cyano-2-(4'-(4-méthylpipérazin-1-ylsulfonyl)biphényl-4-yl)cyclopropyl)-butanamide), $IC_{50}$-CatC= 15 nM) ont été développés, respectivement, par AstraZeneca, Boehringer Ingelheim and Neuprozyme Therapeutics (**Figure 29**).

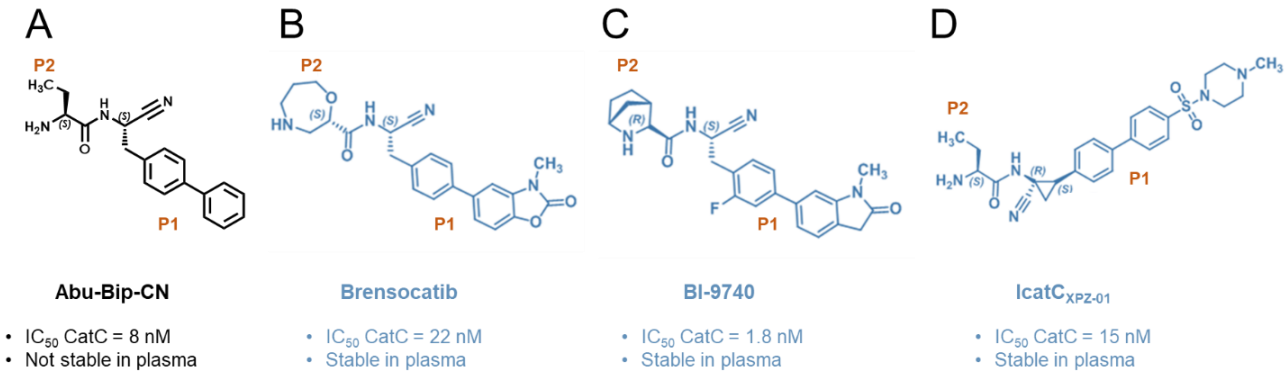


**Figure 29 : Structures chimiques des inhibiteurs de type nitrile de la cathepsine C. (A)** Abu-Bip-CN, **(B)** brensocatib, **(C)** BI-9740, **(D)** IcatC$_{XPZ-01}$.

Les structure 3D des inhibiteurs nitriles complexés avec la CatC ont permis d'élucider leur mécanisme d'interaction, qui résulte de la formation d'un complexe thiomidate entre la cystéine du site actif et la fonction nitrile des inhibiteurs (**Figure 30**) (Korkmaz et al., 2019).

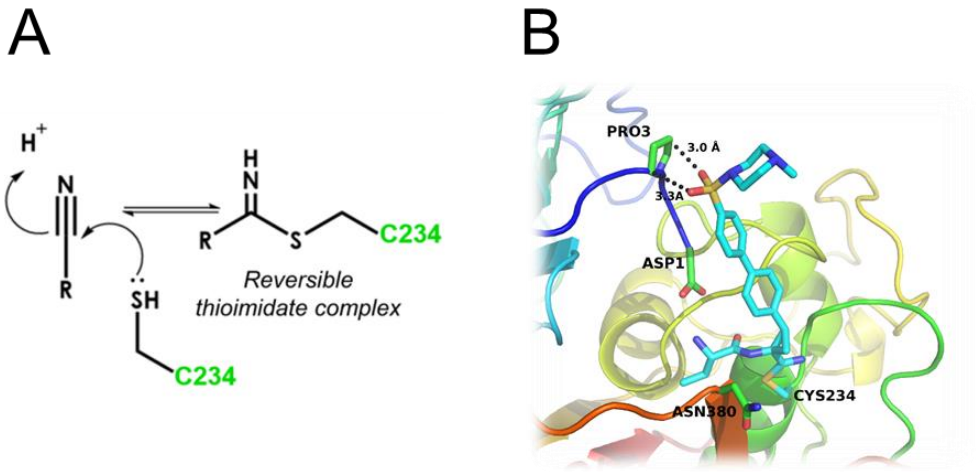


**Figure 30 : Structure cristallisée de l'IcatC$_{XPZ-01}$ complexé au site actif de la cathepsine C humaine. (A)** La formation d'un complexe thioimidate réversible entraînant la réaction de la fonction nitrile avec le site actif cystéine 234. **(B)** La structure de l'IcatC$_{XPZ-01}$ (en turquoise). D'après (Korkmaz et al., 2019).

La CatC est également inhibée par les inhibiteurs irréversibles comme **GSK2793660** (Miller et al., 2017), **le composé 22** (Hou et al., 2019) (**Tableau 5**), **Gly-Phe-diazomethyl cétone**, **biphenyle-Ile-Leu-diazomethyl cétone** (BIL-DMK), **E64**, **E64c**, **E64d** (Methot et al., 2007), mais aussi par les inhibiteurs protéiques comme les stéfines A et B et les cystatines C et F (Korkmaz et al., 2018a).

**Tableau 5 : Inhibiteurs de la cathepsine C en cours d'essais cliniques.**

| | Nature de l'interaction avec la CatC | $IC_{50}$ (nM) | Inhibition de la CatC cellulaire *in vitro* | Inhibition de la CatC *in vivo* Préclinique | Clinique |
|---|---|---|---|---|---|
| **$IcatC_{XPZ-01}$** | Réversible (nitrile) | 15[1] | HL-60[2] ; neutrophiles différentiés des promyéolocytes de la moelle humaine[3]; neutrophiles différentiés des $CD34^{+}$[4] | Souris[1], hamster[5], macaque[3] | - |
| **BI-9740** | Réversible (nitrile) | 1.8[6] | Neutrophile différentié des CD34[6] | Souris, rat | - |
| **BI-1291583** | Réversible (nitrile) | 0.9[7] | U937[7] | Souris[7] | Phase 2[8] |
| **Brensocatib** | Réversible (nitrile) | | Neutrophiles différentiés des $CD34^{+}$ de la moelle humaine[9] | Souris[10], rat[10] | Phase 3[11] |
| **Compound 54** | Réversible (pyridine) | 57.4[12] | HL60[12], THP-1[12], neutrophiles différentiés des promyéolocytes de la moelle murine[12] | Souris[12], rat[12] | Phase 1 |
| **GSK2793660** | Irréversible | 1[13] | Information non disponible | Information non disponible | Phase 1[13] |
| **Compound 22** | Irréversible (acrylamide) | 17.3[14] | THP-1[14], U-937[14] | Mouse[14] | - |

**.** [1](Korkmaz et al., 2019), [2](Hamon et al., 2016c), [3](Guarino et al., 2017), [4](Seren et al., 2018), [5] (Bourgon et al., 2022), [6](Jerke et al., 2022), [7](Kreideweiss et al., 2023), [8](Chalmers et al., 2023), [9] (Doyle et al., 2016), [10](Basso et al., 2023), [11](Cipolla et al., 2023), [12](Chen et al., 2021) [13](Miller et al., 2017), [14](Hou et al., 2019).

### 2.4.2.5 Les fonctions biologiques de la cathepsine C

La CatC possède comme fonction physiologique majeure l'activation des protéases à sérine des cellules hématopoïétiques. Celles-ci sont synthétisées sous forme de pro-protéases (zymogènes inactifs) contenant un di-propeptide. Le clivage du di-propeptide par la CatC entraîne un changement de conformation de la protéase, ce qui la rend protéolytiquement active (Korkmaz et al., 2018a).

*Maturation des protéases à serine des mastocytes* : Les mastocytes possèdent protéase à serine maturées par la CatC dans leurs granules, telle que la chymase, la CatG et les tryptases (**Figure 31**) (Wolters et al., 1998). Les granules sont sécrétés lors de réaction allergique ou anaphylactique, ce qui libère les protéases à serine, ainsi que l'histamine, un composant majeur de ces granules. La dégranulation est engendrée par la fixation d'IgE sur les mastocytes, qui possèdent un très grand nombre de récepteurs à IgE, ce qui explique leur rôle dans la réaction allergique (Douaiher et al., 2014).

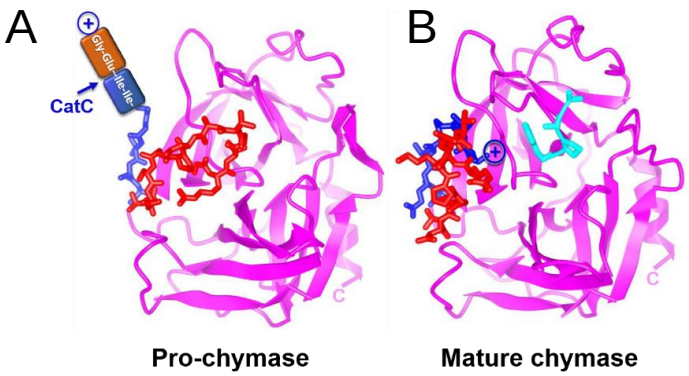


**Figure 31 : Activation de la pro-chymase par la cathepsine C. (A)** Représentation en ruban de la pro-chymase et **(B)** de la chymase mature liée à un inhibiteur peptidique représenté en turquoise. Le clivage par la CatC du peptide Gly-Glu engendre une modification structurelle ce qui libère le site actif de la chymase (PDB ID 1NN6) (Reiling et al., 2003). D'après (Korkmaz et al., 2018a).

*Maturation des protéases à serine du neutrophile (PSN) :* La CatC clive le pro-dipeptide des zymogènes des protéases à serine du neutrophile (PSN) (l'élastase (NE), la proteinase 3 (PR3), la CatG (Adkison et al., 2002a; Pham et al., 2004), la NSP-4 (Perera et al., 2013)) afin de les activer. L'activation des pro-PSN par la CatC se produit lors de la formation des granules azurophiles du PNN. Les propeptides amino-terminaux des PSN sont composés d'acides aminés différents soit : serine-acide glutamique pour la NE ; alanine-acide glutamique pour la PR3 ; glycine-acide glutamique pour la CatG et alanine-glutamine pour la NSP-4 (**Figure 32**).

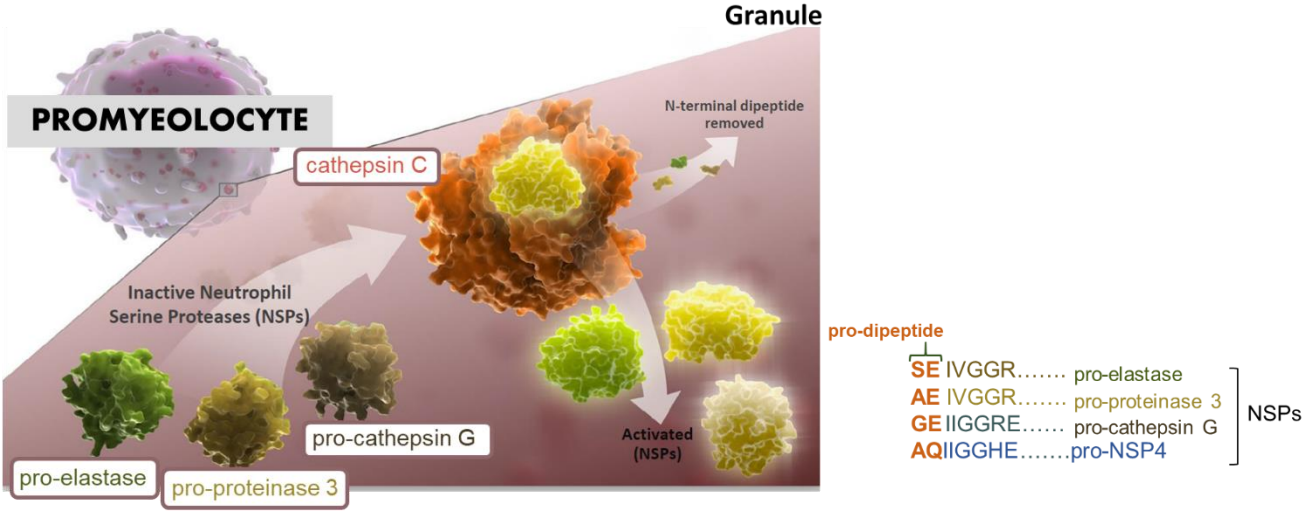


**Figure 32 : Illustration de la maturation des protéases à serine du neutrophile par la cathepsine C dans le promyélocyte.** Les PSN synthétisées avec leurs propeptides et sont maturées par la CatC, libérant ainsi les formes protéolytiquement actives.

Après l'activation par la CatC, les PSN sont stockées dans les granules cytoplasmiques des neutrophiles. La fonction de la CatC dans l'activation des PSN a également été confirmée *in vivo* chez les souris déficientes en CatC ($CatC^{-/-}$). Chez ces souris déficientes, une réduction sévère de l'activité protéolytique des PSN présentes dans des cellules hématopoïétiques a été constatée (Adkison et al., 2002a).

*Maturation des granzymes* :

Les granzymes (Gzms) constituent une famille de protéases à sérine cytotoxiques présentes dans les LT $CD8^+$ cytotoxiques et dans les NK. Les Gzm pro-apoptotiques sont stockées dans les vésicules sécrétoires cytotoxiques sous forme de protéases protéolytiquement actives.
Il y existe cinq Gzms (A, B, H, K et M). Les GzmA et GzmB sont les deux granzymes les plus étudiées. Toutes les Gzms sont produites sous forme de zymogènes, comme les PSN, elles nécessitent le clivage de leur dipropeptide N-terminal pour être actives.

2.4.2.6 Les fonctions pathologiques de la cathepsine C

Une inactivation de la CatC est observée chez les patients atteints du syndrome de Papillon-Lefèvre (SPL), maladie génétique héréditaire rare à transmission autosomique récessive. Cette pathologie se caractérise par une kératodermie palmoplantaire et une parodontite précoce et sévère (**Figure 33**) sans que les patients souffrent d'une infection récurrente (Toomes et al., 1999). Les signes cliniques permettent de poser le diagnostic et pour la plupart des cas, une analyse génétique est également effectuée pour confirmer le diagnostic. Plus de 75 mutations ont été identifiées pour le SPL.

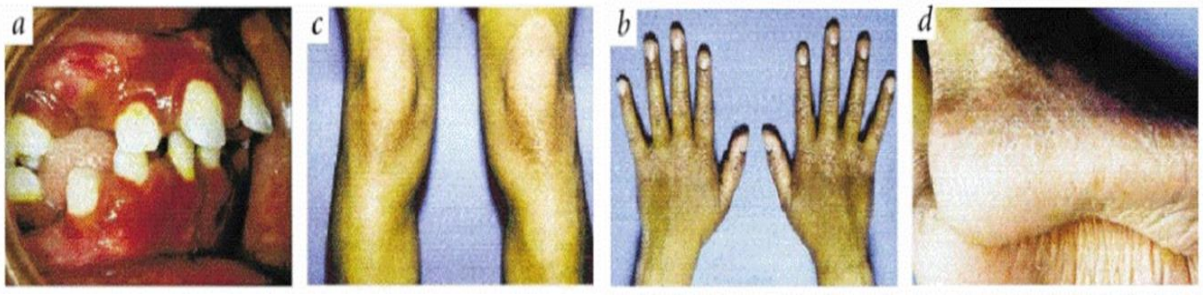


**Figure 33 : Manifestations cliniques des patients atteints du syndrome de Papillon-Lefèvre.** Les signes cliniques des patients atteints du SPL sont une inflammation des gencives entrainant une parodontite et une kératodermie. D'après (Toomes et al., 1999).

L’inactivation de la CatC entraîne, chez les patients SPL, une sévère réduction de la NE, de la PR3, de la CatG (Guarino et al., 2017; Pham et al., 2004) (**Figure 34**) et de la NSP-4 (Perera et al., 2013) dans les PNN circulants. Les données récentes obtenues au sein de notre équipe ont montré que <10% (<10 % PR3, NE et <1 % CatG) des PSN dans les neutrophiles de patients SPL étaient activées par une protéase inconnue (Seren et al., 2018) que nous avons appelée NSPs-AAP pour *Neutrophil Serine Protease Alternative Activating Protease*, c’est-à-dire PSN-Protéase Activatrice Alternative (PSN-AAP). Cela suggère que la CatC est la principale protéase, mais pas la seule, impliquée dans l'activation des proPSN.

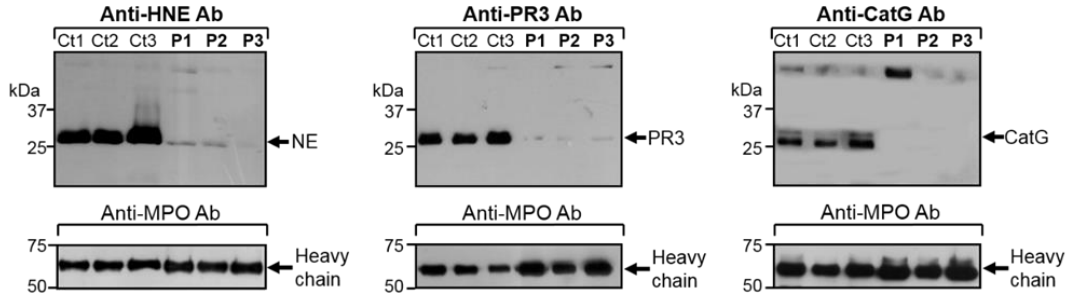


**Figure 34 : Conséquences de l’inactivation génétique de la cathepsine C sur la stabilité des protéases à sérine neutrophiliques humaines.** L’analyse des PSN dans des lysats de PNN isolés de sujets sains (Ct) et de patients SPL (P) par Western-Blot. La MPO est utilisée comme contrôle. D’après (Korkmaz et al., 2018a).

Malgré le faible niveau de la PR3 cellulaire, la quantité de la PR3 constitutive à la surface des PNN quiescents reste comparable à celle des PNN sains avec une distribution bimodale. La distribution bimodale de la PR3 membranaire est causée par l’expression à la régulation épigénétique restreinte à un sous-ensemble du récepteur à la PR3 des neutrophiles, le CD177. Celle-ci entraîne l’apparition de deux sous-ensembles, le $CD177^-$/PR3m(low) et $CD177^+$/PR3m(high) à la surface cellulaire. Suite à une activation par l’ionophore calcique des PNN de patients atteints du SPL, aucune augmentation significative de la PR3 membranaire n’a été observée contrairement aux PNN sains (Seren et al., 2018).

Les conséquences de l’inactivation génétique de la CatC sur les PSN des monocytes ont été étudiées l’équipe du Dr Ralph Kettritz (Nephrology and Intensive Care Medicine, Hôpital Universitaire de la Charité de Berlin). Les monocytes expriment moins de PSN que les neutrophiles. Dans une population de cellules enrichies en monocytes de patients SPL avec une pureté de 80 ± 5 %, une très forte réduction des PSN a été observée. La quantité de la PR3 à la surface des monocytes de patients est sévèrement réduite comparée à celle de sujets sains. (Jerke et al., 2022).

Dans les lymphocytes de patients SPL une réduction modérée en activité protéolytique de la GzmA et la GzmB a été observée (Pham et al., 2004) suggérant ainsi une voie de maturation indépendante de la CatC (**Figure 35**).

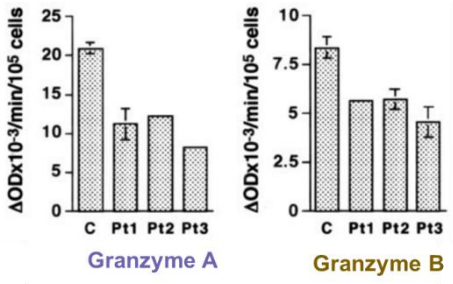


**Figure 35 : Conséquences de l'inactivation génétique de la cathepsine C sur l'activation des granzymes.** L'analyse de l'activité protéolytique de la GzmA et de la GzmB dans des lysats de lymphocytes de sujets sains (C) et de patients SPL (Pt) en utilisant des substrats synthétiques chromogéniques. D'après (Pham et al., 2004).

Un défaut génétique de la CatC tel qu'observé dans le SPL n'empêche pas complètement l'activation des proPSN, et des proGzmsA/B. Les neutrophiles issus de patients atteints du SPL ne présentent pas un défaut dans leur activités antimicrobiennes, ce qui suggère que ces protéases ne représentent pas le principal mécanisme utilisé par les neutrophiles humains pour tuer les bactéries (Sorensen et al., 2014). Les granzymes constituent 90% des granules cytolytiques intracellulaires des lymphocytes T cytotoxiques et des cellules NK, avec des rôles essentiels dans la lutte contre les tumeurs et l'élimination des cellules infectées. La voie d'activation alternative indépendante de la CatC fournit une explication moléculaire à l'absence d'un phénotype d'immunodéficience généralisée des cellules T chez les patients atteints de PLS (Pham et al., 2004) (**Figure 36**).

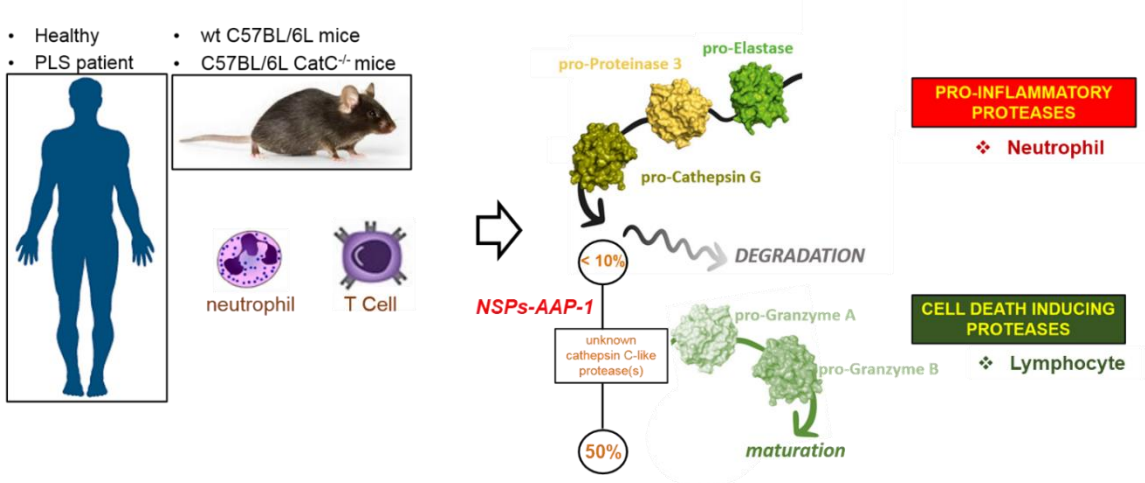


**Figure 36 : Conséquences de l'inactivation génétique chez l'homme ou d'une déplétion chez la souris de la cathepsine C sur l'activation de ses protéases à serine cibles.** Les valeurs sont issues des neutrophiles et des lymphocytes issus de patients SPL.

# 3. Les protéases à sérine maturée par la cathepsine C

## 2.1 Les protéases à sérine du neutrophile

La NE a été identifiée en 1968 par Janoff et Scherer comme une enzyme capable de cliver l'élastine (Janoff and Scherer, 1968). La CatG a été décrite par Starkey et Barrett en 1976 comme une enzyme capable de cliver des substrats synthétiques de la chymotrypsine (Starkey and Barrett, 1976). La PR3 a été identifiée par différents groupes de recherche sous différents noms. La « myéloblastine » est identifiée puis elle a été décrite comme une protéase à serine présente dans les cellules leucémiques promyélocytaires HL-60 (Bories et al., 1989). Mais il a été démontré que la « myéloblastine » est identique à une protéase nommée la PR3 qui avait été étudiée pour son rôle dans l'emphysème (Baggiolini et al., 1978). La NSP4 a été découverte par l'équipe de recherche du Dr Dieter Jenne en 2012 (Perera et al., 2012).

### 3.1.1 La biosynthèse des protéases à sérine du neutrophile

Les PSN sont 4 protéases ayant évolué à partir d'un ancêtre commun par duplication de gènes. Elles sont synthétisées sous forme de pré-pro-protéinase inactive contenant un peptide signal et un prodipeptide en N-terminal (Garwicz et al., 1997). De plus, ces zymogènes contiennent un propeptide en C-terminal dont l'élimination n'est pas nécessaire pour l'activité des protéases. L'activation des PSN est réalisée par la CatC qui clive et élimine le dipropeptide N-terminal des zymogènes. Le propeptide C-terminal des PSN est clivé par une ou plusieurs protéases encore inconnues, bien que cela ne semble pas être nécessaire à l'activité protéolytique (**Figure 37**) (Capizzi et al., 2003; Gullberg et al., 1995).

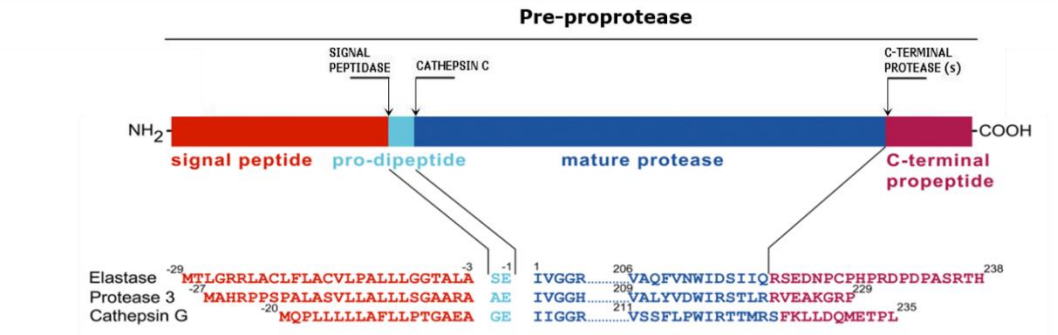


**Figure 37 : Activation des protéases à serine du neutrophile.** Les PSN sont synthétisées sous forme de pré-proprotéases constituées d'un peptide signal, d'un propeptide, de la protéase mature et d'un propeptide en position C-term. Pendant la maturation, le propeptide en N-term est enlevé par le clivage protéolytique de la CatC, la ou les protéase(s) impliquée(s) dans le clivage du propeptide en C-term reste(nt) encore inconnue(s). D'après (Korkmaz et al., 2008).

### 3.2.2 Les caractéristiques structurales des protéases à sérine du neutrophile

Des études de radiocristallographies ont permis d'établir les structures tridimensionnelles des PSN. Ces protéases sont constituées de deux domaines à feuillet β et d'une hélice α C-terminal (Bode et al., 1986; Fujinaga et al., 1996; Hof et al., 1996). La triade catalytique des PSN est située à la jonction des deux tonneaux β et la fente du site actif est perpendiculaire à cette jonction (**Figure 38**). Les PSN sont des protéases hautement cationiques à cause de leurs nombreux résidus chargés positivement dans leur domaine d'activation (Korkmaz et al., 2007). Les PSN sont stabilisées par 3 ou 4 ponts disulfures. Ces protéases existent sous différents isoformes selon leur niveau de glycosylation.

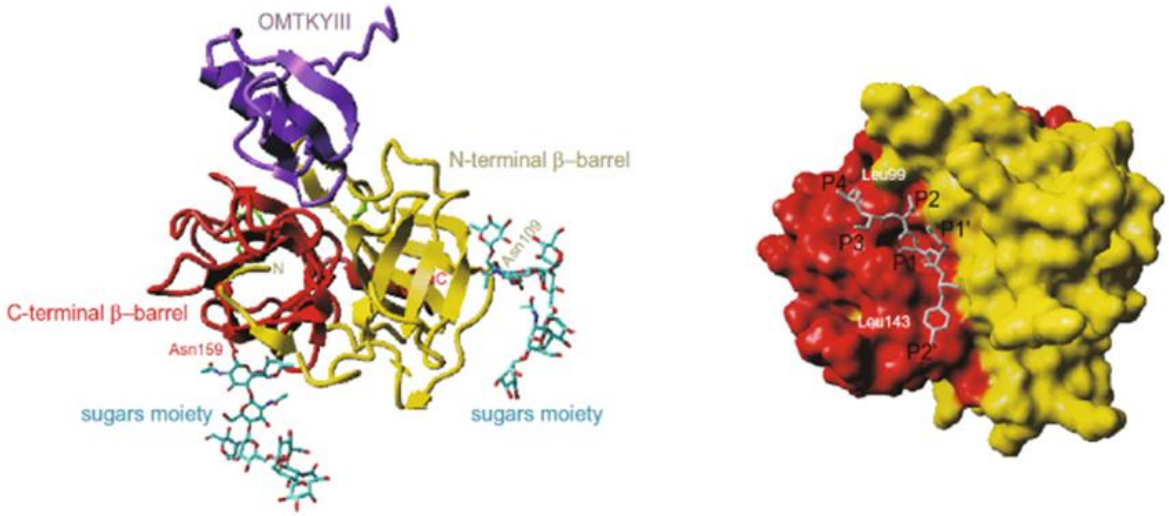


**Figure 38 : Structure tridimensionnelle de l'élastase complexée à l'inhibiteur OMTKYIII.** **(A)** Représentation en ruban de l'élastase complexée à l'inhibiteur réversible OMTKYIII (en violet). Le domaine N-terminal est le domaine C-terminal de l'élastase sont représentés respectivement en jaune et en rouge (PDB ID 1PPF). Les glycosylations sont colorées en turquoises. **(B)** Représentation de la surface de l'élastase avec le même code couleur que précédemment. La bouche inhibitrice de l'inhibiteur OMTKYIII (en gris) dans le complexe avec l'élastase. D'après (Korkmaz and Gauthier, 2013).

### 3.1.3 Les inhibiteurs physiologiques des protéases à sérine du neutrophile

L'activité protéolytique des PSN est régulée en conditions physiologiques par des inhibiteurs naturels présents sur le site inflammatoire. Parmi eux, on retrouve les serpines, inhibiteurs de protéases à serine (alpha-1 antitrypsine, alpha-1 antichymotrypsine) qui représentent environ 10% des protéines sanguines (**Figure 39**), l'alpha-2-macroglobuline, l'élafine et le SLPI (*secretory leukocyte protease inhibitor*) (Korkmaz et al., 2010).

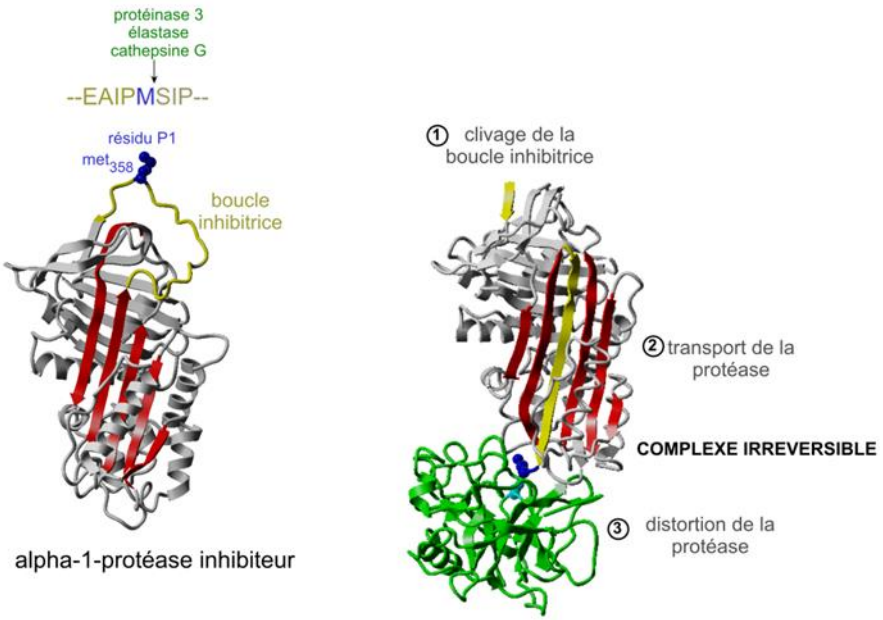


**Figure 39 : Structure et mécanisme d'action des serpines illustrés par l'alpha-1 antitrypsin (AAT).** Représentation en ruban de l'AAT avec sa boucle inhibitrice en jaune. Lors de l'interaction avec les PSN, la boucle inhibitrice de l'AAT est clivée au niveau de la liaison méthionine-sérine. Suite au clivage, la PSN est transportée à l'autre pôle de l'AAT. Le changement de conformation subit par la protéase empêche la déacylation ce qui permet la formation d'une liaison covalente entre l'inhibiteur et la protéase. Les structures ont été générées à partir du PDB ID 1EZX en utilisant le logiciel Yasara. D'après (Dementiev et al., 2006).

### 3.1.4 Les fonctions physiologiques des protéases à sérine du neutrophile

Les PSN jouent un rôle important dans plusieurs processus physiopathologiques tels que la défense antimicrobienne, la régulation de l'activité des cytokines, l'activation cellulaire et le remodelage tissulaire pendant la cicatrisation. Ce sont donc des enzymes multifonctionnelles qui agissent autant dans la destruction des agents pathogènes que dans la régulation du processus inflammatoire (Pham, 2006). Les PSN ont également un rôle dans la chimiotaxie et la migration par le clivage des molécules d'adhésion lors de la diapédèse des PNN (Hermant et al., 2003). Toutefois, le rôle des PSN dans la chimiotaxie reste à confirmer car certaines études le confirment alors que d'autres, où des inhibiteurs de PSN sont utilisés, ne montrent aucun changement dans la migration des PNN (Adkison et al., 2002b; Young et al., 2007).

### 3.1.5 Les fonctions pathologiques des protéases à sérine du neutrophile

De façon générale, l'inflammation est définie comme la réponse de l'organisme aux blessures ou infections. Cependant, l'altération de l'homéostasie cellulaire peut être à l'origine de la sécrétion de signaux déclenchant la réponse inflammatoire (Meizlish et al., 2021). Dans la plupart des cas, l'initiation et la propagation des pathologies chroniques inflammatoires pulmonaires résultent d'une réponse inflammatoire excessive et non contrôlée. Les mécanismes moléculaires et cellulaires au cours des processus inflammatoires ou infectieux contribuent à la chronicité des maladies pulmonaires et peuvent conduire à une insuffisance respiratoire. Dans ce contexte, la BPCO, le déficit en alpha-1 antitrypsine, la bronchiectasie et la mucoviscidose représentent des pathologies typiques d'une dérégulation inflammatoire au niveau pulmonaire (Barnes and Stockley, 2005). Parmi les acteurs responsables de cette « sur-inflammation », le PNN, en dépit de son activité antimicrobienne, semble jouer un rôle central. Le PNN permet la destruction des agents pathogènes par phagocytose quand ceux-ci sont présents dans l'environnement pulmonaire. Mais l'activité excessive des PSN, qu'il libère dans le milieu extracellulaire après son activation, peut conduire à la dégradation protéolytique du tissu pulmonaire (**Figure 40**) et doit donc être maintenue sous contrôle. Les traitements standards actuellement utilisés n'ont aucun effet sur l'inflammation neutrophilique. Par conséquent, de nouveaux traitements anti-inflammatoires sont nécessaires pour améliorer les résultats cliniques.

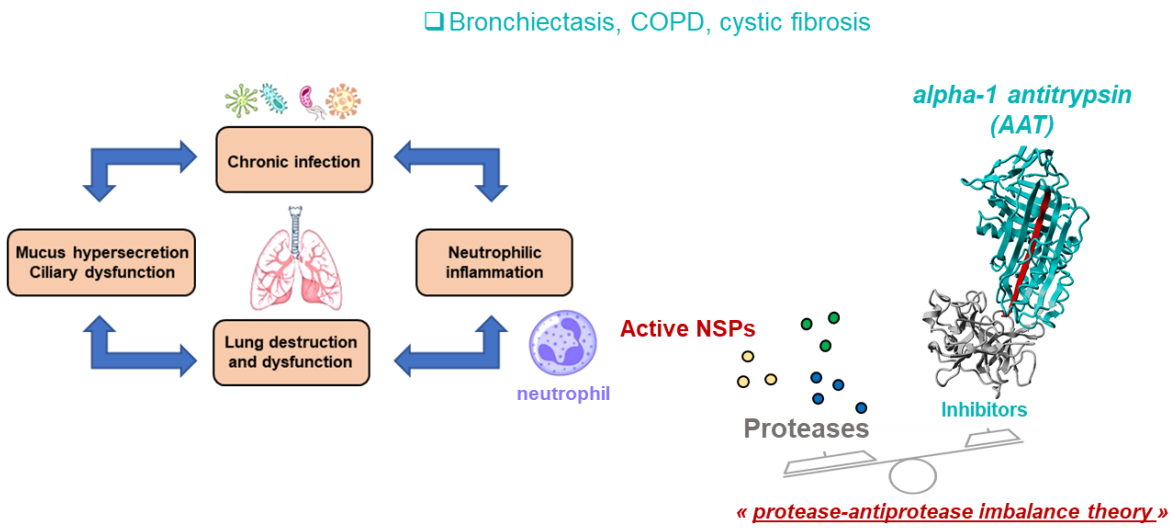


**Figure 40 : Cercle vicieux de l'infection et de l'inflammation dans les pathologies inflammatoires pulmonaires chroniques.** Le déséquilibre de la balance protéase anti-protéase est impliqué dans les maladies inflammatoires pulmonaires chroniques.

Les PSN sont également les acteurs déterminants d'une pathologie auto-immune systémique d'étiologie inconnue, la granulomatose avec polyangéite (GPA) caractérisée par une inflammation de la paroi de certains vaisseaux de petit calibre et une granulomatose. La GPA est après la mucoviscidose une des maladies rares les plus fréquemment rencontrées (1 cas pour 20.000 personnes). Maladie inflammatoire jusqu'à présent incurable, elle affecte principalement le poumon et les reins, nécessitant un traitement de fond à visée immunosuppressive dont les effets secondaires compromettent durablement l'état du malade. Les neutrophiles qui expriment à leur surface l'auto-antigène (la protéase PR3) contre lequel sont dirigés les auto-anticorps (ANCA, Anti-Neutrophil Cytoplasmic Antibodies) responsables du déclenchement du processus inflammatoire, sont des acteurs clés de la pathogénicité dans la GPA (Jenne et al., 1990). L'interaction des ANCAs avec l'auto-antigène membranaire conduit à l'activation des neutrophiles et à la libération de médiateurs pro-inflammatoires (protéases, oxydants…) à l'origine des lésions vasculaires (Falk et al., 1990) (**Figure 41**). L'introduction de la thérapie cytotoxique a changé le pronostic de la GPA qui est devenu une pathologie chronique. Les taux de mortalité restent cependant élevés autour de 13% à un an et de 45% à 10 ans. Il est donc essentiel de mettre au point des thérapies ciblées alternatives pour améliorer le pronostic et diminuer les complications iatrogènes.

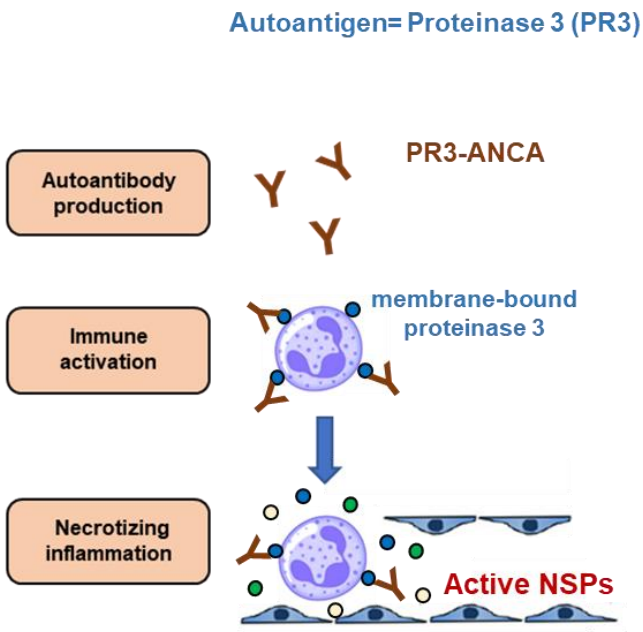


**Figure 41 : Physiopathologie de la granulomatose avec polyangéite**

## 3.2 Les granzymes

Les granzymes (Gzms) constituent une famille de protéases à sérine cytotoxiques présentes dans les lymphocytes T cytotoxiques et les cellules tueuses naturelles (NK).

### 3.2.1 La biosynthèse des granzymes

Les GzmA, B, H, K et M sont les cinq Gzms présentes chez l'Homme alors que les souris en ont 10. Les GzmA et GzmB sont les granzymes les plus étudiées. Les Gzms peuvent être divisées en trois sous-classes selon la localisation chromosomique de leur gène. Le locus Gzm A des Gzms regroupe les GzmA et K et est situé sur le chromosome 13 chez la souris et le chromosome 5 chez l'homme. Le locus Gzm B des Gzms qui regroupe la Gzm B et un nombre variable de Gzm apparentés, est localisé sur le chromosome 14 chez la souris et chez l'Homme. Le locus M, spécifique à la Gzm M, est situé sur le chromosome 10 chez la souris et 19 chez l'Homme (Hay and Slansky, 2022) (**Tableau 6**).

**Tableau 6 : Localisation chromosomique des gènes des granzymes chez la souris et chez l'Homme.** D'après (Hay and Slansky, 2022).

| | ***Chromosome murin*** | ***Chromosome humain*** |
|---|---|---|
| ***Gzm K*** | **13 c** | **5** |
| ***Gzm A*** | **13 c** | **5** |
| ***Gzm B*** | **14c** | **14c** |
| ***Gzm H*** | **-** | **14c** |
| ***Gzm C*** | **14c** | **-** |
| ***Gzm F*** | **14c** | **-** |
| ***Gzm N*** | **14c** | **-** |
| ***Gzm G*** | **14c** | **-** |
| ***Gzm D*** | **14c** | **-** |
| ***Gzm E*** | **14c** | **-** |
| ***Gzm M*** | **10c** | **19c** |

### 3.2.2 Les caractéristiques structurales des granzymes

Toutes les Gzms sont produites sous forme de zymogènes inactifs, comme les PSN, et nécessitent l'élimination d'un dipropeptide N-terminal pour devenir complètement actives et stockées dans les granules cytotoxiques. Les Gzms ont une structure similaire aux PSN, mais possèdent également plusieurs caractéristiques déterminantes. Les résidus aux positions 1 à 4 (généralement Ile-Ile-Gly-Gly) et 9 à 16 sont hautement conservés dans toutes les granzymes

chez l'Homme et chez les rongeurs. Leur séquence propeptidique généralement Gly-Glu ou Glu-Glu est clivée par la CatC. Ils ont généralement trois ponts disulfures conservés, bien que la Gzms A en ait quatre. La Gzm A est la seule Gzm dimérique, en raison d'un pont disulfure intermoléculaire (Hink-Schauer et al., 2003) (**Figure 42**). La Gzm A et la GzmB clivent leurs substrats, respectivement, après les résidus basiques et après les résidus acides, principalement l'aspartate.

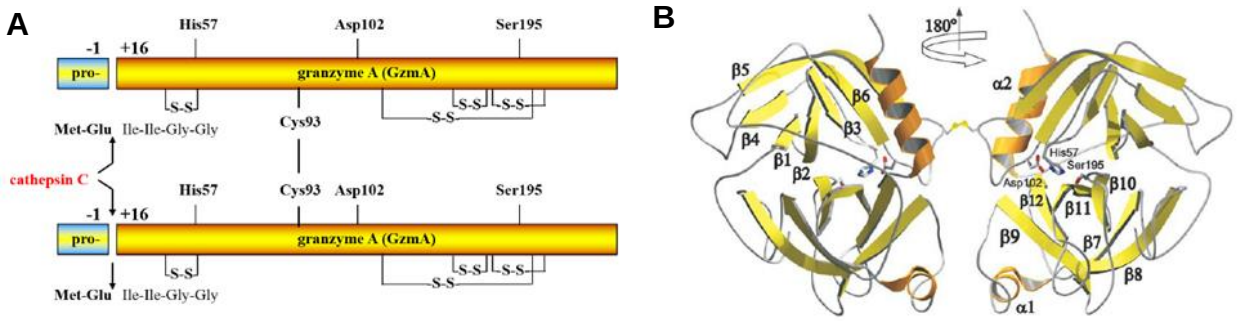


**Figure 42 : Structure de la granzyme A. A**) Représentation du dimère de la granzyme A, relié par un pont disulfure entre les Cys93. **B**) Représentation en ruban de la granzyme A dimérique. Le site actif du monomère de droite est à l'horizontale de la surface moléculaire. Une rotation symétrique permet de visualiser le dos du dimère de gauche. Les structures secondaires en feuillet-β et en hélice-α sont colorés respectivement en jaune et orange. D'après (Hink-Schauer et al., 2003).

### 3.2.2 Les fonctions physiologiques des granzymes

Lorsque les lymphocytes sont activés, un mécanisme d'exocytose des granules cytotoxiques permet aux Gzms d'atteindre la cellule à détruire. Elles pénètrent le cytoplasme grâce à l'action des perforines et induisent ainsi leur action pro-apoptotique. Les Gzms, une fois internalisées dans le cytoplasme de la cellule cible, clivent différents substrats cytoplasmiques, mitochondriaux ou nucléaires pour déclencher les voies apoptotiques. Une fois libérée dans le cytoplasme, la Gzm B va cliver un grand nombre de substrats comme les caspases 3 et 7 ou le DFF45 (*DNA fragmentation factor 45 kDa subunit*) aussi appelé ICAD (Caspase-activated DNase inhibitor), activant ainsi des voies de mort caspases-dépendantes et caspases-indépendantes. La Gzm A ne peut activer que des voies de mort caspases-indépendantes (Martinvalet et al., 2005) (**Figure 43**).

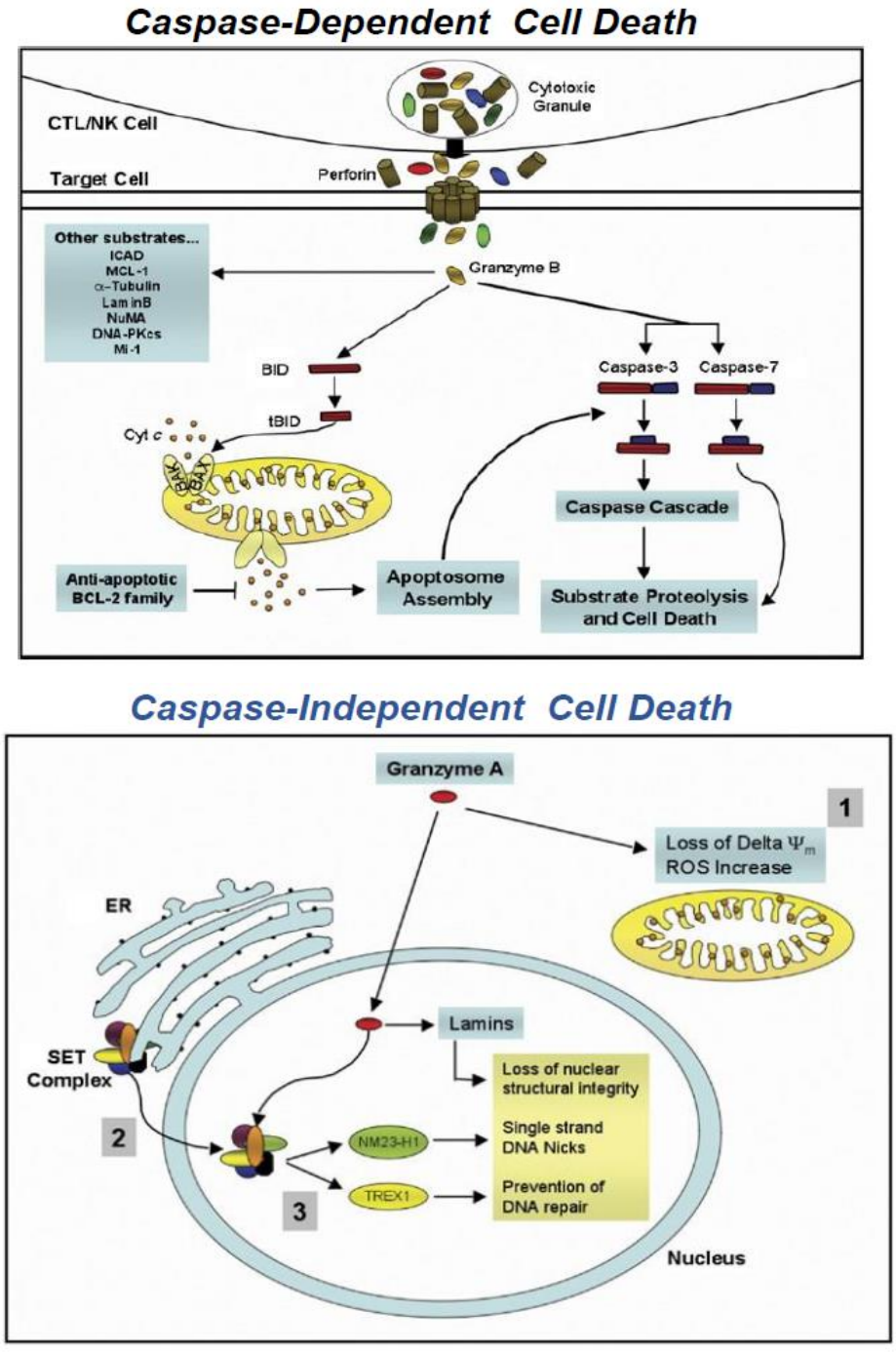


**Figure 43 : Voies de mort cellulaires activées par les granzymes A et B.** D'après (Martinvalet et al., 2005).

## 4. Ciblages pharmacologiques de la cathepsine C

La CatC attire une attention croisée des académiciens et des industriels dû à son rôle dans l'activation des PSN. Plusieurs laboratoires pharmaceutiques (Insmed, Boehringer Ingelheim, Neuprozyme, GlaskoSmithKline) sont actuellement très actifs dans le développement d'inhibiteurs de CatC pour la thérapie des pathologies chroniques inflammatoires pulmonaires dont les soins représentent un marché mondial de plus de 100 milliards d'euros (**Figure 44**).

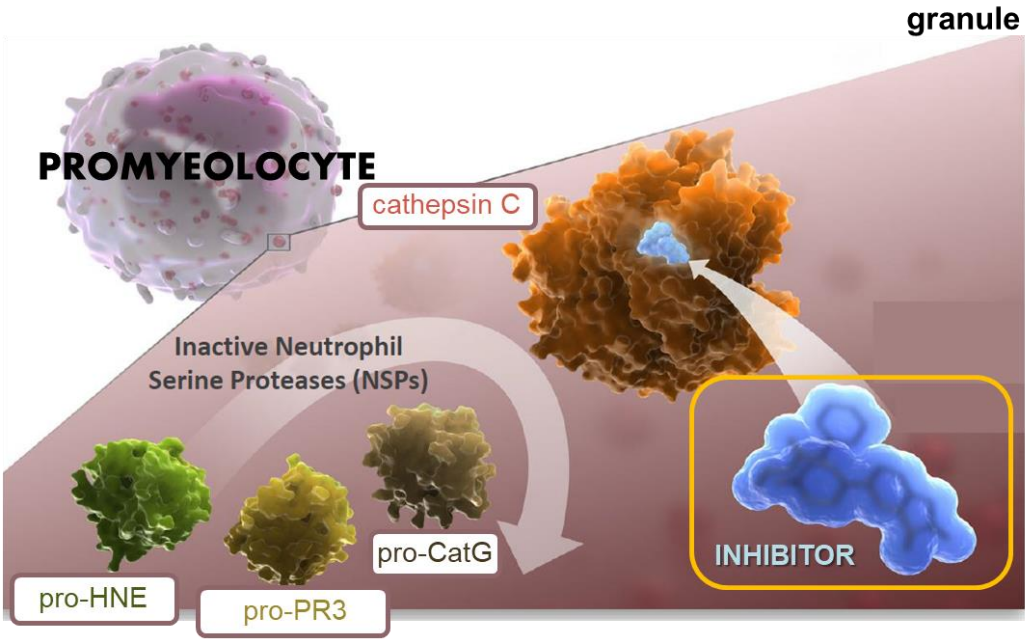


**Figure 44 : Illustration du ciblage pharmacologique des protéases à serine du neutrophile par l'inhibition de cathepsine C dans le promyélocyte à l'aide des inhibiteurs chimiques.**

### 4.1 IcatC$_{XPZ-01}$

**L'IcatC$_{XPZ-01}$** est un inhibiteur réversible de type nitrile puissant et très sélectif de la CatC ($IC_{50}$ : 15 nM). Cet inhibiteur, pénétrant les cellules *in vitro* ne montre pas de toxicité vis-à-vis des cellules en culture (Guarino et al., 2017). L'incubation des cellules $CD34^+$ humaines avec l'**IcatC$_{XPZ-01}$** au cours de la différenciation neutrophilique a résulté en une très forte réduction de la PR3 membranaire, soluble et de son activité protéolytique, sans que cela n'affecte la différenciation des neutrophiles (Seren et al., 2018). Cette étude a suggéré l'inhibition de la NSPs-AAP par l'**IcatC$_{XPZ-01}$**. L'élimination presque complète des proformes de la NE et de la CatG, en présence de l'**IcatC$_{XPZ-01}$** a été également été observé dans les neutrophiles différenciés à partir des promyélocytes de moelle osseuse humaine de donneurs sains ou des cellules $CD34^+$ cultivés en présence de l'**IcatC$_{XPZ-01}$** (Guarino et al., 2017; Seren et al., 2018).

La sécrétion par la voie constitutive de la proforme de la NE depuis l'appareil de Golgi dans le milieu extracellulaire n'est pas compromise, ce qui indique une protéolyse des zymogènes dans les granules intracellulaires (Guarino et al., 2017). Ces résultats ont clairement démontré que la disparition des proformes des PSN n'est pas une conséquence unique de l'inactivation génétique de CatC observés chez les patients atteints de SPL.

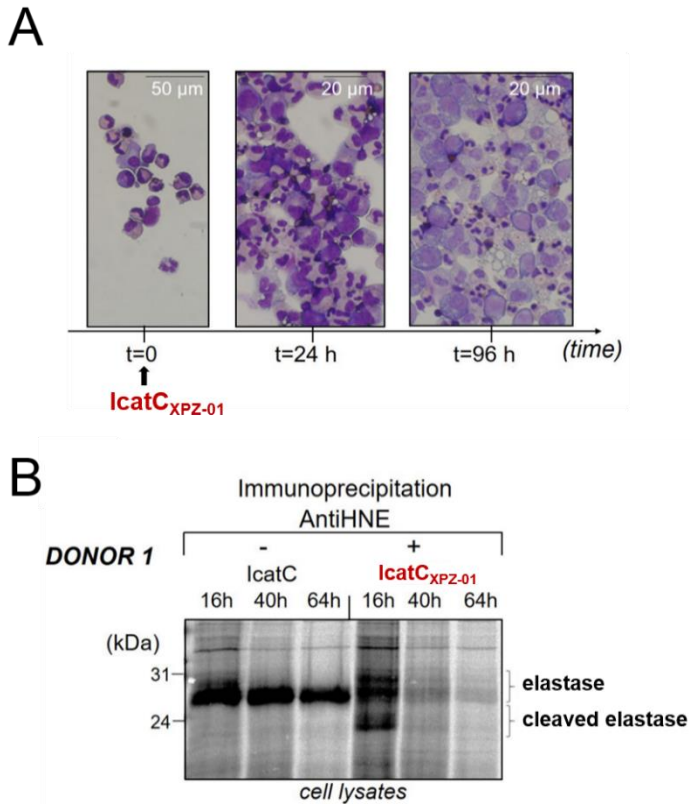


**Figure 45 : Elimination de l'élastase dans les neutrophiles en culture traités avec l'IcatC$_{XPZ-01}$. (A)** Les promyélocytes humains purifiés à partir de la moelle osseuse de donneur sain ont été différenciés en présence de l'**IcatC$_{XPZ-01}$**. Aucune toxicité n'a été détectée à 96h. **(B)** L'élimination protéolytique de l'élastase neutrophilique humaine (hNE) induite par l'**IcatC$_{XPZ-01}$** pendant la différentiation des promyélocytes en PNN. D'après (Guarino et al., 2017).

Des études pharmacocinétiques et pharmacodynamiques chez la souris ont révélé que l'**IcatC$_{XPZ-01}$** s'est accumulé dans la moelle osseuse, atteignant des niveaux appropriés pour l'inhibition de la CatC et par conséquent celle des PSN. L'administration sous-cutanée de l'**IcatC$_{XPZ-01}$** à un modèle murin de polyarthrite rhumatoïde induite au collagène, a entraîné une activité antiarthritique statistiquement significative (Korkmaz et al., 2019). L'inhibition prolongée de la CatC chez le macaque par l'administration de l'**IcatC$_{XPZ-01}$** pendant 12 jours a conduit à l'élimination presque totale des PSN dans les cellules sanguines (**Figure 46**) (Guarino et al., 2017).

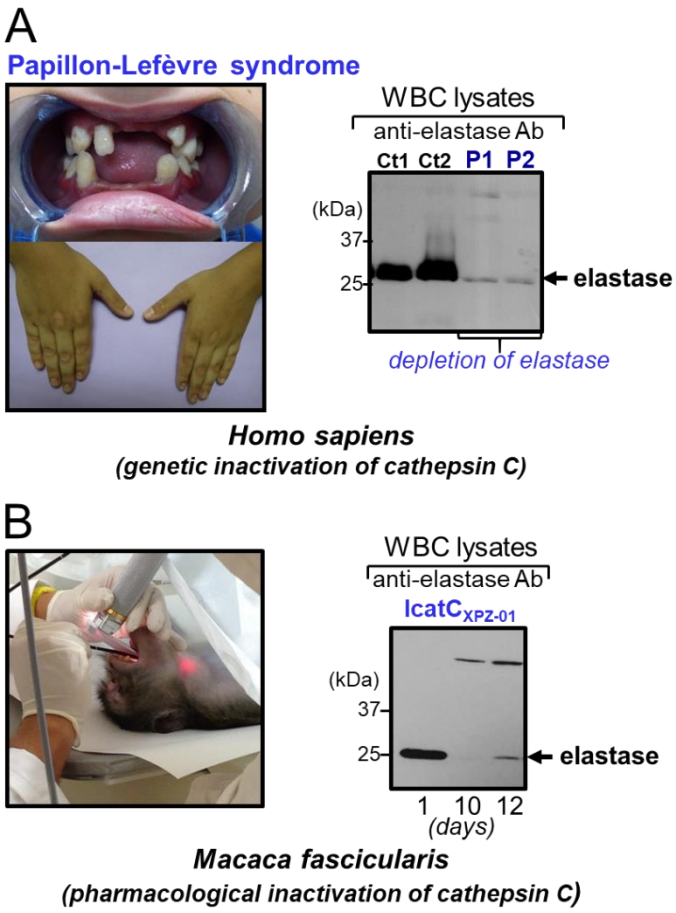


**Figure 46 : Conséquences de l'inactivation génétique ou pharmacologique de cathepsine C. (A)** La déficience génétique en CatC chez l'Homme. Les caractéristiques dentaires et dermatologiques du SPL. L'analyse de l'élastase dans les lysats de globules blancs (WBC) isolés de témoins sains (Ct) et deux patients SPL (P) a été réalisée par western-blot à l'aide d'un anticorps anti-élastase. Les cellules des patients SPL sont déplétées en zymogènes de l'élastase, car dégradés lors de la différenciation des neutrophiles dans la moelle osseuse. **(B)** L'inhibition prolongée de la CatC dans un modèle expérimental d'inflammation pulmonaire aiguë chez le macaque par l'administration de l'**IcatC$_{XPZ-01}$** pendant 12 jours a conduit à l'élimination presque totale de l'élastase dans les lysats de globules blancs. L'image montre un lavage broncho-alvéolaire d'un macaque anesthésié. L'inhibition de la CatC a entraîné l'élimination des zymogènes de l'élastase, comme observé chez les patients SPL. L'analyse de l'élastase dans les lysats des leucocytes a été réalisée comme précédemment. D'après (Korkmaz et al., 2020a).

### 4.2 BI-9740 et BI-1291583

**BI-9740** est un inhibiteur réversible de type nitrile très puissant de la CatC ($IC_{50}$ : 1,8 nM). Cet inhibiteur, pénétrant les cellules *in vitro* ne montre pas de toxicité vis-à-vis des cellules en culture (Jerke et al., 2022). L'incubation des cellules $CD34^+$ humaines avec **BI-9740** au cours de la différenciation neutrophilique a entraîné une très forte réduction des NSPs et de leurs activités protéolytiques, sans que cela affecte la différenciation des neutrophiles. La réduction de la PR3 membranaire atténuait significativement l'activation des neutrophiles en présence

des PR3-ANCA (Jerke et al., 2022). Des études pharmacocinétiques et pharmacodynamiques chez la souris ont révélé que **BI-9740** s'accumule dans la moelle osseuse, atteignant des niveaux appropriés pour l'inhibition de la CatC et donc de celle des PSN (Jerke et al., unpublished).

**BI-1291583** est également un inhibiteur réversible très puissant de la CatC ($IC_{50}$ : 0.9 nM) dont la structure chimique n'est pas encore rendue publique par le laboratoire pharmaceutique. L'incubation des cellules U937 avec **BI-1291583** a pour conséquence une très forte réduction des activités protéolytiques des NSPs. Des études pharmacocinétiques et pharmacodynamiques dans un modèle murin d'infection pulmonaire au lipopolysaccharide ont révélé que **BI-1291583** s'est accumulé dans la moelle osseuse, atteignant des niveaux appropriés pour l'inhibition de la CatC et par conséquence celle des PSN dans les neutrophiles (Kreideweiss et al., 2023). **BI-1291583** est actuellement évalué phase 2 chez les patients atteints de la bronchectasie (Chalmers et al., 2023).

### 4.3 Brensocatib

**Brensocatib** (AZD7986/INS1007) est un inhibiteur réversible de type nitrile de la CatC. L'élimination presque complète des proformes des PSN en présence de **brensocatib** a été observée dans les neutrophiles différenciés à partir des cellules $CD34^+$ de moelle osseuse humaine de donneurs sains cultivés en présence de l'inhibiteur.

Des études pharmacocinétiques/pharmacodynamiques chez la souris et chez le rat ont révélé que **brensocatib** s'accumule dans la moelle osseuse, atteignant des niveaux appropriés pour l'inhibition de la CatC et par conséquent celle des PSN (Basso et al., 2023). Cependant, les souris ont présenté une plus grande réduction des activités PSN que les rats. **Brensocatib** a atténué la néphrite lupique accélérée par l'interféron-α dans un modèle murin (Chen et al., 2023). L'administration de **brensocatib** à des modèles de rongeurs de polyarthrite rhumatoïde a entraîné une activité antiarthritique statistiquement significative (McDonald et al., 2023). Le ciblage de la CatC avec **brensocatib** a supprimé efficacement les métastases pulmonaires du cancer du sein dans un modèle murin (Xiao et al., 2021). De plus, la combinaison de **brensocatib** et de l'anticorps anti-PD-L1 a bloqué les métastases du cancer colorectal chez la souris (Dang et al., 2023).

**Brensocatib** est actuellement évaluée dans de multiples maladies pulmonaires (https://insmed.com/, e.g. bronchectasie, mucoviscidose, rhino-sinusite chronique). Les résultats positifs de l'étude clinique de phase 2 chez les patients atteints de la bronchectasie ont été récemment publiés (Chalmers et al., 2020; Cipolla et al., 2023). L'administration de 25 mg

de **brensocatib** a réduit de ~65% les activités des PSN dans les neutrophiles circulants et de ~90% dans les expectorations pulmonaires. Les résultats ont montré une réduction des pourcentages d'exacerbation avec un allongement du temps entre deux épisodes. **Brensocatib** est actuellement évalué en Phase 3 chez les patients atteints de la bronchectasie. Dans le contexte de la pandémie de COVID-19 (Seren et al., 2021), **brensocatib** a été évalué en Phase 3 chez les patients atteints de la COVID-19 (Keir et al., 2022; Korkmaz et al., 2020b) mais une efficacité clinique n'a pas été observée (Keir et al., 2022).

### 4.4 HSK31858

**HSK31858 (composé 54)**, découvert en Chine, est un « inhibiteur non peptidylique » réversible de la CatC humaine ($IC_{50}$ : 57.4 nM) (Chen et al., 2021). Chez la souris et chez le rat il a été révélé que **HSK31858** s'était accumulé dans la moelle osseuse, atteignant des niveaux appropriés pour l'inhibition de la CatC et par conséquent celle des PSN. Ce composé a montré une activité anti-inflammatoire efficace dans un modèle de la BPCO chez le rat (Chen et al., 2021). **HSK31858** est actuellement évalué en phase clinique 2 chez les patients atteints de la bronchectasie (https://classic.clinicaltrials.gov/ct2/show/NCT05023525).

### 4.5 GSK27936600

**GSK27936600** est un inhibiteur irréversible de la CatC ($IC_{50}$ : 1 nM). C'est le premier inhibiteur de la CatC évalué chez l'Homme. L'essai clinique de la Phase 1 a consisté en une administration orale pendant 21 jours de **GSK27936600.** L'administration de 12 mg de l'inhibiteur a réduit de 20-40% l'activité des PSN dans les PNN circulant alors que l'inhibition de la CatC était supérieure à 90% en moins de 3 heures après l'administration de l'inhibiteur (Miller et al., 2017). Le développement de l'inhibiteur est bloqué à cause d'une mauvaise accumulation dans la moelle osseuse.

### 4.6 Composé 22

Deux inhibiteurs connus du récepteur du facteur de croissance épidermique (EGFR) contenant des ogives acrylamides réactives ont été identifiés comme des inhibiteurs de la CatC (Hou et al., 2019). Le même groupe a rapporté que l'inhibiteur de l'EGFR WZ4002 inhibait la CatC avec un $IC_{50}$ de l'ordre du micromolaire. Une nouvelle série d'inhibiteurs développés sur

cet échafaudage a conduit à l'identification d'un inhibiteur très puissant et sélectif, N-(5-((6-((2-méthoxy-4-(4-méthylpipérazine-1-yl)phényl)amino)- 3-(pipéridin-1-yl) pyridin-2-yl)oxy)-2-méthylphényl)acrylamide (**composé 22**) ($IC_{50}$ : 17.3 nM). L'incubation des cellules U-937 ou THP-1 avec cet inhibiteur irréversible a résulté en une très forte réduction de l'activité de la CatC. Ce composé a montré une activité anti-inflammatoire efficace dans un modèle murin de pancréatite aigu (Hou et al., 2019).

# II. Travaux personnels

# Objectifs de la thèse

Les PSN étant des effecteurs majeurs de la dégradation tissulaire, leur ciblage par des inhibiteurs spécifiques ou polyvalents paraît une approche pertinente de thérapie ciblée. Cependant et en dépit de la simplicité apparente de cette stratégie, les efforts en ce sens ont été jusqu'à présent infructueux. Une solution alternative au ciblage *in situ* des protéases consiste à contrôler leur activité avant leur arrivée sur le site inflammatoire, leur mécanisme d'activation intervenant au cours des stades précoces de maturation des neutrophiles dans la moelle osseuse (Korkmaz et al., 2010). La CatC est une protéase à cystéine qui catalyse la maturation des PSN en libérant spécifiquement les prodipeptides de leurs proformes inactives au niveau de la moelle osseuse. Son inhibition devrait donc réduire drastiquement la quantité de PSN actives véhiculées par les neutrophiles sur les sites inflammatoires et limiter le recrutement délétère des neutrophiles, auto-entretenu par ces mêmes PSN qui participent à l'activation des cytokines/chimiokines pro-inflammatoires. La CatC représente ainsi une cible thérapeutique potentielle dans toutes les pathologies inflammatoires impliquant un recrutement de neutrophiles. L'inactivation pharmacologique de la CatC peut être obtenue soit en utilisant des inhibiteurs ciblant le site actif de la protéase mature (*inhibition directe*), soit en ciblant la ou les protéases de conversion de la proCatC (*inhibition indirecte*). Des inhibiteurs chimiques ciblant le site actif de la CatC (*inhibition direct*) sont actuellement évalués dans les essais précliniques et cliniques (Chalmers et al., 2023; Korkmaz et al., 2020a). L'inhibition d'environ 80% de la maturation de la proCatC (*inhibition indirecte*) dans les cellules leucémiques promyélocytaires HL-60 n'a pas résulté en une inhibition significative des PSN.

Une inactivation génétique de la CatC est observée chez les patients atteints du syndrome de Papillon-Lefèvre (SPL), maladie génétique héréditaire rare à transmission autosomique récessive. Cette pathologie se caractérise par une parodontite précoce et sévère sans que les patients ne souffrent d'infections récurrentes. Dans les neutrophiles sanguins des patients atteints de SPL, seules de faibles quantités de PSN actives sont détectées (<10 % par rapport aux individus sains) (Pham et al., 2004; Seren et al., 2018), ce qui suggère l'implication d'une protéase alternative à la CatC, que nous avons nommé la NSPsAAP-1 (*NSPs-Alternative Activating Protease-1)* impliquée dans l'activation des zymogènes de PSN. Les granzymes (Gzms) sont des protéases à sérine cytotoxiques présentes dans les lymphocytes cytotoxiques et impliquées dans l'élimination des cellules infectées par un virus ou cancéreuses. Les Gzms sont également activées par la CatC. Cependant, la caractérisation enzymatique des Gzms A et

B dans les lymphocytes cytotoxiques de patients atteints du SPL a révélé une voie d'activation indépendante de la CatC (Pham et al., 2004) (**Figure 47**).

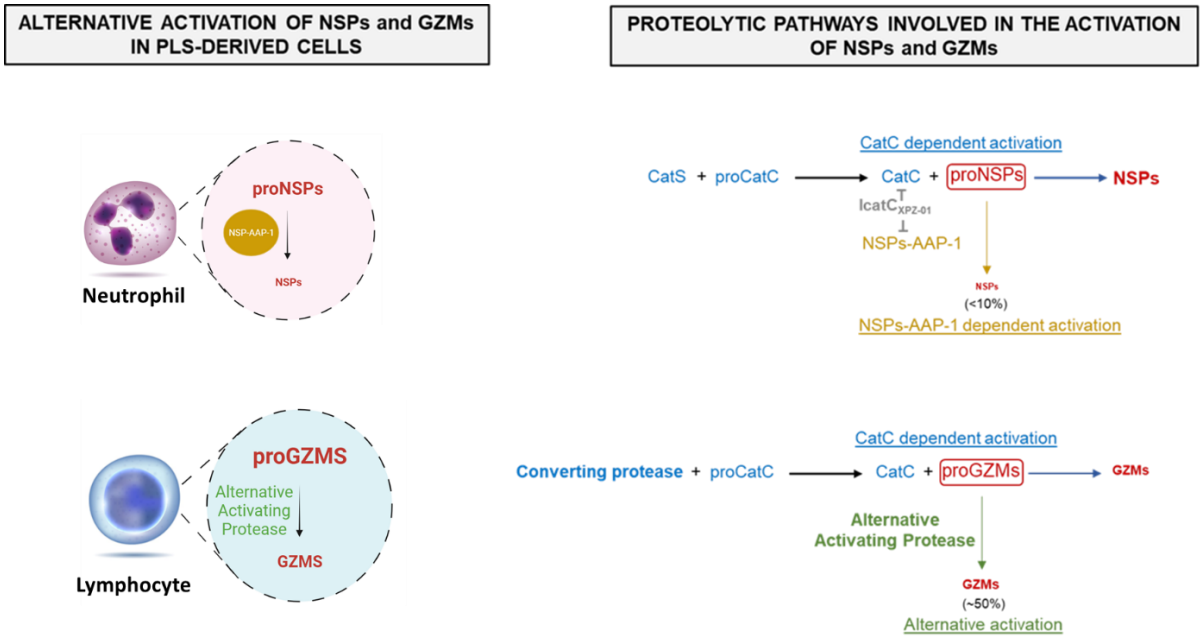


**Figure 47 : Illustration des cascades protéolytiques impliquées dans l'activation des protéases à serine du neutrophile et des granzymes dans des cellules saines ou issues de patients déficitaires en cathepsine C.**

L'identification des processus protéolytiques impliqués dans l'activation des PSN permettrait un meilleur contrôle de ces protéases pro-inflammatoires dans les maladies inflammatoires ou auto-immunes. Un inhibiteur chimique inhibant la CatC, mais également la protéase alternative NSPs-AAP-1 permettrait d'inactiver et d'éliminer totalement les PSN. Une co-inhibition pharmacologique de la CatC et de la NSPs-AAP-1 permettrait d'éliminer la PR3 membranaire, l'auto-antigène majeur des vascularites à PR3-ANCA (Seren et al., 2018). De plus, la connaissance de la nature de la protéase alternative impliquée dans l'activation des Gzms permettrait de concevoir et d'utiliser des inhibiteurs thérapeutiques ciblant seulement la CatC et la NSPs-AAP sans qu'il y ait une altération de l'activité cytotoxique des lymphocytes cytotoxiques liée à une inhibition des Gzms.

**L'objectif principal de cette thèse était d'étudier les processus protéolytiques non-dépendants de la CatC impliqués dans l'activation des PSN et des Gzms.** La NSPs-AAP-1 pourrait être la protéase alternative des lymphocytes cytotoxiques impliquée dans l'activation des Gzms. Pour répondre à cette question scientifique, l'hypothèse de travail était que

l'inactivation pharmacologique de la (des) protéase(s) de conversion impliquée dans la maturation de la proCatC permettrait de bloquer la voie d'activation CatC dépendante des PSN et des Gzms permettant ainsi la caractérisation des voies d'activation CatC indépendante impliquant la ou les protéase(s) alternatives(s).

Les 2 taches principales du sujet de thèse consistaient à :

- Identifier la protéase(s) de conversion de type CatL-Like impliquée dans la maturation de la proCatC dans les neutrophiles, dans les monocytes/macrophages et dans les lymphocytes
- Etudier les conséquences de l'inhibition pharmacologique de la maturation de la CatC sur l'activation des PSN et Gzms afin de connaître la nature de la (des) protéase(s) alternative(s).

# Manuscrit 1

## Pharmacological inhibition of cathepsin S and of NSPs-AAP-1 (a novel, alternative protease driving the activation of neutrophil serine proteases)

Roxane Domain*, Seda Seren*, Uwe Jerke, Manousos Makridakis, Kuan-Ju Chen, Jérôme Zoidakis, Moez Rhimi, Xian Zhang, Tillia Bonvent, Cécile Croix, Loïc Gonzalez, Dedong Li, Jessica Basso, Christophe Paget, Marie-Claude Viaud-Massuard, Gilles Lalmanach, Guo-Ping Shi, Ali Aghdassi, Antonia Vlahou, Patrick P. McDonald, Isabelle Couillin, Rich Williams k, Ralph Kettritz, Brice Korkmaz

**Introduction** : Les protéases à sérine du neutrophile (PSN) (l'élastase neutrophilique (NE), la protéinase 3 (PR3), la cathépsine G (CatG)) sont impliquées dans les pathologies inflammatoires à composante neutrophilique tels que la bronchopneumopathie chronique obstructive pulmonaire (BPCO), le déficit en alpha-1 antitrypsine, la mucoviscidose et la bronchiectasie dans le cadre des pathologies chroniques inflammatoires pulmonaires. Dans ces pathologies, les neutrophiles accumulés dans le tissu pulmonaire relarguent des PSN, entrainant une activité protéolytique non contrôlée qui à terme conduit à la destruction du tissu pulmonaire. Les PSN sont synthétisées sous forme de pro-protéases inactives et sont activées par la cathepsine (CatC) dans les précurseurs neutrophiliques au niveau de la moelle osseuse. Ainsi, la CatC est une cible pharmacologique pour l'inhibition des PSN, comportant l'avantage d'inhiber les trois PSN en ne ciblant qu'une seule protéase. L'inhibition de la CatC comme cible thérapeutique contre les pathologies respiratoires neutrophiliques est actuellement en cours d'essais cliniques. La CatC fait partie des cathepsines à cystéine ayant l'incapacité de s'auto-maturer, car celle-ci possède une activité exopeptidasique, et non endopeptidasique. Récemment, au laboratoire d'accueil, il a été montré que la CatC pouvait être maturée *in vitro* par les 5 protéases CatL-Like (Cathepsines S, L, V, F et K). Les patients atteints du syndrome de Papillon-Lefèvre, une déficience génétique en CatC, ont des taux de PSN actives très faibles dans leurs neutrophiles (PR3 et NE <10% ; CatG <1%), ce qui nous indique l'existence d'une protéase alternative impliquée dans l'activation des PSN que nous avons appelé la NSPs-AAP-1 (*NSPs Activating Alternative Protéase 1*).

L'objectif de ce travail consistait à i) identifier la protéase(s) de conversion de type CatL-Like impliquée dans la maturation de la proCatC dans les neutrophiles, ii) étudier les conséquences de l'inhibition pharmacologique de la maturation de la proCatC sur l'activation des PSN afin de connaître la nature de la NSPs-AAP-1.

**Résultats :** Nous avons identifié la cathépsine S (CatS) comme la protéase de conversion majeure de la proCatC dans la lignée promyélocytaire HL-60. L'**IcatS**$_{\#54}$, un inhibiteur spécifique de la CatS développé au cours de ce projet en collaboration avec le Dr Rich Williams (Queen's University, Belfast), est capable d'inhiber presque totalement la maturation de la proCatC. Cependant, malgré l'absence de CatC active, l'activité des PSN est conservée dans ces cellules, ce qui confirme la présence d'une voie d'activation alternative des PSN catalysée par la NSPs-AAP-1. Nous avons supposé que cette protéase pourrait avoir des caractéristiques communes avec la CatC, étant donné leur fonction commune sur l'activation des PSN. Afin de caractériser la NSPs-AAP-1, nous avons utilisé différents inhibiteurs

réversibles ou irréversibles de la CatC humaine. L'utilisation de l'**Icat$_{XPZ-01}$**, un inhibiteur de type nitrile, ou du **E64d** nous ont permis d'inhiber quasi totalement l'activation des PSN. En revanche, l'utilisation d'inhibiteurs irréversibles n'avait aucune action sur l'activation des PSN dans les cellules HL-60. Par conséquent, nous avons conclu que la NSPs-AAP-1 est une protéase à cystéine inhibée par des inhibiteurs nitrile réversible de la CatC. Les mêmes expérimentations ont été réalisées sur des neutrophiles différentiés à partir des cellules $CD34^+$ issues de sang de cordon ombilical en collaboration avec l'équipe du Dr Ralph Kettritz (Charité, Berlin). De façon similaire, la CatS apparaît comme la protéase majeure responsable de la maturation de la proCatC dans ces cellules. L'utilisation de l'inhibiteur de la CatS, l'**IcatS$_{\#54}$**, permet une inhibition indirecte des PSN d'environ 70%. Lorsque l'**IcatS$_{\#54}$** est combiné avec l'**IcatC$_{XPZ-01}$**, on obtient comme dans la lignée HL-60 une quasi-totale inhibition des PSN.

Nous avons ensuite étudié l'inhibition de la NSPs-AAP-1 murine en présence d'inhibiteurs synthétiques de la CatC humaine *in vitro* et *in vivo*. Dans ces expériences, les neutrophiles murins ont été différenciés à partir de progéniteurs de la moelle osseuse *in vitro* chez des souris de type sauvage ou knock-out ($Ctsc^{-/-}$). Des activités de PSN détectables ont été mesurées dans les neutrophiles $Ctsc^{-/-}$ différenciés (NE : 18% ± 5.4 ; PR3 : 20% ± 6.6 ; CatG 0.1% ± 0,1, par rapport aux neutrophiles des animaux de type sauvage) indiquant la présence de la NSPs-AAP-1 dans les neutrophiles murins. De plus, nous avons observé une inhibition presque totale des activités protéolytiques des PSN lorsque les neutrophiles de type sauvage et $Ctsc^{-/-}$ étaient différenciés en présence de 2 µM d'**IcatC$_{XPZ-01}$** ce qui indique une inhibition de la CatC et de la NSPs-AAP-1.

**Conclusion :** La CatS est la protéase de conversion majeure impliquée dans la maturation de la proCatC dans les précurseurs neutrophiliques humains. L'inhibition de la CatS par l'**IcatS$_{\#54}$** engendre le blocage presque complet de la maturation de la pro-CatC et résulte en une inhibition significative de l'activation des PSN dans les neutrophiles différenciés des cellules $CD34^+$ humaines. La NSPs-AAP-1 est une protéase à cystéine, capable de maturer les PSN, présente également chez la souris. Elle est inhibée par des inhibiteurs de type nitrile réversible de la CatC, tel que l'**IcatC$_{XPZ-01}$**, aussi bien dans le modèle humain, que chez la souris. Un inhibiteur chimique inhibant la CatC, mais également la protéase alternative NSPs-AAP-1 permettrait d'inactiver et d'éliminer totalement les PSN. La combinaison d'un inhibiteur de la CatS et d'un inhibiteur capable d'inhiber la CatC et la NSPs-AAP-1 serait plus efficace pour neutraliser les PSN dans les maladies inflammatoires chroniques et auto-immunes.

Contents lists available at ScienceDirect

Biochemical Pharmacology

journal homepage: www.elsevier.com/locate/biochempharm

# Pharmacological inhibition of cathepsin S and of NSPs-AAP-1 (a novel, alternative protease driving the activation of neutrophil serine proteases)

Roxane Domain [a,b,1], Seda Seren [a,b,1], Uwe Jerke [c], Manousos Makridakis [d], Kuan-Ju Chen [e], Jérôme Zoidakis [d], Moez Rhimi [f], Xian Zhang [g], Tillia Bonvent [a,b], Cécile Croix [a,b], Loïc Gonzalez [a,b], Dedong Li [e], Jessica Basso [e], Christophe Paget [a,b], Marie-Claude Viaud-Massuard [a,b], Gilles Lalmanach [a,b], Guo-Ping Shi [h], Ali Aghdassi [i], Antonia Vlahou [d], Patrick P. McDonald [e], Isabelle Couillin [j], Rich Williams [k], Ralph Kettritz [c,l], Brice Korkmaz [a,b,*]

[a] INSERM UMR-1100, Research Center for Respiratory Diseases, Tours, France
[b] Université de Tours, Tours, France
[c] Experimental and Clinical Research Center, Charité und Max-Delbrück-Centrum für Molekulare Medizin in der Helmholtz-Gemeinschaft (MDC), Berlin, Germany
[d] Biotechnology Division, Biomedical Research Foundation, Academy of Athens, Athens, Greece
[e] Research Department, Insmed Incorporated, Bridgewater, NJ, USA
[f] INRAE UMR-1319, Microbiota Interaction with Human and Animal Team (MIHA), Micalis Institute, AgroParisTech, Université Paris-Saclay, Jouy-en-Josas, France
[g] School of Food and Biological Engineering, Hefei University of Technology, Hefei, Anhui, China
[h] Department of Medicine, Cardiovascular Medicine, Brigham and Women's Hospital and Harvard Medical School, Boston, MA, USA
[i] Department of Medicine A - Gastroenterology, Nephrology, Endocrinology and Rheumatology, University Medicine Greifswald, Greifswald, Germany
[j] CNRS UMR-7355, Experimental and Molecular Immunology and Neurogenetics, Université d'Orléans, Orléans, France
[k] The Patrick G Johnston Center for Cancer Research, Queen's University, Belfast, UK
[l] Nephrology and Intensive Care Medicine, Charité-Universitätsmedizin, Berlin, Germany

ARTICLE INFO

*Keywords:*
Cathepsin C
Cysteine cathepsin
Neutrophil serine protease
Zymogen
Synthetic inhibitor
Therapeutic approach

ABSTRACT

An uncontrolled activity of neutrophil serine proteases (NSPs) contributes to inflammatory diseases. Cathepsin C (CatC) is known to activate NSPs during neutrophilic differentiation and represents a promising pharmacological target in NSP-mediated diseases. In humans, Papillon-Lefèvre syndrome (PLS) patients have mutations in their *CTSC* gene, resulting in the complete absence of CatC activity. Despite this, low residual NSP activities are detected in PLS neutrophils (<10% vs healthy individuals), suggesting the involvement of CatC-independent proteolytic pathway(s) in the activation of proNSPs. This prompted us to characterize CatC-independent NSP activation pathways by blocking proCatC maturation. In this study, we show that inhibition of intracellular CatS almost completely blocked CatC maturation in human promyeloid HL-60 cells. Despite this, NSP activation was not significantly reduced, confirming the presence of a CatC-independent activation pathway involving a CatC-like protease that we termed NSPs-AAP-1. Similarly, when human $CD34^+$ progenitor cells were treated with CatS inhibitors during neutrophilic differentiation *in vitro*, CatC activity was nearly abrogated but ~30% NSP activities remained, further supporting the existence of NSPs-AAP-1. Our data indicate that NSPs-AAP-1 is a cysteine protease that is inhibited by reversible nitrile compounds designed for CatC inhibition. We further established a proof of concept for the indirect, although incomplete, inhibition of NSPs by pharmacological targeting of CatC maturation using CatS inhibitors. This emphasizes the potential of CatS as a therapeutic target for inflammatory

*Abbreviations:* α1PI, alpha1-protease inhibitor; ABZ, *ortho*-aminobenzoic acid; ACT, alpha1-antichymotrypsin; ANCA, anti-neutrophil cytoplasmic autoantibody; BCA, bicinchoninic acid; CatC, cathepsin C; CatG, cathepsin G; DMSO, dimethyl sulfoxide; ECL, enhanced chemiluminescence; EDDnp, *N*-(2.4-dinitrophenyl)ethylenediamine; FRET, fluorescence resonance energy transfer; GPA, granulomatosis with polyangiitis; HBSS, Hank's balanced salt buffer; hNE, human neutrophil elastase; HSC, hematopoietic stem cell; MPO, myeloperoxidase; NETs, neutrophil extracellular traps; NSP, neutrophil serine protease; PBS, phosphate-buffered saline; PLS, Papillon-Lefèvre syndrome; PR3, proteinase 3; $PR3^m$, membrane-bound PR3; RT, room temperature; SDS-PAGE, sodium dodecyl sulfate polyacrylamide gel electrophoresis; WBC, white blood cell.

* Corresponding author at: INSERM UMR-1100 "Research Center for Respiratory Diseases" and Université de Tours, Tours, France.
*E-mail address:* brice.korkmaz@inserm.fr (B. Korkmaz).

[1] Equal contribution

https://doi.org/10.1016/j.bcp.2024.116114
Received 9 November 2023; Received in revised form 14 February 2024; Accepted 5 March 2024

diseases. Thus, preventing proNSP maturation using a CatS inhibitor, alone or in combination with a CatC/NSPs-AAP-1 inhibitor, represents a promising approach to efficiently control the extent of tissue injury in neutrophil-mediated inflammatory diseases.

## 1. Introduction

Neutrophils are the first line of cellular defense against invading pathogens and play an important role in the inflammatory response. They are differentiated from hematopoietic stem cells in the bone marrow and mature neutrophils are released into the blood in humans. Neutrophils mount several functional responses to eliminate pathogens. In addition to phagocytosis, these responses include the secretion of cytotoxic molecules such as neutrophil serine proteases (NSPs) – neutrophil elastase (NE), proteinase 3 (PR3), cathepsin G (CatG), and NSP4; the generation of reactive oxygen species (ROS); and the extrusion of web-like structures of decondensed chromatin decorated with numerous microbicidal proteins, called NETs (for neutrophil extracellular traps) [1]. NSP-mediated proteolysis is controlled endogenously by proteins of the serpin superfamily (including α1-protease inhibitor (α1PI) and α1-antichymotrypsin) as well as by canonical inhibitors such as secretory leukocyte peptide inhibitor (SLPI) and elafin [2,3]. Conversely, dysregulation of NSP activity contributes to the pathogenesis of neutrophil-mediated chronic inflammatory and auto-immune diseases [2,3].

NSPs are synthesized as inactive zymogens (proNSPs) containing an N-terminal two-residue propeptide, which maintains the zymogen in an inactive conformation. Activation of NSP zymogens occurs through the removal of the *N*-terminal dipropeptide by a cysteine protease called cathepsin C (CatC, EC 3.4.14.1; also known as dipeptidyl peptidase 1/DPP1) [4]. CatC is a highly conserved lysosomal dipeptidyl aminopeptidase belonging to the C1 family (clan CA) of cysteine peptidases [5,6]. Eleven cysteine cathepsins that are closely related to papain have been identified in humans [7]. All of them are synthesized as inactive pre-proenzymes containing a signal peptide, a propeptide, and a catalytic domain; the latter corresponding to the mature proteolytically active form [8,9]. Although most of human cysteine cathepsins are endopeptidases, CatB, C, H, and X retain an exopeptidase activity driven by their structural characteristics and are not auto-catalytically activated [7,9–11]. Unlike other cysteine cathepsins, CatC possesses a N-terminal exclusion domain responsible for its diaminopeptidase activity [5], allowing activation of NSP zymogens.

CatC is initially synthesized as a 55-kDa monomeric single chain pro-enzyme. Newly synthesized monomers associate to form proCatC dimers which undergo proteolytic cleavage at several sites to release internal 10-kDa propeptides and finally associate to form a functional tetramer [12]. Human proCatC is not auto-catalytically processed *in vitro* but is instead maturated by CatL-like proteases [13]. These proteases process proCatC in two consecutive steps. The first one releases the exclusion domain along with two peptides of 36 and 33 kDa, each one composed of the truncated propeptide, and the heavy and light chains. The second step involves the release of the heavy chain from each peptide [14–16]. Each mature CatC monomer in the functional tetramer consists of three subunits associated by non-covalent interactions, a 16-kDa N-terminal "exclusion" domain, a 23-kDa heavy chain and a 7.5-kDa light chain [14], with the heavy and the light chains forming a papain-like structure. The best characterized physiological function of active CatC is the activation of pro-inflammatory granular serine proteases of immune cells, including the NSPs [17].

A genetic defect in the *CTSC* gene (which encodes CatC) causes Papillon-Lefèvre syndrome (PLS, OMIM: 245000) or Haim-Munk syndrome in humans [18]. In our previous studies, we investigated the stability of mutated CatC in PLS white blood cells, neutrophils [19] and urines [20]. Nonsense, frameshift and missense mutations all resulted in a total absence of CatC protein in PLS patients [19,20]. Whereas nonsense and frameshift mutations are expected to affect the expression of mutated CatC, it is surprising for missense mutations to alter the stability of mutated proteins. It has been suggested that the latter mutations induce the intracellular proteolytic degradation of CatC [20,21]. In any event, the loss of CatC activity in neutrophils from PLS patients is associated with a strong reduction in NSP proteolytic activities but leaves significant residual activities (<10 % vs healthy individuals) [19,22] (Fig. 1). This suggests that CatC is the major, but not unique, protease involved in the activation of proNSPs [19]. In spite of their deficiency in CatC, PLS patients do not present marked immunodeficiency. This provided the rationale for a transient pharmacological inhibition of CatC activity in precursor cells within the bone marrow as a therapeutic strategy to regulate NSP activity in inflammatory and/or immune disorders [2,13,23].

Pharmacological inhibition of CatC can be achieved either using chemical inhibitors interacting with the mature, functional protease (*direct inhibition*) [24,25], or by impairing the activation of its proform by targeting proCatC-converting protease(s) (*indirect inhibition*) [15]. Potent reversible CatC inhibitors (**IcatC$_{XPZ-01}$** [25], **BI-9740** [26], **BI-1291583** [27], **brensocatib** [28,29] and **HSK31858** [30]) as well as irreversible CatC inhibitors (**GSK2793660** [31] and compound **22** [32]) have been synthetized, some of which are now being tested preclinically and in clinical trials [13,33,34] in patients with non-cystic fibrosis bronchiectasis, cystic fibrosis or chronic rhinosinusitis without nasal polyps (CRSsNP) [35].

Our previous work showed that PLS neutrophils display incompletely suppressed NSP activities despite a loss-of-function CatC mutation [19], which indicates that NSP-driven tissue damage might not be abrogated by blocking CatC alone. Importantly, our findings also suggested the existence of NSPs alternative activating protease(s) (NSPs-AAPs), which should ideally be targeted, along with CatC, to bring about full NSP inhibition. In this study, we investigated the proteolytic processes involved in the generation of active NSPs to generate further experimental evidence of the existence of NSPs-AAP(s), and to identify new therapeutic targets for NSP-mediated inflammatory diseases. To this end, we employed different pharmacological approaches to block pro-CatC maturation. We first used potent, cell-permeable inhibitors and determined the fate of proNSPs in a human promyeloid cell line as well as in neutrophils generated from human hematopoietic stem cells. We then investigated the proteolytic pathways involved in the activation of murine NSPs to understand the pharmacodynamics of CatC inhibitors.

## 2. Materials and methods

### 2.1. Materials

*Substrates*: Gly-Phe-AMC (#AMC-033) and Gly-Arg-AMC (#AMC-031) were from MP Biomedicals (Illkirch, France), ABZ-VAD(nor)VADYQ-EDDnp [36,37], Abz-APQQIMDDQ-EDDnp [36,37], Abz-TPFSGQ-EDDnp [38], Abz-VARCADYQ-EDDnp were from GeneCust (Boynes, France). *Inhibitors*: **E64d** (2*S*,3*S*-trans-(Ethoxycarbonyloxirane-2-carbonyl)-L-leucine-(3-methylbutyl) amide; aloxistatin) (HY-100229) was from MedChemExpress (Sollentuna, Sweden), compound **1** (calpain inhibitor VI, N-(4-fluorophenylsulfonyl)-L-valyl-L-leucinal)) (sc-293979); compound **2** (calpeptin, N-benzyloxycarbonyl-L-leucyl-norleucinal) (sc-202516); compound **3** (N-Acetyl-L-leucyl-L-leucyl-L-methioninal (sc-201268), compound **4** (Z-L-Abu-CONH-ethyl) (sc-301995) and **PD 150606** (3-(4-Iodophenyl)-2-mercapto-(Z)-2-propenoic Acid) (sc-222133) were from Santa Cruz Biotechnology (Heidelberg Germany). **RO5461111** (**IcatS$_{RO-11}$**) was provided by Roche Pharma

Research & Early Development, Roche Innovation Center Basel (Basel, Switzerland). Compound 22 (**IcatC$_{EGFR-22}$**) was kindly provided by Dr Zhiyuan Zhang (National Institute of Biological Sciences (NIBS), China). **IcatC$_{XPZ-01}$** was synthetized as in Guarino et al., [39]. **BI-9740** (**IcatC$_{BI-9740}$**) was obtained *via* Boehringer Ingelheim's innovation platform OpnMe (https://opnme.com) [40]. **GSK2793660** (**IcatC$_{GSK-60}$**) was generously provided by Dr Aili Lazaar from GlaxoSmithKline Pharmaceuticals (Brentford, UK). (L)-Thi-(L)-Phe-CN was was generously provided by Dr Adam Lesner (University of Gdansk/Poland), Biotin-Pro-Tyr-Asp-Ala$^{P}$(O-C$_6$H$_4$-4-Cl)$_2$ was synthetized as in Guarino et al., [39]. Alpha-1-antitrypsin (16–16-011609) and alpha-1-antichymotrypsin (16–16-012400) were from Athens Research & Technology (Athens, Georgia, USA). *Proteases*: mature human CatC was from Unizyme Laboratories (Hørsholm, Denmark). Active human PR3 and NE were from Athens Research & Technology (Athens, Georgia, USA). Active Human CatS and CatG were from Millipore (Molsheim, France). Recombinant human CatL (952CY) was from R&D system (Lille, France) and CatL from human liver (219402) was from Calbiochem® (San Diego, California, USA). *Antibodies*: murine anti-human CatC antibody directed against the heavy chain of CatC [15] (sc-74590), rabbit anti-human MPO antibody directed against the heavy chain (C-16-R, sc-16128-R) and rabbit anti-mouse CatG (sc-33207) were purchased from Santa Cruz Biotechnology (Heidelberg, Germany). Goat anti-human CatS antibody (AF1183) and goat anti-human CatL (AF952) were purchased from R&D system (Lille, France). Rabbit anti-human PR3 [15] (ab133613), rabbit anti-mouse NE antibody (ab68672) and rabbit anti-human CatD (ab75852) were purchased from Abcam (Cambridge, UK). Rabbit anti-human CatG (83578S) and rabbit anti-human NE (63610S) were purchased from Cell Signaling (Beverly, Massachusetts, USA). Murine anti-human β-actin antibody (A2228), peroxidase conjugated rabbit anti-goat IgG antibody (A5420) and peroxidase conjugated sheep anti-mouse IgG antibody (A5906) were purchased from Sigma-Aldrich (Saint-Quentin Fallavier, France). Peroxidase conjugated goat anti-rabbit IgG (H + L) antibody (Affini pure) (111-035-003) was purchased from Jackson ImmunoResearch (Cambridgeshire, UK).

### 2.2. Synthesis of IcatS$_{\#54}$

Boc-Cys-OMe was alkylated under standard basic conditions, followed by removal of Boc protecting group to afford 1. A one pot two-step reductive amination reaction was conducted to install the trifluormethylamino amide isostere. The intermediate acid was then oxidised to the sulfone-acid 2. The acid 2 was coupled to the 4,4-disubstitutedpiperidine under standard conditions to afford compound 3 (**IcatS$_{\#54}$**). Reagents: (a) 2-fluorobenzyl bromide, $K_2CO_3$, DMF, 20 h; (b) 4 N HCl dioxane, 1 h; (c) (i) 4-Fluorotrifluoroacetophenone, $K_2CO_3$, MeOH, 50 °C, 18 h; (ii) $Zn(BH_4)_2$, DME, ACN, −40 °C, 4 h; (d) NaTg, TBAH, $H_2O_2$, EtOAc, 3 h; (e) 4-amino-4-Cyano-*N*-Me-piperidine, HATU, NMM, DMF, 18 h (Fig. 2).

### 2.3. IC$_{50}$ determination

Serial dilutions (0–50 μM for compound **1**, **IcatS$_{\#54}$** and 0–0.5 μM for compound 2) were made in assay buffer in presence of recombinant cysteine proteases at 2 nM (CatB, C, F, K, L, S and V). After 15 min of incubation at 37 °C under low agitation, fluorogenic substrate was added (Gly-Phe-AMC for CatC, Z-Leu-Arg-AMC for CatS and Z-Phe-Arg-AMC for other cysteine cathepsins, 20 μM for each substrate). IC$_{50}$ values were derived by a sigmoidal dose–response (variable slope) curve using GraphPad Prism software. The reported data are average of at least three independent experiments in duplicate.

### 2.4. Blood neutrophil purification

Blood from healthy volunteers from the EFS (Etablissement Français du Sang) and blood from PLS patients (Germany) were collected in EDTA tubes. Neutrophils were isolated from blood using EasySep™ Direct Human Neutrophil Isolation Kit (StemCell Technologies (19666), Saint Égrève, France). This kit isolates neutrophils directly from human whole blood by immunomagnetic negative selection. Unwanted cells are labeled with antibodies EasySep™ Direct RapidSpheres™ and separated using an EasySep™ magnet. Once collected neutrophils were washed with PBS and lysed in 50 mM HEPES buffer, 750 mM NaCl, 0.1 % Nonidet P-40 (NP-40), pH 7.4. Soluble fractions were separated from cell debris by centrifugation at 10,000g for 20 min. Proteins were assayed with a bicinchoninic acid assay (BCA) (23227, Thermo Fisher Scientific, Villebon sur Yvette, France).

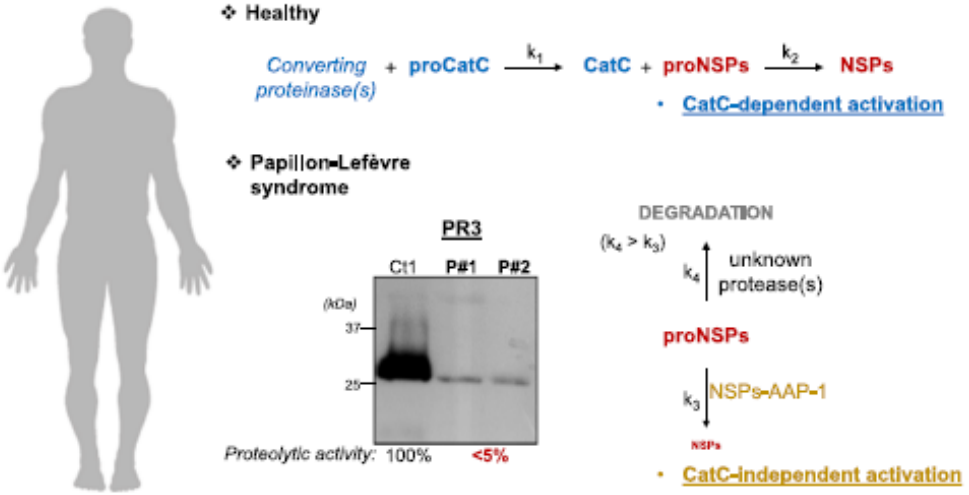


**Fig. 1.** ProNSP processing pathways in human. Characterization of NSPs in neutrophils from PLS patients with CatC deficiency allowed the highlighting of a CatC independent processing and activating pathway (k3) catalyzed by unknown protease(s) [19], called NSPs-AAP-1 in this study. Little amounts of synthesized proNSPs are activated while the rest are eliminated during neutrophil differentiation. The differentiation of isolated human bone-marrow neutrophilic precursors in presence of the cell-permeable CatC inhibitor **IcatC$_{XPZ-01}$** allowed the highlighting of a proteolytic processing pathway (k4) catalyzed by unknown protease(s) in granules [39] responsible for the elimination of NSP zymogens. However, there is no evidence showing that k3 and k4 exist in healthy neutrophilic precursors containing proteolytically active CatC.

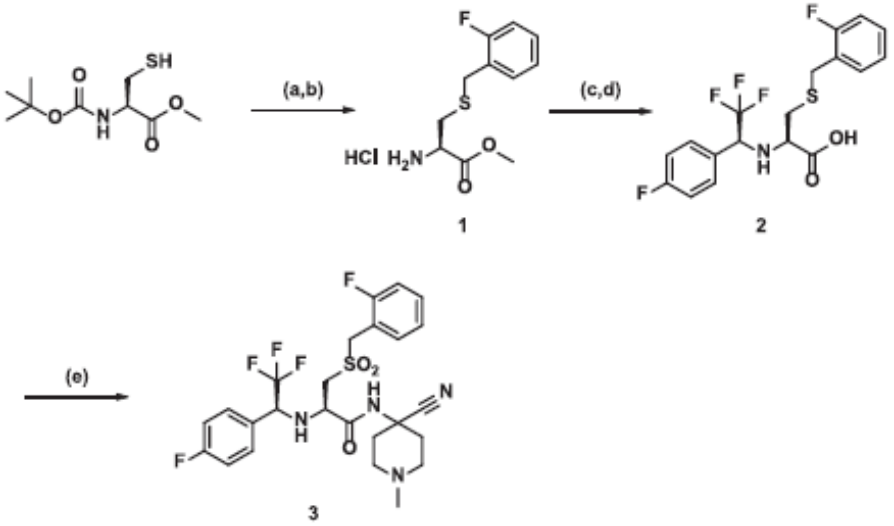


Fig. 2. Synthetic schema for the synthesis of $\mathbf{IcatS}_{\#54}$.

### 2.5. Proteomics and bioinformatics analysis of HL-60 cells

HL-60 cells were cultured in RPMI-1640 GlutaMAX™ supplement (61870044, Gibco™) medium supplemented with 10 % FBS (Fetal Bovine Serum substitute, Fetal + Triple 0.1 μm Sterile Filtered, SERANA®, S-FBSP-EU-015), 50 units/ml penicillin and 50 μg/ml streptomycin at 37 °C in a humidified atmosphere containing 5 % $CO_2$ (passage number < 30). Cell pellets were homogenized in FASP (Filter Aided Sample Preparation) lysis buffer (4 % SDS, 0.1 M DTE, 0.1 M Tris-HCl pH 7.6). Protein concentration was determined by Bradford assay. Protease inhibitors (Roche, Basel, Switzerland) were added at a final concentration of 3.6 % and samples were stored at -80 °C until further use. Protein extracts (200 μg/sample) were processed using filter aided sample preparation (FASP) as described previously [41], with minor modifications [42]. Briefly, buffer exchange was performed in Amicon Ultra Centrifugal filter devices (0.5 ml, 30-kDa MWCO; Merck) at 14.000 rcf for 15 min at room temperature. The protein extract was mixed with urea buffer (8 M urea in 0.1 M Tris-HCl, pH 8.5) and centrifuged. The concentrate was diluted with urea buffer and centrifugation was repeated. Alkylation of proteins was performed with 0.05 M iodoacetamide in urea buffer for 20 min in the dark followed by a centrifugation at 14.000 rcf for 10 min at RT. Additional series of washes were conducted with urea buffer (2 times) and ammonium bicarbonate buffer (50 mM NH4HCO3, pH 8.5, 2 times). Tryptic digestion was performed overnight at RT in the dark, using a trypsin to protein ratio of 1:100. Peptides were eluted by centrifugation at 14.000 rcf for 10 min, lyophilized and stored at -80 °C until further use.

LC-MS/MS experiments were performed on the Dionex Ultimate 3000 UHPLC system coupled with the high-resolution nano-ESI QExactive HF mass spectrometer (Thermo Scientific). Each sample was reconstituted in 200 μL loading solution composed of 0.1 % v/v formic acid. A 5 μL volume was injected and loaded on the Acclaim PepMap 100 (100 μm × 2 cm C18, 5 μm, 100 Å) trapping column with the loading pump operating at a flow rate of 5 μL/min. For the peptide separation the Acclaim PepMap RSLC, 75 μm × 50 cm, C18, 2 μm, 100 Å column was used for multi-step gradient elution. Mobile phase (A) was composed of 0.1 % formic acid and mobile phase (B) was composed of 100 % acetonitrile, 0.1 % formic acid. The peptides were eluted under a 240 min gradient from 2 % (B) to 80 % (B). Flow rate was 300 nL/min and column temperature was set at 35 °C. Gaseous phase transition of the separated peptides was achieved with positive ion electrospray ionization applying a voltage of 2.5 kV. For every MS survey scan, the top 10 most abundant multiply charged precursor ions between *m/z* ratio 300 and 2200 and intensity threshold 500 counts were selected with FT mass resolution of 70.000 and subjected to HCD fragmentation. Tandem mass spectra were acquired with FT resolution of 35.000. Normalized collision energy was set to 33 and already targeted precursors were dynamically excluded for further isolation and activation for 30 sec with 5 ppm mass tolerance.

Raw files were analysed with Proteome Discoverer 1.4 software package (Thermo Finnigan), using the Sequest search engine and the Uniprot human (Homo sapiens) reviewed database, including 20.204 entries. The search was performed using carbamidomethylation of cysteine as static and oxidation of methionine as dynamic modifications. Two missed cleavage sites, a precursor mass tolerance of 10 ppm and fragment mass tolerance of 0.05 Da were allowed. False discovery rate (FDR) validation was based on q value: target FDR: 0.01.

Label free quantification was performed by utilizing the precursor ion area values exported from the total ion chromatogram as defined by the Proteome Discoverer 1.4 software package. Output files from Proteome Discoverer were processed with R programming language for statistical computing (version 4.0.3). Raw protein intensities for each sample were subjected to normalization according to $X' = X/\mathrm{Sum}(Xi) * 10^6$.

### 2.6. Inhibition of proteases in HL-60 cells and human $CD34^+$-derived neutrophils

HL-60 cells (2–3 × $10^6$ cells) were cultured for 72 h and treated with **E64d** (1, 10, 100 μM). Continuous inhibition of CatS was maintained in cell cultures (starting at 2–3 × $10^6$ cells) with the synthetic inhibitors $\mathbf{IcatS}_{\#54}$ ((*R*)-N-(4-cyano-1-methylpiperidin-4-yl)-3-((2-fluorobenzyl) sulfonyl)-2-(((*S*)-2,2,2-trifluoro-1-(4-fluorophenyl)ethyl)amino)propanamide, $\mathbf{IcatS}_{\mathrm{RO\text{-}11}}$ ((2*S*,4*R*)-N-(1-cyanocyclopropyl)-4-((4-(2-methylpyridin-4-yl)-2-(trifluoromethyl)phenyl)sulfonyl)-1-(1-(trifluoromethyl)cyclopropane-carbonyl)pyrrolidine-2-carboxamideo), **IcatS** (*N*-(1-cyanocyclopropyl)-3-((2,3-difluorobenzyl)sulfonyl)-2-((2,2,2-trifluoro-1-(4-fluorophenyl)ethyl)amino)propanamide), compound **1** (2*S*-[[(4-fluorophenyl)sulfonyl]amino]-N-[(1*S*)-1-formyl-3-methylbutyl]-3-methyl-butanamide), compound **2** (calpeptin, N-benzyloxycarbonyl-L-leucyl-norleucinal), compound **3** (N-Acetyl-L-leucyl-L-leucyl-L-methioninal or compound **4** (Z-L-Abu-CONH-ethyl). Continuous direct inhibition of CatC was maintained in cell cultures (starting at 2–3 × $10^6$ cells) with the synthetic inhibitors $\mathbf{IcatC}_{\mathrm{XPZ\text{-}01}}$ (1 μM), $\mathbf{IcatC}_{\mathrm{GSK\text{-}60}}$ (10 μM) or $\mathbf{IcatC}_{\mathrm{EGFR\text{-}22}}$ (0.2 μM). Either compounds **1**, compounds **4**, or $\mathbf{IcatS}_{\#54}$ (10 μM) was supplemented with the CatC

inhibitor, **IcatC**$_{XPZ-01}$ (1 μM) or **IcatC**$_{GSK-60}$ (10 μM).

Umbilical cord blood samples were taken giving informed consent (Ethics vote EA4/025/18). Mononuclear cells were obtained from anti-coagulated cord blood by centrifugation over a LSM1077 (PAA, Paschin, Austria) gradient at 800 × g for 20 min. Cells were washed and stained using the CD34$^+$ progenitor isolation kit (Miltenyi, Bergisch-Gladbach, Germany) and sorted according to the manufacturer's instructions. CD34$^+$ cells were cultivated in stem span serum free medium (Cell Systems, St. Katharinen, Germany) supplemented with Penicillin/Streptomycin, 100 ng/ml SCF, 20 ng/ml TPO and 50 ng/ml FLT3-L (Peprotech, London, UK) for expansion. Neutrophil differentiation was performed in RPMI with 10 % FCS, 10 ng/ml G-CSF (Peprotech), and either DMSO control, **IcatS**$_{\#54}$ (20 μM) or compound **1** (10 μM and 30 μM). **IcatS**$_{\#54}$ and compound **1** were supplemented with **IcatC**$_{XPZ-01}$ (1 μM) and **IcatC**$_{BI-9740}$ (1 μM). Medium was changed every other day. We PR3-phenotyped the neonatal neutrophils obtained from the freshly harvested umbilical cords by flow cytometry prior to the CD34$^+$ HSC isolation. We selected only cord blood where the neonatal neutrophils showed a clear bimodal membrane PR3 pattern.

HL-60 cells were lysed in 50 mM HEPES buffer, 750 mM NaCl, 0.1 % Nonidet P-40 (NP-40), pH 7.4. Soluble fractions were separated from cell debris by centrifugation at 10.000 × g for 20 min. CD34$^+$ or neutrophil-differentiated CD34$^+$ HSC were lysed in 50 mM HEPES buffer, 750 mM NaCl, 0.05 % NP-40, pH 7.4. Soluble fractions were separated from cell debris by centrifugation at 10.000 × g for 20 min and then concentrated by ultrafiltration (Vivaspin (filtration threshold 10-kDa)) in some experiments. Proteins were assayed with a BCA.

### 2.7. Animal experiments

All studies were carried out under approval of: 1. "Comité d'Ethique Appliqué à l'Expérimentation Animale" under the protocols No.: #12504-201720818404277v1, #201604071220401-4885 and #1728), 2. the Care and Use of Laboratory Animals published by the US National Institutes of Health and were approved by the Harvard Medical School Standing Committee on Animals (Protocol No.: #2016N000442). 3. the Institutional Animal Care and Use Committee (IACUC) of Rutgers University Animal Care Committee (Protocol No.: PROTO999900342). Wild-type (WT) male C57BL/6 mice were purchased from Jackson Laboratories, (Bar Harbor, ME) or Janvier Labs (Le Genest-Saint-Isle, France), *Ctsc*$^{-/-}$ and NSP triple knock-out mice on C57BL/6 genetic background were obtained from Washington University (Dr C. Pham) and bred at Charles River Laboratories (Wilmington, MA). The mice used in this study were 11–16 weeks old. Prolonged **IcatC**$_{XPZ-01}$ administration was performed as in [39].

### 2.8. Murine neutrophils differentiation from bone marrow progenitor cells and inhibition of intracellular proteases

WT (n = 5) and *Ctsc*$^{-/-}$ (n = 5) femurs and tibias of both hind limbs were harvested for each animal. The bones were kept on wet ice until processing for bone marrow collection. In brief, bone cutters were used to cut off the epiphysis of the long bones to expose the bone marrow-filled cavity. Each bone cavity was then flushed with 5 ml/bone of PBS through a 40-μm cell strainer and collected in a 50-ml conical tube. Cells were spun down (400 × g, 4 °C, 5 min) and the supernatants were discarded.

For mixed white blood cells (WBC) sample preparation, the bone marrow cells were lysed with 1X red blood cell (RBC) lysis buffer (Sigma R7757) at room temperature for 2 min, followed by the addition of 10 ml PBS to stop RBC lysis. The cell suspension was centrifuged (400 × g, 4 °C, 5 min), resuspended in 1 ml in PBS, and centrifuged (400 × g, 4 °C, 5 min).

For promyelocytes preparation, bone marrow promyelocytes were isolated using Direct Lineage Cell Depletion Kit (Miltenyi, 130–110-470). This kit isolates untouched lineage-negative cells from mouse bone marrow cell suspension using microbeads conjugated to monoclonal antibodies against mature hematopoietic cells, the marked cells are retained in a LS column (Miltenyi, 130–042-401) fixed on a magnet and untouched cells are collected. Briefly, cells were counted and resuspended in ice-cold MACS buffer (pH 7.2 PBS plus 0.5 % BSA and 2 mM EDTA), 80 μL of buffer per 2 × 10$^7$ total cell. Followed by 20 μL per 2 × 10$^7$ total cell of Direct Lineage Cell Depletion Cocktail. The mixture was then incubated for 10 min at 2–8 °C. The cell suspension was applied to the Magnetic separation LS Column (MACS, Miltenyi, 130 042 401). Unlabeled cells representing the enriched promyelocytes were collected from the flow-through. The column was washed with 3 ml of ice-cold MACS buffer three times.

Collected cells were cultured at 200.000 cells/ml in IMDM medium, supplement GlutaMAX™, HEPES (Gibco™, 31980030), 10 % FBS (SERANA®, S-FBSP-EU-015), 1 % Pen Strep (Penicillin Streptomycin, Gibco™, 151–40-122) with 50 ng/ml of Stem cell factor (Recombinant mouse SCF carrier free, BioLegend®, 579704) and 50 ng/ml of Interleukin-3 (Recombinant mouse IL-3 carrier free, BioLegend®, 575504) supplemented or not with chemical inhibitor (**IcatC**$_{XPZ-01}$ (1 μM)) for 3 days. At day 3 cells were counted and resuspended at 200.000 cells/ml with the same medium with 50 ng/ml of SCF, IL-3 and Granulocyte Colony Stimulating Factor (Recombinant mouse G-CSF carrier free, BioLegend®, 574604) and cultured for two days. At day 5 same method were used than at day 3 but medium was supplemented with only 50 ng/ml of G-CSF. At day 7 cells were washed and counted, some of them will be used for FACS analysis and the rest will be lysed. FACS analysis were used to control neutrophil population. Cells were marked with antibodies against CD45 (APC/Cyanine7 anti-mouse CD45, BioLegend®, 103116), Ly6G (FITC anti-mouse Ly6G, BioLegend®, 127606), CD11b (PE/Cy7 anti-mouse/human CD11b, BioLegend®, 101216) and Live/Dead™ (Live/Dead™ Fixable Aqua Dead Cell Stain Kit, Invitrogen, L34957).

Cells were lysed in 50 mM HEPES buffer, 750 mM NaCl, 0.1 % NP-40, pH 7.4. Soluble fractions were separated from cell debris by centrifugation at 15.000 × g for 20 min.

### 2.9. Total protein quantification

The Pierce™ BCA Protein Assay Kit (Thermo Scientific, 23227) was used to measure the total protein of the samples after lysis to allow for subsequent normalization, following the manufacturer's instructions.

### 2.10. Measurements of protease activities in cell lysates

In HL-60 cells, CD34$^+$ or neutrophil-differentiated CD34$^+$ HSC lysates, proteolytic activities of CatC and NSPs were measured as in [15]. Briefly, the CatC activity in cell lysates was measured spectrofluorometrically (Spectra Max Gemini EM) at 460 nm (excitation: 350) with or without the nitrile inhibitor (L)-Thi-(L)-Phe-CN using Gly-Phe-AMC (20 μM final) as substrate in 50 mM sodium acetate, 30 mM NaCl, 1 mM EDTA, 2 mM DTT, pH 5.5 at 37 °C. The PR3 activity in cell lysates was measured at 420 nm (excitation: 320) with or without the PR3 inhibitor Bt-PYDnV$^P$(O-C$_6$H$_4$-4-Cl)$_2$ (nV: norvaline) (1 μM in 50 mM HEPES buffer, 750 mM NaCl, 0.05 % NP40, pH 7.4 at 37 °C) using Abz-VADnVADYQ-EDDnp (20 μM) as substrate. CatG activity was measured at 420 nm (excitation: 320) in 50 mM HEPES buffer, 100 mM NaCl, 0.05 % NP 40, pH 7.4 at 37 °C, in the presence or not of 1 μM anti-chymotrypsin, using Abz-TPFSGQ-EDDnp (20 μM) as substrate. NE activity was measured at 420 nm (excitation: 320) with or without the NE inhibitor Epi-hNE-4 (1 μM in 50 mM HEPES buffer, 750 mM NaCl, 0.05 % NP40, pH 7.4 at 37 °C) using Abz-APQQIMDDQ-EDDnp (20 μM) as substrate.

In murine neutrophils differentiated from bone marrow progenitor cells lysates and bone marrow lysates CatC activity was measured in activity buffer (50 mM sodium acetate, 30 mM NaCl, 1 mM EDTA, 2 mM DTT, pH 5.5 at 37 °C) at 460 nm (excitation: 350) with or without the

nitrile inhibitor (L)-Thi-(L)-Phe-CN using Gly-Arg-AMC (20 μM) as substrate. Activity of NE was measured with a fluorogenic substrate in activity buffer (50 mM HEPES buffer, 750 mM NaCl, 0.05 % NP40, pH 7.4) at 37 °C with or without the inhibitor α1PI (1 μM) at 420 nm (excitation: 320) using Abz-APQQIMDDQ-EDDnp as substrate, PR3 activity was measured in the same conditions using Abz-VARCADYQ-EDDnp as substrate. CatG activity was measured in the same conditions as above.

### 2.11. Western blotting

The pellet of $CD34^+$ HSC or neutrophil-differentiated $CD34^+$ HSC were lysed in sample buffer (20 mM Tris (pH 8,8), 138 mM NaCl, 10 % glycerol, 2 mM EDTA, 1 % Triton-X-100, 1 % NP-40 and protease inhibitor mix). The total protein concentration has been determined by the BCA (Thermo Fisher Scientific, Villebon sur Yvette, France) or Bradford (Bio-Rad, Hercules, USA) assay. HL60 cells lysates, and $CD34^+$ samples were separated by SDS-PAGE under denaturing/reducing conditions and transfered to Hybond-ECL membranes. Free sites were saturated by incubation in PBS, 0.1 % Tween-20, 5 % fat-free milk for 1 h and the membranes were then incubated with goat anti-human CatS antibody (diluted 1:1000), murine anti-human CatC antibody directed against the heavy chain of CatC (diluted 1:1000), rabbit anti-human PR3 [15] (diluted 1:1000), rabbit anti-human CatG (diluted 1:1000), rabbit anti-human NE (diluted 1:1000) or goat anti-human CatL (diluted 1:1000), in PBS, 0.1 % Tween-20, 5 % non-fat milk overnight at 4 °C. The membranes were washed three times in PBS, 0.1 % Tween-20, incubated for 1 h30 with a peroxidase-coupled secondary antibody diluted 1:10000 or 1:5000 in PBS, 0.1 % Tween-20 5 % non-fat milk. For loading control, membranes were stripped with $H_2O_2$ 35 % for 20 min at 37 °C. Then incubated with murine anti-human β-actin antibody (diluted 1:1000) or rabbit anti-human MPO antibody directed against the heavy chain (diluted 1:1000) in PBS, 0.1 % Tween-20, 5 % non-fat milk overnight at 4 °C. The membranes were washed three times in PBS, 0.1 % Tween-20, incubated for 1 h30 with a peroxidase-coupled secondary antibody (diluted 1:5000) in PBS, 0.1 % Tween-20, 5 % non-fat milk.

Murine neutrophils differentiated from bone marrow progenitor cells lysates and bone marrow lysates were treated as above and incubated with murine anti-human CatC antibody (diluted 1:1000), rabbit anti-mouse CatG (diluted 1:500), or rabbit anti-mouse NE antibody (diluted 1:1000) in PBS, 0.1 % Tween-20, 5 % non-fat milk overnight at 4 °C. The membranes were washed three times in PBS, 0.1 % Tween-20, incubated for 1 h30 with a peroxidase-coupled secondary antibody (diluted 1:5000) in PBS, 0.1 % Tween-20, 5 % non-fat milk. For loading control, membranes were stripped with $H_2O_2$ 35 % for 20 min at 37 °C. Then incubated with rabbit anti-human MPO antibody directed against the heavy chain (diluted 1:1000) in PBS, 0.1 % Tween-20, 5 % non-fat milk overnight at 4 °C. The membranes were washed three times in PBS, 0.1 % Tween-20, incubated for 1 h30 with a peroxidase-coupled secondary antibody (diluted 1:5000) in PBS, 0.1 % Tween-20, 5 % non-fat milk.

## 3. Results

### 3.1. ProCatC-converting proteases in human promyelocytic HL-60 precursor cells

We first aimed to identify candidate cysteine proteases that could activate proCatC in HL-60 cells, by immunoblot analysis. CatF, CatK or CatV were not detectable in concentrated cell-free supernatants or in cell lysates (*data not shown*). By contrast, HL-60 cells mainly secreted ~ 42-kDa proCatL whereas the cell lysates contained only the propeptide lacking the ~ 32-kDa single chain of mature CatL (Fig. 3A). Furthermore, HL-60 cells secreted similar amounts of 32-kDa proCatS and ~ 23-kDa mature CatS, whereas the cell lysates contained mainly mature CatS (Fig. 3B). We next broadened our scope and analyzed the entire HL-60 cell proteome, using a mass spectrometry-based proteomic approach. Among the 3693 proteins that were identified [43] (*Data reference*), CatS was the only proCatC-converting CatL-Like protease. Thus, two assays identified CatS as likely the major CatC-activating cysteine protease, whereas CatL could have a small contribution.

To determine whether the CatL and CatS proforms were processed by cysteine proteases, we resorted to the cell-permeable, broad-spectrum cysteine protease inhibitor, **E64d** (Fig. 4). Incubation of HL-60 cells with 100 μM **E64d** for 72 h only delayed proCatS/proCatL processing, resulting in the appearance of low amounts of proCatL (Fig. 3C) and ~ 28-kDa-truncated proCatS (Fig. 3D). This indicated a partial involvement of at least one additional class of proteases. In this regard, CatD was identified in HL-60 cell lysates by both proteomic and immunoblot analyses. However, incubation of HL-60 cells with pepstatin A-penetratin conjugate (an inhibitor of acid proteases) did not alter the processing of proCatS and proCatL, thereby excluding CatD from the maturation pathways of these proteases (*data not shown*).

### 3.2. Impact of pharmacological CatS inhibition on the maturation of proCatC and proNSPs in human promyelocytic HL-60 precursor cells

In our previous study, we used **IcatS** to inhibit CatS [15] whereas in this study, we used two different CatS inhibitors expected to be more cell-permeable. A novel, potent, selective and cell-permeable CatS nitrile inhibitor, termed **IcatS**$_{\#54}$ (Fig. 4), was designed and synthesized, based on the **IcatS** [15]. **IcatS**$_{\#54}$ has improved cellular activity and selectively inhibits human CatS activity among other human cysteine cathepsins and NSPs (Tables 1 and 2). After incubating HL-60 cells with 10 μM **IcatS**$_{\#54}$ for one week (i.e. the time required to allow a complete turnover of pre-existing active CatC and NSPs), we observed an important but still incomplete blockade of proCatC maturation, with accumulation of the previously reported 35-kDa fragment containing the truncated propeptide, the heavy chain and the light chain [21], and a low intensity band corresponding to the heavy chain (Fig. 5A). The proteolytic activity of CatC (monitored using its fluorogenic substrate, Gly-Phe-AMC) was inhibited ~ 95 % relative to control cell lysates. Despite this, the activity of PR3 and CatG were reduced by only 10–15 % (Fig. 5A). **IcatS**$_{\#54}$ also did not interfere with the processing of proCatS into the mature protease, as similar amounts of pro- and mature CatS were detected in treated and control cells by western blot. We confirmed the results using the potent, selective and cell-permeable CatS nitrile inhibitor, **RO5461111** (Roche Pharma Research & Early Development, Roche Innovation Center Basel, hereafter called **IcatS**$_{\text{RO-11}}$, $IC_{50}$CatS = 0.4 nM; $IC_{50}$CatL = 49 μM [44]) which blocked ~ 95 % of CatC activity in cell lysates resulting in the inhibition of PR3 and CatG by only 10–15 % (Fig. 5A). The presence of active PR3 and CatG in **IcatS**$_{\#54}$-treated cell lysates was also confirmed by observing the formation of the ~ 80-kDa irreversible serpin-protease complexes when lysates were incubated with α1PI (Fig. 5B). Similar results were obtained when **IcatS**$_{\text{RO-11}}$-treated cells were incubated with serpins (*data not shown*).

Although this is unlikely, the residual CatC activity (less than 5 %) observed in the presence of **IcatS**$_{\#54}$ or **IcatS**$_{\text{RO-11}}$ may have been enough to fully activate proNSPs. To eliminate this possibility, we next tried to block proCatC maturation completely before measuring NSP activities.

### 3.3. Consequences of total proCatC maturation blockade on proNSPs in human promyelocytic HL-60 precursor cells

We used the cell-permeable aldehyde protease inhibitor, *N*-(4-fluorophenylsulfonyl)-$_L$-valyl-$_L$-leucinal (compound **1**, 2*S*-[[(4-fluorophenyl)sulfonyl]amino]-N-[(1*S*)-1-formyl-3-methylbutyl]-3-methylbutanamide [45]), to inhibit both CatS ($IC_{50}$ = < 1 nM) and CatL ($IC_{50}$ = 1.6 nM [45]) that did not reduce CatC/NSPs activities using purified proteases *in vitro*. Incubating HL-60 cells with compound **1** (10 μM final), resulted in a nearly total abolition of proCatC maturation, with a

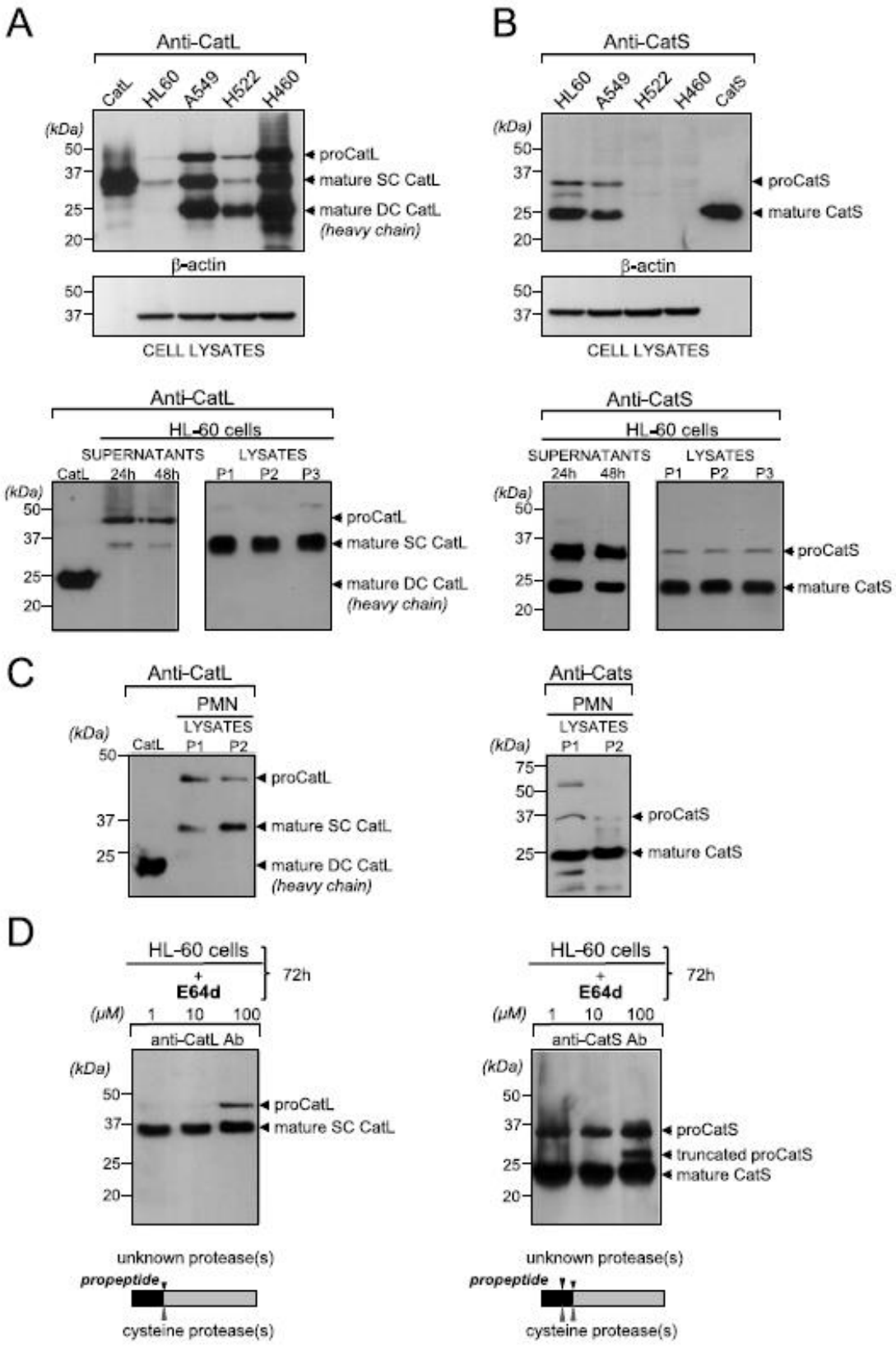


(caption on next page)

**Fig. 3.** CatL and CatS in HL-60 cells. Western blot analysis of 30-fold concentrated HL-60 cells supernatants (50 µg of protein/lane) and cell lysates (50 µg protein/lane) A) using antiCatL or B) antiCatS antibodies. The cells were cultured for 24 h and 48 h. Western blotting were performed in denaturing and reducing conditions using mature double chain purified human liver CatL [61], recombinant CatL and recombinant CatS as controls. Human lung cancer lines A549, H522, H460 expressing both mature single chain (SC) and double chains (DC) CatL were used for comparative analysis. Similar results were obtained in 3 independent experiments. C) Western blot analysis of human polymorphonuclear neutrophil (PMN) lysates using antiCatL or antiCatS antibodies. D) Processing of proCatL and proCatS in HL-60 cells exposed to increasing concentration of **E64d**. HL-60 cells were cultured in the presence of 1, 10 or 100 µM of E64d for 72 h and were lysed. Cell lysates were analyzed by western blotting in denaturing and reducing conditions using antiCatL or antiCatS antibodies. Two bands of ~ 42-kDa and ~ 28-kDa, corresponding, to proCatL and truncated proCatS, respectively, appeared when cells were incubated with 100 µM of **E64d**. Diagrams show the processing of proCatL and proCatS in HL-60 cells. Arrows indicate the cleavage sites in zymogens. As ~ 28-kDa truncated proCatS with comparable molecular weight was also observed during auto-processing [62,63], we assumed that the sequence cleavable by unknown protease(s) in proCatS propeptide segment was also cleaved by cysteine protease(s).

corresponding accumulation of the truncated proCatC fragment as observed by western blot (Fig. 6A). Accordingly, the proteolytic activity of CatC monitored with Gly-Phe-AMC in compound **1**-treated versus control cells was inhibited by ~ 99 %. These effects could not be attributed to compound **1** toxicity, since preliminary experiments showed that it was non-toxic at up to 30 µM in HL-60 cells. Despite its marked inhibition of CatC activity, compound **1** failed to significantly affect PR3 or CatG activities (Fig. 6A). Compound **1** also did not affect the processing of proCatS, as similar amounts of pro- and mature forms were detected in treated and untreated cells by western blot (Fig. 6B). Similar results were obtained with two other aldehyde inhibitors of CatS/CatL, namely N-benzyloxycarbonyl-L-leucyl-norleucinal ($IC_{50}$CatS = 1.2 nM ±, $IC_{50}$CatL = 4 ± nM) and N-Acetyl-L-leucyl-L-leucyl-L-methioninal ($IC_{50}$CatS = 1.5 ± 0.88 nM, $IC_{50}$CatL = 3.2 ± 0.94 nM) or using cell-permeable dipeptidyl α-ketoamide reversible inhibitor Z-L-Abu-CONH-ethyl reported as compound **2**, compound **3** and compound **4**, respectively (Fig. 7). Because aldehyde protease inhibitors can also inhibit calcium-dependent cysteine proteases (calpains) within cells, we tested whether the maturation of proCatC might be affected by **EGTA** (a general calcium-dependent protease inhibitor), or by **PD 150606** (3-(4-iodophenyl)-2-mercapto-(Z)-2-propenoic acid; a cell-permeable, non-competitive, selective, calcium-dependent inhibitor of calpain-1 and calpain-2). Neither inhibitor altered the maturation of proCatC, indicating no implication of calpain-type proteases in this process (*data not shown*).

These data from indirect CatC inhibition studies suggested that at least one additional protease that was not able to hydrolyse the Gly-Phe-AMC CatC substrate, was involved in CatS/CatC-independent maturation of proPR3/proCatG in HL-60 cells. This CatC-like protease(s), now called NSPs-Alternative Activating Protease-1 (NSPs-AAP-1), was capable of activating 80 % of PR3 and CatG when proCatC maturation was almost totally inhibited. We then investigated whether we could inhibit NSPs-AAP-1 using chemical inhibitors targeting CatC, by analyzing NSP activation in HL-60 cells.

### *3.4. Co-inhibition of both CatC and NSPs-AAP-1 in human promyelocytic HL-60 precursor cells by reversible nitrile CatC inhibitor IcatC$_{XPZ-01}$*

Since **IcatC$_{XPZ-01}$**, a potent, reversible, cell-permeable nitrile inhibitor [25] inhibits ~ 95 % of CatC activity in HL-60 cells but in contrast to **IcatS$_{\#54}$**, almost completely prevented proNSPs maturation [15], we hypothesized that **IcatC$_{XPZ-01}$** must inhibit not only CatC, but also NSPs-AAP-1. Indeed, supplementing compound **1** with **IcatC$_{XPZ-01}$** at days 7 and 10 resulted in ~ 95 % inhibition of PR3 and CatG in cell lysates (Fig. 6A). Furthermore, we observed that the combination of both compound **1** and **IcatC$_{XPZ-01}$**, but not the individual inhibitors, partially altered proCatS maturation with appearance of the ~ 28-kDa-truncated proCatS (Fig. 6B). Furthermore, when compound **1** was supplemented with **IcatC$_{XPZ-01}$**, we detected unprocessed, proteolytically inactive PR3 zymogens that were unable to form an irreversible stable complex with α1PI (Fig. 6C).

Thus, NSPs-AAP-1 that, together with CatC, is involved in proPR3/proCatG maturation was inhibited by **IcatC$_{XPZ-01}$** (Fig. 6D). We then analyzed the NSPs-AAP-1 dependent activation of proNSPs using additional CatC inhibitors.

### *3.5. Inhibition of CatC-, but not NSPs-AAP-1-dependent activation of proNSPs, by irreversible CatC inhibitors in human HL-60 cells*

We hypothesized that irreversible CatC inhibitors **GSK-2793660** (**IcatC$_{GSK-60}$**) [31] and EGFR-derived inhibitor (**IcatC$_{EGFR-22}$**) [32], which are structurally distinct from **IcatC$_{XPZ-01}$**, inhibit CatC but not the NSPs-AAP-1 pathway. Incubation of HL-60 cells with **IcatC$_{GSK-60}$** (10 µM) or **IcatC$_{EGFR-22}$** (0.2 µM) for one week resulted in an almost total abolition of the cleavage of Gly-Phe-AMC substrate, indicating effective CatC inhibition (**IcatC$_{EGFR-22}$**: 99.9 ± 0.14 %; **IcatC$_{GSK-60}$**: 98 ± 0.53 %; n = 3 independent experiments). However, cell treatment with **IcatC$_{GSK-60}$** or **IcatC$_{EGFR-22}$** reduced the PR3/CatG activity by only 10–20 %. Therefore, NSPs-AAP-1 contributed to ~ 85 % of PR3 and CatG activation when CatC was almost totally inhibited. Similar results were found when **IcatC$_{GSK-60}$** was supplemented with compound **1**. Unlike **IcatC$_{XPZ-01}$**, the combination of **IcatC$_{GSK-60}$** with compound **1** did not alter proCatS maturation (western blot analysis, n = 3 independent experiments).

These results showed that **IcatC$_{GSK-60}$** and **IcatC$_{EGFR-22}$** inhibited CatC but not the NSPs-AAP-1 activity and confirmed that the latter represents an additional protease involved in the maturation of proNSPs in HL-60 cells. We next investigated consequences of CatC zymogen maturation blockade on NSP maturation in neutrophils generated from human CD34$^+$ progenitor cells.

### *3.6. Consequences of proCatC maturation blockade on proNSP activation in neutrophils generated from human CD34$^+$ progenitor cells*

Human CD34$^+$ HSC were isolated from umbilical cord blood and differentiated into neutrophils in the presence or absence of CatS inhibitor **IcatS$_{\#54}$** (20 µM) (Fig. 8A). Neutrophil differentiation was assessed by the expression of neutrophil surface markers (CD11b, CD15, CD66b) but was not affected by the inhibitory compounds after 10 days (*data not shown*). By western blot, we observed nearly no proCatC maturation as evidenced by minimal accumulation of the 35-kDa truncated proCatC fragment in **IcatS$_{\#54}$**-treated cells (Fig. 8B). Immunoblotting of cell lysates showed no alteration of MPO processing as a control but reduction of the amount of NSP zymogens (Fig. 8C, D). NSP activities in **IcatS$_{\#54}$**-treated cell lysates were significantly but incompletely inhibited (by 62.5 ± 11.7 % for PR3, by 76.4 ± 14.7 % for NE and by 62.4 ± 8.1 % for CatG) as determined by hydrolysis of the sensitive and selective FRET substrates (n = 3 independent experiments) (Fig. 8E). Importantly, combination of **IcatS$_{\#54}$** with **IcatC$_{XPZ-01}$** resulted in almost total inhibition and elimination of NSPs (Fig. 8D and E) without affecting cell differentiation. A similar partial NSPs inhibition was obtained when human CD34$^+$ HSC were differentiated in the presence of compound **1**. Again, when compound **1** was combined with the nitrile CatC inhibitor, **IcatC$_{BI-9740}$**, NSP activities were abrogated (Fig. 9).

In conclusion, we identified CatS as the major human neutrophil proCatC maturating protease involved in proNSP activation, and NSPs-AAP-1 as an additional CatC-independent protease that activates proNSPs and was inhibited by reversible nitrile inhibitors. We next investigated proteolytic pathways involved in the activation of NSPs in mice.

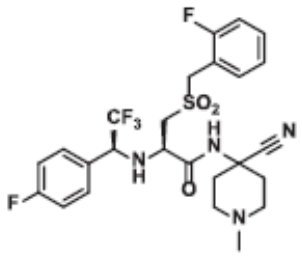

**IcatS**$_{\#54}$

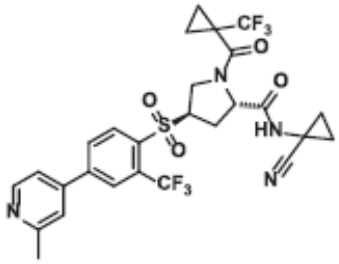

**IcatS**$_{RO-11}$

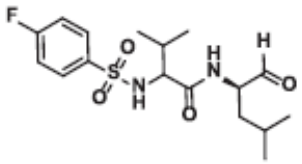

Compound **1**

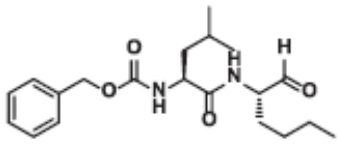

Compound **2**

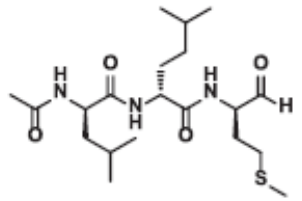

Compound **3**

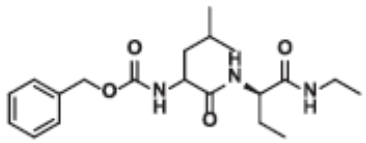

Compound **4**

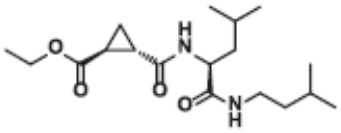

**E64d**

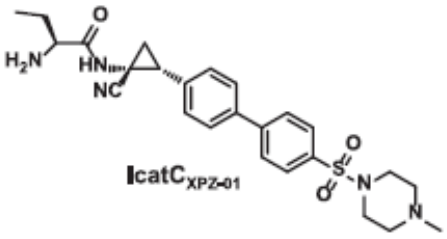

**IcatC**$_{XPZ-01}$

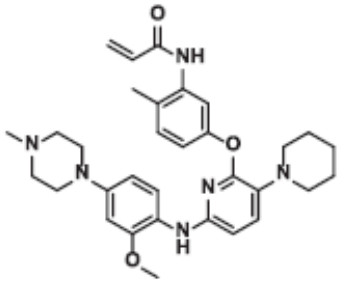

**IcatC**$_{EGFR-22}$

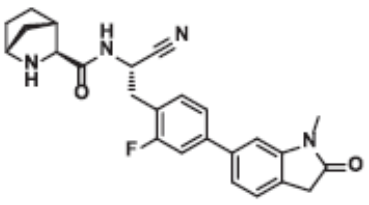

**IcatC**$_{BI-9740}$

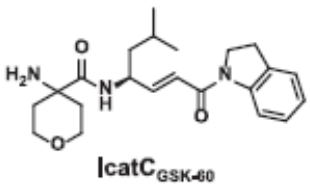

**IcatC**$_{GSK-60}$

*(caption on next page)*

**Fig. 4.** Chemical structures of cell-permeable synthetic protease inhibitors used in this study. **IcatS$_{\#54}$**: (*R*)-N-(4-cyano-1-methylpiperidin-4-yl)-3-((2-fluorobenzyl) sulfonyl)-2-(((*S*)-2,2,2-trifluoro-1-(4-fluorophenyl)ethyl)amino)propenamide, **RO5461111** (**IcatS$_{RO-11}$**): (2*S*,4*R*)-N-(1-cyanocyclopropyl)-4-((4-(2-methylpyridin-4-yl)-2-(trifluoromethyl)phenyl)sulfonyl)-1-(1-(trifluoromethyl)cyclopropane-carbonyl)pyrrolidine-2-carboxamide *(CatS inhibitors)*, Compound 1: 2*S*-[[(4-fluorophenyl)sulfonyl]amino]-N-[(1*S*)-1-formyl-3-methylbutyl]-3-methyl-butanamide, Compound 2: (calpeptin, *N*-benzyloxycarbonyl-L-leucyl-norleucinal); Compound 3: (N-Acetyl-L-leucyl-L-leucyl-L-methioninal, Compound 4: (Z-L-Abu-CONH-ethyl) *(CatS and CatL inhibitors)*, **E64d**: (1*S*,2*S*)-ethyl 2-((((*S*)-1-(isopentylamino)-4-methyl-1-oxopentan-2-yl)carbamoyl)cyclopropanecarboxylate (*broad-spectrum cysteine protease inhibitor*), **IcatC$_{XPZ-01}$**: (*S*)-2-amino-N-((1*R*,2*R*)-1-cyano-2-(4'-(4-methylpiperazin-1-ylsulfonyl)biphenyl-4-yl)cyclopropyl)butanamide, Compound 22 (**IcatC$_{EGFR-22}$**): N-(5-((6-((2-methoxy-4-(4-methylpiperazin-1-yl)phenyl)amino)-3-(piperidin-1-yl)pyridin-2-yl)oxy)-2-methylphenyl)acrylamide, **BI-9740** (**IcatC$_{BI-9740}$**): (1*R*,3*S*,4*S*)-N-((*S*)-1-cyano-2-(2-fluoro-4-(1-methyl-2-oxoindo-lin-6-yl) phenyl)ethyl)-2-azabicyclo[2.2.1]heptane-3-carboxamide, **GSK2793660** (**IcatC$_{GSK-60}$**): (*S*,*E*)-4-amino-*N*-(1-(indolin-1-yl)-6-methyl-1-oxohept-2-en-4-yl)tetrahydro-2*H*-pyran-4-carboxamide *(CatC inhibitors)*.

**Table 1**
Comparative analysis of **IcatS$_{\#54}$** selectivity for human cysteine cathepsins and NSPs.

| Proteases | $IC_{50}$ (nM) |
|---|---|
| CatS | 7.1 |
| CatB | >10.000 |
| CatC | n.i. |
| CatK | >10.000 |
| CatL | 358 |
| CatV | 139 |
| NE | n.i. |
| PR3 | n.i. |
| CatG | n.i. |

$IC_{50}$ concentration of **IcatS$_{\#54}$** resulting in 50% inhibition of proteolytic activity.
n.i.: non inhibition

**Table 2**
Proteases targeted with cell-permeable synthetic inhibitors used in this study.

| Inhibitors | Targeted proteases |
|---|---|
| • *Reversible covalent* | |
| **IcatS$_{\#54}$** | CatS |
| **IcatS$_{RO-11}$** | CatS |
| **Compounds 1–4** | CatS and CatL |
| **IcatC$_{XPZ-01}$** | CatC and NSPs-AAP-1 |
| **IcatC$_{BI-9740}$** | CatC and NSPs-AAP-1 |
| • *Irreversible* | |
| **IcatC$_{EGFR-22}$** | CatC |
| **IcatC$_{GSK-60}$** | CatC |
| **E64d** | Cysteine proteases |

### 3.7. Consequences of CatS genetic depletion on proCatC and proNSP maturation in mice

We investigated whether proCatC/proNSPs were processed and maturated in C57BL/6 CatS knock-out (*Ctss*$^{-/-}$) mice. Western blots using bone marrow and blood WBC lysates from *Ctss*$^{-/-}$ animals showed that proCatC was correctly processed and that amounts of the heavy chains liberated were the same in WT and *Ctss*$^{-/-}$ lysates (Fig. 10A and B). These finding did not eliminate the possibility of temporary CatS involvement, namely in proCatC maturation in promyelocytes, affecting proNSPs conversion into active enzymes. NE was detected in the bone marrow and in blood WBC lysates, and formed irreversible 80-kDa complexes when lysates were incubated with exogenous purified α1PI, as determined by western blot (Fig. 10C). The selectivity of anti-murine NE antibodies was shown in bone marrow-derived WBC or isolated bone marrow neutrophils from NSP triple knock-out mice (*data not shown*). These data suggest that CatS was not the major proCatC maturating protease in mice and not a major contributor to NSPs activation.

### 3.8. Consequences of CatC genetic depletion or pharmacological inhibition on proNSP activation in mice

We next investigated the presence of NSPs-AAP-1 in mice. Bone marrow samples were collected from WT and *Ctsc*$^{-/-}$ C57BL/6 mice and CatC/NSPs were analyzed in cell lysates by immunoblot and fluorogenic substrate assay (Fig. 11). The selectivity of murine NSP FRET substrates and antibodies was checked in bone marrow-derived WBC or isolated neutrophils from NSP triple knock-out mice (n ≥ 3 independent experiments (*data not shown*). Western blots using selective antibodies showed significantly reduced but still detectable NSP proteins (30.7 % ± 2.8 for NE and 20.2 % ± 1.7 for CatG) in samples from *Ctsc*$^{-/-}$ mice (Fig. 11A, middle and lower panels). Moreover, NSPs detected in bone marrow lysates from *Ctsc*$^{-/-}$ mice formed irreversible 80-kDa complexes when lysates were incubated with exogenous purified α1PI or ACT, as determined by western blotting (*data not shown*). Accordingly, significantly reduced but still substantial NSP activities were measured (36.34 % ± 8.62 for NE, 46.2 % ± 6.29 for PR3 and < 1 % for CatG (Fig. 11B)) in bone marrow samples from *Ctsc*$^{-/-}$ mice compared to WT mice. Residual NE and PR3 activities were more pronounced than that of CatG. Residual NSP activities were inhibited in the presence of selective NSP inhibitors (*data not shown*). Collectively, these results showed that CatC was also not the unique protease involved in proNSP maturation in mice, and that an NSPs-AAP-1 was also present in mice and a contributor to NSP activity (Fig. 11C).

We then studied the inhibition of murine NSPs-AAP-1 in the presence of CatC inhibitor **IcatC$_{XPZ-01}$** *in vitro* and *in vivo*. In these experiments, WT or *Ctsc*$^{-/-}$ murine neutrophils were differentiated from bone marrow progenitors *in vitro* in WT. Detectable NSP activities were measured in differentiated *Ctsc*$^{-/-}$ neutrophils (NE: 18.0 ± 5.4 %; PR3: 20.0 ± 6.6 %; CatG 0.1 ± 0.1 %, relative to neutrophils from WT animals) (Fig. 12A) but not in NSP triple knock-out bone marrow isolated mature neutrophils used as controls (n ≥ 3 independent experiments). Moreover, we observed an almost total inhibition of NSP proteolytic activities when WT and *Ctsc*$^{-/-}$ neutrophils were differentiated in the presence of 1 μM of **IcatC$_{XPZ-01}$** that inhibits both CatC and NSPs-AAP-1 in 5 independent experiments (Fig. 12A). Prolonged administration (7 days) of **IcatC$_{XPZ-01}$** (4.8 mg/kg at 10 ml/kg as in [25]) treatment reduced NSP proteolytic activities (by 29.1 ± 8.3 % for NE, 20.4 ± 5.7 % for PR3 and 26.3 ± 9 % for CatG) (Fig. 12B) and NSP proteins (by 81.1 ± 6.8 % for NE and 75.9 ± 8.6 % for CatG) (Fig. 12C) in WT mice as assessed at the end of the treatment period.

## 4. Discussion

In this study, we show (*i*) that CatS, a potent elastinolytic enzyme, is the major druggable converting protease involved in the maturation of human neutrophil proCatC; (*ii*) that an NSPs-AAP-1 activity exists and works independently of CatC in granulocytes; *(iii)* that proNSPs are activated by CatC- and NSPs-AAP-1-dependent proteolytic pathways, which are conserved in both humans and mice; and (*iv*) that pharmacological targeting of CatS in human CD34$^{+}$ hematopoietic stem cell-differentiated neutrophils allows for a sizeable inactivation and elimination of NSPs (~70 %), as well as a further reduction upon additional NSPs-AAP-1 inhibition. These heretofore unknown aspects of the proteolytic pathways involved in proNSP activation have the potential to spawn novel treatment strategies to control NSP-mediated tissue injury that is often associated with the presence of activated neutrophils in numerous chronic inflammatory or autoimmune diseases.

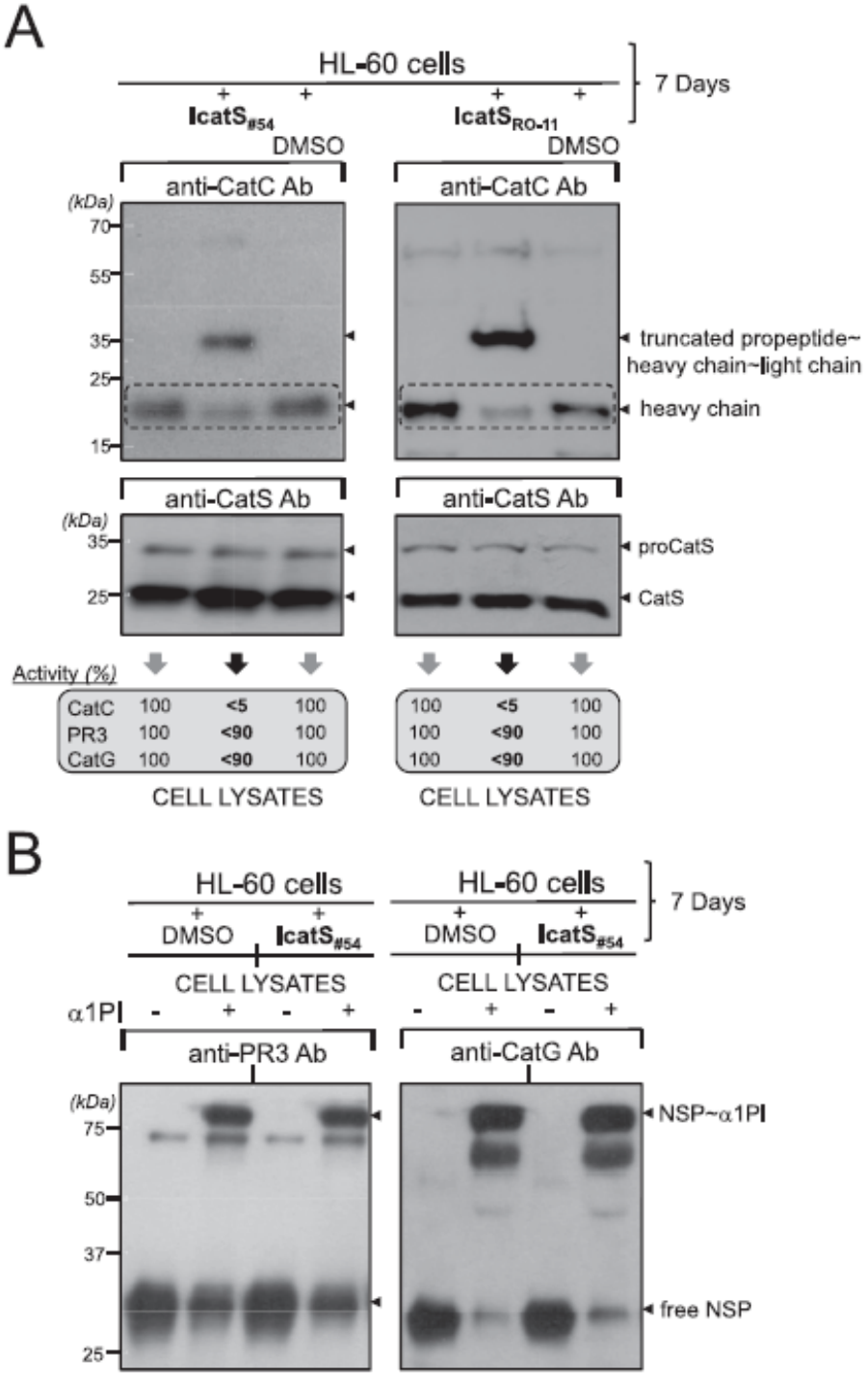


**Fig. 5.** Consequences of pharmacological CatS inhibition on the maturation of proCatC and proNSPs in HL-60 cells. HL-60 cells were cultured for 7 days in the presence of 10 μM of $IcatS_{RO-11}$ or $IcatS_{\#54}$ or after adding DMSO containing medium alone. A) Western blot analysis of cell lysates using antiCatC antibody directed against the 23-kDa heavy chain of CatC demonstrating the accumulation of ~ 35-kDa fragment composed of truncated propeptide, the heavy chain and the light chain in presence of $IcatS_{RO-11}$ or $IcatS_{\#54}$. Western blot analysis of cell lysates using antiCatS antibody as protein control showing not impact of inhibitors on proCatS processing. The percentage of proteolytic activities of CatC, PR3 and CatG was determined using fluorogenic substrates GF-AMC, Abz-VAD(nor)VADYQ-EDDnp, and Abz-TPFSQQ-EDDnp, respectively. Similar results were obtained in three independent experiments. B) Western blot analysis of cell lysates incubated with or without human α1PI using antiPR3 or antiCatG antibody. The *de novo* formation of irreversible α1PI-NSP complexes of about 75-kDa revealing activation of PR3 and CatG in presence of $IcatS_{\#54}$.

CatL and CatS have been previously identified as proCatC-maturating proteases *in vitro* [14]. We have similarly investigated the maturation of proCatC in human neutrophilic precursors at different stages and showed that targeting CatS using a selective cell-permeable nitrile inhibitor (**IcatS**) reduced CatC activity by about 80 % without affecting NSP activities [15]. We had proposed that this incomplete CatC inhibition could be due to the presence of additional proCatC maturating protease(s) resistant to the CatS inhibitor and/or to a limited effect of the

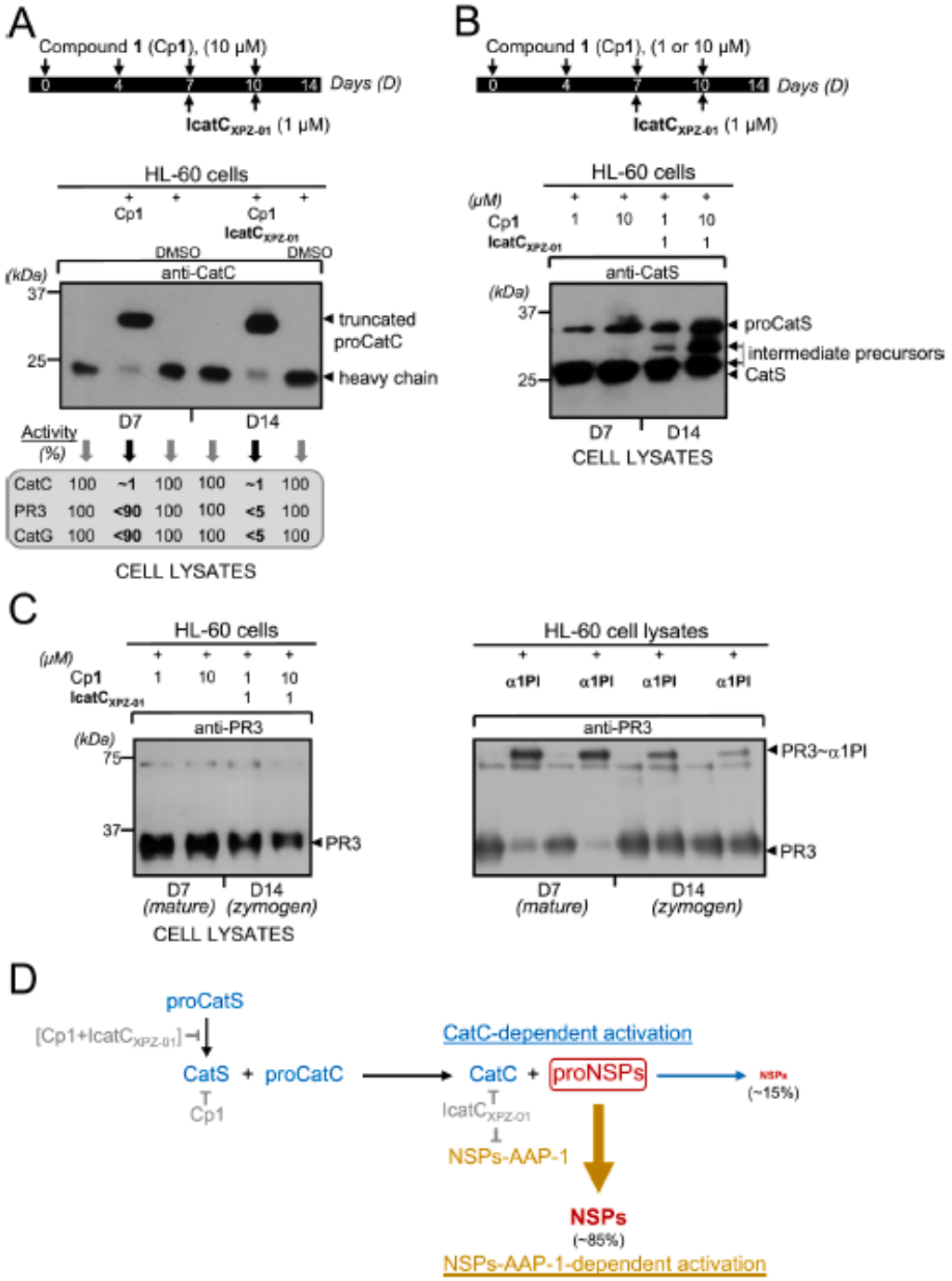


**Fig. 6.** Processing of proCatC, proCatS and proNSPs in HL-60 cells cultured in the presence of compound 1 supplemented with IcatC$_{XPZ-01}$. HL-60 cells were cultured for 14 days in the presence of compound 1 or after adding DMSO containing buffer alone. IcatC$_{XPZ-01}$ was added at day 7. Processing of proCatC, proCatS and proNSPs in cell lysates were analyzed by western blotting. A) Western blot analysis of cell lysates using anti-CatC antibody directed against the 23-kDa heavy chain of CatC demonstrating the accumulation of ~ 35-kDa fragment in presence of compound 1. Proteolytic activities of NSPs are inhibited in presence of compound 1 supplemented with IcatC$_{XPZ-01}$. The percentage of proteolytic activities of CatC, PR3 and CatG was determined as in Fig. 5. Results obtained in three independent experiments were shown. B) Western blot analysis of cell lysates using anti-CatS antibody showing alteration of proCatS processing with accumulation of intermediate precursor in presence of compound 1 supplemented with IcatC$_{XPZ-01}$. Similar results were obtained in three independent experiments. Incubation of cells only with compound 1 (*data not shown*) or IcatC$_{XPZ-01}$ for 14 days did not alter the processing of proCatS (see Fig. 7C). C) Western blot analysis of cell lysates incubated with or without α1PI using anti-PR3 antibody. (*Left*) PR3 stability in cell lysates incubated without α1PI. (*Right*) PR3 in same cell lysates incubated with or without α1PI. The decrease of ~ 75-kDa irreversible α1PI-PR3 complexes formation and the detection of free PR3 in presence of compound 1 supplemented with IcatC$_{XPZ-01}$ revealing unprocessing of PR3 zymogens. Similar results were obtained in three independent experiments. D) Diagram summary of proNSPs activation pathways in HL-60 cells. ProNSPs are activated by CatC (*in blue*) and NSPs-AAP-1 (*in dark yellow*) dependent pathways in HL-60 cells. CatC dependent activation pathway is initiated by proteolytic processing and maturation of proCatS. Combination of compound 1 with IcatC$_{XPZ-01}$ partially inhibits the maturation of proCatS. The nitrile dipeptidyl CatC inhibitor IcatC$_{XPZ-01}$ inhibits both CatC and NSPs-AAP-1 dependent maturation of proNSPs in HL-60 cells.

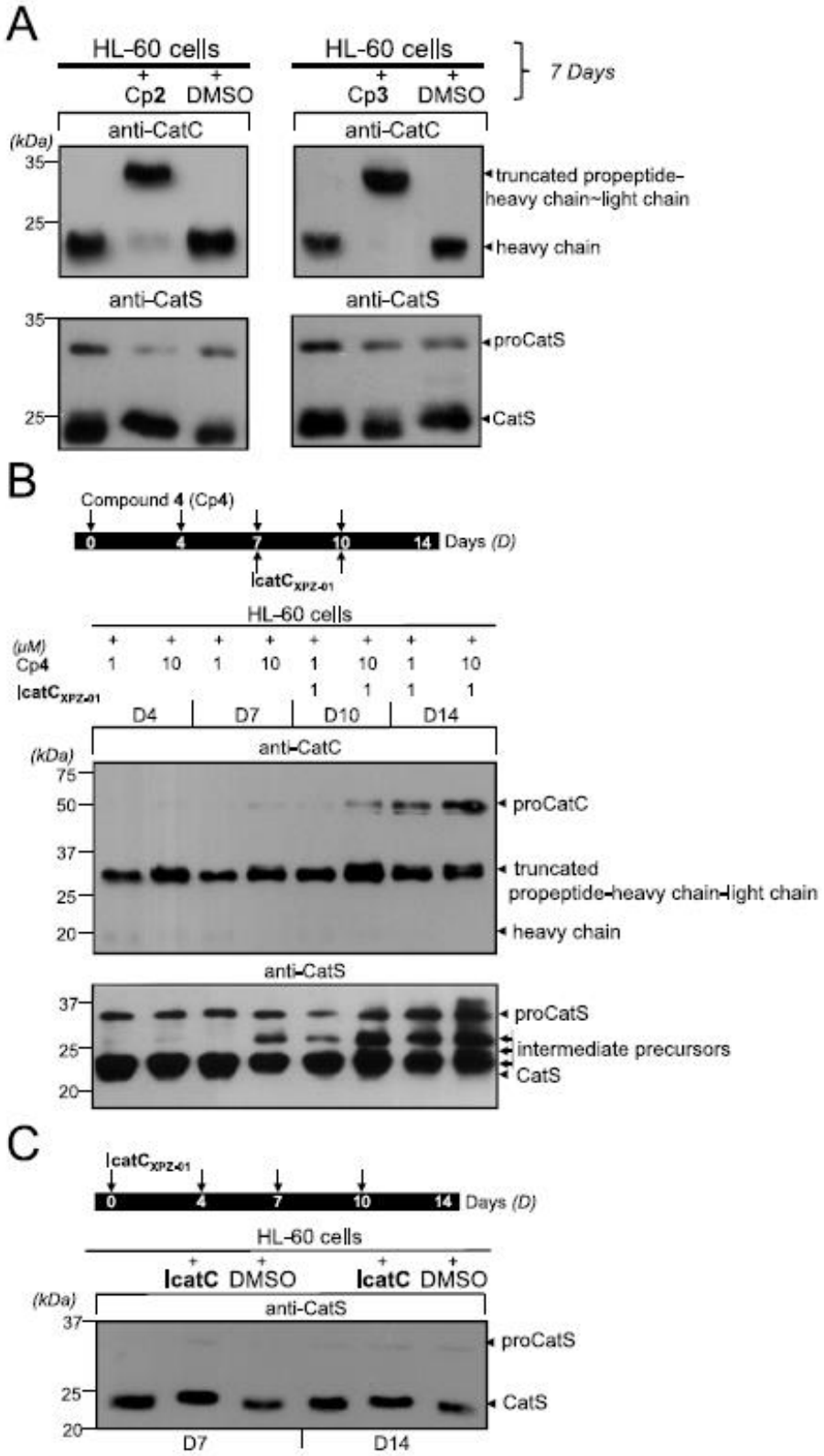


**Fig. 7.** Processing of proCatC and proCatS in HL-60 cells cultured in the presence or absence of synthetic inhibitors. A) HL-60 cells were cultured for 7 days in the presence of compound 2 (Cp2, 10 μM), compound 3 (Cp3, 10 μM) or after adding DMSO containing buffer alone. Cell lysates were analyzed by western blotting using antiCatC antibody. B) HL-60 cells were cultured for 14 days in the presence of compound 4 (Cp4, 1 and 10 μM), or after adding buffer containing DMSO alone. IcatC$_{XPZ-01}$ (1 μM) was added at days 7 and 10. Cell lysates were analyzed by western blotting using antiCatC antibody and antiCatS antibody. C) HL-60 cells were cultured for 14 days in the presence of IcatC$_{XPZ-01}$ (1 μM), or after adding buffer containing DMSO alone. Cell lysates were analyzed by western blotting using antiCatS antibody.

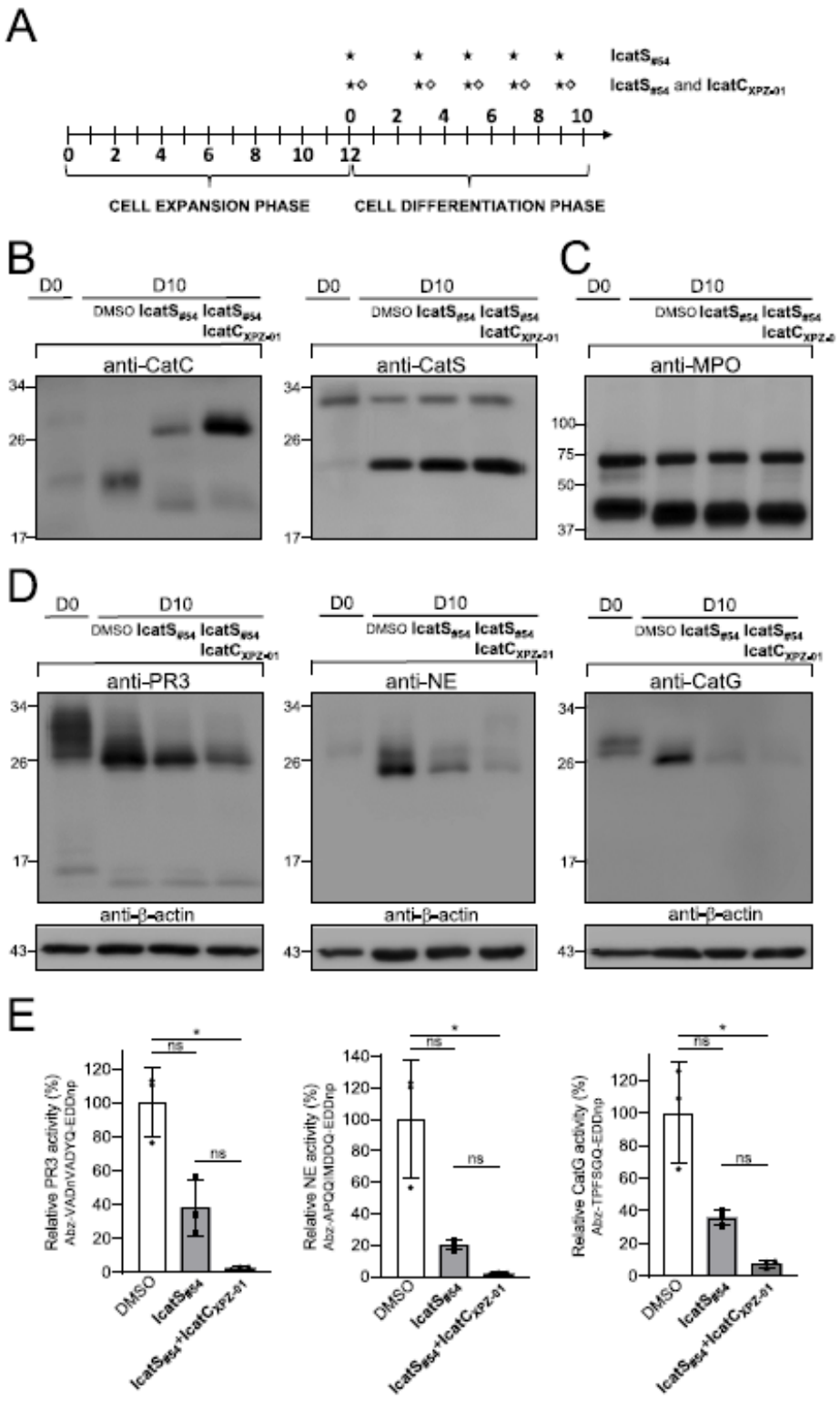


**Fig. 6.** Activation of proNSPs in neutrophils generated from $CD34^+$ hematopoietic stem cells in the presence of $IcatS_{\#54}$. A) $CD34^+$ cells from umbilical cord blood samples of three donors were differentiated over 10 days into neutrophils in medium containing $IcatS_{\#54}$ (20 μM), a mixture of $IcatS_{\#54}$ (20 μM) and $IcatC_{XPZ-01}$ (1 μM), or in DMSO containing buffer, respectively. B) Immune reactive CatC and CatS. C) MPO as a control was not affected by inhibitor treatment. D) PR3, NE and CatG were analyzed in cell lysates in parallel by western blotting using specific antibodies. Anti-β-actin was used as loading control. Western blot analysis of cell lysates demonstrating the elimination of NSP zymogens in presence of inhibitors. E) Proteolytic activity for PR3, NE, and CatG was determined by FRET assay. Proteolytic activity was strongly reduced in the presence of the CatS ($IcatS_{\#54}$) inhibitor alone and almost abrogated by the combination with the CatC inhibitor ($IcatC_{XPZ-01}$). Statistical analysis of the data was performed using a nonparametric test (Kruskal-Wallis test), *$p < 0.1$.

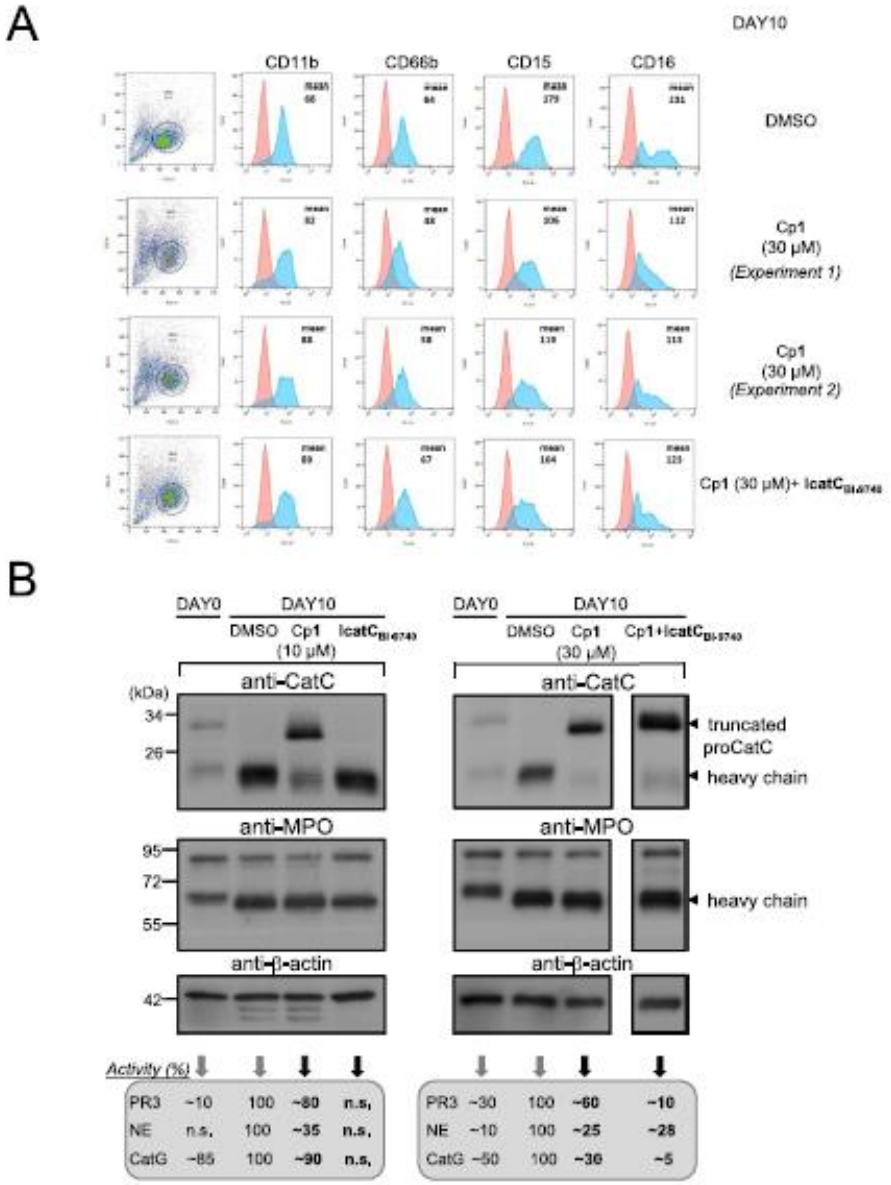


(caption on next page)

**Fig. 9.** Activation of proNSPs in neutrophils generated from CD34$^+$ hematopoietic stem cells in the presence of compound **1** alone and in combination with the reversible nitrile CatC inhibitor **IcatC**$_{BI-9740}$. CD34$^+$ cells from umbilical cord blood samples of three donors were differentiated over 10 days into neutrophils in medium containing compound **1** (Cp1, 10 μM or 30 μM), **IcatC**$_{BI-9740}$ (1 μM), compound **1**/**IcatC**$_{BI-9740}$ or after adding DMSO containing buffer alone. A) Neutrophil differentiation was assessed by the expression of the neutrophil surface markers CD11b, CD66b, CD15 and CD16 (blue) by flow cytometry. Isotype staining in (red). B) Processing of proCatC in cell lysates were analyzed by Western blotting using antiCatC antibody directed against the 23-kDa heavy chain of CatC. Western blot analysis of cell lysates demonstrating the accumulation of the fragment composed of truncated propeptide, the heavy chain and the light chain in presence of compound **1** (10 μM, two independent experiments; 30 μM, one experiment). Anti-myeloperoxidase (MPO) and anti-β-actin used as controls. NSPs activities were determined in the same cell lysates prepared for CatC analysis as in Fig. 8. Incubation of cells with **IcatC**$_{BI-9740}$ alone resulted in complete elimination of NSPs in cell lysates as in [26] (*data not shown*). C) Immune reactive PR3, NE and CatG were analyzed by Western blotting using antiPR3, antiNE and antiCatG antibodies in the same cell lysates prepared for CatC analysis as in Fig. 8. Anti-β-actin used as loading control. Western blot analysis of cell lysates demonstrating the reduction of NSP zymogens in presence of compound **1** alone (30 μM) and complete inhibition in combination with **IcatC**$_{BI-9740}$.

inhibitor in the cell-based assay. In this study, we aimed to block completely the maturation of proCatC using synthetic, cell-permeable cysteine cathepsin inhibitors and to determine the fate of NSPs in human neutrophilic precursors. Though we recently identified CatL-like proteases (CatF, CatK, CatV) as novel putative proCatC activators *in vitro* [21], herein we failed to detect these proteases in HL-60 cell lysates or supernatants. This agrees well with previous studies showing that the CatF gene is not expressed in HL-60 cells or leukocytes [46] while those of CatK and CatV are expressed mainly in osteoclasts [47,48] and in the thymus and testis [49]. CatS (and to a lower extent, CatL) were detected in both HL-60 cells and purified blood neutrophils, emerging as likely candidates to activate proCatC. CatL was detected as a ~ 32-kDa mature single chain (i.e. not processed into two mature 23-kDa chains) in HL-60 cells, much like it is found in fibroblasts [50] and bone marrow dendritic cells [51]. The wide-spectrum cysteine protease inhibitor, **E64d**, only partially altered proCatS and proCatL processing in HL-60 cells, indicating that activation of these two proteases obeys a non-specific proteolytic mechanism.

When we incubated HL-60 cells with **IcatS**$_{\#54}$, the processing and maturation of proCatC were strongly altered and corresponded with the accumulation of a truncated proCatC fragment. This confirmed the prominent role of CatS, and fully agrees with data obtained using another nitrile inhibitor, **IcatS**$_{RO-11}$, which is structurally unrelated to **IcatS**$_{\#54}$ [44,52]. Noteworthy is that a residual CatC activity of about 5 % (vs that of control cells) was still present despite the complete inhibition of CatS by either **IcatS**$_{\#54}$ or **IcatS**$_{\#RO-11}$. More importantly, PR3

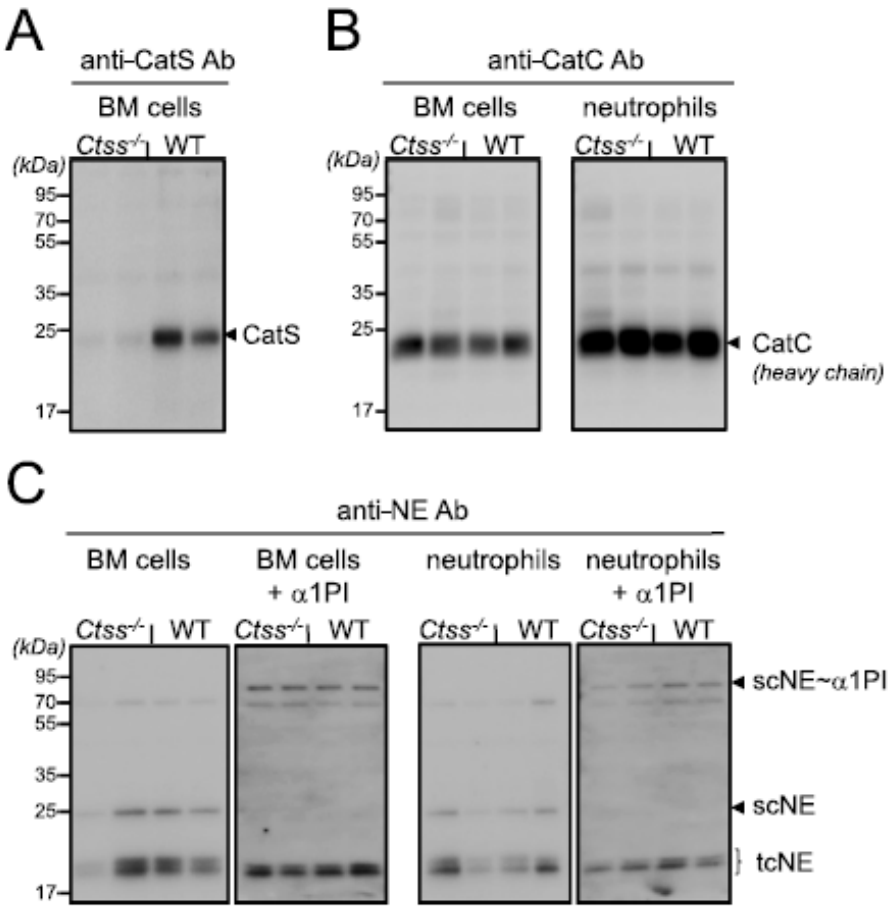


**Fig. 10.** Activation of CatC and NSPs in *Ctss*$^{-/-}$ C57BL/6 mice. A) Western blot analysis of WT and *Ctss*$^{-/-}$ bone marrow (BM) cell lysates using anti-CatS antibodies. B) Western blot analysis of bone marrow cells and blood neutrophils lysates using anti-CatC antibodies. Presence of mature immunoreactive CatC as revealed by the ~ 20-kDa heavy chain in *Ctss*$^{-/-}$ mice indicates that CatS is not required in proCatC maturation. C) Western blot analysis of bone marrow cells and blood neutrophils lysates incubated with or without human α1PI using anti-NE antibodies. The *de novo* formation of irreversible α1PI-scNE complexes of about 80-kDa reveals that NE is proteolytically active despite the absence of CatS. NE produced by murine neutrophils may be present in a cleaved (two-chains (tc)) and uncleaved (single chain (sc)) [64]. Similar results were obtained in three independent experiments.

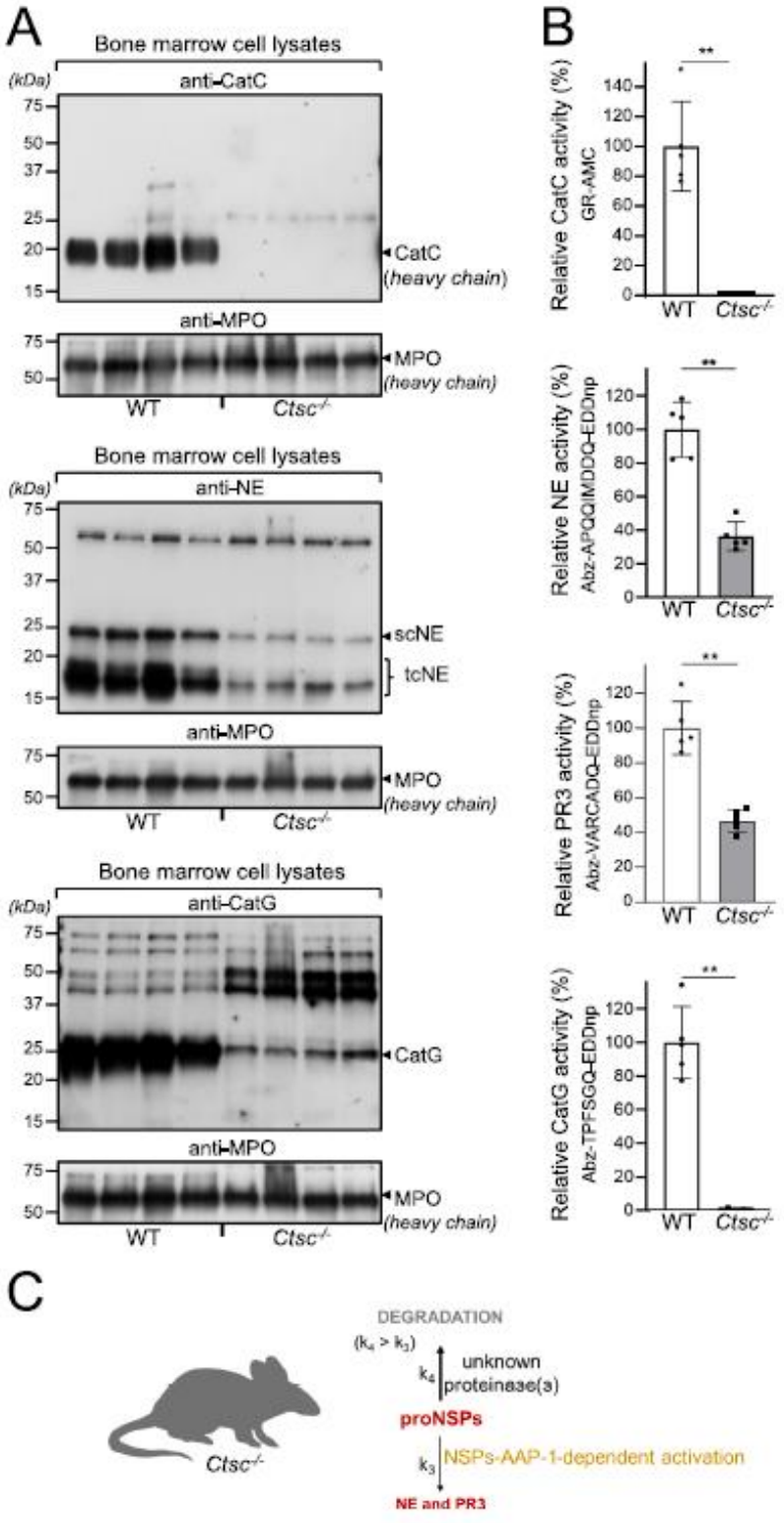


**Fig. 11.** Activation of NSPs in *Ctsc*$^{-/-}$ C57BL/6 mice. A) Western blot analysis of bone marrow cell lysates using antiCatC, antiNE and antiCatG antibodies. Significantly reduced level of immunoreactive NE and CatG in *Ctsc*$^{-/-}$ mice bone marrow lysates compared with WT shows the elimination of NSP zymogens in absence of CatC (n = 4 animals). sc: single chain/tc: two chains (upper and lower bands). Myeloperoxidase (MPO) served as control for protein content. B) Residual activity of CatC, NE, PR3 and CatG in *Ctsc*$^{-/-}$ mice bone marrow lysates. Proteolytic activities were measured using fluorogenic substrates. Monitored selective NE, PR3 and CatG activities indicates the activation of NSPs in absence of CatC. The histograms show the mean ± SD of CatC (n = 5 animals) and NSP activities (n = 5 animals), each done in duplicates. Statistical analysis of the data was performed using a nonparametric test (Mann Whitney test), $^{**}p < 0.01$. C) Consequences of CatC depletion in *Ctsc*$^{-/-}$ mice on the fate of proNSPs. Activation and degradation pathways of proNSPs identified in PLS patients are conserved in CatC deficient mice.

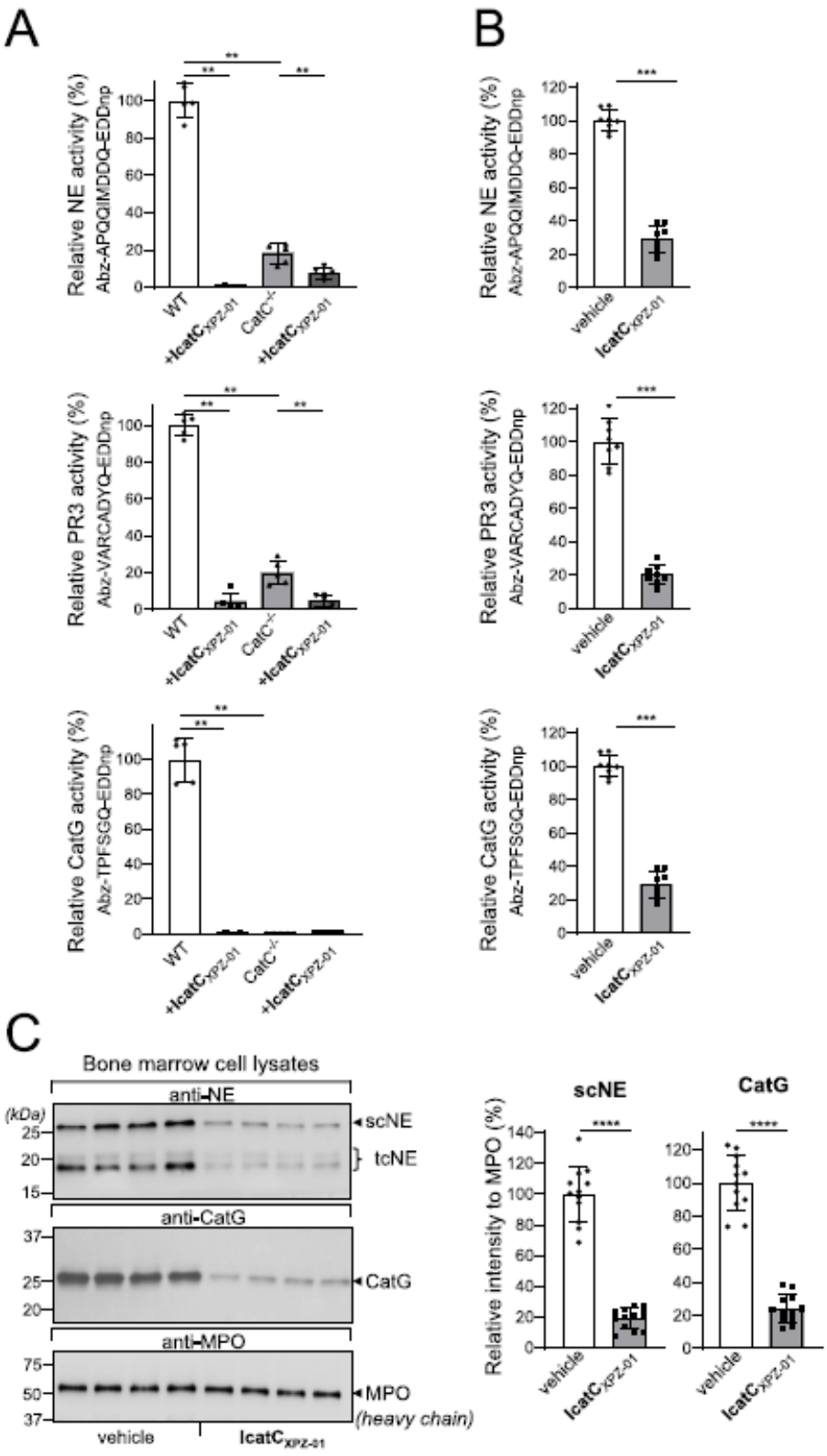


*(caption on next page)*

**Fig. 12.** Murine NSPs activation in presence of **IcatC**$_{XPZ-01}$ in cellular assay *in vitro* and *in vivo*. A) Residual activity of NSPs in murine neutrophils differentiated from WT or *Ctsc*$^{-/-}$ mice bone marrow progenitors in the presence of **IcatC**$_{XPZ-01}$ *in vitro*. Almost total inhibition of NSP proteolytic activities measured using selective FRET substrates were observed. The histograms show the mean ± SD in 5 independent experiments each done in duplicates. Statistical analysis of the data was performed using a nonparametric test (Mann Whitney test), $^{**}p < 0.01$. B) Consequences of prolonged **IcatC**$_{XPZ-01}$ administration into WT mice on NSPs activation. Residual activity of NSPs in bone marrow cell lysates were measured as in A. The histograms show the mean ± SD in 5 independent experiments each done in duplicates. Statistical analysis of the data was performed using a nonparametric test (Mann Whitney test), $^{**}p < 0.01$, $^{***}p < 0.001$. C) Western blot analysis of bone marrow cell lysates using antiNE and antiCatG antibodies. Significantly reduced level of immunoreactive NE and CatG in **IcatC**$_{XPZ-01}$ treated mice bone marrow lysates compared with vehicle treated control mice shows the elimination of NSP zymogens (n = 4 animals). Band intensities were normalized to myeloperoxidase (MPO) as loading control. The histograms show the mean ± SD of 12 independent experiments. Statistical analysis of the data was performed using a nonparametric test (Mann Whitney test), $^{****}p < 0.0001$. sc: single chain/tc: two chains (upper and lower bands).

and CatG (chosen here as representative NSPs) remained fully active.

This raises the question of whether the residual CatC activity observed when CatS is inhibited is sufficient to fully activate NSPs, or whether other protease(s) might compensate for the low level of CatC activity. In this regard, **IcatS**$_{\#54}$ is a reversible inhibitor that could well spare a low level of active CatS, hardly detectable kinetically but sufficient to explain the partial CatC activation. It could also be that CatL, which is present in low amounts in HL-60 cells and is not inhibited by **IcatS**$_{\#54}$, is responsible for this activation. We succeeded in fully blocking proCatC maturation using cell-permeable cysteine protease inhibitors that target both CatS and CatL (compounds **1**–**4**). However, we found again that PR3 and CatG remained almost fully active. Thus, HL-60 cells contain at least one additional protease that can activate proPR3 and proCatG. We and others observed that in neutrophils from PLS patients who totally lack CatC, strongly reduced but still detectable active PR3/NE (0.5 % to 10 % versus healthy controls), and active CatG (<1% versus healthy controls) [19,22] were present. These data strongly suggest the existence of an unknown alternative protease(s) involved in proNSP activation. A CatC-like protease with such a profile, which we termed NSPs-AAP-1, is a cysteine protease inhibited by reversible nitrile inhibitors of CatC, but not by irreversible ones. Interestingly, this proteolytic activity is inhibited by **IcatC**$_{XPZ-01}$ since we observed no significant activation of proPR3 or proCatG when supplementing compounds **1**–**4** with **IcatC**$_{XPZ-01}$. However, whether this inhibition results from a direct or an indirect blockade of this protease by alteration of the maturation process remains to be investigated. In a previous study, we observed that the pharmacological inhibition of CatC with **IcatC**$_{XPZ-01}$ or **IcatC**$_{BI-9740}$ in a stem cell model reduced membrane-bound PR3 more than a CatC loss-of-function mutation [19,26]. In view of the current data, the stronger membrane-bound PR3 reduction achieved with **IcatC**$_{XPZ-01}$ or **IcatC**$_{BI-9740}$ could be explained by the inhibition of NSPs-AAP-1.

Cell-permeable CatC inhibitors blocked the activation of proNSPs in neutrophils differentiated from progenitor cells *in vitro* [19,26,39]. As an alternative approach to the traditional targeting of CatC's active site, we used cell-permeable inhibitors (**IcatS**$_{\#54}$ or compound **1**) targeting proCatC activation during the differentiation of human in CD34$^{+}$ progenitor cells into neutrophils. This almost totally abrogated proCatC maturation and was accompanied by a significant reduction in cellular NSP content and proteolytic activities (~70 %), as opposed to the expected ~ 90 % reduction in NSP activities observed in PLS neutrophils [19,22]. In this regard, it is possible that *in vitro* differentiation of neutrophils may not fully recapitulate the processes occurring in the human bone marrow. For instance, the duration of promyelocytic stage or the

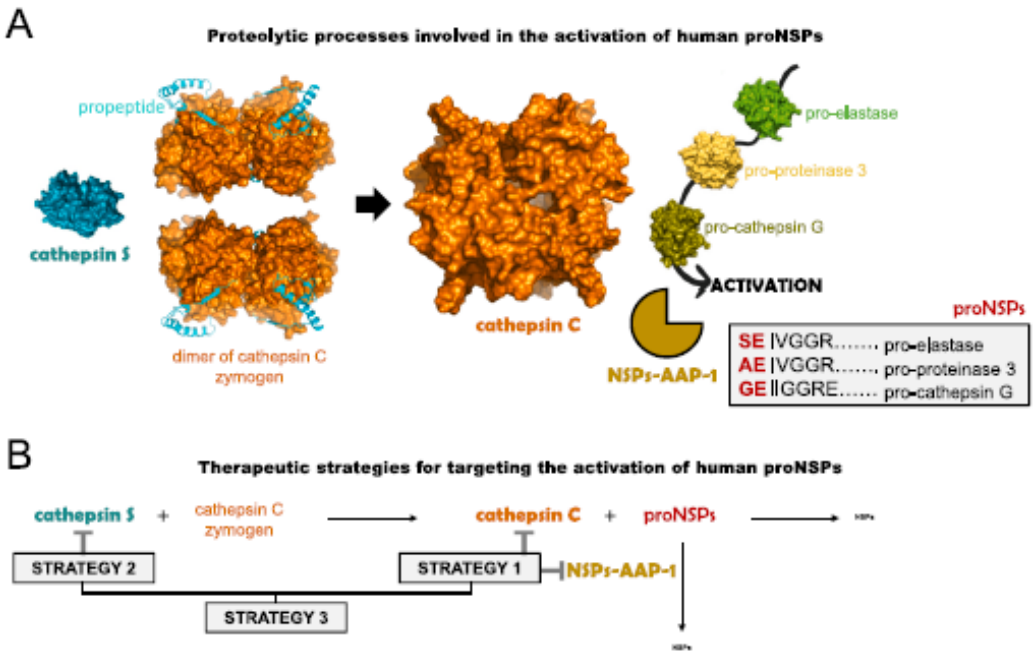


**Fig. 13.** Activation of proNSPs during human neutrophil differentiation. A) NSPs are synthetized in myeloblasts/promyelocytes stages of neutrophil differentiation as inactive zymogens containing a N-terminal dipropeptide in the bone marrow. Our study focusing on proteolytic pathways involved in the activation of proNSPs shows that CatS is the major protease executing proCatC maturation and NSPs-AAP-1 is an additional cysteine protease catalyzing the activation of NSPs. B) New data from the study describing in detail the proteolytic pathways implicated in the activation of proNSPs are important for the design of novel therapeutic approaches. Nitrile inhibitors which are able to inhibit CatC and NSPs-AAP-1 could better inhibit the activation of proNSPs (*therapeutic strategy 1*). CatS, a potent elastinolytic enzyme like NSPs, is a druggable major proCatC converting protease which could be targeted to prevent tissue damages in chronic inflammatory diseases. Inhibition of CatS and by consequence NSPs could be an efficient strategy to neutralize elastinolytic enzymes (*therapeutic strategy 2*). The blockade of proNSPs activation by the combination of a CatC inhibitor with a CatS inhibitor might help to improve control of tissue damage (*therapeutic strategy 3*).

expression/intracellular amounts of NSPs-AAP-1 could differ. The inability of *in vitro* differentiated human neutrophils to generate NETs also suggests that functional differences must exist [53]. Be that as it may, the combination of either **IcatS**$_{\#54}$ with **IcatC**$_{XPZ\text{-}01}$, or of compound **1** with **IcatC**$_{BI\text{-}9740}$, resulted in an almost total inhibition of NSP activity and protein levels; this inhibition of NSPs-AAP-1 also took place without affecting cell differentiation. Thus, from a developmental and clinical viewpoint, nitrile type inhibitors of CatC such as **IcatC**$_{XPZ\text{-}01}$ and **IcatC**$_{BI\text{-}9740}$, which display a dual activity against both CatC and NSPs-AAP-1, could be considered superior to CatC inhibitors which do not affect NSPs-AAP-1 (therapeutic strategy 1) (Fig. 13). Furthermore, our study established a new strategy to inhibit NSPs (therapeutic strategy 2) by blocking the CatC-dependent NSP activation through CatS inhibition. Finally, the combined pharmacological inhibition of CatS and CatC/NSPs-AAP-1 could provide an even more efficient inhibition of NSPs (therapeutic strategy 3), which would be particularly useful in eliminating membrane-bound PR3 in conditions like granulomatosis with polyangiitis.

CatS, which is expressed in a wide variety of immune cells, is a potent elastinolytic and collagenolytic cysteine protease that retains its enzymatic activity at neutral pH, highlighting its involvement in both intra- and extracellular proteolysis. Previous work has shown that CatS is involved in the pathogenesis of several inflammatory lung diseases including chronic obstructive pulmonary disease (COPD) and cystic fibrosis [54–57]. Increased levels of CatS in patient samples correlate significantly with a decline in lung function and increased pulmonary neutrophilic infiltration [58]. Thus, pharmacological inactivation of both CatS and NSP activities (using CatS and CatC/NSPs-AAP-1 inhibitors) could more efficiently counter tissue damage in respiratory diseases. In support of this view, pharmacological inhibition or genetic depletion of CatS in mice were found to reduce inflammation and lung injury in respiratory disease models [59]. Similar observations were made in NE-deficient or in NSP triple knock-out mice [60]. To better interpret the consequences of CatS inactivation in murine disease models, we investigated its involvement in the activation of murine proNSPs. Identification of active CatC and NE (as a representative NSP) in bone marrow and blood neutrophil extracts from CatS-deficient mice showed that CatS was not essential for the activation of proNSPs in mice. Collectively, the above data support an inflammatory role for CatS itself in mouse models, insofar as it does not only rely on NSP activities. Whence the added benefit of targeting CatS in a more comprehensive anti-inflammatory therapeutic approach.

In humans we identified a CatC-independent NSP activation pathway that is catalyzed by NSPs-AAP-1. This cysteine protease could be a direct proNSP activator, like CatC, or involved in proteolytic pathways resulting in the activation of NSPs. Our *Ctsc*$^{-/-}$ mice data suggested that an NSPs-AAP-like enzyme was also present in mice and contributed significantly to the activation of NE and PR3 (30–40 %), but not to that of CatG, during neutrophil differentiation in the bone marrow. In blood neutrophils from PLS patients, CatG is similarly much less activated (<1% versus healthy individuals) compared to NE and PR3 (<10 % versus healthy controls) [19,22]. In this regard, the glycine at P2 position in the N-terminal propeptide (Fig. 13), which is conserved in human and murine proCatG, could delay the processing and activation during neutrophil differentiation in the bone marrow. Moreover, we speculate that NSPs-AAP-1 plays a role in the activation human and murine NSP4 as the two-residue propeptides of NSP4 zymogens do not contain a glycine. In this study, we indeed observed that human and murine NSPs-AAPs were unable to cleave the fluorogenic CatC substrate, Gly-Phe-AMC, which features a glycine at P2 position. Furthermore, mouse NSPs-AAPs-1 was inhibited using **IcatC**$_{XPZ\text{-}01}$ during *in vitro* differentiation of CatC-deficient neutrophils, resulting in the loss of NSP activation. Since both human and mouse NSPs-AAPs were inhibited by **IcatC**$_{XPZ\text{-}01}$, they must be largely conserved homologs. Neutrophils from CatC-deficient mice are reported to generate significantly fewer NETs than those of WT neutrophils [53], which suggests an antimicrobial role for CatC and NSPs in health, but also raises the possibility that these proteases might contribute to chronic inflammation, given the role of NETs therein. And indeed, CatC-deficient mice are protected against experimentally induced neutrophil-mediated diseases [13]. This also reveals that the alternative proNSP activation pathway driven by NSPs-AAP-1, which generates 30–40 % of active NSPs, is insufficient to sustain neutrophil-driven diseases in CatC-deficient mice. This again illustrates the therapeutic benefit of targeting all proteases acting upstream of NSPs, including NSPs-AAP-1, CatC, and CatS.

In conclusion, we showed herein that CatS, a potent elastinolytic enzyme that has been identified as a therapeutic target in chronic inflammation-associated tissue injury, is the physiologic converting protease of human neutrophilic proCatC. Pharmacological targeting of CatS using potent, cell-permeable inhibitors indeed results in a near-total blockade of proCatC maturation, accompanied by a significant inactivation and elimination of NSPs. Preventing proNSP maturation by a CatS inhibitor, alone or in combination with a CatC/NSPs-AAP-1 inhibitor, therefore represents a promising therapeutic approach to efficiently control the extent of tissue damage in neutrophil-mediated chronic inflammatory and auto-immune diseases.

## 5. Financial support

This work was supported by the "Ministère de l'enseignement supérieur, de la recherche et de l'innovation (MESRI)", the "Région Centre-Val de Loire" (Project PIRANA). This project has received funding from the *European Union's Horizon 2020 research and innovation programme* under grant agreement No 668036 (RELENT) and from Roche Pharma Research & Early Development, Roche Innovation Center Basel (Switzerland) for cathepsin C inhibition using **RO5461111**. Responsibility for the information and views set out in this study lies entirely with the authors. Ralph Kettritz was supported by grant KE 576/10-1 from the Deutsche Forschungsgemeinschaft.

## CRediT authorship contribution statement

**Roxane Domain:** Conceptualization, Data curation, Formal analysis, Investigation, Validation, Writing – review & editing. **Seda Seren:** Conceptualization, Data curation, Formal analysis, Investigation, Writing – review & editing. **Uwe Jerke:** Data curation, Formal analysis, Investigation, Methodology, Writing – review & editing. **Manousos Makridakis:** Data curation, Formal analysis, Investigation, Methodology. **Kuan-Ju Chen:** Data curation, Formal analysis, Investigation, Methodology, Writing – review & editing. **Jérôme Zoidakis:** Data curation, Formal analysis, Investigation, Methodology, Supervision, Validation. **Moez Rhimi:** Formal analysis, Resources, Writing – review & editing. **Xian Zhang:** Data curation, Formal analysis, Investigation. **Tillia Bonvent:** Data curation, Formal analysis, Investigation. **Cécile Croix:** Data curation, Formal analysis, Investigation. **Loïc Gonzalez:** Data curation, Formal analysis, Investigation. **Dedong Li:** Data curation, Formal analysis, Investigation. **Jessica Basso:** Data curation, Formal analysis, Investigation. **Christophe Paget:** Resources, Validation. **Marie-Claude Viaud-Massuard:** Data curation, Formal analysis, Validation. **Gilles Lalmanach:** Resources, Validation. **Guo-Ping Shi:** Resources, Supervision, Validation. **Ali Aghdassi:** Resources, Validation. **Antonia Vlahou:** Validation, Writing – review & editing. **Patrick P. McDonald:** Validation, Writing – original draft. **Isabelle Couillin:** Investigation, Resources, Writing – review & editing. **Rich Williams:** Resources, Validation. **Ralph Kettritz:** Conceptualization, Validation, Writing – original draft. **Brice Korkmaz:** Conceptualization, Formal analysis, Funding acquisition, Investigation, Resources, Supervision, Validation, Writing – original draft, Writing – review & editing.

## Declaration of competing interest

The authors declare the following financial interests/personal

relationships which may be considered as potential competing interests: Brice Korkmaz has been paid for the time spent as a committee member for advisory boards (Brensocatib Advisory Board (BRAB), INSMED, USA), other forms of consulting (Boehringer Ingelheim (Germany), Neuprozyme Therapeutics Aps (Denmark), Santhera Pharmaceuticals (Switzerland), Chiesi (Italy), Gerson Lehrman Group (GLG) (USA), Slingshot Insights expert network (USA)), symposium organisation (INSMED, Boehringer Ingelheim, Chiesi) and travel support, lectures or presentations, outside the submitted work. Other authors declare no competing financial interests.

## Data availability

Data will be made available on request.

## Acknowledgments

Brice Korkmaz acknowledges the "Alexandre von Humboldt Foundation" (Germany) for a short institutional informative visits grant (2018) and LE STUDIUM Loire Valley Institute for Advanced Studies for Research Consortium grants (2021-2022 and 2024-2025). The authors thank Dr Thibault Chazeirat (INSERM U-1100) for $IC_{50}$ determination, Lise Vanderlynden (INSERM U-1100) for technical assistance, and Dr Aili Lazaar from GlaxoSmithKline Pharmaceuticals for providing GSK2793660.

*Data reference*

List of identified proteins in 6 biological replicates of HL-60 cells. Relative abundance of proteins in each sample are presented in ppm. https://data.mendeley.com/datasets/tw3759s2nd/1

## References

[1] G.L. Burn, A. Foti, G. Marsman, D.F. Patel, A. Zychlinsky, The neutrophil, Immunity 54 (7) (2021) 1377–1391.
[2] B. Korkmaz, M.S. Horwitz, D.E. Jenne, F. Gauthier, Neutrophil elastase, proteinase 3, and cathepsin G as therapeutic targets in human diseases, Pharmacol. Rev. 62 (4) (2010) 726–759.
[3] B. Korkmaz, A. Lesner, C. Guarino, M. Wysocka, C. Kellenberger, H. Watier, U. Specks, F. Gauthier, D.E. Jenne, Inhibitors and antibody fragments as potential anti-inflammatory therapeutics targeting neutrophil proteinase 3 in human disease, Pharmacol. Rev. 68 (3) (2016) 603–630.
[4] D.E. Jenne, A. Kuhl, Production and applications of recombinant proteinase 3, wegener's autoantigen: problems and perspectives, Clin. Nephrol. 66 (3) (2006) 153–159.
[5] D. Turk, V. Janjic, I. Stern, M. Podobnik, D. Lamba, S.W. Dahl, C. Lauritzen, J. Pedersen, V. Turk, B. Turk, Structure of human dipeptidyl peptidase I (cathepsin C): exclusion domain added to an endopeptidase framework creates the machine for activation of granular serine proteases, EMBO J. 20 (23) (2001) 6570–6582.
[6] H.R. Gutmann, J.S. Fruton, On the proteolytic enzymes of animal tissues; an intracellular enzyme related to chymotrypsin, J. Biol. Chem. 174 (3) (1948) 851–858.
[7] V. Turk, V. Stoka, O. Vasiljeva, M. Renko, T. Sun, B. Turk, D. Turk, Cysteine cathepsins: from structure, function and regulation to new frontiers, BBA 1824 (1) (2012) 68–88.
[8] M. Cygler, J.S. Mort, Proregion structure of members of the papain superfamily. Mode of inhibition of enzymatic activity, Biochimie 79 (11) (1997) 645–652.
[9] B. Turk, D. Turk, V. Turk, Lysosomal cysteine proteases: more than scavengers, BBA 1477 (1–2) (2000) 98–111.
[10] M. Fonovic, B. Turk, Cysteine cathepsins and their potential in clinical therapy and biomarker discovery, Proteomics Clin. Appl. 8 (5-6) (2014) 416–426.
[11] M. Fonovic, B. Turk, Cysteine cathepsins and extracellular matrix degradation, BBA 1840 (8) (2014) 2560–2570.
[12] I. Dolenc, B. Turk, G. Pungercic, A. Ritonja, V. Turk, Oligomeric structure and substrate induced inhibition of human cathepsin C, J. Biol. Chem. 270 (37) (1995) 21626–21631.
[13] B. Korkmaz, G.H. Caughey, I. Chapple, F. Gauthier, J. Hirschfeld, D.E. Jenne, R. Kettritz, G. Lalmanach, A.S. Lamort, C. Lauritzen, M. Legowska, A. Lesner, S. Marchand-Adam, S.J. McKaig, C. Moss, J. Pedersen, H. Roberts, A. Schreiber, S. Seren, N.S. Thakker, Therapeutic targeting of cathepsin C: from pathophysiology to treatment, Pharmacol. Ther. 190 (2018) 202–236.
[14] S.W. Dahl, T. Halkier, C. Lauritzen, I. Dolenc, J. Pedersen, V. Turk, B. Turk, Human recombinant pro-dipeptidyl peptidase I (cathepsin C) can be activated by cathepsins L and S but not by autocatalytic processing, Biochemistry 40 (6) (2001) 1671–1678.
[15] Y. Hamon, M. Legowska, V. Herve, S. Dallet-Choisy, S. Marchand-Adam, L. Vanderlynden, M. Demonte, R. Williams, C.J. Scott, M. Si-Tahar, N. Heuze-Vourc'h, G. Lalmanach, D.E. Jenne, A. Lesner, F. Gauthier, B. Korkmaz, Neutrophilic cathepsin C is maturated by a multistep proteolytic process and secreted by activated cells during inflammatory lung diseases, J. Biol. Chem. 291 (16) (2016) 8486–8499.
[16] B. Korkmaz, A. Lesner, S. Letast, Y.K. Mahdi, M.L. Jourdan, S. Dallet-Choisy, S. Marchand-Adam, C. Kellenberger, M.C. Viaud-Massuard, D.E. Jenne, F. Gauthier, Neutrophil proteinase 3 and dipeptidyl peptidase I (cathepsin C) as pharmacological targets in granulomatosis with polyangiitis (wegener granulomatosis), Semin. Immunopathol. 35 (4) (2013) 411–421.
[17] A.M. Adkison, S.Z. Raptis, D.G. Kelley, C.T. Pham, Dipeptidyl peptidase I activates neutrophil-derived serine proteases and regulates the development of acute experimental arthritis, J. Clin. Invest. 109 (3) (2002) 363–371.
[18] C. Toomes, J. James, A.J. Wood, C.L. Wu, D. McCormick, N. Lench, C. Hewitt, L. Moynihan, E. Roberts, C.G. Woods, A. Markham, M. Wong, R. Widmer, K. A. Ghaffar, M. Pemberton, I.R. Hussein, S.A. Temtamy, R. Davies, A.P. Read, P. Sloan, M.J. Dixon, N.S. Thakker, Loss-of-function mutations in the cathepsin C gene result in periodontal disease and palmoplantar keratosis, Nat. Genet. 23 (4) (1999) 421–424.
[19] S. Seren, M. Rashed Abouzaid, C. Eulenberg-Gustavus, J. Hirschfeld, H. Nasr Soliman, U. Jerke, K. N'Guessan, S. Dallet-Choisy, A. Lesner, C. Lauritzen, B. Schacher, P. Eickholz, N. Nagy, M. Szell, C. Croix, M.C. Viaud-Massuard, A. Al Farraj Aldosari, S. Ragunatha, M. Ibrahim Mostafa, F. Giampieri, M. Battino, H. Cornillier, G. Lorette, J.L. Stephan, C. Goizet, J. Pedersen, F. Gauthier, D. E. Jenne, S. Marchand-Adam, I.L. Chapple, R. Kettritz, B. Korkmaz, Consequences of cathepsin C inactivation for membrane exposure of proteinase 3, the target antigen in autoimmune vasculitis, J. Biol. Chem. 293 (32) (2018) 12415–12428.
[20] Y. Hamon, M. Legowska, P. Fergelot, S. Dallet-Choisy, L. Newell, L. Vanderlynden, A. Kord Valeshabad, K. Acrich, H. Kord, T. Charalampos, F. Morice-Picard, I. Surplice, J. Zoidakis, K. David, A. Vlahou, S. Ragunatha, N. Nagy, K. Farkas, M. Szell, C. Goizet, B. Schacher, M. Battino, A. Al Farraj Aldosari, X. Wang, Y. Liu, S. Marchand-Adam, A. Lesner, E. Kara, S. Korkmaz-Icoz, C. Moss, P. Eickholz, A. Taieb, S. Kavukcu, D.E. Jenne, F. Gauthier, B. Korkmaz, Analysis of urinary cathepsin C for diagnosing papillon-lefevre syndrome, FEBS J. 283 (3) (2016) 498–509.
[21] A.S. Lamort, Y. Hamon, C. Czaplewski, A. Gieldon, S. Seren, L. Coquet, F. Lecaille, A. Lesner, G. Lalmanach, F. Gauthier, D. Jenne, B. Korkmaz, Processing and maturation of cathepsin C zymogen: a biochemical and molecular modeling analysis, Int. J. Mol. Sci. 20 (19) (2019).
[22] C.T. Pham, J.L. Ivanovich, S.Z. Raptis, B. Zehnbauer, T.J. Ley, Papillon-Lefevre syndrome: correlating the molecular, cellular, and clinical consequences of cathepsin C/dipeptidyl peptidase I deficiency in humans, J. Immunol. 173 (12) (2004) 7277–7281.
[23] D. Guay, C. Beaulieu, M.D. Percival, Therapeutic utility and medicinal chemistry of cathepsin C inhibitors, Curr. Top. Med. Chem. 10 (7) (2010) 708–716.
[24] N. Methot, J. Rubin, D. Guay, C. Beaulieu, D. Ethier, T.J. Reddy, D. Riendeau, M. D. Percival, Inhibition of the activation of multiple serine proteases with a cathepsin C inhibitor requires sustained exposure to prevent pro-enzyme processing, J. Biol. Chem. 282 (29) (2007) 20836–20846.
[25] B. Korkmaz, A. Lesner, M. Wysocka, A. Gieldon, M. Hakansson, F. Gauthier, D. T. Logan, D.E. Jenne, C. Lauritzen, J. Pedersen, Structure-based design and in vivo anti-arthritic activity evaluation of a potent dipeptidyl cyclopropyl nitrile inhibitor of cathepsin C, Biochem. Pharmacol. 164 (2019) 349–367.
[26] U. Jerke, C. Eulenberg-Gustavus, A. Rousselle, P. Nicklin, S. Kreideweiss, M. A. Grundl, P. Eickholz, K. Nickles, A. Schreiber, B. Korkmaz, R. Kettritz, Targeting cathepsin C in PR3-ANCA Vasculitis, J. Am. Soc. Nephrol. 33 (5) (2022) 936–947.
[27] S. Kreideweiss, G. Schanzle, G. Schnapp, V. Vintonyak, M.A. Grundl, BI 1291583: a novel selective inhibitor of cathepsin C with superior in vivo profile for the treatment of bronchiectasis, Inflamm. Res. (2023).
[28] K. Doyle, H. Lonn, H. Kack, A. Van de Poel, S. Swallow, P. Gardiner, S. Connolly, J. Root, C. Wikell, G. Dahl, K. Stenvall, P. Johannesson, Discovery of second generation reversible covalent DPP1 inhibitors leading to an oxazepane amidoacetonitrile based clinical candidate (AZD7986), J. Med. Chem. 59 (20) (2016) 9457–9472.
[29] D. Cipolla, J. Zhang, B. Korkmaz, J.D. Chalmers, J. Basso, D. Lasala, C. Fernandez, A. Teper, K.C. Mange, W.R. Perkins, E.J. Sullivan, Dipeptidyl peptidase-1 inhibition with brensocatib reduces the activity of all major neutrophil serine proteases in patients with bronchiectasis: results from the WILLOW trial, Respir. Res. 24 (1) (2023) 133.
[30] X. Chen, Y. Yan, Z. Zhang, F. Zhang, M. Liu, L. Du, H. Zhang, X. Shen, D. Zhao, J. B. Shi, X. Liu, Discovery and in vivo anti-inflammatory activity evaluation of a novel non-peptidyl non-covalent cathepsin C inhibitor, J. Med. Chem. 64 (16) (2021) 11857–11885.
[31] P. Szczesniak, M. Pieczykolan, S. Stecko, The synthesis of alpha, alpha-disubstituted alpha-amino acids via Ichikawa rearrangement, J. Org. Chem. 81 (3) (2016) 1057–1074.
[32] W. Hou, H. Sun, Y. Ma, C. Liu, Z. Zhang, Identification and optimization of novel cathepsin C inhibitors derived from EGFR inhibitors, J. Med. Chem. 62 (12) (2019) 5901–5919.
[33] K.J. Chen, J. Zhang, D. LaSala, J. Basso, D. Chun, Y. Zhou, P.P. McDonald, W. R. Perkins, D.C. Cipolla, Brensocatib, an oral, reversible inhibitor of dipeptidyl peptidase 1, mitigates interferon-alpha-accelerated lupus nephritis in mice, Front. Immunol. 14 (2023) 1185727.
[34] J.D. Chalmers, A. Gupta, S.H. Chotirmall, A. Armstrong, P. Eickholz, N. Hasegawa, P.J. McShane, A.E. O'Donnell, M. Shteinberg, H. Watz, A. Eleftheraki,

C. Diefenbach, W. Sauter, A phase 2 randomised study to establish efficacy, safety and dosing of a novel oral cathepsin C inhibitor, BI 1291583, in adults with bronchiectasis: airleaf, ERJ Open Res 9 (3) (2023).
[35] J.D. Chalmers, R. Kettritz, B. Korkmaz, Dipeptidyl peptidase 1 inhibition as a potential therapeutic approach in neutrophil-mediated inflammatory disease, Front. Immunol. 14 (2023) 1239151.
[36] B. Korkmaz, S. Attucci, M.A. Juliano, T. Kalupov, M.L. Jourdan, L. Juliano, F. Gauthier, Measuring elastase, proteinase 3 and cathepsin G activities at the surface of human neutrophils with fluorescence resonance energy transfer substrates, Nat. Protoc. 3 (6) (2008) 991–1000.
[37] B. Korkmaz, S. Attucci, E. Hazouard, M. Ferrandiere, M.L. Jourdan, M. Brillard-Bourdet, L. Juliano, F. Gauthier, Discriminating between the activities of human neutrophil elastase and proteinase 3 using serpin-derived fluorogenic substrates, J. Biol. Chem. 277 (42) (2002) 39074–39081.
[38] S. Attucci, B. Korkmaz, L. Juliano, E. Hazouard, C. Gïrardin, M. Brillard-Bourdet, S. Rehault, P. Anthonioz, F. Gauthier, Measurement of free and membrane-bound cathepsin G in human neutrophils using new sensitive fluorogenic substrates, Biochem. J. 366 (Pt 3) (2002) 965–970.
[39] C. Guarino, Y. Hamon, C. Croix, A.S. Lamort, S. Dallet-Choisy, S. Marchand-Adam, A. Lesner, T. Baranek, M.C. Viaud-Massuard, C. Lauritzen, J. Pedersen, N. Heuze-Vourc'h, M. Si-Tahar, E. Firatli, D.E. Jenne, F. Gauthier, M.S. Horwitz, N. Borregaard, B. Korkmaz, Prolonged pharmacological inhibition of cathepsin C results in elimination of neutrophil serine proteases, Biochem. Pharmacol. 131 (2017) 52–67.
[40] A. Gollner, M. Koster, P. Nicklin, T. Trieselmann, E. Klein, J. Vlach, C. Heine, M. Grundl, J. Ramharter, D. Wyatt, M. Chaturvedi, A. Ciulli, K.C. Carter, S. Muller, D. Bischoff, P. Ettmayer, E. Haaksma, J. Mack, D. McConnell, D. Stenkamp, H. Weinstabl, M. Zentgraf, C.R. Wood, F. Montel, opnMe.com: a digital initiative for sharing tools with the biomedical research community, Nat. Rev. Drug Discov. 21 (7) (2022) 475–476.
[41] J.R. Wisniewski, A. Zougman, N. Nagaraj, M. Mann, Universal sample preparation method for proteome analysis, Nat. Methods 6 (5) (2009) 359–362.
[42] P.E. Nikolaou, N. Mylonas, M. Makridakis, M. Makrecka-Kuka, A. Iliou, S. Zerikiotis, P. Efentakis, S. Kampoukos, N. Kostomitsopoulos, R. Vilskersts, I. Ikonomidis, V. Lambadiari, C.J. Zuurbier, A. Latosinska, A. Vlahou, G. Dimitriadis, E.K. Iliodromitis, I. Andreadou, Cardioprotection by selective SGLT-2 inhibitors in a non-diabetic mouse model of myocardial ischemia/reperfusion injury: a class or a drug effect? Basic Res. Cardiol. 117 (1) (2022) 27.
[43] **J. Zoidakis, List of identified proteins in 6 biological replicates of HL-60 cells. Relative abundance of proteins in each sample are presented in ppm, 2023.**
[44] K.V. Rupanagudi, O.P. Kulkarni, J. Lichtnekert, M.N. Darisipudi, S.R. Mulay, B. Schott, S. Gruner, W. Haap, G. Hartmann, H.J. Anders, Cathepsin S inhibition suppresses systemic lupus erythematosus and lupus nephritis because cathepsin S is essential for MHC class II-mediated CD4 T cell and B cell priming, Ann. Rheum. Dis. 74 (2) (2015) 452–463.
[45] J. Inoue, M. Nakamura, Y.S. Cui, Y. Sakai, O. Sakai, J.R. Hill, K.K. Wang, P. W. Yuen, Structure-activity relationship study and drug profile of N-(4-fluorophenylsulfonyl)-L-valyl-L-leucinal (SJA6017) as a potent calpain inhibitor, J. Med. Chem. 46 (5) (2003) 868–871.
[46] I. Santamaria, G. Velasco, A.M. Pendas, A. Paz, C. Lopez-Otin, Molecular cloning and structural and functional characterization of human cathepsin F, a new cysteine proteinase of the papain family with a long propeptide domain, J. Biol. Chem. 274 (20) (1999) 13800–13809.
[47] D. Bromme, K. Okamoto, Human cathepsin O2, a novel cysteine protease highly expressed in osteoclastomas and ovary molecular cloning, sequencing and tissue distribution, Bio. Chem. Hoppe-Seyler 376 (6) (1995) 379–384.
[48] B.D. Gelb, G.P. Shi, M. Heller, S. Weremowicz, C. Morton, R.J. Desnick, H. A. Chapman, Structure and chromosomal assignment of the human cathepsin K gene, Genomics 41 (2) (1997) 258–262.
[49] D. Bromme, Z. Li, M. Barnes, E. Mehler, Human cathepsin V functional expression, tissue distribution, electrostatic surface potential, enzymatic characterization, and chromosomal localization, Biochemistry 38 (8) (1999) 2377–2385.
[50] S. Gal, M.C. Willingham, M.M. Gottesman, Processing and lysosomal localization of a glycoprotein whose secretion is transformation stimulated, J. Cell Biol. 100 (2) (1985) 535–544.
[51] R. Maehr, H.C. Hang, J.D. Mintern, Y.M. Kim, A. Cuvillier, M. Nishimura, K. Yamada, K. Shirahama-Noda, I. Hara-Nishimura, H.L. Ploegh, Asparagine endopeptidase is not essential for class II MHC antigen presentation but is required for processing of cathepsin L in mice, J. Immunol. 174 (11) (2005) 7066–7074.
[52] S. Kumar Vr, M.N. Darisipudi, S. Steiger, S.K. Devarapu, M. Tato, O.P. Kukarni, S. R. Mulay, D. Thomasova, B. Popper, J. Demleitner, G. Zuchtriegel, C. Reichel, C. D. Cohen, M.T. Lindenmeyer, H. Liapis, S. Moll, E. Reid, A.W. Stitt, B. Schott, S. Gruner, W. Haap, M. Ebeling, G. Hartmann, H.J. Anders, Cathepsin S cleavage of protease-activated Receptor-2 on endothelial cells promotes microvascular diabetes complications, J Am Soc Nephrol 27 (6) (2016) 1635–1649.
[53] H. Yan, H.F. Zhou, A. Akk, Y. Hu, L.E. Springer, T.L. Ennis, C.T.N. Pham, Neutrophil proteases promote experimental abdominal aortic aneurysm via extracellular trap release and plasmacytoid dendritic cell activation, Arterioscler. Thromb. Vasc. Biol. 36 (8) (2016) 1660–1669.
[54] R. Brown, S. Nath, A. Lora, G. Samaha, Z. Elgamal, R. Kaiser, C. Taggart, S. Weldon, P. Geraghty, Cathepsin S: investigating an old player in lung disease pathogenesis, comorbidities, and potential therapeutics, Respir. Res. 21 (1) (2020) 111.
[55] M.C. McKelvey, S. Weldon, D.F. McAuley, M.A. Mall, C.C. Taggart, Targeting proteases in cystic fibrosis lung disease. Paradigms, progress, and potential, Am J Respir Crit Care Med 201 (2) (2020) 141–147.
[56] R. Brown, D.M. Small, D.F. Doherty, L. Holsinger, R. Booth, R. Williams, R. J. Ingram, J.S. Elborn, M.A. Mall, C.C. Taggart, S. Weldon, Therapeutic inhibition of cathepsin S reduces inflammation and mucus plugging in adult betaENaC-tg mice, Mediators Inflamm. 2021 (2021) 6682657.
[57] D.F. Doherty, S. Nath, J. Poon, R.F. Foronjy, M. Ohlmeyer, A.J. Dabo, M. Salathe, M. Birrell, M. Belvisi, N. Baumlin, M.D. Kim, S. Weldon, C. Taggart, P. Geraghty, Protein phosphatase 2A reduces cigarette smoke-induced cathepsin S and loss of lung function, Am. J. Respir. Crit. Care Med. 200 (1) (2019) 51–62.
[58] S. Weldon, P. McNally, D.F. McAuley, I.K. Oglesby, C.L. Wohlford-Lenane, J. A. Bartlett, C.J. Scott, N.G. McElvaney, C.M. Greene, P.B. McCray Jr., C.C. Taggart, miR-31 dysregulation in cystic fibrosis airways contributes to increased pulmonary cathepsin S production, Am. J. Respir. Crit. Care Med. 190 (2) (2014) 165–174.
[59] T. Zheng, M.J. Kang, K. Crothers, Z. Zhu, W. Liu, C.G. Lee, L.A. Rabach, H. A. Chapman, R.J. Homer, D. Aldous, G.T. De Sanctis, S. Underwood, M. Graupe, R. A. Flavell, J.A. Schmidt, J.A. Elias, Role of cathepsin S-dependent epithelial cell apoptosis in IFN-gamma-induced alveolar remodeling and pulmonary emphysema, J. Immunol. 174 (12) (2005) 8106–8115.
[60] N. Guyot, J. Wartelle, L. Malleret, A.A. Todorov, G. Devouassoux, Y. Pacheco, D. E. Jenne, A. Belaaouaj, Unopposed cathepsin G, neutrophil elastase, and proteinase 3 cause severe lung damage and emphysema, Am. J. Pathol. 184 (8) (2014) 2197–2210.
[61] R.W. Mason, G.D. Green, A.J. Barrett, Human liver cathepsin L, Biochem. J. 226 (1) (1985) 233–241.
[62] J. Sage, F. Mallevre, F. Barbarin-Costes, S.A. Samsonov, J.P. Gehrcke, M. T. Pisabarro, E. Perrier, S. Schnebert, A. Roget, T. Livache, C. Nizard, G. Lalmanach, F. Lecaille, Binding of chondroitin 4-sulfate to cathepsin S regulates its enzymatic activity, Biochemistry 52 (37) (2013) 6487–6498.
[63] Z. Tber, M. Wartenberg, J.E. Jacques, V. Roy, F. Lecaille, D. Warszycki, A. J. Bojarski, G. Lalmanach, L.A. Agrofoglio, Selective inhibition of human cathepsin S by 2,4,6-trisubstituted 1,3,5-triazine analogs, Bioorg. Med. Chem. 26 (14) (2018) 4310–4319.
[64] T. Dau, R.S. Sarker, A.O. Yildirim, O. Eickelberg, D.E. Jenne, Autoprocessing of neutrophil elastase near its active site reduces the efficiency of natural and synthetic elastase inhibitors, Nat. Commun. 6 (2015) 6722.

# Manuscrit 2

## Activation of neutrophil elastase-related serine proteases in myelomonocytic cells

Roxane Domain[1,2], Thibault Chazeirat[1,2§], Quentin Guilbert[1,2§], Lise Vanderlynden[1,2], Patrick P. McDonald[5], Rich Williams[4] and Brice Korkmaz[1,2*]

**Introduction** : L'élastase neutrophilique (NE), la protéinase 3 (PR3), la cathepsine G (CatG) et la NSP4 sont des protéases à sérine du neutrophile (PSN) que l'on trouve dans les granules des promyélocytes au cours de la différenciation des neutrophiles dans la moelle osseuse. La grande majorité des PSN sont activées par la cathepsine C (CatC) et, dans une moindre mesure, par la NSPs-AAP-1 (NSP-Alternative Activating Protease-1). Le monocyte, précurseur du macrophage, exprime les PSN, mais en quantités largement moindres comparées au neutrophile.

L'objectif de ce travail consistait à i) identifier la protéase(s) de conversion de type CatL-Like impliquée dans la maturation de la proCatC dans des lignées cellulaires pro-monocytaires (U937, THP-1) et dans des macrophages dérivés de monocytes et ii) étudier les conséquences de l'inhibition pharmacologique de la maturation de la proCatC sur l'activation des PSN dans ces cellules.

**Résultats** : Nous avons identifié la CatS comme la protéase de conversion majeure impliquée dans la maturation de la proCatC dans les cellules U937. Dans ces cellules, nous avons observé une activation des PSN impliquant la CatC et la NSPs-AAP-1 comme observée dans les neutrophiles. Dans les cellules THP-1, la NE et la PR3 ont été générées par la CatC et une protéase alternative inconnue différente de la NSPs-AAP-1 que nous avons appelé la NSPs-AAP-2, tandis que la CatG a été activée par la CatC. En outre, nous avons montré que les formes actives de la PR3 et de la CatG n'étaient pas stables et étaient dégradées par protéolyse dans les cellules THP-1, ce qui explique l'expression relativement faible de ces PSN dans cette lignée cellulaire, par rapport à d'autres cellules myélomonocytaires.

**Conclusions** : Notre étude montre que l'activation des PSN dans les cellules myélomonocytaires est dépendante du type cellulaire et, plus important encore, que le génome humain contient au moins trois protéases impliquées dans l'activation des PSN.

# Activation of neutrophil elastase-related serine proteases in myelomonocytic cells

Roxane Domain[1,2], Thibault Chazeirat[1,2§], Quentin Guilbert[1,2§], Lise Vanderlynden[1,2], Patrick P. McDonald[3], Rich Williams[4] and Brice Korkmaz[1,2*]

[1]INSERM UMR-1100, "Research Center for Respiratory Diseases", Tours, France

[2]University of Tours, Tours, France

[3]Université de Sherbrooke, Quebec, Canada

[4]The Patrick G Johnston Centre for Cancer Research, Queen's University, Belfast, UK

[§]Equal contribution

*To whom correspondence should be addressed: Brice Korkmaz, INSERM UMR-1100 "Research Center for Respiratory Diseases" and Université de Tours, Tours, France. Faculty of Medicine, 10 Bld. Tonnellé, 37032, Tours, France; e-mail: brice.korkmaz@inserm.fr; Tel: 0033 2 47 36 63 86

**Abstract**

Elastase, proteinase 3, cathepsin G and NSP4 (Neutrophil Serine Protease 4) are pro-inflammatory serine proteases found within the granules of promyelocytes during neutrophil differentiation in the bone marrow. The vast majority of NSPs are activated by cathepsin C and, to a much lesser degree, by NSPs-AAP-1 (NSP-Alternative Activating Protease-1) from their inactive precursor forms via proteolytic cleavage of their prodipeptides. In this work, we investigated the respective roles of cathepsin C and NSPs-AAP in the activation of NSPs in pro-monocytic cell lines (U937, THP-1) and in primary monocyte-derived macrophages. In U937 cells, we observed a neutrophil-like activation of NSPs involving cathepsin C and NSPs-AAP-1. In THP-1 cells, elastase and proteinase 3 were generated by cathepsin C and a unknown protease called NSPs-AAP-2, while cathepsin G was activated by cathepsin C. Furthermore, we showed that active forms of proteinase 3 and cathepsin G were not stable and proteolytically degraded in THP-1 cells, which explains the relatively low abundance of these NSPs in this cell line, compared to other myelomonocytic cells. In conclusion, our study shows that NSP activation in myelomonocytic cells is cell type-dependent and more importantly, that the human genome contains at least three proteases involved in NSP activation.

## INTRODUCTION

Neutrophil elastase (NE, EC.3.4.21.37), proteinase 3 (PR3, EC.3.4.21.76), cathepsin G (CatG, EC3.4.21.20) and NSP4 (Neutrophil Serine Protease 4) are the four serine proteases produced at the promyelocyte stage of neutrophil differentiation in the bone marrow. Proteolytically active neutrophil serine proteases (NSPs) are localized in cytoplasmic granules of mature neutrophils; they are secreted into the extracellular medium following neutrophil degranulation (1), or within the phagolysosome during phagocytosis. Most NSPs are typically expressed in neutrophils and, to a much lesser degree, in certain monocyte populations (2). NSPs are known to be involved in pathogen killing and to participate in modulating inflammatory processes. NSPs display proteolytic activity against a variety of extracellular matrix proteins. As a result, uncontrolled NSP activation by endogenous protease inhibitors can induce tissue damage, such as that observed in chronic inflammatory diseases (3).

Genes encoding NSPs consist of five exons and four introns (4-6). The NE, PR3 and NSP4 genes are localized on chromosome 19 while the gene encoding CatG is located on chromosome 14. NSPs are synthetized as proteolytically inactive pre-pro-proteases in the endoplasmic reticulum, and feature a N-terminal signal peptide, a prodipeptide, and a C-terminal extension (7). Hematopoietic progenitor cells have been widely used to investigate the conformational and physico-chemical properties of NSPs in relation to their intracellular trafficking (8-10). Processing and removal of the signal peptide leads to generation of a pro-protease (zymogen) containing the N-terminal prodipeptide and the C-terminal extension. NE, PR3 and NSP4 additionally contain two N-glycosylation sites, while CatG contains only one such site. Complex oligosaccharide side chains are formed in the Golgi apparatus. The pro-protease conformation of NSPs keeps the zymogens catalytically inactive without altering their targeting to cytoplasmic granules (11). N-terminal prodipeptides of inactive glycosylated NSP precursors are cleaved by cathepsin C (CatC, also known as dipeptidyl peptidase-1 (DPP-1)) (12) in the trans-side of the Golgi and within cytoplasmic granules. Approximately 60% of unprocessed, proNSPs are secreted by constitute secretion into extracellular medium (7).

CatC is a *ubiquitously expressed* lysosomal amino-peptidase found in cells of the myeloid lineage including neutrophils, monocytes, macrophages, mast cells, and their precursors (13). CatC is initially synthesized as a 55-kDa monomeric single-chain pro-protease. Monomers associate to form proCatC dimers, which undergo proteolytic cleavage at several sites to release internal 10-kDa propeptides and finally associate to form functional tetramers (14). Human

proCatC dimer is processed by CatL-like proteases (CatF, CatK, CatL, CatS and CatV) in two consecutive steps *in vitro (15)*. In human neutrophils, proCatC is mainly maturated by CatS[1]. Loss-of-function mutations of CatC gene in Papillon-Lefèvre syndrome (PLS) patients are associated with severe reduction in the inactivation of NSPs in both neutrophils and monocytes (2,16,17). Unprocessed proNSPs with prodipeptides are normally proteolytically degraded during cell differentiation in the bone marrow (18). In neutrophils from PLS patients however, the loss of CatC activity does not totally prevent proNSP activation as illustrated by the finding that residual proteolytic activities can still be measured (<5% NE and PR3; <1% CatG) (19). A cysteine protease termed NSPs-AAP (NSPs-Alternative Activating Protease), which is conserved in mice, is also involved in the maturation of proNSPs in human neutrophils[2]. Human and mouse NSPs-AAPs can be inhibited using **IcatC$_{XPZ-01}$**, a cell-permeable, reversible dipeptidyl cyclopropyl nitrile inhibitor of CatC in cellular assays[1].

CatC is a potential therapeutic target in several NSP-mediated chronic inflammatory diseases (20). A total blockade of neutrophil CatC activity may be achieved directly using an active-site directed specific inhibitor (20) or by preventing its maturation using a CatS inhibitor. In cells of the monocyte-macrophage lineage however, the picture is less clear. We hypothesized that proteolytic mechanisms involved in the activation of proNSPs in neutrophil precursors are conserved in myelomonocytic cells. For this purpose, we investigated the proteolytic processes generating active CatC and NSPs in various monocyte-macrophage cells.

[1] Domain et al., unpublished
[2] Domain et al., unpublished

## RESULTS

### Activation of NSPs in U937 cells

We first investigated CatC and NSP levels in U937 culture supernatants and cell lysates by Western blot. U937 cells constitutively secreted ~60 kDa proCatC and glycosylated proNSPs (~28 kDa proPR3, ~32 kDa proNE and ~27 kDa proCatG), whereas the cell lysates contained mainly mature proteases, as well as some proNE. In cell lysates, we further analyzed the proteolytic activities of CatC and NE/CatG using selective fluorogenic substrates and found that they are all catalytically active.

The candidate CatL-like proteases acting upon proCatC in U937 cells were identified by immunoblot analysis. As shown in **Figure 1**, cell lysates contained mature CatS, CatL, CatF and CatV. Next, we investigated the effect on CatC maturation of broad-spectrum cysteine protease inhibitors, such as the cell-permeable aldehyde protease inhibitors, *N*-(4-fluorophenylsulfonyl)-$_L$-valyl-$_L$-leucinal (compound **1**, 2S-[[(4-fluorophenyl)sulfonyl]amino]-N-[(1S)-1-formyl-3-methylbutyl]-3-methyl-butanamide (21)), or N-Benzyloxycarbonyl-$_L$-leucyl-norleucinal, ($IC_{50}$CatS < 1nM, $IC_{50}$CatL = 1.6 nM); and of the selective CatS inhibitor, **IcatS$_{\#54}$** ((*R*)-N-(4-cyano-1-methylpiperidin-4-yl)-3-((2-fluorobenzyl)sulfonyl)-2-(((*S*)-2,2,2-trifluoro-1-(4-fluorophenyl)ethyl)amino)propenamide. Incubating U937 cells with compound **1**, compound **2** or **IcatS$_{\#54}$** resulted in a near total blockade of proCatC maturation with a matching accumulation of the truncated proCatC fragment, as determined by Western blot. This indicates that CatS is the major protease involved in proCatC maturation in these cells (**Figure 2A**). Accordingly, the proteolytic activity of CatC was almost totally inhibited by **IcatS$_{\#54}$** when monitored using the fluorogenic substrate, Gly-Phe-AMC. The processing and activation of NSPs was also studied using α1-PI in U937 cell lysates. In the absence of mature CatC, NSPs were able to form irreversible complexes with α1-PI and to cleave selective FRET substrates, indicating that CatC was not the unique protease involved in the activation of these proteases in U937 cells (**Figure 2B**).

In HL-60 cells, CatC and a cysteine protease called NSPs-AAP-1 were both implicated in the activation of elastase-related serine proteases. **IcatC$_{XPZ-01}$**, a potent, reversible, cell-permeable nitrile inhibitor (22) was shown to block~95% of CatC activity in HL-60 cells and to almost completely inhibit NSP activation (23). However, the structurally-unrelated, irreversible CatC inhibitor, **GSK-2793660** (**IcatC$_{GSK-60}$**) (24), inhibits CatC but not the NSPs-AAP pathway in HL-60 cells[1]. We therefore hypothesized that NSPs-AAP-dependent

activation of NSPs could similarly occur in U937 cells. For this purpose, we analyzed the NSPs-AAP-dependent activation by selectively blocking CatC-activity with **IcatC$_{XPZ-01}$** or **IcatC$_{GSK-60}$**. As shown in **Figure 3A**, incubating U937 cells with either inhibitor resulted in a total blockade of CatC activity. By contrast, NSP activation was inhibited by **IcatC$_{XPZ-01}$** but not **IcatC$_{GSK-60}$** (**Figure 3A, B**). Furthermore, proPR3 but not proNE/proCatG were degraded (**Figure 3B**).

Thus, we identified CatS as the major proCatC maturating enzyme in U937 cells and showed that both CatC-dependent and -independent pathways are involved in the activation of elastase-related serine protease zymogens.

**Activation of neutrophil serine proteases in THP-1 cells**

U937 cells are of tissue origin, thus at more mature stage, whereas THP-1 cells originate from a blood leukemia origin at less mature stage with immature phenotype (25). To determine whether the above findings could be a general feature of promonocytic cells despite different origins and maturation stages, we next conducted similar experiments in the THP-1 cell line. Investigation of THP-1 cell lysates revealed very low amounts of active NSPs (**Suppl. Figure 4**, in preparation) which failed to cleave selective FRET substrates. THP-1 cells secreted highly glycosylated proNSPs (~31 kDa proPR3, ~35 kDa and 37 kDa proNE, ~31 kDa proCatG), which were detectable after 24 h of cell culture in the supernatants (**Supp. Figure 4**, in preparation). Thus, THP-1 cells differ from U937 cells regarding CatC and NSP abundance, distribution, and activity.

In THP-1 cells, CatS and CatL were identified as candidate cysteine proteases for processing proCatC, as determined by immunoblot. Accordingly, incubating THP-1 cells with compound **1** or compound **2** resulted in significant blockade of proCatC maturation (65.8± 8.7% of CatC activity with compound **1** and 79.6±12.1% with compound **2**) with a matching accumulation of the truncated proCatC fragment, as determined by Western blot (**Figure 4A**). The selective CatS inhibitor, **IcatS$_{\#54}$**, did not alter the maturation of proCatC. Unexpectedly, when we measured NSP proteolytic activities in cells treated with compound **1** or compound **2**, we observed significantly more activities versus control cells (**Figure 4C**). Western blot analysis of cell lysates revealed the apparition of a 24-kDa, low glycosylated, active PR3 in addition to the 28-kDa high glycosylated PR3 zymogens when cells were treated with compound **1** or compound **2** (**Figure 4D**). The 24-kDa low glycosylated active PR3 was not found in cell supernatants, in contrast to the high glycosylated PR3 zymogens. Inhibition of

proteolytic enzymes using compound **1** or compound **2** may account for the appearance of undegraded 24-kDa low glycosylated active PR3. Similar results were obtained for *NE and* CatG (**Figure 4D**).

We then investigated NSP activation in the presence of **IcatC$_{GSK-60}$** or **IcatC$_{XPZ-01}$**. Both inhibitors totally blocked CatC activity in THP-1 cells (**Figure 5A**). Incubating cells with **IcatC$_{GSK-60}$** or **IcatC$_{XPZ-01}$** did not block the activation of PR3 and NE as they were able to form irreversible complexes with exogenous α1-PI (**Figure 5B**). The activation of CatG was blocked in the presence of **IcatC$_{GSK-60}$** or **IcatC$_{XPZ-01}$**. Furthermore, we observed the apparition of undegraded 24-kDa low glycosylated active PR3 and 27-kDa low glycosylated pro-CatG in **IcatC$_{XPZ-01}$**-treated THP-1 cells (**Figure 5B**).

These results established that CatC is the unique protease involved in the activation of CatG while a CatC/NSPs-AAP-independent pathway particiates in the activation of PR3 and NE zymogens in THP-1 cells. This unknown protease was called NSPs-AAP-2.

## EXPERIMENTAL PROCEDURES

***Materials***- *Substrates*: Gly-Phe-AMC (#AMC-033) was from MP Biomedicals (Illkirch, France), ABZ-VAD(nor)VADYQ-EDDnp (26,27), ABZ-APQQIMDDQ-EDDnp (26,27), ABZ-TPFSGQ-EDDnp (28) were from GeneCust (Boynes, France). *Inhibitors*: compound **1** (calpain inhibitor VI, *N*-(4-fluorophenylsulfonyl)-$_L$-valyl-$_L$-leucinal)) (sc-293979); compound **2** (calpeptin, *N*-benzyloxycarbonyl-$_L$-leucyl-norleucinal) (sc-202516) were from Santa Cruz Biotechnology (Heidelberg Germany). **IcatC$_{XPZ-01}$** was synthetized in (18). **IcatC$_{GSK-60}$** was generously provided by Dr Aili Lazara from GSK laboratory (Brentford, UK). (L)-Thi-(L)-Phe-CN was generously provided by Dr Adam Lesner (University of Gdansk/Poland), Bt-PYDA$^P$(O-$C_6H_4$-4-Cl)$_2$ was synthetized as in (49). Alpha-1-antitrypsin (16-16-011609) and alpha-1-Antichymotrypsin (16-16-012400) were from Athens Research & Technology (Athens, Georgia, USA). *Purified proteases*: mature human CatC was from Unizyme Laboratories (Hørsholm, Denmark). Active human PR3 and NE were from Athens Research & Technology (Athens, Georgia, USA). Active Human CatS and CatG were from Millipore (Molsheim, France). *Antibodies*: murine anti-human CatC antibody directed against the heavy chain of CatC (23) (sc-74590) was purchased from Santa Cruz Biotechnology (Heidelberg, Germany). Goat anti-human CatS antibody (AF1183) and goat anti-human CatL (AF952) were purchased from R&D system (Lille, France). Rabbit anti-human PR3 (23) (ab-133613) was

purchased from Abcam (Cambridge, UK). Rabbit anti-human CatG (83578S) and rabbit anti-human NE (63610S) were purchased from Cell Signaling (Beverly, Massachusetts, USA). Murine anti-human GAPDH was purchased from Proteintech (60004-1-IG). Murine anti-human β–actin antibody (A2228), peroxidase-conjugated rabbit anti-goat IgG antibody (A5420) and peroxidase-conjugated sheep anti-mouse IgG antibody (A5906) were purchased from Sigma-Aldrich (Saint-Quentin Fallavier, France). Peroxidase-conjugated goat anti-rabbit IgG (H+L) antibody (Affini pure) was purchased from Jackson ImmunoResearch (Cambridgeshire, UK).

***Inhibition of intracellular proteases-*** U937 cells were cultured in RPMI-1640 medium supplemented with 10% FBS (Fetal Bovine Serum substitute, Fetal+Triple 0.1 µm Sterile Filtered, SERANA®, S-FBSP-EU-015), 50 U/mL penicillin and 50 µg/mL streptomycin at 37°C in a humidified atmosphere containing 5% $CO_2$. THP-1 cells were cultured under the same conditions, except that the culture medium was also supplemented with 50 µM β-2-mercaptoethanol. Continuous inhibition of CatS and C was maintained in cell cultures (starting at 3 x $10^6$ cells) with or without the synthetic inhibitors, compounds **Cp1, Cp2, IcatS$_{\#54}$** (10 µM), I**catC$_{GSK-60}$** (5µM) and **IcatC$_{XPZ-01}$** (10 µM).

Cells were lysed in 50 mM HEPES buffer, 750 mM NaCl, 0.1% Nonidet P-40 (NP-40), pH 7.4. for 5 min under shaking at RT. Soluble fractions were separated from cell debris by centrifugation at 10,000 x g for 20 min. Proteins were assayed using the BCA method, and kinetic assays were conducted using equal protein amounts across samples.

***Measurements of protease activities in cell lysates-*** Proteolytic activities of CatC and NSPs were measured as in (23). Briefly, CatC activity in cell lysates was measured spectrofluorometrically (Spectra Max Gemini EM) at 460 nm with or without the nitrile inhibitor (L)-Thi-(L)-Phe-CN using Gly-Phe-AMC (50 µM final) as substrate in 50 mM sodium acetate, 30 mM NaCl, 1 mM EDTA, 2 mM DTT, pH 5.5 at 37°C. The PR3 activity in cell lysates was measured at 420 nm with or without the PR3 inhibitor Bt-PYDA$^P$(O-$C_6H_4$-4-Cl)$_2$ (1 µM in 50 mM Hepes buffer, 750 mM NaCl, 0.05% NP40, pH 7.4 at 37°C) using Abz-VADnVADYQ-EDDnp (20 µM) as substrate. CatG activity was measured at 420 nm in 50 mM Hepes buffer, 100 mM NaCl, 0.05% NP 40, pH 7.4 at 37°C, in the presence or not of 1 µM antichymotrypsin, using Abz-TPFSGQ-EDDnp (20 µM) as substrate. NE activity was measured at 420 nm with or without the NE inhibitor Epi-HNE-4 (1 µM in 50 mM Hepes buffer,

750 mM NaCl, 0.05% NP40, pH 7.4 at 37°C) using Abz-APQQIMDDQ-EDDnp (20 µM) as substrate.

***Western blotting-*** The total protein concentration in THP-1 and U937 lysates was determined by the BCA assay (Thermo Fisher Scientific, Villebon-sur-Yvette, France), and samples (xx µg/sample ) were separated by SDS-PAGE under reducing conditions and transferred to Hybond-ECL membranes. Free sites were saturated by incubation in PBS, 0.1% Tween-20, 5% fat-free milk for 1 h and the membranes were then incubated overnight at 4°C in PBS, 0.1% Tween, 5% non-fat milk with goat anti-human CatS antibody (diluted 1:1000), murine anti-human CatC antibody directed against the heavy chain of CatC (diluted 1:1000), rabbit anti-human PR3 (23) (diluted 1:1000), rabbit anti-human CatG (diluted 1:1000), rabbit anti-human NE (diluted 1:1000) or goat anti-human CatL (diluted 1:1000). The membranes were washed three times how long? in PBS, 0.1% Tween, and incubated for 90 min with a peroxidase-coupled secondary antibody diluted 1:10000 or 1:5000 in PBS, 0.1% Tween 5% non-fat milk. Il manque la détection (ECL?). For loading control, membranes were stripped with $H_20_2$ 35% for 20 min at 37°C, then incubated with murine anti-human β-actin antibody (diluted 1:1000) in PBS, 0.1% Tween, 5% non-fat milk overnight at 4°C. The membranes were washed three times in PBS, 0.1% Tween, incubated for 1h30 with a peroxidase-coupled secondary antibody diluted 1:5000 in PBS, 0.1% Tween 5% non-fat milk.

**Acknowledgments:** This work was supported by the "*Ministère* de l'*Enseignement Supérieur* et de la Recherche", the "Région Centre-Val de Loire" (Project PIRANA). The authors thank Catherine Girardin Neau (INSERM U-1100) for technical assistance.

**Conflicts of interest:** The authors declare no competing financial interests. Patrick. P. McDonald is also employed as Executive Director, Research at Insmed Inc. Insmed was however not involved in this work; did not fund it; and does not endorse it, implicitly or otherwise.

**Authorship contributions:** Brice Korkmaz supervised the work. Brice Korkmaz and Roxane Domain participated in the research design. Roxane Domain, Thibault Chazeiret, Quentin Guilbert, Lise Vanderlynden conducted the experiments. Brice Korkmaz, Roxane Domain, Patrick P. McDonald, Rich Williams performed data analyses. Brice Korkmaz wrote the manuscript. All authors contributed to the writing and revision of the manuscript.

## REFERENCES


1. Korkmaz, B., Lamort, A. S., Domain, R., Beauvillain, C., Gieldon, A., Yildirim, A. O., Stathopoulos, G. T., Rhimi, M., Jenne, D. E., and Kettritz, R. (2021) Cathepsin C inhibition as a potential treatment strategy in cancer. *Biochem Pharmacol* **194**, 114803
2. Jerke, U., Eulenberg-Gustavus, C., Rousselle, A., Nicklin, P., Kreideweiss, S., Grundl, M. A., Eickholz, P., Nickles, K., Schreiber, A., Korkmaz, B., and Kettritz, R. (2022) Targeting Cathepsin C in PR3-ANCA Vasculitis. *J Am Soc Nephrol* **33**, 936-947
3. Korkmaz, B., Horwitz, M. S., Jenne, D. E., and Gauthier, F. (2010) Neutrophil elastase, proteinase 3, and cathepsin G as therapeutic targets in human diseases. *Pharmacol Rev* **62**, 726-759
4. Zimmer, M., Medcalf, R. L., Fink, T. M., Mattmann, C., Lichter, P., and Jenne, D. E. (1992) Three human elastase-like genes coordinately expressed in the myelomonocyte lineage are organized as a single genetic locus on 19pter. *Proc Natl Acad Sci U S A* **89**, 8215-8219
5. Perera, N. C., Schilling, O., Kittel, H., Back, W., Kremmer, E., and Jenne, D. E. (2012) NSP4, an elastase-related protease in human neutrophils with arginine specificity. *Proc Natl Acad Sci U S A* **109**, 6229-6234
6. Caughey, G. H., Schaumberg, T. H., Zerweck, E. H., Butterfield, J. H., Hanson, R. D., Silverman, G. A., and Ley, T. J. (1993) The human mast cell chymase gene (CMA1): mapping to the cathepsin G/granzyme gene cluster and lineage-restricted expression. *Genomics* **15**, 614-620
7. Gullberg, U., Bengtsson, N., Bulow, E., Garwicz, D., Lindmark, A., and Olsson, I. (1999) Processing and targeting of granule proteins in human neutrophils. *J Immunol Methods* **232**, 201-210
8. Lindmark, A., Gullberg, U., and Olsson, I. (1994) Processing and intracellular transport of cathepsin G and neutrophil elastase in the leukemic myeloid cell line U-937-modulation by brefeldin A, ammonium chloride, and monensin. *J Leukoc Biol* **55**, 50-57
9. Garwicz, D., Lindmark, A., Hellmark, T., Gladh, M., Jogi, J., and Gullberg, U. (1997) Characterization of the processing and granular targeting of human proteinase 3 after transfection to the rat RBL or the murine 32D leukemic cell lines. *J Leukoc Biol* **61**, 113-123
10. Gullberg, U., Lindmark, A., Lindgren, G., Persson, A. M., Nilsson, E., and Olsson, I. (1995) Carboxyl-terminal prodomain-deleted human leukocyte elastase and cathepsin G are efficiently targeted to granules and enzymatically activated in the rat basophilic/mast cell line RBL. *J Biol Chem* **270**, 12912-12918
11. Gullberg, U., Andersson, E., Garwicz, D., Lindmark, A., and Olsson, I. (1997) Biosynthesis, processing and sorting of neutrophil proteins: insight into neutrophil granule development. *Eur J Haematol* **58**, 137-153
12. Pham, C. T., Ivanovich, J. L., Raptis, S. Z., Zehnbauer, B., and Ley, T. J. (2004) Papillon-Lefevre syndrome: correlating the molecular, cellular, and clinical consequences of cathepsin C/dipeptidyl peptidase I deficiency in humans. *J Immunol* **173**, 7277-7281
13. Rao, N. V., Rao, G. V., Marshall, B. C., and Hoidal, J. R. (1996) Biosynthesis and processing of proteinase 3 in U937 cells. Processing pathways are distinct from those of cathepsin G. *J Biol Chem* **271**, 2972-2978
14. Dolenc, I., Turk, B., Pungercic, G., Ritonja, A., and Turk, V. (1995) Oligomeric structure and substrate induced inhibition of human cathepsin C. *J Biol Chem* **270**, 21626-21631

15. Lamort, A. S., Hamon, Y., Czaplewski, C., Gieldon, A., Seren, S., Coquet, L., Lecaille, F., Lesner, A., Lalmanach, G., Gauthier, F., Jenne, D., and Korkmaz, B. (2019) Processing and Maturation of Cathepsin C Zymogen: A Biochemical and Molecular Modeling Analysis. *Int J Mol Sci* **20**
16. Hart, T. C., Hart, P. S., Bowden, D. W., Michalec, M. D., Callison, S. A., Walker, S. J., Zhang, Y., and Firatli, E. (1999) Mutations of the cathepsin C gene are responsible for Papillon-Lefevre syndrome. *J Med Genet* **36**, 881-887
17. Toomes, C., James, J., Wood, A. J., Wu, C. L., McCormick, D., Lench, N., Hewitt, C., Moynihan, L., Roberts, E., Woods, C. G., Markham, A., Wong, M., Widmer, R., Ghaffar, K. A., Pemberton, M., Hussein, I. R., Temtamy, S. A., Davies, R., Read, A. P., Sloan, P., Dixon, M. J., and Thakker, N. S. (1999) Loss-of-function mutations in the cathepsin C gene result in periodontal disease and palmoplantar keratosis. *Nat Genet* **23**, 421-424
18. Guarino, C., Hamon, Y., Croix, C., Lamort, A. S., Dallet-Choisy, S., Marchand-Adam, S., Lesner, A., Baranek, T., Viaud-Massuard, M. C., Lauritzen, C., Pedersen, J., Heuze-Vourc'h, N., Si-Tahar, M., Firatli, E., Jenne, D. E., Gauthier, F., Horwitz, M. S., Borregaard, N., and Korkmaz, B. (2017) Prolonged pharmacological inhibition of cathepsin C results in elimination of neutrophil serine proteases. *Biochem Pharmacol* **131**, 52-67
19. Seren, S., Rashed Abouzaid, M., Eulenberg-Gustavus, C., Hirschfeld, J., Nasr Soliman, H., Jerke, U., N'Guessan, K., Dallet-Choisy, S., Lesner, A., Lauritzen, C., Schacher, B., Eickholz, P., Nagy, N., Szell, M., Croix, C., Viaud-Massuard, M. C., Al Farraj Aldosari, A., Ragunatha, S., Ibrahim Mostafa, M., Giampieri, F., Battino, M., Cornillier, H., Lorette, G., Stephan, J. L., Goizet, C., Pedersen, J., Gauthier, F., Jenne, D. E., Marchand-Adam, S., Chapple, I. L., Kettritz, R., and Korkmaz, B. (2018) Consequences of cathepsin C inactivation for membrane exposure of proteinase 3, the target antigen in autoimmune vasculitis. *J Biol Chem* **293**, 12415-12428
20. Korkmaz, B., Caughey, G. H., Chapple, I., Gauthier, F., Hirschfeld, J., Jenne, D. E., Kettritz, R., Lalmanach, G., Lamort, A. S., Lauritzen, C., Legowska, M., Lesner, A., Marchand-Adam, S., McKaig, S. J., Moss, C., Pedersen, J., Roberts, H., Schreiber, A., Seren, S., and Thakker, N. S. (2018) Therapeutic targeting of cathepsin C: from pathophysiology to treatment. *Pharmacol Ther* **190**, 202-236
21. Inoue, J., Nakamura, M., Cui, Y. S., Sakai, Y., Sakai, O., Hill, J. R., Wang, K. K., and Yuen, P. W. (2003) Structure-activity relationship study and drug profile of N-(4-fluorophenylsulfonyl)-L-valyl-L-leucinal (SJA6017) as a potent calpain inhibitor. *J Med Chem* **46**, 868-871
22. Korkmaz, B., Lesner, A., Wysocka, M., Gieldon, A., Hakansson, M., Gauthier, F., Logan, D. T., Jenne, D. E., Lauritzen, C., and Pedersen, J. (2019) Structure-based design and in vivo anti-arthritic activity evaluation of a potent dipeptidyl cyclopropyl nitrile inhibitor of cathepsin C. *Biochem Pharmacol* **164**, 349-367
23. Hamon, Y., Legowska, M., Herve, V., Dallet-Choisy, S., Marchand-Adam, S., Vanderlynden, L., Demonte, M., Williams, R., Scott, C. J., Si-Tahar, M., Heuze-Vourc'h, N., Lalmanach, G., Jenne, D. E., Lesner, A., Gauthier, F., and Korkmaz, B. (2016) Neutrophilic Cathepsin C Is Maturated by a Multistep Proteolytic Process and Secreted by Activated Cells during Inflammatory Lung Diseases. *The Journal of biological chemistry* **291**, 8486-8499
24. Szczesniak, P., Pieczykolan, M., and Stecko, S. (2016) The Synthesis of alpha,alpha-Disubstituted alpha-Amino Acids via Ichikawa Rearrangement. *J Org Chem* **81**, 1057-1074

25. Akula, S., Lara, S., Olsson, A. K., and Hellman, L. (2022) Quantitative Analysis of the Transcriptome of Two Commonly Used Human Monocytic Cell Lines-THP-1 and Mono Mac 6-Reveals Their Arrest during Early Monocyte/Neutrophil Differentiation. *Int J Mol Sci* **23**
26. Korkmaz, B., Attucci, S., Juliano, M. A., Kalupov, T., Jourdan, M. L., Juliano, L., and Gauthier, F. (2008) Measuring elastase, proteinase 3 and cathepsin G activities at the surface of human neutrophils with fluorescence resonance energy transfer substrates. *Nature protocols* **3**, 991-1000
27. Korkmaz, B., Attucci, S., Hazouard, E., Ferrandiere, M., Jourdan, M. L., Brillard-Bourdet, M., Juliano, L., and Gauthier, F. (2002) Discriminating between the activities of human neutrophil elastase and proteinase 3 using serpin-derived fluorogenic substrates. *J Biol Chem* **277**, 39074-39081
28. Attucci, S., Korkmaz, B., Juliano, L., Hazouard, E., Girardin, C., Brillard-Bourdet, M., Rehault, S., Anthonioz, P., and Gauthier, F. (2002) Measurement of free and membrane-bound cathepsin G in human neutrophils using new sensitive fluorogenic substrates. *Biochem J* **366**, 965-970

**FIGURE LEGENDS**

**FIGURE 1. CatL-like proteases in U-937 and THP-1 cells.** Western blot analysis of U-937 cell lysates (5, 10, 20, 30, 50 and 100 µg of total protein) and THP-1 cell lysates (5, 10, 30, 50 and 100 µg of total protein) using anti-CatS, anti-CatL, anti-CatV, anti-CatF, or anti-CatK antibodies.

**FIGURE 2. Consequences of pharmacological blockade of proCatC maturation on proNSPs activation in U-937 cells.** U-937 cells were cultured for 7 days in the presence of 10 µM compound **1** (Cp**1**), compound **2** (Cp**2**), **IcatS**$_{\#54}$ or after adding DMSO containing buffer alone. **A)** Western-blot analysis of cell lysates using anti-CatC antibody directed against the 23-kDa heavy chain of CatC demonstrating the accumulation of ~35-kDa fragment composed of truncated propeptide, the heavy chain and the light chain in presence of chemical inhibitors. Anti-GAPDH antibody was used as loading control. The percentage of CatC activity in treated cell lysates was determined using Gly-Phe-AMC fluorogenic substrate. **B)** Western blot analysis of cell lysates incubated with or without α1PI using anti-PR3, anti-NE or anti-CatG antibodies. The formation of NSP-α1PI irreversible complexes revealing processed active of NSPs in absence of mature CatC. Similar results were obtained in three independent experiments.

**FIGURE 3. Activation of proNSPs in U-937 cells cultured in the presence of CatC inhibitors IcatC$_{GSK-60}$ or IcatC$_{XPZ-01}$.** U-937 cells were cultured for 7 days in the presence of **IcatC**$_{GSK-60}$ (5µM), **IcatC**$_{XPZ-01}$ (10 µM) or after adding DMSO containing buffer alone. The percentage of CatC, NE and CatG relative activities in treated cell lysates was determined using selective fluorogenic substrates. **B)** Western-blot analysis of cell lysates incubated with or without α1PI using anti-PR3 antibody. The decrease of ~75 kDa irreversible α1PI-PR3 complexes formation and of the free PR3 in presence of **IcatC**$_{XPZ-01}$ revealing unprocessing of PR3 zymogens and elimination of zymogens. Similar results were obtained in three independent experiments.

**FIGURE 4. Processing of proCatC and proNSPs in THP-1 cells cultured in presence of compound 1, compound 2, or IcatS$_{\#54}$ on maturation on proNSPs activation.** THP-1 cells were cultured for 7 days in the presence of 10 µM of compound 1 (Cp**1**), compound **2** (Cp**2**),

**IcatS$_{\#54}$** or after adding DMSO containing buffer alone. **A)** Western-blot analysis of cell lysates using antiCatC antibody directed against the 23-kDa heavy chain of CatC demonstrating the accumulation of ~35-kDa fragment composed of truncated propeptide, the heavy chain and the light chain in presence of Cp**1** and Cp**2**. **B)** The percentage of CatC activity in treated cell lysates was determined using Gly-Phe-AMC fluorogenic substrate. **C)** The percentage of NE, PR3 and CatG relative activities to Cp**1** in treated cell lysates was determined using selective fluorogenic substrates. **D)** Western-blot analysis of cell lysates incubated with or without α1PI using anti-PR3 antibody revealed the apparition of 24-kDa low glycosylated active PR3 in addition to 28-kDa high glycosylated PR3 zymogens in presence of Cp**1** or Cp**2**. 24-kDa low glycosylated active PR3 was not found in cell free supernatants unlike high glycosylated PR3 zymogens which are constitutively secreted.

**FIGURE 5. Activation of proNSPs in THP-1 cells cultured in the presence of CatC inhibitors IcatC$_{GSK-60}$ or IcatC$_{XPZ-01}$.** THP-1 cells were cultured for 7 days in the presence of **IcatC$_{GSK-60}$** (5 µM), **IcatC$_{XPZ-01}$** (10 µM) or after adding DMSO containing buffer alone. **A)** The percentage of CatC activity in treated cell lysates was determined using Gly-Phe-AMC fluorogenic substrate. **B)** Western-blot analysis of cell lysates incubated with or without α1PI using anti-PR3, anti-NE or anti-CatG antibodies. Anti-GAPDH antibody was used as loading control.

**FOOTNOTES**

The abbreviations used are: ABZ, *ortho*-aminobenzoic acid; BCA, bicinchoninic acid; CatC, cathepsin C; CatG; cathepsin G; DMSO, dimethyl sulfoxide; ECL, enhanced *chemiluminescence*; EDDnp, *N*-(2.4-dinitrophenyl)ethylenediamine; FRET, fluorescence resonance energy transfer; HBSS, Hank's balanced salt buffer; NE, neutrophil elastase; NSP; neutrophil serine protease; PBS, phosphate-buffered saline; PLS, Papillon-Lefèvre syndrome; PR3, proteinase 3; PR3$^{m}$, membrane-bound PR3; RT, room temperature; SDS-PAGE, sodium dodecyl sulfate polyacrylamide gel electrophoresis.

**FIGURE 1**

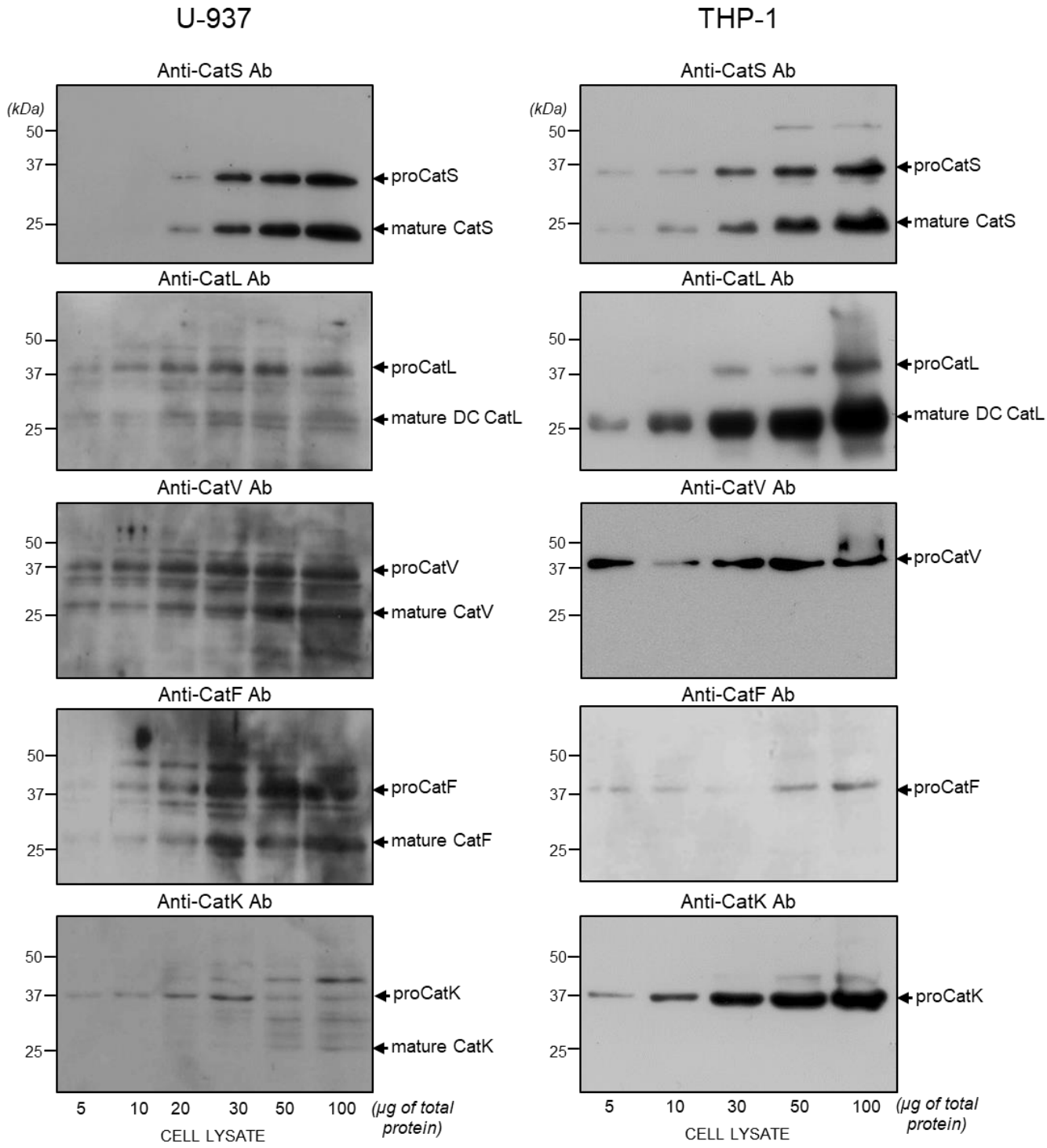
U-937
THP-1
Anti-CatS Ab
(kDa)
50
37
25
proCatS
mature CatS
Anti-CatL Ab
proCatL
mature DC CatL
Anti-CatV Ab
proCatV
mature CatV
Anti-CatF Ab
proCatF
mature CatF
Anti-CatK Ab
proCatK
mature CatK
5
10
20
30
50
100
(µg of total protein)
CELL LYSATE

**FIGURE 2**

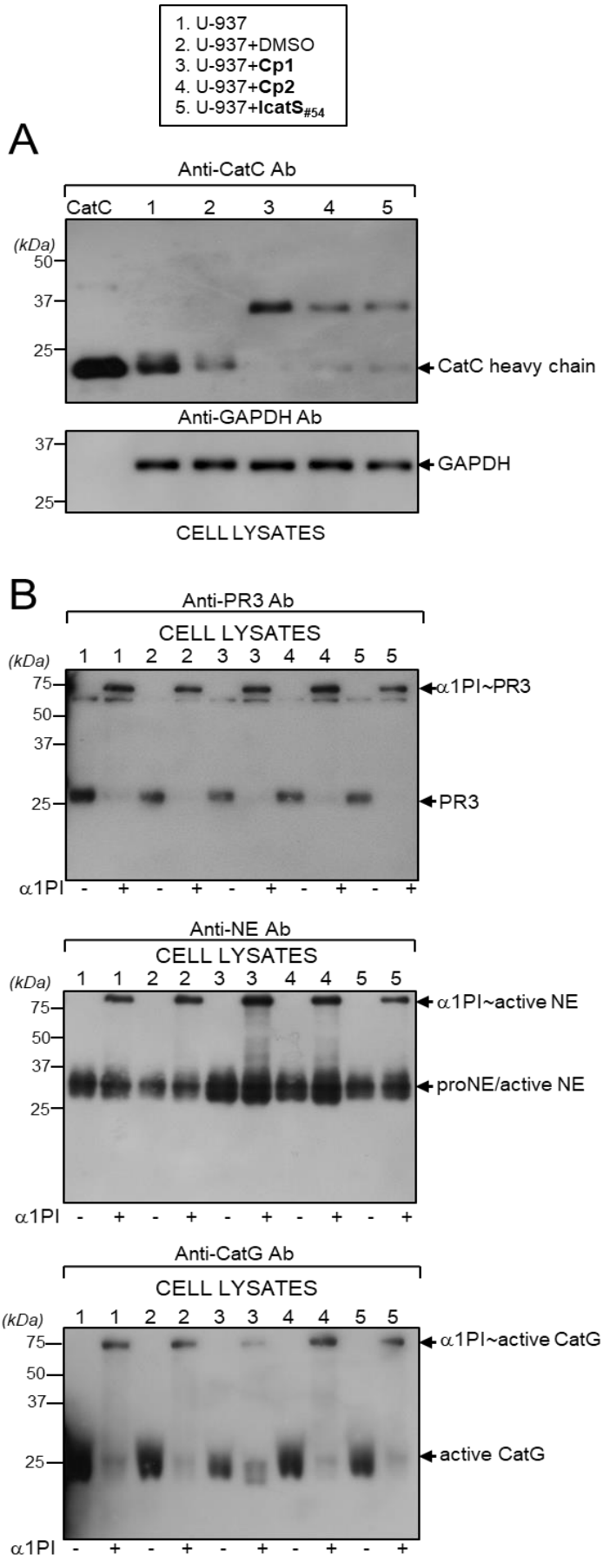
1. U-937
2. U-937+DMSO
3. U-937+Cp1
4. U-937+Cp2
5. U-937+IcatS#54
A
Anti-CatC Ab
CatC 1 2 3 4 5
(kDa)
50
37
25
CatC heavy chain
Anti-GAPDH Ab
37
25
GAPDH
CELL LYSATES
B
Anti-PR3 Ab
CELL LYSATES
(kDa)
1 1 2 2 3 3 4 4 5 5
75
50
37
25
α1PI~PR3
PR3
α1PI - + - + - + - + - +
Anti-NE Ab
CELL LYSATES
(kDa)
1 1 2 2 3 3 4 4 5 5
75
50
37
25
α1PI~active NE
proNE/active NE
α1PI - + - + - + - + - +
Anti-CatG Ab
CELL LYSATES
(kDa)
1 1 2 2 3 3 4 4 5 5
75
50
37
25
α1PI~active CatG
active CatG
α1PI - + - + - + - + - +

**FIGURE 3**

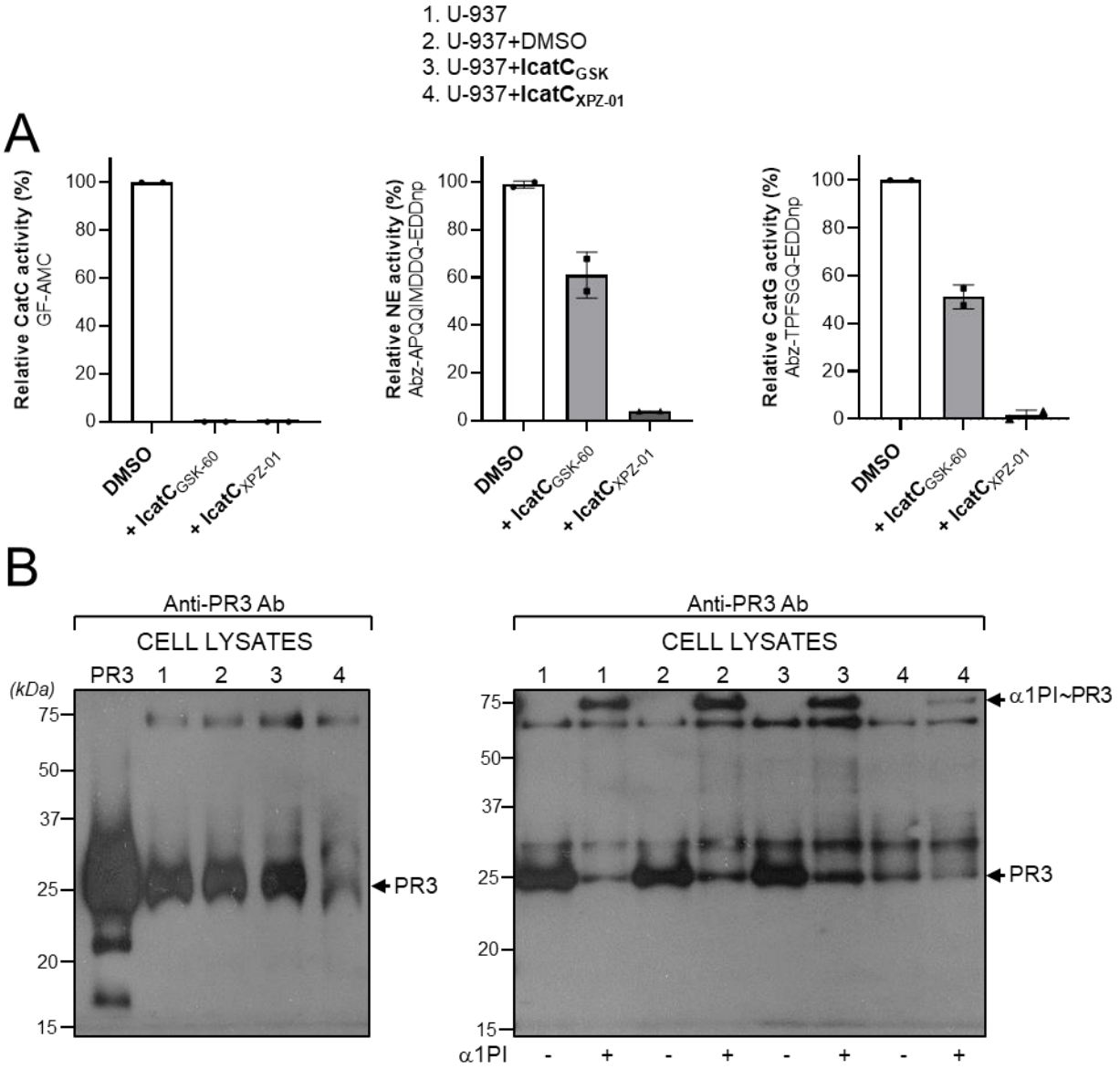
1. U-937
2. U-937+DMSO
3. U-937+IcatC$_{GSK}$
4. U-937+IcatC$_{XPZ-01}$
A
Relative CatC activity (%)
GF-AMC
Relative NE activity (%)
Abz-APQQIMDDQ-EDDnp
Relative CatG activity (%)
Abz-TPFSGQ-EDDnp
100
80
60
40
20
0
DMSO
+ IcatC$_{GSK-60}$
+ IcatC$_{XPZ-01}$
B
Anti-PR3 Ab
CELL LYSATES
PR3 1 2 3 4
(kDa)
75
50
37
25
20
15
PR3
1 1 2 2 3 3 4 4
α1PI~PR3
α1PI - + - + - + - +

**FIGURE 4**

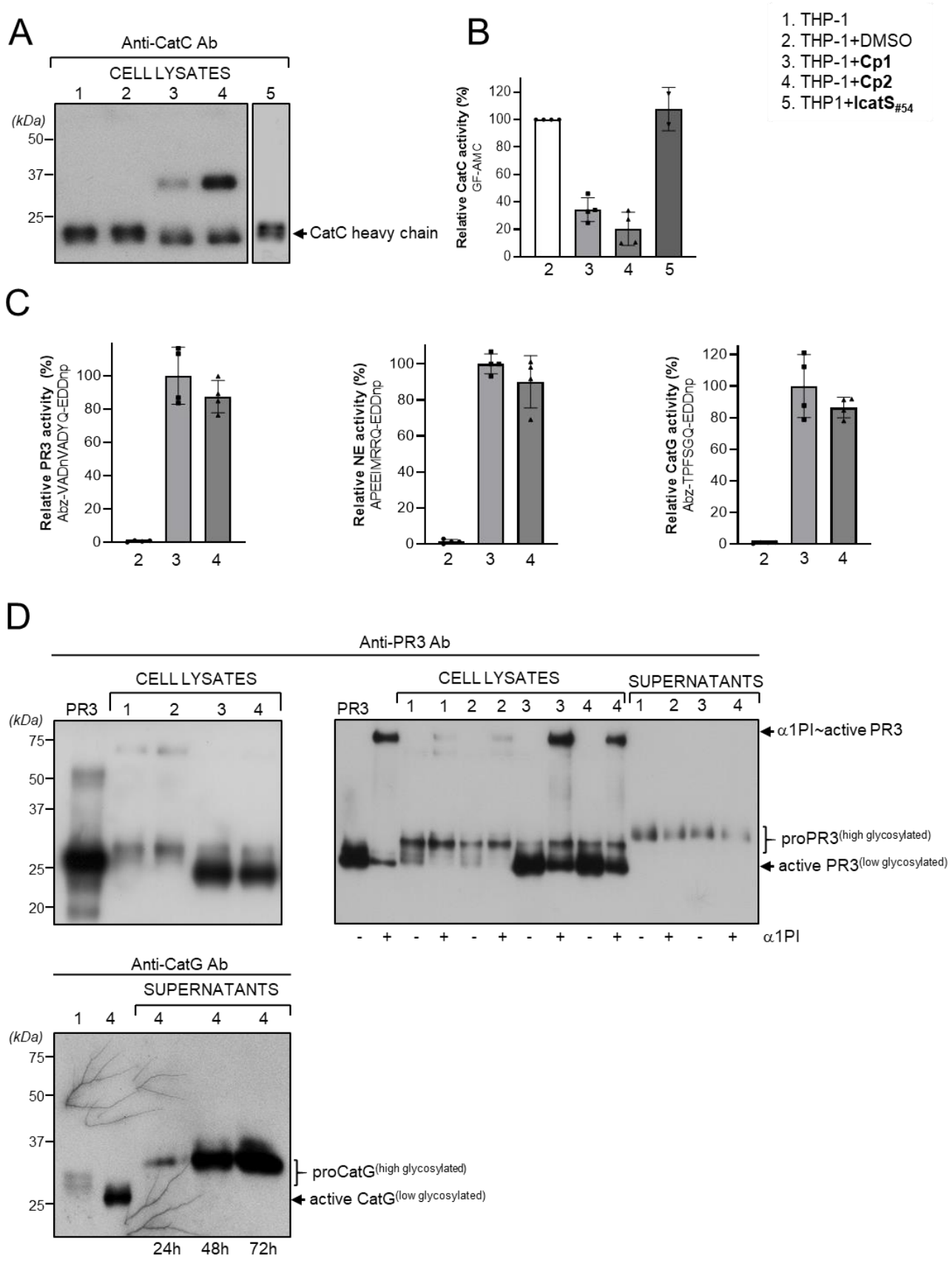
A
Anti-CatC Ab
CELL LYSATES
1 2 3 4 5
(kDa)
50
37
25
CatC heavy chain
B
Relative CatC activity (%)
GF-AMC
120
100
80
60
40
20
0
2 3 4 5
1. THP-1
2. THP-1+DMSO
3. THP-1+Cp1
4. THP-1+Cp2
5. THP1+IcatS#54
C
Relative PR3 activity (%)
Abz-VADnVADYQ-EDDnp
Relative NE activity (%)
APEEIMRRQ-EDDnp
Relative CatG activity (%)
Abz-TPFSGQ-EDDnp
2 3 4
D
Anti-PR3 Ab
CELL LYSATES
SUPERNATANTS
PR3
1 2 3 4
1 1 2 2 3 3 4 4
(kDa)
75
50
37
25
20
α1PI~active PR3
proPR3(high glycosylated)
active PR3(low glycosylated)
- + - + - + - + - + - + - + α1PI
Anti-CatG Ab
SUPERNATANTS
1 4 4 4 4
proCatG(high glycosylated)
active CatG(low glycosylated)
24h 48h 72h

**FIGURE 5**

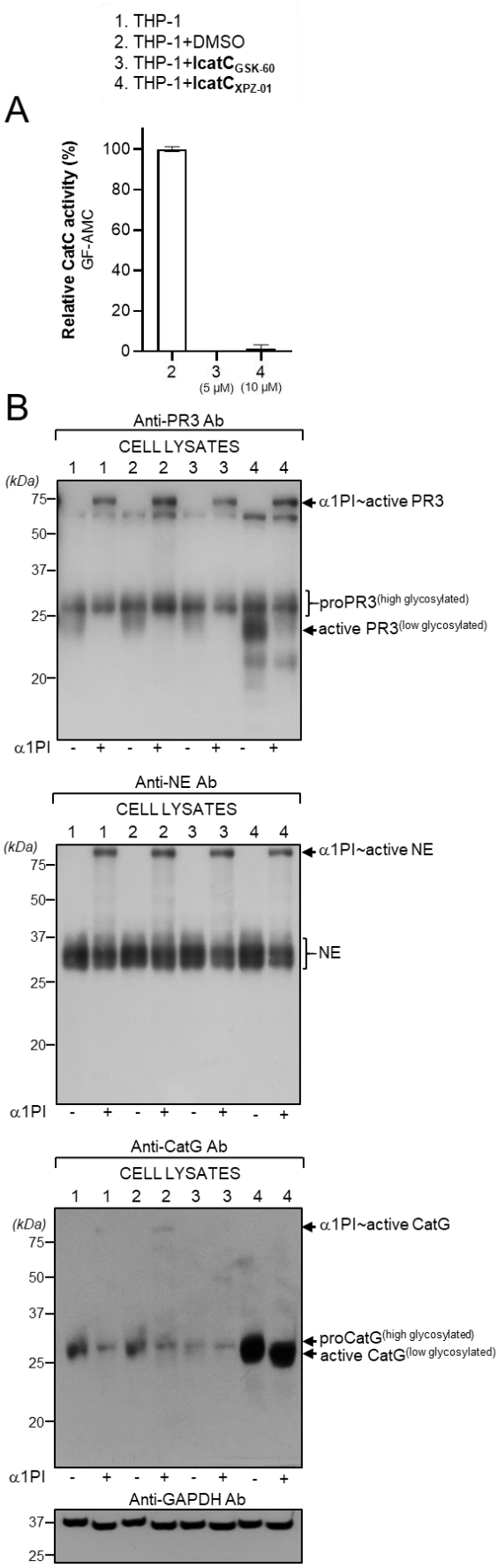
1. THP-1
2. THP-1+DMSO
3. THP-1+IcatC$_{GSK-60}$
4. THP-1+IcatC$_{XPZ-01}$
A
Relative CatC activity (%)
GF-AMC
100
80
60
40
20
0
2
3
4
(5 μM)
(10 μM)
B
Anti-PR3 Ab
CELL LYSATES
1 1 2 2 3 3 4 4
(kDa)
75
50
37
25
20
α1PI~active PR3
proPR3(high glycosylated)
active PR3(low glycosylated)
α1PI - + - + - + - +
Anti-NE Ab
CELL LYSATES
1 1 2 2 3 3 4 4
(kDa)
75
50
37
25
20
α1PI~active NE
NE
α1PI - + - + - + - +
Anti-CatG Ab
CELL LYSATES
1 1 2 2 3 3 4 4
(kDa)
75
50
37
25
20
α1PI~active CatG
proCatG(high glycosylated)
active CatG(low glycosylated)
α1PI - + - + - + - +
Anti-GAPDH Ab
37
25

# Manuscrit 3

## Activation of granzymes in cytotoxic lymphocytes

Roxane Domain[1,2], Loïc Gonzalez[1,2], Jérôme Zoidakis[3], Antonia Vlahou[3], Peter Eickholz[4], Patrick P. McDonald[5], Rich Williams[6], Christophe Paget[1,2] and Brice Korkmaz[1,2*]

**Introduction** : Les granzymes (Gzms) sont des protéases à serine apparentées à l'élastase, présentes dans les lymphocytes cytotoxiques (LC) et impliquées dans l'élimination des cellules infectées par des virus et des cellules cancéreuses. Dans les lymphocytes cytotoxiques, les granzymes sont conservées dans des granules sous leur forme active. Les Gzms sont relarguées avec des perforines, capables de former des pores dans les cellules cibles, ce qui permet aux Gzms de pénétrer dans la cellule et de déclencher la mort cellulaire.

Comme d'autres protéases à serine homologues dérivées des cellules immunitaires, les Gzms sont maturées par la cathepsine C (CatC). En outre, la caractérisation enzymatique des Gzms A et B dans les lymphocytes cytotoxiques de patients atteints du syndrome de Papillon-Lefèvre (SPL) et présentant un déficit en CatC a révélé l'existence d'une voie d'activation indépendante de la CatC. Il existe donc une voie alternative à la CatC permettant l'activation des Gzms. Dans le cas de l'activation des PSN, une voie alternative à la CatC et impliquant une protéase à cystéine appelée la NSP-APP-1 a été mise en évidence dans les neutrophiles.

Au cours de ce travail, dans un premier temps, nous avons identifié les protéases de conversion de la proCatC et dans un deuxième temps nous avons évalué les conséquences du blocage pharmacologique de la maturation de la proCatC sur l'activation des proGzms.

**Résultats :** Des lymphocytes issus de sang de patients SPL et de donneurs sains ont été cultivés pendant 8 jours avec des concentrations élevées en Interleukine-2 afin d'obtenir des cellules activées LAK (Lymphokine Activated Killer Cell) » (cellules LAK). En comparant le protéome des lymphocytes avec celui des cellules LAK, nous avons observé qu'il y a significativement plus de Gzms A et B dans les cellules LAK que dans les lymphocytes. De plus, cela nous a permis d'identifier la CatS et la CatL comme protéases CatL-Like capables de maturer de la CatC dans les lymphocytes. L'activité protéolytique de la CatC dans les lysats de cellules LAK des deux patients atteints du SPL était indétectable confirmant la déficience en CatC. En comparaison, l'activité de la GzmA a été réduite de 49,9 % et l'activité de la GzmB de 66,3 % dans les lysats de cellules LAK des patients. Ces résultats confirment l'existence d'une voie d'activation indépendante de la CatC impliquée dans l'activation des Gzms dans les LC.

Des cellules mononuclées du sang périphérique (PBMC) de donneurs sains ont été cultivées en présence d'IL-2 pendant 2 jours, en présence ou en l'absence d'**E64d**, un inhibiteur de protéase à cystéine à large spectre et perméable aux cellules, afin de déterminer si la proCatC

est convertie en sa forme active par les protéases à cystéine. Le traitement des cellules avec **E64d** a entraîné un blocage presque total de la génération de la chaîne lourde de la CatC et par conséquent une accumulation de la proCatC tronquée, comme l'a montré l'analyse par western blot. En conséquence, l'activité de la CatC a été totalement bloquée dans les cellules traitées avec **E64d**. Nous avons ensuite cherché à identifier des protéases CatL-Like candidates qui pourraient activer la proCatC dans les cellules LAK. Nous avons détecté principalement la CatS et la CatL dans les lysats cellulaires. Une approche protéomique basée sur la spectrométrie de masse a également été utilisée pour analyser le protéome des cellules LAK à la recherche de protéases de type CatL qui pourraient convertir la proCatC. Des PBMC provenant de donneurs sains ont été cultivées en l'absence ou en présence du **composé 1** (2S-[[(4-fluorophényl)sulfonyl]amino]-N-[(1S)-1-formyl-3-méthylbutyl]-3-méthyl-butanamide), qui inhibe à la fois CatS (($IC_{50}$ = < 1nM) et CatL ($IC_{50}$ = 1.6 nM (36)), ou de l'inhibiteur sélectif de la CatS, l'**IcatS$_{\#54}$**. L'activité protéolytique de CatC a été inhibée de 75 % dans les cellules traitées par **le composé 1** et de 60 % dans les cellules traitées par l'**IcatS$_{\#54}$**. L'inhibition maximale de la CatC s'est produite lorsque les cellules ont été traitées avec **le composé 1** et l'inhibiteur sélectif de la CatC, **IcatC$_{XPZ-01}$**. L'incubation des cellules avec des inhibiteurs n'a pas modifié la viabilité ou l'activation des cellules en LAK. Ces résultats suggèrent que CatS et CatL sont toutes deux impliquées dans la maturation de la proCatC.

Pour déterminer si la protéase(s) alternative(s) impliquée(s) dans l'activation des proGzms est une protéase à cystéine, des PBMC de donneurs sains et de patients SPL ont été cultivés avec de l'IL-2, en l'absence ou en présence de l'**IcatC$_{XPZ-01}$** pendant 8 jours. **IcatC$_{XPZ-01}$** a inhibé 49.6 ± 6 % de GzmA et 66,7 ± 9 % de GzmB dans les cellules LAK saines. Les activités granzymes résiduelles des cellules LAK de patients SPL n'ont pas été inhibées. Des résultats similaires ont été obtenus avec l'**E64d**, ce qui indique que la protéase(s) alternative(s) impliquée(s) dans la maturation des Gzms dans les LC n'est pas une protéase(s) à cystéine.

**Conclusion :** La voie alternative de l'activation des Gzms dans les LC est médiée par une protéase résistante aux inhibiteurs de protéase à cystéine. Cette étude suggère que le ciblage pharmacologique de CatC pour bloquer les PSN dans les maladies inflammatoires chroniques ne devrait pas altérer l'activité des LC.

# Activation of granzymes in cytotoxic lymphocytes

Roxane Domain[1,2], Loïc Gonzalez[1,2], Jérôme Zoidakis[3], Antonia Vlahou[3], Peter Eickholz[4], Patrick P. McDonald[5], Rich Williams[6], Christophe Paget[1,2] and Brice Korkmaz[1,2*]

[1]INSERM UMR-1100, "Research Center for Respiratory Diseases", Tours, France

[2]Université de Tours, Tours, France

[3]Biotechnology Division, Biomedical Research Foundation, Academy of Athens, Athens, Greece

[4]Department of Periodontology, Hospital of the Johann-Wolfgang-Goethe University, Frankfurt, Germany

[5]Université de Sherbrooke, Sherbrooke, Québec, Canada

[6]The Patrick G Johnston Centre for Cancer Research, Queen's University, Belfast, UK

*To whom correspondence should be addressed: Brice Korkmaz, INSERM UMR-1100 "Research Center for Respiratory Diseases" and Université de Tours, Tours, France. Faculty of Medicine, 10 Bld. Tonnellé, 37032, Tours, France; e-mail: brice.korkmaz@inserm.fr; Tel: 0033 2 47 36 63 86

## Abstract

Granzymes are elastase-related serine proteases present in cytotoxic lymphocytes and involved in eliminating virus-infected and cancerous cells. Like other related immune cell-derived serine proteases, granzymes are maturated by a cysteine protease called cathepsin C (CatC). In addition, enzymatic characterization of granzymes A and B in cytotoxic lymphocytes from Papillon-Lefèvre syndrome (PLS) patients with CatC deficiency revealed the existence of a CatC-independent processing and activation pathway. This was mediated by a CatC-like protease resistant to inhibition by nitrile CatC inhibitors or by the cysteine protease inhibitor, E64d. This study suggests that pharmacological targeting of CatC to block neutrophil elastase-related serine proteases in chronic inflammatory diseases is unlikely to alter cytotoxic T-cell activity.

## INTRODUCTION

Granzymes (Gzms) constitute a family of serine proteases found in cytotoxic lymphocytes (CLs) – mainly $CD8^+$ T and natural killer (NK) cells, which are known to eliminate virus-infected or transformed cells through their granule cell death pathway. In CLs, pro-apoptotic Gzms are stored in cytotoxic secretory vesicles in a proteolytically active form. Gzms are released together with the pore-forming protein, perforin, which is required for their penetration into the cytosol of *target cells. Once in the cytosol, Gzms initiate cytotoxic cell death by processing their selective substrates (1).*

There exist 5 Gzms (A, B, H, K, and M) in humans whereas mice have 10 Gzms. GzmA and GzmB are the best studied, and cleave their substrates by acting after basic residues (GzmA) or after acidic residues, primarily aspartate (GzmB) (2). All Gzms are produced as zymogens that require the removal of a N-terminal dipropeptide to become fully activated, much like other related immune cell-associated serine proteases such as neutrophil elastase (1,3,4). The dipropeptide, which is largely conserved amongst Gzms, is cleaved by a cysteine protease called cathepsin C (CatC) (1). CatC deficiency in humans causes Papillon-Lefèvre syndrome (PLS), a rare genetic disease characterized by severe early-onset periodontitis and palmoplantar hyperkeratosis (5). Intriguingly, in *vitro* activated lymphocytes from PLS patients contain proteolytically active GzmA and GzmB and can kill target cells with similar efficiency as those from healthy controls (6). Furthermore, lymphocytes from CatC knock-out mice possess reduced (but still detectable) proteolytically active GzmB and kill target cells almost as efficiently as wild-type mice (7). These studies clearly suggest that proteases other than CatC are involved in Gzm maturation (**Figure 1**), and CatH was suspected to be able to activate GzmB zymogen (7,8).

*CatC is not the sole protease executing the activation of elastase-related neutrophil serine proteases (NSPs). In purified blood neutrophils from PLS patients,* low amounts of active NSPs are detected (*<10% vs healthy individuals)*, suggesting the involvement of a CatC-like protease that we termed NSPs-Alternative Activating Protease-1 (NSPs-AAP-1) (**Figure 1**). NSPs-AAP-1 is a cysteine protease that is inhibited by reversible nitrile compounds designed for CatC inhibition, such as **IcatC**$_{\mathbf{XPZ\text{-}01}}$ (Domain et al., unpublished). Moreover, characterization of NSP zymogen activation in monoblastic cell lines highlighted a second alternative NSP-activating protease called NSPs-AAP-2, which is different from NSPs-AAP-1 (Domain et al., unpublished). Investigation of NSPs and granzymes in neutrophils (derived from PLS patients and activated

lymphocytes, respectively) likewise showed the presence of additional proteases involved in zymogen activation, which may or may not include NSPs-AAP-1 and NSPs-AAP-2.

In this study, we investigated proteolytic processes involved in the generation of active GzmA and GrzB in human CLs. Specifically, we studied the maturation of proCatC and proGzms using potent and specific synthetic cell-permeable inhibitors in human lymphokine-activated killer cells (also known as LAK cells).

## RESULTS

- **CatC and granzymes in PLS LAK cells**

When peripheral blood mononuclear cells (PBMCs) from healthy volunteers and from two identified PLS patients with c.755 A4T 5 Q252L and c.947 T4Gn 7 L316Rw mutations were analyzed by flow cytometry, no differences were observed in the relative proportions of T and NK cells (**Figure 2A**). To generate LAK cells, PBMCs were cultured with high-dose recombinant human IL-2 for 8 days. This treatment induced a high enrichment for T cells while NK cell frequency was largely unaffected (**Figure 2A**). Importantly, the proportion of lymphocyte subsets upon culture was similar between healthy donors and PLS patients. is regimen had no specific outcome using PB, the similar proportions of were obtained in healthy donors and PLS patients (**Figure 2A)**.

Analysis of protein expression in cell lysates showed that LAK cells from healthy donors expressed significantly higher amounts of CatC and granzymes than matched purified blood lymphocytes (day 0), as determined by western blot (**Figure 2B)** and by a mass spectrometry-based proteomic approach (**Table 1**). In contrast, western blot analysis revealed the absence of CatC in LAK cell lysates from both PLS patients. Proteolytic activity of CatC in LAK cells lysates of the two PLS patients was likewise undetectable (**Figure 2C**), confirming CatC deficiency and the selectivity of the dipeptidyl substrate. By comparison, GzmA activity (measured using N-benzyloxycarbonyl-L-lysine thiobenzyl ester) was reduced by 49,9 %, and GzmB activity (measured using Ac-IEPD-pNA substrate) by 66,3 %, in LAK cell lysates from the PLS patients. This however did not reflect reduced amounts of immunoreactive granzymes in PLS LAK cell lysates compared to healthy cells (**Figure 2C**).

These results confirmed the existence of a CatC-independent activation pathway involved in Gzm activation in CLs and prompted us to investigate the proteolytic cascades involved in the maturation of pro-CatC and pro-granzymes.

- **Pro-CatC maturation in LAK cells**

Healthy PBMC were cultured in presence of IL-2 for 2 days in the presence or absence of the cell-permeable broad-spectrum cysteine protease inhibitor, **E64d** (100 µM), to determine whether proCatC would be converted into its active form by cysteine proteases. As shown in **Fig 3A/B**, cell treament with **E64d** resulted in an almost total blockade of CatC heavy chain generation and a corresponding accumulation of the truncated proCatC, as determined by western blot analysis. Accordingly, CatC activity measured using a fluorogenic substrate was totally blocked in cells treated with **E64d** (**Figure 3A**). We next sought to identify candidate Cat-L like proteases that could activate proCatC in LAK cells. We detected mainly CatS and CatL in cell lysates (**Supp.Figure 1**). A mass spectrometry-based proteomic approach was also used to analyze the LAK cell proteome for proCatC-converting, CatL-like proteases. 4761 proteins were thusly identified (***Supp.Material***), including CatS and CatL as (**Table 1**). To gain further insight into the matter, PBMCs from healthy donors were cultured in the absence or presence of compound **1** (2S-[[(4-fluorophenyl)sulfonyl]amino]-N-[(1S)-1-formyl-3-methylbutyl]-3-methyl-butanamide), which inhibits both CatS (IC50 <1 nM) and CatL (IC50 = 1.6 nM (36)), or the selective CatS inhibitor, **IcatS**$_{\#54}$. As shown in **Fig X**, CatC proteolytic activity was inhibited by 75% in compound **1**-treated cells and by 60% in **IcatS**$_{\#54}$-treated cells. The maximal inhibition of CatC occurred when cells were treated with compound **1** and the selective CatC inhibitor, **IcatC**$_{XPZ-01}$ (**Figure 3**). Incubation of cells with inhibitors did not alter LAK cell viability or activation (not shown). These results suggest that both CatS and CatL are involved in proCatC maturation.

- **Activation of pro-granzymes in LAK cells**

To determine whether the additional proteases involved in pro-Gzm activation are cysteine proteases, PBMCs from healthy donors and PLS patients were cultured along with IL-2, in the absence or presence of **IcatC**$_{XPZ-01}$ (20 µM) for 8 days. As shown in **Fig XX**, the inhibitor blocked ~40% of GzmA and 60% of GzmB in healthy LAK cells. The remaining granzyme activities were not inhibited in LAK cells from PLS patients. Similar resuts were obtained using **E-64d**, indicating that the additional protease(s) involved in the maturation of granzymes in cytotoxic lymphocytes was not a cysteine protease.

**EXPERIMENTAL PROCEDURES**

**Materials-** *Substrates and inhibitors*: the fluorogenic substrate, Gly-Phe-AMC (#AMC-033) was from MP Biomedicals (Illkirch, France). Chromogenic substrates Ac-Ile-Glu-Pro-Asp-pNA (4030485.0005) and Z-L-Lys-SBzl hydrochloride (C3647) were from Bachem (Bubendorf, Switzerland) and Sigma-Aldrich (Saint-Quentin Fallavier, France), respectively. **E64d** (2*S*,3*S*-trans-(Ethoxycarbonyloxirane-2-carbonyl)-L-leucine-(3-methylbutyl) amide; Aloxistatin) was from MedChemExpress (Sollentuna, Sweden). **Compound 1** (Calpain inhibitor VI, *N*-(4-fluorophenylsulfonyl)-$_{L}$-valyl-$_{L}$-leucinal)) (sc-293979) was from Santa Cruz (Heidelberg, Germany). *Antibodies*: mature human CatC was from Unizyme Laboratories (Hørsholm, Denmark). Murine anti-human CatC antibody directed against the heavy chain of CatC (9) (sc-74590) was purchased from Santa Cruz. Goat anti-human CatS antibody (AF1183) and goat anti-human CatL (AF952) were purchased from R&D systems (Lille, France). Rabbit anti-human Granzyme A antibody (ab209205) and rabbit anti-human Granzyme B antibody (ab243879) were from Abcam (Cambridge, UK). Murine anti-human β–actin antibody (A2228), peroxidase conjugated rabbit anti-goat IgG antibody (A5420) and peroxidase conjugated sheep anti-mouse IgG antibody (A5906) were all from Sigma-Aldrich (Saint-Quentin Fallavier, France). Peroxidase conjugated goat anti-rabbit IgG (H+L) antibody (Affini pure) was from Jackson ImmunoResearch (Cambridgeshire, UK).

**Blood lymphocyte isolation-** Blood from healthy volunteers from the EFS (Etablissement français du sang) and from PLS patients were collected in Vacutainer tubes with EDTA as anticoagulant. Lymphocytes were purified using lymphocyte separation medium d = 1.077 (Eurobio Scientific, CMSMSL01). Briefly, blood was mixed with physiological serum v/v. Lymphocyte separation medium (3 mL) was deposited at the bottom of a xx-ml tube, then 4 ml of blood were overlaid slowly. Tubes were then centrifugated (room temperature, 40 min, 400g). The PBMC rings were then carefully collected and washed twice with HBSS by centrifuging at 160g for 10 min. Some of the cells were directly analyzed by flow cytometry, and the rest was cultured to obtain LAK (Lymphokine Activated Killer) cells.

**LAK cell culture**- Lymphocytes were cultured in high-dose rh IL-2 for 8 days (1000 U/ml rh IL-2; Miltenyi #130-097-748) in RPMI 1640 + GlutaMAX (Gibco #61870-010), 10% FBSS (Fetal Bovine Serum substitute, Fetal+ Triple 0.1 µm sterile-filtered, SERANA #S-FBSP-EU-015), 1% Penicillin-Streptomycin (Gibco #151-40-122) supplemented or not with chemical inhibitors or their diluents. At day 4, medium was changed and fresh inhibitors were added.

LAK cell amplification and non-toxicity of the inhibitors were assessed by flow cytometry. To this end, cells were stained with antibodies against CD45 (APC/Cyanine7 anti-human CD45, BioLegend #368516), CD3 (APC anti-human CD3, BioLegend #317318), NK-p46 (PE anti-human CD335, BD Pharmingen #557991), CD19 (V450 anti-human CD19, BD Horizon #560354) and Live/Dead™ (Invitrogen #L34957).

**Measurement of protease activities in cell lysates-** Cells pellets were lysed in 50 mM HEPES buffer, 750 mM NaCl, 0.1% Nonidet P-40 (NP-40), pH 7.4. Soluble fractions were separated from cell debris by centrifugation at 10,000g for 20 min (température?). Protein concentrations were assayed with a bicinchoninic acid assay (BCA) (Thermo Fisher Scientific, Villebon-sur-Yvette, France). The CatC activity in cell lysates was measured spectrofluorometrically (Spectra Max Gemini EM) at 460 nm with or without the nitrile inhibitor, (L)-Thi-(L)-Phe-CN, using Gly-Phe-AMC (20 µM final) as substrate in 50 mM sodium acetate, 30 mM NaCl, 1 mM EDTA, 2 mM DTT, pH 5.5 at 37°C. Granzyme B activity in cell lysates was measured at 420 nm in 50 mM Hepes buffer, 750 mM NaCl, 0.05% NP40, pH 7.4 at 37°C) using Ac-Ile-Glu-Pro-Asp-pNA as substrate. Granzyme A activity in cell lysates was measured at 420 nm in 50 mM Hepes buffer, 750 mM NaCl, 0.05% NP40, pH 7.4 at 37°C) chromogenic substrate Z-L-Lys-SBzl hydrochloride as substrate.

**Western blotting-** Lymphocytes and LAK cells lysates were separated by SDS-PAGE under reducing conditions and transfered to Hybond-ECL membranes. Free sites were saturated by incubation in Blocking Buffer (PBS with 0.1% Tween-20, 5% fat-free milk) for 1 h and the membranes were then incubated with goat anti-human CatS antibody (diluted 1:1000), murine anti-human CatC antibody directed against the heavy chain of CatC (diluted 1:1000), Granzyme A antibody (diluted 1:1000) and Granzyme B antibody (diluted 1:1000) or goat anti-human CatL (diluted 1:1000), in Blocking Buffer overnight at 4°C. The membranes were washed three times in PBS, 0.1% Tween, and incubated for 90 min with a peroxidase-coupled secondary antibody diluted 1:10000 or 1:5000 in Blocking Buffer. For loading control, membranes were stripped with $H_20_2$ 35% for 20 min at 37°C, then incubated with murine anti-human β–actin antibody (diluted 1:1000) in Blocking Buffer overnight at 4°C. The membranes were washed three times in PBS, 0.1% Tween, and incubated for 90 min with a peroxidase-coupled secondary antibody diluted 1:5000 in Blocking Buffer.

**Proteomics and Bioinformatics analysis of lymphocytes and LAK-** Cell pellets were homogenized, proteins extracted and after digestion with trypsin, peptides were isolated according to the FASP (Filter Aided Sample Preparation) approach (54). Peptides were analyzed on a Q-Exactive HF mass spectrometer and the resulting spectra were deconvoluted with the Proteome Discoverer 1.4 in order to obtain a list of identified proteins with corresponding quantitation data. R-scripts were used to identify differentially expressed proteins with the following criteria: Mann Whitney p-value < 0.05 and ratio > 1.5 or < 0.67. Enrichment analyses were performed in Metascape (55) utilizing the Custom analysis for *Homo sapiens*. The differentially abundant proteins (Mann Whitney p-value < 0.05 and ratio > 1.5 or < 0.67) from each comparison were used as input (Lymphocytes controls vs Lymphokine Activated Killer (LAK) cells: 1652 features). For the enrichment analyses, only the GO Biological Processes database was used to retrieve pathways and a minimum overlap of 10 features was set. For the remaining options, default settings were used. For each analysis, all statistically enriched terms (GO Biological Processes) were identified and accumulative hypergeometric p-values and enrichment factors were calculated and used for filtering. Remaining significant terms were then hierarchically clustered into a tree based on kappa-statistical similarities among their gene memberships. Then 0.3 kappa score was applied as the threshold to cast the tree into 20 term clusters. The most statistically significant term within a cluster was chosen to represent the cluster. For the networks, each term is represented by a circle node, where its size is proportional to the number of input genes fall under that term, and its color represents its cluster identity. Terms with a similarity (kappa) score > 0.3 are linked by an edge (the thickness of the edge represents the similarity score).

**Acknowledgments:** This work was supported by the “Ministère de l'enseignement supérieur et de la recherche”, the “Région Centre-Val de Loire” (Project PIRANA).

**Conflicts of interest:** The authors declare no competing financial interests. PPMcD is also employed as Executive Director, Research at Insmed Inc. Insmed was however not involved in this work; did not fund it; and does not endorse it, implicitly or otherwise.

**Authorship contributions:** Brice Korkmaz supervised the work. Brice Korkmaz and Roxane Domain participated in the research design. Roxane Domain, Loïc Gonzalez, Jérôme Zoidakis, conducted the experiments. Brice Korkmaz, Christophe Paget, Antonia Vlahou, Rich Williams, Peter Eickholz, Patrick P. McDonald performed data analyses. Brice Korkmaz wrote the initial manuscript and Patrick McDonald made extensive revisions. All authors contributed to the writing and revision processes of the manuscript.

**FIGURE LEGEND**

**Figure 1. Proteolytic cascades involved in the activation of NSPs and granzymes.**

**Figure 2. CatC and granzymes in LAK cells. A)** Lymphocytes from blood healthy volunteers and PLS patients were analysed by flow cytometry. CD45 live and dead cells are represented in the histogram on the left and the proportions of T cells and NK cells of CD45 live cells are representated on the right. After differentiation into LAK cells (8 days), cells were analysed again by FACS as previously (day 0). **B)** Lymphocytes and LAK cells lysates were assayed by western blot using anti-CatC, anti-GzmB and anti-GzmA antibodies. **C**) Activity of CatC, GzmA ans GzmB from LAK cells lysates of healthy donnors and PLS patient. CatC activity was measured using Gly-Phe-AMC fluorogenic substrate, GzmA and GzmB were measured using chromogenic substrate Z-L-Lys-SBzl and Ac-IEPD-pNA respectfully.

**Figure 3. Processing and maturation of proCatC in LAK cells cultured in presence of chemical inhibitors. A)** Healthy PBMCs were cultured for 2 days in the presence of 100 µM **E64d** or **B)** for 8 days in the presence of 2 µM **IcatC$_{XPZ-01}$**, 10 µM compound **1** ("Cp1"), a mixture of 10 µM compound **1** and 10 µM **IcatC$_{XPZ-01}$**, 10 µM **IcatS$_{\#54}$**, or their diluent (DMSO xx%, v/v). Cell lysates were then processed for western blot analysis using an antibody directed against the 23-kDa heavy chain of CatC that also recognizes a ~35-kDa fragment composed of a truncated propeptide, the heavy chain and the light chain. Cell lysates were also assessed for CatC proteolytic activity using the fluorogenic substrate, GF-AMC.

**Figure 4. Activation of granzyme B in LAK cells cultured in presence of chemical inhibitors. A)** Healthy PBMCs were cultured for 8 days in the presence of 2 µM **IcatC$_{XPZ-01}$**, 10 µM compound **1** ("Cp1"), a mixture of 10 µM compound **1** and 2 µM **IcatC$_{XPZ-01}$**, 10 µM **IcatS$_{\#54}$**, or their diluent (DMSO v/v). Cell lysates were then processed for western blot analysis using an anti-GzmB antibody, or assessed for GzmB proteolytic activity using the chromogenic substrate, Ac-IEPD-pNA.

**Table 1.**

| Description | Gene Symbol | Average Abundance Lympho | Average Abundance LAK | Mann Whitney p value LAK vs Lympho | Ratio_LAK vs Lympho |
|---|---|---|---|---|---|
| ***Granzymes*** | | | | | |
| GzmA | *GZMA* | 186 | 4408 | 0,0159 | 23.7618 |
| GzmB | *GZMB* | 70 | 2610 | 0,0195 | 37,0906 |
| GzmH | *GZMH* | 132 | 173 | 0,4127 | 1,3144 |
| GzmK | *GZMK* | 131 | 7 | 0,0179 | 0,0547 |
| GzmM | *GZMM* | 25 | 12 | 0,7012 | 0,4999 |
| ***Cysteine cathepsins*** | | | | | |
| CatC | *CTSC* | 145 | 286 | 0,1905 | 1,9777 |
| CatS | *CTSS* | 94 | 34 | 0,0317 | 0,3630 |
| CatB | *CTSB* | 99 | 18 | 0,0159 | 0,1817 |
| CatW | *CTSW* | 59 | 217 | 0,0317 | 3,65 |
| Pro-catH | *CTSH* | 24 | 0 | 0,0442 | only in Lympho |
| CatZ | *CTSZ* | 85 | 6 | 0,0159 | 0,0719 |

## REFERENCES


1. Hay, Z. L. Z., and Slansky, J. E. (2022) Granzymes: The Molecular Executors of Immune-Mediated Cytotoxicity. *Int J Mol Sci* **23**
2. Trapani, J. A., and Sutton, V. R. (2003) Granzyme B: pro-apoptotic, antiviral and antitumor functions. *Curr Opin Immunol* **15**, 533-543
3. Caputo, A., Garner, R. S., Winkler, U., Hudig, D., and Bleackley, R. C. (1993) Activation of recombinant murine cytotoxic cell proteinase-1 requires deletion of an amino-terminal dipeptide. *J Biol Chem* **268**, 17672-17675
4. Smyth, M. J., McGuire, M. J., and Thia, K. Y. (1995) Expression of recombinant human granzyme B. A processing and activation role for dipeptidyl peptidase I. *J Immunol* **154**, 6299-6305
5. Toomes, C., James, J., Wood, A. J., Wu, C. L., McCormick, D., Lench, N., Hewitt, C., Moynihan, L., Roberts, E., Woods, C. G., Markham, A., Wong, M., Widmer, R., Ghaffar, K. A., Pemberton, M., Hussein, I. R., Temtamy, S. A., Davies, R., Read, A. P., Sloan, P., Dixon, M. J., and Thakker, N. S. (1999) Loss-of-function mutations in the cathepsin C gene result in periodontal disease and palmoplantar keratosis. *Nat Genet* **23**, 421-424
6. Pham, C. T., Ivanovich, J. L., Raptis, S. Z., Zehnbauer, B., and Ley, T. J. (2004) Papillon-Lefevre syndrome: correlating the molecular, cellular, and clinical consequences of cathepsin C/dipeptidyl peptidase I deficiency in humans. *J Immunol* **173**, 7277-7281
7. Sutton, V. R., Waterhouse, N. J., Browne, K. A., Sedelies, K., Ciccone, A., Anthony, D., Koskinen, A., Mullbacher, A., and Trapani, J. A. (2007) Residual active granzyme B in cathepsin C-null lymphocytes is sufficient for perforin-dependent target cell apoptosis. *J Cell Biol* **176**, 425-433
8. D'Angelo, M. E., Bird, P. I., Peters, C., Reinheckel, T., Trapani, J. A., and Sutton, V. R. (2010) Cathepsin H is an additional convertase of pro-granzyme B. *J Biol Chem* **285**, 20514-20519
9. Hamon, Y., Legowska, M., Herve, V., Dallet-Choisy, S., Marchand-Adam, S., Vanderlynden, L., Demonte, M., Williams, R., Scott, C. J., Si-Tahar, M., Heuze-Vourc'h, N., Lalmanach, G., Jenne, D. E., Lesner, A., Gauthier, F., and Korkmaz, B. (2016) Neutrophilic Cathepsin C Is Maturated by a Multistep Proteolytic Process and Secreted by Activated Cells during Inflammatory Lung Diseases. *The Journal of biological chemistry* **291**, 8486-8499

**FIGURE 1**

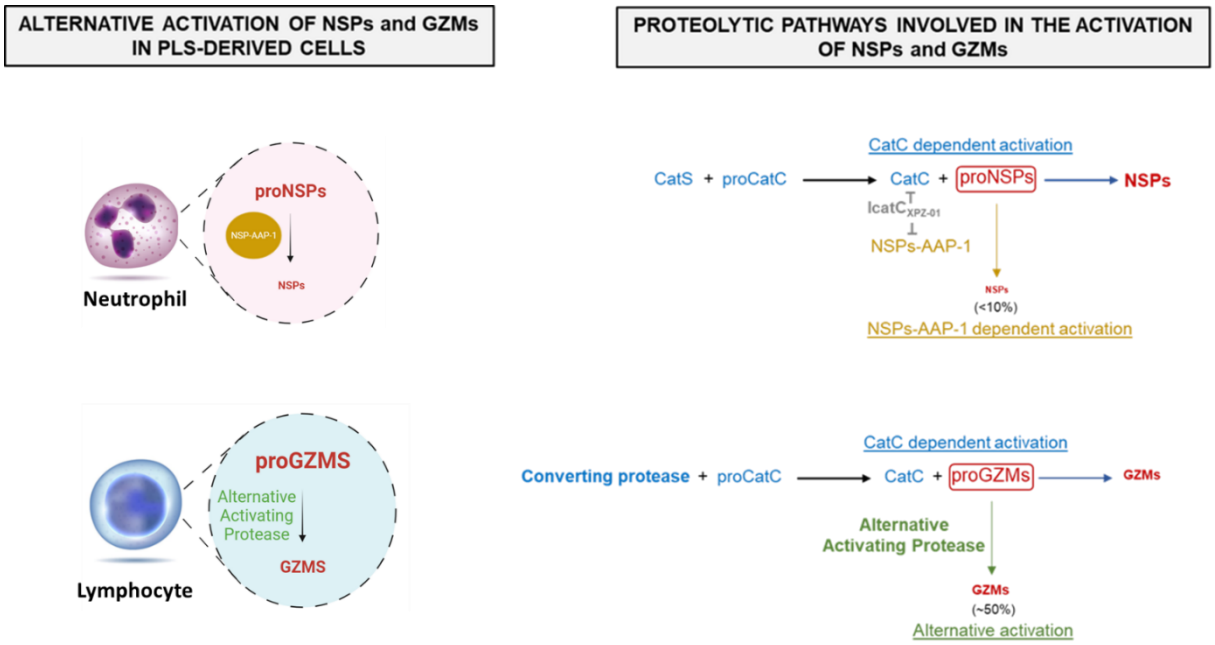
ALTERNATIVE ACTIVATION OF NSPs and GZMs IN PLS-DERIVED CELLS
PROTEOLYTIC PATHWAYS INVOLVED IN THE ACTIVATION OF NSPs and GZMs
proNSPs
NSP-AAP-1
NSPs
Neutrophil
CatC dependent activation
CatS + proCatC
CatC + proNSPs
NSPs
IcatC XPZ-01
NSPs-AAP-1
NSPs
(<10%)
NSPs-AAP-1 dependent activation
proGZMS
Alternative Activating Protease
GZMS
Lymphocyte
CatC dependent activation
Converting protease + proCatC
CatC + proGZMs
GZMs
Alternative Activating Protease
GZMs
(~50%)
Alternative activation

**FIGURE 2**

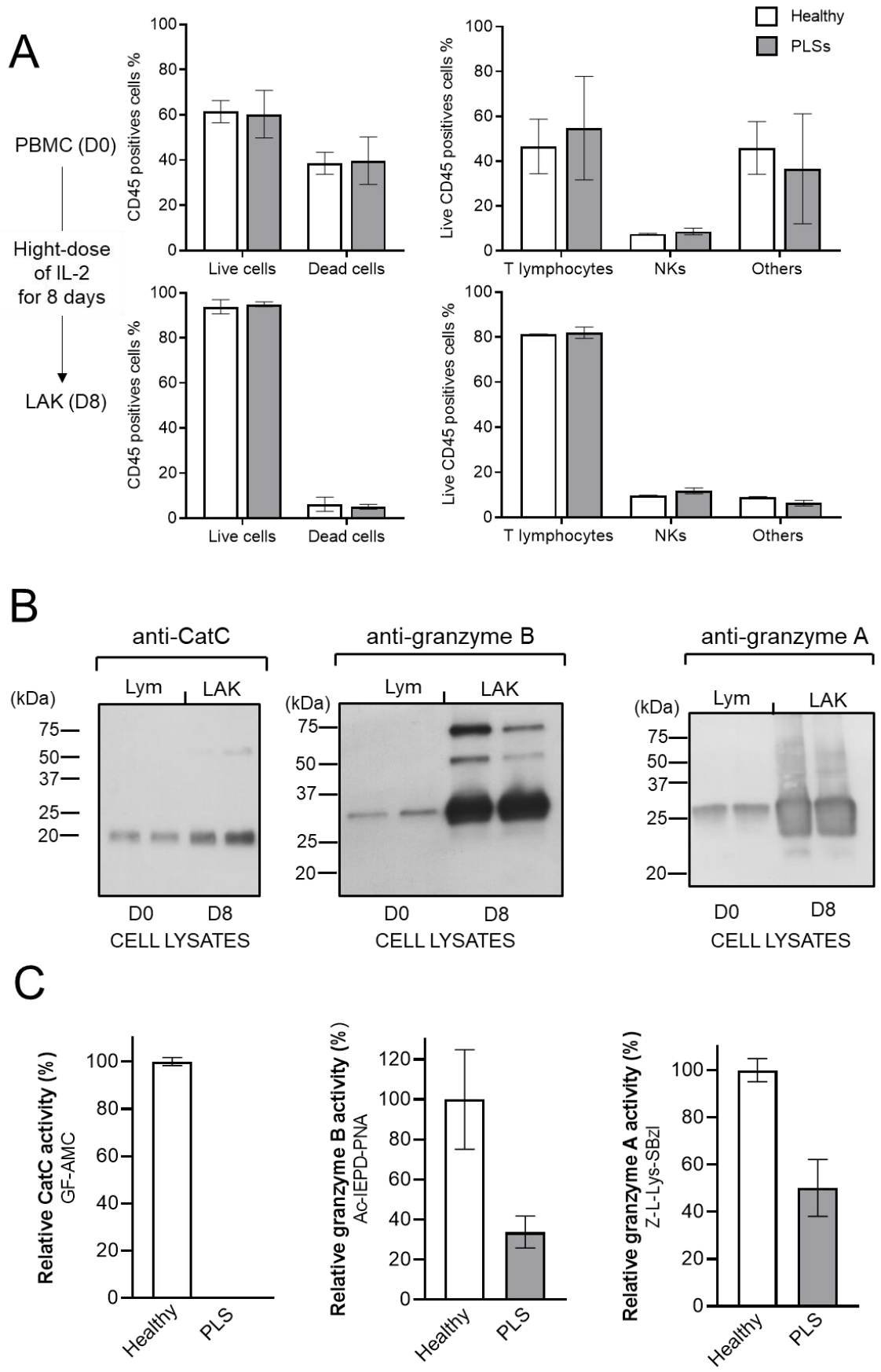
A
PBMC (D0)
Hight-dose of IL-2 for 8 days
LAK (D8)
CD45 positives cells %
Live cells
Dead cells
Live CD45 positives cells %
T lymphocytes
NKs
Others
Healthy
PLSs
B
anti-CatC
anti-granzyme B
anti-granzyme A
(kDa)
Lym
LAK
75
50
37
25
20
D0
D8
CELL LYSATES
C
Relative CatC activity (%)
GF-AMC
Relative granzyme B activity (%)
Ac-IEPD-PNA
Relative granzyme A activity (%)
Z-L-Lys-SBzl
Healthy
PLS

**FIGURE 3**

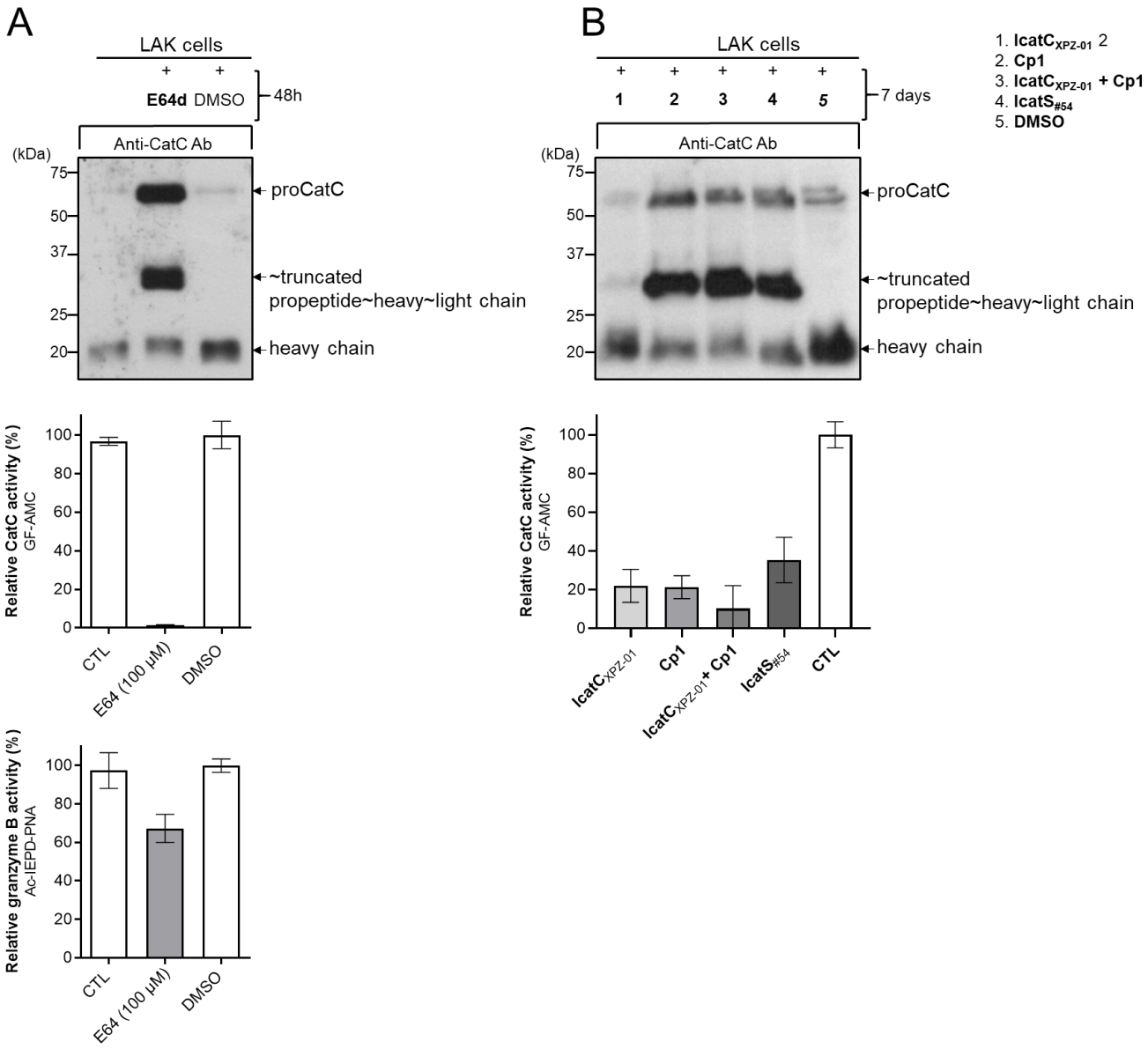
A
LAK cells
+ +
E64d DMSO
48h
Anti-CatC Ab
(kDa)
75
50
37
25
20
proCatC
~truncated propeptide~heavy~light chain
heavy chain
Relative CatC activity (%) GF-AMC
100
80
60
40
20
0
CTL
E64 (100 µM)
DMSO
Relative granzyme B activity (%) Ac-IEPD-PNA
B
LAK cells
+ + + + +
1 2 3 4 5
7 days
1. IcatC$_{XPZ-01}$ 2
2. Cp1
3. IcatC$_{XPZ-01}$ + Cp1
4. IcatS$_{\#54}$
5. DMSO
IcatC$_{XPZ-01}$
Cp1
IcatC$_{XPZ-01}$+ Cp1
IcatS$_{\#54}$
CTL

**FIGURE 4**

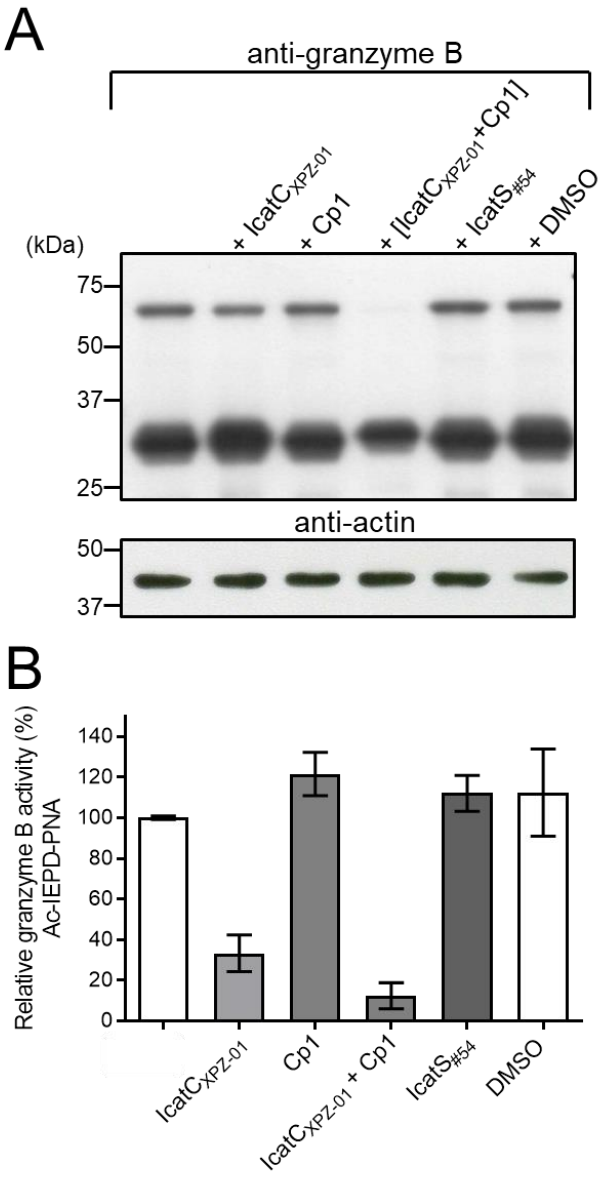
A
anti-granzyme B
+ IcatC$_{XPZ-01}$
+ Cp1
+ [IcatC$_{XPZ-01}$+Cp1]
+ IcatS$_{\#54}$
+ DMSO
(kDa)
75
50
37
25
anti-actin
50
37
B
Relative granzyme B activity (%)
Ac-IEPD-PNA
140
120
100
80
60
40
20
0
IcatC$_{XPZ-01}$
Cp1
IcatC$_{XPZ-01}$ + Cp1
IcatS$_{\#54}$
DMSO

**Supp.FIGURE 1**

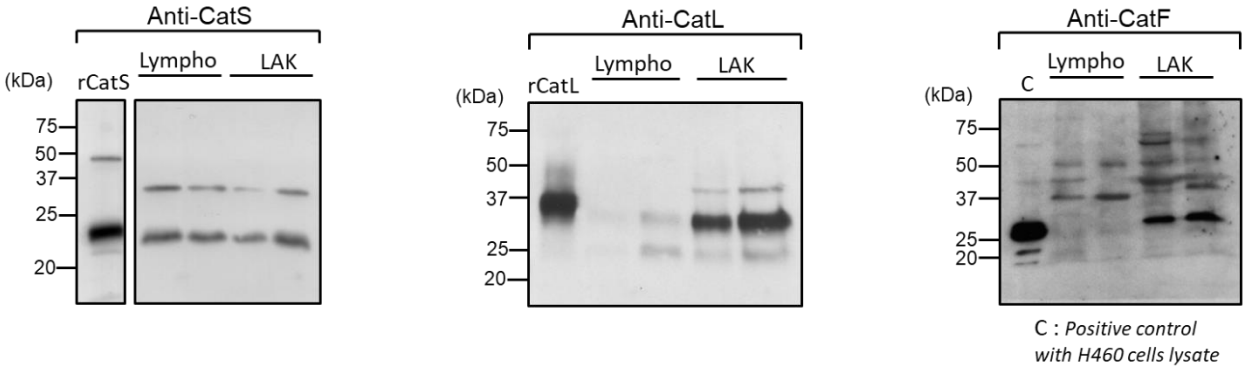

# III. Discussion, conclusion et perspectives

Dans cette étude, nous démontrons (i) que la CatS, une puissante enzyme élastinolytique, est la principale protéase de conversion impliquée dans la maturation de la proCatC des neutrophiles et des lymphocytes ; (ii) qu'il existe deux protéases alternatives de nature différente impliquées dans l'activation des PSN (NSPs-AAP-1) et Gzms dans les neutrophiles et lymphocytes, respectivement; (iii) que la NSPs-AAP-1 est conservée chez la souris ; (iv) que le ciblage pharmacologique de la CatS dans les neutrophiles humains différenciés des $CD34^+$ entraîne une inactivation et une élimination significatives des PSN (~70%). Ces aspects jusqu'ici inconnus des voies protéolytiques impliquées dans l'activation des proPSN ont le potentiel d'engendrer de nouvelles stratégies de traitement pour contrôler les lésions tissulaires médiées par les PSN qui sont souvent associées à la présence de neutrophiles activés dans de nombreuses maladies inflammatoires ou auto-immunes chroniques.

***Maturation de la pro-cathepsine C et activation des protéases à serine des neutrophiles par la cathepsine C et la NSP-AAP-1 dans les neutrophiles***

La maturation de la proCatC dans des précurseurs de neutrophile humain à différents stades a permis de montrer que le ciblage de la CatS par un inhibiteur nitrile sélectif et perméable, **IcatS**, réduisait l'activité de la CatC d'environ 80 % sans affecter l'activité des PSN (Hamon et al., 2016c). Cette inhibition incomplète de la CatC pourrait être due à la présence d'une ou plusieurs protéases supplémentaires capables de maturer la proCatC, résistantes à l'inhibiteur de la CatS et/ou à un effet limité de l'inhibiteur sur les cellules. Dans notre étude, nous avons envisagé de bloquer complètement la maturation de la proCatC à l'aide d'inhibiteurs synthétiques perméables aux cellules et de déterminer le devenir des PSN dans les précurseurs neutrophiliques humains. En plus des CatS et CatL les cathepsines F (CatF), K (CatK) et V (CatV), ont récemment été identifiées comme de nouveaux activateurs putatifs de la proCatC *in vitro* (Lamort et al., 2019), mais nous n'avons pas réussi à détecter ces protéases dans les lysats de cellules HL-60 ni dans leurs surnageants concentrés. Ceci est en accord avec des études antérieures montrant que le gène de CatF n'était pas exprimé dans les cellules/leucocytes HL-60 (Santamaria et al., 1999) et que ceux de CatK et CatV étaient exprimés principalement dans les ostéoclastes (Bromme and Okamoto, 1995; Gelb et al., 1997) et le thymus/testicules (Bromme et al., 1999). La CatS et, dans une moindre mesure, la CatL ont été détectées dans les cellules HL-60 et dans les neutrophiles sanguins purifiés et sont donc apparus comme des cibles prometteuses pour maturer la proCatC. L'inhibiteur des protéases à cystéine à large spectre,

E64d, n'a modifié que partiellement la maturation de la proCatS et de la proCatL dans les cellules HL-60, indiquant que l'activation de ces protéases obéit à un mécanisme protéolytique non spécifique.

Nous avons incubé les cellules HL-60 avec l'**IcatS$_{\#54}$**, un nouvel inhibiteur nitrile perméable aux cellules, puissant et hautement sélectif, qui a efficacement inhibé la CatS *in cellulo*. Nous avons observé que la maturation de la proCatC étaient fortement impactée par l'accumulation d'un fragment tronqué de la proCatC, ce qui confirme le rôle de la CatS et son inhibition intracellulaire effective. Des résultats similaires ont été obtenus avec l'inhibiteur nitrile l'**IcatS$_{\#RO-11}$** qui est structurellement différent de l'**IcatS$_{\#54}$**. Cependant, une activité résiduelle de la CatC, d'environ 5 % par rapport à celle des cellules témoins, était toujours présente malgré l'inhibition complète de la CatS en présence d'**IcatS$_{\#54}$** ou d'**IcatS$_{\#RO-11}$**. De plus, la PR3 et la CatG, choisis comme PSN représentatives, étaient pleinement actives. Et contrairement à **E64d**, l'**IcatS$_{\#54}$** n'a pas modifié la maturation de la proCatS dans les cellules HL-60. La proCatS, comme les autres cathepsines à cystéine avec une activité endopeptidase, est capable de s'auto-activer. La maturation de la proCatS dans les cellules HL-60 n'étant pas modifiée par l'**IcatS$_{\#54}$**, suggère l'implication de protéases à cystéine supplémentaires dans la maturation de celle-ci.

La question qui se pose alors est de savoir si l'activité résiduelle de la CatC est capable d'activer pleinement les PSN, ou si une ou plusieurs autre(s) protéase(s) compenseraient la faible activité de la CatC. En effet, l'**IcatS#54** est un inhibiteur réversible qui pourrait bien maintenir un faible niveau de CatS active, difficilement détectable cinétiquement, mais suffisant pour expliquer l'activation partielle de la CatC. Il se pourrait également que la CatL, présente en faible quantité dans les cellules HL-60 et non inhibée par l'**IcatS#54**, soit responsable de cette activation. Nous avons réussi à bloquer complètement la maturation de la proCatC en utilisant des inhibiteurs de protéases à cystéine perméables aux cellules, non-toxiques et irréversibles qui inhibent à la fois la CatS et la CatL. Cependant, nous avons constaté, à nouveau, que la PR3 et la CatG étaient presque pleinement actives. Ainsi, les cellules HL-60 contiennent au moins une protéase supplémentaire capable d'activer les proPR3/proCatG. Ceci est en accord avec l'observation selon laquelle, chez les neutrophiles de patients atteints du syndrome de Papillion-Lefèvre (SPL), une maladie autosomique récessive entrainant la perte de fonction de la CatC, nous avons détecté l'activité fortement réduite mais toujours détectable de la PR3 (<10%) et, dans une moindre mesure, de la CatG. Il est donc concevable que l'activation résiduelle des proPSN puisse être réalisée par d'autres enzymes protéolytiques en l'absence d'activité de la CatC. Toutes ces données soutiennent la présence

dans le génome humain d'une ou plusieurs protéases de conversion inconnues impliquées dans l'activation des proPSN. Nous avons appelé, la ou les protéase(s) CatC-like, capable d'activer les PSN, la NSPs-Alternative Activating Protease 1 (NSPs-AAP-1). La suite de l'étude consistait donc à caractériser la NSPs-AAP-1.

Nous avons pu conclure que la NSPs-AAP-1 est une protéase à cystéine, inhibée par des inhibiteurs nitriles réversibles, mais pas par des inhibiteurs irréversibles de la CatC. Il est intéressant de noter que cette activité protéolytique est inhibée par l'**IcatC$_{XPZ-01}$**, en effet nous n'avons observé aucune activation significative de la proPR3 et de la proCatG lors de la supplémentation des inhibiteurs de la CatS avec l'**IcatC$_{XPZ-01}$**. Cependant, il reste à déterminer si cette inhibition résulte d'un blocage direct et/ou indirect de cette protéase par l'altération du processus de maturation.

Il a été montré que l'incubation de cellules HL-60 avec l'inhibiteur nitrile **IcatS** entraînait une altération partielle de la maturation de la proCatC où 20 % de la proCatC était convertie en forme active. La combinaison de l'**IcatS** avec l'**IcatC$_{XPZ-01}$** a presque complètement bloqué la maturation de la proCatC (Hamon et al., 2016c). Nos données expérimentales dans la présente étude ont clairement indiqué que la CatS (et éventuellement la CatL) était impliquée dans la maturation de la proCatC dans les cellules HL-60. Par conséquent, les protéases affectées par l'**IcatC$_{XPZ-01}$** entrainant l'abrogation totale de la maturation de la proCatC pourraient être les CatS/CatL. Étant donné que les CatS/CatL matures n'étaient pas inhibées par l'**IcatC$_{XPZ-01}$** *in vitro*, nous avons montré que la combinaison d'**IcatS$_{\#54}$** ou du composé **1-4** avec l'**IcatC$_{XPZ-01}$** affectait le processus de maturation des proCatS/proCatL.

La CatS, exprimée dans une grande variété de cellules immunitaires, est une puissante cathepsine à cystéine qui conserve son activité enzymatique élastinolytique et collagénolytique dans des environnements à pH neutre, soulignant son activité protéolytique aussi bien intracellulaires qu'extracellulaires. Des travaux antérieurs ont démontré que la CatS est impliquée dans la pathogenèse de plusieurs maladies pulmonaires inflammatoires, notamment la bronchopneumopathie chronique obstructive (BPCO) (Andrault et al., 2019). Les niveaux accrus de CatS dans les échantillons des patients sont significativement corrélés à un déclin de la fonction pulmonaire et à une augmentation de l'infiltration neutrophilique dans les poumons. De plus, l'inhibition pharmacologique ou la déplétion génétique de la CatC chez la souris ont réduit l'inflammation et les lésions pulmonaires dans les modèles de maladies respiratoires. Des observations similaires ont été faites chez des souris déficientes en élastase ou triplement

déficientes en PSN. Pour mieux interpréter les conséquences de l'inactivation de la CatS dans des modèles murins de maladies, nous avons étudié son implication dans l'activation des proPSN murines. L'identification de la CatC et de l'élastase actives représentatives en tant que PSN dans des extraits de moelle osseuse et de neutrophiles sanguins de souris déficientes en CatS a montré que la CatS n'était pas essentielle à l'activation des proPSN chez la souris.

Comme dit précédemment, chez l'homme, nous avons identifié une voie de maturation des PSN indépendante de la CatC, catalysée par la ou le(s) NSPs-AAP-1(s) et inhibée par l'**IcatC$_{XPZ-01}$**. Nous avons donc poursuivi notre étude afin de déterminer si cette voie était conservée dans un modèle murin et si celle-ci était la NSPs-AAP-1. Nos données, utilisant des souris déficientes en CatC, suggèrent que la ou le(s) NSPs-AAP-1(s) sont également présentes chez les souris et contribue de manière significative à l'activation de la NE et de la PR3 (30 à 40 %) mais pas de la CatG, lors de la différenciation des neutrophiles dans la moelle osseuse. Les neutrophiles stimulés provenant de souris déficientes en CatC génèrent beaucoup moins de NETs que chez les souris WT (Yan et al., 2016). De plus, les souris déficientes en CatC sont protégées contre les maladies médiées par les neutrophiles induites expérimentalement (Korkmaz et al., 2018a). Chez les souris déficientes en CatC, la voie d'activation des proPSN dépendante de(s) NSPs-AAP-1(s) générant 30 à 40 % de protéase active n'est pas suffisante pour induire des maladies neutrophiliques dépendantes. Chez la souris, l'**IcatC$_{XPZ-01}$** atteint la moelle osseuse ce qui permet d'inhiber la CatC et l'activation des PSN de manière significative. La disparition des zymogènes des PSN a été observée chez les souris traitées avec l'**IcatC$_{XPZ-01}$**. L'**IcatC$_{XPZ-01}$** a aussi été testé sur des hamsters dans le but d'inhiber l'inflammation neutrophilique délétère lors d'une infection à SARS-COV2 (Bourgon et al., 2022). L'utilisation de cet inhibiteur a permis de réduire significativement l'invasion neutrophilique au niveau de l'épithélium olfactif et de diminuer la propagation de l'infection virale (Bourgon et al., 2022) (**Annexe 3**). À la suite de la caractérisation des PSN de rat (**Annexe 4**), un autre inhibiteur nitrile réversible de la CatC, **BI-9740**, a été utilisé afin d'atténuer le dysfonctionnement vasculaire de lésion d'ischémie-reperfusion (**Annexe 5**). Comme chez la souris, l'administration de l'inhibiteur de la CatC a permis de diminuer l'expression et l'activité de la NE (58% d'activité résiduelle) et de la CatG (46% d'activité résiduelle) dans les moelles osseuses. On peut émettre l'hypothèse qu'une voie indépendante de la CatC est conservée dans l'activation des PSN chez le rat, mais d'autres expérimentations sont nécessaires pour confirmer cette théorie. Cependant l'administration prolongée d'**IcatC$_{XPZ-01}$** chez *Macaca fascicularis* a

entraîné une inhibition presque totale des PSN (Guarino et al., 2017), indiquant une faible contribution de la NSPs-AAP-1 chez les primates.

Pour conclure, nous avons montré ici que la CatS, une puissante enzyme élastinolytique identifiée comme cible thérapeutique des lésions tissulaires chroniques induites par l'inflammation, est la protéinase de conversion physiologique de la proCatC des neutrophiles humains. Le ciblage pharmacologique de la CatS à l'aide d'inhibiteurs puissants et perméables aux cellules entraîne un blocage presque total de la maturation de la proCatC. Cette étude a atteint une preuve de concept *in vitro* démontrant que l'inhibition pharmacologique de la CatS peut conduire à une inactivation et une élimination significative des PSN. Le blocage de l'activation des proPSN par un inhibiteur de la CatS ou par la combinaison d'un inhibiteur de la CatC avec un inhibiteur de la CatS pourrait aider à contrôler efficacement les lésions tissulaires dans les maladies médiées par les neutrophiles (**Manuscrit 1**).

***Stabilisation et activation des protéases à serine des neutrophiles dans les monocytes-macrophages***

La CatC est une protéase ubiquitaire et son rôle dans les autres cellules immunitaires telles que les monocytes, les macrophages et les lymphocytes ne doit pas être négligé. En effet bien qu'en très faible quantité les PSN sont présentes dans les monocytes, mais leur rôle demeure incertain, nous avons donc choisi de caractériser la maturation de la pro-CatC et l'activation des PSN dans ces cellules. Les monocytes sont des cellules de l'immunité innée, elles font partie des cellules recrutées en réponse à un danger pour l'organisme bactéries, virus, ou blessure. Les monocytes sont produits lors de l'hématopoïèse dans la moelle osseuse, une fois sur le site de l'infection, ils sont convertis en macrophage en fonction de leur exposition à des chimiokines. Les monocytes peuvent dériver en différents types de macrophage pro- ou anti-inflammatoire en fonction du type de chimiokines auxquelles ils ont été exposés, pouvant à la fois exacerber l'inflammation ou faciliter la réparation tissulaire. Leurs rôles variés tant dans l'homéostasie tissulaire que dans la réaction de l'immunité innée, font de ces cellules des cibles thérapeutiques intéressantes, d'autant plus qu'elles sont impliquées dans de nombreuses pathologies. Comme notamment la BPCO, en effet la CatS excrétée par les macrophages altère la perméabilité de l'épithélium pulmonaire, ce qui entraîne la disruption de la barrière épithéliale et favorise l'aggravation de l'inflammation dans cette pathologie (Bigot et al., 2022). L'utilisation d'un inhibiteur de la CatS et donc très séduisant dans cette pathologie, compte tenu

de son effet sur les macrophages, cependant l'effet que celui-ci pourrait avoir sur la maturation de la pro-CatC dans ces cellules reste à déterminer.

Afin de caractériser la maturation de la pro-CatC dans les monocytes, nous avons utilisé deux modèles cellulaires, les U-937 et les THP-1. Dans les cellules U-937, nous avons pu montrer la présence des CatS, L, V, F et K. L'utilisation d'un inhibiteur de ces protéases a permis d'empêcher la maturation de la pro-CatC dans ces cellules, de plus l'utilisation de l'inhibiteur sélectif de la CatS, l'**IcatS$_{\#54}$**, a entraîné l'inhibition quasi-totale de la CatC, ce qui nous laisse à penser que comme dans les HL-60, la CatS est la protéase majeure impliquée dans la maturation de la pro-CatC dans les cellules U-937. À l'image des résultats obtenus avec les cellules HL-60, l'activité des PSN n'a pas été impactée lors de l'utilisation de ces inhibiteurs, la présence de la NSPs-AAP-1 dans ces cellules a donc été envisagée. Afin de confirmer la présence de la NSPs-AAP-1, nous avons administré deux inhibiteurs dans ces cellules, l'**IcatC$_{XPZ-01}$** capable d'inhiber la CatC et la NSPs-AAP-1 et l'**IcatC$_{GSK-60}$** inhibant la CatC mais non la NSPs-AAP-1. En présence de l'**IcatC$_{XPZ-01}$**, l'activité de la NE et de la CatG sont presque totalement abrogées, en revanche en présence de l'**IcatC$_{GSK-60}$** l'activité est diminuée, mais une grande partie de celle-ci demeure. On retrouve le même profil que chez les HL-60, nous confortant dans l'idée de la présence de la NSPs-AAP-1 dans les cellules U-937.

L'étude a été poursuivie avec les THP-1 dans lesquelles nous avons pu montrer la présence des CatS et CatL matures, ainsi que les pro-CatV, pro-CatF et pro-CatK. La CatL semble être beaucoup plus exprimée dans les THP-1 que dans les U-937 ou les HL-60. Afin de caractériser la maturation de la pro-CatC dans les THP-1, nous avons utilisé les mêmes inhibiteurs que ceux utilisés précédemment avec les U-937. Le composé **1**, l'inhibiteur de la CatS et de la CatL a permis d'inhiber la maturation de la pro-CatC, mais de façon incomplète, le composé **2** a permis d'augmenter cette inhibition, en revanche l'inhibiteur spécifique de la CatS, l'**IcatS$_{\#54}$**, n'a pas eu d'effet sur la maturation de la pro-CatC. Contrairement aux cellules HL-60 et U-937, la CatS n'est pas la protéase majeure responsable de la maturation de la pro-CatC dans les THP-1. Nous n'avons pas encore déterminé si la CatL assure la majeure partie de cette fonction dans ces cellules, pour cela d'autres expérimentations seront nécessaires, mais elle est notre meilleure candidate.

De façon surprenante, même si l'activité de la CatC n'est que partiellement inhibée en présence des inhibiteurs, composé **1** et composé **2**, l'activité des PSN est drastiquement augmentée. Ces résultats inédits et contre-intuitifs d'activité enzymatique, nous ont encouragés

à regarder l'effet de ces inhibiteurs en termes de quantité protéique de PSN. L'analyse des Western Blot des lysats cellulaires montre une augmentation de la quantité de PR3 et de CatG en présence des inhibiteurs. Elles sont présentes sous deux formes de poids moléculaires différents, variant par leur glycosylation. La forme avec le plus haut poids moléculaire est hautement glycosylée et ne forme pas de complexe avec l'α-antitrypsine, ce qui signifie qu'elle n'est pas active. C'est un zymogène hautement glycosylé, appelé pro-PR3$^{(\text{high glycosylated})}$. La forme de bas poids moléculaire est moins glycosylée, elle forme un complexe avec l'α-antitrypsine, ce qui signifie qu'elle est active. De ce fait, elle est nommée active PR3$^{(\text{low glycosylated})}$. Le traitement des THP-1 par les composés **1** et **2**, induit une augmentation de la quantité de la forme active PR3$^{(\text{low glycosylated})}$. Les mêmes résultats ont été obtenus avec la CatG. Ces résultats sont en accord avec les activités des PSN mesurées en présence de ces inhibiteurs. Ces données nous amènent à suggérer l'hypothèse selon laquelle les composés **1** et **2**, inhibent des protéases impliquées dans la dégradation de la forme active des PSN. Une altération de la dégradation des PSN, nous permet d'expliquer leur augmentation en présence des inhibiteurs. Les formes glycosylées renforcent cette hypothèse. Classiquement, la glycosylation des protéines permet de les protéger de la dégradation enzymatique. La persistance des formes actives peu glycosylées, encourage l'idée d'un défaut de dégradation des PSN en présence des inhibiteurs. Pour confirmer cette hypothèse, nous commencerons par vérifier l'expression des PSN, car nous ne pouvons pas exclure la possibilité que les PSN soient surexprimées en présence des composés **1** et **2**. L'étude du trafic cellulaire que les PSN empruntent dans les THP-1 pourrait aussi nous aider à confirmer ou non notre hypothèse.

Il n'en demeure pas moins, que l'inhibition de la CatC, bien qu'incomplète, n'impacte pas l'activation des PSN, ce qui suggère une voie d'activation indépendante de la CatC, et donc peut être la NSPs-AAP-1, à l'image des cellules U-937 et HL-60. Afin de répondre à ces questions nous avons traité les THP-1 avec les inhibiteurs **IcatC$_{\text{XPZ-01}}$** et l'**IcatC$_{\text{GSK-60}}$**, de la même façon qu'avec les U-937. Le traitement avec les inhibiteurs a permis d'abroger totalement l'activité de la CatC. L'inhibition par l'**IcatC$_{\text{GSK-60}}$**, n'a pas eu d'effet sur la PR3 et la NE, mais semble avoir empêché l'activation de la CatG. En revanche, l'**IcatC$_{\text{XPZ-01}}$** a entrainé l'augmentation protéique de la PR3$^{(\text{low glycosylated})}$ active et de celle de la CatG, seulement sous une forme inactive. Le traitement n'a cependant pas eu d'effet sur la NE. Les résultats chez les souris et les patients SPL, nous indique que la NSPs-AAP-1 n'est pas capable d'activer la CatG *in vivo*, ceci pouvant être expliquer par la présence d'une glycine dans son pro-dipeptide. L'absence d'activité de la CatG, lorsque la CatC est totalement inhibée, nous laisse penser à

une activation spécifique par cette protéase. En revanche, la PR3 et la NE ne sont pas inhibée en présence d'**IcatC$_{XPZ-01}$**, alors que celui-ci inhibe la CatC et la NSPs-AAP-1. Ce qui nous permet de conclure à l'existence d'une activation indépendante de la CatC et de la NSPs-AAP-1 dans les cellules THP-1, que nous avons nommé la NSPs-AAP-2. Il semblerait que la NSPs-AAP-2 ne soit pas capable, comme la NSPs-AAP-1, d'activer la CatG. Non seulement l'**IcatC$_{XPZ-01}$** n'a pas permis d'inhiber la PR3et la NE, il a entraîné l'augmentation protéique de la PR3 et de la CatG. Potentiellement, l'**IcatC$_{XPZ-01}$** impacterait la voie de dégradation des PSN comme les composés **1** et **2**.

Pour conclure, la CatS est la protéase majeure impliquée dans la maturation de la pro-CatC dans les cellules U-937, mais pas dans les cellules THP-1. La voie NSPs-AAP-1 est importante dans la maturation des PSN dans les cellules U-937, en revanche, elle ne l'est pas dans les cellules THP-1. Ce qui a permis de mettre en évidence une seconde activation des PSN indépendante de la CatC que nous avons nommé la NSPs-AAP-2. Les stades de différentiation de ces deux lignées cellulaires pourraient expliquer les différences dans l'activation des PSN. Un stade pro-monocytaire (U-937) semble avoir un profil similaire au HL-60, en revanche un stade un peu plus précoce pro-monocytaire (THP-1) affiche des caractéristiques totalement différentes. La différenciation des U-937 et des cellules THP-1 est une perspective intéressante pour mieux caractériser ces deux voies. Nous envisageons de compléter cette étude sur les processus protéolytiques dans des monocytes issus de donneur sain et de patients SPL, ainsi que leur différenciation en macrophage (**Manuscrit 2**).

### *Maturation de la pro-cathepsine C et son implication dans l'activation des granzymes dans les lymphocytes cytotoxiques*

Il existe également une voie alternative à la CatC, impliquée dans la maturation des Gzms dans les lymphocytes cytotoxiques. L'étude de cette voie pourrait nous apporter des éclaircissements sur la NSPs-AAP-1 ou la NSPs-AAP-2. De plus l'impact d'inhibiteurs tel que l'**IcatC$_{XPZ-01}$** pourrait avoir un effet délétère sur l'activité des lymphocytes cytotoxique, si la voie alternative impliquée dans l'activation des Gzms est réalisée par la NSPs-AAP-1. D'où la nécessité d'étudier la maturation de pro-CatC et les mécanismes protéolytiques impliqués dans l'activation des Gzms dans les lymphocytes cytotoxiques. Les lymphocytes cytotoxiques et les natural killer, permettent l'élimination des cellules infectées par les virus et des cellules cancéreuses. Dans les lymphocytes cytotoxiques, les Gzms sont stockées dans des granules sous

leur forme active. Les Gzms sont des protéases à serine qui sont relarguées avec des perforines, entrainant la formation de pores dans les cellules cibles, ce qui permet aux Gzms de pénétrer dans la cellule et de déclencher la mort cellulaire. Afin d'être active, comme les PSN, les Gzm ont besoin que leur pro-dipeptide soit clivé. De la même façon que pour les PSN, cette action est réalisée par la CatC. En effet, chez les patients atteints du syndrome de Papillon-Lefèvre, une déficience génétique autosomique récessive en CatC, l'activité des Gzms A et B dans les lymphocytes cytotoxiques est diminuée d'environ 50% comparée à des contrôles sains. La CatC est donc une des protéases responsables de l'activation des granzymes dans les lymphocytes cytotoxiques, mais elle n'est pas l'unique protéases impliquée. Démontrant la présence d'une voie alternative à la CatC permettant l'activation des granzymes que nous avons introduite précédemment.

Afin d'étudier la maturation de la pro-CatC et les mécanismes protéolytiques impliquée dans l'activation des Grzms, nous avons utilisé des cellules LAK, pour *Activated Lymphokine Killer cells*. Les cellules LAK sont un mélange de lymphocytes T et de natural killers issus de sang humain et activés par un excès d'interleukine-2. Activation en cellule LAK permet l'augmentation de l'expression des Grzms A et B ce qui nous permet d'étudier les mécanismes impliqués dans leur activation, et de mesurer leur activité puisqu'elles sont présentes en grande quantité. Nous avons pu montrer la présence des cathepsines S et L dans les cellules LAK. Afin d'étudier la maturation de la pro-CatC nous avons utilisé les mêmes inhibiteurs que précédemment, et nous avons pu déterminer que la CatS est la protéase majeure impliquée dans la maturation de la pro-CatC à l'image des neutrophiles et des cellules U-937. De plus, l'activité des Gzms A et B n'a pas été modifiée par ces inhibiteurs, ce qui nous laisse suppose de la présence d'une voie d'activation indépendante de la CatC dans ces cellules. En revanche, la maturation de la pro-CatC n'est pas complètement inhibée par ces inhibiteurs, en effet une activité résiduelle de la CatC est présente.

Nous avons donc utilisé des cellules LAK issues de patient SPL, et nous avons pu confirmer les résultats de la littérature, à savoir une activité résiduelle des Gzms A et B d'environ 60% et 40% respectivement, ce qui confirme la présence de la voie alternative à la CatC dans ces cellules. Afin de caractériser cette voie, nous avons utilisé l'**IcatC$_{XPZ-01}$**, bien que celui a permis d'inhiber la CatC dans ces cellules, nous avons retrouvé les mêmes résultats que chez les patients atteints du syndrome de Papillon-Lefèvre, ce qui nous permet de conclure que la voie alternative impliquée dans l'activation des Gzms A et B est différente de la NSPs-AAP-1. De plus, l'utilisation de l'inhibiteur de protéase à cystéine **E64**d, a eu le même effet que l'**IcatC$_{XPZ}$**-

**01**, nous confirmant un peu plus que la NSPs-AAP-1 n'est pas impliquée dans l'activation des Gzms et que la ou les protéase(s) impliquée(s) n'est probablement pas une protéase à cystéine. Il n'est pas improbable que ce soit la NSPs-AAP-2 qui soit, comme dans les THP-1, responsable de l'activation des Gzms A et B, cependant nous n'avons pas encore caractérisé suffisamment cette voie pour pouvoir l'affirmer. Cependant, ces résultats nous permettent de supposer que l'utilisation de traitement thérapeutique ciblant la CatS et la CatC, dans le but d'inhiber indirectement les PSN, n'aura pas d'effets délétères sur l'activité cytotoxique des lymphocytes (**Manuscrit 3**).

***Conclusion finale et perspectives***

Ces travaux de thèse nous ont permis de mettre en évidence la CatS comme cible thérapeutique intéressante pour l'inhibition de PSN dans les pathologies inflammatoires neutrophiliques. L'utilisation synergique d'inhibiteurs de CatS et de CatC semble être une stratégie thérapeutique innovante dans l'amélioration des traitements des pathologies telle que la BPCO. Les voies alternatives indépendantes de la CatC à l'activation des PSN et des Gzms ont commencé à être caractérisées. Les NSPs-AAP-1 et 2, demeurent cependant inconnues, mais la poursuite de ces travaux de thèse permettra peut-être de les identifier. Pour ce faire, l'utilisation des cellules HL-60, THP-1 et U-937 déplétées génétiquement en CatS et CatC, par CRISPR-CAS9, sont en cours de préparation. De plus, les inhibiteurs de la CatC, mais pas **Gly**-Phe-DMK, a permis d'inhiber l'activation des PSN dans les cellules U-937 (Methot et al., 2007). Nous supposons que l'inhibiteur **Ala**-Phe-DMK agit sur la CatC et la NSPs-AAP-1, à l'image de l'**IcatC$_{XPZ-01}$**, cependant sa fixation irréversible et la possibilité de son marquage radioactif, pourraient nous permettre d'isoler la NSPs-AAP-1 et de la séquencer.

# Références Bibliographiques

Abel AM, Yang C, Thakar MS and Malarkannan S (2018) Natural Killer Cells: Development, Maturation, and Clinical Utilization. *Front Immunol* **9**:1869.

Adkison AM, Raptis SZ, Kelley DG and Pham CT (2002a) Dipeptidyl peptidase I activates neutrophil-derived serine proteases and regulates the development of acute experimental arthritis. *J Clin Invest* **109**:363-371.

Adkison AM, Raptis SZ, Kelley DG and Pham CT (2002b) Dipeptidyl peptidase I activates neutrophil-derived serine proteases and regulates the development of acute experimental arthritis. *J Clin Invest* **109**:363-371.

Akula S, Lara S, Olsson AK and Hellman L (2022) Quantitative Analysis of the Transcriptome of Two Commonly Used Human Monocytic Cell Lines-THP-1 and Mono Mac 6-Reveals Their Arrest during Early Monocyte/Neutrophil Differentiation. *Int J Mol Sci* **23**.

Amar S, Smith L and Fields GB (2017) Matrix metalloproteinase collagenolysis in health and disease. *Biochim Biophys Acta Mol Cell Res* **1864**:1940-1951.

Andrault PM, Schamberger AC, Chazeirat T, Sizaret D, Renault J, Staab-Weijnitz CA, Hennen E, Petit-Courty A, Wartenberg M, Saidi A, Baranek T, Guyetant S, Courty Y, Eickelberg O, Lalmanach G and Lecaille F (2019) Cigarette smoke induces overexpression of active human cathepsin S in lungs from current smokers with or without COPD. *Am J Physiol Lung Cell Mol Physiol* **317**:L625-L638.

Babior BM (1984) Oxidants from phagocytes: agents of defense and destruction. *Blood* **64**:959-966.

Baggiolini M, Bretz U, Dewald B and Feigenson ME (1978) The polymorphonuclear leukocyte. *Agents Actions* **8**:3-10.

Bainton DF and Farquhar MG (1966) Origin of granules in polymorphonuclear leukocytes. Two types derived from opposite faces of the Golgi complex in developing granulocytes. *J Cell Biol* **28**:277-301.

Barnas JL, Looney RJ and Anolik JH (2019) B cell targeted therapies in autoimmune disease. *Curr Opin Immunol* **61**:92-99.

Barnes PJ and Stockley RA (2005) COPD: current therapeutic interventions and future approaches. *Eur Respir J* **25**:1084-1106.

Basso J, Chen KJ, Zhou Y, Mark L, LaSala D, Dorfman A, Atalla M, Chun D, Viramontes V, Chang C, Leifer F, McDonald PP and Cipolla DC (2023) The pharmacokinetic profile of brensocatib and its effect on pharmacodynamic biomarkers including NE, PR3, and CatG in various rodent species. *Front Pharmacol* **14**:1208780.

Bigot P, Chesseron S, Saidi A, Sizaret D, Parent C, Petit-Courty A, Courty Y, Lecaille F and Lalmanach G (2022) Cleavage of Occludin by Cigarette Smoke-Elicited Cathepsin S Increases Permeability of Lung Epithelial Cells. *Antioxidants (Basel)* **12**.

Bode W, Wei AZ, Huber R, Meyer E, Travis J and Neumann S (1986) X-ray crystal structure of the complex of human leukocyte elastase (PMN elastase) and the third domain of the turkey ovomucoid inhibitor. *Embo J* **5**:2453-2458.

Bondebjerg J, Fuglsang H, Valeur KR, Pedersen J and Naerum L (2006) Dipeptidyl nitriles as human dipeptidyl peptidase I inhibitors. *Bioorg Med Chem Lett* **16**:3614-3617.

Bone HG, McClung MR, Roux C, Recker RR, Eisman JA, Verbruggen N, Hustad CM, DaSilva C, Santora AC and Ince BA (2010) Odanacatib, a cathepsin-K inhibitor for osteoporosis: a two-year study in postmenopausal women with low bone density. *J Bone Miner Res* **25**:937-947.

Bories D, Raynal MC, Solomon DH, Darzynkiewicz Z and Cayre YE (1989) Down-regulation of a serine protease, myeloblastin, causes growth arrest and differentiation of promyelocytic leukemia cells. *Cell* **59**:959-968.

Borregaard N (2010) Neutrophils, from marrow to microbes. *Immunity* **33**:657-670.

Borregaard N and Cowland JB (1997) Granules of the human neutrophilic polymorphonuclear leukocyte. *Blood* **89**:3503-3521.

Borregaard N, Sorensen OE and Theilgaard-Monch K (2007) Neutrophil granules: a library of innate immunity proteins. *Trends Immunol* **28**:340-345.

Bossard MJ, Tomaszek TA, Thompson SK, Amegadzie BY, Hanning CR, Jones C, Kurdyla JT, McNulty DE, Drake FH, Gowen M and Levy MA (1996) Proteolytic activity of human osteoclast cathepsin K. Expression, purification, activation, and substrate identification. *J Biol Chem* **271**:12517-12524.

Bourgon C, Albin AS, Ando-Grard O, Da Costa B, Domain R, Korkmaz B, Klonjkowski B, Le Poder S and Meunier N (2022) Neutrophils play a major role in the destruction of the olfactory epithelium during SARS-CoV-2 infection in hamsters. *Cell Mol Life Sci* **79**:616.

Brinkmann V, Reichard U, Goosmann C, Fauler B, Uhlemann Y, Weiss DS, Weinrauch Y and Zychlinsky A (2004) Neutrophil extracellular traps kill bacteria. *Science* **303**:1532-1535.

Bromme D (2001) Papain-like cysteine proteases. *Curr Protoc Protein Sci* **Chapter 21**:Unit 21 22.

Bromme D, Li Z, Barnes M and Mehler E (1999) Human cathepsin V functional expression, tissue distribution, electrostatic surface potential, enzymatic characterization, and chromosomal localization. *Biochemistry* **38**:2377-2385.

Bromme D and Okamoto K (1995) Human cathepsin O2, a novel cysteine protease highly expressed in osteoclastomas and ovary molecular cloning, sequencing and tissue distribution. *Biol Chem Hoppe Seyler* **376**:379-384.

Brown GR, McGuire MJ and Thiele DL (1993) Dipeptidyl peptidase I is enriched in granules of in vitro- and in vivo-activated cytotoxic T lymphocytes. *J Immunol* **150**:4733-4742.

Butler GS, Overall CM (2013) Matrix metalloproteinase processing of signaling molecules to regulate inflammation. *Periodontol 2000* **63**(1):123-48

Capizzi SA, Viss MA, Hummel AM, Fass DN and Specks U (2003) Effects of carboxy-terminal modifications of proteinase 3 (PR3) on the recognition by PR3-ANCA. *Kidney Int* **63**:756-760.

Chalmers JD, Gupta A, Chotirmall SH, Armstrong A, Eickholz P, Hasegawa N, McShane PJ, O'Donnell AE, Shteinberg M, Watz H, Eleftheraki A, Diefenbach C and Sauter W (2023) A Phase 2 randomised study to establish efficacy, safety and dosing of a novel oral cathepsin C inhibitor, BI 1291583, in adults with bronchiectasis: Airleaf. *ERJ Open Res* **9**.

Chalmers JD, Haworth CS, Metersky ML, Loebinger MR, Blasi F, Sibila O, O'Donnell AE, Sullivan EJ, Mange KC, Fernandez C, Zou J, Daley CL and Investigators W (2020) Phase 2 Trial of the DPP-1 Inhibitor Brensocatib in Bronchiectasis. *N Engl J Med*.

Cham BP, Gerrard JM and Bainton DF (1994) Granulophysin is located in the membrane of azurophilic granules in human neutrophils and mobilizes to the plasma membrane following cell stimulation. *Am J Pathol* **144**:1369-1380.

Chen KJ, Zhang J, LaSala D, Basso J, Chun D, Zhou Y, McDonald PP, Perkins WR and Cipolla DC (2023) Brensocatib, an oral, reversible inhibitor of dipeptidyl peptidase 1, mitigates interferon-alpha-accelerated lupus nephritis in mice. *Front Immunol* **14**:1185727.

Chen X, Yan Y, Zhang Z, Zhang F, Liu M, Du L, Zhang H, Shen X, Zhao D, Shi JB and Liu X (2021) Discovery and In Vivo Anti-inflammatory Activity Evaluation of a Novel Non-peptidyl Non-covalent Cathepsin C Inhibitor. *J Med Chem* **64**:11857-11885.

Choe Y, Leonetti F, Greenbaum DC, Lecaille F, Bogyo M, Bromme D, Ellman JA and Craik CS (2006) Substrate profiling of cysteine proteases using a combinatorial peptide library identifies functionally unique specificities. *J Biol Chem* **281**:12824-12832.

Chwieralski CE, Welte T and Buhling F (2006) Cathepsin-regulated apoptosis. *Apoptosis* **11**:143-149.

Cieutat AM, Lobel P, August JT, Kjeldsen L, Sengelov H, Borregaard N and Bainton DF (1998) Azurophilic granules of human neutrophilic leukocytes are deficient in lysosome-associated membrane proteins but retain the mannose 6-phosphate recognition marker. *Blood* **91**:1044-1058.

Cigic B and Pain RH (1999) Location of the binding site for chloride ion activation of cathepsin C. *Eur J Biochem* **264**:944-951.

Cipolla D, Zhang J, Korkmaz B, Chalmers JD, Basso J, Lasala D, Fernandez C, Teper A, Mange KC, Perkins WR and Sullivan EJ (2023) Dipeptidyl peptidase-1 inhibition with brensocatib reduces the activity of all major neutrophil serine proteases in patients with bronchiectasis: results from the WILLOW trial. *Respir Res* **24**:133.

Coillard A and Segura E (2019) In vivo Differentiation of Human Monocytes. *Front Immunol* **10**:1907.

Coulombe R, Grochulski P, Sivaraman J, Menard R, Mort JS and Cygler M (1996) Structure of human procathepsin L reveals the molecular basis of inhibition by the prosegment. *EMBO J* **15**:5492-5503.

Cowland JB and Borregaard N (2016) Granulopoiesis and granules of human neutrophils. *Immunol Rev* **273**:11-28.

Cutolo M, Campitiello R, Gotelli E and Soldano S (2022) The Role of M1/M2 Macrophage Polarization in Rheumatoid Arthritis Synovitis. *Front Immunol* **13**:867260.

Cygler M and Mort JS (1997) Proregion structure of members of the papain superfamily. Mode of inhibition of enzymatic activity. *Biochimie* **79**:645-652.

Dahl SW, Halkier T, Lauritzen C, Dolenc I, Pedersen J, Turk V and Turk B (2001) Human recombinant pro-dipeptidyl peptidase I (cathepsin C) can be activated by cathepsins L and S but not by autocatalytic processing. *Biochemistry* **40**:1671-1678.

Dang YZ, Chen XJ, Yu J, Zhao SH, Cao XM and Wang Q (2023) Cathepsin C promotes colorectal cancer metastasis by regulating immune escape through upregulating CSF1. *Neoplasma* **70**:123-135.

Das A, Sinha M, Datta S, Abas M, Chaffee S, Sen CK and Roy S (2015) Monocyte and macrophage plasticity in tissue repair and regeneration. *Am J Pathol* **185**:2596-2606.

Dementiev A, Dobo J and Gettins PG (2006) Active site distortion is sufficient for proteinase inhibition by serpins: structure of the covalent complex of alpha1-proteinase inhibitor with porcine pancreatic elastase. *J Biol Chem* **281**:3452-3457.

Deu E, Verdoes M and Bogyo M (2012) New approaches for dissecting protease functions to improve probe development and drug discovery. *Nat Struct Mol Biol* **19**:9-16.

Dolenc I, Turk B, Pungercic G, Ritonja A and Turk V (1995) Oligomeric structure and substrate induced inhibition of human cathepsin C. *J Biol Chem* **270**:21626-21631.

Douaiher J, Succar J, Lancerotto L, Gurish MF, Orgill DP, Hamilton MJ, Krilis SA and Stevens RL (2014) Development of mast cells and importance of their tryptase and chymase serine proteases in inflammation and wound healing. *Adv Immunol* **122**:211-252.

Doyle K, Lonn H, Kack H, Van de Poel A, Swallow S, Gardiner P, Connolly S, Root J, Wikell C, Dahl G, Stenvall K and Johannesson P (2016) Discovery of Second Generation Reversible Covalent DPP1 Inhibitors Leading to an Oxazepane Amidoacetonitrile Based Clinical Candidate (AZD7986). *J Med Chem* **59**:9457-9472.

Drake FH, Dodds RA, James IE, Connor JR, Debouck C, Richardson S, Lee-Rykaczewski E, Coleman L, Rieman D, Barthlow R, Hastings G and Gowen M (1996) Cathepsin K, but not cathepsins B, L, or S, is abundantly expressed in human osteoclasts. *J Biol Chem* **271**:12511-12516.

Egesten A, Breton-Gorius J, Guichard J, Gullberg U and Olsson I (1994) The heterogeneity of azurophil granules in neutrophil promyelocytes: immunogold localization of myeloperoxidase, cathepsin G, elastase, proteinase 3, and bactericidal/permeability increasing protein. *Blood* **83**:2985-2994.

Erez E, Fass D and Bibi E (2009) How intramembrane proteases bury hydrolytic reactions in the membrane. *Nature* **459**:371-378.

Erickson AH, Isidoro C and Mach LM, J.S. (2013) *Proteases: Structure and Function*, Springer.

Falk RJ, Terrell RS, Charles LA and Jennette JC (1990) Anti-neutrophil cytoplasmic autoantibodies induce neutrophils to degranulate and produce oxygen radicals in vitro. *Proc Natl Acad Sci U S A* **87**:4115-4119.

Mikkel Faurschou, Niels Borregaard, (2003) Neutrophil granules and secretory vesicles in inflammation, *Microbes and Infection,*Volume 5, Issue 14, 1317-1327.

Filippi MD (2016) Mechanism of Diapedesis: Importance of the Transcellular Route. *Adv Immunol* **129**:25-53.

Fingleton B (2017) Matrix metalloproteinases as regulators of inflammatory processes. *Biochim Biophys Acta Mol Cell Res* **1864**:2036-2042.

Flannery T, McQuaid S, McGoohan C, McConnell RS, McGregor G, Mirakhur M, Hamilton P, Diamond J, Cran G, Walker B, Scott C, Martin L, Ellison D, Patel C, Nicholson C, Mendelow D, McCormick D and Johnston PG (2006) Cathepsin S expression: An independent prognostic factor in glioblastoma tumours--A pilot study. *Int J Cancer* **119**:854-860.

Fonovic M and Turk B (2014) Cysteine cathepsins and extracellular matrix degradation. *Biochim Biophys Acta* **1840**:2560-2570.

Fujinaga M, Chernaia MM, Halenbeck R, Koths K and James MN (1996) The crystal structure of PR3, a neutrophil serine proteinase antigen of Wegener's granulomatosis antibodies. *J Mol Biol* **261**:267-278.

Gal S, Willingham MC and Gottesman MM (1985) Processing and lysosomal localization of a glycoprotein whose secretion is transformation stimulated. *J Cell Biol* **100**:535-544.

Ganz T, Selsted ME, Szklarek D, Harwig SS, Daher K, Bainton DF and Lehrer RI (1985) Defensins. Natural peptide antibiotics of human neutrophils. *J Clin Invest* **76**:1427-1435.

Garwicz D, Lindmark A, Hellmark T, Gladh M, Jogi J and Gullberg U (1997) Characterization of the processing and granular targeting of human proteinase 3 after transfection to the rat RBL or the murine 32D leukemic cell lines. *J Leukoc Biol* **61**:113-123.

Gelb BD, Shi GP, Heller M, Weremowicz S, Morton C, Desnick RJ and Chapman HA (1997) Structure and chromosomal assignment of the human cathepsin K gene. *Genomics* **41**:258-262.

Guarino C, Hamon Y, Croix C, Lamort AS, Dallet-Choisy S, Marchand-Adam S, Lesner A, Baranek T, Viaud-Massuard MC, Lauritzen C, Pedersen J, Heuze-Vourc'h N, Si-Tahar M, Firatli E, Jenne DE, Gauthier F, Horwitz MS, Borregaard N and Korkmaz B (2017) Prolonged pharmacological inhibition of cathepsin C results in elimination of neutrophil serine proteases. *Biochem Pharmacol* **131**:52-67.

Guglani L, Khader SA (2010) Th17 cytokines in mucosal immunity and inflammation. *Curr Opin HIV AIDS* **5**(2):120-7.

Guicciardi ME, Leist M and Gores GJ (2004) Lysosomes in cell death. *Oncogene* **23**:2881-2890.

Gullberg U, Lindmark A, Lindgren G, Persson AM, Nilsson E and Olsson I (1995) Carboxyl-terminal prodomain-deleted human leukocyte elastase and cathepsin G are efficiently

targeted to granules and enzymatically activated in the rat basophilic/mast cell line RBL. *J Biol Chem* **270**:12912-12918.

Guncar G, Pungercic G, Klemencic I, Turk V and Turk D (1999) Crystal structure of MHC class II-associated p41 Ii fragment bound to cathepsin L reveals the structural basis for differentiation between cathepsins L and S. *EMBO J* **18**:793-803.

Hamon Y, Legowska M, Fergelot P, Dallet-Choisy S, Newell L, Vanderlynden L, Kord Valeshabad A, Acrich K, Kord H, Charalampos T, Morice-Picard F, Surplice I, Zoidakis J, David K, Vlahou A, Ragunatha S, Nagy N, Farkas K, Szell M, Goizet C, Schacher B, Battino M, Al Farraj Aldosari A, Wang X, Liu Y, Marchand-Adam S, Lesner A, Kara E, Korkmaz-Icoz S, Moss C, Eickholz P, Taieb A, Kavukcu S, Jenne DE, Gauthier F and Korkmaz B (2016a) Analysis of urinary cathepsin C for diagnosing Papillon-Lefevre syndrome. *FEBS J* **283**:498-509.

Hamon Y, Legowska M, Herve V, Dallet-Choisy S, Marchand-Adam S, Vanderlynden L, Demonte M, Williams R, Scott CJ, Si-Tahar M, Heuze-Vourc'h N, Lalmanach G, Jenne DE, Lesner A, Gauthier F and Korkmaz B (2016b) Neutrophilic cathepsin C is maturated by a multi-step proteolytic process and secreted by activated cells during inflammatory lung diseases. *J Biol Chem*.

Hamon Y, Legowska M, Herve V, Dallet-Choisy S, Marchand-Adam S, Vanderlynden L, Demonte M, Williams R, Scott CJ, Si-Tahar M, Heuze-Vourc'h N, Lalmanach G, Jenne DE, Lesner A, Gauthier F and Korkmaz B (2016c) Neutrophilic Cathepsin C Is Maturated by a Multistep Proteolytic Process and Secreted by Activated Cells during Inflammatory Lung Diseases. *J Biol Chem* **291**:8486-8499.

Han L, Yang J, Wang X, Li D, Lv L, Li B (2015) Th17 cells in autoimmune diseases. *Front Med* **9**(1):10-9.

Hara K, Kominami E and Katunuma N (1988) Effect of proteinase inhibitors on intracellular processing of cathepsin B, H and L in rat macrophages. *FEBS Lett* **231**:229-231.

Hay ZLZ and Slansky JE (2022) Granzymes: The Molecular Executors of Immune-Mediated Cytotoxicity. *Int J Mol Sci* **23**.

Hedstrom L (2002) Serine Protease Mechanism and Specificity. *Chem Rev* **102**:4501-4523.

Helske S, Syvaranta S, Lindstedt KA, Lappalainen J, Oorni K, Mayranpaa MI, Lommi J, Turto H, Werkkala K, Kupari M and Kovanen PT (2006) Increased expression of elastolytic cathepsins S, K, and V and their inhibitor cystatin C in stenotic aortic valves. *Arterioscler Thromb Vasc Biol* **26**:1791-1798.

Hermant B, Bibert S, Concord E, Dublet B, Weidenhaupt M, Vernet T and Gulino-Debrac D (2003) Identification of proteases involved in the proteolysis of vascular endothelium cadherin during neutrophil transmigration. *J Biol Chem* **278**:14002-14012.

Hickey MJ, Kubes P. Intravascular immunity: the host-pathogen encounter in blood vessels. Nat Rev Immunol. 2009 May;9(5):364-75.

Hink-Schauer C, Estebanez-Perpina E, Kurschus FC, Bode W and Jenne DE (2003) Crystal structure of the apoptosis-inducing human granzyme A dimer. *Nat Struct Biol* **10**:535-540.

Hof P, Mayr I, Huber R, Korzus E, Potempa J, Travis J, Powers JC and Bode W (1996) The 1.8 A crystal structure of human cathepsin G in complex with Suc-Val-Pro-PheP-(OPh)2: a Janus-faced proteinase with two opposite specificities. *Embo J* **15**:5481-5491.

Hou W, Sun H, Ma Y, Liu C and Zhang Z (2019) Identification and Optimization of Novel Cathepsin C Inhibitors Derived from EGFR Inhibitors. *J Med Chem* **62**:5901-5919.

Itoh R, Kawamoto S, Adachi W, Kinoshita S, Okubo K (1999) Genomic organization and chromosomal localization of the human cathepsin L2 gene. *DNA Res* **6**(2):137-40.

Janoff A and Scherer J (1968) Mediators of inflammation in leukocyte lysosomes. IX. Elastinolytic activity in granules of human polymorphonuclear leukocytes. *J Exp Med* **128**:1137-1155.

Jenne DE, Tschopp J, Ludemann J, Utecht B and Gross WL (1990) Wegener's autoantigen decoded. *Nature* **346**:520.

Jerke U, Eulenberg-Gustavus C, Rousselle A, Nicklin P, Kreideweiss S, Grundl MA, Eickholz P, Nickles K, Schreiber A, Korkmaz B and Kettritz R (2022) Targeting Cathepsin C in PR3-ANCA Vasculitis. *J Am Soc Nephrol* **33**:936-947.

Kaulmann G, Palm GJ, Schilling K, Hilgenfeld R and Wiederanders B (2006) The crystal structure of a Cys25 -> Ala mutant of human procathepsin S elucidates enzyme-prosequence interactions. *Protein Sci* **15**:2619-2629.

Kaushansky K (2006) Lineage-specific hematopoietic growth factors. *N Engl J Med* **354**:2034-2045.

Keir HR, Long MB, Abo-Leyah H, Giam YH, Vadiveloo T, Pembridge T, Hull RC, Delgado L, Band M, McLaren-Neil F, Adamson S, Lahnsteiner E, Gilmour A, Hughes C, New BJ, Connell D, Dowey R, Turton H, Richardson H, Cassidy D, Cooper J, Suntharalingam J, Diwakar L, Russell P, Underwood J, Hicks A, Dosanjh DP, Sage B, Dhasmana D, Spears M, Thompson AR, Brightling C, Smith A, Patel M, George J, Condliffe AM, Shoemark A, MacLennan G, Chalmers JD and Investigators S-C (2022) Dipeptidyl peptidase-1 inhibition in patients hospitalised with COVID-19: a multicentre, double-blind, randomised, parallel-group, placebo-controlled trial. *Lancet Respir Med* **10**:1119-1128.

Ketterer S, Gomez-Auli A, Hillebrand LE, Petrera A, Ketscher A and Reinheckel T (2017) Inherited diseases caused by mutations in cathepsin protease genes. *FEBS J* **284**:1437-1454.

Kitamoto S, Sukhova GK, Sun J, Yang M, Libby P, Love V, Duramad P, Sun C, Zhang Y, Yang X, Peters C and Shi GP (2007) Cathepsin L deficiency reduces diet-induced atherosclerosis in low-density lipoprotein receptor-knockout mice. *Circulation* **115**:2065-2075.

Kjeldsen L, Johnsen AH, Sengelov H and Borregaard N (1993) Isolation and primary structure of NGAL, a novel protein associated with human neutrophil gelatinase. *J Biol Chem* **268**:10425-10432.

Koike M, Shibata M, Ezaki J, Peters C, Saftig P, Kominami E and Uchiyama Y (2013) Differences in expression patterns of cathepsin C/dipeptidyl peptidase I in normal, pathological and aged mouse central nervous system. *Eur J Neurosci* **37**:816-830.

Kolaczkowska E and Kubes P (2013) Neutrophil recruitment and function in health and inflammation. *Nat Rev Immunol* **13**:159-175.

Korkmaz B, Caughey GH, Chapple I, Gauthier F, Hirschfeld J, Jenne DE, Kettritz R, Lalmanach G, Lamort AS, Lauritzen C, Legowska M, Lesner A, Marchand-Adam S, McKaig SJ, Moss C, Pedersen J, Roberts H, Schreiber A, Seren S and Thakker NS (2018a) Therapeutic targeting of cathepsin C: from pathophysiology to treatment. *Pharmacol Ther* **190**:202-236.

Korkmaz B, Caughey GH, Chapple I, Gauthier F, Hirschfeld J, Jenne DE, Kettritz R, Lalmanach G, Lamort AS, Lauritzen C, Legowska M, Lesner A, Marchand-Adam S, McKaig SJ, Moss C, Pedersen J, Roberts H, Schreiber A, Seren S and Thakker NS (2018b) Therapeutic targeting of cathepsin C: from pathophysiology to treatment. *Pharmacol Ther*.

Korkmaz B, Hajjar E, Kalupov T, Reuter N, Brillard-Bourdet M, Moreau T, Juliano L and Gauthier F (2007) Influence of charge distribution at the active site surface on the

substrate specificity of human neutrophil protease 3 and elastase. A kinetic and molecular modeling analysis. *J Biol Chem* **282**:1989-1997.
Korkmaz B, Horwitz MS, Jenne DE and Gauthier F (2010) Neutrophil elastase, proteinase 3, and cathepsin G as therapeutic targets in human diseases. *Pharmacol Rev* **62**:726-759.
Korkmaz B, Lamort AS, Domain R, Beauvillain C, Gieldon A, Yildirim AO, Stathopoulos GT, Rhimi M, Jenne DE and Kettritz R (2021) Cathepsin C inhibition as a potential treatment strategy in cancer. *Biochem Pharmacol* **194**:114803.
Korkmaz B, Lesner A, Marchand-Adam S, Moss C and Jenne DE (2020a) Lung Protection by Cathepsin C Inhibition: A New Hope for COVID-19 and ARDS? *J Med Chem* **63**:13258-13265.
Korkmaz B, Lesner A, Marchand-Adam S, Moss C and Jenne DE (2020b) Lung Protection by Cathepsin C Inhibition: A New Hope for COVID-19 and ARDS? *J Med Chem*.
Korkmaz B, Lesner A, Wysocka M, Gieldon A, Hakansson M, Gauthier F, Logan DT, Jenne DE, Lauritzen C and Pedersen J (2019) Structure-based design and in vivo anti-arthritic activity evaluation of a potent dipeptidyl cyclopropyl nitrile inhibitor of cathepsin C. *Biochem Pharmacol* **164**:349-367.
Korkmaz B, Moreau T and Gauthier F (2008) Neutrophil elastase, proteinase 3 and cathepsin G: physicochemical properties, activity and physiopathological functions. *Biochimie* **90**:227-242.
Kouzehkanan ZM, Saghari S, Tavakoli S, Rostami P, Abaszadeh M, Mirzadeh F, Satlsar ES, Gheidishahran M, Gorgi F, Mohammadi S and Hosseini R (2022) A large dataset of white blood cells containing cell locations and types, along with segmented nuclei and cytoplasm. *Sci Rep* **12**:1123.
Kramer L, Turk D and Turk B (2017) The Future of Cysteine Cathepsins in Disease Management. *Trends Pharmacol Sci* **38**:873-898.
Kratofil RM, Kubes P and Deniset JF (2017) Monocyte Conversion During Inflammation and Injury. *Arterioscler Thromb Vasc Biol* **37**:35-42.
Kreideweiss S, Schanzle G, Schnapp G, Vintonyak V and Grundl MA (2023) BI 1291583: a novel selective inhibitor of cathepsin C with superior in vivo profile for the treatment of bronchiectasis. *Inflamm Res*.
Kumar BV, Connors TJ and Farber DL (2018) Human T Cell Development, Localization, and Function throughout Life. *Immunity* **48**:202-213.
Lambeth JD (2007) Nox enzymes, ROS, and chronic disease: an example of antagonistic pleiotropy. *Free Radic Biol Med* **43**:332-347.
Lamort AS, Hamon Y, Czaplewski C, Gieldon A, Seren S, Coquet L, Lecaille F, Lesner A, Lalmanach G, Gauthier F, Jenne D and Korkmaz B (2019) Processing and Maturation of Cathepsin C Zymogen: A Biochemical and Molecular Modeling Analysis. *Int J Mol Sci* **20**.
LeBien TW and Tedder TF (2008) B lymphocytes: how they develop and function. *Blood* **112**:1570-1580.
Lecaille F, Kaleta J and Bromme D (2002) Human and parasitic papain-like cysteine proteases: their role in physiology and pathology and recent developments in inhibitor design. *Chem Rev* **102**:4459-4488.
Lecaille F, Weidauer E, Juliano MA, Bromme D and Lalmanach G (2003) Probing cathepsin K activity with a selective substrate spanning its active site. *Biochem J* **375**:307-312.
Legowska M, Hamon Y, Wojtysiak A, Grzywa R, Sienczyk M, Burster T, Korkmaz B and Lesner A (2016) Development of the first internally-quenched fluorescent substrates of human cathepsin C: The application in the enzyme detection in biological samples. *Arch Biochem Biophys* **612**:91-102.

Levy O (2004) Antimicrobial proteins and peptides: anti-infective molecules of mammalian leukocytes. *J Leukoc Biol* **76**:909-925.
Ley K, Laudanna C, Cybulsky MI and Nourshargh S (2007) Getting to the site of inflammation: the leukocyte adhesion cascade updated. *Nat Rev Immunol* **7**:678-689.
Li Z, Hou WS, Escalante-Torres CR, Gelb BD and Bromme D (2002) Collagenase activity of cathepsin K depends on complex formation with chondroitin sulfate. *J Biol Chem* **277**:28669-28676.
Lindahl C, Simonsson M, Bergh A, Thysell E, Antti H, Sund M and Wikstrom P (2009) Increased levels of macrophage-secreted cathepsin S during prostate cancer progression in TRAMP mice and patients. *Cancer Genomics Proteomics* **6**:149-159.
Löwe J, Stock D, Jap B, Zwickl P, Baumeister W, Huber R (1995) Crystal structure of the 20S proteasome from the archaeon T. acidophilum at 3.4 A resolution. *Science* **268**(5210):533-9.
Lopez-Otin C and Bond JS (2008) Proteases: multifunctional enzymes in life and disease. *J Biol Chem* **283**:30433-30437.
Lukacs-Kornek V and Turley SJ (2008) Immunology. Chaperone puts the brakes on. *Science* **322**:1640-1641.
Marino-Puertas L, Goulas T and Gomis-Ruth FX (2017) Matrix metalloproteinases outside vertebrates. *Biochim Biophys Acta Mol Cell Res* **1864**:2026-2035.
Martinvalet D, Zhu P and Lieberman J (2005) Granzyme A induces caspase-independent mitochondrial damage, a required first step for apoptosis. *Immunity* **22**:355-370.
Mauri C and Bosma A (2012) Immune regulatory function of B cells. *Annu Rev Immunol* **30**:221-241.
McDonald AG and Tipton KF (2014) Fifty-five years of enzyme classification: advances and difficulties. *FEBS J* **281**:583-592.
McDonald PP, Leifer FG, Basso J, Lasala D, Li D, Chen KJ, Zhang J, Perkins WR and Cipolla DC (2023) Brensocatib (an oral, reversible inhibitor of dipeptidyl peptidase-1) attenuates disease progression in two animal models of rheumatoid arthritis. *Front Immunol* **14**:1231047.
McGuire MJ, Lipsky PE and Thiele DL (1993) Generation of active myeloid and lymphoid granule serine proteases requires processing by the granule thiol protease dipeptidyl peptidase I. *J Biol Chem* **268**:2458-2467.
Medzhitov R (2008) Origin and physiological roles of inflammation. *Nature* **454**(7203):428-35
Meitei HT, Lal G (2023) T cell receptor signaling in the differentiation and plasticity of CD4+ T cells. *Cytokine Growth Factor Rev* **69**:14-27.
Meizlish ML, Franklin RA, Zhou X and Medzhitov R (2021) Tissue Homeostasis and Inflammation. *Annu Rev Immunol* **39**:557-581.
Menard R, Carmona E, Takebe S, Dufour E, Plouffe C, Mason P and Mort JS (1998) Autocatalytic processing of recombinant human procathepsin L. Contribution of both intermolecular and unimolecular events in the processing of procathepsin L in vitro. *J Biol Chem* **273**:4478-4484.
Methot N, Rubin J, Guay D, Beaulieu C, Ethier D, Reddy TJ, Riendeau D and Percival MD (2007) Inhibition of the activation of multiple serine proteases with a cathepsin C inhibitor requires sustained exposure to prevent pro-enzyme processing. *J Biol Chem* **282**:20836-20846.
Miller BE, Mayer RJ, Goyal N, Bal J, Dallow N, Boyce M, Carpenter D, Churchill A, Heslop T and Lazaar AL (2017) Epithelial desquamation observed in a phase I study of an oral cathepsin C inhibitor (GSK2793660). *Br J Clin Pharmacol* **83**:2813-2820.
Mitchell AJ, Roediger B and Weninger W (2014) Monocyte homeostasis and the plasticity of inflammatory monocytes. *Cell Immunol* **291**:22-31.

Molgaard A, Arnau J, Lauritzen C, Larsen S, Petersen G and Pedersen J (2007) The crystal structure of human dipeptidyl peptidase I (cathepsin C) in complex with the inhibitor Gly-Phe-CHN2. *Biochem J* **401**:645-650.

Musil D, Zucic D, Turk D, Engh RA, Mayr I, Huber R, Popovic T, Turk V, Towatari T, Katunuma N and et al. (1991) The refined 2.15 A X-ray crystal structure of human liver cathepsin B: the structural basis for its specificity. *EMBO J* **10**:2321-2330.

Nagler DK, Sulea T and Menard R (1999) Full-length cDNA of human cathepsin F predicts the presence of a cystatin domain at the N-terminus of the cysteine protease zymogen. *Biochem Biophys Res Commun* **257**:313-318.

Nauseef WM (2007) How human neutrophils kill and degrade microbes: an integrated view. *Immunol Rev* **219**:88-102.

O'Brien KL and Finlay DK (2019) Immunometabolism and natural killer cell responses. *Nat Rev Immunol* **19**:282-290.

Oliveira M, Torquato RJ, Alves MF, Juliano MA, Bromme D, Barros NM and Carmona AK (2010) Improvement of cathepsin S detection using a designed FRET peptide based on putative natural substrates. *Peptides* **31**:562-567.

Oorni K, Sneck M, Bromme D, Pentikainen MO, Lindstedt KA, Mayranpaa M, Aitio H and Kovanen PT (2004) Cysteine protease cathepsin F is expressed in human atherosclerotic lesions, is secreted by cultured macrophages, and modifies low density lipoprotein particles in vitro. *J Biol Chem* **279**:34776-34784.

Othman A, Sekheri M, Filep JG (2022) Roles of neutrophil granule proteins in orchestrating inflammation and immunity. *FEBS J*. **289**(14):3932-3953.

Pagani M, Rossetti G, Panzeri I, de Candia P, Bonnal RJ, Rossi RL, Geginat J, Abrignani S. Role of microRNAs and long-non-coding RNAs in CD4(+) T-cell differentiation. Immunol Rev. 2013 May;253(1):82-96.

Parker H, Albrett AM, Kettle AJ and Winterbourn CC (2012) Myeloperoxidase associated with neutrophil extracellular traps is active and mediates bacterial killing in the presence of hydrogen peroxide. *J Leukoc Biol* **91**:369-376.

Patel AA, Zhang Y, Fullerton JN, Boelen L, Rongvaux A, Maini AA, Bigley V, Flavell RA, Gilroy DW, Asquith B, Macallan D, Yona S (2017) The fate and lifespan of human monocyte subsets in steady state and systemic inflammation. *J Exp Med* **214**(7):1913-1923.

Perera NC, Schilling O, Kittel H, Back W, Kremmer E and Jenne DE (2012) NSP4, an elastase-related protease in human neutrophils with arginine specificity. *Proc Natl Acad Sci U S A* **109**:6229-6234.

Perera NC, Wiesmuller KH, Larsen MT, Schacher B, Eickholz P, Borregaard N and Jenne DE (2013) NSP4 is stored in azurophil granules and released by activated neutrophils as active endoprotease with restricted specificity. *J Immunol* **191**:2700-2707.

Pham CT (2006) Neutrophil serine proteases: specific regulators of inflammation. *Nat Rev Immunol* **6**:541-550.

Pham CT, Armstrong RJ, Zimonjic DB, Popescu NC, Payan DG and Ley TJ (1997) Molecular cloning, chromosomal localization, and expression of murine dipeptidyl peptidase I. *J Biol Chem* **272**:10695-10703.

Pham CT, Ivanovich JL, Raptis SZ, Zehnbauer B and Ley TJ (2004) Papillon-Lefevre syndrome: correlating the molecular, cellular, and clinical consequences of cathepsin C/dipeptidyl peptidase I deficiency in humans. *J Immunol* **173**:7277-7281.

Pieper K, Grimbacher B and Eibel H (2013) B-cell biology and development. *J Allergy Clin Immunol* **131**:959-971.

Pillay J, den Braber I, Vrisekoop N, Kwast LM, de Boer RJ, Borghans JA, Tesselaar K and Koenderman L (2010) In vivo labeling with 2H2O reveals a human neutrophil lifespan of 5.4 days. *Blood* **116**:625-627.

Pilsczek FH, Salina D, Poon KK, Fahey C, Yipp BG, Sibley CD, Robbins SM, Green FH, Surette MG, Sugai M, Bowden MG, Hussain M, Zhang K and Kubes P (2010) A novel mechanism of rapid nuclear neutrophil extracellular trap formation in response to Staphylococcus aureus. *J Immunol* **185**:7413-7425.

Plitas G, Rudensky AY (2016) Regulatory T Cells: Differentiation and Function. *Cancer Immunol Res* **4**(9):721-5.

Poreba M, Mihelic M, Krai P, Rajkovic J, Krezel A, Pawelczak M, Klemba M, Turk D, Turk B, Latajka R and Drag M (2014) Unnatural amino acids increase activity and specificity of synthetic substrates for human and malarial cathepsin C. *Amino Acids* **46**:931-943.

Portaro FC, Santos AB, Cezari MH, Juliano MA, Juliano L and Carmona E (2000) Probing the specificity of cysteine proteinases at subsites remote from the active site: analysis of P4, P3, P2' and P3' variations in extended substrates. *Biochem J* **347 Pt 1**:123-129.

Puzer L, Cotrin SS, Alves MF, Egborge T, Araujo MS, Juliano MA, Juliano L, Bromme D and Carmona AK (2004) Comparative substrate specificity analysis of recombinant human cathepsin V and cathepsin L. *Arch Biochem Biophys* **430**:274-283.

Rao NV, Rao GV and Hoidal JR (1997) Human dipeptidyl-peptidase I. Gene characterization, localization, and expression. *J Biol Chem* **272**:10260-10265.

Rawlings ND, Barrett AJ and Finn R (2016) Twenty years of the MEROPS database of proteolytic enzymes, their substrates and inhibitors. *Nucleic Acids Res* **44**:D343-350.

Raza Y, Salman H, Luberto C. (2021) Sphingolipids in Hematopoiesis: Exploring Their Role in Lineage Commitment. *Cells* **10**(10):2507.

Reiling KK, Krucinski J, Miercke LJ, Raymond WW, Caughey GH and Stroud RM (2003) Structure of human pro-chymase: a model for the activating transition of granule-associated proteases. *Biochemistry* **42**:2616-2624.

Ruffell B, Affara NI, Cottone L, Junankar S, Johansson M, DeNardo DG, Korets L, Reinheckel T, Sloane BF, Bogyo M and Coussens LM (2013) Cathepsin C is a tissue-specific regulator of squamous carcinogenesis. *Genes Dev* **27**:2086-2098.

Sage J, Mallevre F, Barbarin-Costes F, Samsonov SA, Gehrcke JP, Pisabarro MT, Perrier E, Schnebert S, Roget A, Livache T, Nizard C, Lalmanach G and Lecaille F (2013) Binding of chondroitin 4-sulfate to cathepsin S regulates its enzymatic activity. *Biochemistry* **52**:6487-6498.

Sage J, Renault J, Domain R, Bojarski KK, Chazeirat T, Saidi A, Leblanc E, Nizard C, Samsonov SA, Kurfurst R, Lalmanach G, Lecaille F. Modulation of the expression and activity of cathepsin S in reconstructed human skin by neohesperidin dihydrochalcone. Matrix Biol. 2022 Mar;107:97-112.

Santamaria I, Velasco G, Cazorla M, Fueyo A, Campo E and Lopez-Otin C (1998) Cathepsin L2, a novel human cysteine proteinase produced by breast and colorectal carcinomas. *Cancer Res* **58**:1624-1630.

Santamaria I, Velasco G, Pendas AM, Paz A and Lopez-Otin C (1999) Molecular cloning and structural and functional characterization of human cathepsin F, a new cysteine proteinase of the papain family with a long propeptide domain. *J Biol Chem* **274**:13800-13809.

Satpathy AT, Wu X, Albring JC and Murphy KM (2012) Re(de)fining the dendritic cell lineage. *Nat Immunol* **13**:1145-1154.

Schwann T (1836) Ueber das Wesen des Verdauungsprocesses. *Ann Phys Chem* **114**:358–364.

Schechter I and Berger A (1967) On the size of the active site in proteases. I. Papain. *Biochem Biophys Res Commun* **27**:157-162.

Schmitz J, Furtmann N, Ponert M, Frizler M, Loser R, Bartz U, Bajorath J and Gutschow M (2015) Active Site Mapping of Human Cathepsin F with Dipeptide Nitrile Inhibitors. *ChemMedChem* **10**:1365-1377.

Seren S, Derian L, Keles I, Guillon A, Lesner A, Gonzalez L, Baranek T, Si-Tahar M, Marchand-Adam S, Jenne DE, Paget C, Jouan Y and Korkmaz B (2021) Proteinase release from activated neutrophils in mechanically ventilated patients with non-COVID-19 and COVID-19 pneumonia. *Eur Respir J*.

Seren S, Rashed Abouzaid M, Eulenberg-Gustavus C, Hirschfeld J, Nasr Soliman H, Jerke U, N'Guessan K, Dallet-Choisy S, Lesner A, Lauritzen C, Schacher B, Eickholz P, Nagy N, Szell M, Croix C, Viaud-Massuard MC, Al Farraj Aldosari A, Ragunatha S, Ibrahim Mostafa M, Giampieri F, Battino M, Cornillier H, Lorette G, Stephan JL, Goizet C, Pedersen J, Gauthier F, Jenne DE, Marchand-Adam S, Chapple IL, Kettritz R and Korkmaz B (2018) Consequences of cathepsin C inactivation for membrane exposure of proteinase 3, the target antigen in autoimmune vasculitis. *J Biol Chem* **293**:12415-12428.

Shapouri-Moghaddam A, Mohammadian S, Vazini H, Taghadosi M, Esmaeili SA, Mardani F, Seifi B, Mohammadi A, Afshari JT and Sahebkar A (2018) Macrophage plasticity, polarization, and function in health and disease. *J Cell Physiol* **233**:6425-6440.

Sims AH, Robson GD, Hoyle DC, Oliver SG, Turner G, Prade RA, Russell HH, Dunn-Coleman NS and Gent ME (2004) Use of expressed sequence tag analysis and cDNA microarrays of the filamentous fungus Aspergillus nidulans. *Fungal Genet Biol* **41**:199-212.

Sioud M and Hansen MH (2001) Profiling the immune response in patients with breast cancer by phage-displayed cDNA libraries. *Eur J Immunol* **31**:716-725.

Somoza JR, Palmer JT and Ho JD (2002) The crystal structure of human cathepsin F and its implications for the development of novel immunomodulators. *J Mol Biol* **322**:559-568.

Sorensen OE, Clemmensen SN, Dahl SL, Ostergaard O, Heegaard NH, Glenthoj A, Nielsen FC and Borregaard N (2014) Papillon-Lefevre syndrome patient reveals species-dependent requirements for neutrophil defenses. *J Clin Invest* **124**:4539-4548.

Starkey PM and Barrett AJ (1976) Human cathepsin G. Catalytic and immunological properties. *Biochem J* **155**:273-278.

Sun L, Su Y, Jiao A, Wang X and Zhang B (2023) T cells in health and disease. *Signal Transduct Target Ther* **8**:235.

Szecsi PB (1992) The aspartic proteases. *Scand J Clin Lab Invest Suppl* **210**:5-22.

Tak T, Drylewicz J, Conemans L, de Boer RJ, Koenderman L, Borghans JAM, Tesselaar K (2017) Circulatory and maturation kinetics of human monocyte subsets in vivo. *Blood* **130**(12):1474-1477.

Thaler B, Hohensinner PJ, Krychtiuk KA, Matzneller P, Koller L, Brekalo M, Maurer G, Huber K, Zeitlinger M, Jilma B, Wojta J, Speidl WS (2016) Differential in vivo activation of monocyte subsets during low-grade inflammation through experimental endotoxemia in humans. *Sci Rep* **6**:30162.

Thome JJ, Yudanin N, Ohmura Y, Kubota M, Grinshpun B, Sathaliyawala T, Kato T, Lerner H, Shen Y and Farber DL (2014) Spatial map of human T cell compartmentalization and maintenance over decades of life. *Cell* **159**:814-828.

Toomes C, James J, Wood AJ, Wu CL, McCormick D, Lench N, Hewitt C, Moynihan L, Roberts E, Woods CG, Markham A, Wong M, Widmer R, Ghaffar KA, Pemberton M, Hussein IR, Temtamy SA, Davies R, Read AP, Sloan P, Dixon MJ and Thakker NS (1999) Loss-of-function mutations in the cathepsin C gene result in periodontal disease and palmoplantar keratosis. *Nat Genet* **23**:421-424.

Tran TV, Ellis KA, Kam CM, Hudig D and Powers JC (2002) Dipeptidyl peptidase I: importance of progranzyme activation sequences, other dipeptide sequences, and the N-

terminal amino group of synthetic substrates for enzyme activity. *Arch Biochem Biophys* **403**:160-170.

Turk D, Janjic V, Stern I, Podobnik M, Lamba D, Dahl SW, Lauritzen C, Pedersen J, Turk V and Turk B (2001a) Structure of human dipeptidyl peptidase I (cathepsin C): exclusion domain added to an endopeptidase framework creates the machine for activation of granular serine proteases. *EMBO J* **20**:6570-6582.

Turk V, Stoka V, Vasiljeva O, Renko M, Sun T, Turk B and Turk D (2012) Cysteine cathepsins: from structure, function and regulation to new frontiers. *Biochim Biophys Acta* **1824**:68-88.

Turk V, Turk B and Turk D (2001b) Lysosomal cysteine proteases: facts and opportunities. *EMBO J* **20**:4629-4633.

Vanlaere I, Libert C (2009) Matrix metalloproteinases as drug targets in infections caused by gram-negative bacteria and in septic shock. *Clin Microbiol Rev* **22**(2):224-39.

Verma S, Dixit R, Pandey KC (2016) Cysteine Proteases: Modes of Activation and Future Prospects as Pharmacological Targets. *Front Pharmacol* **7**:107.

Walker JA, McKenzie ANJ (2018) TH2 cell development and function. *Nat Rev Immunol* **18**(2):121-133.

Wex T, Levy B, Wex H and Bromme D (1999) Human cathepsins F and W: A new subgroup of cathepsins. *Biochem Biophys Res Commun* **259**:401-407.

Wiederanders B and Kirschke H (1989) The processing of a cathepsin L precursor in vitro. *Arch Biochem Biophys* **272**:516-521.

Wilkinson RD, Williams R, Scott CJ and Burden RE (2015) Cathepsin S: therapeutic, diagnostic, and prognostic potential. *Biol Chem* **396**:867-882.

Wolters PJ, Raymond WW, Blount JL and Caughey GH (1998) Regulated expression, processing, and secretion of dog mast cell dipeptidyl peptidase I. *J Biol Chem* **273**:15514-15520.

Woo YD, Jeong D and Chung DH (2021) Development and Functions of Alveolar Macrophages. *Mol Cells* **44**:292-300.

Wu Y, Yuan M, Wang C, Chen Y, Zhang Y and Zhang J (2023) T lymphocyte cell: A pivotal player in lung cancer. *Front Immunol* **14**:1102778.

Xiao Y, Cong M, Li J, He D, Wu Q, Tian P, Wang Y, Yang S, Liang C, Liang Y, Wen J, Liu Y, Luo W, Lv X, He Y, Cheng DD, Zhou T, Zhao W, Zhang P, Zhang X, Xiao Y, Qian Y, Wang H, Gao Q, Yang QC, Yang Q and Hu G (2021) Cathepsin C promotes breast cancer lung metastasis by modulating neutrophil infiltration and neutrophil extracellular trap formation. *Cancer Cell* **39**:423-437 e427.

Yan H, Zhou HF, Akk A, Hu Y, Springer LE, Ennis TL and Pham CTN (2016) Neutrophil Proteases Promote Experimental Abdominal Aortic Aneurysm via Extracellular Trap Release and Plasmacytoid Dendritic Cell Activation. *Arterioscler Thromb Vasc Biol* **36**:1660-1669.

Young RE, Voisin MB, Wang S, Dangerfield J and Nourshargh S (2007) Role of neutrophil elastase in LTB4-induced neutrophil transmigration in vivo assessed with a specific inhibitor and neutrophil elastase deficient mice. *Br J Pharmacol* **151**:628-637.

Zamai L, Ahmad M, Bennett IM, Azzoni L, Alnemri ES, Perussia B (1998) Natural killer (NK) cell-mediated cytotoxicity: differential use of TRAIL and Fas ligand by immature and mature primary human NK cells. *J Exp Med* **188**(12):2375-80.

Zhang M and Zhang S (2020) T Cells in Fibrosis and Fibrotic Diseases. *Front Immunol* **11**:1142.

Zhu J (2018) T Helper Cell Differentiation, Heterogeneity, and Plasticity. *Cold Spring Harb Perspect Biol* **10**(10):a030338.

# Annexes

# Annexe 1

Biochemical Pharmacology 194 (2021) 114803

Contents lists available at ScienceDirect

Biochemical Pharmacology

journal homepage: www.elsevier.com/locate/biochempharm

Review

# Cathepsin C inhibition as a potential treatment strategy in cancer

Brice Korkmaz [a,*], Anne-Sophie Lamort [b,1], Roxane Domain [a,1], Céline Beauvillain [c], Artur Gieldon [d], Ali Önder Yildirim [b], Georgios T. Stathopoulos [b], Moez Rhimi [e], Dieter E. Jenne [b,f], Ralph Kettritz [g,h]

[a] INSERM UMR-1100, "Research Center for Respiratory Diseases" and University of Tours, 37032 Tours, France
[b] Comprehensive Pneumology Center (CPC) and Institute for Lung Biology and Disease (iLBD), Helmholtz Center Munich-German Research Center for Environmental Health (HMGU) and Ludwig-Maximilian-University (LMU), Munich, Bavaria 81377, Germany[2]
[c] University of Angers, University of Nantes, Angers University Hospital, INSERM UMR-1232, CRCINA, Innate Immunity and Immunotherapy, SFR ICAT, 49000 Angers, France
[d] Faculty of Chemistry, University of Gdansk, 80-308 Gdansk, Poland
[e] Microbiota Interaction with Human and Animal Team (MIHA), Micalis Institute, AgroParisTech, Université Paris-Saclay, INRAE, Jouy-en-Josas, France
[f] Max Planck Institute of Neurobiology, 82152 Planegg-Martinsried, Germany
[g] Experimental and Clinical Research Center, Charité und Max-Delbrück-Centrum für Molekulare Medizin in der Helmholtz-Gemeinschaft (MDC), Berlin, Germany
[h] Nephrology and Intensive Care Medicine, Charité-Universitätsmedizin, Berlin, Germany

ARTICLE INFO

*Keywords:*
Protease
Inhibitor
Neutrophil
Treatment strategy
Inflammation
Cancer

ABSTRACT

Epidemiological studies established an association between chronic inflammation and higher risk of cancer. Inhibition of proteolytic enzymes represents a potential treatment strategy for cancer and prevention of cancer metastasis. Cathepsin C (CatC) is a highly conserved lysosomal cysteine dipeptidyl aminopeptidase required for the activation of pro-inflammatory neutrophil serine proteases (NSPs, elastase, proteinase 3, cathepsin G and NSP-4). NSPs are locally released by activated neutrophils in response to pathogens and non-infectious danger signals. Activated neutrophils also release neutrophil extracellular traps (NETs) that are decorated with several neutrophil proteins, including NSPs. NSPs are not only NETs constituents but also play a role in NET formation and release. Although immune cells harbor large amounts of CatC, additional cell sources for this protease exists. Upregulation of CatC expression was observed in different tissues during carcinogenesis and correlated with metastasis and poor patient survival. Recent mechanistic studies indicated an important interaction of tumor-associated CatC, NSPs, and NETs in cancer development and metastasis and suggested CatC as a therapeutic target in a several cancer types. Cancer cell-derived CatC promotes neutrophil recruitment in the inflammatory tumor microenvironment. Because the clinical consequences of genetic CatC deficiency in humans resulting in the elimination of NSPs are mild, small molecule inhibitors of CatC are assumed as safe drugs to reduce the NSP burden. Brensocatib, a nitrile CatC inhibitor is currently tested in a phase 3 clinical trial as a novel anti-inflammatory therapy for patients with bronchiectasis. However, recently developed CatC inhibitors possibly have protective effects beyond inflammation. In this review, we describe the pathophysiological function of CatC and discuss molecular mechanisms substantiating pharmacological CatC inhibition as a potential strategy for cancer treatment.

*Abbreviations:* BAL, broncho-alveolar lavage; Cat, cathepsin; IL, interleukin; MMP, matrix metalloproteinase; NE, neutrophil elastase; NETs, neutrophil extracellular traps; NSP, neutrophil serine protease; PDB, Protein Data Bank; PLS, Papillon-Lefèvre syndrome; PR3, proteinase 3; $PR3^{mb}$, membrane-bound PR3.

* Corresponding author at: INSERM UMR-1100, "Research Center for Respiratory Diseases", University of Tours, Faculty of Medicine, 10 Bld. Tonnellé, 37032 Tours, France.
*E-mail address:* brice.korkmaz@inserm.fr (B. Korkmaz).

[1] Equal contribution.
[2] A member of the German Center for Lung Research (DZL).

https://doi.org/10.1016/j.bcp.2021.114803
Received 9 August 2021; Received in revised form 30 September 2021; Accepted 4 October 2021
Available online 20 October 2021
0006-2952/© 2021 Elsevier Inc. All rights reserved.

## 1. Introduction

Cancer represents a global health problem and is ranked as the second most common cause of death by the World Health Organization. Among the different cancer types, lung cancer contributed worldwide to more than 2 million new cases in 2020 with an unfavorable survival rate [1,2]. Substantial efforts have been made to better characterize lung cancer subtypes by the identification of key mutation patterns [3,4] and deciphering molecular disease mechanisms [5] particularly with respect to metastases. Upon adhesion molecule loss, cancer cells from the primary tumor disseminate outside the original tissue where they can remain dormant and clinically undetectable for many years before they generate secondary tumors or metastases. In addition to harboring primary tumors, the lungs are commonly affected by metastases originating from different primary cancer locations including kidney, stomach, pancreas, bladder, male and female genitourinary tract, breast, liver, head and neck [6]. Evolution and progression of several cancer types correlate with smoking, inflammation and tumor-associated immune cells [5,7]. These immune cells are involved in both pro-tumorigenic and anti-tumorigenic roles. Among these immune cells, neutrophils present in the tumor microenvironment are referred to as tumor-associated neutrophils (TANs), which are further categorized as anti-tumoral and pro-tumoral. Mimicking the dichotomy of macrophages into M1 and M2, a nomenclature of N1 and N2 has been proposed to define anti- or pro-tumor neutrophils respectively. However, given the complexity of the activation and differentiation states of the TAN population that includes also granulocytic myeloid-derived suppressor cells (G-MDSCs), the population is best summarized as pro- and anti-tumor TANs [5,8]. Antitumor neutrophils inhibit tumor cell proliferation and survival both directly and indirectly by recruiting additional immune cells. On the contrary, pro-tumoral neutrophils induce immunosuppression and promote tumor invasion, metastasis and angiogenesis through their release of various compounds such as MMP9, elastase, HMGB1, S100A8, S100A9 and BV8 [7,9–12]. Smoking leading to chronic lung inflammation is also associated with higher risk of recurrence and death in breast cancer patients. Epidemiological studies revealed that the increased risk of cancer recurrence after a period of clinical remission may be linked to inflammation [13–15]. Neutrophil recruitment to the tumor site *via* chemokine interactions with their corresponding receptors leads to poor patient outcome [16,17]. These myeloid cells then generate a microenvironment and biological niche that favors cancer progression. Yet, the exact chemokine network and the pathways sustaining recruitment of these cells to the tumor remains largely unknown [18]. Among recruited immune cells, neutrophils were identified as critical actors in experimental models for cancer cell awakening [7] as well as cancer-associated thrombosis [19]. The latter causes significant morbidity and mortality in cancer patients. Activated neutrophils release neutrophil extracellular traps (NETs) that are decorated with several neutrophil proteins, including neutrophil serine proteases (NSPs) maturated by cathepsin C (CatC, (EC 3.4.14.1)) [20] (Fig. 1) and tissue factor [21]. Consequently, NET formation by blood neutrophils exerts procoagulant and prothrombin effects suggesting that NETs may provide a therapeutic target to inhibit cancer-related thrombosis. Enhanced susceptibility of neutrophils to form NETs is observed in several preclinical cancer models suggesting systemic and local cancer effects, which stimulate neutrophils to release NETs that in turn promote the inflammatory and prothrombotic environment. These observations suggest a pivotal role for neutrophils in cancer biology. Proteases released from activated or dying neutrophils provide candidates promoting both primary tumors and metastasis.

Cancer development and metastasis rely on increased expression and proteolytic activity of several proteases. Cathepsin D, an aspartyl protease, was shown to promote breast cancer metastasis [22]. Cysteine proteases are additional actors in the metastatic process [23,24]. For example, cathepsin B expression is increased in a variety of human tumors and is involved in tumor invasion and metastasis, potentially by degrading basement membranes and extracellular matrix. Moreover, recent data implicating NSPs and their maturating cysteine protease CatC (Fig. 1) in cancer development raised a new interest in exploring these proteases both as disease mediators and pharmacological targets.

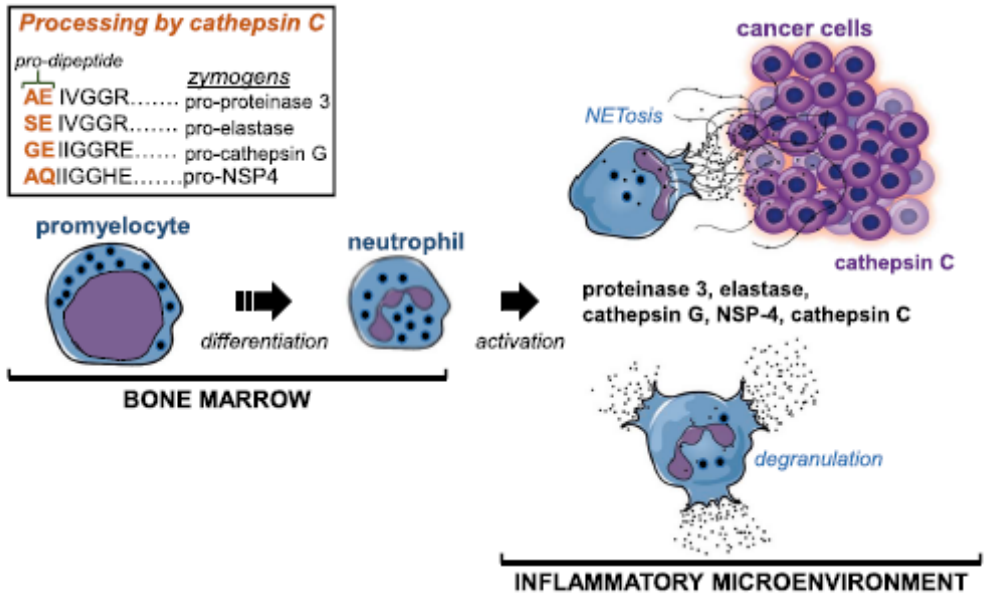


**Fig. 1.** NSPs and CatC in the inflammatory tumor microenvironment. *(Left)* Maturation of NSPs. NSP zymogens are processed and converted to active enzymes by CatC during the promyelocytic stage of neutrophil differentiation in the bone marrow. Pro-dipeptides of NSPs, removed by CatC, are shown in orange. *(Right)* Release of NSPs and CatC from activated neutrophils. Mature NSPs and CatC stored in intracellular granules are released from activated neutrophils following degranulation. NSPs are also detected in the inflammatory tumor microenvironment on neutrophil extracellular traps (NETs) consisting of extracellular nuclear DNA from activated neutrophils. Expression and release of cancer cell-derived CatC. Cancer cells can secrete mature and/or proCatC. (For interpretation of the references to color in this figure legend, the reader is referred to the web version of this article.)

In addition, plasminogen and metalloprotease family members are of importance because of their ability to degrade basement membrane and extracellular matrix components [25–28]. Inhibition of MMPs (matrix metalloproteases) in cancer tissue resulted in reduced tumor invasion, angiogenesis and migration [23,24]. These experimental data that clearly established the importance of proteases in cancer, together with the fact that existing protease inhibitors, mainly metalloprotease inhibitors, failed in previous clinical studies [29], underscore the need for new, more effective protease inhibitors suitable for preclinical and clinical exploration. Additional research aspects include inhibitor specificity and determination of the optimal disease stage for inhibitor administration.

We next focus on NSPs and CatC, and their mechanistic involvement in cancer biology and discuss the potential of pharmacological CatC inhibition for cancer treatment.

## 2. Neutrophil serine proteases in cancer

The neutrophil serine protease family includes neutrophil elastase (NE, EC 3.4.21.37), proteinase 3 (PR3, EC 3.4.21.76), cathepsin G (CatG, EC 3.4.21.20) [30,31], and recently discovered neutrophil serine protease-4 (NSP-4) [32,33]. NSPs belong to the chymotrypsin family and are synthetized as inactive precursors in promyelocytes containing an N-terminal prodipeptide to avoid unwanted protein degradation in the endoplasmic reticulum or Golgi apparatus (Fig. 1). N-terminal propeptides are removed in post-Golgi organelles by CatC. The X-ray three-dimensional structures of mature NSPs have the two six-stranded β-barrel domains typical of chymotrypsin-like serine proteases. The active-site residues are located in a crevice between the two β-barrels [30,34] (Fig. 2).

Activated neutrophils release NSPs either as soluble molecules or attached to NETs. NETs are involved in killing of invading microorganisms [20] but also in thrombosis [35,36] and tissue injury in autoimmune vasculitis [37]. NE not only decorates NETs but is also essential for NETs formation by promoting nuclear chromatin decondensation [38,39]. The proteolytic activities of NSPs are mainly regulated by serpin (serine protease inhibitors) and chelonianin families [30,31]. NSPs participate in intracellular and extracellular pathogen killing, but also shape the inflammatory response [40,41] by cleavage of extracellular matrix proteins and processing of inflammatory mediators as shown in inflammatory and autoimmune diseases [30,42–44]. Additionally, activated neutrophils transfer proteolytically active NSPs to neighboring cells, as sown for endothelial cells, resulting in cleavage of intracellular substrates and subsequently endothelial cell injury [45]. Thus, neutrophils create an microenvironment that, at least in part, depends on NSPs and NETs.

Recent data suggest that the neutrophil-associated inflammatory microenvironment, including NSPs and NETs, is not only involved in inflammatory diseases but also in cancer [5]. Extracellular proteolytically active NSPs were detected in several cancer types and correlate with poor prognosis. Zoidakis *et al.* identified PR3 as an antigenic marker of bladder cancer by urinary proteome analysis [46]. PR3 was frequently elevated in the urine of bladder cancer patients but not detected in the urine of healthy controls. Guarino *et al.* showed that urinary PR3 is proteolytically active and originates from cancer-associated neutrophils as NE and myeloperoxidase (MPO), additional markers of neutrophil activation, were also present in the urine of patients with bladder cancer [47]. Urine samples from patients with a bladder cancer were concentrated, and both PR3 protein as well as proteolytic PR3 activity was monitored using a selective PR3-FRET substrate. Active PR3 concentration was detected in the cancer patient samples and estimated to be 0.1–1 nM based on the rate of substrate hydrolysis (Fig. 3). NE is detected in broncho-alveolar lavage (BAL) fluids from patients with lung cancer [48]. Furthermore, the amount of NE and MPO in the BAL fluid was significantly higher in patients with lung cancer compared to COPD (chronic obstructive pulmonary disease)

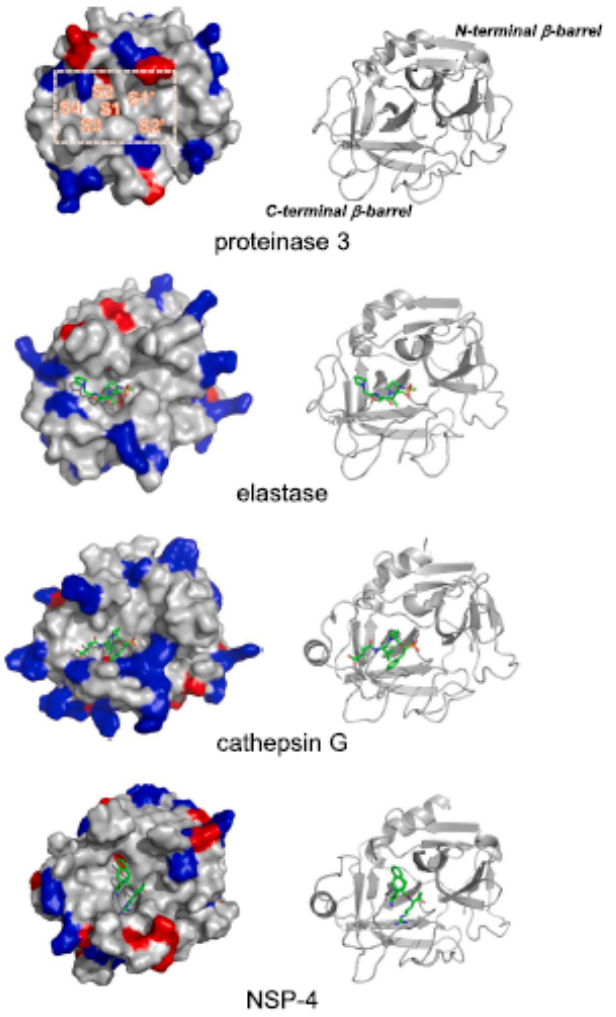


**Fig. 2.** Three-dimensional structures of human NSPs. *(Left)* Solvent accessible surfaces and *(Right)* ribbon plots of NSPs. The depicted 3D structures are based on the 3D atomic coordinates of PR3 [Protein Data Bank (PDB) code: 1FUJ, [97]], NE in complex with inhibitor GW475151 [PDB code: 1H1B [98]], CatG in complex with the peptidyl phosphonate inhibitor Suc-Val-Pro-Phe$^{P}$-$(OPh)_2$ [PDB code: 1CGH, [99]] and NSP4 in complex with the chloromethylketone inhibitor Phe-Phe-Arg-CMK [PDB code: 4Q7Z, [100]]. The structures on the left show the positive (blue) and negative (red) electrostatic surface potential. Ribbon plots of NSPs show the characteristics of the trypsin/chymotrypsin family, the two asymmetric β-barrels, and the C-terminal α-helix. Positions of the subsites S4 to S2′ in the active site region of PR3 are shown in orange [101]. Bound inhibitors are shown as green stick models. (For interpretation of the references to color in this figure legend, the reader is referred to the web version of this article.)

patients. Recently, Lerman and Hammes reviewed the current evidence for NE involvement in primary tumor growth and secondary organ metastasis [49]. As highlighted in several studies, pharmacological inhibition or gene-deletion of NE reduced cancer progression in *in vivo* mouse models [10,49]. Furthermore, the cleavage pattern of peptides found in cancer tissue revealed a strong preference for small hydrophobic residues at P1 residues, making NE the most likely candidate involved in the observed cancer-specific proteolytic processing [50]. Albrengues *et al.* showed that sustained experimental lung inflammation induced by lipopolysaccharide (LPS) administration or tobacco smoke exposure promotes NET-formation and that these NETs in turn awaken dormant malignant mammary cancer cells [7]. Mechanistic analysis in

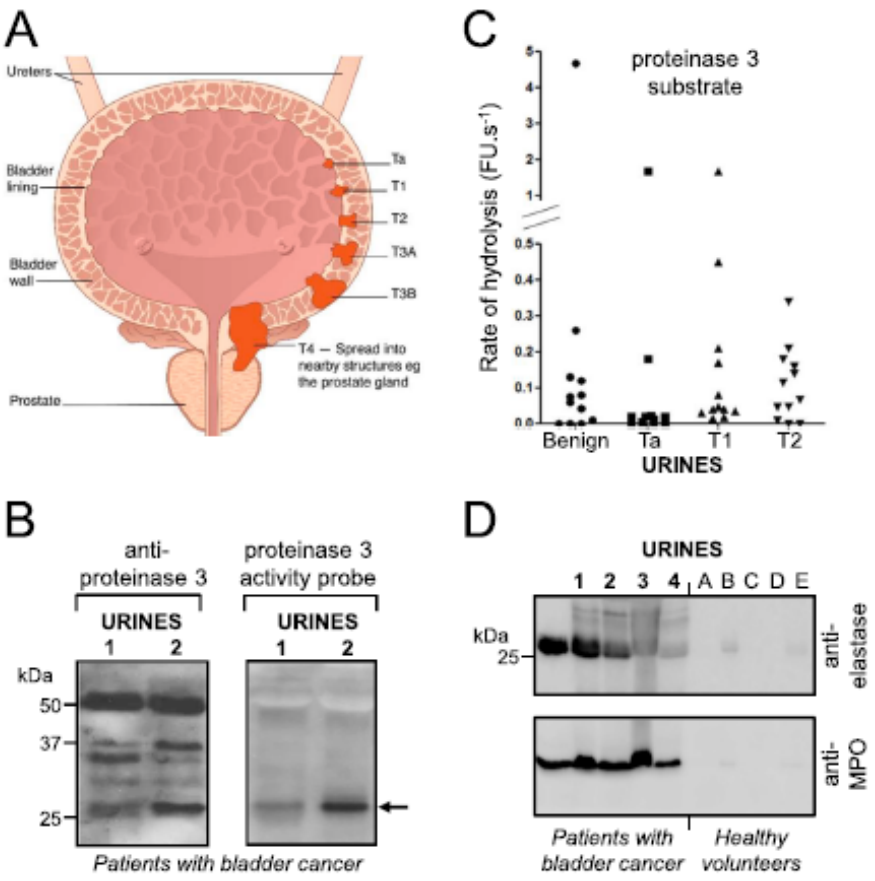


**Fig. 3.** NSP expression in human bladder cancer. (A) Schematic representation of different bladder cancer stages progressing from Ta to T4. Ta: This stage refers to noninvasive papillary carcinoma; T1: The tumor has spread to the connective tissue called the lamina propria that separates the lining of the bladder from the muscles beneath, but does not involve the bladder wall muscle; T2: The tumor has spread to the muscle of the bladder wall; T3: The tumor has grown into the perivesical tissue that surrounds the bladder; T3A: Microscopic perivesical tissue infiltration; T3B: Macroscopic perivesical tissue infiltration; T4: The tumor has spread to any of the following: the abdominal or pelvic wall, prostate or seminal vesicles, uterus, or vagina. (B) Western blot detection of secreted PR3 in 10x concentrated urine samples of patients with bladder cancer using an anti-PR3 antibody (*left*). Selective labeling of PR3 using the activity-based probe biotin-Pro-Tyr-Asp-Ala$^{P}$-(O-$C_6H_4$-4-Cl)$_2$ [47] in concentrated (10x) urine samples. (C) Activity determination of secreted PR3 in the urine of patients with different stages of bladder cancers. Rate of hydrolysis of selective PR3 substrate ABZ-VAD(nor)VADYQ-EDDnp in concentrated (10x) urine from patients with bladder cancer. Proteolytically active PR3 in unconcentrated urine was 0.1–1 nM based on the rate of substrate hydrolysis. Immunodetection and PR3 activity quantification in urine according to cancer stages (numbers of patients displaying benign lesions, n = 11, and early stages of bladder cancer; Ta, n = 10, T1, n = 12, and T2, n = 12) [47] (D) Western blot analyses of NE (*upper panel*) and myeloperoxidase (MPO) (*lower panel*) in concentrated (10x) urine samples from healthy volunteers and patients with bladder cancer.

murine models revealed that inflammation-activated neutrophils drive cancer cell awakening by laminin processing *via* NET-associated NE and MMP-9 [7]. The neo epitopes generated upon proteolytic laminin cleavage induced transformation of the previously dormant cancer cells into aggressively growing metastases by activating integrin signaling. Furthermore, Teijeira *et al.* showed that NETs secreted by inflammation-activated neutrophils surrounded cancer cells and blocked the cytotoxic anti-cancer effects of immune cells, which impaired tumor clearance [51,52]. Inhibition of NE reduced the extension of cancer cell-induced NETs and NETs-mediated cancer cell invasion. Thus, NE and NETs promote pro-tumorigenic actions of neutrophils and are therefore considered as therapeutic targets for multiple cancer types [7,49].

In addition to their validated functional roles in tumor biology discussed above, it appears that *CTSC*, *ELANE*, *PRTN3*, *CTSG*, and *PRSS57* genes are frequently co-mutated in a significant proportion (6.1%) of human cancers from the cancer genome atlas (TCGA) pan-cancer dataset [53,54]. Most changes were copy number alterations, either deletions or amplifications (Fig. 4). Interestingly, NSP gene-alterations are enriched in some tumor types, like ovarian carcinomas, sarcomas, melanomas, and esophageal carcinomas that feature alteration frequencies of more than 10%. A number of additional cancers, like endometrial, bladder, cervical, and lung carcinomas show alterations in 5–10% of the cases, whereas other cancers, like mesothelioma, thyroid, renal, and pancreatic carcinomas have virtually none of these abnormalities (Fig. 5). In addition to copy number alterations, single nucleotide variants (SNPs) are seen in all five genes (*CTSC*, *ELANE*, *PRTN3*, *CTSG*, and *PRSS57*), which do not feature mutational hotspots (Fig. 6). Interestingly, patients with NSP-alterations were of a younger age at diagnosis, had higher indices of genomic alteration, aneuploidy, and hypermutation, as well as elevated hypoxia scores compared to patients without such changes (not shown). These findings suggest that cancers with NSP mutations represent a subclass of particularly aggressive tumors. This conclusion is also supported by clinical observations, since NSP-altered TCGA pan-cancer patients display higher relapse rates, higher tumor grade, and decreased progression-free survival. Moreover, specifically *CTSC* and *PRTN3*-altered patients also exhibit decreased overall survival (Fig. 7). While all the above observations need to be confirmed in additional cohorts, and while the variable distribution of NSP alterations across human cancer types may confound these results, a number of future research questions arise. For example, do the observed NSP gene mutations occur in tumor or stromal cells? The first possibility of NSP gene mutations occurring in cancer cells calls for studies exploring intracellular (cell-autonomous) versus paracrine NSP effects on tumor biology. No such studies have been reported so far. The second, more unlikely but not yet excluded possibility for NSP gene mutations in tumor-infiltrating stromal cells also warrants further investigation. Conceivably, neutrophils with abundant transcription of NSP genes also acquire mutations in these genes similar to what has been discovered for epithelial tissues [55]. Together, these clinical and experimental data establish mechanistic NSP implications in a variety of cancers and suggest that reducing NSPs has beneficial anti-tumor effects.

## 3. Neutrophil cathepsin C

CatC, also known as dipeptidyl peptidase 1 (DPP1, EC 3.4.14.1), is a ubiquitously expressed (Fig. 8) lysosomal aminopeptidase belonging to the C1 family of papain-like cysteine peptidases [56]. CatC catalyzes the removal of dipeptides from the N-terminal end of peptides and proteins. CatC is highly, but not exclusively, expressed in immune cells and has a role in shaping innate immune responses. The best-characterized

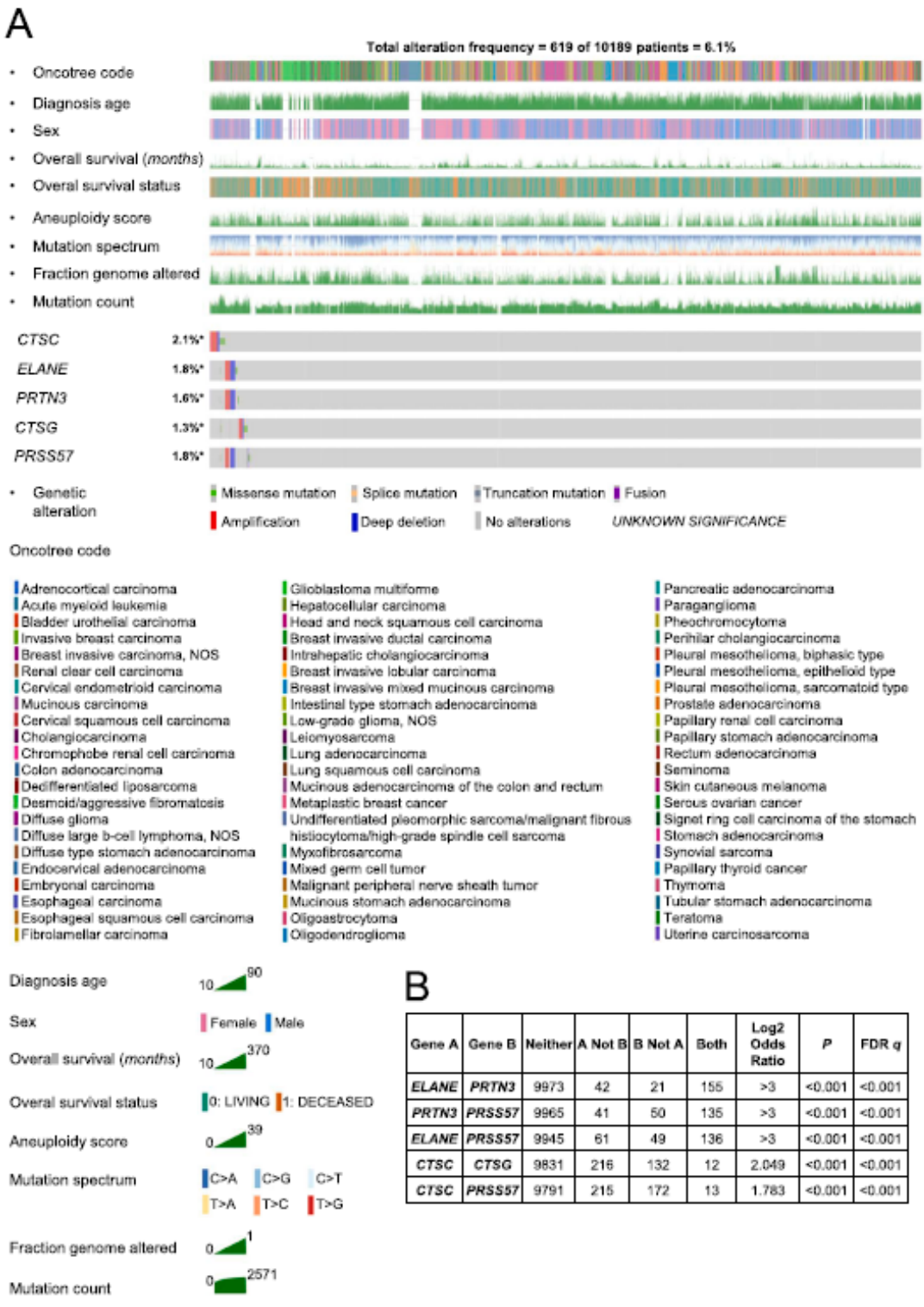


B

| Gene A | Gene B | Neither | A Not B | B Not A | Both | Log2 Odds Ratio | *P* | FDR *q* |
|---|---|---|---|---|---|---|---|---|
| ***ELANE*** | ***PRTN3*** | 9973 | 42 | 21 | 155 | >3 | <0.001 | <0.001 |
| ***PRTN3*** | ***PRSS57*** | 9965 | 41 | 50 | 135 | >3 | <0.001 | <0.001 |
| ***ELANE*** | ***PRSS57*** | 9945 | 61 | 49 | 136 | >3 | <0.001 | <0.001 |
| ***CTSC*** | ***CTSG*** | 9831 | 216 | 132 | 12 | 2.049 | <0.001 | <0.001 |
| ***CTSC*** | ***PRSS57*** | 9791 | 215 | 172 | 13 | 1.783 | <0.001 | <0.001 |

**Fig. 4.** Alteration of NSPs in human cancers. Shown are *CTSC*, *ELANE*, *PRTN3*, *CTSG*, and *PRSS57* mutation frequencies in the cancer genome atlas (TCGA) pan-cancer dataset (n = 10.189 patients), in form of a clinical and molecular data plot with alteration frequencies (A) and co-mutation matrix (B). Columns represent patients and rows clinical/molecular features. Data were accessed at https://www.cbioportal.org/ on March 1st 2021. TCGA acronyms were from https://gdc.cancer.gov/resources-tcga-users/tcga-code-tables/tcga-study-abbreviations accessed on the same date. *P*, probability, hypergeometric test; FDR *q*, probability, false discovery rate.

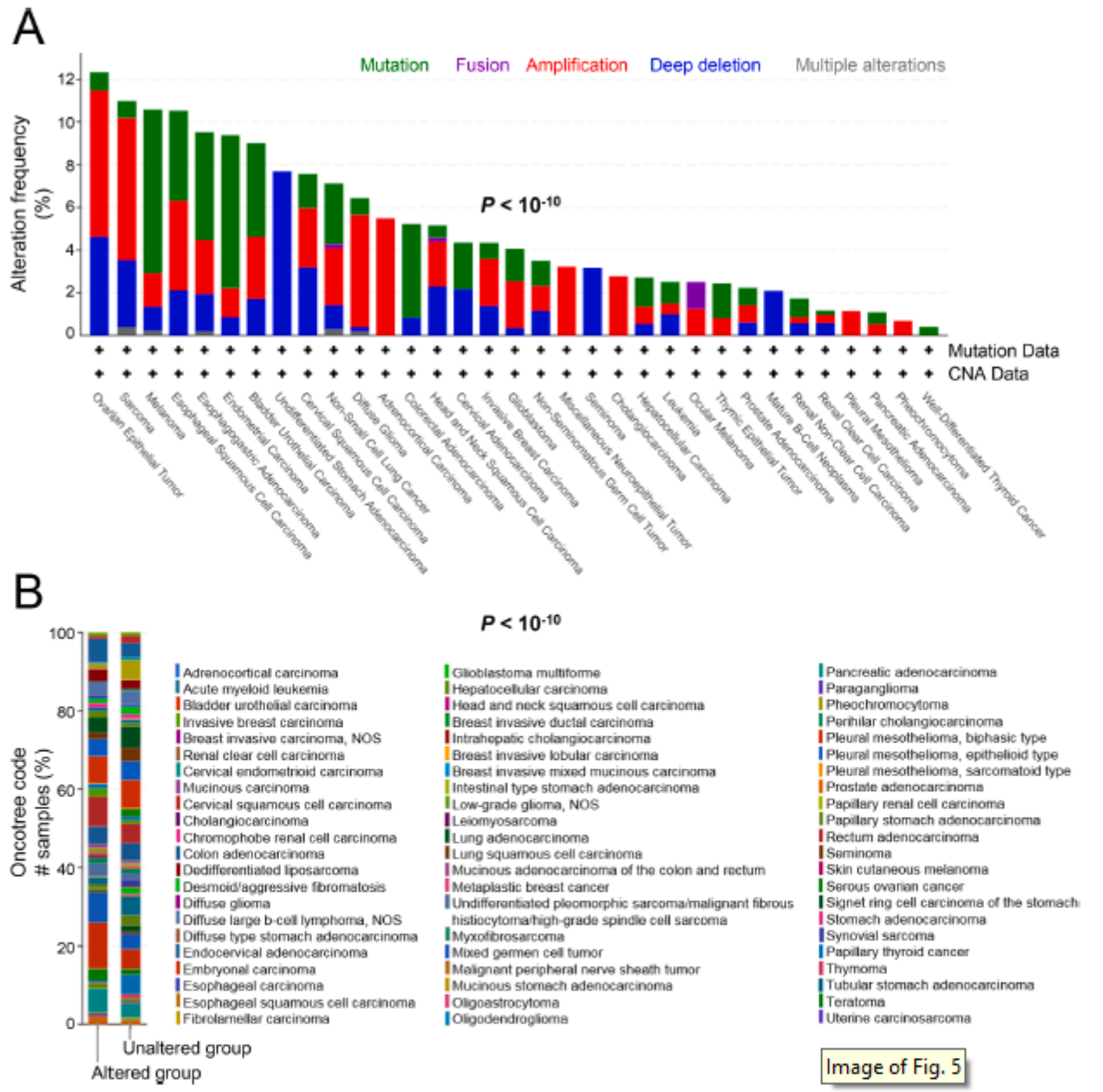


**Fig. 5.** NSP gene-alteration in cancer types. Cumulative *CTSC*, *ELANE*, *PRTN3*, *CTSG*, and *PRSS57* mutation frequencies across cancer types from the TCGA pan-cancer dataset (n = 10.189) (A, B). Data were accessed at https://www.cbioportal.org/ on March 1st 2021. TCGA acronyms were from https://gdc.cancer.gov/resources-tcga-users/tcga-code-tables/tcga-study-abbreviations accessed on the same date. *P*, probability, $\chi^2$ test. CNA, Copie Number Alteration.

physiological function of CatC is the activation of immune cell-associated serine proteases, including NSPs [57,58], mast cell chymase [59] and lymphocyte granzymes [60,61]. CatC is a unique member of the cysteine cathepsins that functions as a tetrameric protease [56].

CatC is initially synthetized as a single chain ~60-kDa monomer (Fig. 8C) that spontaneously associates to form proteolytically inactive proCatC homodimers [62] (Fig. 9). The sequence of proCatC (residues: 1–439) is partitioned into three instead of two domains, namely a ~16-kDa N-terminal exclusion domain (1–119), a ~11-kDa internal propeptide (120–206), and a ~30-kDa C-terminal catalytic domain (207–439) with a papain-like structure. The proteolytically active homotetrameric CatC is generated by the proteolytic removal of its propeptide segment and the processing of the catalytic domain into a heavy (207–370) and light chain (371–439) [56]. Cathepsin-like proteases are identified as proCatC processing and activating proteases *in vitro* [62,63]. The propeptide of proCatC is involved in the formation of a stable dimer and in two consecutive steps of the proCatC maturation process. The removal of the propeptides occurs during the first step. The processing of the catalytic domain generating heavy and light chains during the second step is essential for the final homo-tetrameric active conformation [63]. Molecular modeling analysis suggests that the tetrameric structure of CatC stabilizes the exclusion domain in the correct position conferring CatC its aminopeptidase activity [63]. The carboxylic group of the Asp1 side chain of CatC activation domain

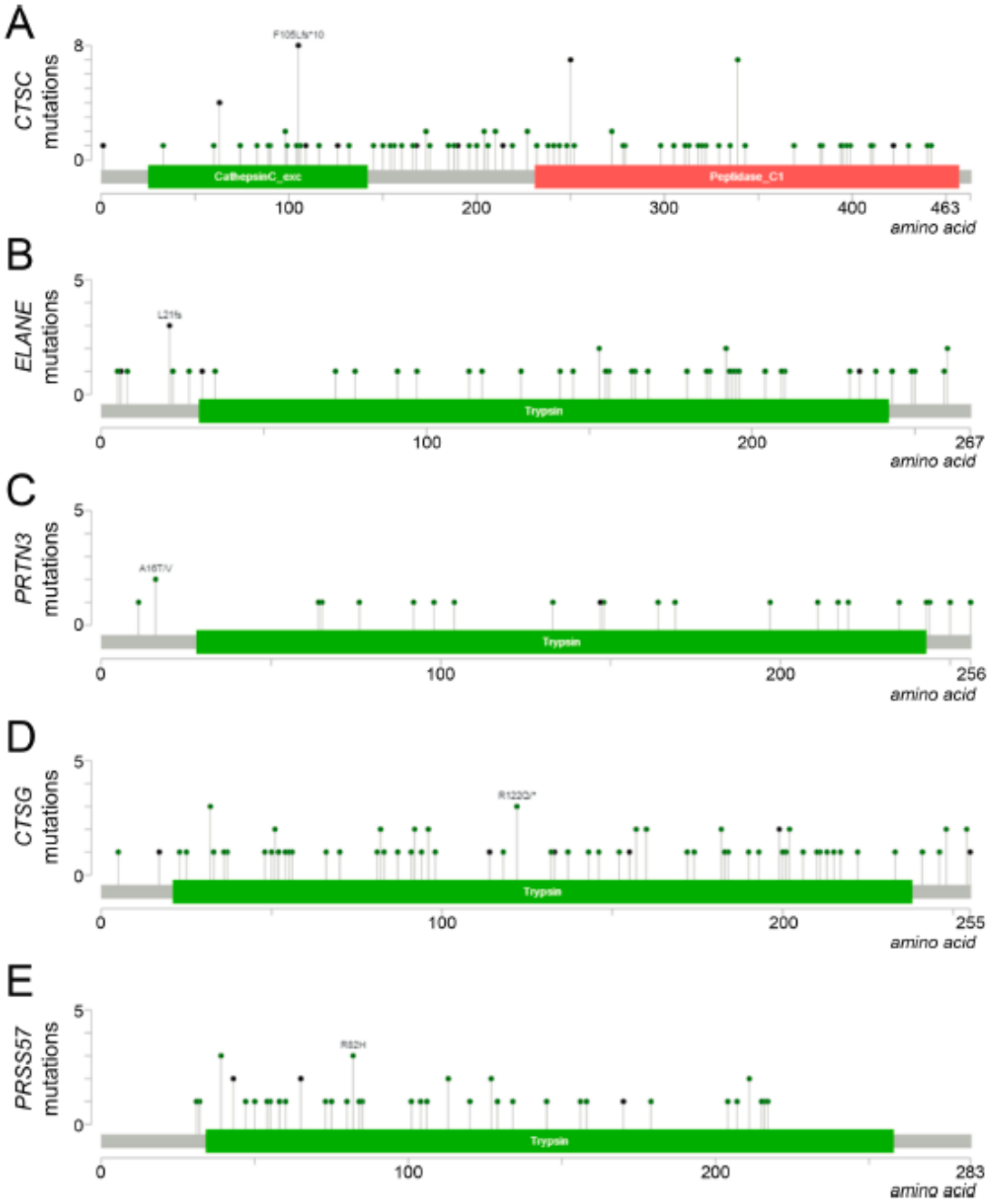


**Fig. 6.** NSPs mutations in human cancers. Lollipop plots of *CTSC* (A), *ELANE* (B), *PRTN3* (C), *CTSG* (D), and *PRSS57* (E) mutations across cancer types from the TCGA pan-cancer dataset (n = 10.189). Data were accessed at https://www.cbioportal.org/ on March 1st 2021. TCGA acronyms were from https://gdc.cancer.gov/resources-tcga-users/tcga-code-tables/tcga-study-abbreviations accessed on the same date.

sequences, is responsible for the anchoring of the N-terminal amino group of CatC substrates [64] (Fig. 10).

Mature CatC converts proNSPs into their proteolytically active forms during neutrophil differentiation in the bone marrow [57,58]. After liberation of their N-terminal propeptides by CatC, NSPs undergo an important conformational change and adopt a stable mature conformation [40]. Once matured, CatC and active NSPs are stored together in cytoplasmic granules [65]. Activated neutrophils secrete mature CatC into the extracellular milieu together with other granule-associated proteases. In patients with neutrophilic lung inflammation, mature CatC is found in sputa from cystic fibrosis and asthma patients [65], in tracheal aspirates from mechanically ventilated patients with pneumonia [66], and in the BAL fluid from patients with non-small lung cancer, even when containing only low neutrophil numbers [65]. Because proCatC but not mature CatC, is constitutively secreted by bronchial epithelial cells present in lung secretions from healthy individuals, mature CatC is considered as a biomarker of active pulmonary neutrophilic inflammation [65]. However, the functional role of

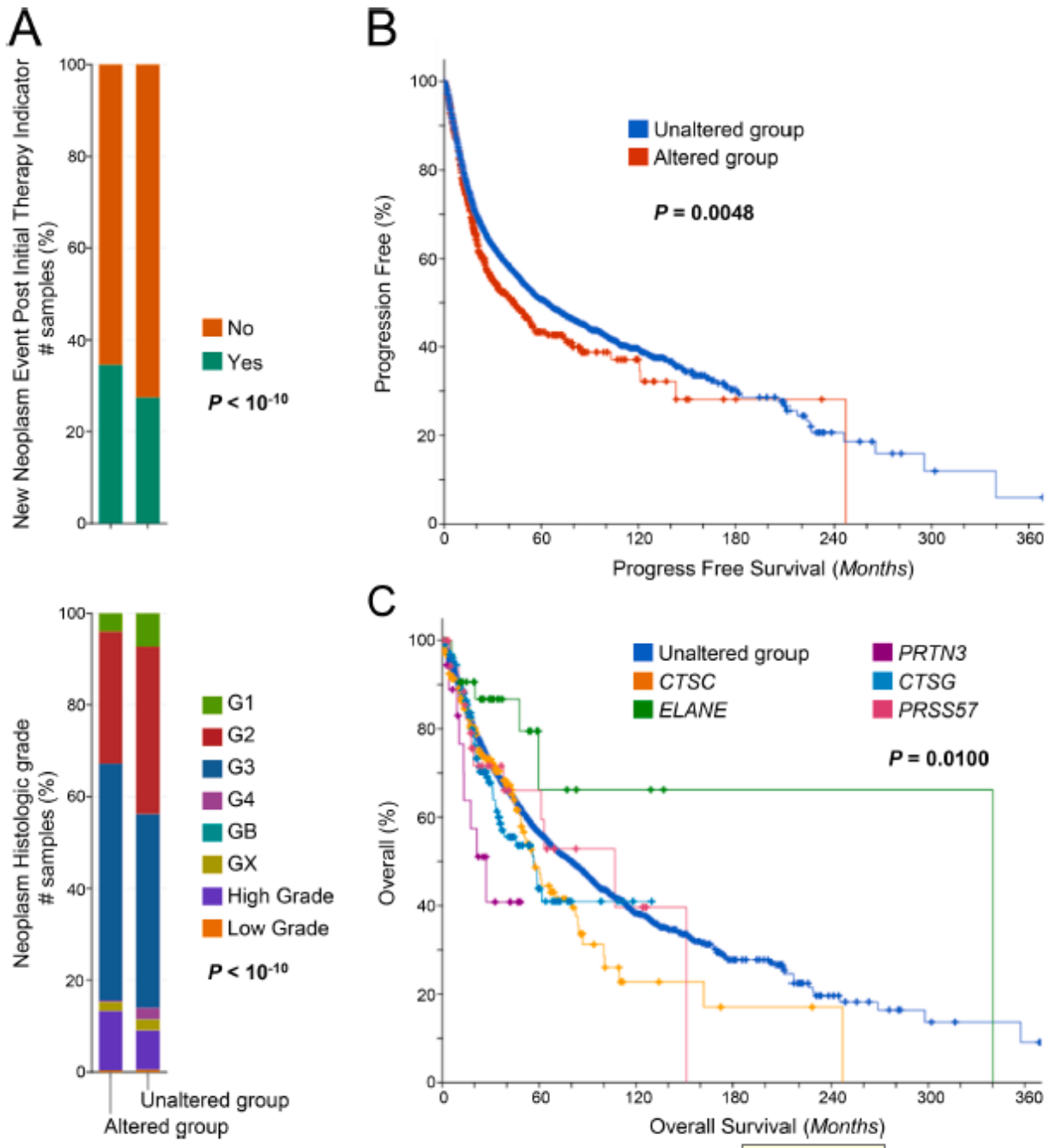


**Fig. 7.** Frequency distributions of CatC/NSP mutations and progression-free patient survival. (A) Frequency d[Image of Fig. 7]*ELANE*, *PRTN3*, *CTSG*, and *PRSS57* mutant cancers compared with non-altered cancers from the TCGA pan-cancer dataset (n = 10.189) according to relapse (*top*) and cancer grades G1 (considered as a low grade) to GX (considered as a high grade) (*bottom*). G1: well differentiated (low grade); G2: moderately differentiated (intermediate grade); G3: poorly differentiated (high grade); G4: undifferentiated (high grade); GB: grade borderline; GX: grade cannot be assessed (undetermined grade). (B, C) CatC and NSP mutations characterize high-grade human cancers that tend to relapse. Progression-free survival of patients with *CTSC*, *ELANE*, *PRTN3*, *CTSG* and *PRSS57* mutant cancers compared with patients with non-altered cancers (B) and overall survival of patients with *CTSC*, *ELANE*, *PRTN3*, *CTSG*, *PRSS57*, or none of the above mutations (C) in the TCGA pan-cancer dataset (n = 10.189). *CTSC* and *PRTN3*-mutant cancers are associated with decreased patient survival. Shown are Kaplan-Meier survival estimates. Data were accessed at https://www.cbioportal.org/ on March 1st 2021. *P*, probability, $\chi^2$ test (A) and log-rank test (B, C).

extracellular CatC originating from neutrophils at the inflammatory sites remains unknown.

Loss of function mutations in the CatC gene *CTSC* cause PLS characterized by severe pre-pubertal periodontitis and palmoplantar keratoderma without marked immunodeficiency [67,68]. PLS white blood cell lysates from a cohort of 24 patients with established missense, frameshift or nonsense *CTSC* mutations did not contain CatC activity or immunoreactive CatC protein [69]. The missense mutation Leu172Pro within the propeptide segment altered the proCatC stability as well as the *in vitro* maturation of the recombinant zymogen [63]. Mutated CatC

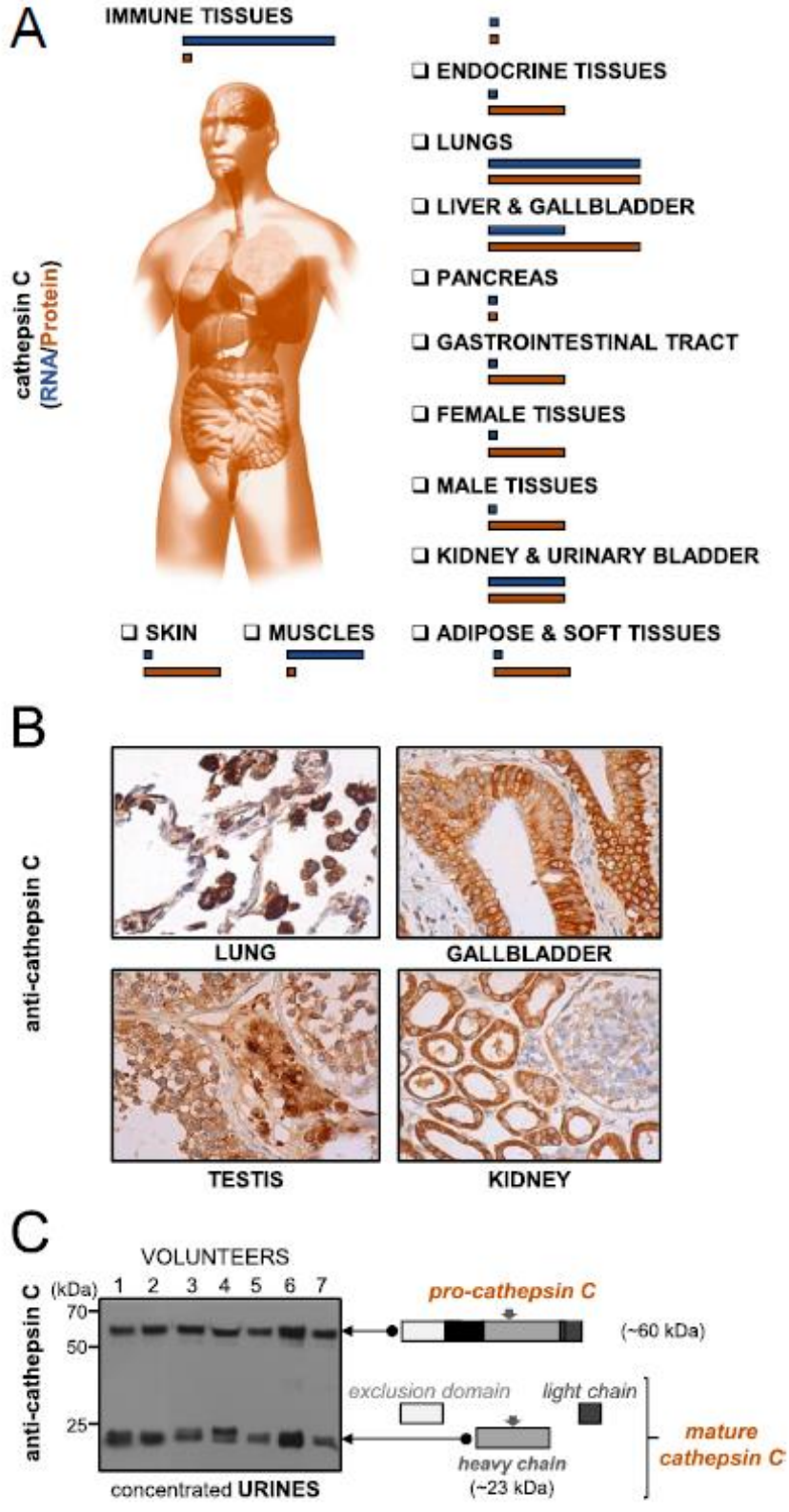


**Fig. 6.** Physiologic CatC expression in different tissues. (A) *CTSC* mRNA (blue) and protein (brown) expression were ranked as low (little square), medium (middle-long bar), and high (long horizontal bar). Low mRNA, <25 normalized transcripts per million; medium, 25–50 normalized transcripts per million; high, greater than50 normalized transcripts per million. Low protein, expression by <25% of individuals tested; medium, protein expression by 25–50% of individuals tested; high, protein expression by >50% of individuals tested. RNA-seq and immunohistochemistry data were from The Human Protein Atlas (https://www.proteinatlas.org/). (B) Immunoperoxidase detection of CatC (brown) in diverse healthy organs lung, gallbladder, testis, kidney) using anti-CatC sc-74590 HRP. Images provided by Charline Bubel (Santa Cruz Biotechnology). (C) Western blot analysis of secreted CatC in 10x concentrated urine samples of seven healthy donors using an anti-CatC antibody (sc-74590) directed against the 23 kDa CatC heavy chain. The samples are concentrated 10 times [102]. The unprocessed pro-CatC single chain and the heavy chain liberated upon processing are detected in urine samples. The diagram on the right illustrates the processing of the 60 kDa proCatC into the mature CatC. The arrow indicates the CatC heavy chain. (For interpretation of the references to color in this figure legend, the reader is referred to the web version of this article.)

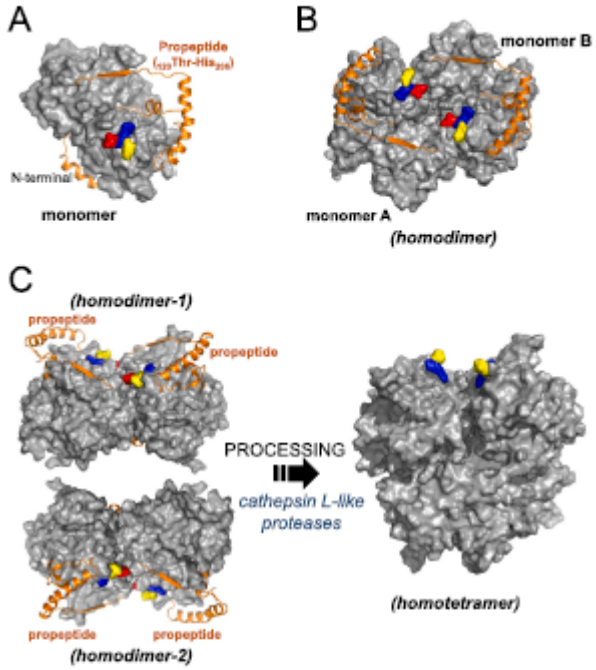


**Fig. 9.** Human proCatC and mature CatC structures. (A) Model structure of human proCatC monomer. The surface representation of the exclusion domain and papain-like catalytic domain is shown and colored in grey. The ribbon plot shows the topology of the propeptide (residues $_{120}$Thr-His$_{206}$) in orange. Leu, Arg and Asp ($_{369}$Leu-Arg/Asp$_{371}$, the sequence containing the cleavage sites of proCatC maturating proteases between the heavy and light chains) are colored in yellow, blue and red respectively. (B) ProCatC homodimer constituted of monomers A and B in surface representation with the same color coding as in A is shown. (C) Processing by CatL-like proteases of two homodimers and their association to form proteolytically mature tetrameric CatC. The models [63] were based on the crystal structures of human CatC (PDB code: 3PDF [103]), and the crystal structures of trypanosome brucei proCatB (PDB code: 4HWY [104]). (For interpretation of the references to color in this figure legend, the reader is referred to the web version of this article.)

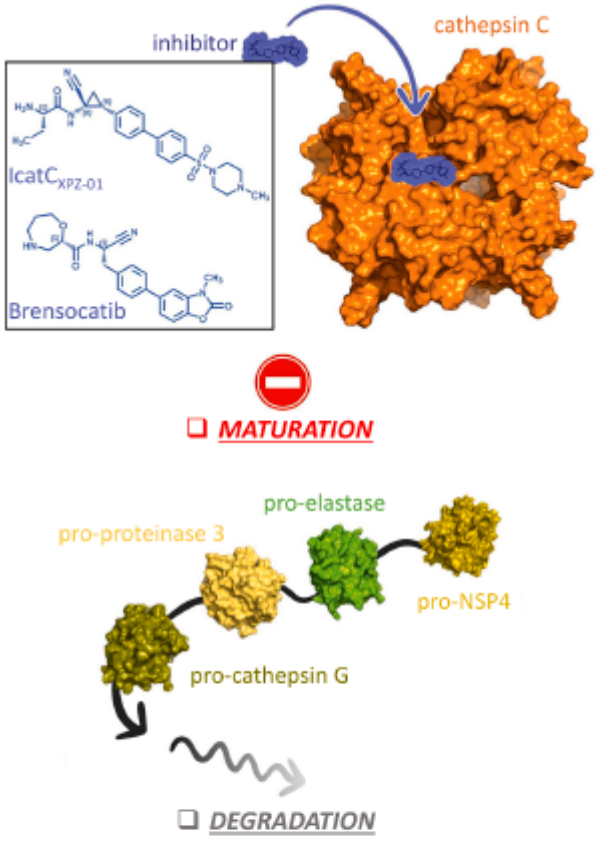


**Fig. 10.** NSP degradation as a result of CatC inhibition. Structure of two CatC inhibitors, IcatC$_{XPZ-01}$ [90] and brensocatib [91].

with missense mutations is suspected to be degraded during neutrophil differentiation [69,70]. The lack of CatC activity reduces both the activity and the amount of NSPs in neutrophils from PLS patients [33,58,69]. Using a highly sensitive and selective PR3 substrate, PR3 activity in a cohort of 20 PLS patients amounted to only 1% to 4% compared to those of healthy controls [69] indicating that CatC is the major but not unique proNSPs maturating protease. Furthermore, proteomic analysis of azurophil granule proteins in healthy versus PLS patient samples showed that approximately 15 proteins were differentially expressed [70]. Importantly, two different teams showed that PLS neutrophils are incapable of forming NETs due to lack of NE activity [70,71].

These data establish the importance of neutrophil CatC for NSP maturation and suggest that NSPs abrogation does not cause severe infections.

## 4. Tumor cell-derived cathepsin C

Although neutrophils and other immune cells harbor large amounts of CatC, additional sources for this protease exist. Upregulation of CatC expression was observed in different tissues during carcinogenesis. Ruffell *et al.* investigated the function of CatC in breast cancer and squamous cell carcinoma in mice and found increased CatC protein and proteolytic activity in both types of these tumor tissues compared to healthy control tissues [72]. Results from *Ctsc*$^{-/+}$ and *Ctsc*$^{-/-}$ mice revealed a tissue-specific role of CatC in squamous cell but not breast cancer development. Moreover, immune cell and fibroblast CatC was reported to be critical for promoting angiogenesis and tumor growth [72]. Zhang *et al.* investigated the differential expression of CatC in hepatocellular carcinoma (HCC) and normal liver tissues by bioinformatic tools and tissue microarrays [73]. CatC was upregulated in HCC patients and correlated with poor prognosis. Using gain/loss-of-function assays, the authors identified CatC as an oncogenic protein that promoted the proliferation and metastasis of HCC cancer cells. Mechanistically, overexpression of CatC activated the TNF-α/p38 MAPK pathway that assisted HCC growth and metastasis. The tumor-promoting role of CatC was also shown for renal carcinoma cells by Chiang *et al.* [74]. Kim *et al.* [75] and Pal Khalet *et al.* [76] reported the role of CatC in the regulation of autophagy-mediated cancer cell proliferation.

Recently, Xiao *et al.* highlight the potential of tumor cell-secreted mature CatC to promote lung metastasis of breast cancer cells [77]. The authors first identified proteins that were regulated in human breast cancers and murine breast cancer cell lines with lung metastatic capacities. CatC was amongst the highest regulated proteins and its expression and secretion were elevated in lung metastases of breast cancer. Moreover, high CatC expression in primary tumors was negatively correlated with patients' overall survival. Hence, tumor-derived CatC provides a prognostic survival marker. In addition, in experimental murine breast cancer models, a strong correlation was observed between CatC expression and infiltrating neutrophils that deposited NETs in both primary tumors and lung metastasis. The authors reported the dual function of tumor-secreted mature CatC in neutrophil recruitment to metastatic niches and NETosis induction. To elucidate how mature CatC affects neutrophil functions, Xiao *et al.* explored the

possibility that neutrophil membrane-bound NSP zymogens were proteolytically activated by tumor cell-derived CatC. They suggest that indeed a conversion of membrane-bound PR3 ($PR3^{mb}$) from the zymogen into the mature form by tumor derived CatC activity occurs, and that this effect provides a mechanistic link to neutrophil infiltration and NET formation. The authors proposed that the $PR3^{mb}$ zymogen, predominantly detected as a 34-kDa molecule that is distinct from the 27-kDa mature granule-stored form, was the result of differential post-translational modifications. The authors argue that the tumor CatC-mediated activation of $PR3^{mb}$ resulted in IL-1β processing and NFκb activation in the neutrophils. In the proposed scheme, this activation leads to the secretion of IL-6 and CCL3 further enhancing neutrophil recruitment to metastatic niches. The CatC-PR3-IL-1β axis was also suggested to contribute to p38 activation and ROS (reactive oxygen species) production resulting in NET formation that in turn support metastatic growth of tumor cells. In a final pursuit to confirm that proteolytic PR3 activity is essential for neutrophil IL-1β production, recombinant active *human* PR3 was added to conditioned medium from *CTSC*-silenced cancer cells supplemented with fetal bovine or horse serum. The authors observed that active PR3 indeed restored IL-1β generation even in the absence of tumor cell-derived CatC.

The data obtained by Xiao *et al.* identified CatC as a potentially important actor in breast cancer. However, a note of caution is warranted with respect to the proposed molecular mechanisms in neutrophils. The authors suggest that the main action of tumor-secreted mature CatC on local and systemic neutrophil functions is caused by the small pool of inactive proPR3 on the neutrophil surface that is activated by CatC. In our view, this mechanistic concept is highly speculative and needs further critical evaluation. For example, using mice with myeloid cells deficient in PR3 as tumor recipients would reveal additional information. PR3-deficient neutrophils are expected to show significantly less IL-1β generation in response to tumor cell-derived CatC thereby strengthening the specific role of PR3 in this process. Additional concerns pertain to the suggested role of proPR3 on the neutrophil surface. We agree with the authors that most $PR3^{mb}$ on quiescent human neutrophils is proteolytically inactive. In fact, we and others suspected previously that constitutively expressed $PR3^{mb}$ on quiescent human neutrophils could be the zymogen form of PR3 [78,79] and, in addition, PR3 becomes inactivated by binding to the neutrophil-specific CD177 membrane receptor [80]. In contrast, large amounts of active PR3 are translocated from the intracellular granules to the cell membrane during neutrophil activation. Unlike constitutive $PR3^{mb}$, induced $PR3^{mb}$ exposed on activated neutrophils is proteolytically active [78,79]. However, we are concerned firstly, about the high molecular weight of murine $PR3^{mb}$ observed by Xiao *et al.* Granule-associated PR3 and $PR3^{mb}$ have similar molecular weights and no major post-translational differences despite their different destinations after sorting and targeting of PR3 to either the outer leaflet of cellular membranes or to granules. Secondly, only a very small fraction of the total neutrophil PR3 pool is exposed and accessible on the cell surface of human neutrophils [69]. Activation of such a small amount of $PR3^{mb}$ by tumor-derived CatC leading to the observed tumor-associated activities *in vivo* is implausible. Importantly, almost no $PR3^{mb}$ is exposed on the surface of murine neutrophils because the hydrophobic patch of human PR3 that mediates membrane association is not conserved in murine PR3 [81,82]. Thirdly, in our hands, it is not easy to activate proPR3 and related proNSPs by CatC, even under controlled laboratory conditions in solution. High concentrations of the substrates (at least 0.3 mg/ml) and optimal acidic conditions are required (personal observation by D.E. Jenne). It is unlikely that such conditions exist in the tumor environment. Moreover, it is very difficult to distinguish mouse PR3 from mouse NE at low concentrations using activity measurements, as mouse PR3 is more similar to mouse NE than human PR3 is to human NE [30,40]. In fact, the PR3 substrate used in the Xiao *et al.* study was designed to be specific for human PR3 and it is not cleaved by mouse PR3 [83,84]. A better approach would be to employ catalytically active and inactive murine PR3 and murine proPR3 as a control. Finally, recombinant active PR3 was added to cell cultures containing fetal bovine or horse serum rich in the main physiological PR3 inhibitor alpha-1 antitrypsin, and exogenous active *human* PR3 was administered intravenously. In both circumstances, the presence of high alpha-1 antitrypsin concentrations rapidly inhibits the proteolytic PR3 activity and we cannot see how it possibly can exert its functions in the neutrophil. Thus, we believe that tumor-derived CatC within the inflammatory tumor microenvironment employs other molecules than $PR3^{mb}$ to activate neutrophils that in turn promote lung metastasis.

Together these data support the notion that tumor-derived CatC promotes growth and metastasis of several cancer types and that CatC inhibition has beneficial anti-tumor effects.

## 5. Pharmacological inhibition of cathepsin C

CatC is increasingly recognized as a pharmacological target for blocking NSP activity and NETosis in neutrophil-driven inflammatory and autoimmune diseases [30,43]. The observation that CatC knock-out mice were protected in NSPs-driven experimental inflammation models supports the therapeutic strategy of CatC inhibition in these diseases [42,43,57]. Because of the discussed role of CatC, NE, and NETs in cancer, pharmacological CatC inhibition can also be envisioned as a therapeutic strategy to prevent primary tumor growth and metastasis [85]. While several CatC inhibitors have been discovered and tested in preclinical models (including $IcatC_{XPZ\text{-}01}$, BI-9740 (Jerke *et al., in preparation*), EGFR-derived inhibitor [86], non-peptidyl non-covalent CatC inhibitor [87], GSK-2793660 [88] and brensocatib [89] have advanced the furthest in clinical development.

Two dipeptidyl nitrile inhibitors $IcatC_{XPZ\text{-}01}$ ((*S*)-2-amino-*N*-((1*R*,2*R*)-1-cyano-2-(4′-(4-methylpiperazin-1-ylsulfonyl)biphenyl-4-yl) cyclopropyl)butanamide), $IC_{50}$.CatC = 15 nM) [90] and brensocatib (formerly INS1007/AZD7986, (*S*)-N-((*S*)-1-Cyano-2-(4-(3-methyl-2-oxo-2,3-dihydrobenzo-[d]oxazol-5-yl)phenyl)ethyl)-1,4-oxazepane-2-carboxamide, $IC_{50}$.CatC = 22 nM) [91] were recently shown to effectively block the maturation of NSP zymogens *in vitro* and *in vivo* (Fig. 10). Nitrile compounds are the best investigated group of CatC inhibitors [43]. The nitrile group of these compounds reacts with the active Cys234 site resulting in the reversible formation of a thioimidate adduct (Fig. 11). In rodents, $IcatC_{XPZ\text{-}01}$ [90] and brensocatib [91] reached sufficient levels in the bone marrow to inhibit CatC and downstream NSPs activation. In a murine model of rheumatoid arthritis, prolonged administration of $IcatC_{XPZ\text{-}01}$ resulted in sustained anti-arthritic activity [90]. $IcatC_{XPZ\text{-}01}$ was also evaluated in an orthotopic mouse lung transplantation (LTx) model after 18 h cold storage of the graft [92]. Recipient mice treated with $IcatC_{XPZ\text{-}01}$ prior to LTx showed improved early graft function. Furthermore, prolonged administration of $IcatC_{XPZ\text{-}01}$ in *Macaca fascicularis* resulted in almost complete elimination of NSPs in white blood cells confirming that a reduction in NSPs, comparable to that seen in PLS patients, is possible using pharmacological CatC inhibitors [93]. Zymogen conformations of NSPs are susceptible to proteolysis leading to their proteolytic degradation within intracellular granules at very early stages of neutrophil maturation [69,93]. Xiao *et al.* showed that systemic administration of brensocatib effectively inhibited breast cancer lung metastasis in their mouse model, preserved body weight, and enhanced overall animal survival time [77]. This effect is encouraging, even though the underlying molecular mechanisms need to be better characterized.

Brensocatib was the first nitrile CatC inhibitor that was assessed in clinical trials [91]. The safety, tolerability and pharmacokinetics/pharmacodynamics of single and multiple oral doses were evaluated in a randomized, placebo-controlled, phase 1 study started in 2014. Daily doses of 10, 25 and 40 mg brensocatib in 81 healthy subjects treated for 28 days resulted in significant reduction of neutrophil NE activity without serious side effects [94]. Safety, efficacy and pharmacokinetics of brensocatib were then evaluated in the WILLOW phase 2 study, an

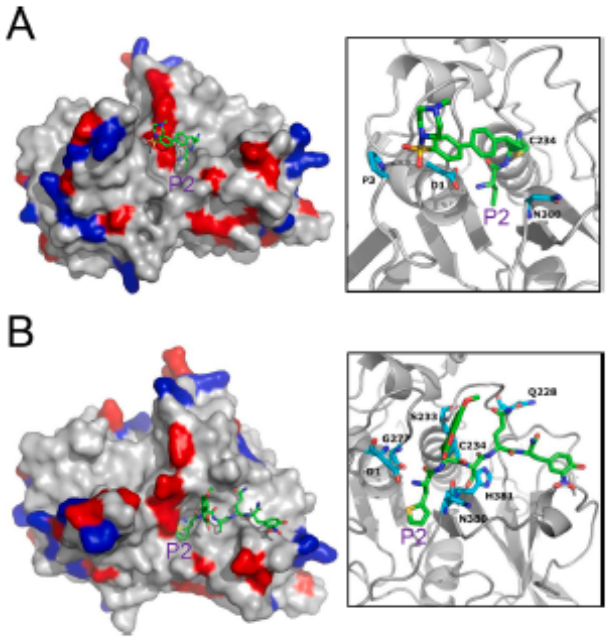


**Fig. 11.** Model structure of the complex formed between $IcatC_{XPZ-01}$ or a FRET substrate and human CatC. (*Left*) Solvent accessible surface of CatC colored according to its positive (blue) and negative (red) electrostatic potential. (*Right*) The carbon atoms of CatC and compounds are shown in turquoise and green, respectively. Oxygen, nitrogen, sulfur atoms are colored in red, blue and yellow, respectively. Critical residues in the vicinity of the active site involved in binding e.g. Asp-1 (D1) and Pro-3 (P3) are labeled in black. The position P2 according to the nomenclature of Schechter and Berger [105] is highlighted by the violet label "P2" and shows residues of the compounds interacting with CatC. (A) The coordinates of CatC complex with amino-N-((1*R*,2*R*)-1-cyano-2-(4′-((4-methylpiperazin-1-yl)sulfonyl)-[1′-biphenyl]-4-yl)cyclopropyl)cyclohexane-1-carboxamide (PDB code: 6IC7 [90]) was used for molecular modeling. (B) The model of internally-quenched fluorescent substrate Thi-Ala(Mca)-Ser-Gln-Tyr(3-$NO_2$)-$NH_2$ in complex with CatC [106] (based on PDB code: 2DJF [64]). The presence of the exclusion domain blocks the enzyme active site beyond the S2 subsite, making it only accessible to the N-terminus of its substrates. The CatC S2 subsite is the deepest site and it has the shape of a pocket. (For interpretation of the references to color in this figure legend, the reader is referred to the web version of this article.)

international, randomized, double-blind placebo-controlled trial [89]. 256 adults with non-cystic fibrosis bronchiectasis, a chronic inflammatory lung disease defined as a permanent dilatation of the bronchi [95], were treated once daily for 24 weeks with 10 mg or 25 mg brensocatib or placebo. Brensocatib reduced the primary endpoint, namely the time to first pulmonary exacerbation, and a key secondary study endpoint, namely the rate of pulmonary exacerbations, and significantly reduced sputum NE by approximately ~85% [89]. The efficacy, safety, and tolerability of brensocatib is currently being evaluated in a global, randomized, double-blind, placebo-controlled phase 3 trial termed ASPEN (NCT number: NCT04594369). Patients with non-cystic fibrosis bronchiectasis were randomized to receive brensocatib 10 mg, 25 mg, or placebo once daily for 52 weeks. Acute respiratory distress syndrome (ARDS), a severe outcome of COVID-19 is also associated with neutrophilic inflammation. Elimination of NSPs may reduce lung injury and thereby prevent the irreversible pulmonary failure in COVID-19 patients [66,96]. To explore this effect further, brensocatib is currently being evaluated in the STOP-COVID19 (Superiority Trial of Protease inhibition in COVID-19, EudraCT Number: 2020–001643-13) trial in 300 hospitalized patients with COVID-19 pneumonia [96].

## 6. Conclusion

The best-characterized function of CatC is the activation of immune cell-associated serine proteinases. However, additional CatC roles, particularly in non-immune cells, are beginning to emerge. Recent analyses in cancer patients revealed increased CatC expression in some malignant cells that correlated with metastasis and poor survival implicating CatC as a biomarker. Mechanistically, tumor-derived CatC was suggested to regulate immune cell functions in the tumor microenvironment thereby promoting tumor growth and metastasis. Specifically, tumor CatC, in addition to neutrophil CatC, may control NSPs and NETs formation – both implicated in cancer biology. Synthetic compounds are now available to inhibit CatC in neutrophils, tumors and other host tissues. Brensocatib is a CatC inhibitor that is currently being evaluated in a phase 3 clinical trial in patients with non-cystic fibrosis bronchiectasis. If effective in preclinical cancer models, brensocatib could possibly be repurposed for treatment of cancer patients.

## Author contributions

All authors contributed to the writing and revision process of the manuscript. B. Korkmaz supervised the work.

## Support statement

This work was supported by the "Ministère de l'Enseignement Supérieur et de la Recherche" and the "Région Centre Val de Loire" (Project PIRANA, 2019–00134916) (to BK); the Graduate College (Graduiertenkolleg, GRK) #2338 of the German Research Society (Deutsche Forschungsgemeinschaft, DFG), the target validation project for pharmaceutical development ALTERNATIVE of the German Ministry for Education and Research (Bundesministerium für Bildung und Forschung, BMBF), a Translational Research Grant by the German Centre for Lung Research (Deutsches Zentrum für Lungenforschung, DZL) (to GTS), by the grant KE 576/10-1 and 394046635 -SFB 1365 from the Deutsche Forschungsgemeinschaft (DFG) to R.K.

## Declaration of Competing Interest

B. Korkmaz has been paid for the time spent as a committee member for advisory boards (INSMED Inc., NJ, USA), other forms of consulting (Neuprozyme Therapeutics Aps (Denmark), Santhera Pharmaceuticals (Switzerland)), symposium organization (INSMED Inc., NJ, USA) and travel support, lectures or presentations, outside the submitted work. R. K served on the INSMED advisory board.

## Acknowledgment

The authors thank Guillaume Parrot (University of Tours - SID'com) for his contribution to the figure preparation.

## References

[1] H. Sung, J. Ferlay, R.L. Siegel, M. Laversanne, I. Soerjomataram, A. Jemal, F. Bray, Global cancer statistics 2020: GLOBOCAN estimates of incidence and mortality worldwide for 36 cancers in 185 countries, CA Cancer J. Clin. 71 (3) (2021) 209–249.
[2] Y.H. Luo, L. Luo, J.A. Wampfler, Y. Wang, D. Liu, Y.M. Chen, A.A. Adjei, D. E. Midthun, P. Yang, 5-year overall survival in patients with lung cancer eligible or ineligible for screening according to US Preventive Services Task Force criteria: a prospective, observational cohort study, Lancet Oncol. 20 (8) (2019) 1098–1108.
[3] U. Testa, G. Castelli, E. Pelosi, Lung cancers: molecular characterization, clonal heterogeneity and evolution, and cancer stem cells, Cancers (Basel) 10 (2018) 248.
[4] K. Wadowska, I. Bil-Lula, L. Trembecki, M. Sliwinska-Mosson, Genetic markers in lung cancer diagnosis: a review, Int. J. Mol. Sci. 21 (13) (2020) 4569.
[5] S. Jaillon, A. Ponzetta, D. Di Mitri, A. Santoni, R. Bonecchi, A. Mantovani, Neutrophil diversity and plasticity in tumour progression and therapy, Nat. Rev. Cancer 20 (9) (2020) 485–503.

[6] A. Jamil, A. Kasi, Lung Metastasis, StatPearls, Treasure Island (FL), 2021.
[7] J. Albrengues, M.A. Shields, D. Ng, C.G. Park, A. Ambrico, M.E. Poindexter, P. Upadhyay, D.L. Uyeminami, A. Pommier, V. Kuttner, E. Bruzas, L. Maiorino, C. Bautista, E.M. Carmona, P.A. Gimotty, D.T. Fearon, K. Chang, S.K. Lyons, K. E. Pinkerton, L.C. Trotman, M.S. Goldberg, J.T. Yeh, M. Egeblad, Neutrophil extracellular traps produced during inflammation awaken dormant cancer cells in mice, Science 361 (6409) (2018) eaao4227.
[8] V. Audrito, A. Manago, F. Gaudino, L. Sorci, V.G. Messana, N. Raffaelli, S. Deaglio, NAD-biosynthetic and consuming enzymes as central players of metabolic regulation of innate and adaptive immune responses in cancer, Front. Immunol. 10 (2019) 1720.
[9] H. Nozawa, C. Chiu, D. Hanahan, Infiltrating neutrophils mediate the initial angiogenic switch in a mouse model of multistage carcinogenesis, Proc. Natl. Acad. Sci. U. S. A. 103 (33) (2006) 12493–12498.
[10] A.M. Houghton, D.M. Rzymkiewicz, H. Ji, A.D. Gregory, E.E. Egea, H.E. Metz, D. B. Stolz, S.R. Land, L.A. Marconcini, C.R. Kliment, K.M. Jenkins, K.A. Beaulieu, M. Mouded, S.J. Frank, K.K. Wong, S.D. Shapiro, Neutrophil elastase-mediated degradation of IRS-1 accelerates lung tumor growth, Nat. Med. 16 (2) (2010) 219–223.
[11] S. Tohme, H.O. Yazdani, A.B. Al-Khafaji, A.P. Chidi, P. Loughran, K. Mowen, Y. Wang, R.L. Simmons, H. Huang, A. Tsung, Neutrophil extracellular traps promote the development and progression of liver metastases after surgical stress, Cancer Res. 76 (6) (2016) 1367–1380.
[12] F. Shojaei, M. Singh, J.D. Thompson, N. Ferrara, Role of Bv8 in neutrophil-dependent angiogenesis in a transgenic model of cancer progression, Proc. Natl. Acad. Sci. U. S. A. 105 (7) (2008) 2640–2645.
[13] N.P. McAndrew, L. Bottalico, C. Mesaros, I.A. Blair, P.Y. Tsao, J.M. Rosado, T. Ganguly, S.J. Song, P.A. Gimotty, J.J. Mao, A. DeMichele, Effects of systemic inflammation on relapse in early breast cancer, npj Breast Cancer 7 (1) (2021) 7.
[14] A. Varkaris, A. Katsiampoura, J.S. Davis, N. Shah, M. Lam, R.L. Frias, C. Ivan, M. Shimizu, J. Morris, D. Menter, M. Overman, H. Tran, J. Heymach, Y.S. Chun, J.-N. Vauthey, G. Calin, S. Kopetz, Circulating inflammation signature predicts overall survival and relapse-free survival in metastatic colorectal cancer, Br. J. Cancer 120 (3) (2019) 340–345.
[15] A.E. Tuomisto, M.J. Makinen, J.P. Vayrynen, Systemic inflammation in colorectal cancer: Underlying factors, effects, and prognostic significance, World J. Gastroenterol. 25 (31) (2019) 4383–4404.
[16] .
[17] A.J. Gentles, A.M. Newman, C.L. Liu, S.V. Bratman, W. Feng, D. Kim, V.S. Nair, Y. Xu, A. Khuong, C.D. Hoang, M. Diehn, R.B. West, S.K. Plevritis, A.A. Alizadeh, The prognostic landscape of genes and infiltrating immune cells across human cancers, Nat. Med. 21 (8) (2015) 938–945.
[18] H. Gonzalez, C. Hagerling, Z. Werb, Roles of the immune system in cancer: from tumor initiation to metastatic progression, Genes Dev. 32 (19–20) (2018) 1267–1284.
[19] C. Thalin, Y. Hisada, S. Lundstrom, N. Mackman, H. Wallen, Neutrophil extracellular traps: villains and targets in arterial, venous, and cancer-associated thrombosis, Arterioscler. Thromb. Vasc. Biol. 39 (9) (2019) 1724–1738.
[20] V. Brinkmann, U. Reichard, C. Goosmann, B. Fauler, Y. Uhlemann, D.S. Weiss, Y. Weinrauch, A. Zychlinsky, Neutrophil extracellular traps kill bacteria, Science 303 (5663) (2004) 1532–1535.
[21] L. Badimon, G. Vilahur, Neutrophil extracellular traps: a new source of tissue factor in atherothrombosis, Eur. Heart J. 36 (22) (2015) 1364–1366.
[22] A. Eatemadi, H.T. Aiyelabegan, B. Negahdari, M.A. Mazloomi, H. Daraee, N. Daraee, R. Eatemadi, E. Sadroddiny, Role of protease and protease inhibitors in cancer pathogenesis and treatment, Biomed. Pharmacother. 86 (2017) 221–231.
[23] T.P. Khaket, T.K. Kwon, S.C. Kang, Cathepsins: Potent regulators in carcinogenesis, Pharmacol. Ther. 198 (2019) 1–19.
[24] O.C. Olson, J.A. Joyce, Cysteine cathepsin proteases: regulators of cancer progression and therapeutic response, Nat. Rev. Cancer 15 (12) (2015) 712–729.
[25] C. Verollet, G.M. Charriere, A. Labrousse, C. Cougoule, V. Le Cabec, I. Maridonneau-Parini, Extracellular proteolysis in macrophage migration: losing grip for a breakthrough, Eur. J. Immunol. 41 (10) (2011) 2805–2813.
[26] M.D. Roycik, X. Fang, Q.X. Sang, A fresh prospect of extracellular matrix hydrolytic enzymes and their substrates, Curr. Pharm. Des. 15 (12) (2009) 1295–1308.
[27] V. Christiaens, H.R. Lijnen, Role of the fibrinolytic and matrix metalloproteinase systems in development of adipose tissue, Arch. Physiol. Biochem. 112 (4-5) (2006) 254–259.
[28] A.C.P. Riddick, C.J. Shukla, C.J. Pennington, R. Bass, R.K. Nuttall, A. Hogan, K. K. Sethia, V. Ellis, A.T. Collins, N.J. Maitland, R.Y. Ball, D.R. Edwards, Identification of degradome components associated with prostate cancer progression by expression analysis of human prostatic tissues, Br. J. Cancer 92 (12) (2005) 2171–2180.
[29] R.E. Vandenbroucke, C. Libert, Is there new hope for therapeutic matrix metalloproteinase inhibition? Nat. Rev. Drug Discov. 13 (12) (2014) 904–927.
[30] B. Korkmaz, M.S. Horwitz, D.E. Jenne, F. Gauthier, D. Sibley, Neutrophil elastase, proteinase 3 and cathepsin G as therapeutic targets in human diseases, Pharmacol. Rev. 62 (4) (2010) 726–759.
[31] B. Korkmaz, T. Moreau, F. Gauthier, Neutrophil elastase, proteinase 3 and cathepsin G: physicochemical properties, activity and physiopathological functions, Biochimie 90 (2) (2008) 227–242.
[32] N.C. Perera, O. Schilling, H. Kittel, W. Back, E. Kremmer, D.E. Jenne, NSP4, an elastase-related protease in human neutrophils with arginine specificity, Proc. Natl. Acad. Sci. U. S. A. 109 (16) (2012) 6229–6234.
[33] N.C. Perera, K.-H. Wiesmüller, M.T. Larsen, B. Schacher, P. Eickholz, N. Borregaard, D.E. Jenne, NSP4 is stored in azurophil granules and released by activated neutrophils as active endoprotease with restricted specificity, J. Immunol. 191 (5) (2013) 2700–2707.
[34] B. Korkmaz, A. Lesner, C. Guarino, M. Wysocka, C. Kellenberger, H. Watier, U. Specks, F. Gauthier, D.E. Jenne, D.R. Sibley, Inhibitors and antibody fragments as potential anti-inflammatory therapeutics targeting neutrophil proteinase 3 in human disease, Pharmacol. Rev. 68 (3) (2016) 603–630.
[35] M. Demers, D.S. Krause, D. Schatzberg, K. Martinod, J.R. Voorhees, T.A. Fuchs, D. T. Scadden, D.D. Wagner, Cancers predispose neutrophils to release extracellular DNA traps that contribute to cancer-associated thrombosis, Proc. Natl. Acad. Sci. U. S. A. 109 (32) (2012) 13076–13081.
[36] T.A. Fuchs, A. Brill, D. Duerschmied, D. Schatzberg, M. Monestier, D.D. Myers Jr., S.K. Wrobleski, T.W. Wakefield, J.H. Hartwig, D.D. Wagner, Extracellular DNA traps promote thrombosis, Proc. Natl. Acad. Sci. U. S. A. 107 (36) (2010) 15880–15885.
[37] A. Schreiber, A. Rousselle, J.U. Becker, A. von Massenhausen, A. Linkermann, R. Kettritz, Necroptosis controls NET generation and mediates complement activation, endothelial damage, and autoimmune vasculitis, Proc. Natl. Acad. Sci. U. S. A. 114 (45) (2017) E9618–E9625.
[38] V. Papayannopoulos, K.D. Metzler, A. Hakkim, A. Zychlinsky, Neutrophil elastase and myeloperoxidase regulate the formation of neutrophil extracellular traps, J. Cell Biol. 191 (3) (2010) 677–691.
[39] K. Metzler, C. Goosmann, A. Lubojemska, A. Zychlinsky, V. Papayannopoulos, A myeloperoxidase-containing complex regulates neutrophil elastase release and actin dynamics during NETosis, Cell Rep. 8 (3) (2014) 883–896.
[40] S.A.I. Weiss, S.R.T. Rehm, N.C. Perera, M.L. Biniossek, O. Schilling, D.E. Jenne, Origin and expansion of the serine protease repertoire in the myelomonocyte lineage, Int. J. Mol. Sci. 22 (4) (2021) 1658.
[41] K. Kessenbrock, T. Dau, D.E. Jenne, Tailor-made inflammation: how neutrophil serine proteases modulate the inflammatory response, J. Mol. Med. (Berl.) 89 (1) (2011) 23–28.
[42] A. Schreiber, C.T. Pham, Y. Hu, W. Schneider, F.C. Luft, R. Kettritz, Neutrophil serine proteases promote IL-1beta generation and injury in necrotizing crescentic glomerulonephritis, J. Am. Soc. Nephrol. 23 (3) (2012) 470–482.
[43] B. Korkmaz, G.H. Caughey, I. Chapple, F. Gauthier, J. Hirschfeld, D.E. Jenne, R. Kettritz, G. Lalmanach, A.S. Lamort, C. Lauritzen, M. Legowska, A. Lesner, S. Marchand-Adam, S.J. McKaig, C. Moss, J. Pedersen, H. Roberts, A. Schreiber, S. Seren, N.S. Thakker, Therapeutic targeting of cathepsin C: from pathophysiology to treatment, Pharmacol. Ther. 190 (2018) 202–236.
[44] R. Kettritz, Neutral serine proteases of neutrophils, Immunol. Rev. 273 (1) (2016) 232–248.
[45] U. Jerke, D.P. Hernandez, P. Beaudette, B. Korkmaz, G. Dittmar, R. Kettritz, Neutrophil serine proteases exert proteolytic activity on endothelial cells, Kidney Int. 88 (4) (2015) 764–775.
[46] J. Zoidakis, M. Makridakis, P.G. Zerefos, V. Bitsika, S. Esteban, M. Frantzi, K. Stravodimos, N.P. Anagnou, M.G. Roubelakis, M. Sanchez-Carbayo, A. Vlahou, Profilin 1 is a potential biomarker for bladder cancer aggressiveness, Mol. Cell. Proteomics 11 (4) (2012) M111–009449.
[47] C. Guarino, M. Legowska, C. Epinette, C. Kellenberger, S. Dallet-Choisy, M. Sieńczyk, G. Gabant, M. Cadene, J. Zoidakis, A. Vlahou, M. Wysocka, S. Marchand-Adam, D.E. Jenne, A. Lesner, F. Gauthier, B. Korkmaz, New selective peptidyl di(chlorophenyl) phosphonate esters for visualizing and blocking neutrophil proteinase 3 in human diseases, J. Biol. Chem. 289 (46) (2014) 31777–31791.
[48] N. Vaguliene, M. Zemaitis, S. Lavinskiene, S. Miliauskas, R. Sakalauskas, Local and systemic neutrophilic inflammation in patients with lung cancer and chronic obstructive pulmonary disease, BMC Immunol. 14 (2013) 36.
[49] I. Lerman, S.R. Hammes, Neutrophil elastase in the tumor microenvironment, Steroids 133 (2018) 96–101.
[50] M. Kistowski, J. Dębski, J. Karczmarski, A. Paziewska, J. Olędzki, M. Mikula, J. Ostrowski, M. Dadlez, A strong neutrophil elastase proteolytic fingerprint marks the carcinoma tumor proteome, Mol. Cell. Proteomics 16 (2) (2017) 213–227.
[51] A. Teijeira, S. Garasa, M. Gato, C. Alfaro, I. Migueliz, A. Cirella, C. de Andrea, M. C. Ochoa, I. Otano, I. Etxeberria, M.P. Andueza, C.P. Nieto, L. Resano, A. Azpilikueta, M. Allegretti, M. de Pizzol, M. Ponz-Sarvise, A. Rouzaut, M. F. Sanmamed, K. Schalper, M. Carleton, M. Mellado, M.E. Rodriguez-Ruiz, P. Berraondo, J.L. Perez-Gracia, I. Melero, CXCR1 and CXCR2 chemokine receptor agonists produced by tumors induce neutrophil extracellular traps that interfere with immune cytotoxicity, Immunity 52 (5) (2020), 856-871 e8.
[52] A.S. Ireland, T.G. Oliver, Neutrophils create an ImpeNETrable shield between tumor and cytotoxic immune cells, Immunity 52 (5) (2020) 729–731.
[53] E. Cerami, J. Gao, U. Dogrusoz, B.E. Gross, S.O. Sumer, B.A. Aksoy, A. Jacobsen, C.J. Byrne, M.L. Heuer, E. Larsson, Y. Antipin, B. Reva, A.P. Goldberg, C. Sander, N. Schultz, The cBio cancer genomics portal: an open platform for exploring multidimensional cancer genomics data, Cancer Discov. 2 (5) (2012) 401–404.
[54] J. Gao, B.A. Aksoy, U. Dogrusoz, G. Dresdner, B. Gross, S.O. Sumer, Y. Sun, A. Jacobsen, R. Sinha, E. Larsson, E. Cerami, C. Sander, N. Schultz, Integrative analysis of complex cancer genomics and clinical profiles using the cBioPortal, Sci. Signal 6 (269) (2013) pl1.
[55] M. Imielinski, G. Guo, M. Meyerson, Insertions and deletions target lineage-defining genes in human cancers, Cell 168 (3) (2017), 460-472 e14.
[56] D. Turk, V. Janjic, I. Stern, M. Podobnik, D. Lamba, S.W. Dahl, C. Lauritzen, J. Pedersen, V. Turk, B. Turk, Structure of human dipeptidyl peptidase I (cathepsin C): exclusion domain added to an endopeptidase framework creates

the machine for activation of granular serine proteases, EMBO J. 20 (23) (2001) 6570–6582.
[57] A.M. Adkison, S.Z. Raptis, D.G. Kelley, C.T.N. Pham, Dipeptidyl peptidase I activates neutrophil-derived serine proteases and regulates the development of acute experimental arthritis, J. Clin. Invest. 109 (3) (2002) 363–371.
[58] C.T. Pham, J.L. Ivanovich, S.Z. Raptis, B. Zehnbauer, T.J. Ley, Papillon-Lefevre syndrome: correlating the molecular, cellular, and clinical consequences of cathepsin C/dipeptidyl peptidase I deficiency in humans, J. Immunol. 173 (12) (2004) 7277–7281.
[59] P.J. Wolters, C.T.N. Pham, D.J. Muilenburg, T.J. Ley, G.H. Caughey, Dipeptidyl peptidase I is essential for activation of mast cell chymases, but not tryptases, in mice, J. Biol. Chem. 276 (21) (2001) 18551–18556.
[60] M.J. Smyth, M.J. McGuire, K.Y. Thia, Expression of recombinant human granzyme B. A processing and activation role for dipeptidyl peptidase I, J. Immunol. 154 (12) (1995) 6299–6305.
[61] V.R. Sutton, N.J. Waterhouse, K.A. Browne, K. Sedelies, A. Ciccone, D. Anthony, A. Koskinen, A. Muilbacher, J.A. Trapani, Residual active granzyme B in cathepsin C-null lymphocytes is sufficient for perforin-dependent target cell apoptosis, J. Cell Biol. 176 (4) (2007) 425–433.
[62] S.W. Dahl, T. Halkier, C. Lauritzen, I. Dolenc, J. Pedersen, V. Turk, B. Turk, Human recombinant pro-dipeptidyl peptidase I (cathepsin C) can be activated by cathepsins L and S but not by autocatalytic processing, Biochemistry 40 (6) (2001) 1671–1678.
[63] A.S. Lamort, Y. Hamon, C. Czaplewski, A. Gieldon, S. Seren, L. Coquet, F. Lecaille, A. Lesner, G. Lalmanach, F. Gauthier, D. Jenne, B. Korkmaz, Processing and maturation of Cathepsin C Zymogen: a biochemical and molecular modeling analysis, Int. J. Mol. Sci. 20 (19) (2019) 4747.
[64] A. Molgaard, J. Arnau, C. Lauritzen, S. Larsen, G. Petersen, J. Pedersen, The crystal structure of human dipeptidyl peptidase I (cathepsin C) in complex with the inhibitor Gly-Phe-CHN2, Biochem. J. 401 (3) (2007) 645–650.
[65] Y. Hamon, M. Legowska, V. Hervé, S. Dallet-Choisy, S. Marchand-Adam, L. Vanderlynden, M. Demonte, R. Williams, C.J. Scott, M. Si-Tahar, N. Heuzé-Vourc'h, G. Lalmanach, D.E. Jenne, A. Lesner, F. Gauthier, B. Korkmaz, Neutrophilic cathepsin C is maturated by a multi-step proteolytic process and secreted by activated cells during inflammatory lung diseases, J. Biol. Chem. 291 (16) (2016) 8486–8499.
[66] S. Seren, L. Derian, I. Keleş, A. Guillon, A. Lesner, L. Gonzalez, T. Baranek, M. Si-Tahar, S. Marchand-Adam, D.E. Jenne, C. Paget, Y. Jouan, B. Korkmaz, Proteinase release from activated neutrophils in mechanically ventilated patients with non-COVID-19 and COVID-19 pneumonia, Eur. Respir. J. 57 (4) (2021), 2003755.
[67] C. Toomes, J. James, A.J. Wood, C.L. Wu, D. McCormick, N. Lench, C. Hewitt, L. Moynihan, E. Roberts, C.G. Woods, A. Markham, M. Wong, R. Widmer, K. A. Ghaffar, M. Pemberton, I.R. Hussein, S.A. Temtamy, R. Davies, A.P. Read, P. Sloan, M.J. Dixon, N.S. Thakker, Loss-of-function mutations in the cathepsin C gene result in periodontal disease and palmoplantar keratosis, Nat. Genet. 23 (4) (1999) 421–424.
[68] T.C. Hart, P.S. Hart, D.W. Bowden, M.D. Michalec, S.A. Callison, S.J. Walker, Y. Zhang, E. Firatli, Mutations of the cathepsin C gene are responsible for Papillon-Lefevre syndrome, J. Med. Genet. 36 (12) (1999) 881–887.
[69] S. Seren, M. Rashed Abouzaid, C. Eulenberg-Gustavus, J. Hirschfeld, H. Nasr Soliman, U. Jerke, K. N'Guessan, S. Dallet-Choisy, A. Lesner, C. Lauritzen, B. Schacher, P. Eickholz, N. Nagy, M. Szell, C. Croix, M.-C. Viaud-Massuard, A. Al Farraj Aldosari, S. Ragunatha, M. Ibrahim Mostafa, F. Giampieri, M. Battino, H. Cornillier, G. Lorette, J.-L. Stephan, C. Goizet, J. Pedersen, F. Gauthier, D. E. Jenne, S. Marchand-Adam, I.L. Chapple, R. Kettritz, B. Korkmaz, Consequences of cathepsin C inactivation for membrane exposure of proteinase 3, the target antigen in autoimmune vasculitis, J. Biol. Chem. 293 (32) (2018) 12415–12428.
[70] O.E. Sorensen, S.N. Clemmensen, S.L. Dahl, O. Ostergaard, N.H. Heegaard, A. Glenthoj, F.C. Nielsen, N. Borregaard, Papillon-Lefevre syndrome patient reveals species-dependent requirements for neutrophil defenses, J. Clin. Invest. 124 (10) (2014) 4539–4548.
[71] H. Roberts, P. White, I. Dias, S. McKaig, R. Veeramachaneni, N. Thakker, M. Grant, I. Chapple, Characterization of neutrophil function in Papillon-Lefevre syndrome, J. Leukoc. Biol. 100 (2) (2016) 433–444.
[72] B. Ruffell, N.I. Affara, L. Cottone, S. Junankar, M. Johansson, D.G. DeNardo, L. Korets, T. Reinheckel, B.F. Sloane, M. Bogyo, L.M. Coussens, Cathepsin C is a tissue-specific regulator of squamous carcinogenesis, Genes Dev. 27 (19) (2013) 2086–2098.
[73] G.P. Zhang, X. Yue, S.Q. Li, Cathepsin C interacts with TNF-alpha/p38 MAPK signaling pathway to promote proliferation and metastasis in hepatocellular carcinoma, Cancer Res. Treat. 52 (1) (2020) 10–23.
[74] K.-C. Chiang, C.-Y. Lai, H.-L. Chiou, C.-L. Lin, Y.-S. Chen, S.-H. Kao, Y.-H. Hsieh, Timosaponin AIII inhibits metastasis of renal carcinoma cells through suppressing cathepsin C expression by AKT/miR-129-5p axis, J. Cell. Physiol. 234 (8) (2019) 13332–13341.
[75] S. Kim, S.I. Lee, N. Kim, M. Joo, K.H. Lee, M.W. Lee, H.J. Jeon, H. Ryu, J.M. Kim, J.Y. Sul, G.Y. Song, J.Y. Kim, H.J. Lee, Decursin inhibits cell growth and autophagic flux in gastric cancer via suppression of cathepsin C, Am. J. Cancer Res. 11 (4) (2021) 1304–1320.
[76] T.P. Khaket, M.P. Singh, I. Khan, M. Bhardwaj, S.C. Kang, Targeting of cathepsin C induces autophagic dysregulation that directs ER stress mediated cellular cytotoxicity in colorectal cancer cells, Cell. Signal. 46 (2018) 92–102.
[77] Y. Xiao, M. Cong, J. Li, D. He, Q. Wu, P.u. Tian, Y. Wang, S. Yang, C. Liang, Y. Liang, J. Wen, Y. Liu, W. Luo, X. Lv, Y. He, D.-D. Cheng, T. Zhou, W. Zhao, P. Zhang, X. Zhang, Y. Xiao, Y. Qian, H. Wang, Q. Gao, Q.-C. Yang, Q. Yang, G. Hu, Cathepsin C promotes breast cancer lung metastasis by modulating neutrophil infiltration and neutrophil extracellular trap formation, Cancer Cell 39 (3) (2021) 423–437.e7.
[78] B. Korkmaz, J. Jaillet, M.-L. Jourdan, A. Gauthier, F. Gauthier, S. Attucci, Catalytic activity and inhibition of wegener antigen proteinase 3 on the cell surface of human polymorphonuclear neutrophils, J. Biol. Chem. 284 (30) (2009) 19896–19902.
[79] B. Korkmaz, A. Lesner, S. Letast, Y.K. Mahdi, M.-L. Jourdan, S. Dallet-Choisy, S. Marchand-Adam, C. Kellenberger, M.-C. Viaud-Massuard, D.E. Jenne, F. Gauthier, Neutrophil proteinase 3 and dipeptidyl peptidase I (cathepsin C) as pharmacological targets in granulomatosis with polyangiitis (Wegener granulomatosis), Semin. Immunopathol. 35 (4) (2013) 411–421.
[80] U. Jerke, S.F. Marino, O. Daumke, R. Kettritz, Characterization of the CD177 interaction with the ANCA antigen proteinase 3, Sci. Rep. 7 (2017) 43328.
[81] H. Pfister, M. Ollert, L.F. Frohlich, L. Quintanilla-Martinez, T.V. Colby, U. Specks, D.E. Jenne, Antineutrophil cytoplasmic autoantibodies against the murine homolog of proteinase 3 (Wegener autoantigen) are pathogenic in vivo, Blood 104 (5) (2004) 1411–1418.
[82] B. Korkmaz, D.E. Jenne, F. Gauthier, Relevance of the mouse model as a therapeutic approach for neutrophil proteinase 3-associated human diseases, Int. Immunopharmacol. 17 (4) (2013) 1198–1205.
[83] B. Korkmaz, E. Hajjar, T. Kalupov, N. Reuter, M. Brillard-Bourdet, T. Moreau, L. Juliano, F. Gauthier, Influence of charge distribution at the active site surface on the substrate specificity of human neutrophil protease 3 and elastase. A kinetic and molecular modeling analysis, J. Biol. Chem. 282 (3) (2007) 1989–1997.
[84] T. Kalupov, M. Brillard-Bourdet, S. Dade, H. Serrano, J. Wartelle, N. Guyot, L. Juliano, T. Moreau, A. Belaaouaj, F. Gauthier, Structural characterization of mouse neutrophil serine proteases and identification of their substrate specificities: relevance to mouse models of human inflammatory diseases, J. Biol. Chem. 284 (49) (2009) 34084–34091.
[85] B. Korkmaz, I. Keles, Cathepsin C as pharmacological target in cancer, <http://online.cancerresearch2021.org/hibrit/pdf/dijital-kitap.pdf> (2021).
[86] W. Hou, H. Sun, Y. Ma, C. Liu, Z. Zhang, Identification and optimization of novel cathepsin C inhibitors derived from EGFR inhibitors, J. Med. Chem. 62 (12) (2019) 5901–5919.
[87] X. Chen, Y. Yan, Z. Zhang, F. Zhang, M. Liu, L. Du, H. Zhang, X. Shen, D. Zhao, J. B. Shi, X. Liu, Discovery and in vivo anti-inflammatory activity evaluation of a novel non-peptidyl non-covalent cathepsin C inhibitor, J. Med. Chem. 64 (16) (2021) 11857–11885.
[88] S.A. Miller, D.D. Dykes, H.F. Polesky, A simple salting out procedure for extracting DNA from human nucleated cells, Nucleic Acids Res. 16 (3) (1988) 1215.
[89] J.D. Chalmers, C.S. Haworth, M.L. Metersky, M.R. Loebinger, F. Blasi, O. Sibila, A. E. O'Donnell, E.J. Sullivan, K.C. Mange, C. Fernandez, J. Zou, C.L. Daley, W. Investigators, Phase 2 trial of the DPP-1 inhibitor brensocatib in bronchiectasis, N. Engl. J. Med. 383 (22) (2020) 2127–2137.
[90] B. Korkmaz, A. Lesner, M. Wysocka, A. Gieldon, M. Håkansson, F. Gauthier, D. T. Logan, D.E. Jenne, C. Lauritzen, J. Pedersen, Structure-based design and in vivo anti-arthritic activity evaluation of a potent dipeptidyl cyclopropyl nitrile inhibitor of cathepsin C, Biochem. Pharmacol. 164 (2019) 349–367.
[91] K. Doyle, H. Lönn, H. Käck, A. Van de Poël, S. Swallow, P. Gardiner, S. Connolly, J. Root, C. Wikell, G. Dahl, K. Stenvall, P. Johannesson, Discovery of second generation reversible covalent DPP1 inhibitors leading to an oxazepane amidoacetonitrile based clinical candidate (AZD7986), J. Med. Chem. 59 (20) (2016) 9457–9472.
[92] S.R.T. Rehm, N.F. Smirnova, C. Morrone, J. Gotzfried, A. Feuchtinger, J. Pedersen, B. Korkmaz, A.O. Yildirim, D.E. Jenne, Premedication with a cathepsin C inhibitor alleviates early primary graft dysfunction in mouse recipients after lung transplantation, Sci. Rep. 9 (1) (2019) 9925.
[93] C. Guarino, Y. Hamon, C. Croix, A.-S. Lamort, S. Dallet-Choisy, S. Marchand-Adam, A. Lesner, T. Baranek, M.-C. Viaud-Massuard, C. Lauritzen, J. Pedersen, N. Heuzé-Vourc'h, M. Si-Tahar, E. Firath, D.E. Jenne, F. Gauthier, M.S. Horwitz, N. Borregaard, B. Korkmaz, Prolonged pharmacological inhibition of cathepsin C results in elimination of neutrophil serine proteases, Biochem. Pharmacol. 131 (2017) 52–67.
[94] R. Palmér, J. Mäenpää, A. Jauhiainen, B. Larsson, J. Mo, M. Russell, J. Root, S. Prothon, L. Chialda, P. Forte, T. Egelrud, K. Stenvall, P. Gardiner, Dipeptidyl peptidase 1 inhibitor AZD7986 induces a sustained, exposure-dependent reduction in neutrophil elastase activity in healthy subjects, Clin. Pharmacol. Ther. 104 (6) (2018) 1155–1164.
[95] A.F. Barker, Bronchiectasis, N. Engl. J. Med. 346 (18) (2002) 1383–1393.
[96] B. Korkmaz, A. Lesner, S. Marchand-Adam, C. Moss, D.E. Jenne, Lung protection by cathepsin C inhibition: a new hope for COVID-19 and ARDS? J. Med. Chem. 63 (22) (2020) 13258–13265.
[97] M. Fujinaga, M.M. Chernaia, R. Halenbeck, K. Koths, M.N.G. James, The crystal structure of PR3, a neutrophil serine proteinase antigen of Wegener's granulomatosis antibodies, J. Mol. Biol. 261 (2) (1996) 267–278.
[98] S.J.F. Macdonald, M.D. Dowle, L.A. Harrison, G.D.E. Clarke, G.G.A. Inglis, M. R. Johnson, P. Shah, R.A. Smith, A. Amour, G. Fleetwood, D.C. Humphreys, C. R. Molloy, M. Dixon, R.E. Godward, A.J. Wonacott, O.M.P. Singh, S.T. Hodgson, G.W. Hardy, Discovery of further pyrrolidine trans-lactams as inhibitors of human neutrophil elastase (HNE) with potential as development candidates and the crystal structure of HNE complexed with an inhibitor (GW475151), J. Med. Chem. 45 (18) (2002) 3878–3890.
[99] P. Hof, I. Mayr, R. Huber, E. Korzus, J. Potempa, J. Travis, J.C. Powers, W. Bode, The 1.8 A crystal structure of human cathepsin G in complex with Suc-Val-Pro-

PheP-(OPh)2: a Janus-faced proteinase with two opposite specificities, EMBO J. 15 (20) (1996) 5481–5491.
[100] S.J. Lin, K. Dong, C. Eigenbrot, M. van Lookeren Campagne, D. Kirchhofer, Structures of neutrophil serine protease 4 reveal an unusual mechanism of substrate recognition by a trypsin-fold protease, Structure 22 (9) (2014) 1333–1340.
[101] B. Korkmaz, S. Attucci, T. Moreau, E. Godat, L. Juliano, F. Gauthier, Design and use of highly specific substrates of neutrophil elastase and proteinase 3, Am. J. Respir. Cell Mol. Biol. 30 (6) (2004) 801–807.
[102] Y. Hamon, M. Legowska, P. Fergelot, S. Dallet-Choisy, L. Newell, L. Vanderlynden, A. Kord Valeshabad, K. Acrich, H. Kord, T. Charalampos, F. Morice-Picard, I. Surplice, J. Zoidakis, K. David, A. Vlahou, S. Ragunatha, N. Nagy, K. Farkas, M. Szell, C. Goizet, B. Schacher, M. Battino, A. Al Farraj Aldosari, X. Wang, Y. Liu, S. Marchand-Adam, A. Lesner, E. Kara, S. Korkmaz-Icoz, C. Moss, P. Eickholz, A. Taieb, S. Kavukcu, D.E. Jenne, F. Gauthier, B. Korkmaz, Analysis of urinary cathepsin C for diagnosing Papillon-Lefevre syndrome, FEBS J. 283 (3) (2016) 498–509.
[103] D. Laine, M. Palovich, B. McCleland, E. Petitjean, I. Delhom, H. Xie, J. Deng, G. Lin, R. Davis, A. Jolit, N. Nevins, B. Zhao, J. Villa, J. Schneck, P. McDevitt, R. Midgett, C. Kmett, S. Umbrecht, B. Peck, A.B. Davis, D. Bettoun, Discovery of novel cyanamide-based inhibitors of cathepsin C, ACS Med. Chem. Lett. 2 (2) (2011) 142–147.
[104] L. Redecke, K. Nass, D.P. DePonte, T.A. White, D. Rehders, A. Barty, F. Stellato, M. Liang, T.R.M. Barends, S. Boutet, G.J. Williams, M. Messerschmidt, M. M. Seibert, A. Aquila, D. Arnlund, S. Bajt, T. Barth, M.J. Bogan, C. Caleman, T.-C. Chao, R.B. Doak, H. Fleckenstein, M. Frank, R. Fromme, L. Galli, I. Grotjohann, M.S. Hunter, L.C. Johansson, S. Kassemeyer, G. Katona, R.A. Kirian, R. Koopmann, C. Kupitz, L. Lomb, A.V. Martin, S. Mogk, R. Neutze, R.L. Shoeman, J. Steinbrener, N. Timneanu, D. Wang, U. Weierstall, N.A. Zatsepin, J.C. H. Spence, P. Fromme, I. Schlichting, M. Duszenko, C. Betzel, H.N. Chapman, Natively inhibited Trypanosoma brucei cathepsin B structure determined by using an X-ray laser, Science 339 (6116) (2013) 227–230.
[105] I. Schechter, A. Berger, On the size of the active site in proteases. I. Papain, Biochem. Biophys. Res. Commun. 27 (2) (1967) 157–162.
[106] M. Legowska, Y. Hamon, A. Wojtysiak, R. Grzywa, M. Sienczyk, T. Burster, B. Korkmaz, A. Lesner, Development of the first internally-quenched fluorescent substrates of human cathepsin C: the application in the enzyme detection in biological samples, Arch. Biochem. Biophys. 612 (2016) 91–102.

# Annexe 2




# Modulation of the expression and activity of cathepsin S in reconstructed human skin by neohesperidin dihydrochalcone

**J. Sage [a,*], J. Renault [b,c,*], R. Domain [b,c], K.K. Bojarski [d], T. Chazeirat [b,c], A. Saidi [b,c], E. Leblanc [a], C. Nizard [a], S.A. Samsonov [d], R. Kurfurst [a], G. Lalmanach [b,c] and F. Lecaille [b,c]**

***a* - LVMH-Recherche,** *Saint Jean de Braye F-45800, France*
***b* - Université de Tours,** *Tours, France*
***c* - INSERM,** *Centre d'Etude des Pathologies Respiratoires, Team Mécanismes Protéolytiques dans l'Inflammation, UMR 1100, Tours F-37032, France*
***d* - Faculty of Chemistry,** *University of Gdańsk, Gdańsk 80-308, Poland*

***Corresponding to Fabien Lecaille:*** *Fabien Lecaille, Université de Tours, INSERM, UMR 1100, CEPR, 10 Boulevard Tonnellé, F-37032 Tours cedex, France.* *fabien.lecaille@univ-tours.fr.*
https://doi.org/10.1016/j.matbio.2022.02.003

## Abstract

Dysregulation of cathepsin S (Cat S), a cysteine protease involved in extracellular-matrix and basement membrane (BM) degradation, is a concomitant feature of several inflammatory skin diseases. Therefore, Cat S has been suggested as a potential therapeutic target. Flavonoids, which were identified as regulatory molecules of various proteolytic enzymes, exert beneficial effects on skin epidermis. Herein, thirteen flavonoid compounds were screened *in vitro* and *in silico* and neohesperidin dihydrochalcone (NHDC) was identified as a potent, competitive, and selective inhibitor ($K_i$=8±1 μM) of Cat S. Furthermore, Cat S-dependent hydrolysis of nidogen-1, a keystone protein of BM architecture, as well elastin, collagens I and IV was impaired by NHDC, while both expression and activity of Cat S were significantly reduced in NHDC-treated human keratinocytes. Moreover, a reconstructed human skin model showed a significant decrease of both mRNA and protein levels of Cat S after NHDC treatment. Conversely, the expression of nidogen-1 was significantly increased. NHDC raised IL-10 expression, an anti-inflammatory cytokine, and mediated STAT3 signaling pathway, which in turn dampened Cat S expression. Our findings support that NHDC may represent a valuable scaffold for structural improvement and development of Cat S inhibitors to preserve the matrix integrity and favor skin homeostasis during inflammatory events.

© 2022 Elsevier B.V. All rights reserved.

## Introduction

Human cathepsin S (Cat S, EC 3.4.22.27) is a non-glycosylated lysosomal papain-like cysteine protease that is primarily expressed in many antigen presenting cells (dendritic cells, macrophages, and B cells) and participates in MHC-II antigen presentation (for review: [1]. In addition, Cat S is found in a range of resident cells including keratinocytes, and its expression can be induced by pro-inflammatory stimuli. Among the members of human cysteine cathepsin family (cathepsins B, C, H, F, K, L, O, S, V, W, and X), Cat S has the unique property to be highly active and stable at neutral pH, supporting its potential involvement in extracellular proteolytic activities [2,3]. Moreover, some cells (i.e., macrophages, osteoclasts, tumor cells) express vacuolar-type $H^+$-ATPase pumps that lower the pericellular pH, thus subsequently triggering cysteine cathepsin activity [4–7]. Accordingly, Cat S participates in matrix remodeling by the degradation at acidic and neutral pH of extracellular matrix (ECM) constituents such as elastin and collagen type I, as well basement membrane (BM) components, including laminins, collagen type IV, and nidogen-1 (nid-1) [8–10]. More specifically, beside other proteases (e.g.

MMP-1, -3, -9, elastase, cysteine cathepsins B, K, L, and V), Cat S contributes to highly specific intra- and extracellularly proteolytic processes in human skin, supporting that Cat S represents a major regulator of barrier function and immune homeostasis [11,12]. Aberrant expression and activity of Cat S is related to the pathogenesis of autoimmune diseases in skin (e.g. psoriasis, atopic dermatitis), highlighting its potential as an attractive therapeutic target [13–21].

Beside synthetic chemicals, it is now well admitted that numerous natural compounds with high bioavailability and low cytotoxicity can provide a wide range of potential health benefits. Flavonoid compounds, which are extensively present in the kingdom of plants, have sparked great attention in recent years, considering their potent antioxidant, metal chelation, anti-inflammatory, antimicrobial, antifungal, anticancer, and antiviral properties (for review: [22]. Moreover, flavonoids exert powerful anti-aging and photoprotective effects on the skin through the regulation of various proteolytic enzyme types, including metallo-, serine, aspartic proteases as well cysteine cathepsins B, H, K, L, and V (for review: [23]. Despite their ability to inhibit Cat S has never been investigated, flavonoids may represent promising candidates to modulate Cat S extracellular activity and to preserve BM integrity at the dermal epidermal junction (DEJ). Therefore, this work aimed to analyze the ability of five representative chemical classes of thirteen commercial flavonoids including flavones (chrysin and apigenin), flavanones (naringenin, hesperitin, eriodictyol, neohesperidin), flavanols (gallocatechin, neohesperidin epigallocathechin 3-gallate), flavonols (myricetin, quercetin, kaempferol), and dihydrochalcones (cardamonin, neohesperidin dihydrochalcone) to inhibit Cat S activity. Among these compounds, neohesperidin dihydrochalcone (NHDC) displayed the most potent inhibitory activity against Cat S. The mechanism of inhibition was determined by *in vitro* kinetics analysis, and interactions between Cat S and NHDC were evaluated *in silico* by molecular docking. Moreover, consequences of NDHC-dependent Cat S inhibition on keratinocytes and a reconstructed human skin (RHS) model were examined as well the signaling pathway underlying the modulation of Cat S expression. Our results suggested that NHDC may provide an effective scaffold for development of specific and selective small Cat S inhibitors as skin therapeutic agents, which could be further exploited in topical formulations during inflammatory skin disorders.

## Results and discussion

### Screening of flavonoids for inhibitory activity against Cat S

Except epigallocathechin 3-gallate (EGCG) and to a less extent kaempferol and cardamonin, all tested compounds showed some dose-dependent inhibitory effect toward Cat S activity (Supplementary Fig. 1). Among them, neohesperidin dihydrochalcone (NHDC), was the most potent inhibitor of Cat S-mediated Z-FR-AMC hydrolysis. The inhibition constant (Ki) values were further determined, and results reported in Table 1. NHDC inhibited Cat S according to a reversible mechanism with a $K_i$ of 8±1 μM, while neohesperidin (NHP) was less effective with a $K_i$ of 27±9 μM, suggesting that linearization of the pyrane ring C (see the nomenclature of chrysin and NHDC structures, Table 1), which leads to a ~2.5-fold increase of the dipolar moment, may assist interactions with the enzyme (Supplementary Table 1). Also, hesperetin, the aglycone form of NHP, had a weaker inhibitory capacity ($K_i$=127±23 μM) *in vitro*, suggesting that the substitution of the benzene ring A by a sugar moiety (i.e., 4'-((2-*O*-[6-Deoxy-α-L-mannopyranosyl]-β-D-glucopyranosyl) oxy)) could favor inhibition of Cat S. The low potency of cardamonin, a chalcone aglycone, to inhibit Cat S ($K_i$=327±56 μM) corroborated the likely importance of this structural feature.

### Competitive inhibition of Cat S by NHDC

NHDC inhibited Cat S in a competitive manner, since the vertical axis intercept (1/Vm) remained while the horizontal axis intercept (-1/Km) increased with NHDC concentration (Fig. 1A). The secondary plot of slopes of Lineweaver-Burk ($K_{app}$) *vs.* [NHDC] was linearly fitted (shown in the inset), which indicated that NHDC bound to the substrate binding site of Cat S. Conversely, Cat S inhibition by flavones, flavanones, flavanols and flavonols best corresponded to a non-competitive mechanism (data not shown). Preincubation (0-120 min) of Cat S with NHDC at a concentration eliciting ~50% inhibition of its peptidase activity revealed that Cat S inhibition was highly stable, since ≥99% NHDC inhibitory potential was retrieved after 2h-incubation (Fig. 1B). On the other hand, NHDC remained an effective inhibitor of Cat S at pH 7.4 ($K_i$=40±6 μM), supporting its potential to reduce extracellularly the proteolysis of ECM components by Cat S. NHDC was also tested at pH 5.5 against closely related human cathepsins L (Cat L) and B (Cat B), which are the two prevalent and ubiquitous papain-like cysteine proteases expressed by keratinocytes in skin epidermis [10,24]. The inhibitory effect of NHDC on both Cat L and Cat B was substantially weaker than that of Cat S, with a ~18-20-fold $K_i$ increase (Cat L: $K_i$=144±22 μM, Cat B: $K_i$=167±11 μM) assessing a fairly selectivity towards Cat S (Fig. 1C). Moreover, NHDC demonstrated a substantially weaker inhibitory activity ($K_i$=61±16 μM) towards the related cathepsin-L like enzyme, human cathepsin K at pH 5.5. Likewise, NHDC inhibited in a dose dependent manner hydrolysis of fluorogenic substrates derived from

**Table 1.** *Ki* values for inhibition of Cat S by flavonoids.

| | # | Compound | Structure | *Ki* (μM) |
|---|---|---|---|---|
| *Flavones* | 1 | Chrysin | 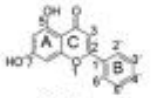 | 111±36 |
| | 2 | Apigenin | 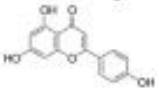 | 96±7 |
| *Flavanones* | 3 | Naringenin | 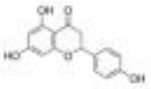 | 109±33 |
| | 4 | Hesperetin | 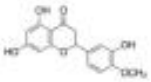 | 127±23 |
| | 5 | Eriodictyol | 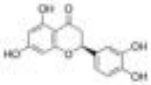 | 162±45 |
| | 6 | Neohesperidin (NHP) | 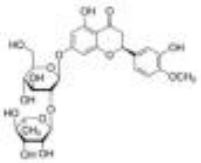 | 27±9 |
| *Flavanols* | 7 | Gallocatechin | 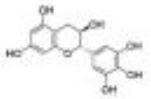 | 86±24 |
| | 8 | Epigallocathe-chin 3-gallate (EGCG) | 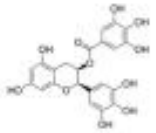 | 326±22 |
| *Flavonols* | 9 | Myricetin | 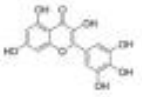 | 72±10 |
| | 10 | Quercetin | 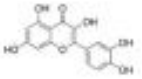 | 73±12 |
| | 11 | Kaempferol | 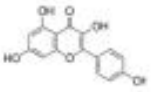 | 132±37 |
| *Dihydrochal-cones* | 12 | Cardamonin | 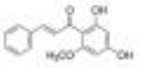 | 327±56 |

(continued)

**Table 1** (*Continued*)

| # | Compound | Structure | *Ki* (μM) |
|---|---|---|---|
| 13 | Neohesperidin dihydrochalcone (NHDC) | 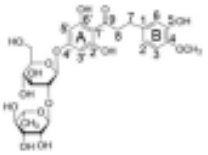 | 8±1 |

Basic flavonoid structure corresponds to a fifteen-carbon skeleton consisting of two benzene rings (A and B as shown in chrysin) linked via a heterocyclic pyrane ring (C).

elastin, collagens type I and IV, supporting that NHDC could effectively impair both elastinolytic and collagenolytic activities of Cat S, besides its peptidase activity (Fig. 2). Moreover, proteolysis of nidogen-1 (nid-1), a key protein in BM assembly and a specific substrate of Cat S [10,25], is readily prevented by NHDC (100 μM).

### Identification of putative binding sites of NHDC on Cat S

Molecular docking simulations were performed to provide intermolecular insights in the interactions between flavonoids and Cat S. Molecular docking of the thirteen flavonoids predicted binding affinity ($\Delta G_{calc}$) in a similar range for all examined complexes (difference magnitude ± 2 kcal/mol) with a preference in the substrate-binding site (catalytic cavity) of the enzyme (supplementary Table 1). Interestingly, among the flavonoids tested, only chrysin, naringenin, kaempferol, and NHDC were docked exclusively in the active site of Cat S, with NHDC poses in the top-ranking binding scores ($\Delta G_{calc}$=-7.4 kcal/mol). In addition, docking scores positively correlated with experimental free binding energy ($\Delta G_{exp}$) (Pearson correlation: r=0.707, p=0.007). Principal component analysis (PCA) was then used to identify molecular descriptors of flavonoids that may be important in the inhibition of Cat S. A linear positively relationship (r=0.78, p=0.0017) was established between $\Delta G_{exp}$ and the partition coefficient in octanol/water (LogP), while a negative correlation was measured between $\Delta G_{exp}$ and polar surface area (r=-0.66, p=0.014) (Fig. 3A, B). Moreover, $\Delta G_{exp}$ correlated negatively with mass (r=-0.68, p=0.010), accessible surface area (r=-0.68, p=0.01), H-bond acceptor (r=-0.69, p=0.008), and orientable bonds (r=-0.63, p=0.02) of tested compounds. Results indicated that large and polar flavonoid compounds with the lowest lipophilicity, i.e., NHDC, constituted the most efficient inhibitors of Cat S. Molecular dynamics (MD) was used to give a better view on stability of NHDC-Cat S complexes than that obtained from molecular docking. As depicted inFig. 3 C, MD unveiled that NHDC likely bound to the active site rather than other sites located on the protein surface. Indeed, mean values of five binding free energies obtained from 20 ns MD simulation at pH 7 of NHDC in the active and non-active site were ΔG=-24.7±4 kcal/mol and ΔG=-22.0±4.5 kcal/mol, respectively. The competitive inhibition mode of Cat S by NHDC deduced from kinetic studies was consistent with MD analysis. NHDC exhibited a binding pose covering preferentially the central region of the Cat S substrate-binding site, by establishing hydrogen bonds with residues Q19, G23, G65, and G69 (Fig. 3D). Regarding the disaccharide moiety of NHDC (4'-((2-*O*-[6-Deoxy-α-L-mannopyranosyl]-β-D-glucopyranosyl) oxy), deoxy-α-L-mannopyranose bound preferentially to the S2 pocket of Cat S, while β-D-glucopyranose bound preferentially to the S1 subsite.

### Effect of NHDC on Cat S in human keratinocytes

After assessing that NHDC was a relevant inhibitor of Cat S *in vitro* and *in silico*, we investigated its cellular effects on keratinocytes, the predominant cell type in epidermis (Fig. 4). First, we analyzed the cell viability of normal human epidermal keratinocytes (NHEK), following a treatment by NHDC (0, 100 μM, and 500 μM) for 24 h. No significant cell cytotoxicity at high concentration was measured, and relatively homogenous monolayers of small (10-20 μm) cells were observed in the absence and presence of NHDC (Fig. 4A). These results corroborated previous findings on the safety profile of NHDC on different cell types (fibroblasts, stem cells) [26,27], contrasting to several structurally related polyphenols (i.e., apigenin, naringenin, eriodictyol, kaempferol, quercetin) that exhibited at high concentrations deleterious effect on cell viability of numerous human cells, including HaCaT keratinocytes [28,29]. Then, impact of NHDC on Cat S expression (mRNA, protein) and activity of growing NHEK was evaluated. Both mRNA expression and intracellular protein level were reduced ($p<0.05$) in cell lysates of NHDC-treated keratinocytes compared with the control group, reaching a ~1.6-fold decrease with 500 μM NHDC (Fig. 4B, C). Consistently, specific enzymatic activity of secreted Cat S, using Z-LR-AMC as substrate, decreased in a dose-dependent manner under treatment with NHDC ($p<0.001$)

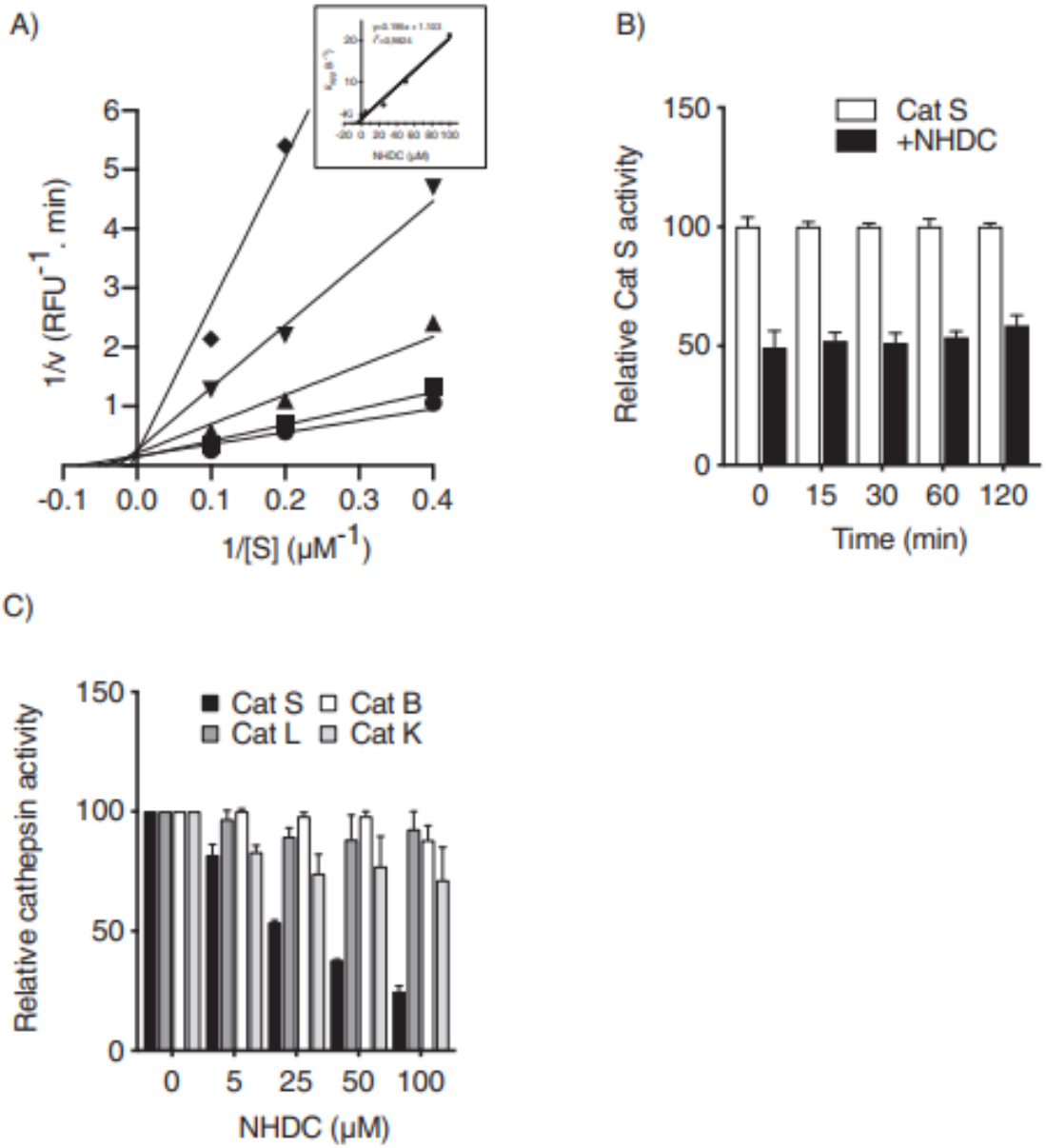


**Fig. 1.** Competitive and selective inhibition of Cat S by NHDC. A) Lineweaver-Burk plots analysis of Cat S inhibition. To determine the nature of inhibition of Cat S by NHDC, the rate of Cat S (0.2 nM) was measured with Z-FR-AMC at different concentrations in the presence of NHDC (0 μM:•; 5 μM:■; 25 μM:▲; 50 μM:▼ and 100 μM:◆). Enzyme activity was expressed as RFU/min (relative fluorescence units of AMC released per unit of time). Results are the mean of 3 experiments conducted in triplicates. The values of $K_{app}$ were calculated by double reciprocal plots at four concentrations of substrate Z-FR-AMC and in presence of five different concentrations of NHDC (insert). Intersection of the slope with x axis corresponds to -$K_i$. B) Stability of NHDC (50 μM) to inhibit Cat S (0.5 nM) at pH 5.5 over time. Cat S activity: data assays were normalized to 100% of the respective value at t=0 min, in the absence of NHDC. C) Inhibition of the peptidase activity (Z-FR-AMC: 10 μM) of Cat B, Cat L, Cat K, and Cat S (final concentration: 0.5 nM) with NHDC in the activity buffer (pH 5.5). The activity is expressed as a percentage and compared to the control without NHDC (100% activity).

(Fig. 4D). Data indicated that a relatively short-term (24 h) treatment by NHDC can down regulate Cat S expression in keratinocytes, supporting that NHDC could be a valuable reagent for the regulation of Cat S in inflammatory responses. These findings prompted us to explore whether a long-term treatment with NHDC might unveil a direct inhibitory effect on the Cat S expression in skin, consequently associated to a reduction in the remodeling and/or degradation of matrix (BM and ECM) components.

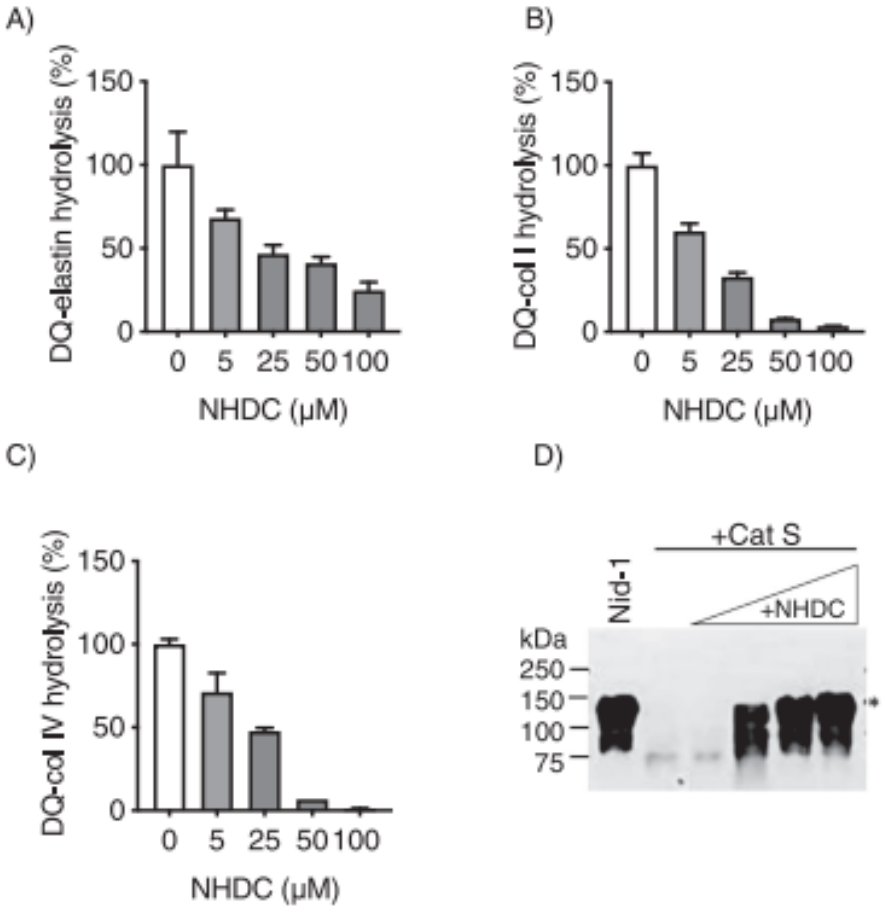


**Fig. 2.** Inhibition of the proteolytic activity of Cat S by NHDC. Cat S (0.5 nM) was incubated in the activity buffer pH (5.5) in the absence and presence of NHDC (5, 25, 50, and 100 μM). Collagenase and elastase activities of Cat S were measured with the following fluorogenic substrates: A) DQ-elastin (10 μg/mL), B) DQ-collagen I (10 μg/mL), C) DQ-collagen IV (10 μg/mL). The activity was expressed as a percentage and compared to the control without NHDC (100% activity). Results are expressed as mean±standard deviation (SD) of three independent experiments, each performed in duplicate. D) Representative western-blot of nidogen-1 (nid-1, 50 ng) incubated 30 min in the activity buffer (pH 5.5) or in the presence of Cat S (10 nM) with increasing concentrations of NHDC (from left to right: 1 μM, 50 μM, 100 μM, and 200 μM). Star indicates the location of nid-1.

### Effect of NHDC on Cat S and matrix components in reconstructed human skin (RHS) model

A biologically relevant model of reconstructed human skin (RHS) consisting of an epidermis and dermis separated by a basement membrane (BM) and populated with human skin cells (keratinocytes and fibroblasts) was previously developed [30]. Accordingly, RHS could represent an appropriate template to identify and characterize changes in Cat S expression and BM protein integrity following exposure to NHDC (100 μM) for 14 days. Histological examination revealed a completely stratified epithelium in *de novo* RHS, which closely resembled normal human epidermis (Fig. 5A). Immunostaining of RHS cryosections with anti-human Cat S antibodies revealed that Cat S, which was broadly expressed in epidermis and to a lesser extent in dermis, was significantly reduced in NHDC-treated RHS compared to control (Fig. 5B), consistent with the observed decrease in Cat S levels in NHDC-treated keratinocytes. Conversely, a noticeable changed in the amount of specific BM constituents was observed. A significant increase of nid-1 and laminin-1, but not collagen type IV was measured in the dermal epidermal junction (DEJ) of NHDC-treated RHS. In addition, immunohistochemistry (IHC) analysis of ECM proteins in dermis revealed that elastin, fibronectin, and collagen type I staining was significantly increased after 14 days of NHDC treatment (Fig. 5B), while collagen type VII, and fibrillin levels were unchanged (data not shown). IHC results for both Cat S and nid-1 were confirmed by sandwich ELISA in RHS lysates (Fig. 5C). One

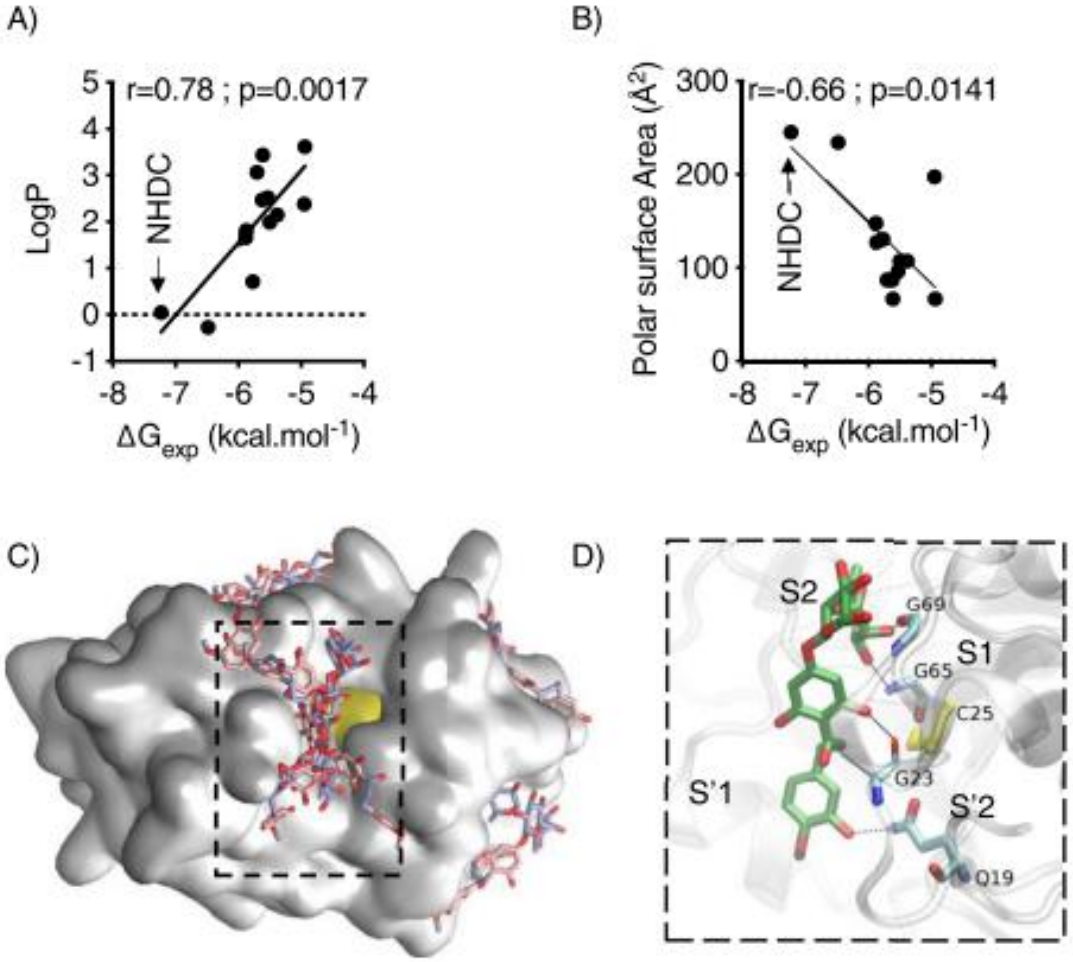


**Fig. 3.** Docking model of NHDC with Cat S. A) Experimental Gibbs free energy ($\Delta G_{exp}$) of the thirteen flavonoids were plotted against partition coefficient (LogP). $\Delta G_{exp}$ was obtained from experimental Ki, using the formula $\Delta G = R.T.\ln(Ki)$. B) Correlation between polar surface area and $\Delta G_{exp}$. The significance of the correlation was assessed with Pearson coefficient (r). C) Top 10 dock poses of NHDC (pink and cyan sticks) on Cat S (light grey surface) with a focus of the active site (dotted square). Cysteine 25 (C25) of the catalytic site is depicted in yellow. D) Hydrogen bonds between NHDC (green sticks) and residues Q19, G23, G65, and G69 of the active cleft of Cat S are shown. Subsites S2, S1, S'1, and S'2 are depicted.

can suggest that the increased or unchanged expression of these matrix components, identified as biologically relevant targets of Cat S, can be attributed in part to the decrease of expression/activity of the enzyme by NHDC. Whether downregulation of Cat S secretion is directly triggered by NHDC or depends on other matrix-degrading enzymes will require further investigation.

### NHDC exposure altered Cat S expression in RHS through IL-10/STAT3 axis

NHDC, like other flavonoid compounds, encompasses anti-inflammatory effects in various human cells by modulating the expression and secretion of cytokines [31–34]. Furthermore, there is some evidence that specific cytokines regulate Cat S expression [35]. Accordingly, previous studies reported that interferon-gamma (IFN-γ), a pro-inflammatory cytokine, induces selectively Cat S expression in keratinocytes [13,24], while exposure to interleukin IL-10, a potent anti-inflammatory cytokine, downregulates its expression in macrophages [36]. To further confirm whether the production of these two crucial cytokines is dysregulated in NDHC-treated RHS, we performed a multiplex cytokine analysis. Following NHDC (100 μM) treatment for 14 days, RHS supernatants showed a significant increased release of IL-10 (40.49±2.92 pg/mL) compared to control groups (28.01±2.70 pg/mL), while NHDC successfully reduced expression of IFN-γ (p=0.011) (Fig. 5C). In the same line, NHDC (100

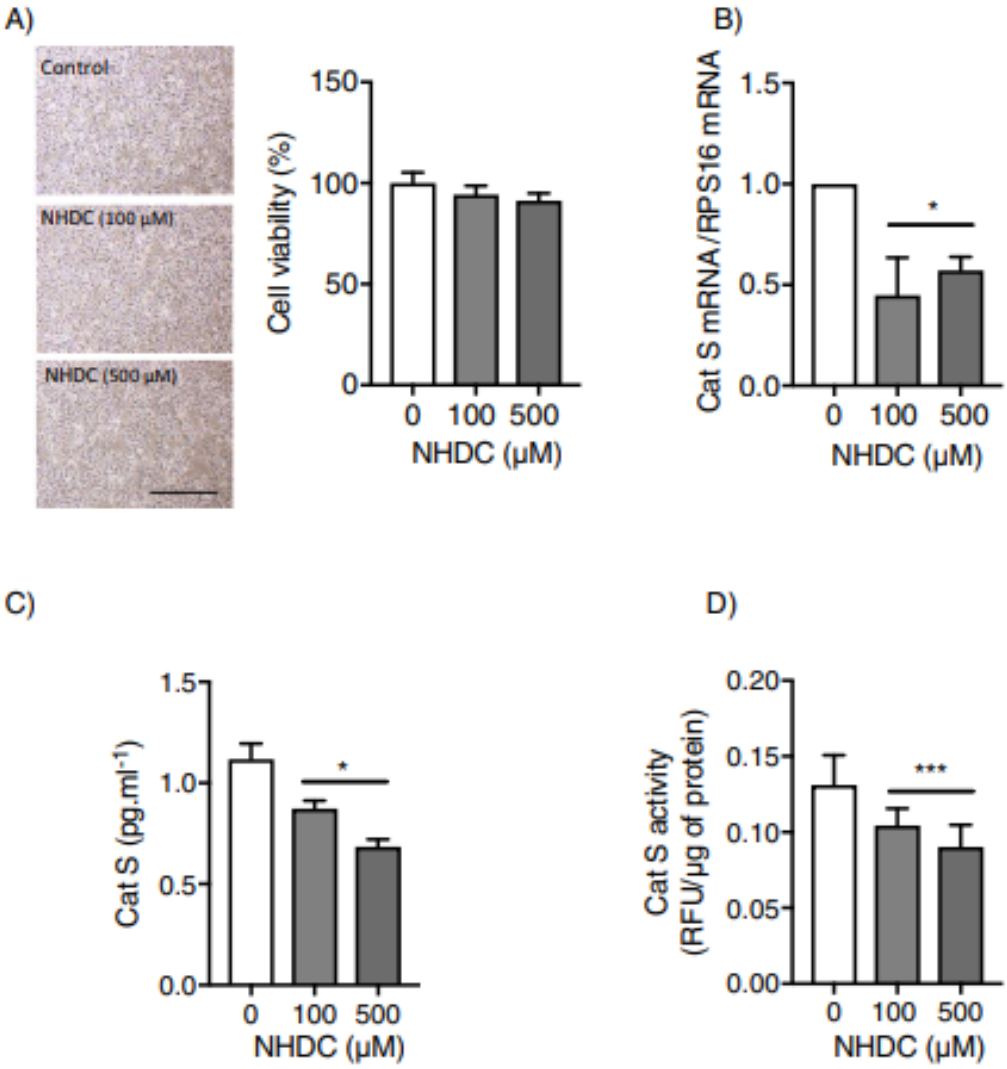


**Fig. 4.** Effect of NHDC on Cat S expression/activity in human keratinocytes. A) General morphology of normal human epidermal keratinocytes (NHEK) grown during 24 h in the absence (control) or with NHDC (100 and 500 µM). Cells in monolayer culture were photographed using light microscopy (scale bar: 200 µm). Cell viability of NHDC was performed by WST-1 assays (n=3). Data are expressed as a percentage and compared to the control without NHDC (100%). B) Cat S mRNA levels were analyzed by RT-qPCR and normalized to the levels of RPS16 mRNA. C) Cat S protein levels (ELISA) in NHEK lysates, (n=3, duplicate). D) Cat S activity in cell-free supernatants. Supernatants were pretreated in the presence of proteases inhibitors cocktail. Cat S activity (relative fluorescence unit: RFU) in supernatant (30 µg of protein deposited) was monitored using Z-Leu-Arg-AMC (30 µM) (n=3, duplicate) (see material and methods for details). Error bars represent median values±S.D. Statistical significance was assessed between NHDC-treated cells and non-treated cells using the non-parametric Mann-Whitney U-test (*$P < 0.05$; *** $P < 0.001$).

µM) did not alter pro-inflammatory cytokine IL-6 secretion, as reported elsewhere in LPS-stimulated murine macrophages model [31] (Supplementary Fig. 2A). A similar result was observed for IL-8 (Supplementary Fig. 2B). In addition to suppress IFN-γ signaling, a previous report indicated that IL-10 activates its primary mediator, signal transducer and activator of transcription 3 (STAT3), concomitantly with the down expression of Cat S in human macrophages [36]. To examine whether NHDC could upregulate STAT3 in epidermis, we performed western-blot analysis on untreated and NHDC-treated RHS lysates. As shown in Fig. 5D, treatment with NHDC triggered STAT3 phosphorylation (P-STAT3). Conversely, activation of STAT3 led to a marked decrease in Cat S protein levels in NHDC-treated RHS lysates, corroborating ELISA experiments (Fig. 5C). Taken together, this result

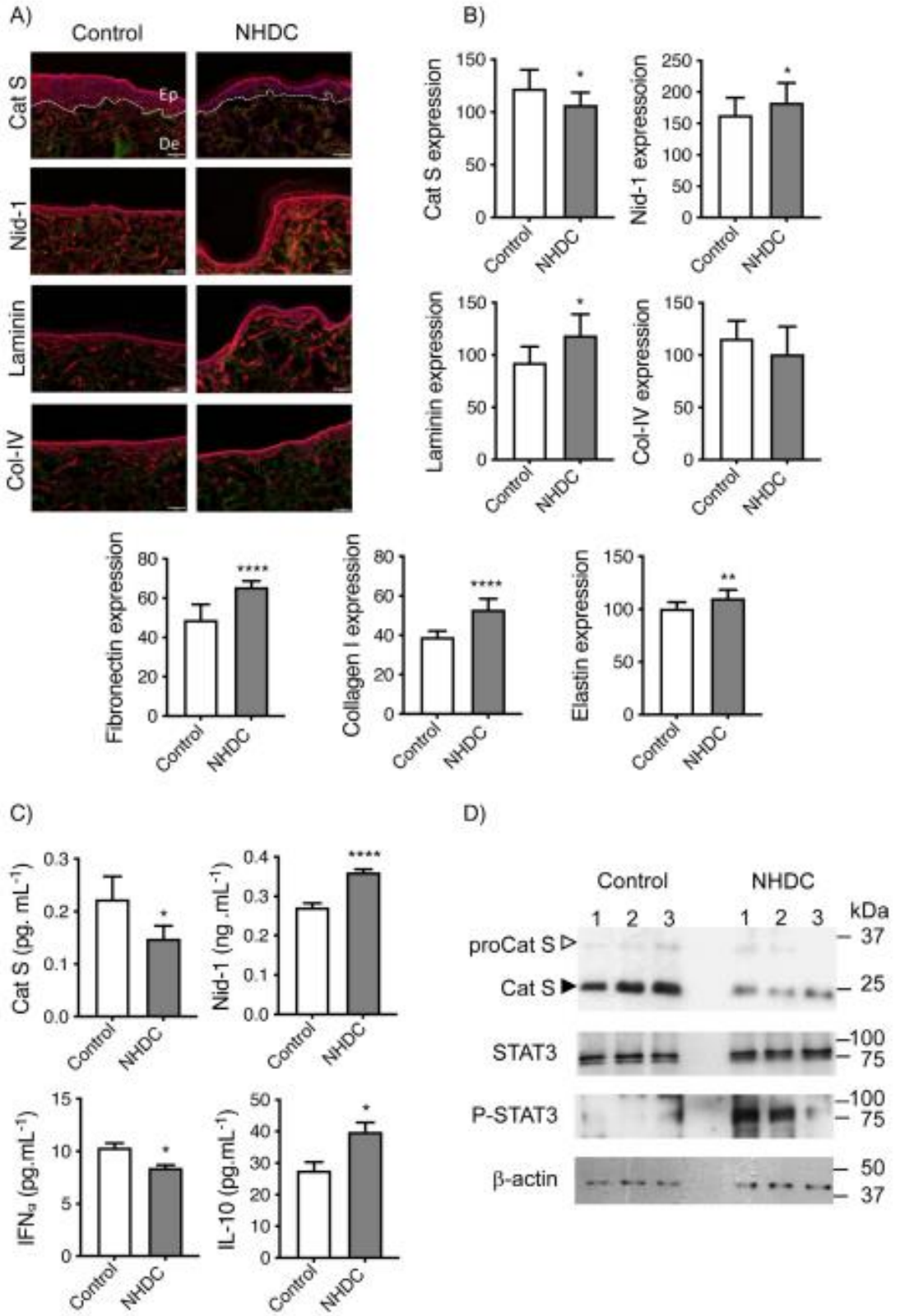


**Fig. 5.** Effect of NHDC on Cat S and BM components expression in reconstructed human skin. A) Representative image of immunofluorescence staining of Cat S, nidogen-1, laminin-332/-511, and collagen-IV in reconstructed human

supported that the downregulation of Cat S by NHDC in RHS is associated with the IL-10/STAT3 axis. Nevertheless, it cannot be excluded that NHDC could also interfere with other potential cellular pathways involved in the regulation of cathepsin expression.

## Conclusions

Over the last 20 years, extensive efforts have been devoted to the search and the development of synthetic or natural derivative inhibitors of Cat S, leading to the discovery of potent and selective covalent and non-covalent inhibitors (for review: [37]). However, no study has investigated the inhibitory potency of the flavonoids on Cat S, contrary to its counterparts cathepsins B, L, K, and V (for review: [23]). In the present work, among thirteen commercial flavonoids from five chemical subclasses, we identified NHDC as a potent reversible and competitive inhibitor of Cat S at both acidic and neutral pH. Moreover, NHDC displayed a reasonable selectivity for Cat S *vs* human Cat B and Cat L at acidic pH. *In silico* analysis supported kinetics data and suggested that NHDC interacted within the active site of Cat S by establishing hydrogen bonds. Electrostatic and van der Waals interactions may also contribute to the overall binding affinity of NHDC toward Cat S.

Based on prior studies supporting that NHDC has no toxicity on cells and animals [38,39], we examined the consequences of exposure of human keratinocytes to NHDC on Cat S expression and the impact of Cat S inhibition in a reconstructed human skin (RHS) model. Treatment of keratinocytes and RHS with NHDC resulted in a significant reduction of Cat S expression, whereas levels of major ECM and BM constituents in epidermis (i.e. nid-1, laminin-1, elastin, fibronectin, and collagen type I), were noticeably increased. Moreover, Cat S downregulation is associated to IL-10-induced STAT3 activation, as previously reported in primary human blood macrophages [36]. Accordingly, the Fig. 6 summarizes a putative signaling pathway in epidermis. Alternatively, NHDC may also have an indirect effect of cathepsin S expression by modulating other cofactors and cellular mechanisms. For instance,

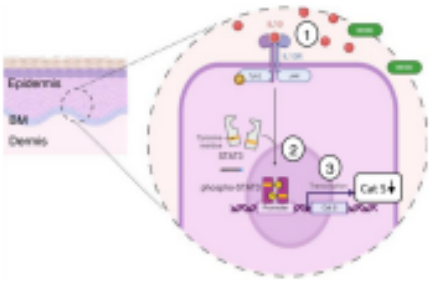


**Fig. 6.** Putative model of NHDC-induced down expression of Cat S in human skin. We propose that NHDC induces the production of IL-10 (1), which binds to its receptor and subsequently activates STAT3 (2). Phosphorylation of STAT3 downregulates Cat S expression (3). Figure was created by BioRender.com. BM: basement membrane.

Cat S may be secreted via secretory lysosomes upon elevation of intracellular $Ca^{2+}$ levels, which favors its release into the extracellular space [40]. Interestingly, some natural flavonoids change the intracellular $Ca^{2+}$ homeostasis linked to functional alterations of the mitochondria, $Ca^{2+}$ channels and $Ca^{2+}$ pumps [41], supporting that NHDC may also modify calcium homeostasis. Accordingly, analysis of the regulation of $Ca^{2+}$ by NHDC could be the purpose of further study. Finally, besides its antioxidative, anti-inflammatory, and anti-apoptotic properties [34], NHDC may have therapeutic activity by reducing Cat S expression/activity during skin inflammatory diseases. Conceivably, NHDC could be used as a lead framework for the further development of a more specific and selective Cat S inhibitor to prevent dysregulated ECM and BM proteolysis mediated by overexpressed Cat S during skin diseases, including psoriasis and atopic dermatitis.

## Experimental procedures

### Enzymes, substrates, and inhibitors

All the chemicals were of analytical grade. Human cysteine cathepsins B, L, and S were supplied by Calbiochem (VWR International S.A.S., France) and their active site titration was determined using L-3-carboxy-trans-2, 3-epoxy-propionylleucylamide-(4-guanido)-

skin (RHS) model. RHS were cultivated 14 days in the absence (control, n=3) or with NHDC (100 μM, n=3). Scale bar = 100 μm. B) Following confocal laser microscopy acquisition pictures (four randomly chosen areas from each RHS) were analyzed, and relative expression of Cat S was quantified and standardized to the epidermis surface. Quantification of basement membrane proteins expression was standardized to the dermal–epidermal junction surface. Relative expression of fibronectin, collagen type I, and elastin was quantified and standardized to the dermis surface. C) The cell culture from RHS was analyzed for Cat S, nidogen-1 content (lysates), and cytokines (supernatants) using dedicated ELISA kits. Data represent the mean±S.D. D) Western blot analysis of Cat S, STAT3, and P-STAT3 in lysates of three RHS treated or not with NHDC. β-actin served as a loading control. Data are representative of at least three biological independent repeats. (*$p<0.05$; **$p<0.01$; ****$p<0.0001$). Epidermis (Ep), dermal-epidermal junction (dashed line), and dermis (De).

butane (E-64) (Sigma-Aldrich, Saint-Quentin Fallavier, France). Human cathepsin K was produced as described elsewhere [42]. 7-amino-4-methylcoumarin (AMC) was supplied by Sigma-Aldrich, while peptidyl-AMC substrates: Z-FR-AMC and Z-LR-AMC (benzyloxycarbonyl-Phe/Leu-Arg-7-amino-4-methyl coumarin) came from R&D System (Abingdon, UK). Activity assays were performed in the following buffer: 100 mM acetate sodium buffer, pH 5.5, 2 mM dithiothreitol (DTT), and 0.01% Brij35 or in 100 mM Hepes buffer, pH 7.4, 2 mM DTT, and 0.01% Brij35. Enzymatic assays were carried out at 37°C in the activity buffer, using Z-FR-AMC or Z-LR-AMC ($\lambda_{ex}$=350 nm, $\lambda_{em}$=460 nm). DQ-elastin, DQ-collagen types I and IV were purchased from Molecular Probes (Life Technologies, Saint Aubin, France). Elastinolytic and collagenolytic assays were monitored using a 96-well microplate reader spectrofluorometer (SpectraMax Gemini, Molecular Devices, Saint Gregoire, France) ($\lambda_{ex}$=495 nm, $\lambda_{em}$=515 nm). Recombinant human nidogen-1 was from R&D System. Pepstatin A, ethylene diamine tetraacetic acid (EDTA), AEBSF (Pefabloc), and S-methyl thiomethanesulfonate (MMTS) were from Sigma-Aldrich. Morpholinourea-leucinyl-homophenylalanine-vinyl-sulfone phenyl inhibitor (LHVS) was provided by Dr. J. H. McKerrow (Skaggs School of Pharmacy and Pharmaceutical Sciences, University of California, San Diego, USA).

### Flavonoids

Thirteen flavonoids were provided by Sigma-Aldrich (purity>95%) including chrysin (MW: 254.24 g/mol), apigenin (MW: 270.24 g/mol), naringenin (MW: 272.25 g/mol), hesperetin (MW: 302.28 g/mol), eriodictyol (MW: 288.25 g/mol), neohesperidin (NHP) (MW: 610.56 g/mol), gallocatechin (MW: 306.27 g/mol), epigallocathechin 3-gallate (EGCG) (MW: 458.37 g/mol), myricetin (MW: 318.24 g/mol), quercetin (MW: 302.24 g/mol), kaempferol (MW: 286.24 g/mol), cardamonin (270.28 g/mol), and neohesperidin dihydrochalcone (MW: 612.58 g/mol).

### Enzyme inhibition studies

First, Cat S (0.2 nM) was incubated with each flavonoid (0-100 μM) in the activity buffer (pH 5.5) at 37°C for 10 min to screen their potent inhibitory potency. After addition of Z-FR-AMC (10 μM) the residual enzymatic activity of Cat S was followed by monitoring the fluorescence release of AMC. The experiments were performed in triplicate for each concentration. Then, Cat S (0.5 nM) was incubated with each flavonoid (0-100 μM) in the activity buffer (pH 5.5) at 37°C for 10 min before adding various amount of Z-FR-AMC (1-10 μM) to determine the type of inhibition. All assays were carried out in triplicate for each concentration of flavonoid and averaged before further calculations. Inhibition constant ($K_i$) values were calculated using Lineweaver-Burk plots, plotting 1/v against 1/Z-FR-AMC. The $K_i$ value for NHDC was also determined at pH 7.4 for Cat S and at pH 5.5 for Cat L, Cat B, and Cat K. The data were further analyzed by Dixon plots (1/v=f(flavonoid)) and non-linear regression analyses to ascertain the modality of inhibitor binding (GraphPad Prism, San Diego, CA, USA).

### Correction of fluorescence quenching in Cat S kinetics

Considering the overlay of absorbance wavelength of AMC-derived substrates and some flavonoids (apigenin, eriodictyol, EGCG, myricetin, quercetin, and kaempferol), their effect on fluorescence release was corrected by plotting standard fluorescence curves of free AMC (1-10 μM) in the presence of flavonoid at the concentrations used in our assays. Quenching values were expressed as percent decrease in the AMC fluorescent signal and were calculated using the formula: $(100 - ((F_1/F_0) \times 100))$ (with $F_1$=fluorescence of the AMC group in the presence of the flavonoid and $F_0$=fluorescence of the AMC group in the absence of the flavonoid). The other flavonoids had negligeable effect on the fluorescence of AMC.

### Hydrolysis of ECM and BM-derived components by Cat S in the presence of NHDC

Elastinolytic and collagenolytic activities of Cat S (0.5 nM) were measured with the following fluorogenic substrates DQ-collagen I (10 μg/mL), DQ-collagen IV (10 μg/mL), and DQ-elastin (10 μg/mL) in the absence and presence of NHDC (5-100 μM). Alternatively, nidogen-1 (50 ng protein) was incubated with Cat S (10 nM) in the presence of increasing concentrations of NHDC (1-200 μM) in the activity buffer (pH 5.5) for 30 min at 37°C. Samples were separated by SDS-PAGE (10%) and transferred to nitrocellulose membranes for nidogen-1 immunodetection according to [10].

### Molecular docking

Flavonoids were modelled with the use of Avogadro software [43](Hanwell et al., 2012). Charges and geometry parameters required for molecular dynamics (MD) simulations were calculated with the antechamber module of AMBER16 [45]. Molecular docking of flavonoids was performed to Cat S (PDB: 2C0Y) using Autodock Vina, with default parameters and a grid box covering the entire enzyme [44]. The 10 top docked poses were further analyzed. The standard Gibbs free energy (ΔG) change of binding for flavonoids to Cat S was calculated from the experimental values using the following equation: ΔG=R.T.ln(Ki). Principal Component Analysis (PCA)

for flavonoids was performed with the KNIME software with a linear regression model [46], using the following parameters: mass, accessible surface area, charge, dipole moment, number of aromatic rings, number of hydrogen bonds donors, acceptors, partition coefficient, solubility, number of rotatable bonds, dissociation constant, polar surface area, and normalized number of hydrogen bonds). Twenty nanosecond MD simulations and free energy calculations were performed using the protocols as described [47].

### Ethic statements

Cells were isolated from skin samples collected from patients undergoing surgery and were considered as "waste" and thus were exempt from ethical approval. Helsinki principles were adhered to, and participants gave written, informed consent to provide samples for research.

### Cell culture

Normal human epidermal keratinocytes (NHEK) were isolated from abdominal skin of healthy donor (26 years) undergoing abdominal plastic surgery, as described elsewhere [48]. NHEK were grown to 90% confluence in keratinocyte serum-free medium (KSFM, Invitrogen, Cergy Pontoise, France) supplemented with epidermal growth factor (EGF, 5 ng/mL, Invitrogen), bovine pituitary extract (50 mg/mL, Invitrogen), penicillin (100 U/mL, Invitrogen) and streptomycin (100 U/mL, Invitrogen) at 37°C in a 5% $CO_2$ atmosphere. After determination of non-cytotoxic doses by a viability test (Premix WST-1 Cell Proliferation Assay, Takara Bio Inc, Kusatsu, Japan), keratinocytes were treated or not with NHDC (100, 500 μM) for 24 h. Supernatants and cells were harvested in a preservative buffer (100 mM sodium acetate buffer, pH 5.5, 0.5 mM Pefabloc SC, 0.5 mM EDTA, 1 mM MMTS and 0.04 mM pepstatin A) and stored at -80°C. The protein concentrations in supernatants and cell lysates were determined with the bicinchoninic acid assays kit (BCA protein assay kit, Interchim, Montluçon, France).

### Reconstructed human skin (RHS) model

Normal human fibroblasts, isolated from the foreskin of a one-year-old donor, were seeded onto a dermal substrate made of collagen-matrix (Integra LifeSciences, Princeton, NJ, USA). This dermal equivalent was grown for 20 days at 37°C in a 5% $CO_2$ atmosphere in Dulbecco's modified Eagle's medium (DMEM with Glutamax-1, Life Technologies, Cergy Pontoise, France) supplemented with 10% fetal bovine serum (FBS) (Sigma-Aldrich), 50 μg/mL streptomycin, 50 U/mL penicillin and 1 μg/mL amphotericin B (Life Technologies). The fibroblast media was supplemented with 50 μg/mL L-ascorbic acid (Sigma-Aldrich) and changed every day. On day 20, normal human keratinocytes (from the same donor as for fibroblasts) were seeded on the dermal equivalent and were grown in a proprietary keratinocyte-media as previously reported [30], and changed every day. After three days of submerged culture, RHS were elevated at the air-liquid interface and cultured in defined keratinocyte serum-free medium changed every two days. On day 27, RHS were treated in the absence or presence of NHDC (100 μM) in simplified keratinocyte medium, with a renewal of treatment every 48 h for two weeks. At the end of the experiment, on day 41, supernatants were collected for further cytokines assays and stored at -80°C. One-half of RHS (n=3 per condition) was harvested for immunohistology studies, while the other half was harvested to proceed to protein extraction. Briefly, RHS were homogenized in cold buffer containing 10 mM Hepes/KOH, pH 7.9, 10 mM KCl, 2 mM $MgCl_2$, 0.1 mM DTT, 0.1% (v/v) Nonidet P40, in presence of protease inhibitors cocktail (0.5 mM Pefabloc SC, 0.5 mM EDTA, 1 mM MMTS, 0.04 mM pepstatin A). After centrifugation (12,000 x g) during 2 min, supernatants were collected and stored at -80°C. The protein concentrations in cell-free supernatants of RHS were determined with the bicinchoninic acid assays kit.

### Antibodies

For western-blot studies, anti-Cat S and anti-nidogen-1 antibodies were from R&D Systems (Minneapolis, MN, USA) (dilution 1:1,000). Anti-β-actin (1:1000) was from R&D Systems. Anti-STAT3 (1:1,000) was from BD Biosciences (Le Pont de Claix, France). Anti-phospho-STAT3 (Tyr705, 1:1,000) was from Cell Signaling Technology Europe (Leiden, The Netherlands). For immunofluorescence studies, anti-Cat S and anti-nidogen-1 antibodies were diluted 1:100 and 1:250, respectively. Anti-collagen type I, anti-collagen type IV, and anti-elastin antibodies (1:500) were from Novotec (Reuver, Netherlands). Anti-laminin-1 and anti-fibrillin-1 antibodies (1:200) were from ThermoFisher Scientific (Fremont, CA, USA). Anti-fibronectin (1:500) was from Abcam (Cambridge, UK). The secondary antibodies used for WB (1:5,000) and IF (1:200) were respectively from R&D Systems and Life technologies (ThermoFisher Scientific).

### Multiplex cytokines, Cat S and nidogen-1 quantification in RHS

Levels of IL-6, IL-8, IL-10 and IFN-γ in RHS supernatants were quantified using the MILLIPLEX Multi-Analyte Profiling (MAP) Human Cytokine/Chemokine assay kit (HCYTOMAG-60K, Millipore) and MAGPIX Multiplexing System (Luminex Corporation, Austin,

TX, USA) according to the manufacturer's instructions. Data were analyzed using xPONENT 4.2 software. Cat S and nidogen-1 were quantified using sandwich ELISA DuoSet kits (R&D Systems).

*Immunofluorescence in RHS:* RHS were embedded in tissue freezing medium (Leica, Wetzlar, Germany) and stored at -80°C before being cut with a cryostat in sections of 20 μm thickness, and analyzed as previously reported [25]. Briefly, quantification of Cat S was standardized to the epidermis surface. Quantification of basement membrane proteins (nid-1, laminin-1, and collagen type IV) was standardized to the dermal-epidermal junction surface. Elastin, collagen type I, fibronectin, and fibrillin quantification were standardized to the dermis surface (Leica QWin digital image processing and analysis software).

*Expression and activity of Cat S in NHEK and RHS model:* Total RNAs were extracted from NHEK using RNA purification kit (Macherey-Nagel, Hoerdt, France) according to the manufacturer's instructions. cDNA was synthetized using 0.5 μg of RNA and RevertAid reverse transcriptase (Thermo Fisher Scientific). The relative transcript expression of Cat S was measured with the LightCycler 480 system (Roche Diagnostics GmbH, Mannheim, Germany) using specific primers [25] and the Powerup SYBR green master mix (Thermo Fisher Scientific). For quantification of relative expression levels, the ΔΔCt method was used (normalization gene, human ribosomal protein S16 (RPS16)). The protein concentration of Cat S in NHEK supernatants and lysates, and in RHS lysates were performed using a sandwich ELISA DuoSet kit (R&D Systems). Following running of RHS cell-free supernatants (100 μg of total protein/well; 12% SDS-PAGE under reducing conditions) Cat S was immunodetected by anti-Cat S primary antibody incubated overnight at 4°C. Horseradish peroxidase (HRP)−conjugated anti−IgG antibody was incubated for 1 h at room temperature, and immune−positive bands were visualized using an enhanced chemiluminescence assay kit (ECL Plus Western blotting detection system; Amersham Biosciences, UK). In addition, western-blot detection of STAT-3, phospho-STAT-3, and β-actin were performed in RHS. Following one-hour incubation of NHEK supernatants (30 μg of total protein) and RHS supernatants (100 μg of total protein) in 100 mM Hepes buffer, pH 7.4, 10 mM DTT, and 0.01% Brij35 at 37°C, Cat S activity was monitored using Z-LR-AMC (30 μM). Specific activity of Cat S was checked using the inhibitor LHVS (10 nM) as reported elsewhere [49].

### Statistical analysis

Data were expressed as median ± SD unless indicated and analyzed by non-parametric Mann-Whitney U test. Statistical analysis was performed using GraphPad Prism (GraphPad software, San Diego, CA, USA). Differences at a p-value $< 0.05$ were considered significant.

## Author contributions

FL supervised research; JS, EL, SAS, RK, GL, and FL designed research; JR, JS, EL, RD, KKB, AS, and TC performed research; RK, CN, and FL contributed new reagents; JR, JS, RK, SAS, GL, and FL analyzed data; FL wrote the paper. JS, RK, SAS, and GL revised the paper. All authors approved the final version of the manuscript mmc1.docx

## Declaration of interests

The authors declare that they have no competing interests.

## Acknowledgments

This work was supported by LVMH Recherche (Saint Jean de Braye, France) and by institutional funding from the Institut National de la Santé et de la Recherche Médicale (INSERM) and the University of Tours. TC holded a doctoral fellowship from MESRI (Ministère de l'Enseignement Supérieur, de la Recherche et de l'Innovation, France). KKB holded a BMN (Badania Młodych Naukowców) grant from the Faculty of Chemistry, University of Gdańsk (BMN-538-8370-B249-18) and a grant (UMO-2018/31/N/ ST4/01677) from the National Science Centre of Poland (Narodowe Cenrtum Nauki). SAS received funding (grant UMO-2018/30/E/ST4/00037) from the National Science Centre of Poland (Narodowe Centrum Nauki). We are grateful to Maïlys Gaudet and Titouan Lescop for their technical help with keratinocytes and RHS experiments. Authors acknowledge Dr. Fabrice Gouilleux (Groupe Innovation et Ciblage Cellulaire, University of Tours, France) for providing STAT3 and pSTAT3 antibodies.

## Supplementary materials

Supplementary material associated with this article can be found, in the online version, at doi:10.1016/j.matbio.2022.02.003.

*Received 14 December 2021;*
*Received in revised form 7 February 2022;*
*Accepted 9 February 2022*
Available online 12 February 2022

***Keywords:***
Basement membrane;
Epidermis;
Extracellular-matrix;
Inhibition;
Keratinocyte;
Flavonoid;
Nidogen;
Protease

***Abbreviations:***
AEBSF, 4-(2-aminoethyl) benzenesulfonyl fluoride hydrochloride; BM, basement membrane; CA-074, N-(L-3-trans-propylcarbamoyloxirane-2-carbonyl)-L-isoleucyl-L-proline; Cat, cathepsin; EGCG, epigallocathechin 3-gallate; ECM, extracellular-matrix; LHVS, Morpholinourea-leucinyl-homophenylalanine-vinyl-sulfone; MMP, matrix metalloproteinase; MMTS, S-Methyl thiomethanesulfonate; NHDC, neohesperidin dihydrochalcone; NHP, neohesperidin; NSP, neutrophil serine proteases; NHEK, normal human epidermal keratinocytes; PMSF, phenylmethylsulfonyl fluoride; RHS, reconstructed human skin

*Authors contributed equally to this manuscript.

## References

[1] R.D.A. Wilkinson, R. Williams, C.J. Scott, R.E. Burden, Cathepsin S: therapeutic, diagnostic, and prognostic potential, Biol. Chem. 396 (2015) 867–882, doi: 10.1515/hsz-2015-0114.

[2] H. Kirschke, B. Wiederanders, D. Brömme, A. Rinne, Cathepsin S from bovine spleen. Purification, distribution, intracellular localization and action on proteins, Biochem. J. 264 (1989) 467–473, doi: 10.1042/bj2640467.

[3] G.P. Shi, J.S. Munger, J.P. Meara, D.H. Rich, H.A. Chapman, Molecular cloning and expression of human alveolar macrophage cathepsin S, an elastinolytic cysteine protease, J. Biol. Chem. 267 (1992) 7258–7262.

[4] A. Punturieri, S. Filippov, E. Allen, I. Caras, R. Murray, V. Reddy, S.J. Weiss, Regulation of elastinolytic cysteine proteinase activity in normal and cathepsin K-deficient human macrophages, J. Exp. Med. 192 (2000) 789–799.

[5] V.Y. Reddy, Q.Y. Zhang, S.J. Weiss, Pericellular mobilization of the tissue-destructive cysteine proteinases, cathepsins B, L, and S, by human monocyte-derived macrophages, Proc. Natl. Acad. Sci. U. S. A. 92 (1995) 3849–3853, doi: 10.1073/pnas.92.9.3849.

[6] D.Q. Yang, S. Feng, W. Chen, H. Zhao, C. Paulson, Y.-P. Li, V-ATPase subunit ATP6AP1 (Ac45) regulates osteoclast differentiation, extracellular acidification, lysosomal trafficking, and protease exocytosis in osteoclast-mediated bone resorption, J. Bone Miner. Res. 27 (2012) 1695–1707, doi: 10.1002/jbmr.1623.

[7] M.M. Mohamed, B.F. Sloane, Cysteine cathepsins: multifunctional enzymes in cancer, Nat. Rev. Cancer. 6 (2006) 764–775.

[8] H.A. Chapman, R.J. Riese, G.P. Shi, Emerging roles for cysteine proteases in human biology, Annu. Rev. Physiol. 59 (1997) 63–88, doi: 10.1146/annurev.physiol.59.1.63.

[9] G.P. Shi, J.A. Villadangos, G. Dranoff, C. Small, L. Gu, K.J. Haley, R. Riese, H.L. Ploegh, H.A. Chapman, Cathepsin S required for normal MHC class II peptide loading and germinal center development, Immunity 10 (1999) 197–206, doi: 10.1016/s1074-7613(00)80020-5.

[10] J. Sage, E. Leblanc-Noblesse, C. Nizard, T. Sasaki, S. Schnebert, E. Perrier, R. Kurfurst, D. Brömme, G. Lalmanach, F. Lecaille, Cleavage of nidogen-1 by cathepsin S impairs its binding to basement membrane partners, PLoS One 7 (2012) e43494, doi: 10.1371/journal.pone.0043494.

[11] E. Vidak, U. Javoršek, M. Vizovišek, B. Turk, Cysteine cathepsins and their extracellular roles: shaping the microenvironment, Cells 8 (2019) E264, doi: 10.3390/cells8030264.

[12] M. Vizovišek, E. Vidak, U. Javoršek, G. Mikhaylov, A. Bratovs, B. Turk, Cysteine cathepsins as therapeutic targets in inflammatory diseases, Expert Opin. Ther. Targets 24 (2020) 573–588, doi: 10.1080/14728222.2020.1746765.

[13] G. Schwarz, W.-H. Boehncke, M. Braun, C.J. Schröter, T. Burster, T. Flad, D. Dressel, E. Weber, H. Schmid, H. Kalbacher, Cathepsin S activity is detectable in human keratinocytes and is selectively upregulated upon stimulation with interferon-gamma, J. Invest. Dermatol. 119 (2002) 44–49, doi: 10.1046/j.1523-1747.2002.01800.x.

[14] G.-P. Shi, G.K. Sukhova, M. Kuzuya, Q. Ye, J. Du, Y. Zhang, J.-H. Pan, M.L. Lu, X.W. Cheng, A. Iguchi, S. Perrey, A.M.-E. Lee, H.A. Chapman, P. Libby, Deficiency of the cysteine protease cathepsin S impairs microvessel growth, Circ. Res. 92 (2003) 493–500, doi: 10.1161/01.RES.0000060485.20318.96.

[15] J.A. Joyce, A. Baruch, K. Chehade, N. Meyer-Morse, E. Giraudo, F.-Y. Tsai, D.C. Greenbaum, J.H. Hager, M. Bogyo, D. Hanahan, Cathepsin cysteine proteases are effectors of invasive growth and angiogenesis during multistage tumorigenesis, Cancer Cell 5 (2004) 443–453, doi: 10.1016/s1535-6108(04)00111-4.

[16] A. Schönefuss, W. Wendt, B. Schattling, R. Schulten, K. Hoffmann, M. Stuecker, C. Tigges, H. Lübbert, C. Stichel, Upregulation of cathepsin S in psoriatic keratinocytes, Exp. Dermatol. 19 (2010) e80–e88, doi: 10.1111/j.1600-0625.2009.00990.x.

[17] V.B. Reddy, S.G. Shimada, P. Sikand, R.H. Lamotte, E.A. Lerner, Cathepsin S elicits itch and signals via protease-activated receptors, J. Invest. Dermatol. 130 (2010) 1468–1470, doi: 10.1038/jid.2009.430.

[18] N. Kim, K.B. Bae, M.O. Kim, D.H. Yu, H.J. Kim, H.S. Yuh, Y.R. Ji, S.J. Park, S. Kim, K.-H. Son, S.-J. Park, D. Yoon, D.-S. Lee, S. Lee, H.-S. Lee, T.-Y. Kim, Z.Y. Ryoo, Overexpression of cathepsin S induces chronic atopic dermatitis in mice, J. Invest. Dermatol. 132 (2012) 1169–1176, doi: 10.1038/jid.2011.404.

[19] J.S. Ainscough, T. Macleod, D. McGonagle, R. Brakefield, J.M. Baron, A. Alase, M. Wittmann, M. Stacey, Cathepsin S is the major activator of the psoriasis-associated proinflammatory cytokine IL-36γ, Proc. Natl. Acad. Sci. U. S. A. 114 (2017) E2748–E2757, doi: 10.1073/pnas.1620954114.

[20] K. Chung, T. Pitcher, A.D. Grant, E. Hewitt, E. Lindstrom, M. Malcangio, Cathepsin S acts via protease-activated receptor 2 to activate sensory neurons and induce itch-like behaviour, Neurobiol. Pain 6 (2019) 100032, doi: 10.1016/j.ynpai.2019.100032.

[21] P. Panwar, T. Hedtke, A. Heinz, P.-M. Andrault, W. Hoehenwarter, D.J. Granville, C.E.H. Schmelzer, D. Brömme, Expression of elastolytic cathepsins in human skin and their involvement in age-dependent elastin degradation, Biochim. Biophys. Acta Gen. Subj. 1864 (2020) 129544, doi: 10.1016/j.bbagen.2020.129544.

[22] A.N. Panche, A.D. Diwan, S.R. Chandra, Flavonoids: an overview, J. Nutr. Sci. 5 (2016) e47, doi: 10.1017/jns.2016.41.

[23] A. Vidal-Albalat, F.V. González, Atta-ur Rahman, Chapter 6 - Natural Products as Cathepsin Inhibitors, Studies in Natural Products Chemistry, Elsevier, 2016, pp. 179–213, doi: 10.1016/B978-0-444-63749-9.00006-2.

[24] W.-H. Boehncke, F. Ochsendorf, I. Paeslack, R. Kaufmann, T.M. Zollner, Decorative cosmetics improve the quality of life in patients with disfiguring skin diseases, Eur. J. Dermatol. 12 (2002) 577–580.

[25] J. Sage, D. De Quéral, E. Leblanc-Noblesse, R. Kurfurst, S. Schnebert, E. Perrier, C. Nizard, G. Lalmanach, F. Lecaille, Differential expression of cathepsins K, S and V between young and aged Caucasian women skin epidermis, Matrix Biol. 33 (2014) 41–46, doi: 10.1016/j.matbio.2013.07.002.

[26] K. Schueller, J. Hans, S. Pfeiffer, J. Walker, J.P. Ley, V. Somoza, Identification of Interleukin-8-Reducing Lead Compounds Based on SAR Studies on Dihydrochalcone-Related Compounds in Human Gingival Fibroblasts (HGF-1 cells) In Vitro, Molecules 25 (2020) E1382, doi: 10.3390/molecules25061382.

[27] G.E. Han, H.-T. Kang, S. Chung, C. Lim, J.A. Linton, J.-H. Lee, W. Kim, S.-H. Kim, J.H. Lee, Novel Neohesperidin Dihydrochalcone Analogue Inhibits Adipogenic Differentiation of Human Adipose-Derived Stem Cells through the Nrf2 Pathway, Int. J. Mol. Sci. 19 (2018) E2215, doi: 10.3390/ijms19082215.

[28] E.-R. Lee, Y.-J. Kang, J.-H. Kim, H.T. Lee, S.-G. Cho, Modulation of apoptosis in HaCaT keratinocytes via differential regulation of ERK signaling pathway by flavonoids, J. Biol. Chem. 280 (2005) 31498–31507, doi: 10.1074/jbc.M505537200.

[29] M. Matsuo, N. Sasaki, K. Saga, T. Kaneko, Cytotoxicity of flavonoids toward cultured normal human cells, Biol. Pharm. Bull. 28 (2005) 253–259, doi: 10.1248/bpb.28.253.

[30] E. Noblesse, V. Cenizo, C. Bouez, A. Borel, C. Gleyzal, S. Peyrol, M.-P. Jacob, P. Sommer, O. Damour, Lysyl oxidase-like and lysyl oxidase are present in the dermis and epidermis of a skin equivalent and in human skin and are associated to elastic fibers, J. Invest. Dermatol. 122 (2004) 621–630, doi: 10.1111/j.0022-202X.2004.22330.x.

[31] S. Choi, S. Yu, J. Lee, W. Kim, Effects of Neohesperidin Dihydrochalcone (NHDC) on Oxidative Phosphorylation, Cytokine Production, and Lipid Deposition, Foods 10 (2021) 1408, doi: 10.3390/foods10061408.

[32] M. Comalada, I. Ballester, E. Bailón, S. Sierra, J. Xaus, J. Gálvez, F.S. de Medina, A. Zarzuelo, Inhibition of pro-inflammatory markers in primary bone marrow-derived mouse macrophages by naturally occurring flavonoids: analysis of the structure-activity relationship, Biochem. Pharmacol. 72 (2006) 1010–1021, doi: 10.1016/j.bcp.2006.07.016.

[33] S. Crouvezier, B. Powell, D. Keir, P. Yaqoob, The effects of phenolic components of tea on the production of pro- and anti-inflammatory cytokines by human leukocytes in vitro, Cytokine 13 (2001) 280–286, doi: 10.1006/cyto.2000.0837.

[34] Q. Shi, X. Song, J. Fu, C. Su, X. Xia, E. Song, Y. Song, Artificial sweetener neohesperidin dihydrochalcone showed antioxidative, anti-inflammatory and anti-apoptosis effects against paraquat-induced liver injury in mice, Int. Immunopharmacol. 29 (2015) 722–729, doi: 10.1016/j.intimp.2015.09.003.

[35] P. Geraghty, C.M. Greene, M. O'Mahony, S.J. O'Neill, C.C. Taggart, N.G. McElvaney, Secretory leucocyte protease inhibitor inhibits interferon-gamma-induced cathepsin S expression, J. Biol. Chem. 282 (2007) 33389–33395, doi: 10.1074/jbc.M706884200.

[36] L.L.Y. Chan, B.K.W. Cheung, J.C.B. Li, A.S.Y. Lau, A role for STAT3 and cathepsin S in IL-10 down-regulation of IFN-gamma-induced MHC class II molecule on primary human blood macrophages, J. Leukoc. Biol. 88 (2010) 303–311, doi: 10.1189/jlb.1009659.

[37] N. Fuchs, M. Meta, D. Schuppan, L. Nuhn, T. Schirmeister, Novel Opportunities for Cathepsin S Inhibitors in Cancer Immunotherapy by Nanocarrier-Mediated Delivery, Cells 9 (2020) E2021, doi: 10.3390/cells9092021.

[38] D.H. Waalkens-Berendsen, M.E.M. Kuilman-Wahls, A. Bär, Embryotoxicity and teratogenicity study with neohesperidin dihydrochalcone in rats, Regul. Toxicol. Pharmacol. 40 (2004) 74–79, doi: 10.1016/j.yrtph.2004.05.007.

[39] B.A. Lina, H.C. Dreef-van der Meulen, D.C. Leegwater, Subchronic (13-week) oral toxicity of neohesperidin dihydrochalcone in rats, Food Chem. Toxicol. 28 (1990) 507–513, doi: 10.1016/0278-6915(90)90121-3.

[40] A. Rodríguez, P. Webster, J. Ortego, N.W. Andrews, Lysosomes behave as Ca2+-regulated exocytic vesicles in fibroblasts and epithelial cells, J. Cell Biol. 137 (1997) 93–104, doi: 10.1083/jcb.137.1.93.

[41] M. Ontiveros, D. Rinaldi, M. Marder, M.V. Espelt, I. Mangialavori, M. Vigil, J.P. Rossi, M. Ferreira-Gomes, Natural flavonoids inhibit the plasma membrane Ca2+-ATPase, Biochem. Pharmacol. 166 (2019) 1–11, doi: 10.1016/j.bcp.2019.05.004.

[42] C.J. Linnevers, M.E. McGrath, R. Armstrong, F.R. Mistry, M.G. Barnes, J.L. Klaus, J.T. Palmer, B.A. Katz, D. Brömme, Expression of human cathepsin K in Pichia pastoris and preliminary crystallographic studies of an inhibitor complex, Protein Sci. 6 (1997) 919–921, doi: 10.1002/pro.5560060421.

[43] M.D. Hanwell, D.E. Curtis, D.C. Lonie, T. Vandermeersch, E. Zurek, G.R. Hutchison, Avogadro: an advanced semantic chemical editor, visualization, and analysis platform, J. Cheminform. 4 (2012) 17, doi: 10.1186/1758-2946-4-17.

[44] O. Trott, A.J. Olson, AutoDock Vina: improving the speed and accuracy of docking with a new scoring function, efficient optimization and multithreading, J. Comput. Chem. 31 (2010) 455–461, doi: 10.1002/jcc.21334.

[45] D.A. Case, R.M. Betz, D.S. Cerutti, T.E. Cheatham, T.A. Darden, R.E. Duke, T.J. Giese, H. Gohlke, A.W. Goetz, N. Homeyer, S. Izadi, P. Janowski, J. Kaus, A. Kovalenko, T.S. Lee, S. LeGrand, P. Li, C. Lin, T. Luchko, R. Luo, B. Madej, D. Mermelstein, K.M. Merz, G. Monard, H. Nguyen, H.T. Nguyen, Y. Omelyan, A. Onufriev, D.R. Roe, A. Roitberg, C. Sagui, C.L. Simmerling, W.M. Botello-Smith, J. Swails, R.C. Walker, J. Wang, R.M. Wolf, X. Wu, L. Xiao, P.A. Kollman, 2016. doi:https://doi.org/10.13140/RG.2.2.27958.70729.

[46] C. Dietz, M.R. Berthold, KNIME for Open-Source Bioimage Analysis: A Tutorial, Adv. Anat. Embryol. Cell Biol. 219 (2016) 179–197, doi: 10.1007/978-3-319-28549-8_7.

[47] F. Lecaille, T. Chazeirat, K.K. Bojarski, J. Renault, A. Saidi, V.G.N.V. Prasad, S. Samsonov, G. Lalmanach, Rat cathepsin K: Enzymatic specificity and regulation of its collagenolytic activity, Biochim. Biophys. Acta Proteins Proteom. 1868 (2020) 140318, doi: 10.1016/j.bbapap.2019.140318.

[48] T. Zuliani, V. Denis, E. Noblesse, S. Schnebert, P. Andre, M. Dumas, M.-H. Ratinaud, Hydrogen peroxide-induced cell death in normal human keratinocytes is differentiation dependent, Free Radic. Biol. Med. 38 (2005) 307–316, doi: 10.1016/j.freeradbiomed.2004.09.021.

[49] P.-M. Andrault, A.C. Schamberger, T. Chazeirat, D. Sizaret, J. Renault, C.A. Staab-Weijnitz, E. Hennen, A. Petit-Courty, M. Wartenberg, A. Saidi, T. Baranek, S. Guyetant, Y. Courty, O. Eickelberg, G. Lalmanach, F. Lecaille, Cigarette smoke induces overexpression of active human cathepsin S in lungs from current smokers with or without COPD, Am. J. Physiol. Lung Cell. Mol. Physiol. 317 (2019) L625–L638, doi: 10.1152/ajplung.00061.2019.

# Annexe 3

Cellular and Molecular Life Sciences (2022) 79:616
https://doi.org/10.1007/s00018-022-04643-1



ORIGINAL ARTICLE

# Neutrophils play a major role in the destruction of the olfactory epithelium during SARS-CoV-2 infection in hamsters

Clara Bourgon[1] · Audrey St Albin[1] · Ophélie Ando-Grard[1] · Bruno Da Costa[1] · Roxane Domain[2] · Brice Korkmaz[2] · Bernard Klonjkowski[3] · Sophie Le Poder[3] · Nicolas Meunier[1]

Received: 8 June 2022 / Revised: 2 November 2022 / Accepted: 22 November 2022
© The Author(s), under exclusive licence to Springer Nature Switzerland AG 2022

## Abstract

The loss of smell (anosmia) related to SARS-CoV-2 infection is one of the most common symptoms of COVID-19. Olfaction starts in the olfactory epithelium mainly composed of olfactory sensory neurons surrounded by supporting cells called sustentacular cells. It is now clear that the loss of smell is related to the massive infection by SARS-CoV-2 of the sustentacular cells in the olfactory epithelium leading to its desquamation. However, the molecular mechanism behind the destabilization of the olfactory epithelium is less clear. Using golden Syrian hamsters infected with an early circulating SARS-CoV-2 strain harboring the D614G mutation in the spike protein; we show here that rather than being related to a first wave of apoptosis as proposed in previous studies, the innate immune cells play a major role in the destruction of the olfactory epithelium. We observed that while apoptosis remains at a low level in the damaged area of the infected epithelium, the latter is invaded by Iba1$^+$ cells, neutrophils and macrophages. By depleting the neutrophil population or blocking the activity of neutrophil elastase-like proteinases, we could reduce the damage induced by the SARS-CoV-2 infection. Surprisingly, the impairment of neutrophil activity led to a decrease in SARS-CoV-2 infection levels in the olfactory epithelium. Our results indicate a counterproductive role of neutrophils leading to the release of infected cells in the lumen of the nasal cavity and thereby enhanced spreading of the virus in the early phase of the SARS-CoV-2 infection.

**Keywords** Post-viral olfactory disorder (PVOD) · Pathophysiology · Innate immunity

**Abbreviations**

| | |
|---|---|
| OE | Olfactory epithelium |
| OSN | Olfactory sensory neuron |
| MPO | Myeloperoxidase |

## Introduction

Loss of smell (anosmia) is a major symptom of COVID-19 pandemic. With omicron's increased transmission, hundreds of thousands of people per day still get infected worldwide. Despite omicron's reduced anosmia prevalence [1], loss of smell will likely affect millions more [2, 3] and 10% of anosmic patients might not recover their sense of smell 6 months after the disease onset [4, 5]. The full olfactory recovery could even take up to 1 year and some patients may never recover their sense of smell [6]. A recent study estimates that in the USA about 720,000 people actually suffer from chronic olfactory disorder related to COVID-19 [7]. The loss of smell negatively impacts life quality by disrupting feeding behavior potentially leading to malnutrition; and by exposing to food poisoning and to inhalation of dangerous chemicals [8]. In severe and persistent cases, anosmic patients could possibly suffer from chronic depression [9]. It is thus crucial to understand the cellular basis of anosmia.

Olfaction starts in the olfactory epithelium (OE) which contains olfactory sensory neurons (OSNs) surrounded by supporting cells called sustentacular cells. Both cell types are regenerated regularly due to multipotent basal cells [10]. Among these cells, only sustentacular cells express significantly angiotensin-converting enzyme 2 (ACE2) and transmembrane serine protease 2 (TMPRSS2) required for

✉ Nicolas Meunier
nicolas.meunier@inrae.fr

1 Unité de Virologie et Immunologie Moléculaires (UR892), INRAE, Université Paris-Saclay, Jouy-en-Josas, France

2 INSERM UMR-1100, "Research Center for Respiratory Diseases" and University of Tours, 37032 Tours, France

3 UMR 1161 Virologie, INRAE-ENVA-ANSES, École Nationale Vétérinaire d'Alfort, Maisons-Alfort, 94704 Paris, France

Published online: 03 December 2022

SARS-CoV-2 cellular entrance [11–13]. We and others observed in the golden Syrian hamster model that SARS-CoV-2 infects massively the sustentacular cells in the OE leading to its desquamation as well as olfactory neurons deciliation and death [14–16]. Although very rarely OSNs may be infected by SARS-CoV-2 [17], a recent study in humans confirms that anosmia arises primarily from infection of sustentacular cells of the OE followed by the disruption of OE integrity without OSN infection [18].

In this study, we focused on the early events following SARS-CoV-2 infection of the nasal cavity to explore the mechanism of the unusually extensive OE damage following SARS-CoV-2 infection. Several studies reported that most cells of the infected OE including OSNs undergo apoptosis [19–22]. A similar phenomenon has been reported during influenza infection [23] and has been considered for SARS-CoV-2 as a defense mechanism to limit a potential invasion of the central nervous system by pathogens using the olfactory route [24]. Alternatively, innate immune cells could trigger directly the desquamation of the OE through inflammation as observed in the lung [25]. Indeed, innate immune cells invade massively the SARS-CoV-2-infected OE [14]. Iba1 (ionized calcium-binding adapter molecule 1) is a marker of microglia/macrophages [26] which are the most studied innate immune cells in the nasal cavity [23]. In the central nervous system, $Iba1^+$ microglial cells ensure viral clearance by phagocytizing viral particles and infected cells [27, 28] and can induce cell death as observed in the hippocampus using the Theiler's virus model of encephalitis [29]. As the OE is not protected by the blood–brain barrier, neutrophils and monocytes/macrophages classically recruited during the early event of inflammation could also be involved in the OE damage following SARS-CoV-2 infection [30, 31]. Neutrophils are well known for their ability to induce tissue damage, notably through the release of elastase-like proteinases [32, 33] as well as the production of reactive oxygen species (ROS) by the myeloperoxidase (MPO) and formation of toxic neutrophil extracellular traps [34, 35]. Macrophages are known for their ability to phagocyte pathogens, produce cytokines and activate other immune cells [36]. Although they are involved in the regeneration of the OE [37, 38], they can also lead to tissue damage during viral infections notably through NLRP3 (NOD-, LRR- and pyrin domain-containing protein 3) inflammasome activation and metalloproteinases activity [31].

In the current work, we observed that apoptosis remains at a low level in the infected areas of the OE while innate immune cells were systematically present in the damaged area of the OE. By manipulating neutrophil activity by two different complementary approaches, we show that they play a major role in the early events of OE destabilization following SARS-CoV-2 infection.

## Material and methods

### Study design

The study was performed to understand the cellular mechanisms leading to the SARS-CoV-2-induced damage in the OE using hamsters as an animal model. Hamsters experiments were planned in accordance with the principles of the 3Rs (replacement, reduction and refinement). Body weight and animal behavior were monitored before and during the experiments. Different parameters in the nasal cavity were measured by quantitative polymerase chain reaction (qPCR) and by immunohistochemistry. SARS-CoV-2 replication was measured in vitro to evaluate a potential inhibition by the drugs used to modulate neutrophils activity. Sample size for each experiment is indicated in figure legends. During analysis, all data points were included except because of technical failure to process the sample. Animals were randomized to the experimental groups. All analyses were performed blindly of the treatment.

### SARS-CoV-2 Isolates

In vivo experiments were carried out with SARS-CoV-2 strain BetaCoV/France/IDF/200107/2020, which was isolated by Dr. Paccoud from the La Pitié-Salpétrière Hospital in France. This strain was kindly provided by the Urgent Response to Biological Threats (CIBU) hosted by Institut Pasteur (Paris, France), headed by Dr. Jean-Claude Manuguerra. Cell culture experiments were performed with the SARS-CoV-2 strain France/IDF0372/2020 kindly provided by Sylvie van der Werf. Both strains have been isolated in the beginning of the pandemic in Europe in March 2020.

### Animals

Fifty-six 8-week-old male hamsters were purchased from Janvier's breeding Center (Le Genest, St Isle, France). Animal experiments were carried out in the animal biosafety level 3 facility of the UMR Virologie (ENVA, Maisons-Alfort); approved by the ANSES/EnvA/UPEC Ethics Committee (CE2A16) and authorized by the French ministry of Research under the number APAFIS#25384-2020041515287655.

Infection was achieved by nasal instillation (40 µL in each nostril with $5.10^3$ $TCID_{50}$ of SARS-CoV2 strain BetaCoV/France/IDF/200107/2020) on anesthetized animals under isoflurane. Such viral infection dose gives robust infection level in the nasal cavity [14, 39]. Seven mock-infected animals received only Dulbecco's minimal essential medium.

For neutrophil depletion experiments, hamsters were injected intraperitoneally with either PBS or 150 mg/kg

and 100 mg/kg of cyclophosphamide (CAS: 6055-19-2; PHR1404; Sigma-Aldrich), respectively, at 3 and 1 days before SARS-CoV-2 infection. Animals were sacrificed at 1 dpi (days post-infection) and at 2 dpi ($n=4$ in each group).

To inhibit neutrophil elastase-like proteases, we used a specific synthetic cathepsin C inhibitor ($IcatC_{XPZ-01}$; [40]) diluted in 10% (2-Hydroxypropyl)-β-cyclodextrin (CAS: 128446-35-5; C0926; Sigma-Aldrich) suspended in citrate buffer 50 mM at pH 5 (vehicle) as described previously [41]. Hamsters were injected intraperitoneally twice a day with either vehicle ($n=4$) or $IcatC_{XPZ-01}$ at 4.5 mg/kg for 10 days before infection by SARS-CoV-2 ($n=4$). Animals were sacrificed at 1 dpi.

For all experiments except $IcatC_{XPZ-01}$ treatment, the head was divided sagittally into two halves, of which one was used for immunohistochemistry experiments. Nasal turbinates were extracted from the other half for qPCR analysis. Only histological analysis was performed on tissues from $IcatC_{XPZ-01}$ treatment experiments.

## Histology, immunohistochemistry and quantifications

The immunohistochemistry analysis of the olfactory mucosa tissue sections was performed as described previously in mice [43]. Briefly, the animal hemi-heads were fixed for 3 days at room temperature in 4% paraformaldehyde (PFA) and decalcified in Osteosoft (101728; Merck Millipore; Saint-Quentin Fallavier; France) for 3 weeks. Blocks were cryo-protected in 30% sucrose. Cryo-sectioning (12 µm) was performed in coronal sections of the nasal cavity, perpendicular to the hard palate in order to examine the vomeronasal organ (VNO), olfactory epithelium (OE), Steno's gland and olfactory bulb. Sections were stored at − 80 °C until use.

Non-specific staining was blocked by incubation with 2% bovine serum albumin (BSA) and 0.05% Tween. The sections were then incubated overnight with primary antibodies directed against SARS nucleocapsid protein (1/500; mouse monoclonal; clone 1C7C7; Sigma-Aldrich), ionized calcium-binding adapter molecule 1 (Iba1) (1/500; rabbit monoclonal; clone EPR16588; Abcam), myeloperoxidase protein (MPO) (1/500; rabbit monoclonal; clone EPR20257; Abcam), CD68 (1/200; rabbit polyclonal; PA1518; Boster), cleaved caspase 3 (C3C) (1/200; rabbit polyclonal; #9661; Cell signaling), $G_{olf}$ (1/300; rabbit polyclonal; C-18; Santa Cruz), Olfactory Marker Protein (OMP) (1/500; goat polyclonal; 544-10001; Wako) and CK18 (1:50; mouse polyclonal; MAB3234—RGE53, Sigma-Aldrich). Fluorescence staining was performed using goat anti-mouse-A555; goat anti-rabbit-A488 and donkey anti-goat-A546 (1/800; Molecular Probes A21422; A11056; A11008, respectively; Invitrogen).

Images were taken using a 1X71 Olympus microscope equipped with an Orca ER Hamamatsu cooled CCD camera (Hamamatsu Photonics France; Massy; France) or with a Zeiss LSM 700 confocal 187 microscope for cleaved caspase 3 co-staining with either OMP or CK18 experiment and MPO co-staining with Hoechst stained multi-lobal nuclei (MIMA2 Platform, INRAe). Whole section images were reconstructed from 3 images taken at × 50 magnification using a Leica MZ10F Fluorescent binocular microscope. We used these images to display the level of infection revealed by TRITC fluorescence. As this binocular did not possess any UV filter to display Hoechst fluorescence, we used the FITC channel green autofluorescence to display the turbinates structures.

To assess olfactory epithelium damage, we scored the integrity of the OE from 1 to 9 based on Hoechst staining according to missing nuclei area, irregularity of the OE structure and increased distance between nuclei indicating loosening of the epithelium leading to desquamation (Supp. Fig. 1). To evaluate the correlation of apoptosis and innate immune cell presence with damage, OE areas were divided in two groups: undamaged areas (damage score equal to 1 or 2) and damaged areas (damage score between 5 and 9). Apoptosis level, infiltration of immune cells in the OE and its underlying lamina propria were quantified as the percentage of the area positive for C3C (cleaved caspase 3); Iba1 (macrophages/microglia), CD68 (activated bone-marrow-derived macrophages) and MPO (neutrophils). For each animal, the percentage of stained OE was averaged over 4 distinct areas in the beginning of olfactory turbinates at 1 dpi and in the medial part of the nasal cavity containing Steno's gland and NALT at 2 dpi.

In cyclophosphamide and in $IcatC_{XPZ-01}$ experiments, we performed both IHC and classical hematoxylin and eosin (HE) staining as described previously [42]. We examined two independent sections of nasal turbinates (separated by 500 µm) in the middle of the nasal cavity containing NALT and Steno's gland. For each section, we measured the total infected area of the OE, the area of desquamated cells in the lumen (based on Hoechst nuclear staining) and the percentage of infected desquamated cells in the lumen (based on N protein immunostaining). These experiments were designed to measure the global damage of the OE following SARS-CoV-2 infection when neutrophil action was impaired. At 2 dpi, the level of neutrophil infiltration was so high that complete quantification could not be achieved. Instead, we set a global score from 1 to 9 of $^{1/}$OE damage based on the integrity of the OE and $^{2/}$neutrophil infiltration based on the overall presence of MPO signal in nasal mucosa and in nasal cavity lumen. We verified that our scoring system and total quantification gave similar results for $MPO^+$ cells presence at 1 dpi where infection is restricted to the most ventro rostral part of the nasal turbinates.

All quantifications were made with ImageJ (Rasband, W.S., ImageJ, US National Institutes of Health, Bethesda, Maryland, USA, http://imagej.nih.gov/ij/, 1997–2012) to threshold specific staining and performed blindly of the treatment.

### RNA extraction and RT-qPCR analysis

Total RNA was extracted from frozen nasal turbinates using the Trizol-chloroforme method as described previously [43]. Oligo-dT first strand cDNA synthesis was performed from 5 µg total RNA with iScript Advance cDNA Synthesis Kit for RT-qPCR (BioRad; #1725038) following manufacturer's recommendations. qPCR was carried out using 125 ng of cDNA added to a 15 µL reaction mix. This reaction mix contained 10 µL iTaq Universal Sybr Green SuperMix (Bio-Rad; #1725124), and primers at 500 nM (sequences in Supp Table 1). The reaction was performed with a thermocycler (Mastercycler ep Realplex, Eppendorf). Fluorescence during qPCR reaction was monitored and measured by Realplex Eppendorf software. A dissociation curve was plotted at the end of the forty amplification cycles of the qPCR to check the ability of theses primers to amplify a single and specific PCR product.

Quantification of initial specific RNA concentration was done using the ΔΔCt method. Standard controls of specificity and efficiency of the qPCR were performed. The mRNA expression of each gene was normalized with the expression level of G3PDH. A correction factor was applied to each primer pair according to their efficiency [44].

### Measure of antiviral activity of cyclophosphamide and cathepsin C inhibitor against SARS-CoV-2 in cell culture

Vero E6 cells (CRL-1586, ATCC maintained at 37 °C; 5% $CO_2$) were seeded at $2.10^4$ cells per well in a 96-well plate in Dulbecco's Modified Eagle's Medium, 5% fetal bovine serum (FBS-12A, Capricorn Scientific, Clinisciences). For cyclophosphamide antiviral activity evaluation, cells were treated with 0.15 mg/mL (corresponding to the maximum dose potentially present in hamsters) or 0.45 mg/mL cyclophosphamide diluted in sterile PBS. For $IcatC_{XPZ-01}$ antiviral activity evaluation, cells were treated with 4.5 µg/mL (corresponding to the maximum dose potentially present in hamsters) or 13.5 µg/mL $IcatC_{XPZ-01}$ diluted in 10% dextrin, citrate buffer 50 mM, pH = 5. Cells were treated with PBS as control ($n = 6$ for each condition) and molecule cytotoxicity was tested as well without infection at the highest used concentration. All treatments were started one hour prior to infection with SARS-CoV-2 strain France/IDF0372/2020 at $5\times 10^3$ pfu per well diluted in DMEM, 10% fetal bovine serum. Loss of cell viability reflecting the efficiency of viral infection was measured 3 days after infection by adding 100 µL Cell Titer-Glo reagent to each well (CellTiterGlo Luminescent Cell Viability Assay, Promega #G7571), according to the manufacturer's protocol. Cell luminescence of each well was then quantified using an Infinite M200Pro TECAN and normalized to the control condition.

### Statistical analysis

All comparisons were made using Prism 5.0 (GraphPad). Statistical significance between groups was assessed using nonparametric Mann–Whitney tests. For correlation analyses, we used Spearman nonparametric test. Error bars indicate the SEM. Detailed information on statistical test used, sample size and P value are provided in the figure legends.

## Results

### Apoptosis occurs after cell desquamation following SARS-CoV-2 infection of the olfactory epithelium

We previously observed that as soon as two days following nasal instillation of SARS-CoV-2 in Syrian gold hamsters, the sustentacular cells of the OE were massively infected along with strong cellular loss and cellular debris filling the lumen of the nasal cavity [14]. In order to understand the events leading to this desquamation, we chose to focus on the early stages of infection at 1 and 2 dpi. To evaluate the importance of apoptosis in the damage of the OE following SARS-CoV-2 infection, we measured the level of cleaved caspase 3 signal in uninfected animals, and in infected zones of the OE that were either intact or damaged (Fig. 1). Basal level of apoptosis occurring in the OE was not increased in either zone at 1 or 2 dpi (Fig. 1D). However, we observed a strong cleaved caspase 3 signal co-localizing partly with desquamated cell in the lumen of the nasal cavity. The cleaved caspase 3 signal in the lumen of the nasal cavity was increased 5- and 14-fold compared to the OE at 1 and 2 dpi, respectively, which was statistically significant at 2 dpi (Mann–Whitney, $p = 0.0286$) and nearly significant at 1 dpi ($p = 0.0525$). In order to examine the potential OE origin of the C3C positive cells, we performed double staining with cleaved caspase 3 and CK18 or OMP (specific markers of sustentacular cells and OSN, respectively). We observed that most apoptotic cells co-stained with OMP but not with CK18, indicating that OSN but not sustentacular cells undergo Caspase 3 apoptosis once released in the lumen of the nasal cavity (Supp. Fig. 2).

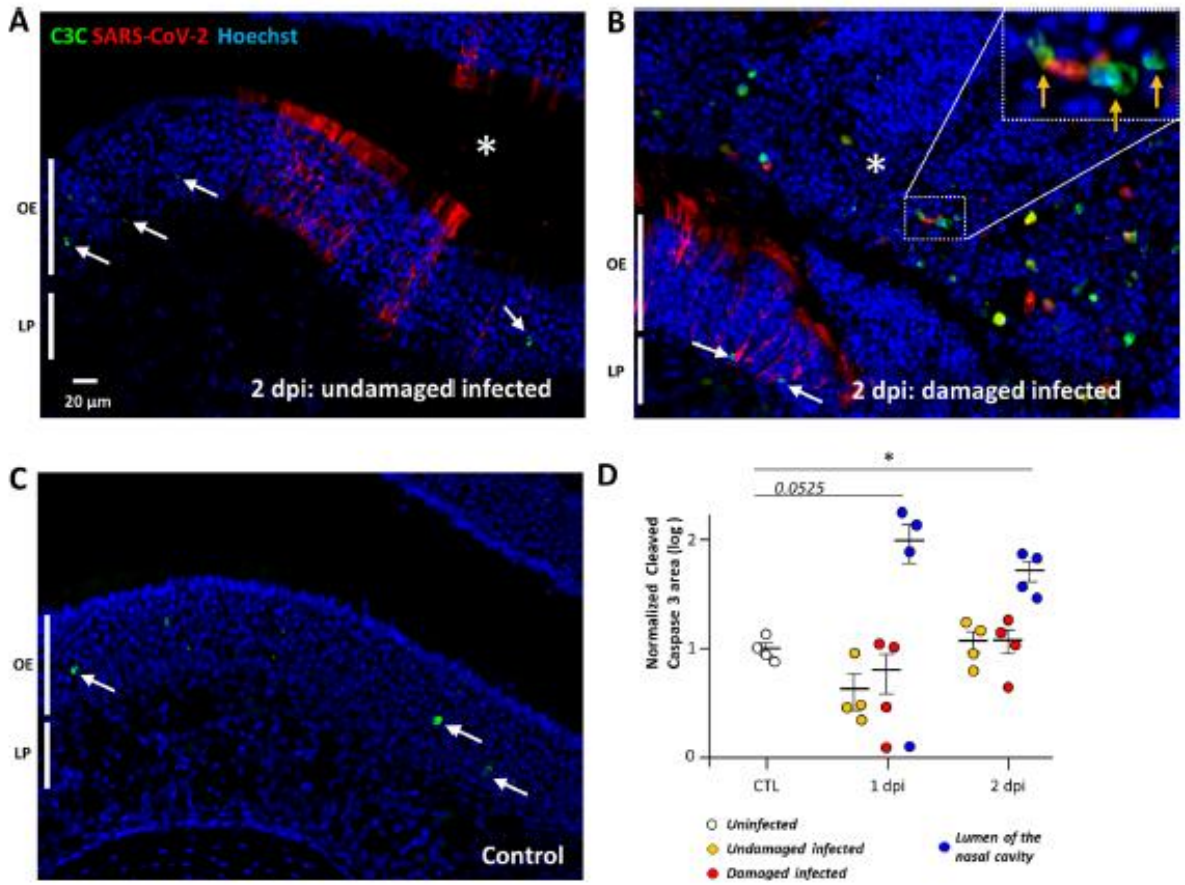


**Fig. 1** Apoptosis occurs in desquamated cells in the lumen of the nasal cavity following SARS-CoV-2 infection but not in the olfactory epithelium. Representative images of an infected intact (**A**), infected damaged (**B**) area of the olfactory epithelium at 2 days post-infection (dpi) and in a control animal (**C**). Apoptotic cells in the olfactory epithelium are indicated by a white arrow (OE: olfactory epithelium/LP lamina propria). The lumen of the nasal cavity is indicated by a white asterisk and is filled with cells, some of which colocalize in their nucleus cleaved caspase 3 signal (orange arrow). (**D**) Cleaved caspase 3 signal in the olfactory epithelium normalized to control (log 10, Mean ± SEM, $n = 4$, $^*p < 0.01$ (Mann–Whitney test))

## Damage of the infected olfactory epithelium is correlated with infiltration of innate immune cells

Since apoptosis does not significantly occur in the OE during the initial phase of infection, the desquamation of the infected OE may be related to immune cell infiltration [14, 15]. So far, the immune cells in the nasal cavity have been poorly characterized. Neutrophils and macrophages are known for their importance in clearing infected tissue [45], but only $Iba1^+$ cells presence is well characterized in the OE [23]. $Iba1^+$ cells are described as microglia/macrophages, but CD68 is more classically used as a marker of monocytes and macrophages [46]. Concerning neutrophils, the presence of neutrophil cytosol factor 2 (Ncf2; [47]) and myeloperoxidase (MPO) have been used successfully to characterize these cells in hamsters [48]. As MPO is only expressed during neutrophil maturation in the bone marrow [49], we used Ncf2 as a marker of neutrophil presence by qPCR and MPO by immunohistochemistry.

We first evaluated at 1 dpi and 2 dpi by qPCR the expression of Iba1, CD68 and Ncf2 along with classical inflammatory markers (TNFα and IL6) and the presence of the virus (Supp. Fig. 3). At 1 dpi, SARS Nucleocapsid protein (SARS N) was already abundantly expressed in the OE at a similar level as at 2 dpi, and TNFα and IL6 transcripts increased gradually (Mann–Whitney, $p < 0.05$). Iba1 and CD68 expression related to macrophage presence in the OE did not rise significantly at 1 dpi compared to control (Mann–Whitney, $p = 0.164$ and 0.128, respectively) but did at 2 dpi (Mann–Whitney, $p < 0.05$). Concerning neutrophils, Ncf2 expression was strongly enhanced at 1 dpi and was still increasing at 2 dpi (Mann–Whitney, $p < 0.05$). These

results suggest that neutrophils are already recruited at 1 dpi and that their recruitment continues at 2 dpi along with the arrival of Iba1$^+$ and CD68$^+$ cells.

We next focused on immunostaining to characterize the presence of Iba1$^+$, CD68$^+$ and MPO$^+$ cells. In the OE of an uninfected hamster, Iba1$^+$ cells were already present and mainly localized in the lamina propria while CD68 signal was absent (Fig. 2A), indicating that Iba1$^+$ cells do not express the classical CD68 marker of macrophages. This was confirmed in the infected areas of the OE where we observed a very different presence of Iba1$^+$ and CD68$^+$ cells. Iba1$^+$ cells were massively present as soon as 1 dpi in the damaged parts of the infected OE as well as in the desquamated cells in the lumen of the nasal cavity. CD68$^+$ cells were less abundant in the damaged part of the OE and mainly present in the desquamated cells filling the lumen of

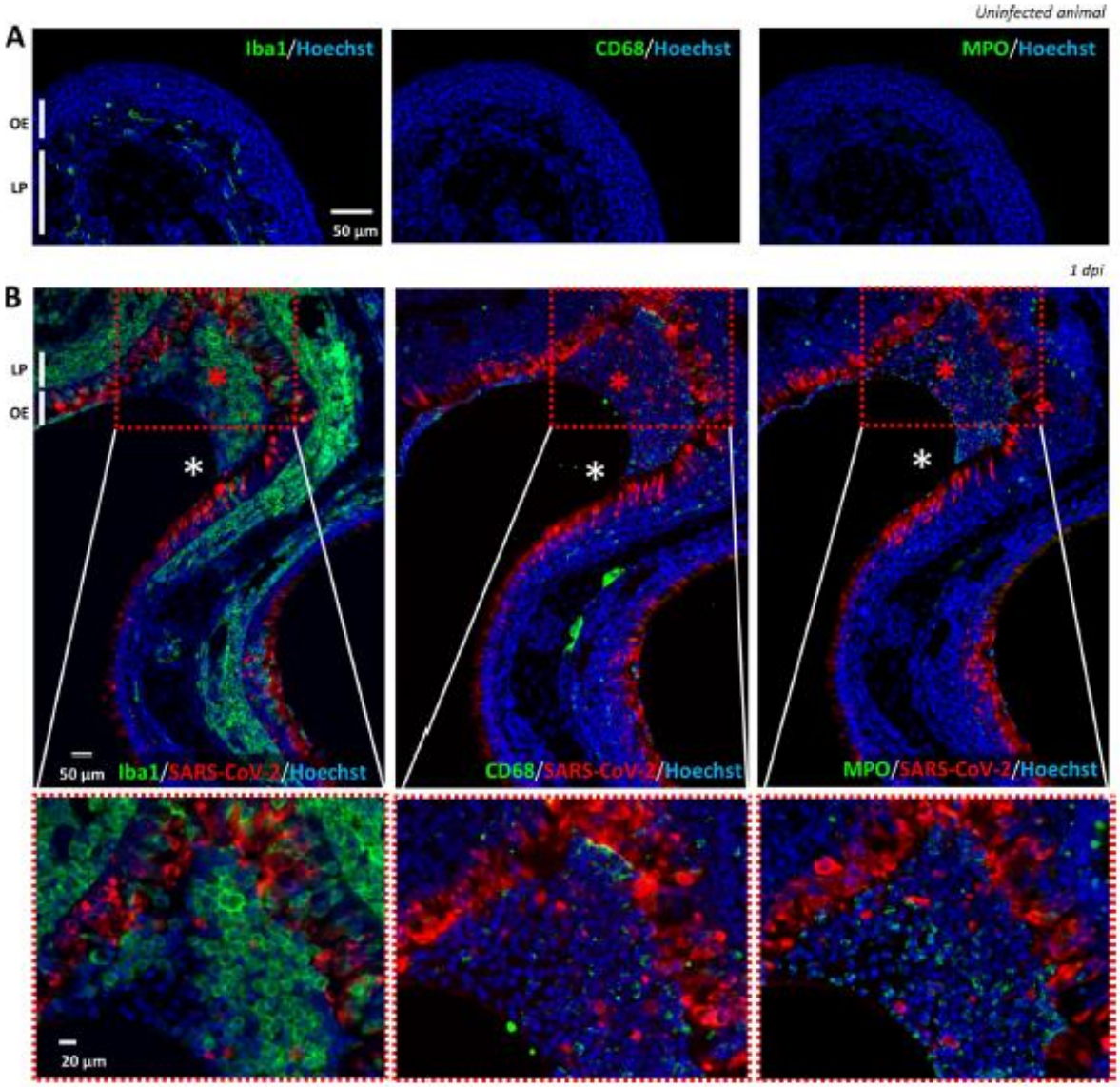


**Fig. 2** Iba1$^+$ (microglia/monocyte lineage), CD68$^+$ (macrophages) and MPO$^+$ (neutrophils) cells presence in the olfactory epithelium before and during SARS-CoV-2 infection. Immunostaining on successive slides of the olfactory epithelium from a non-infected (**A**) or 1 dpi hamster (**B**). Only Iba1$^+$ cells are present in the uninfected olfactory epithelium (OE) and in the lamina propria (LP). In the infected epithelium, Iba1$^+$ cells are massively present in the OE while CD68$^+$ and MPO cells are mostly present in the desquamated cells (red asterisk) in the lumen of the nasal cavity (white asterisk)

the nasal cavity (Fig. 2B). A double staining against Iba1 and CD68 of the desquamated cells in the lumen of the nasal cavity did not reveal any overlap of the two markers (Supp. Fig. 4), showing that Iba1$^+$ cells do not express CD68 once they are located among the desquamated cells. Similar to CD68, MPO signal was absent in uninfected OE and appears during infection partly in the damaged OE and mainly in the lumen of the nasal cavity along with desquamated cells. The MPO$^+$ cells possess typical multi-lobal nuclei characteristic of neutrophils (Supp. Fig. 5). Overall, these results show that Iba1$^+$ cells are much more abundant in the infected OE than CD68$^+$ macrophages and MPO$^+$ neutrophils cells, both being mainly present in the desquamated cells filling the lumen of the SARS-CoV-2-infected nasal cavity.

If these innate immunity cells are involved in the desquamation of the OE, we should always observe their presence in the damaged infected area of the OE. To investigate their infiltration in the OE and its correlation with damage, we focused on three zones similarly as for apoptosis quantification: 1/uninfected, infected 2/without or 3/with damage at 1 and 2 dpi. The infiltration level of Iba1$^+$ cells in the OE was increased in the damaged infected zone but not in the undamaged one (Fig. 3). This difference was statistically significant at 2 dpi (Mann–Whitney, $p=0.0286$) and nearly significant at 1 dpi ($p=0.0525$). The infiltration of these cells was similarly increased in the lamina propria underneath the previous OE zones with a significant difference at 2 dpi ($p=0.0286$). We observed a significant correlation between the damage of the OE and their presence in both the OE and the underlying lamina propria (Spearman test, $p=0.0098$ and 0.0006, respectively).

We similarly examined whether the presence of CD68$^+$ macrophages and MPO$^+$ neutrophils in the OE was associated with the damage of the OE after SARS-CoV-2 infection. Both CD68 and MPO signals were increased in the damaged infected zone but not in the undamaged one (Fig. 4). This difference was statistically significant in the infected damaged zones at 1 and 2 dpi for both markers compared to control and infected undamaged zones of the OE and lamina propria (Mann–Whitney, $p<0.05$). We observed a significant correlation between the damage of the OE and the presence of both CD68$^+$ and MPO$^+$ cells in the OE and the lamina propria (Spearman test, $p<0.001$).

## Neutropenia reduces damage of the OE related to SARS-CoV-2 infection as well as OE infected area

Neutrophils are the main actors of damage to the olfactory epithelium during Poly(I:C)-induced inflammation [50]. We therefore evaluated whether a neutropenic treatment based on cyclophosphamide would reduce the damage induced by SARS-CoV-2 infection in the OE. Such treatment causes apoptosis of bone-marrow-derived cells and has previously been used successfully on hamsters to induce neutropenia [48]. We first monitored in control animals how the treatment impacts circulating immune cells. Neutrophils population was decreased by ~ tenfold, lymphocytes were also decreased by ~ threefold, and monocytes by ~ fivefold (Supp. Fig. 6A). Since cyclophosphamide can impact basal cell proliferation and thus OE structure, we examined its effect in uninfected animals and did not observe any evident damage on the OE structure (Supp Fig. 6B). We next examined the impact of this treatment on the expression of genes related to the innate immune system in the nasal turbinates during SARS-CoV-2 infection. At 1 dpi, the expression of Iba1 and CD68 was not statistically different between vehicle and cyclophosphamide treated animals but a decrease of Ncf2 expression reflecting a reduced presence of neutrophils almost reached significance (Mann–Whitney; $p=0.0571$; Fig. 5A). We observed a tendency of TNFα and IL6 expression reduction which did not reach significance either ($p=0.1143$). Despite the overall tendency of a decrease of innate immune system response at 1 dpi, the level of SARS-CoV-2 infection reflected by N protein expression was decreased and the difference almost reached significance ($p=0.0571$). At 2 dpi, the expression of all genes related to innate immune cell presence as well as TNFα was decreased ($p<0.05$). We examined histologically the neutrophil presence, damage, level of infection in the OE (Fig. 5B, C and Supp. Figs. 6C, 7). MPO signal was significantly decreased at 1 dpi in the OE of cyclophosphamide treated animals compared to control ($p<0.05$) (Fig. 5D$_1$). The damage in the OE was significantly decreased at 1 and 2 dpi ($p<0.01$ and $p<0.05$, respectively) (Fig. 5D$_2$ and Supp. Figs. 8, 9). The reduction tendency of the virus presence measured by the N protein expression was confirmed by immunostaining in the OE at 1 dpi only ($p<0.05$; Fig. 5D$_3$) and seems specific to the OE as the infection of the Steno's gland epithelium lining the maxillary sinus was similar in both conditions (Supp. Fig. 8). We hypothesize that this reduction could be linked to less infected desquamated cells released into the lumen of the nasal cavity following the OE damage induced by the neutrophils. We thus quantified the area of desquamated cells in the lumen which was significantly decreased at 1 dpi and almost reached significance at 2 dpi (Fig. 5D$_4$; $p<0.001$ and $p=0.0905$, respectively). In the desquamated cells of the lumen, the percentage of infected cells was significantly diminished at 1 dpi (Fig. 5D$_5$; $p<0.001$) but not at 2 dpi when infected desquamated cells were in the lumen of the nasal cavity in some treated animals (Supp Fig. 6C). Since the reduction of OE infected area of immunocompromised animal was unexpected, we verified that a dose three times higher than the maximum dose of cyclophosphamide potentially present in the hamsters during infection did not limit the virus replication in vitro (Supp. Fig. 10A, C).

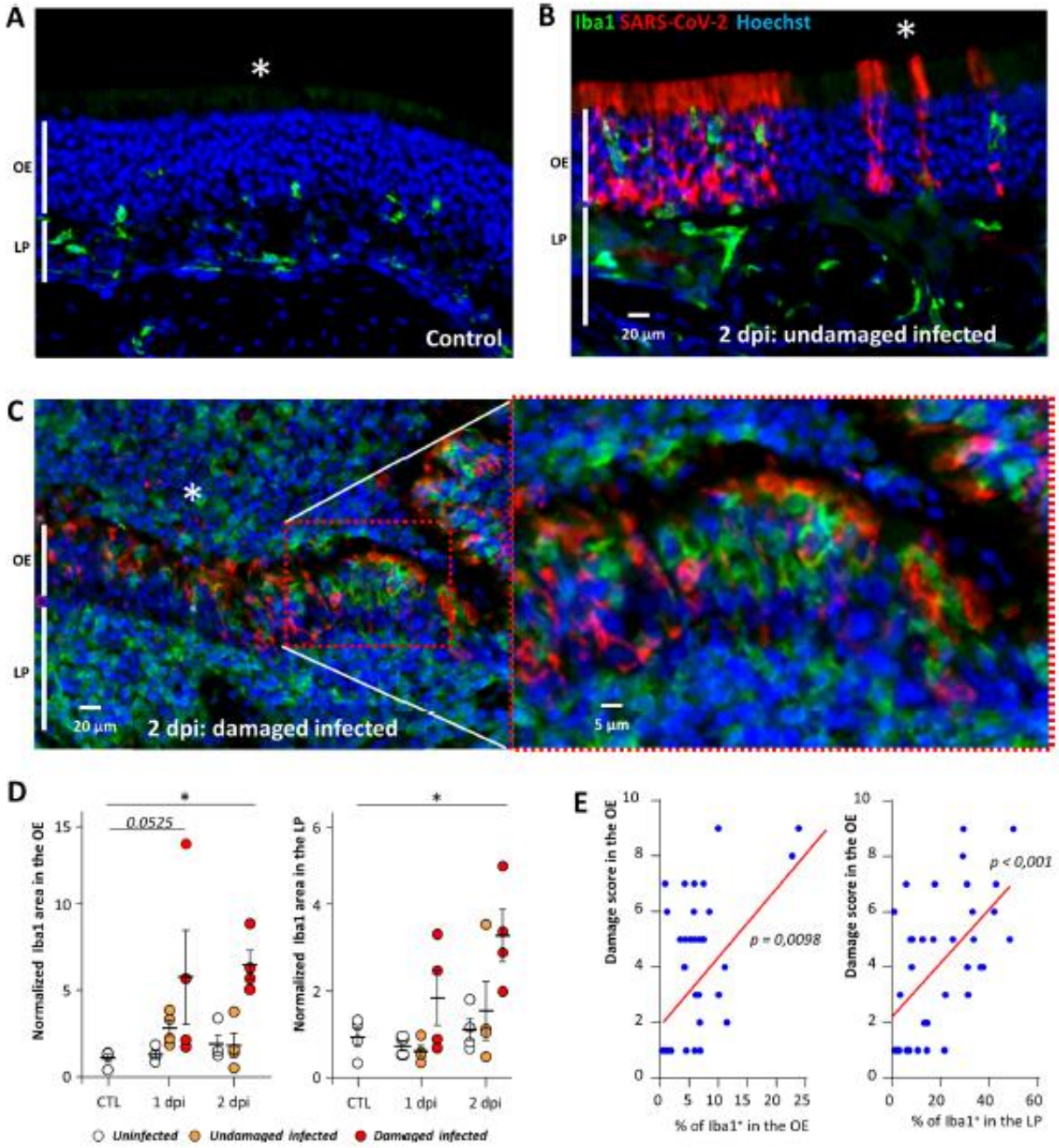


**Fig. 3** Iba1$^+$ cell infiltration increases with the damage in the OE. Representative images of the olfactory epithelium from an uninfected animal (**A**), infected but undamaged (**B**) and infected and damaged (**C**) area of the olfactory epithelium (OE) at 2 days post-infection (dpi). The lumen of the nasal cavity is indicated by a white asterisk. (**D**) Iba1$^+$ signal in the olfactory epithelium (OE, left) and lamina propria (LP, right) in control animals (CTL) or at 1 or 2 dpi (Mean normalized to control ± SEM, $n = 4$, *$p < 0.01$ (Mann–Whitney test)). (**E**) Correlation between score damage of the olfactory epithelium and the percentage of Iba1$^+$ signal in the olfactory epithelium (left panel) and the lamina propria (right panel). Spearman test $p$ value

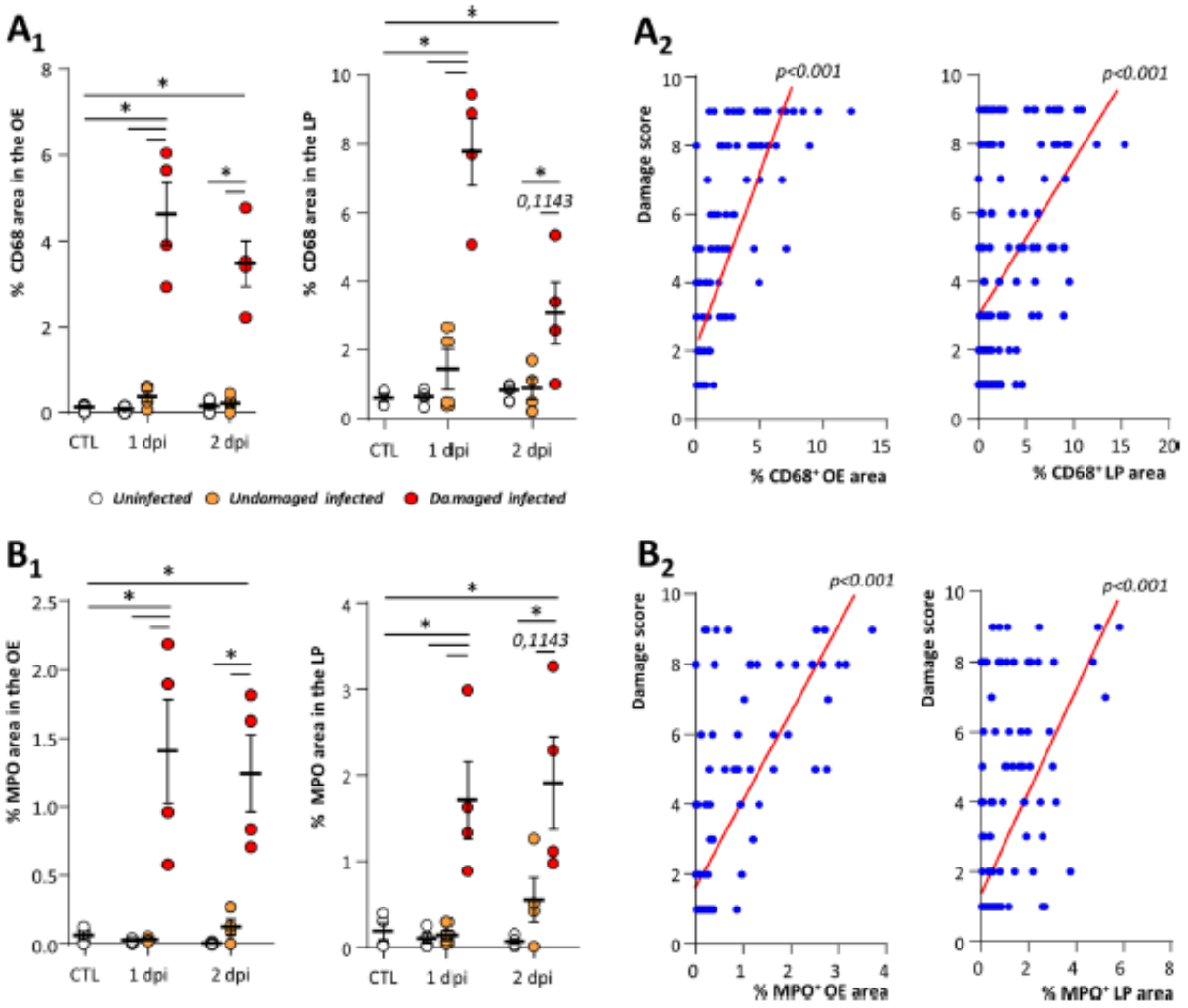


**Fig. 4** $CD68^+$ macrophage and $MPO^+$ neutrophil cells are associated with damage of the olfactory epithelium during SARS-CoV-2 infection. $CD68^+$ ($\mathbf{A_1}$) and $MPO^+$ ($\mathbf{B_2}$) signal in the olfactory epithelium (OE, left) and lamina propria (LP, right) in either control animals (CTL) or at 1 or 2 days post-infection (dpi) (Mean normalized to control ± SEM, $n = 4$, $^*p < 0.05$ (Mann–Whitney test)). Correlation between score damage and percentage of $CD68^+$ ($\mathbf{A_1}$) and $MPO^+$ ($\mathbf{B_2}$) signal in the olfactory epithelium (left panel) and the lamina propria (right panel). Spearman test $p$ value

## Inhibition of neutrophil proteinases reduces damage of the OE related to SARS-CoV-2 infection as well as infected OE area

In order to confirm our results on cyclophosphamide treatment which affects immune cells other than neutrophils, we treated animals with an inhibitor of cathepsin C ($IcatC_{XPZ-01}$) which is essential for the maturation of elastase-like proteinases of neutrophils. This inhibitor has been used successfully to almost completely eliminate the elastase-like activity of neutrophils in vivo [41]. We chose to focus on the histological impact of $IcatC_{XPZ-01}$ treatment at 1 dpi as it gave the most significant results during cyclophosphamide treatment. The inhibition of elastase-like proteinases of neutrophils gave similar results as cyclophosphamide with the exception of some limited neutrophil infiltration in the infected OE (Fig. 6A, B). Globally, the $MPO^+$ neutrophil presence in the nasal turbinates and the damage in the infected area of the OE were significantly reduced compared to vehicle treated animals (Fig. $6C_1$ and Supp. Figs. 11 and 12; Mann–Whitney; $p < 0.01$). We also observed significantly less desquamated cells in the lumen of the nasal cavity which were also less infected (Fig. $6C_2$; Mann–Whitney; $p < 0.01$). Since we observed again that the inhibition of neutrophil action limited SARS-CoV-2 presence in the OE, we verified that a dose three times higher than the maximum

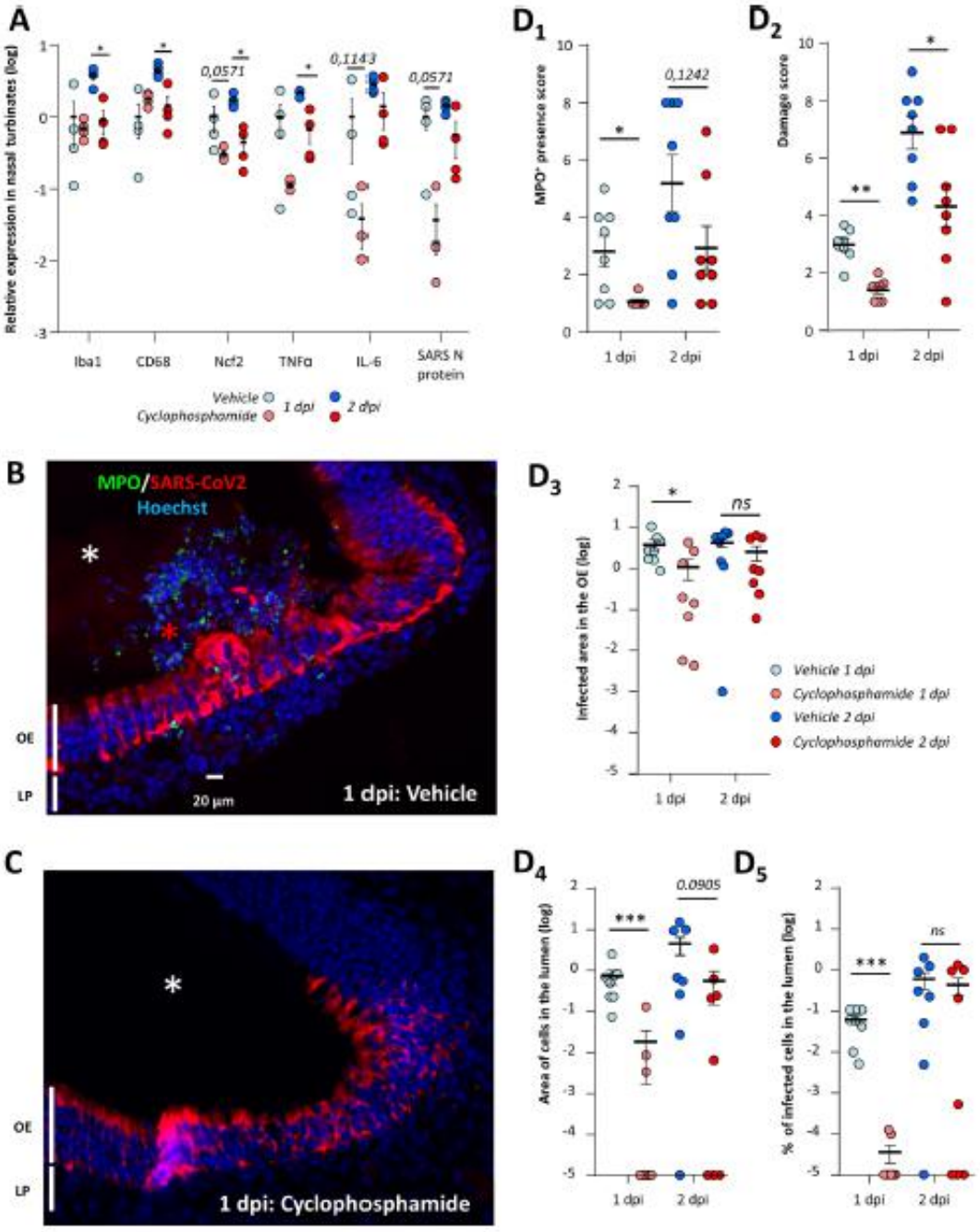


dose of IcatC$_{XPZ-01}$ potentially present in the hamsters during infection did not impair the virus replication in vitro (Supp. Fig. 10B, C). We also observed that the reduction of SARS-CoV-2 infection by IcatC$_{XPZ-01}$ was specific to the OE as the infection of Steno's gland epithelium was not affected in presence of cathepsin C inhibitor (Supp. Fig. 11).

## Discussion

The anosmia induced by SARS-CoV-2 infection is now clearly linked to the infection of the olfactory epithelium with a main tropism for sustentacular cells [18, 51]. We and others have observed that following this infection, the OE undergoes massive damage leading to cell desquamation and

◂**Fig. 5** Immunosuppression induced by cyclophosphamide reduces damage of the olfactory epithelium as well as OE infection area. (**A**) Expression of innate immune genes in the nasal turbinates with or without cyclophosphamide treatment at 1 and 2 days post-infection (dpi). Iba1, CD68 and Ncf2 are related to the presence of microglia/macrophages, monocytes/macrophages and neutrophils, respectively; TNFα and IL6 are two cytokines expressed during inflammation; SARS-CoV-2 N expression is related to the SARS-CoV-2 infection. Results represent the Mean ± SEM relative to vehicle-treated hamsters ($n=4$, $^{*}p<0.05$; Mann–Whitney test). Representative images of the infected olfactory epithelium immunostained for MPO (neutrophil marker) and SARS-CoV-2 N protein in (**B**) vehicle and (**C**) cyclophosphamide treated animal (olfactory epithelium (OE), lamina propria (LP)). In the vehicle condition, the lumen (white asterisk) is filled with desquamated cells (red asterisk) containing MPO signal. In the cyclophosphamide condition, MPO signal is absent and the lumen is mostly free of cellular debris. Quantification in the OE of ($\mathbf{D_1}$) $MPO^{+}$ neutrophil presence ($\mathbf{D_2}$) damage score ($\mathbf{D_3}$) SARS-CoV-2-infected area and in the lumen of the nasal cavity of ($\mathbf{D_4}$) desquamated cells area and ($\mathbf{D_5}$) percentage of SARS-CoV-2-infected area in the desquamated cells (Mean ± SEM, $n=8$ areas of the nasal cavity from 4 different animals, $^{*}p<0.05$, $^{**}p<0.01$, $^{***}p<0.001$ (Mann–Whitney))

cellular debris filling the lumen of the nasal cavity [14, 21, 22], but the mechanism of this destruction is less clear.

Several studies reported an increase in apoptosis especially in olfactory sensory neurons [20–22] and assumed that it led to the destruction of the OE. Here, we first examined the apoptosis level based on cleaved caspase 3 level in the OE of uninfected animals and infected areas of the OE, either intact or damaged. If apoptosis initiates the desquamation process then it should increase in the damaged areas of the OE. However, we observed a similar level of apoptosis level in all these areas (Fig. 1D), which was consistent with the basal level of apoptosis that we previously measured in adult mice and rats OE [42, 52]. While the apoptosis in the infected damaged OE was low, we observed an increased level of apoptosis in cells present in the lumen of the nasal cavity. The discrepancy with previous studies may be due to different models as some were performed using transgenic mice expressing hACE2, but it should be noted that these studies did not perform any quantification and observed as well apoptosis staining in the lumen of the nasal cavity [22]. We observed that most apoptotic cells co-stained with OMP specifically expressed by mature OSNs but not CK18 specific of sustentacular cells (Supp Fig. 2B), indicating that the OSNs undergo C3C-linked apoptosis once released in the lumen of the nasal cavity. The induction of apoptosis by loss of cell contact is well described [53], a phenomenon known as anoikis [54] and observed in human airway epithelial cells during SARS-CoV-2 infection [55]. Desquamated cells in the OE may thus be sufficiently preserved to be able to enter apoptosis after the desquamation process is initiated following OE SARS-CoV-2 infection. The C3C-linked apoptosis may also be related to inflammation as well described for SARS-CoV-2 infection [56]. The remaining cells ongoing apoptosis in the lumen may be immune cells as described during SARS-CoV-2 infection [57] and further experiments are required to identify them.

Since we previously observed that the infected area of the OE is infiltrated by immune cells [14], we next explored whether innate immune cells are involved in this process, especially macrophages and neutrophils known to be involved in damage of epithelial cells during acute inflammation [30, 31, 58]. If so, we should systematically observe their presence in the damaged area of the OE. We first characterized the presence of these cells in the infected OE (Fig. 2). We observed that CD68, a classical marker of macrophages [46], was expressed in a different population than $Iba1^{+}$ cells previously described as a microglia/macrophages cellular population [26]. We observed a continuum of $Iba1^{+}$ cells staining in the OE and in the olfactory bulb similarly as others [59], indicating that they may be more related to microglia than activated macrophages but they require further phenotyping. In the following, we will thus distinguish $Iba1^{+}$ cells and macrophages as $CD68^{+}$ cells to avoid confusion between these two cells types. Immunostaining revealed that at 1 dpi, some parts of the OE in the most rostral part of the nasal cavity were already significantly damaged. We observed that in the infected and damaged area of the OE, $Iba1^{+}$ cells were mainly recruited while macrophages and neutrophils appeared in the zones desquamating toward the lumen of the nasal cavity. While our qPCR results indicate that neutrophils are recruited more abundantly at 1 dpi than $Iba1^{+}$ cells and macrophages (Supp. Fig. 3), we observed that contrary to macrophages and neutrophils, $Iba1^{+}$ cells are already present in the lamina propria of uninfected zones and are rapidly gathering in the infected part of the OE (Fig. 3). The basal presence of $Iba1^{+}$ cells in the lamina propria could explain the apparent discrepancy between qPCR and immunohistochemistry results. Indeed, at the beginning of infection, the increase of $Iba1^{+}$ cells could simply arise from infiltration of adjacent cells in the nasal turbinates, while macrophages and neutrophils may migrate from the blood following chemotaxis. We can thus hypothesize that $Iba1^{+}$ cells are first infiltrating the SARS-CoV-2-infected OE. Similarly, $Iba1^{+}$ microglia are recruited around infected cells of the central nervous system within hours [27], which is consistent with our observation in the OE. Further studies are required to decipher the origin and specific role of these three cells population during the early events of SARS-CoV-2 infection in the infected nasal turbinates.

Neutrophils are known to induce epithelial damage and an elegant study demonstrated their major role during Poly(I:C) (an artificial double-stranded RNA agonist of TLR3 receptor) nasal instillation leading to damage of the OE [50]. In order to evaluate the importance of the neutrophils in the damage induced by SARS-CoV-2, we first induced neutropenia based on cyclophosphamide treatment successfully used

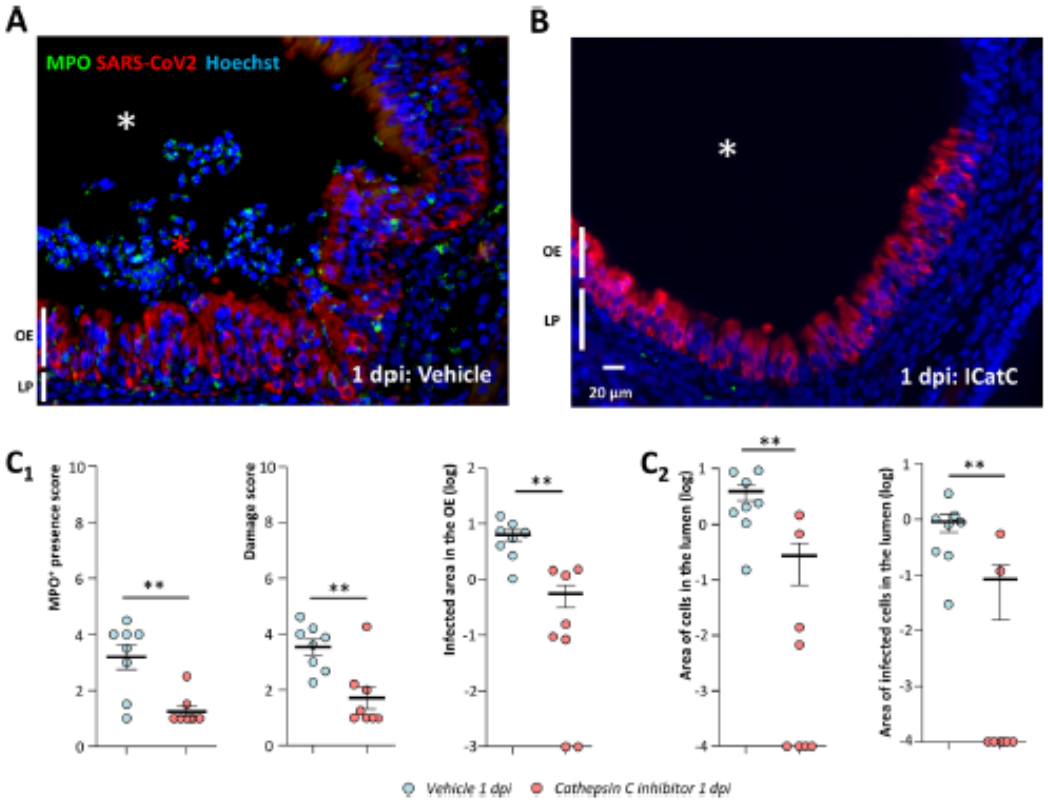


**Fig. 6** Inhibition of neutrophil proteinases reduces damage of the olfactory epithelium as well as infected area. Representative images of the infected olfactory epithelium immunostained for MPO (neutrophil marker) and SARS-CoV-2 N protein in (**A**) vehicle and (**B**) cathepsin C inhibitor ($IcatC_{XPZ-01}$) treated animal (olfactory epithelium (OE), lamina propria (LP)). In the vehicle condition, the lumen (white asterisk) is filled with desquamated cells (red asterisk) containing MPO signal. Under cathepsin C inhibition, MPO signal is less abundant and the lumen is mostly free of cellular debris. Quantification ($C_1$) in the OE of $MPO^+$ neutrophil presence; damage score; SARS-CoV-2-infected area and ($C_2$) in the lumen of the nasal cavity of desquamated cell area and percentage of SARS-CoV-2-infected area in the desquamated cells (Mean ± SEM, $n = 8$ areas of the nasal cavity from 4 different animals, $^*p < 0.05$, $^{**}p < 0.01$, $^{***}p < 0.001$ (Mann–Whitney test))

in hamsters [48]. We confirmed that such treatment mainly affects neutrophils but also reduced to a lesser degree other leucocyte populations (Fig. 5A). As expected such treatment reduced neutrophil infiltration in infected areas of the OE and we observed that damage of the infected OE was significantly reduced as well (Fig. $5D_1, D_2$). In order to confirm the role of neutrophils in the damage of the OE following SARS-CoV-2 infection, we treated hamsters with an inhibitor of cathepsin C ($IcatC_{XPZ-01}$) specifically reducing the neutrophil elastase-like proteinases activity [60]. We observed that similar to cyclophosphamide treatment, the damage of the OE was greatly reduced in this context (Fig. $6C_1$). Surprisingly, the global infiltration of neutrophils was reduced as well, even though we observed that some neutrophils were still present in the most infected area of the OE. Since neutrophils are mainly present among the desquamated cells present in the lumen of the nasal cavity, the reduction in neutrophil infiltration during $IcatC_{XPZ-01}$ treatment may be linked to a decrease in the OE damage as elastase-like proteinase action increases inflammation [61]. It suggests that the damage of the OE initiated by neutrophils may participate in the increase in infiltration of neutrophils leading *in fine* to massive damage of the infected OE areas. Additionally, part of the damage of the OE could simply reflect the destruction of sustentacular cells by SARS-CoV-2 as the treatments on neutrophils that we used were not sufficient to completely eliminate neutrophils or their proteases activity. Overall, these results show that neutrophils have a major causative role in the destruction of the OE following SARS-CoV-2 infection by releasing elastase-like proteinases. $Iba1^+$ cells and macrophages seem clearly to be involved as well as they are recruited during the event leading to the damage of the infected OE. Our results with histochemistry show that $Iba1^+$ cells arrive earlier than neutrophils and macrophages.

Iba1$^+$ cells could be involved in the initial events leading to the damage of the OE as well as phagocytosis. However, their importance in the OE damage should be much lower than neutrophils. Indeed, in the CP treatment which did not impact Iba1$^+$ cell presence in the OE at 1 dpi, we still observed a ~ threefold OE damage reduction with only partial inhibition of neutrophils. In the central nervous system, Iba1$^+$ cells are essential to trigger innate immunity response [28]. We can thus hypothesize that Iba1$^+$ cells may play a chemo-attractive role for macrophages and neutrophils in the infected area of the OE. Further experiments are required to decipher their precise importance in the event leading to OE damage following SARS-CoV-2 infection.

We observed that at 1 dpi, the level of SARS-CoV-2 infection was reduced in cyclophosphamide and Icat$C_{XPZ-01}$-treated hamsters (Figs. 5$D_3$ and 6$C_1$). Such a result was unexpected as neutrophils should effectively destroy infected cells and thus their action should reduce infection progression. We observed that these treatments did not impair SARS-CoV-2 replication in the Steno's gland epithelium and in vitro at a dose three times higher than the maximum dose potentially circulating in hamsters during infection (Supp. Fig. 10). As both treatments act on neutrophils, we thus hypothesize that neutrophils damage of the infected OE may have a counterproductive effect by releasing infected cells into the lumen of the nasal cavity. These infected cells could allow the virus to spread more easily in the OE as it was recently observed in human airway epithelial cells during SARS-CoV-2 infection [55]. This process may also be enhanced by the recently demonstrated impairment of mucociliary clearance during SARS-CoV-2 infection [62]. Such a hypothesis is consistent with our results, showing that cyclophosphamide and Icat$C_{XPZ-01}$ treatment significantly reduced the amount of infected desquamated cells filling the lumen of the nasal cavity (Figs. 5$D_4$, $D_5$ and 6$C_2$). The shedding of SARS-CoV-2 by release of damaged infected cells has been observed recently in vitro in respiratory epithelial cell culture where infection is enhanced in the presence of neutrophils [63]. In this preliminary study, SARS-CoV-2 alone did not significantly increase cytokine production but the neutrophil presence did, showing a major role of the neutrophils in the epithelial response to SARS-CoV-2 infection. In our study, at 2 dpi, the cyclophosphamide treatment inducing neutropenia was less effective than at 1 dpi to prevent OE damage related to SARS-CoV-2 infection (Fig. 5$D_2$). As the neutropenia was only partial, the remaining neutrophils may be more effectively recruited when infection progresses (Fig. 5$D_1$) showing the strong ability of SARS-CoV-2 infection in the OE to recruit innate immune cells.

Overall, our results show that the SARS-CoV-2 infection does not directly induce the massive damage of the OE but that neutrophils play a major role by releasing elastase-like proteinase in the infected OE. This probably leads to the destabilization of the OE structures and shedding of infected cells. In the early phase of the infection, the shedding of infected cells could enhance the virus spread in the OE (Fig. 7). We observed damaged areas of the OE as soon as 1

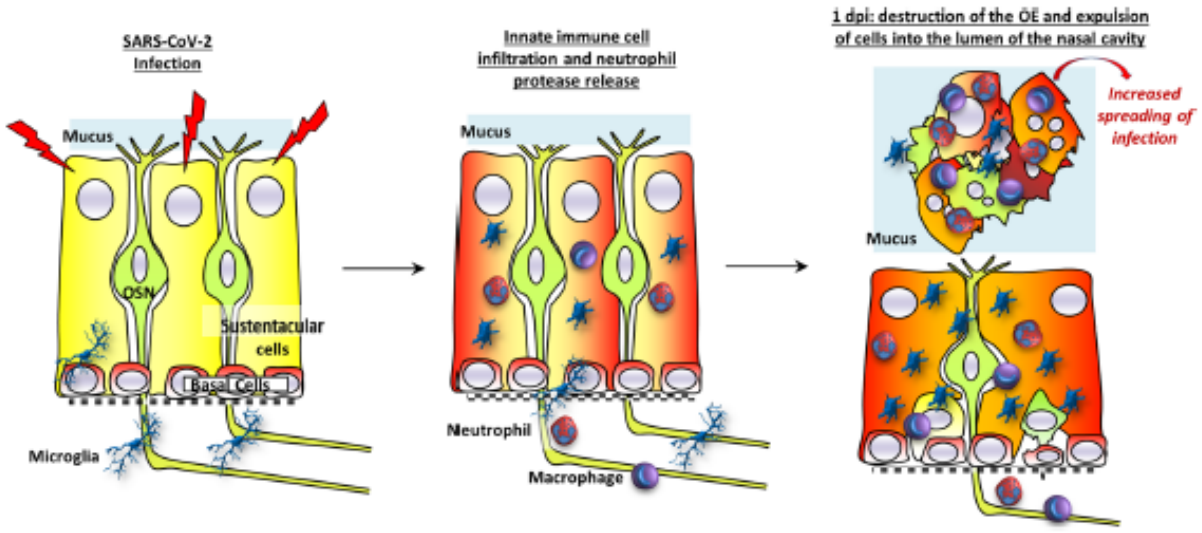


**Fig. 7** Model of innate immune cell signaling leading to olfactory epithelium desquamation. The olfactory epithelium is mainly composed of olfactory sensory neurons (OSN) surrounded by supporting cells (sustentacular cells) and basal cells able to regenerate all cell types of the epithelium. During the infection of sustentacular cells (turning red), Iba1$^+$ cells become activated and infiltrate the olfactory epithelium followed by neutrophils and macrophages. Neutrophils release elastase-like proteinase leading to destabilization of the epithelium structures and the expulsion of cells including non-infected neurons into the lumen of the nasal cavity. The release of infected cells may contribute to an increased spreading of the virus in the OE

dpi, indicating that the innate immune system is extremely efficient in detecting SARS-CoV-2-infected cells to destroy them. The signal triggering this very fast action remains to be explored. The host's immune defense system that may be present to prevent pathogen invasion from the nose to the brain seems beneficial for SARS-CoV-2 to achieve a much more extensive infection of the OE than any previous virus, resulting in unprecedented olfactory dysfunction in the COVID-19 pandemic.

**Supplementary Information** The online version contains supplementary material available at https://doi.org/10.1007/s00018-022-04643-1.

**Acknowledgements** We would like to thank all VIM members for their helpful discussion, Christopher von Bartheld and Birte Nielsen for improvement of the manuscript, Dr Pierre Deshuillers from the BioPole plateform of the National Veterinary School of Alfort for hamsters' blood count, and all the people from the PRBM platform of ENVA who helped us in the BSL3 animal facility. We would also like to thank Bertrand Bryche, Georges Saade, Mustapha Si-Tahar, Laëtitia Merle and Déborah Diakite for their helpful discussion and technical help.

**Author contribution** NM and CB were involved in conceptualization; CB, ASA, OAG, BDC, RD, BK, BK, SLP, and NM helped in investigation; CB and NM contributed to formal analysis; NM and CB helped in writing with input from all authors.

**Funding** NM is supported by INRAe SA department and ANR (Grant CORAR). CB is supported by the "DIM One Health." BK is supported by the "Région Centre Val de Loire (Project Pirana).

**Availability of data and material** Data will be made available on reasonable request, not applicable for material.

## Declarations

**Conflict of interest** All authors do not have conflict of interest.

**Ethics approval and consent to participate** Not applicable.

**Consent for publication** Not applicable.

## References

1. Butowt R, Bilińska K, von Bartheld C (2022) Why does the omicron variant largely spare olfactory function? Implications for the pathogenesis of anosmia in COVID-19. J Infect Dis. https://doi.org/10.1093/infdis/jiac113
2. von Bartheld CS, Hagen MM, Butowt R (2020) Prevalence of chemosensory dysfunction in COVID-19 patients: a systematic review and meta-analysis reveals significant ethnic differences. ACS Chem Neurosci. https://doi.org/10.1021/acschemneuro.0c00460
3. Vaira LA, De Vito A, Lechien JR et al (2021) New onset of smell and taste loss are common findings also in patients with symptomatic COVID-19 after complete vaccination. Laryngoscope. https://doi.org/10.1002/lary.29964
4. Boscolo-Rizzo P, Menegaldo A, Fabbris C et al (2021) Six-month psychophysical evaluation of olfactory dysfunction in patients with COVID-19. Chem Senses. https://doi.org/10.1093/chemse/bjab006
5. Lechien JR, Chiesa-Estomba CM, Beckers E et al (2021) Prevalence and 6-month recovery of olfactory dysfunction: a multicentre study of 1363 COVID-19 patients. J Intern Med. https://doi.org/10.1111/joim.13209
6. Renaud M, Thibault C, Le Normand F et al (2021) Clinical outcomes for patients with anosmia 1 year after COVID-19 diagnosis. JAMA Netw Open 4:e2115352. https://doi.org/10.1001/jamanetworkopen.2021.15352
7. Khan AM, Kallogjeri D, Piccirillo JF (2021) Growing public health concern of COVID-19 chronic olfactory dysfunction. JAMA Otolaryngol Head Neck Surg. https://doi.org/10.1001/jamaoto.2021.3379
8. Meunier N, Briand L, Jacquin-Piques A et al (2021) COVID 19-induced smell and taste impairments: putative impact on physiology. Front Physiol. https://doi.org/10.3389/fphys.2020.625110
9. Rebholz H, Braun RJ, Ladage D et al (2020) Loss of olfactory function-early indicator for Covid-19, other viral infections and neurodegenerative disorders. Front Neurol 11:569333. https://doi.org/10.3389/fneur.2020.569333
10. Schwob JE, Jang W, Holbrook EH et al (2017) Stem and progenitor cells of the mammalian olfactory epithelium: taking poietic license. J Comp Neurol 525:1034–1054. https://doi.org/10.1002/cne.24105
11. Bilinska K, Jakubowska P, Bartheld CS, Butowt R (2020) Expression of the SARS-CoV-2 entry proteins, ACE2 and TMPRSS2, in cells of the olfactory epithelium: identification of cell types and trends with age. ACS Chem Neurosci. https://doi.org/10.1021/acschemneuro.0c00210
12. Brann DH, Tsukahara T, Weinreb C et al (2020) Non-neuronal expression of SARS-CoV-2 entry genes in the olfactory system suggests mechanisms underlying COVID-19-associated anosmia. Sci Adv. https://doi.org/10.1126/sciadv.abc5801
13. Fodoulian L, Tuberosa J, Rossier D et al (2020) SARS-CoV-2 receptors and entry genes are expressed in the human olfactory neuroepithelium and brain. iScience. https://doi.org/10.1016/j.isci.2020.101839
14. Bryche B, St Albin A, Murri S et al (2020) Massive transient damage of the olfactory epithelium associated with infection of sustentacular cells by SARS-CoV-2 in golden Syrian hamsters. Brain Behav Immun 89:579–586. https://doi.org/10.1016/j.bbi.2020.06.032
15. Urata S, Kishimoto-Urata M, Kagoya R et al (2021) Prolonged and extended impacts of SARS-CoV-2 on the olfactory neurocircuit. bioRxiv. https://doi.org/10.1101/2021.11.04.467274
16. Storm N, Crossland NA, McKay LGA, Griffiths A (2022) Comparative pathogenicity of SARS-CoV-2 Omicron and Delta variants in Syrian hamsters mirrors the attenuated clinical outlook of Omicron in COVID-19 irrespective of age. Microbiology 24:103530
17. Butowt R, Meunier N, Bryche B, von Bartheld CS (2021) The olfactory nerve is not a likely route to brain infection in COVID-19: a critical review of data from humans and animal models. Acta Neuropathol 141:809–822. https://doi.org/10.1007/s00401-021-02314-2
18. Khan M, Yoo S-J, Clijsters M et al (2021) Visualizing in deceased COVID-19 patients how SARS-CoV-2 attacks the respiratory and olfactory mucosae but spares the olfactory bulb. Cell. https://doi.org/10.1016/j.cell.2021.10.027
19. Seo JS, Yoon SW, Hwang SH et al (2021) The microvillar and solitary chemosensory cells as the novel targets of infection of SARS-CoV-2 in Syrian golden hamsters. Viruses. https://doi.org/10.3390/v13081653
20. Ye Q, Zhou J, He Q et al (2021) SARS-CoV-2 infection in the mouse olfactory system. Cell Discovery 7:49. https://doi.org/10.1038/s41421-021-00290-1

21. Yu P, Deng W, Bao L et al (2022) Comparative pathology of the nasal epithelium in K18-hACE2 Tg mice, hACE2 Tg mice, and hamsters infected with SARS-CoV-2. Vet Pathol. https://doi.org/10.1177/03009858211071016
22. Zhang AJ, Lee AC-Y, Chu H et al (2021) Severe acute respiratory syndrome coronavirus 2 infects and damages the mature and immature olfactory sensory neurons of hamsters. Clin Infect Dis 73:e503–e512. https://doi.org/10.1093/cid/ciaa995
23. Mori I, Goshima F, Imai Y et al (2002) Olfactory receptor neurons prevent dissemination of neurovirulent influenza A virus into the brain by undergoing virus-induced apoptosis. J Gen Virol 83:2109–2116. https://doi.org/10.1099/0022-1317-83-9-2109
24. Le Bon SD, Horoi M (2020) Is anosmia the price to pay in an immune-induced scorched-earth policy against COVID-19? Med Hypotheses 143:109881. https://doi.org/10.1016/j.mehy.2020.109881
25. Burgoyne RA, Fisher AJ, Borthwick LA (2021) The role of epithelial damage in the pulmonary immune response. Cells 10:2763. https://doi.org/10.3390/cells10102763
26. Imai Y, Ibata I, Ito D et al (1996) A novel geneiba1in the major histocompatibility complex class III region encoding an EF hand protein expressed in a monocytic lineage. Biochem Biophys Res Commun 224:855–862. https://doi.org/10.1006/bbrc.1996.1112
27. Fekete R, Cserép C, Lénárt N et al (2018) Microglia control the spread of neurotropic virus infection via P2Y12 signalling and recruit monocytes through P2Y12-independent mechanisms. Acta Neuropathol 136:461–482. https://doi.org/10.1007/s00401-018-1885-0
28. Wheeler DL, Sariol A, Meyerholz DK, Perlman S (2018) Microglia are required for protection against lethal coronavirus encephalitis in mice. J Clin Invest 128:931–943. https://doi.org/10.1172/JCI97229
29. Käufer C, Chhatbar C, Bröer S et al (2018) Chemokine receptors CCR2 and CX3CR1 regulate viral encephalitis-induced hippocampal damage but not seizures. Proc Natl Acad Sci USA 115:E8929–E8938. https://doi.org/10.1073/pnas.1806754115
30. Kolaczkowska E, Kubes P (2013) Neutrophil recruitment and function in health and inflammation. Nat Rev Immunol 13:159–175. https://doi.org/10.1038/nri3399
31. Meidaninikjeh S, Sabouni N, Marzouni HZ et al (2021) Monocytes and macrophages in COVID-19: friends and foes. Life Sci 269:119010. https://doi.org/10.1016/j.lfs.2020.119010
32. Janoff A (1972) Human granulocyte elastase. Further delineation of its role in connective tissue damage. Am J Pathol 68:579–592
33. Kawabata K, Hagio T, Matsuoka S (2002) The role of neutrophil elastase in acute lung injury. Eur J Pharmacol 451:1–10. https://doi.org/10.1016/S0014-2999(02)02182-9
34. Brinkmann V, Reichard U, Goosmann C et al (2004) Neutrophil extracellular traps kill bacteria. Science 303:1532–1535. https://doi.org/10.1126/science.1092385
35. Saffarzadeh M, Juenemann C, Queisser MA et al (2012) Neutrophil extracellular traps directly induce epithelial and endothelial cell death: a predominant role of histones. PLoS ONE 7:e32366. https://doi.org/10.1371/journal.pone.0032366
36. Arango Duque G, Descoteaux A (2014) Macrophage cytokines: involvement in immunity and infectious diseases. Front Immunol. https://doi.org/10.3389/fimmu.2014.00491
37. Borders AS, Getchell ML, Etscheidt JT et al (2007) Macrophage depletion in the murine olfactory epithelium leads to increased neuronal death and decreased neurogenesis. J Comp Neurol 501:206–218. https://doi.org/10.1002/cne.21252
38. Borders AS, Hersh MA, Getchell ML et al (2007) Macrophage-mediated neuroprotection and neurogenesis in the olfactory epithelium. Physiol Genomics 31:531–543. https://doi.org/10.1152/physiolgenomics.00008.2007
39. Hoagland DA, Moller R, Uhl SA et al (2021) Leveraging the antiviral type I interferon system as a first line of defense against SARS-CoV-2 pathogenicity. Immunity. https://doi.org/10.1016/j.immuni.2021.01.017
40. Korkmaz B, Lesner A, Wysocka M et al (2019) Structure-based design and in vivo anti-arthritic activity evaluation of a potent dipeptidyl cyclopropyl nitrile inhibitor of cathepsin C. Biochem Pharmacol 164:349–367. https://doi.org/10.1016/j.bcp.2019.04.006
41. Guarino C, Hamon Y, Croix C et al (2017) Prolonged pharmacological inhibition of cathepsin C results in elimination of neutrophil serine proteases. Biochem Pharmacol 131:52–67. https://doi.org/10.1016/j.bcp.2017.02.009
42. Bryche B, Dewaele A, Saint-Albin A et al (2019) IL-17c is involved in olfactory mucosa responses to Poly(I:C) mimicking virus presence. Brain Behav Immun. https://doi.org/10.1016/j.bbi.2019.02.012
43. Bryche B, Fretaud M, Saint-Albin Deliot A et al (2019) Respiratory syncytial virus tropism for olfactory sensory neurons in mice. J Neurochem. https://doi.org/10.1111/jnc.14936
44. Muller PY, Janovjak H, Miserez AR, Dobbie Z (2002) Processing of gene expression data generated by quantitative real-time RT-PCR. Biotechniques 32:1372–1374 (**1376, 1378–1379**)
45. Bouchery T, Harris N (2019) Neutrophil–macrophage cooperation and its impact on tissue repair. Immunol Cell Biol 97:289–298. https://doi.org/10.1111/imcb.12241
46. Holness C, Simmons D (1993) Molecular cloning of CD68, a human macrophage marker related to lysosomal glycoproteins. Blood 81:1607–1613. https://doi.org/10.1182/blood.V81.6.1607.1607
47. Leto TL, Lomax KJ, Volpp BD et al (1990) Cloning of a 67-kD neutrophil oxidase factor with similarity to a noncatalytic region of p60 c-src. Science 248:727–730. https://doi.org/10.1126/science.1692159
48. Peniche AG, Bonilla DL, Palma GI et al (2017) A secondary wave of neutrophil infiltration causes necrosis and ulceration in lesions of experimental American cutaneous leishmaniasis. PLoS ONE 12:e0179084. https://doi.org/10.1371/journal.pone.0179084
49. Borregaard N, Theilgaard-Mönch K, Sørensen OE, Cowland JB (2001) Regulation of human neutrophil granule protein expression. Curr Opin Hematol 8:23–27. https://doi.org/10.1097/00062752-200101000-00005
50. Kanaya K, Kondo K, Suzukawa K et al (2014) Innate immune responses and neuroepithelial degeneration and regeneration in the mouse olfactory mucosa induced by intranasal administration of Poly(I:C). Cell Tissue Res 357:279–299. https://doi.org/10.1007/s00441-014-1848-2
51. Fumagalli V, Ravà M, Marotta D et al (2022) Administration of aerosolized SARS-CoV-2 to K18-hACE2 mice uncouples respiratory infection from fatal neuroinvasion. Sci Immunol 7:eabl9929. https://doi.org/10.1126/sciimmunol.abl9929
52. Raynaud A, Meunier N, Acquistapace A, Bombail V (2015) Chronic variable stress exposure in male Wistar rats affects the first step of olfactory detection. Behav Brain Res 291:36–45. https://doi.org/10.1016/j.bbr.2015.05.013
53. Bates RC, Buret A, van Helden DF et al (1994) Apoptosis induced by inhibition of intercellular contact. J Cell Biol 125:403–415. https://doi.org/10.1083/jcb.125.2.403
54. Frisch S, Francis H (1994) Disruption of epithelial cell-matrix interactions induces apoptosis. J Cell Biol 124:619–626. https://doi.org/10.1083/jcb.124.4.619
55. Morrison CB, Edwards CE, Shaffer KM et al (2022) SARS-CoV-2 infection of airway cells causes intense viral and cell shedding, two spreading mechanisms affected by IL-13. Proc Natl Acad Sci USA 119:e2119680119. https://doi.org/10.1073/pnas.2119680119

56. Li S, Zhang Y, Guan Z et al (2020) SARS-CoV-2 triggers inflammatory responses and cell death through caspase-8 activation. Sig Transduct Target Ther 5:235. https://doi.org/10.1038/s41392-020-00334-0
57. Junqueira C, Crespo Â, Ranjbar S et al (2022) FcγR-mediated SARS-CoV-2 infection of monocytes activates inflammation. Nature. https://doi.org/10.1038/s41586-022-04702-4
58. Hasegawa-Ishii S, Shimada A, Imamura F (2017) Lipopolysaccharide-initiated persistent rhinitis causes gliosis and synaptic loss in the olfactory bulb. Sci Rep 7:11605. https://doi.org/10.1038/s41598-017-10229-w
59. Ueha R, Ito T, Furukawa R et al (2022) Oral SARS-CoV-2 inoculation causes nasal viral infection leading to olfactory bulb infection: an experimental study. Front Cell Infect Microbiol 12:924725. https://doi.org/10.3389/fcimb.2022.924725
60. Guarino C, Legowska M, Epinette C et al (2014) New selective peptidyl di(chlorophenyl) phosphonate esters for visualizing and blocking neutrophil proteinase 3 in human diseases. J Biol Chem 289:31777–31791. https://doi.org/10.1074/jbc.M114.591339
61. Döring G (1994) The role of neutrophil elastase in chronic inflammation. Am J Respir Crit Care Med 150:S114–S117. https://doi.org/10.1164/ajrccm/150.6_Pt_2.S114
62. Li Q, Vijaykumar K, Philips SE et al (2022) Mucociliary transport deficiency and disease progression in Syrian hamsters with SARS-CoV-2 infection. Microbiology 5:562
63. Calvert B, Quiroz E, Lorenzana Z et al (2021) Neutrophilic inflammation promotes SARS-CoV-2 infectivity and augments the inflammatory responses in airway epithelial cells. https://doi.org/10.1101/2021.08.09.455472

**Publisher's Note** Springer Nature remains neutral with regard to jurisdictional claims in published maps and institutional affiliations.

Springer Nature or its licensor (e.g. a society or other partner) holds exclusive rights to this article under a publishing agreement with the author(s) or other rightsholder(s); author self-archiving of the accepted manuscript version of this article is solely governed by the terms of such publishing agreement and applicable law.

# Annexe 4

JOURNAL OF SURGICAL RESEARCH • MARCH 2023 (283) 953–964

Available online at www.sciencedirect.com

ScienceDirect

journal homepage: www.JournalofSurgicalResearch.com

# Alpha-1-Antitrypsin Protects Vascular Grafts of Brain-Dead Rats Against Ischemia/Reperfusion Injury

*Qingwei Ding, MD,*[a] *Sivakkanan Loganathan, MD,*[a,b] *Pengyu Zhou, MD,*[a] *Alex Ali Sayour, MD,*[a,c] *Paige Brlecic, MD,*[a] *Tamás Radovits, MD, PhD,*[c] *Roxane Domain, MSc,*[d] *Brice Korkmaz, PhD,*[d] *Matthias Karck, MD,*[a] *Gábor Szabó, MD, PhD,*[a,b] *and Sevil Korkmaz-Icöz, PhD*[a,b,*]

[a] *Department of Cardiac Surgery, University Hospital Heidelberg, Heidelberg, Germany*
[b] *Department of Cardiac Surgery, University Hospital Halle (Saale), Halle, Germany*
[c] *Heart and Vascular Center, Semmelweis University, Budapest, Hungary*
[d] *INSERM UMR-1100, "Research Center for Respiratory Diseases" and University of Tours, Tours, France*

ARTICLE INFO

*Article history:*
Received 12 November 2021
Received in revised form
4 November 2022
Accepted 20 November 2022
Available online xxx

*Keywords:*
Alpha-1-antitrypsin
Brain death
Endothelial function
Heart transplantation
Ischemia/reperfusion

ABSTRACT

*Introduction:* Endothelial dysfunction is a potential side effect of brain death (BD). Ischemia/reperfusion (IR) injury during heart transplantation may lead to further endothelial damage. Protective effects of alpha-1-antitrypsin (AAT), a human neutrophil serine protease inhibitor, have been demonstrated against IR injury. We hypothesized that AAT protects brain-dead rats' vascular grafts from IR injury.

*Methods:* Donor rats were subjected to BD by inflation of a subdural balloon. After 5.5 h, aortic rings were immediately mounted in organ baths (BD, $n = 6$ rats) or preserved in saline, supplemented either with vehicle (BD-IR, $n = 8$ rats) or AAT (BD-IR + AAT, $n = 14$ rats) for 24 h. During organ bath experiment, rings from both IR groups were exposed to hypochlorite to simulate warm reperfusion-associated endothelial injury. Endothelial function was measured *ex vivo*. Immunohistochemical staining for caspases was carried out and DNA-strand breaks were evaluated using terminal deoxynucleotidyl transferase-mediated dUTP nick-end labeling. Data are presented as median (interquartile range).

*Results:* AAT improved IR-induced decreased maximum endothelium-dependent vasorelaxation to acetylcholine in the BD-IR + AAT aortas compared to the BD-IR group (BD: 83 (9-28) % *versus* BD-IR: 49 (39-60) % *versus* BD-IR + AAT: 64 (24-42) %, $P < 0.05$). Additionally, an increase in the rings' sensitivity to acetylcholine was noted after AAT ($pD_2$-value: BD-IR + AAT: 7.35 (7.06-7.89) *versus* BD-IR: 6.96 (6.65-7.21), $P < 0.05$). Caspase-3, -8, -9, and -12 immunoreactivity and the number of terminal deoxynucleotidyl transferase-mediated dUTP nick-end labeling-positive cells were significantly decreased by AAT.

*Conclusions:* AAT alleviates endothelial dysfunction, prevents increased caspase-3, -8, -9, and -12 levels, and decreases apoptotic DNA breakage due to BD and IR injury. This

* *Corresponding author.* Laboratory of Cardiac Surgery, Department of Cardiac Surgery, University Hospital Heidelberg, INF 326, 69120, Heidelberg, Germany. Tel.: +49 6221 566246.
E-mail address: korkmaz@uni-heidelberg.de (S. Korkmaz-Icöz).
0022-4804/$ – see front matter © 2022 Elsevier Inc. All rights reserved.
https://doi.org/10.1016/j.jss.2022.11.047

suggests that AAT treatment may be therapeutically beneficial to reduce IR-induced vascular damage.

© 2022 Elsevier Inc. All rights reserved.

## Introduction

Heart transplantation remains an effective treatment for patients with end-stage heart failure.[1] Brain-dead donors are currently the main organ source for heart transplantation. However, endothelial dysfunction is a well-described phenomenon in transplanted hearts[2] and has also been shown following brain death (BD).[3] BD is associated with a massive release of catecholamine. This results in a tachycardia, peripheral vasoconstriction, and a rise in intracranial pressure, which initially increases arterial blood pressure to maintain adequate cerebral perfusion pressure.[4] This hypertensive phase is followed by systemic hypotension.[5] BD additionally leads to an increase in systemic inflammatory state. Graft dysfunction, resulting from ischemia/reperfusion (IR) injury, is a key issue in heart transplantation. IR-induced endothelial dysfunction is caused by mitochondrial dysfunction, excess endoplasmic reticulum stress, calcium overload resulting in high-energy phosphate depletion,[6] production of reactive oxygen species, the generation of inflammatory cytokines and infiltration of neutrophils,[7] which enhance apoptosis.[8] Cold preservation followed by warm reperfusion, as occurs during heart transplantation, may further aggravate BD-induced vascular damage. To date, vascular structural and functional changes during IR injury following BD have not been fully explored.[9]

Alpha-1-antitrypsin (AAT), an acute-phase response protein, is predominantly produced by hepatocytes in the liver and released into the bloodstream during an inflammatory response or infection.[10] It protects tissues against enzymatic digestion by neutrophil serine proteases, such as neutrophil elastase, cathepsin G, and proteinase 3.[11-13] Intravenous injection of this natural human neutrophil serine protease inhibitor has already been approved to treat emphysema in patients with AAT deficiency.[14] AAT has been shown to have highly effective anti-inflammatory[12,15] and antiapoptotic[16] properties. It reduces reactive oxygen species production as well.[17] Previous studies have shown that AAT protects against the lung[18,19] and renal[20] IR injury. It was demonstrated to prevent the development of adverse left-ventricular remodeling following myocardial infarction.[21] Even though after cardiac transplantation[22] endothelial dysfunction is frequently described and BD impairs coronary endothelial dysfunction,[3] the effects of AAT on vascular grafts obtained following BD in *ex vivo* static cold storage have not been investigated. If initial endothelial dysfunction caused by hypothermia during organ preservation followed by warm reperfusion could be prevented, a higher protection would be obtained.

Based on the above mentioned findings, we hypothesized that adding AAT to physiological saline solution protects vascular grafts of BD rats from IR injury. Furthermore, because of the role apoptosis plays following BD and IR injury, we aimed to explore the effect of AAT on apoptosis-related caspases.

## Materials and Methods

### *Animals*

Male Lewis rats (weighing 250-350 g) were obtained from Janvier Labs (Saint-Berthevin, France) with prior ethical approval (G37/14). All animals received humane care in compliance with the "Principles of Laboratory Animal Care", formulated by the National Society for Medical Research, and with the "Guide for the Care and Use of Laboratory Animals", prepared by the Institute of Laboratory Animal Resources and published by the National Institutes of Health (NIH Publication, 8th Edition, 2011) and EU Directive 2010/63/EU. The ethical approval was obtained by the Ethical Committee of the Regional Council of Karlsruhe, Germany for Animal Experimentation (G37/14).

### *Rat BD model*

As previously reported,[23] the donor rats were anesthetized with an intraperitoneal injection of sodium pentobarbital (60 mg/kg, intraperitoneally), then intubated and ventilated by a respirator (Harvard Apparatus, Holliston, MA, USA). The right carotid artery was cannulated using 2F-microtip pressure-volume conductance catheter for blood pressure and heart rate monitoring (SPR-838, Millar Instruments, Houston, Texas, USA) and the left external jugular vein was used for ringer infusion. The core temperature, measured via a rectal thermometer, was maintained between 36.5°C and 37.5°C with a heating pad. A Fogarty-4F balloon catheter was introduced subdurally through a drilled parietal hole and inflated with 15 μL of saline per min until a total volume of 600 μL was reached. BD was confirmed by maximum pupil dilatation, sustained absence of spontaneous breathing and reflexes. A decrease in systolic blood pressure <60 mmHg was avoided by Ringer administration without inotropic/vasoactive agents. Nonbrain-dead control (sham-operated) rats underwent the same surgical procedure without balloon catheter insertion. Hemodynamic parameters were continuously monitored for 5.5 h.

### In vitro *vascular IR injury*

#### *Aortic ring preparation*

At 5.5 h postsham operation or BD induction, the descending thoracic aorta was explanted, placed in petri dishes either with cold oxygenated Krebs–Henseleit solution (KHL in mM: 118 NaCl, 4.7 KCl, 1.2 $KH_2PO_4$, 1.2 $MgSO_4$, 1.77 $CaCl_2$, 25 $NaHCO_3$, and 11.4 glucose) or physiological saline solution. Periadventitial fat and connective tissue were removed under magnification, and then sectioned into 4-mm long rings.

#### *Cold preservation of aortic rings and experimental groups*

As previously described,[24] the aortic rings from BD rats were placed in test tubes containing 0.9% saline (BD-IR group, 8 rats)

or 1 mg/mL AAT (Prolastin, Grifols, Germany) (BD-IR + AAT group, 14 rats), which was gassed with nitrogen to extrude oxygen, then stored at 4°C. After 24 h of ischemic conservation, the rings were mounted on stainless steel hooks in tissue chambers (emka Technologies S.A.S, Paris, France) containing 20 mL of KHL, and continuously provided 95% $O_2$ and 5% $CO_2$ at 37°C. To mimic free radical generation and endothelial injury, as that occur during reperfusion and reoxygenation *in vivo*, sodium hypochlorite was added to the organ bath chambers (200 μM, 30 min). Aortic rings from BD (BD group, 6 rats) and sham-operated (sham group, 6 rats) rats were immediately mounted in isolated organ baths without cold ischemic storage and hypochlorite incubation. Isometric contractions were recorded using isometric force transducers, digitized, stored, and displayed with IOX Software (emka Technologies S.A.S, Paris, France). The final concentration of the AAT used in the present study was chosen based on previously published study.[19] The experimental protocol is shown in Figure 1.

### Ex vivo *organ bath tension measurements*

Table 1 summarizes the experimental protocol. Briefly, as previously reported,[23] after mounting in organ chambers, four rings from the same aorta were allowed to equilibrate at a resting tension for 20 min. This is necessary to restore ionic gradients, which were altered during cold preservation/conservation. The rings were placed under the optimal basal tension of 2 g (found optimal in preliminary experiments) for an additional 60 min of equilibration, and KHL was changed at 30-min intervals, a precaution against interfering metabolites. First, a precontraction was achieved by adding potassium chloride (KCl, 80 mM) to the organ baths to ensure tissue viability and prepare the rings for stable contraction. After the contractile response had stabilized for approximately 30 min, aortic rings were washed every 15 min until resting tension was reached. Next, the same rings were contracted with an α-adrenergic receptor agonist, phenylephrine (PE) ($10^{-9}$-$10^{-5}$ M) until a stable plateau was reached, and the relaxation responses were investigated by adding cumulative concentrations of the endothelium-dependent vasorelaxant acetylcholine (ACh, $10^{-9}$-$10^{-4}$ M). Then, the aortic rings were rinsed several times with KHL and equilibrated for 30 min until the tension returned to baseline before precontraction with $10^{-6}$ M PE. When the contraction achieved a plateau, for testing relaxation responses of smooth muscle cells, an endothelium-independent dilator sodium nitroprusside (SNP, $10^{-10}$-$10^{-5}$ M) was used in PE ($10^{-6}$ M)-precontracted aortic rings. Noncontracting rings and rings with technical difficulties that prohibited mounting were removed from the analysis. The contractility of PE was evaluated as a percentage of the KCl response and as absolute value in gram, and relaxation was expressed as a percentage of the contraction induced by PE. Half-maximal response ($EC_{50}$) to PE, ACh, or SNP were determined from each individual concentration-response curve by sigmoidal fits using Origin 7.0 (MicroCal Software, Northampton, Massachusetts, USA). The sensitivity $pD_2$ ($-\log EC_{50}$) was then calculated.

### *Immunohistochemical staining for caspase-3, -8, -9, and -12*

Distal regions of the aortic segments were fixed in a buffered paraformaldehyde solution (4%) and embedded in paraffin. As previously reported,[23] hydrogen peroxide (3%) was used to quench the endogenous peroxidase activity for 30 min. Then, the sections were pretreated using heat-induced antigen retrieval with sodium citrate buffer (pH = 6) for 20 min in a microwave oven at 700 W, and 2% normal serum in buffer to block sections for 30 min at room temperature. After that, the sections were incubated with mouse monoclonal IgG anti-caspase-3 (1:1000; antibodies-online GmbH, Aachen, Germany), rabbit polyclonal IgG anti-caspase-8 (1:1000; Novus Biologicals, Littleton, Colorado, USA), mouse monoclonal IgG anti-caspase-9 (1:50; Santa Cruz Biotechnology, Dallas, Texas, USA), and rabbit polyclonal IgG anti-caspase-12 (1:200; Novus Biologicals, Littleton, Colorado, USA) antibodies for 2h at room temperature. Then, biotinylated secondary antibody was diluted in blocking serum buffer (1:50), and sections were covered for 30 min at room temperature. The biotinylated secondary antibody was detected by the avidin-biotinylated complex reagent (VECTASTAIN universal elite avidin-biotinylated complex kit, Burlingame, USA). Afterward, slides were developed with 3,3-diaminobenzidine substrate that produced a dark brown reaction product in the presence

**Table 1 – *Ex vivo* organ baths: experimental design.**

| Steps | | Function |
|---|---|---|
| 1 | KCl (80 mM) | - To ensure tissue viability<br>- To prepare the rings for stable contraction<br>- To assess membrane depolarization-induced smooth muscle contraction |
| 2 | Wash | |
| 3 | Phenylephrine ($10^{-9}$-$10^{-5}$ M) | - To investigate agonist-induced smooth muscle contraction |
| 4 | Acetylcholine ($10^{-9}$-$10^{-4}$ M) | - To assess endothelium-dependent vasorelaxation |
| 5 | Wash | |
| 6 | Phenylephrine ($10^{-6}$ M) | - To investigate agonist-induced smooth muscle contraction |
| 7 | Sodium nitroprusside ($10^{-10}$-$10^{-5}$ M) | - To assess endothelium-independent vasorelaxation |
| 8 | End | |

Vascular smooth muscle cell contraction and relaxation were investigated in the isolated organ bath on isolated thoracic aortic rings of male Lewis rats.

of horseradish peroxidase enzyme and was used in double labeling applications (Vector DAB kit, Burlingame, USA). Finally, slides were dehydrated, cleared, and permanently mounted with ProTaqs Mount Aqua (Quartett, Berlin, Germany). Counterstaining was performed with hematoxylin. Semiquantitative immunohistochemical analysis was performed using conventional microscopy based on the intensity score multiplied by area score (0-12). The evaluation was conducted by two examiners blinded to the experimental groups from 4 randomized nonoverlapping fields per aorta per rat.

### *Terminal deoxynucleotidyl transferase-mediated dUTP nick-end labeling staining*

We performed terminal deoxynucleotidyl transferase-mediated dUTP nick-end labeling (TUNEL) assay to detect DNA strand breaks, as previously described,[25] by using a commercially available kit (Roche Diagnostics Indianapolis, IN, USA). Sections were deparaffinized with xylene and passaged through decreasing concentrations of ethanol, washed with phosphate-buffered saline (PBS) buffer and digested by diluted DNase-free proteinase-K (1:10, Millipore, 21,627) to retrieve antigenic epitopes for 20 min, RT. Then, sections were washed with 1X PBS for 2 × 5 min. After blocking endogenous peroxidases with 3% hydrogen peroxide for 5 min in the dark, sections were washed in PBS-buffer 2 × 5 min. Besides, positive and negative controls were prepared by adding 50 μL DNase I for positive and 50 μL of pure labeling reagent for negative control followed by 5 min washing in PBS-buffer. Then, sections were incubated with TUNEL reaction mixture (Roche Diagnostics, Mannheim, Germany) in humidified atmosphere for 60 min at 37°C in the dark. The sections were then washed with PBS buffer for 3 × 5 min. The slides were mounted using 4′, 6-diamidino-2-phenylindole (DAPI)-Fluoromount-GTM (SouthernBiotech, Birmingham, USA), covered with cover glass and analyzed under a fluorescence microscope. The number of TUNEL-positive cells was analyzed under a fluorescence microscope and expressed as the ratio of DAPI-TUNEL double-labeled nuclei to the total number of nuclei stained with DAPI. The evaluation was done by two examiners blinded to the experimental groups from 4 randomized nonoverlapping fields per aorta per rat.

### *Measurement of neutrophil elastase and cathepsin G activities*

*Western blot*: Bone marrow cell lysates (20-100 μg of total proteins) from rats were incubated in PBS with or without human AAT (hAAT) (5 μM) for 2 h at 37°C with gentle shaking. Irreversible hAAT-rat protease complexations were confirmed by western-blot using selective antibodies (anti-cathepsin G: Santa Cruz, sc-33207 and anti-neutrophil elastase: Abcam, ab-68672).

Fluorescence resonance energy transfer *assays*: Rat neutrophil elastase and cathepsin G activities in bone marrow lysates treated (1 h at 37°C) or not with hAAT were measured spectrofluorometrically (Ex = 320 nm and Em = 420 nm) using fluorescence resonance energy transfer substrates as previously described.[26] Neutrophil elastase activity in bone marrow cell lysates (2.5 μg of total proteins) was measured with or without hAAT (5 μM in HEPES 50 mM, NaCl 0.75 M, NP40 0.05 %, pH 7,4) using Abz-APQQIMDDQ-EDDnp (20 μM) as substrate. Cathepsin G activity was measured in bone marrow cell lysates (1 μg of total proteins) in HEPES 50 mM, NaCl 100 mM, NP40 0.05 %, pH 7,4 completed with or not hAAT (5 μM) using Abz-TPFSGQ-EDDnp (20 μM) as substrate.

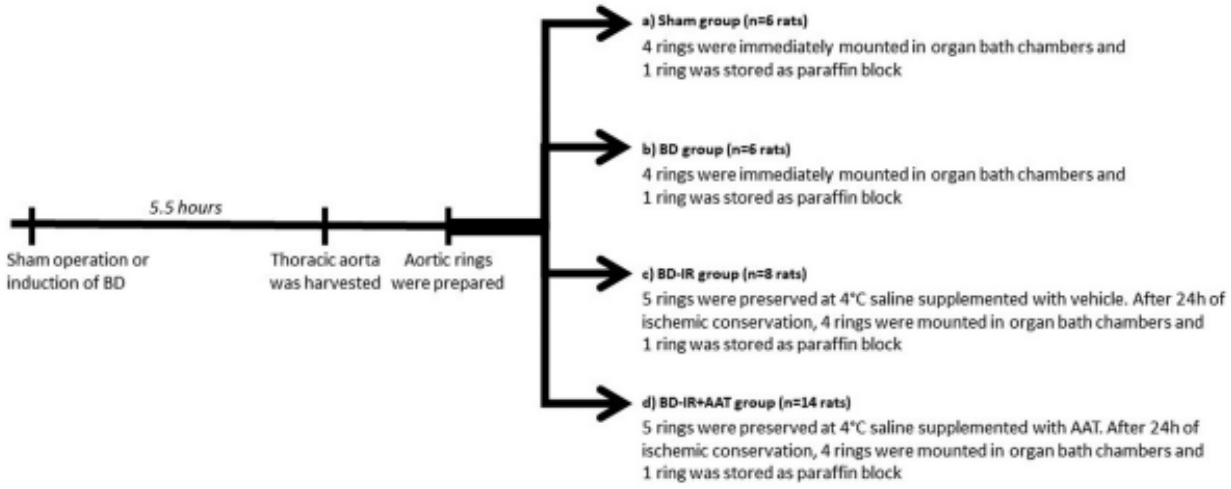


**Fig. 1 – Experimental protocol. Donor rats were subjected to sham operation or brain death by inflation of a subdural balloon. After 5.5 h, the thoracic aorta was harvested, four aortic rings were prepared from each thoracic aorta and immediately mounted in organ baths (sham and BD groups, n = 6 rats/group) or preserved in saline, supplemented either with a vehicle (BD-IR-groups, n = 8 rats) or AAT (BD-IR + AAT group, n = 14 rats) for 24 h. Additionally, in each experimental group, distal regions of the aortic segments were fixed in a buffered paraformaldehyde solution (4%), embedded in paraffin and stored for further analysis. The rings were excluded from the organ bath experiments if they did not contract or after technical problem, and they were accepted as damaged.**

### *Statistical data analysis*

Data are presented as median (interquartile range). Statistical analyses were performed using GraphPad Prism software, version 7.02 (GraphPad Software, Inc, CA, USA) and graphs were created with Origin 7.0 (MicroCal Software, Northampton, Massachusetts, USA). Comparing two experimental groups: data were tested for normality using Shapiro–Wilk test before statistical tests. Two-sample Student's test was used to analyze the differences between sham-operated and BD groups and a nonparametric Mann–Whitney test was applied if data were not normally distributed. Comparing three experimental groups: for hemodynamic parameters, contractile responses to KCl, $pD_2$ values and histological results, the Shapiro–Wilk normality test was used to assess normality of data distribution. For data with normal distribution, one-way analysis of variance followed by Tukey's post hoc test was carried out for multiple comparisons. If the data were not normally distributed, the nonparametric Kruskal–Wallis test followed by Dunn's post hoc test was used. In cases of cumulative concentration-response curves to phenylephrine, ACh, and SNP, a two-factor mixed analysis of variance (factors: AAT and concentration of reagents [PE, ACh, and SNP]) and followed by Tukey's post hoc test was used for multiple comparisons. For organ bath experiments, results are represented as median (interquartile range) of all rings in each experimental group. A value of P less than 0.05 was considered significant.

## Results

### *Characterization of rat model of BD*

*Effect of BD on hemodynamic parameters*

After 5.5 h of BD or sham operation, hemodynamic parameters were measured. Systolic blood pressure [64 (61-70) *versus* 130 (125-140) mmHg, $P < 0.05$], diastolic blood pressure [30 (26-42) *versus* 109 (84-110) mmHg, $P < 0.05$], and mean arterial pressure [43 (38-51) *versus* 117 (98-120) mmHg, $P < 0.05$] were significantly reduced in the BD rats compared to the sham-operated controls.

*Contractile and relaxation responses of BD rat aortic rings*

Smooth muscle contraction, triggered by high potassium ($K^+$)-induced depolarization (Fig. 2A) and by PE [expressed in g [2.79 (2.39-3.30) *versus* 1.52 (1.2-2.0), $P < 0.05$], and as percentage of the maximum contraction-induced by KCl (Fig. 2B)], was significantly higher in the BD group compared to sham-operated rats. The cumulative concentration-response curve

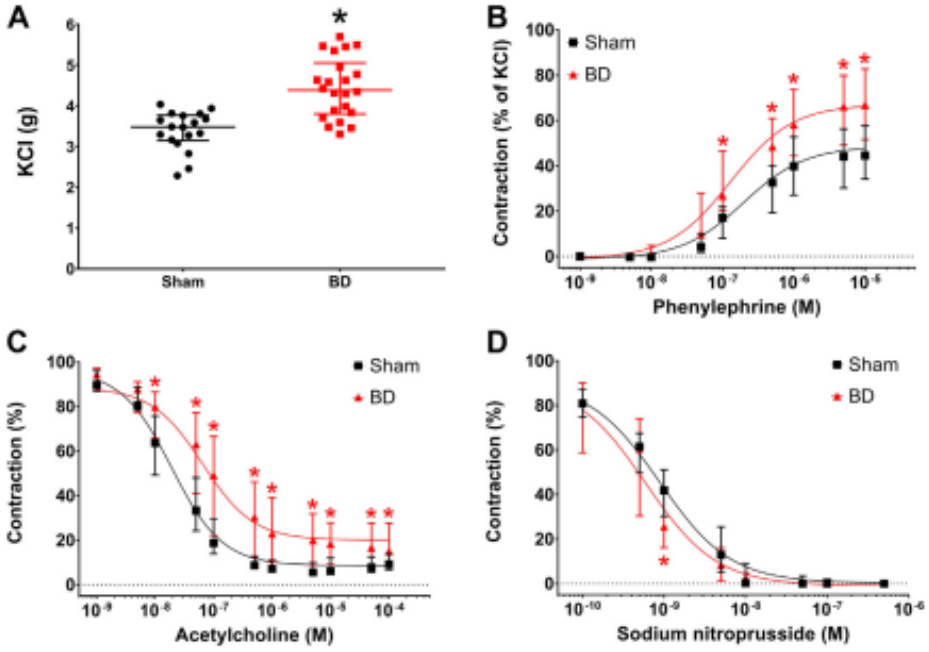


**Fig. 2 – Effect of brain death on vascular contractile and relaxation responses. Contractile responses (A) to high potassium ($K^+$)-induced depolarization and (B) PE (expressed as percentage of the maximum contraction induced by 80 mM potassium chloride (KCl), and (C) acetylcholine-induced endothelium-dependent- and (D) sodium nitroprusside-induced endothelium-independent vasorelaxation of isolated thoracic aortic rings from sham-opareted ($n = 18$ rings from 6 animals) and brain-dead (BD) rats ($n = 22$ rings from 6 animals). Data was tested for normality using Shapiro–Wilk test before statistical tests. For contractile responses to KCl two-sample Student's test was used to analyze the differences between sham-operated and BD groups and a nonparametric Mann–Whitney test was applied if data were not normally distributed. In cases of cumulative concentration-response curves to PE, acetylcholine and sodium nitroprusside, a two-factor mixed ANOVA (factors: brain death and concentration of reagents [PE, acetylcholine, nitroprusside) and followed by Tukey's post-hoc test was used for multiple comparisons. Results are represented as median (interquartile range) of all rings.*$P < 0.05$ *versus* Sham.**

(Fig. 2C) and aortic sensitivity [$pD_2$-value: 7.18 (6.70-7.63) *versus* 7.72 (7.44-7.89), $P < 0.05$] to ACh were significantly decreased in the BD aortic rings compared to the sham-operated controls. Although maximum vasorelaxation to SNP did not differ between the two groups (Fig. 2D), BD resulted in a left-shifted concentration-response curve compared with the sham-operated rats [$pD_2$-value: 9.18 (8.99-9.33) *versus* 9.00 (8.92-9.15), $P < 0.05$]. It should be noted that some rings could not be mounted in the organ baths due to technical difficulties, and rings were excluded from the analysis if they did not contract. Thus, in the sham and BD groups ($n = 6$ rats/group) 18 rings and 22 rings, respectively, were mounted in the organ baths; however, no ring was excluded during the analysis. In the BD-IR group ($n = 8$ rats), 32 rings were mounted in the organ baths, 5 rings were eliminated due to the KCl, PE, or ACh analysis and 11 rings due to the SNP analysis. BD-IR + AAT group ($n = 14$ rats), 52 rings were mounted in the organ baths, 13 rings were eliminated due to the KCl, PE, or ACh analysis and 16 rings due to the SNP analysis.

*Effect of BD on apoptosis-related caspases*

Immunoreactivity for caspase-3 [score: 4.5 (2.5-5) *versus* 1.5 (1-3.5), $P < 0.05$], caspase-8 [score: 4 (3.5–6) *versus* 2 (1.25-3.5), $P < 0.05$], caspase-9 [score: 4 (2.25-4) *versus* 2 (2-2.5), $P < 0.05$], and caspase-12 [score: 4 (4-6) *versus* 2 (2-4), $P < 0.05$] was significantly higher in the BD group compared to the sham-operated animals.

*Effect of BD on DNA-strand breaks in the aorta*

The number of TUNEL-positive nuclei was significantly increased in the BD rings compared to controls [52 (45-64) % *versus* 40 (33-50) %, $P < 0.05$].

### *Effect of AAT on IR in BD rats' aorta*

*Effects of AAT on contractile responses*

Smooth muscle contraction triggered by KCl was significantly decreased in the BD-IR group compared to BD rings, and AAT had no effect (Table 1, Fig. 3A). An increased maximum contractile response to PE at a concentration of $10^{-5}$ M in the BD-IR compared to BD aortas was significantly decreased by AAT (Table 2). However, AAT has not effect on significantly increased cumulative concentration-response curves (Fig. 3B) and aortic ring sensitivity ($pD_2$-value) (Table 2) to PE in the BD-IR + AAT rings compared to the BD-IR group.

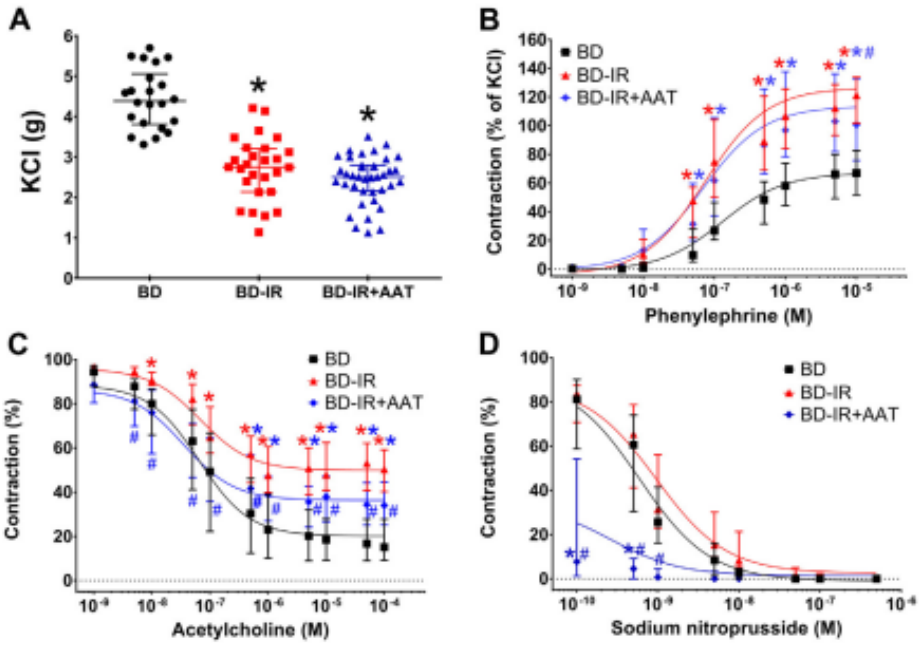


**Fig. 3 – Effect of alpha-1 antitrypsin (AAT) on vascular contractile and relaxation responses against IR injury in aortic rings from brain-dead rats. Contractile responses (A) to high potassium ($K^+$)-induced depolarization and (B) PE (expressed as percentage of the maximum contraction induced by 80 mM KCl, and (C) acetylcholine-induced endothelium-dependent vasorelaxation (BD, $n = 22$ rings from 6 rats; BD-IR, $n = 27$ rings from 8 rats; BD-IR + AAT, $n = 39$ rings from 14 rats) and (D) sodium nitroprusside-induced endothelium-independent vasorelaxation (BD, $n = 22$ rings from 6 rats; BD-IR, $n = 21$ rings from 8 rats; BD-IR + AAT, $n = 36$ rings from 14 rats) of isolated thoracic aortic rings from BD rats. For contractile responses to KCl, the Shapiro–Wilk normality test was used to assess normality of data distribution. For data with normal distribution, one-way ANOVA followed by Tukey's post-hoc test was carried out for multiple comparisons. If the data were not normally distributed, the nonparametric Kruskal–Wallis test followed by Dunn's post-hoc test was used. In cases of cumulative concentration-response curves to phenylephrine, acetylcholine and sodium nitroprusside, a two-factor mixed ANOVA (factors: AAT and concentration of reagents [phenylephrine, acetylcholine, sodium nitroprusside]) and followed by Tukey's post hoc test was used for multiple comparisons. Results are represented as median (interquartile range) of all rings in each experimental group. *$P < 0.05$ *versus* BD; #$P < 0.05$ *versus* BD-IR. ANOVA, analysis of variance.**

**Table 2 – Quantitative analysis of vascular evaluation: effect of AAT on vascular function after IR injury in aortic rings from brain-dead rats.**

| | BD | BD-IR | BD-IR + AAT |
|---|---|---|---|
| Phenylephrine (g) | 2.8 (2.4-3.3) | 3.4 (2.9-3.8) | 2.6 (2.0-3.2)† |
| Phenylephrine (% to KCl) | 67 (52-83) | 121 (102-134)* | 103 (82 -136)*,† |
| $pD_2$ to PE | 6.81 (6.71-7.12) | 7.16 (6.91-7.37)* | 7.15 (6.81-7.31)* |
| KCl (g) | 4.4 (3.8-5.1) | 2.8 ± (2.1-3.2)* | 2.5 (2.2-2.8)* |
| $R_{max}$ to ACh (%) | 83 (9-28) | 49 (39-60)* | 64 (24-42)*,† |
| $pD_2$ to ACh | 7.18 (6.70-7.63) | 6.96 (6.65-7.21) | 7.35 (7.06-7.89)† |
| $R_{max}$ to SNP (%) | 100 (0-0) | 100 (0-0) | 100 (0-0) |
| $pD_2$ to SNP | 9.18 (8.99-9.33) | 9.12 (8.66-9.40) | 9.31 (9.19-9.67)† |

Contractile responses to PE was expressed as gram and as percentage of the maximum contraction induced by 80 mM KCl. Maximum relaxation to acetylcholine (ACh) (BD, $n = 22$ rings from 6 rats; BD-IR, $n = 27$ rings from 8 rats; BD-IR + AAT, $n = 39$ rings from 14 rats) and sodium nitroprusside (SNP) (BD, $n = 22$ rings from 6 rats; BD-IR, $n = 21$ rings from 8 rats; BD-IR + AAT, $n = 36$ rings from 14 rats) was expression as a percentage of the contraction induced by PE. $R_{max}$ indicates maximal relaxation and $pD_2$, negative logarithm of the corresponding half-maximal response ($EC_{50}$). The Shapiro–Wilk normality test was used to assess normality of data distribution. For data with normal distribution, one-way ANOVA followed by Tukey's post-hoc test was carried out for multiple comparisons. If the data were not normally distributed, the nonparametric Kruskal–Wallis test followed by Dunn's post-hoc test was used. Results are represented as median (interquartile range) of all rings in each experimental group.

*$P < 0.05$ *versus* BD.

†$P < 0.05$ *versus* BD-IR.

*Effect of AAT on endothelial function*

Significantly reduced ACh-induced vasorelaxation in the BD-IR group compared to BD rings was significantly improved by AAT (Table 1, Fig. 3C). Furthermore, decreased aortic sensitivity ($pD_2$-value) to ACh seen after BD and IR injury was significantly ameliorated by AAT (Table 2).

*Effects of AAT on smooth muscle relaxation*

Although maximum relaxation to SNP did not differ among the groups, the cumulative concentration-response curve to this relaxant agent in the BD-IR + AAT rings was significantly shifted to the left compared to BD + IR rats (Table 2, Fig. 3D).

*Effects of AAT on aortic caspase-3, -8, -9, and -12 immunoreactivity*

Immunohistochemical analysis for apoptosis-related caspases showed that increased caspase-3, -8, -9, and -12 immunoreactivity in the BD-IR group compared to the BD rings was significantly decreased with AAT (Fig. 4).

*Effects of AAT on DNA strand breaks in the aortic rings*

Even though IR injury had no effect on the inherently elevated TUNEL positivity in the BD group, we observed a significant decrease in the number of TUNEL-positive cells following AAT treatment (Fig. 5).

***Effect of human AAT on rat bone marrow cell lysates***

The activity of two neutrophil serine proteases, including neutrophil elastase and cathepsin G, was determined using hAAT in lysates obtained from rat bone marrow lysates. Our results showed that the activity of these proteases from bone marrow rat lysates were decreased when hAAT was used (Fig. 6).

## Discussion

In the current study, we investigated whether adding AAT to physiological saline solution protects vascular graft function of BD rats from *in vitro* cold ischemia followed by warm reperfusion injury. Furthermore, we hypothesized that AAT has relevant antiapoptotic effect in addition to its known antiprotease functions. To our knowledge, this is first preclinical study showing that the preservation of aortic rings of BD rats with AAT (at a final concentration of 1 mg/mL) alleviates endothelial dysfunction. The study supports a direct antiapoptotic mechanism of AAT against endothelial damage in the aorta injured by both BD and IR injury.

The endothelium plays a key role in various physiological functions, including vascular tone, permeability, anticoagulation, monocyte/leukocyte adhesion, and angiogenesis. Three major relaxing factors produced by the endothelial cells, working cooperatively and causing relaxation of vascular smooth muscle, are nitric oxide (NO),[27,28] prostacyclin,[29] and endothelium-derived hyperpolarizing factor.[30] Stimulation of muscarinic receptor by ACh activates endothelial NO synthase, which releases NO from the endothelial cells. NO diffuses into the underlying smooth muscle cells, where it binds and activates guanylyl cyclase, and increases synthesis of cyclic guanosine monophosphate. Activation of protein kinase G by cGMP decreases intracellular calcium concentration, leading to relaxation of the smooth muscle cells. NO also activates potassium channels, which leads to hyperpolarization and relaxation. prostacyclin, synthesized by cyclooxygenase in endothelial cells, elicits smooth muscle relaxation by stimulating adenylyl cyclase and thereby generating cyclic adenosine monophosphate . The exact chemical identity of endothelium-derived hyperpolarizing factor remains elusive, although several candidates have been proposed including cytochrome P450-derived arachidonic

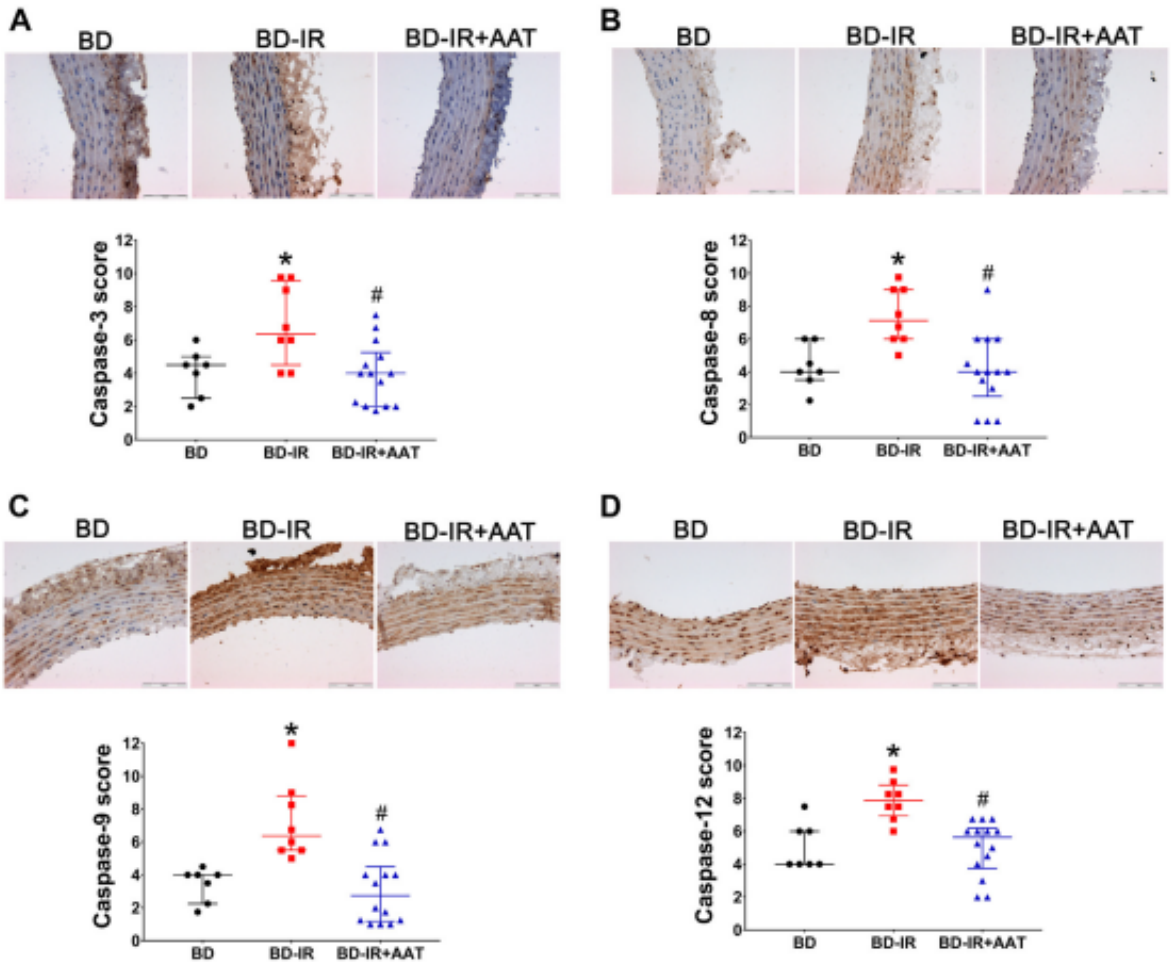


**Fig. 4 – Effect of AAT on apoptosis-related caspases against ischemia/reperfusion (IR) injury in aortic rings from brain-dead rats. Representative images of (A) caspase-3, (B) caspase-8, (C) caspase-9, and (D) caspase-12 immunohistochemical staining (brown staining, x 20, bar = 100 μm) followed by semiquantitative analysis in isolated thoracic aortic rings from BD rats. The Shapiro–Wilk normality test was used to assess normality of data distribution. For data with normal distribution, one-way ANOVA followed by Tukey's post hoc test was carried out for multiple comparisons. If the data were not normally distributed, the nonparametric Kruskal–Wallis test followed by Dunn's post hoc test was used. Results are represented as median (interquartile range) in 4 randomly nonoverlapping fields per aorta per rat (BD, *n* = 7 rats; BD-IR, *n* = 8 rats; BD-IR + AAT, *n* = 14 rats). *P < 0.05 *versus* BD; #P < 0.05 *versus* BD-IR. The evaluation was done in a blinded fashion.**

epoxide, anandamide, endothelial potassium, hydrogen peroxide, and C-type natriuretic peptide.[31] We have previously shown that BD in potential organ donors leads to severe endothelial dysfunction.[3,23] Impaired endothelial cell ability to release relaxing (e.g., nitric oxide) and contracting (e.g., endothelin-1) factors,[32] hormone depletion,[33] inflammatory reaction cascade,[34] oxidative stress, and apoptosis[35,36] among others are important mechanisms involved in BD-induced vascular dysfunction. In the current work, we confirmed that BD caused hemodynamic changes,[37] vascular endothelial and contractile dysfunction.[23] Upon examination of aortic tissue, we demonstrated that BD was associated with increased caspase-3, -8, -9, and -12 levels and DNA strand breaks compared to controls. Endothelial dysfunction is a key problem at different stages of heart transplantation. To optimize preservation of grafts and subsequently improve clinical outcomes,[38] novel strategies are required to attenuate cellular injury during both BD and IR.

It is well documented that intravenous infusions of AAT are most commonly used to treat patients with emphysema seen in AAT deficiency. In the present study, an isolated tissue bath system has allowed *ex vivo* assessment of the effect AAT has on both BD and IR injury-induced vascular dysfunction. Our results showed that endothelium-dependent vasorelaxation and the aortas' sensitivity ($pD_2$-value) to ACh in rings from BD rats were increased by adding AAT (1 mg/mL) to clinically used 0.9% saline during cold storage, indicating an improvement in endothelial function. Furthermore, only at a concentration of $10^{-5}$ M an α1-adrenergic receptor agonist PE-induced increased contraction in the BD-IR compared to BD aortas that was significantly decreased by AAT. It should be noted that in the BD-IR groups, 32 rings were mounted in

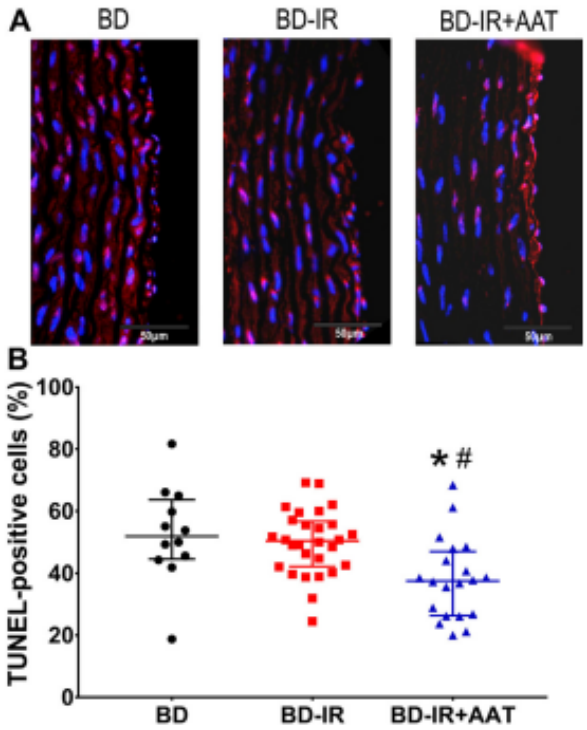


**Fig. 5 – Effects of AAT on DNA strand breaks against IR injury in aortic rings from brain-dead rats. (A) Representative merged micrographs of aortic tissue show pink nuclei with fragmented DNA, visualized by TUNEL) staining and blue nuclei represents 4′,6-diamino-2-phenylindole staining (magnification x40; scale bar: 50 μm) followed by (B) Quantification of TUNEL-positive cells. The Shapiro–Wilk normality test was used to assess normality of data distribution. For data with normal distribution, one-way ANOVA followed by Tukey's post hoc test was carried out for multiple comparisons. If the data were not normally distributed, the nonparametric Kruskal–Wallis test followed by Dunn's post-hoc test was used. Results are represented as median (interquartile range) and correspond to the mean of all rings. *$P < 0.05$ *versus* BD; #$P < 0.05$ *versus* BD-IR. BD, $n = 12$ rings; BD-IR, $n = 28$ rings; BD-IR + AAT, $n = 20$ rings.**

organ bath chambers. Of these, 21 rings were used for SNP analysis and 27 rings for KCl, PE, and ACh analysis (34% drop-out). In contrast, in the BD-IR + AAT group, 52 rings were mounted in organ baths. Of these, 36 rings were analyzed for SNP and 39 rings for KCl, PE, and ACh (~31% drop-out). In the sham and BD groups all the mounted rings were included in the analysis. We therefore believe that IR injury, not the incubation of the aortic rings with AAT, adversely affects the vasoreactivity of the aortic rings. Recently, Götzfried *et al.* have shown that perfusion and the preservation of donor lungs with a conservation solution containing 1 mg/mL AAT improves primary graft function and reduced the inflammatory response after lung transplantation in a preclinical model.[19] Furthermore, Gao *et al.* have demonstrated that intravenous administration of 50 mg/kg AAT before ischemia inhibits lung injury in an *in situ* pulmonary IR model in rats.[14] Additionally, *in vivo* administration of hAAT (80 mg/kg) improves renal function in a mouse model of bilateral kidney IR injury.[20] In a study reported by Toldo *et al.* exogenous administration of clinical grade AAT (60 mg/kg) resulted in better cardiac function and prevented adverse cardiac remodeling in an experimental model of acute myocardial infarction.[21] These findings together suggest that applications of AAT can be expanded for other indications beyond emphysema.

Cellular damage induced by reperfusion injury and BD may lead to apoptosis, also known as programmed cell death. Apoptosis is mediated through three pathways: cytokines/Fas-mediated extrinsic pathway (through caspase-8), mitochondrial-mediated intrinsic pathway (through caspase-9), and endoplasmic reticulum/calcium-mediated pathway (through caspase-12), resulting in caspase-3 activation, and subsequently cell death. AAT has been shown to reduce simulated IR-induced cell death via caspase-3 inhibition in an *in vitro* cell culture model.[18] A previous study has suggested that AAT has intracellular antiproteolytic activity by binding and inactivating caspase-3 activation, thereby preventing apoptosis in lung microvascular endothelial cells.[16] In line with these observations, in the present study, caspase-3, -8, -9 and -12 immunoreactivity, DNA breakage/nuclear fragmentation (detected by TUNEL assay) were significantly decreased by AAT, indicating that AAT reduced apoptosis in the aorta injured by BD and IR. Serban and Petrache have shown that AAT prevents apoptosis in lung endothelial cells.[39] This function was largely dependent on uptake of the AAT from the circulation via both clathrin- and, in part, caveolae-mediated endocytosis and by inhibiting not only serine proteases (with great specificity against neutrophil elastase) but also cysteine proteases (caspase-3, -6, and -7).[39] Additionally, Zhang *et al.* have demonstrated that AAT enters beta cells and directly inhibits caspase-3 activity, leading to protection against apoptosis.[40] Rat AAT has been characterized in 1981[41]: from 330 mL of rat serum, 222 mg of A1AT has been isolated and purified with an overall yield of approximately 20%. Selective substrates for mice neutrophil serine proteases were developed.[42,43] These substrates are also selective to rat neutrophil serine proteases. Our results showed that the activity of neutrophil elastase and cathepsin G from bone marrow rat lysates were decreased when hAAT was used. In our study, we speculate that *in vitro* preservation of vascular grafts of brain-dead rats after IR injury with AAT may be, in part, due to its ability to physically enter vascular endothelial and smooth muscle cells, then to reduce apoptosis.[40] However, further studies are needed. During reperfusion it has been shown that the antiprotease shield of AAT against elastase and other neutrophil serine proteases may represent the main mechanisms of lung preservation.[19] In addition to its antiprotease functions, we have demonstrated another important function of AAT, an antiapoptotic ability that protects tissue against BD and IR injury. However, the exact underlying cellular and molecular mechanisms involved in the vascular protective effect of AAT in our experimental model are still unknown. Potential off-target effects in addition to its protease-mediated function may account for these findings.

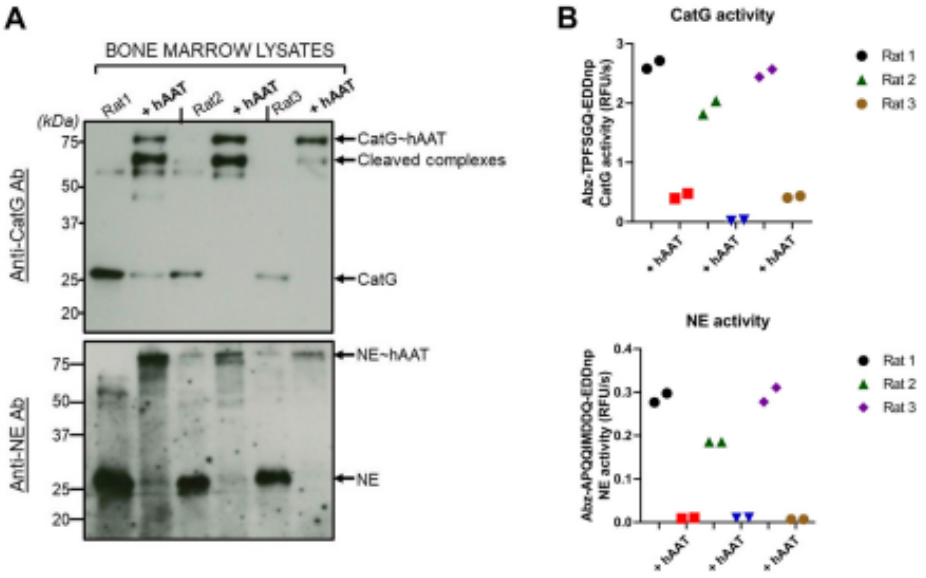


**Fig. 6 – Western-blot and FRET assay analysis of rat bone marrow neutrophil serine proteases inhibition with human alpha-1 antitrypsin (hAAT). (A) Western blotting of bone marrow cell lysates from 3 different rats (Rat Nr. 1, 2, and 3) using anti-cathepsin G (top) and anti-neutrophil elastase (NE, bottom) antibodies incubated with or without hAAT. The de novo formation of irreversible hAAT-protease complexes of about 75 kDa reveals that hAAT inhibits rat CatG and NE. (B) Rat bone marrow CatG and NE activities in the presence or absence of hAAT. Proteolytic activities in rat bone marrow cell lysates (Rat Nr. 1, 2, and 3) are significantly inhibited in presence of hAAT. Results represent two measurements for each rat.**

Sex-specific patterns play a major role in cardiac and vascular changes. Expression or abundance of sex hormone receptors in vascular smooth muscle differs between males and females, causing important variations in vascular function.[44] Female subjects are less susceptible to renal IR injury or delayed graft function after transplantation.[45] It is also clear that there are sex-related differences in the myocardial response to acute IR injury.[46] To distinguish the specific effects of IR injury in this study, additional factors, such as female cycle and related hormone profiles, were avoided and only male rats were used. Although good reasons exist to study males alone, sex-related differences in the effect of AAT inhibitor in brain-dead rats' vascular grafts submitted to IR injury need to be investigated in future studies.

This study has some limitations. First, it would have been more appropriate to use the left anterior descending coronary artery rather than the aorta. However, coronary arteries from rat could not be used due their small size in our setting. Despite that, the present model is a simple and reproducible to test pharmacological approaches to reduce IR injury in vascular grafts. Second, an *in vivo* vascular IR injury model is required as an *ex vivo* organ bath system does not involve nonaortic tissues, blood flow, and activation of leukocytes. Third, even though storage at 4°C for 24h does not follow clinical practice, it is a reliable standardized *in vitro* model for vascular IR injury with significant endothelial damage. Fourth, it would have been interesting to compare the effects of AAT with another serine protease inhibitor on vascular grafts of brain-dead rats against IR injury; however, we do not have evidence at this stage. Fifth, AAT in the preservation solution may penetrate more easily into aortic tissue than into a solid organ, such as the heart. Therefore, an experimental cardiac transplantation model is necessary to extrapolate the results of the present study. Finally, other mechanisms need to be considered that may play a role in the beneficial effect AAT has on vascular grafts after BD and IR injury.

## Conclusions

In summary, our findings support a novel antiapoptotic function of AAT in the aorta injured by BD and IR. AAT exposure was associated with an alleviation of endothelial dysfunction, associated with a preservation of an increase in caspase-3, caspase-8, and caspase-12 levels, and associated with a decreased DNA-breakage due to BD and IR injury. This is not the sole mechanism responsible for AAT-mediated protection against both BD and IR injury-induced endothelial dysfunction and requires further investigation. Currently, brain-dead donors constitute the major source of heart transplantation. However, BD may induce hemodynamic instability and neuroendocrine alterations, which may lead to post-transplant graft dysfunction. Additionally, myocardial IR injury at the time of transplantation leads to further impairments. Taken together, this can contribute to adverse short- and long-term graft outcomes in the recipients. As future potential application, further studies should investigate whether hypothermic preservation or perfusion of brain-dead donor hearts with AAT improves graft dysfunction in a preclinical model of cardiac transplantation. From the clinical point of view, if tissue damage caused by hypothermia in organ preservation and warm reperfusion could be prevented, higher protection would be obtained, and the risk of post-transplant organ dysfunction would be reduced.

## Author Contributions

Conception and design: BK, GS, SKI. Analysis and interpretation: QD, SL, AAS, SKI, RD. Data collection: QD, SL, PZ, SKI, RD. Writing the manuscript: SL, AAS, PB, TR, BK, MK, GS, SKI. Critical revision: QD, SL, AAS, PB, TR, BK, MK, GS, SKI. Approval of the manuscript: QD, SL, PZ, AAS, PB, TR, BK, MK, GS, SKI.

## Acknowledgments

The expert technical assistance of Patricia Kraft, Karin Sonnenberg, Lutz Hoffmann, and Tobias Mayer is gratefully acknowledged.

## Disclosure

None declared.

## Funding

This study was supported by the State of Baden-Württemberg, Germany, by the Medical Faculty of the University of Heidelberg, Germany (to S. Korkmaz-Icöz). Project no. NVKP_16-1–2016-0017 ('National Heart Program') has been implemented with the support provided from the National Research, Development and Innovation Fund of Hungary, financed under the NVKP_16 funding scheme. Project no. RRF-2.3.1-21-2022-00003 (National Cardiovascular Laboratory) has been implemented with the support provided by the European Union. TKP2021-EGA-23 has been implemented with the support provided by the Ministry of Innovation and Technology of Hungary from the National Research, Development and Innovation Fund, financed under the TKP2021-EGA funding scheme. This project was supported by a grant from the National Research, Development and Innovation Office (NKFIH) of Hungary (K134939 to T. Radovits).

## REFERENCES

1. Metra M, Ponikowski P, Dickstein K, et al. Advanced chronic heart failure: a position statement from the study group on advanced heart failure of the heart failure association of the European society of cardiology. *Eur J Heart Fail*. 2007;9:684–694.
2. Hollenberg SM, Klein LW, Parrillo JE, et al. Coronary endothelial dysfunction after heart transplantation predicts allograft vasculopathy and cardiac death. *Circulation*. 2001;104:3091–3096.
3. Szabo G, Buhmann V, Bahrle S, Vahl CF, Hagl S. Brain death impairs coronary endothelial function. *Transplantation*. 2002;73:1846–1848.
4. Smith M. Physiologic changes during brain stem death–lessons for management of the organ donor. *J Heart Lung Transpl*. 2004;23:S217–S222.
5. Bugge JF. Brain death and its implications for management of the potential organ donor. *Acta Anaesthesiol Scand*. 2009;53:1239–1250.
6. Kuznetsov AV, Javadov S, Margreiter R, Grimm M, Hagenbuchner J, Ausserlechner MJ. The role of mitochondria in the mechanisms of cardiac ischemia-reperfusion injury. *Antioxidants*. 2019;8:454.
7. Schofield ZV, Woodruff TM, Halai R, Wu MC, Cooper MA. Neutrophils–a key component of ischemia-reperfusion injury. *Shock*. 2013;40:463–470.
8. Eefting F, Rensing B, Wigman J, et al. Role of apoptosis in reperfusion injury. *Cardiovasc Res*. 2004;61:414–426.
9. Parolari A, Rubini P, Cannata A, et al. Endothelial damage during myocardial preservation and storage. *Ann Thorac Surg*. 2002;73:682–690.
10. Dickson I, Alper CA. Changes in serum proteinase inhibitor levels following bone surgery. *Clin Chim Acta*. 1974;54:381–385.
11. Carrell RW, Jeppsson JO, Laurell CB, et al. Structure and variation of human alpha 1-antitrypsin. *Nature*. 1982;298:329–334.
12. Hunt JM, Tuder R. Alpha 1 anti-trypsin: one protein, many functions. *Curr Mol Med*. 2012;12:827–835.
13. Korkmaz B, Horwitz MS, Jenne DE, Gauthier F. Neutrophil elastase, proteinase 3, and cathepsin G as therapeutic targets in human diseases. *Pharmacol Rev*. 2010;62:726–759.
14. Petrache I, Hajjar J, Campos M. Safety and efficacy of alpha-1-antitrypsin augmentation therapy in the treatment of patients with alpha-1-antitrypsin deficiency. *Biologics*. 2009;3:193–204.
15. Daemen MA, Heemskerk VH, van't Veer C, et al. Functional protection by acute phase proteins alpha(1)-acid glycoprotein and alpha(1)-antitrypsin against ischemia/reperfusion injury by preventing apoptosis and inflammation. *Circulation*. 2000;102:1420–1426.
16. Petrache I, Fijalkowska I, Medler TR, et al. alpha-1 antitrypsin inhibits caspase-3 activity, preventing lung endothelial cell apoptosis. *Am J Pathol*. 2006;169:1155–1166.
17. Bucurenci N, Blake DR, Chidwick K, Winyard PG. Inhibition of neutrophil superoxide production by human plasma alpha 1-antitrypsin. *FEBS Lett*. 1992;300:21–24.
18. Gao W, Zhao J, Kim H, et al. alpha1-Antitrypsin inhibits ischemia reperfusion-induced lung injury by reducing inflammatory response and cell death. *J Heart Lung Transpl*. 2014;33:309–315.
19. Gotzfried J, Smirnova NF, Morrone C, et al. Preservation with alpha1-antitrypsin improves primary graft function of murine lung transplants. *J Heart Lung Transpl*. 2018;35:913–921.
20. Maicas N, van der Vlag J, Bublitz J, et al. Human Alpha-1-Antitrypsin (hAAT) therapy reduces renal dysfunction and acute tubular necrosis in a murine model of bilateral kidney ischemia-reperfusion injury. *PLoS One*. 2017;12:e0168981.
21. Toldo S, Seropian IM, Mezzaroma E, et al. Alpha-1 antitrypsin inhibits caspase-1 and protects from acute myocardial ischemia-reperfusion injury. *J Mol Cell Cardiol*. 2011;51:244–251.
22. Treasure CB, Vita JA, Ganz P, et al. Loss of the coronary microvascular response to acetylcholine in cardiac transplant patients. *Circulation*. 1992;86:1156–1164.
23. Korkmaz-Icoz S, Zhou P, Guo Y, et al. Mesenchymal stem cell-derived conditioned medium protects vascular grafts of brain-dead rats against in vitro ischemia/reperfusion injury. *Stem Cell Res Ther*. 2021;12:144.
24. Veres G, Hegedus P, Barnucz E, et al. Addition of vardenafil into storage solution protects the endothelium in a hypoxia-reoxygenation model. *Eur J Vasc Endovasc Surg*. 2013;46:242–248.
25. Li S, Korkmaz S, Loganathan S, et al. Acute ethanol exposure increases the susceptibility of the donor hearts to ischemia/

reperfusion injury after transplantation in rats. *PLoS One*. 2012;7:e49237.
26. Korkmaz B, Attucci S, Juliano MA, et al. Measuring elastase, proteinase 3 and cathepsin G activities at the surface of human neutrophils with fluorescence resonance energy transfer substrates. *Nat Protoc*. 2008;3:991–1000.
27. Furchgott RF, Vanhoutte PM. Endothelium-derived relaxing and contracting factors. *Faseb J*. 1989;3:2007–2018.
28. Ignarro LJ, Buga GM, Wood KS, Byrns RE, Chaudhuri G. Endothelium-derived relaxing factor produced and released from artery and vein is nitric oxide. *Proc Natl Acad Sci USA*. 1987;84:9265–9269.
29. Moncada S, Gryglewski R, Bunting S, Vane JR. An enzyme isolated from arteries transforms prostaglandin endoperoxides to an unstable substance that inhibits platelet aggregation. *Nature*. 1976;263:663–665.
30. Griffith TM. Endothelium-dependent smooth muscle hyperpolarization: do gap junctions provide a unifying hypothesis? *Br J Pharmacol*. 2004;141:881–903.
31. Ahluwalia A, Hobbs AJ. Endothelium-derived C-type natriuretic peptide: more than just a hyperpolarizing factor. *Trends Pharmacol Sci*. 2005;26:162–167.
32. Stankevicius E, Kevelaitis E, Vainorius E, Simonsen U. [Role of nitric oxide and other endothelium-derived factors]. *Medicina (Kaunas)*. 2003;39:333–341.
33. Vargas F, Fernandez-Rivas A, Garcia Estan J, Garcia del Rio C. Endothelium-dependent and endothelium-independent vasodilation in hyperthyroid and hypothyroid rats. *Pharmacology*. 1995;51:308–314.
34. Kusaka M, Pratschke J, Wilhelm MJ, et al. Activation of inflammatory mediators in rat renal isografts by donor brain death. *Transplantation*. 2000;69:405–410.
35. Stiegler P, Sereinigg M, Puntschart A, et al. Oxidative stress and apoptosis in a pig model of brain death (BD) and living donation (LD). *J Transl Med*. 2013;11:244.
36. Konukoglu D, Uzun H. Endothelial dysfunction and hypertension. *Adv Exp Med Biol*. 2017;956:511–540.
37. Li S, Korkmaz-Icoz S, Radovits T, et al. Donor preconditioning after the onset of brain death with dopamine derivate n-octanoyl dopamine improves early posttransplant graft function in the rat. *Am J Transpl*. 2017;17:1802–1812.
38. Wilbring M, Tugtekin SM, Zatschler B, et al. Even short-time storage in physiological saline solution impairs endothelial vascular function of saphenous vein grafts. *Eur J Cardio Thorac Surg*. 2011;40:811–815.
39. Serban KA, Petrache I. Alpha-1 antitrypsin and lung cell apoptosis. *Ann Am Thorac Soc*. 2016;13(Suppl 2):S146–S149.
40. Zhang B, Lu Y, Campbell-Thompson M, et al. Alpha1-antitrypsin protects beta-cells from apoptosis. *Diabetes*. 2007;56:1316–1323.
41. Roll DE, Glew RH. Isolation and characterization of rat alpha-1-antitrypsin. *J Biol Chem*. 1981;256:8190–8196.
42. Hajjar E, Korkmaz B, Reuter N. Differences in the substrate binding sites of murine and human proteinase 3 and neutrophil elastase. *FEBS Lett*. 2007;581:5685–5690.
43. Kalupov T, Brillard-Bourdet M, Dade S, et al. Structural characterization of mouse neutrophil serine proteases and identification of their substrate specificities: relevance to mouse models of human inflammatory diseases. *J Biol Chem*. 2009;284:34084–34091.
44. Tamaya T, Wada K, Nakagawa M, et al. Sexual dimorphism of binding sites of testosterone and dihydrotestosterone in rabbit model. *Comp Biochem Physiol A Comp Physiol*. 1993;105:745–749.
45. Hosszu A, Fekete A, Szabo AJ. Sex differences in renal ischemia-reperfusion injury. *Am J Physiol Ren Physiol*. 2020;319:F149–F154.
46. Wang M, Baker L, Tsai BM, Meldrum KK, Meldrum DR. Sex differences in the myocardial inflammatory response to ischemia-reperfusion injury. *Am J Physiol Endocrinol Metab*. 2005;288:E321–E326.

# Annexe 5

Liu et al. Journal of Translational Medicine (2023) 21:799
https://doi.org/10.1186/s12967-023-04659-6

Journal of
Translational Medicine

RESEARCH Open Access

# Pharmacological inhibition of the cysteine protease cathepsin C improves graft function after heart transplantation in rats

Baoer Liu[1,2], Brice Korkmaz[3], Patricia Kraft[1], Tobias Mayer[1], Alex A. Sayour[4], Marc A. Grundl[5], Roxane Domain[3], Matthias Karck[1], Gábor Szabó[1,2] and Sevil Korkmaz-Icöz[1,2*]

## Abstract

**Background** Heart transplantation (HTX) is the standard treatment for end-stage heart failure. However, reperfusion following an ischemic period can contribute to myocardial injury. Neutrophil infiltration, along with the subsequent release of tissue-degrading neutrophil elastase (NE)-related serine proteases and oxygen-derived radicals, is associated with adverse graft outcomes. The inhibition of cathepsin C (CatC) has been shown to block NE-related protease activation. We hypothesized that the CatC inhibitor BI-9740 improves graft function after HTX.

**Methods** In a rat model of HTX, the recipient Lewis rats were orally administered with either a placebo (n = 12) or BI-9740 (n = 11, 20 mg/kg) once daily for 12 days. Donor hearts from untreated Lewis rats were explanted, preserved in a cardioplegic solution, and subsequently heterotopically implanted. In vivo left-ventricular (LV) graft function was assessed after 1 h of reperfusion. The proteolytic activity of neutrophil serine proteases was determined in bone marrow lysates from BI-9740-treated and control rats. Additionally, myocardial morphological changes were examined, and heart samples underwent immunohistochemistry and western blot analysis.

**Results** The NE-related proteolytic activity in bone marrow cell lysates was markedly decreased in the BI-9740-treated rats compared to those of the placebo group. Histopathological lesions, elevated CatC and myeloperoxidase-positive cell infiltration, and nitrotyrosine immunoreactivity with an increased number of poly(ADP-ribose) polymerase (PARP)-1-positive cells were lowered in the hearts of animals treated with BI-9740 compared to placebo groups. Regarding the functional parameters of the implanted graft, improvements were observed in both systolic function (LV systolic pressure 110 ± 6 vs 74 ± 6 mmHg; $dP/dt_{max}$ 2782 ± 149 vs 2076 ± 167 mmHg/s, LV developed pressure, at an intraventricular volume of 200 µl, $p < 0.05$) and diastolic function in the hearts of BI-9740 treated animals compared with those receiving the only placebo. Furthermore, the administration of BI-9740 resulted in a shorter graft re-beating time compared to the placebo group. However, this study did not provide evidence of DNA fragmentation, the generation of both superoxide anions and hydrogen peroxide, correlating with the absence of protein alterations related to apoptosis, as evidenced by western blot in grafts after HTX.

**Conclusions** We provided experimental evidence that pharmacological inhibition of CatC improves graft function following HTX in rats.

**Keywords** Heart transplantation, Ischemia, Reperfusion injury, Cathepsin C, Neutrophil elastase

*Correspondence:
Sevil Korkmaz-Icöz
korkmaz@uni-heidelberg.de
Full list of author information is available at the end of the article

© The Author(s) 2023. **Open Access** This article is licensed under a Creative Commons Attribution 4.0 International License, which permits use, sharing, adaptation, distribution and reproduction in any medium or format, as long as you give appropriate credit to the original author(s) and the source, provide a link to the Creative Commons licence, and indicate if changes were made. The images or other third party material in this article are included in the article's Creative Commons licence, unless indicated otherwise in a credit line to the material. If material is not included in the article's Creative Commons licence and your intended use is not permitted by statutory regulation or exceeds the permitted use, you will need to obtain permission directly from the copyright holder. To view a copy of this licence, visit http://creativecommons.org/licenses/by/4.0/. The Creative Commons Public Domain Dedication waiver (http://creativecommons.org/publicdomain/zero/1.0/) applies to the data made available in this article, unless otherwise stated in a credit line to the data.

## Background

Heart transplantation (HTX) is recognized as an optimal therapy for patients with end-stage heart diseases. However, ischemia/reperfusion (IR) injury during HTX is inevitable and associated with postoperative complications, such as graft dysfunction and reduced graft survival [1, 2]. Researchers have devoted significant effort to understand the underlying cellular and molecular mechanisms governing IR injury. Intracellular calcium accumulation, cardiac metabolic alterations, generation of reactive oxygen species (ROS), production of inflammatory cytokines, and activation of inflammatory cells have been suggested as major contributors to myocardial IR injury [3–7]. Besides macrophages, especially neutrophils [8], have been hypothesized to contribute to reperfusion injury by acting as early responders to inflammatory stimuli. They increase proteolytic activity at the site of inflammation via release of pro-inflammatory proteases, in addition to increasing ROS activity.

Pro-inflammatory neutrophil serine proteases (NSPs), including neutrophil elastase (NE), proteinase 3, cathepsin G (CatG), and the recently discovered NSP4, are initially synthesized as inactive zymogens [9, 10] that are converted into their mature active form by cathepsin C (CatC, also known as dipeptidyl peptidase I (DPPI)) within neutrophil progenitor cells before the mature neutrophils are released from the bone marrow into circulation [11, 12]. Under physiological conditions, these mature NSPs play important roles in both intracellular and extracellular bacteria killing, as well as the regulation of inflammatory processes [13, 14]. However, under pathological conditions, data indicates they can contribute to chronic inflammatory diseases, auto-immune diseases, and cancer [9, 10, 15], when massive release of active NSPs is not counterbalanced and regulated by the presence of endogenous serine protease inhibitors [10]. In order to inhibit the activation of these NSPs during neutrophil maturation, hence reducing the overall release of proteolytically active NSPs at the site of inflammation and re-establishing a balanced protease-antiprotease environment, CatC inhibitors have been investigated. As a result, several small molecule inhibitors of CatC are currently undergoing preclinical and clinical trials to evaluate their efficacy in several indications [9, 15, 16]. We investigated a novel concept in our rat model of heterotopic HTX by targeting the uncontrolled NSPs through direct inhibition of their activation via the enzyme CatC [10]. This study aimed to explore the impact of NSPs' activity on IR injury.

Based on these findings, we hypothesized that administering the novel nitrile CatC inhibitor, BI-9740, to the heart transplant recipients improves left-ventricular (LV) graft function in a rat model of HTX.

## Methods

### Animals

Male Lewis rats weighing 250–300 g (Janvier Labs, Saint Berthevin, France) were housed at a constant temperature of 20–24 ℃ with a 12-h of light/dark cycles and were acclimatized for at least 1 week. Standard laboratory rodent diet and water were supplied ad libitum. All animals received human care in consistency with the "Principles of Laboratory Animal Care" defined by the National Society for Medical Research, as well as the "Guide for the Care and Use of Laboratory Animals" arranged by the Institute of Laboratory Animal Resources and distributed by the National Institutes of Health (NIH Publication, 8th Edition, 2011). Approval for animal experimentation was granted by the Ethical Committee of the Regional Council of Karlsruhe, Germany (G257/20).

### Preparation of CatC Inhibitor BI-9740

The small molecule CatC inhibitor BI-9740, obtained for free via Boehringer-Ingelheim Pharma's (Ingelheim am Rhein, Germany) open innovation portal OpnMe (https://opnme.com), was dissolved in a solution containing 0.5% Natrosol™ 250 HX Pharm (Pharmacy of the University Hospital Heidelberg, Germany) and 0.015% Tween-80 (Merck KGaA, Darmstadt, Germany). This vehicle solution was generated and employed in line with the standard protocol used for pharmacodynamics and pharmacokinetic studies with BI-9740 at Boehringer-Ingelheim. Briefly, the vehicle solution was added to the weighted BI-9740 compound and vortexed. Gradually, hydrochloric acid was introduced to adjust the pH value to 4.0 while stirring. This mixture was vortexed and sonicated until a clear solution was obtained and stored at room temperature in the dark for a maximum of 3 days. The concentration of the stock solutions was 2 mg/ml.

In mice, BI-9740 inhibits CatC with an $IC_{50}$ (half-maximal inhibitory concentration) of 0.6 nM, while rats exhibited a value of 2.6 nM (~ fourfold difference). Mice displayed a plasma protein binding rate of 97.7%, whereas rats showed 99.9%, a difference of ~ 20 fold regarding the unbound concentration of BI-9740. In an efficacy model in mice, administration of BI-9740 led to a reduction of NE activity by 91%, proteinase 3 by 97%, and CatG by 100% at a dosage of 0.5 mg/kg. Considering this in vivo activity in mice, the very similar reported oral bioavailability of BI-9740 in mouse and rats, as well as the aforementioned species difference in potency of fourfold between and a difference of 20 fold in free, not plasma bound concentration, we in first approximation assumed that a dose of 20 mg/kg in rats should be sufficient to lead to a significant level of CatC and hence NSP inhibition in rats comparable to the 0.5 mg/kg does in mice. Detailed data on the structure, potency, and plasma protein

binding is available at https://opnme.com/molecules/cathepsin-c-inhibitor-bi-9740.

### Heterotopic HTX model

#### *Experimental groups*

The animals were randomly divided into three groups. The recipient rats were administered with either BI-9740 (HTX + BI-9740 group, n = 11; 20 mg/kg body weight and administration volume: 1 ml/100 g body weight) or an equal volume of 0.5% Natrosol™ 250 HX Pharm vehicle (HTX group, n = 12) once daily for 12 days prior to transplantation. In the control group (n = 10), rats neither received treatment nor underwent transplantation.

#### *Heterotopic HTX in rats*

The model was established as previously described [17]. Briefly, donor Lewis rats were anesthetized with 3% isoflurane gas in a chamber, and maintained with inhalation from a connected tube with 1.75–2.5% in $O_2$, and heparinized (400 IU/kg). Custodiol solution (Dr. Franz Köhler, Chemie GmbH, Bensheim, Germany) was used to induce cardiac arrest and to preserve the explanted heart at 4 °C. On day 13, recipient Lewis rats were anesthetized and heparinized, as described above. The donor heart's aorta was anastomosed to the recipient's abdominal aorta, and the pulmonary artery was anastomosed to the inferior vena cava. The duration of cold ischemia is standardized to 60 min, including both explantation and preservation time, followed by 30 min of implantation. Blood reperfusion was standardized to 60 min and the re-beating time (time to restoration of heartbeat) was also recorded. Additionally, the graft survival rate (i.e. a functioning graft at the time of cardiac function measurement) was calculated.

#### *Post-transplant graft function measurements*

Graft function was measured in vivo 60 min after reperfusion, as we previously described [17]. A 3F balloon catheter (Dispomedica, Hamburg, Germany) and a 2F Millar microprobe pressure catheter (SPR-320NR, Millar Instruments, Houston, TX, USA) were inserted into the left ventricle via the apex. The intraventricular volume was determined using the volume of the deflated balloon (0.02 ml) plus the volume of saline injected into the balloon, with 0.03 ml added each time from 0 to 0.18 ml, resulting in a gradual increase of the final intraventricular volume from 0.02 to 0.20 ml. LV systolic pressure (LVSP), the maximal rate of rise of LV pressure ($dP/dt_{max}$) and the maximum rate of fall of LV pressure ($dP/dt_{min}$) were measured at different LV volumes. Following the hemodynamic measurements, all rats were humanely sacrificed under anesthesia by bleeding. Subsequently, the transplanted hearts were excised for further analysis. At the end of the study, the rat cadavers were placed in a −20 °C freezer for preservation and later transferred to the designated animal carcass processing facility.

### Measurement of selective NE and CatG proteolytic activities

Rat NE and CatG activities in bone marrow lysates from BI-9740-treated and control rats were measured spectrofluorometrically (Ex: 320 nm and Em: 420 nm) using Abz-peptidyl-EDDnp fluorescence resonance energy transfer substrates, as described previously [18]. Briefly, bone-marrow cells were lysed on ice and the soluble fractions were separated from cell debris by centrifugation. NE activity (10 µg of total proteins) was measured with or without human alpha-1 antitrypsin (Sigma-Aldrich, SRP6312) (5 µM, 1 h at 37 °C, in HEPES 50 mM, NaCl 0.75 M, NP40 0.05%, pH 7.4) using Abz-APQQIMDDQ-EDDnp (20 µM) as substrate. CatG activity (0.5 µg of total proteins) was measured with or without human AAT (5 µM, 1 h at 37 °C, in HEPES 50 mM, NaCl 100 mM, NP40 0.05%, pH 7.4) using Abz-TPFSGQ-EDDnp (20 µM) as substrate.

### Histological process

Upon completion of functional measurements, the transplanted heart samples were immediately explanted, fixed in a buffered paraformaldehyde solution (4%), embedded in paraffin, and cut using a microtome. Then, 4-µm thick sections were placed onto adhesive slides. These samples were stained with hematoxylin and eosin (HE) for histopathological examination. Immunohistochemical staining was performed for nitrotyrosine (1:1000; Ab7048, Abcam, Berlin, Germany), MPO (1:100, Abcam, Berlin, Germany), poly(ADP-ribose) polymerase (PARP)-1 (1:1000, Abcam, Berlin, Germany) and CatC (1:300, Santa Cruz Biotechnology, Inc., Heidelberg, Germany). The presence of ROS was determined in situ using the oxidative fluorescent dye dihydroethidium [19]. To detect DNA strand breaks, the Terminal deoxynucleotidyl transferase-mediated dUTP nick-end labeling (TUNEL) assay was performed, as we previously described [20].

### Quantification of immunohistochemical staining

HE staining was used to examine the morphology of myocardial tissue. The number of MPO-, CatC-, PARP-1, and TUNEL-positive cells were counted. The quantification of MPO-positive cells was based on the total numbers of MPO-positive cells, whereas CatC-, PARP-1, and TUNEL-positive cells were expressed as a percentage over the total cell count. Quantitative evaluation was performed using Image J software (NIH, Maryland, USA). A semi-quantitative evaluation of nitrotyrosine expression was conducted by assessing both the staining intensity

(with 0 indicating absolute negativity, 1 for low positivity, 2 for medium positivity and 3 for high positivity) and the number of the labeled target protein (with 0 for negative, 1 for 1–5, 2 for 6–10, 3 for 11–15, 4 for greater than 15). The total score for each field was calculated by multiplying the intensity score by the area score (0–12). The fluorescence intensity score (ranging from 0 to 3) within myocardial sections stained with dihydroethidium was visualized using a fluorescence microscope (Olympus Model BX51, Japan). The evaluation was performed in a blinded manner, with randomly selected non-overlapping fields per myocardium per rat.

### Sodium dodecyl sulfate (SDS)—polyacrylamide gel electrophoresis (PAGE) and immunoblotting analysis

Bone marrow lysates were separated on a 12% SDS-PAGE in reducing/denaturing conditions (50 µg of protein/lane) and blotted onto nitrocellulose membranes. The membranes were then saturated with phosphate-buffered saline (PBS), 0.1% Tween, 5% nonfat milk and incubated with NE-antibody (1:800 diluted in PBS, 0.1% Tween, 5% nonfat milk) overnight at 4 °C. Following this, the membranes were washed 3 times in PBS, 0.1% Tween and then incubated for 1.5 h with a peroxidasecoupled secondary antibody (anti-rabbit IgG-horseradish peroxidase, Jackson ImmunoResearch, 111-035-003) diluted 1:5000 in PBS, 0.1% Tween and 5% nonfat milk. The membranes were washed again as previously described, and the detection was performed using the Enhanced Chemiluminescence system (Cytiva, RPN2232). The same membranes were stripped using hydrogen peroxide 35% for 20 min at 37 °C and immunoblotting was performed using an anti-myeloperoxidase antibody (MPO) (Santa Cruz, sc-16128-R) (1:1000 diluted in PBS, 0.1% Tween, 5% nonfat milk) in the same conditions as before. Densitometry was performed using ImageJ software and the NE/MPO ratio was analyzed.

Proteins were extracted from the myocardial tissue in RIPA buffer (Melford, Ipswich, UK). The protein concentration was determined using the Pierce™ BCA Protein Assay Kit (Thermo Fisher Scientific, Karlsruhe, Germany). Total protein homogenates 20 µg/30 µl were denatured, separated on SDS-PAGE electrophoresis gels, and subsequently transferred onto a polyvinylidene fluoride membrane (Millipore, Darmstadt, Germany). The membrane was blocked with 5% bovine serum albumin (BSA) in Tris-buffered saline (TBS) containing Tween 20 for 1 h, followed by overnight incubation at 4 °C with caspase-3 antibody (1:1000 in 2,5% BSA/TBS-Tween, abcam Cambridge, UK), bcl-2 (1:1000 in 2,5% BSA/TBS-Tween, abcam Cambridge, UK) and bax (1:1000 in 2,5% BSA/TBS-Tween, abcam Cambridge, UK). After washing the blots to remove excessive binding of the primary antibody, the blots were incubated for 1 h with a horseradish peroxidase-conjugated secondary antibody at room temperature. Glyceraldehyde-3-phosphate dehydrogenase (GAPDH) and beta-actin, housekeeping proteins, were used as loading controls and for protein normalization. The immunoreactive protein bands were developed using the Enhanced Chemiluminescence system (PerkinElmer, Rodgau-Juegesheim, Germany). The intensity of the immunoblot bands was detected using a Chemismart 5100.

### Statistical analysis

Data are expressed as mean ± standard error of the mean (SEM). Statistical analyses were conducted using SPSS version 24 (IBM SPSS Statistics, New York, USA). The normality of data distribution was assessed using the Shapiro–Wilk normality test. In cases where the data exhibited a normal distribution, the two-sample student t-test was employed to examine the differences between the two groups. If the assumption of normality was not met, a nonparametric Mann–Whitney test was utilized. For graft function measurements, including LVSP, developed pressure, $dP/dt_{max}$, rate pressure product, and $dP/dt_{min}$, a two-factor mixed analysis of variance (ANOVA) and Tukey's post-hoc test were carried out for multiple comparisons. To detect differences among the three experimental groups, a one-way ANOVA and Tukey's post-hoc-test were conducted. If the data did not pass the normality test, the nonparametric Kruskal–Wallis test followed by Dunn's post-hoc-test was used. A $p < 0.05$ was considered statistically significant.

## Results

### Effect of prolonged BI-9740 administration on body weight and NSP activity

Oral administration of BI-9740 at a dose of 20 mg/kg body weight for a duration of 12 days did not have any effect on the body weight when compared to the placebo-treated animals (312 ± 3.3 g vs 311 ± 5 g, $p > 0.05$). As the pharmacological blockade of CatC should occur in the bone marrow, blood and bone-marrow exposure to BI-9740 after 12 days of treatment was assessed. The proteolytic activity of two major NSPs was determined in bone marrow lysates from BI-9740- and placebo-treated rats. Our results showed that BI-9740 treatment significantly reduced the activity of NE and CatG (by 42 ± 2% for NE, 54 ± 4% for CatG, all $p < 0.0001$) in comparison to the placebo group (Fig. 1A). Furthermore, Western blotting showed reduced NE protein (by 46 ± 5%, $p = 0.0015$) in the BI-9740-treated rats compared to the placebo rats (Fig. 1B). Thus, 12 days of BI-9740 administration were well-tolerated without obvious adverse events, did not

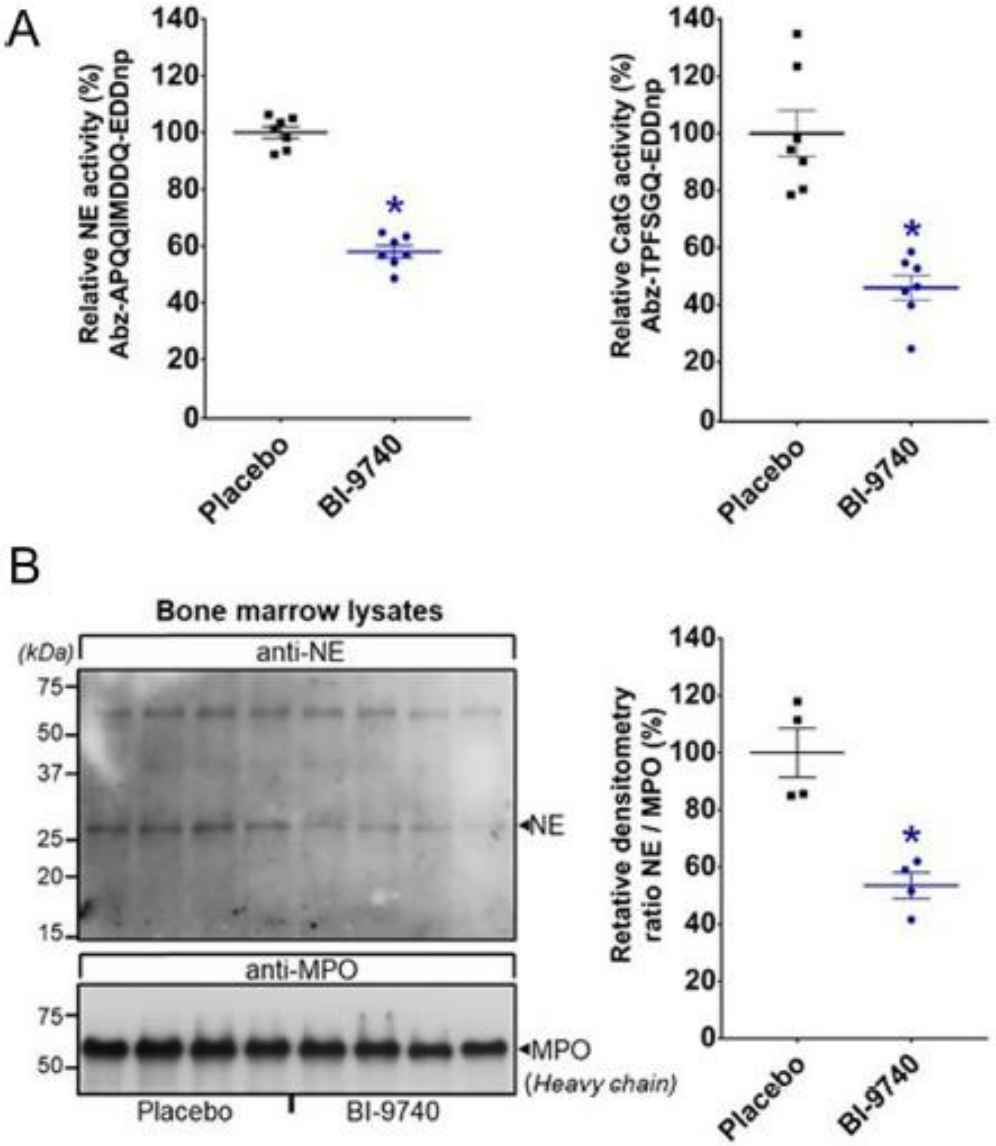


**Fig. 1** Effect of BI-9740 on bone marrow neutrophil serine protease activation. **A** Activities of neutrophil elastase (NE) and cathepsin G (CatG) and **B** Western blotting analysis of NE in bone marrows from placebo and BI-9740-treated rats. The upper blot was incubated with anti-NE, and the lower blot was incubated with anti-myeloperoxidase (MPO) for use as the loading control. Values are presented as mean ± SEM. *$p < 0.05$ vs. placebo

induce any wasting, and significantly reduced bone-marrow NSP proteolytic activities.

### Effect of BI-9740 administration on myocardial morphology after HTX

In the HE staining images, nuclei are stained blue, cytoplasm is stained red, and collagen fibers display varying shades of red. In the control group, the morphology of the myocardial tissue was normal (Fig. 2A). Cardiomyocytes are orderly and closely arranged, with a small intercellular space, and no edema is present between cells (Fig. 2A). In contrast, the HTX group showed disorganization of myofibers, which is related to a dense infiltration of inflammatory cells and interstitial edema (Fig. 2A). BI-9740 treatment exhibited reduced irregularly arranged fiber, decreased inflammatory infiltrate, and less edema in the grafts after HTX (Fig. 2A). Figure 2B illustrates the effect of

A

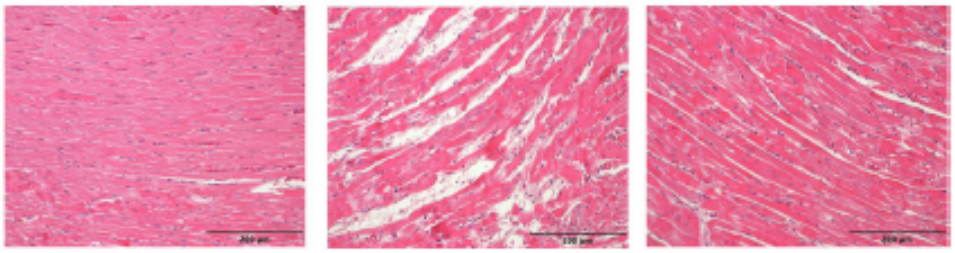


B

| Groups | Edema | Irregular myocardial fiber | Inflammatory infiltrate | Enlarged intracellular space |
|---|---|---|---|---|
| Control | A | A | A | A |
| HTX | +++ | ++ | +++ | ++ |
| HTX+BI | ++ | + | ++ | ++ |

**Fig. 2** Effect of BI-9740 (BI) on myocardial morphology in grafts after heart transplantation (HTX). **A** Representative images of hematoxylin and eosin (HE) staining (×200, scale bar: 200 μm) on cardiac tissue samples from the control group (41 pictures from 7 rats), HTX group (66 pictures from 11 rats) and HTX + BI group (44 pictures from 8 rats). In the HE staining images, nuclei are stained blue, cytoplasm is stained red, and collagen fibers display varying shades of red. **B** The degree of histopathological changes was assessed by examiners who were blinded to the experimental groups. The evaluation was conducted across 3–8 randomly selected, non-overlapping fields within each rat's myocardial tissue. A indicates no changes; +, mild changes; + +, moderate changes; and + + +, marked changes

BI-9740 on the extent of histological changes in myocardial tissues.

### Effect of BI-9740 on CatC, MPO, nitrotyrosine and PARP-1 immunoreactivity after HTX

Immunohistochemical analysis revealed an increase in the number of myocardial CatC-positive cells after HTX compared to control hearts. This increase was significantly decreased by BI-9740 treatment (Fig. 3A). When the cells were counted, an elevation in the number of MPO-positive cells was found in the graft after HTX, indicating infiltrating neutrophils, which was significantly decreased by BI-9740 administration (Fig. 3B). Additionally, the increased immunoreactivity of nitrotyrosine, a biomarker of peroxynitrite, and the increased PARP-1-positive cells, an indicator of apoptotic responses, in the HTX hearts were significantly attenuated by BI-9740 administration (Fig. 4A, B). Therefore, 12 days of BI-9740 treatment was shown to decrease myocardial neutrophil infiltration and nitro-oxidative stress with a decrease in the number of PARP-1-positive cells.

### Effect of BI-9740 on ROS generation and DNA strand breaks after HTX

We have performed dihydroethidium staining to identify ROS generation and TUNEL assay to detect DNA strand breaks. The generation of both superoxide anion and hydrogen peroxide was found to be similar among all the experimental groups (Additional file 1: Figure S1A). Furthermore, quantification of TUNEL-positive nuclei revealed no significant difference among the groups (Additional file 1: Figure S1B).

### Effect of BI-9740 on protein expression of Bax, Bcl-2 and caspase-3 after HTX

Since oxidative stress induces apoptosis, we evaluated the effect of BI-9740 on Bax and Bcl-2 levels, as well as procaspase-3 cleavage, which serves as an indicator of procaspase-3 activation. Consistent with the results from ROS generation and TUNEL assay experiments, our Western blot and densitometric analysis of these tested proteins did not reveal significant differences among the groups (Fig. 5).

### Effect of BI-9740 on heart rate and re-beating time after HTX

Treatment did not affect the baseline heart rate values between HTX + BI-9740 and HTX groups (216 ± 13 vs 239 ± 13 beats/min, $p > 0.05$). However, administration of BI-9740 to the recipient rats was associated with a significant shortening in graft re-beating time after reperfusion compared to the placebo group (first beat: 14.6 ± 1.6 s vs.

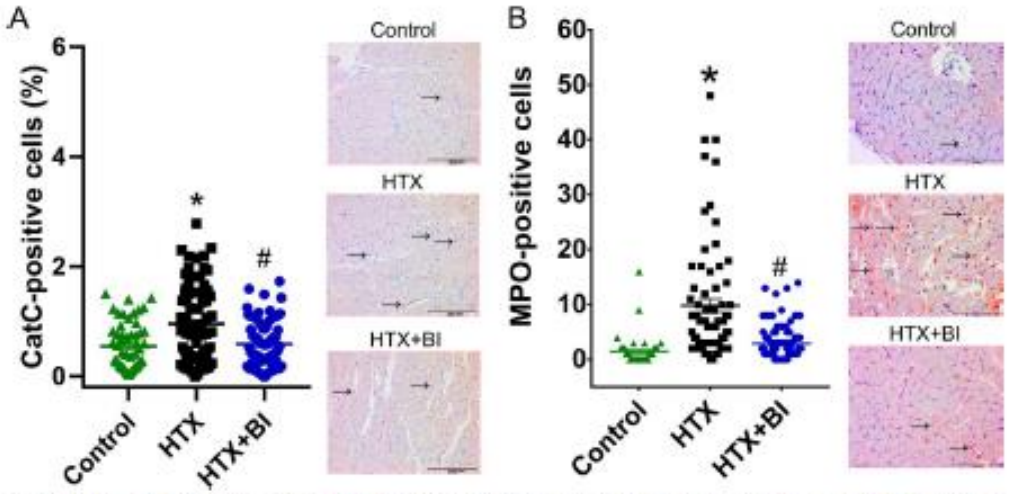


**Fig. 3** Effect of BI-9740 (BI) on cathepsin C (CatC) and myeloperoxidase (MPO) expression in grafts after heart transplantation (HTX). Representative images of **A** CatC (× 200, scale bar: 200 µm) and **B** MPO (× 400, scale bar: 100 µm) immunostaining followed by quantification based on the percentage of CatC-positive cells over the total cell count (control: 56 pictures from 7 rats; HTX: 80 pictures from 10 rats; HTX + BI: 76 pictures from 10 rats) and the total number of MPO-positive cells in the tissue section (control: 47 pictures from 6 rats; HTX: 72 pictures from 9 rats; HTX + BI: 88 pictures from 11 rats). The samples were assessed by two examiners who were blinded to the experimental groups. The evaluation was carried out on 4–8 randomly selected non-overlapping fields within each rat's myocardial tissue. Values are expressed as mean ± SEM and correspond to the mean of all pictures. $^{*}p < 0.05$ vs. control, $^{\#}p < 0.05$ vs HTX

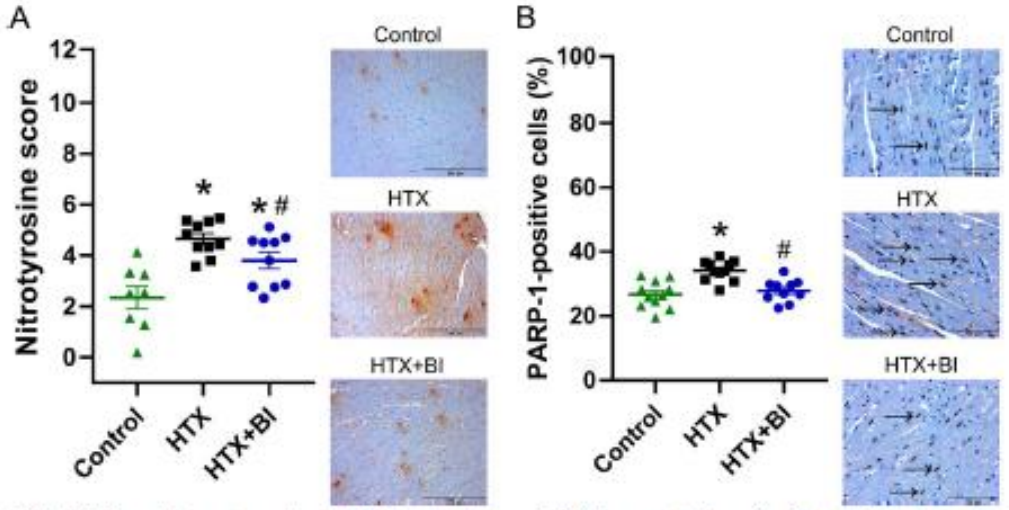


**Fig. 4** Effect of BI-9740 (BI) on nitrotyrosine and poly(ADP-ribose) polymerase (PARP)-1 expression in grafts after heart transplantation (HTX). Representative images of **A** nitrotyrosine (× 100, scale bar: 500 µm) and **B** PARP-1 (× 400, scale bar: 100 µm) immunostaining are shown, along with semi-quantitative analysis of nitrotyrosine immunoreactivity (control: 8 rats, HTX: 10 rats, HTX + BI: 10 rats) and quantification of PARP-1-positive cells (control: 10 rats, HTX: 11 rats, HTX + BI: 10 rats). The samples were assessed by two examiners who were blinded to the experimental groups. The evaluation was conducted on 4–8 randomly selected non-overlapping fields per rat's myocardial tissue. Values are expressed as mean ± SEM. $^{*}p < 0.05$ vs. control, $^{\#}p < 0.05$ vs HTX

21.7 ± 2.8 s and regular beating: 29.5 ± 1.8 s vs. 43.7 ± 3.5 s, $p < 0.05$). Additionally, the graft survival rate (i.e. a functioning graft at the time of cardiac function measurement) was 100% in both the HTX and HTX + BI-9740 groups.

### Effect of BI-9740 on graft function after HTX

In the implanted graft, LV post-transplant systolic function was significantly improved, as evidenced by increased LVSP, developed pressure, and $dP/dt_{max}$ (Fig. 6A–C). Moreover, the rate pressure product, a

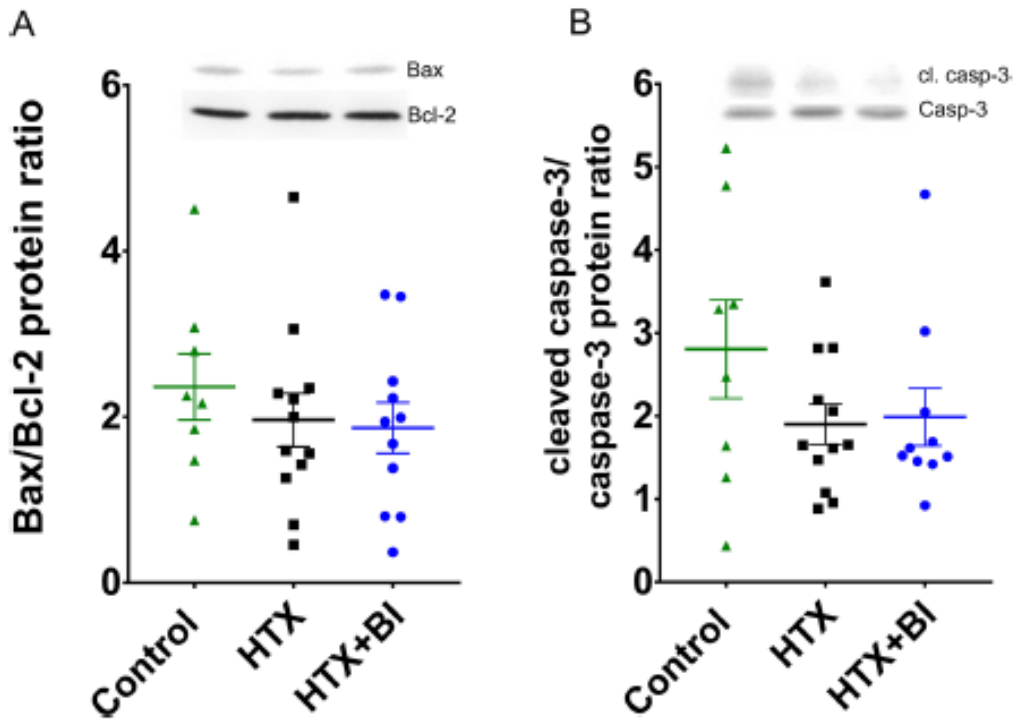


**Fig. 5** Effect of BI-9740 on protein expression of bcl-2, bax, and caspase-3 (casp-3) in grafts after heart transplantation (HTX). Quantification of the protein bands showing **A** bax-to-bcl-2 ratio, and **B** cleaved (cl.) caspase-3-to-caspase-3 ratio. Values are expressed as mean ± SEM

reliable direct indicator of myocardial oxygen demand, was significantly higher in the BI-9740 hearts compared to the placebo group (Fig. 6D). Active myocardial relaxation, evaluated by $dP/dt_{min}$, was also significantly improved with BI-9740 treatment as compared to the placebo group (Fig. 6E).

## Discussion

The purpose of this study was to examine the effects of recipient treatment with a chemical nitrile CatC inhibitor in a rat model of HTX. To the best of our knowledge, this is the first piece of work to suggest that inhibiting CatC with BI-9740 results in diminished major NSP proteolytic activities, ameliorated histopathological changes, reduced neutrophil infiltration, and lowered nitro-oxidative stress in the myocardium with a decrease in the number of the PARP-1-positive cells. Subsequently, this leads to an improved functional recovery of grafts after cardioplegic arrest, followed by ex vivo hypothermic storage and in vivo myocardial blood reperfusion.

Currently, the hearts of brain-dead donors are the major source for HTX. However, brain death is associated with systemic inflammation leading to worse graft outcomes. To distinguish the specific effects of brain death and IR injury, we avoided additional factors that could influence our hypothesis. After short periods of cold ischemia (30 min, 1 h, 1.5 h) reperfusion in rat cardiac allografts results in a significant increase in superoxide production, cardiomyocyte apoptosis, and inflammatory response [21]. Rapid recovery of myocardial function plays a crucial role in determining long-term outcomes because severe hemodynamic changes take place during the early phase following HTX. Therefore, in the present study, the cold ischemia time has been fixed to 1 h and graft function was evaluated 1 h after warm blood reperfusion [17].

Primary graft failure, a frequent complication occurring in the immediate post-operative period, continues to be the main cause of death within the first 30 days after HTX [22]. Given these observations, potential therapeutic strategies are required to protect the grafts by treating the recipients, subsequently improving patient outcomes. The data on the underlying biology associated with primary graft failure, especially the NSP angle, overlaps with the biological profile of CatC inhibitors currently under investigation in the clinic for the inflammatory pulmonary disease non-cystic fibrosis bronchiectasis. Two CatC inhibitors, Brensocatib (Phase 3; ClinicalTrials.gov Identifier: NCT04594369) [23] and BI 1291583 (Phase 2; ClinicalTrials.gov Identifier: NCT05238675), are presently in clinical trials for this indication. In addition, some preclinical results

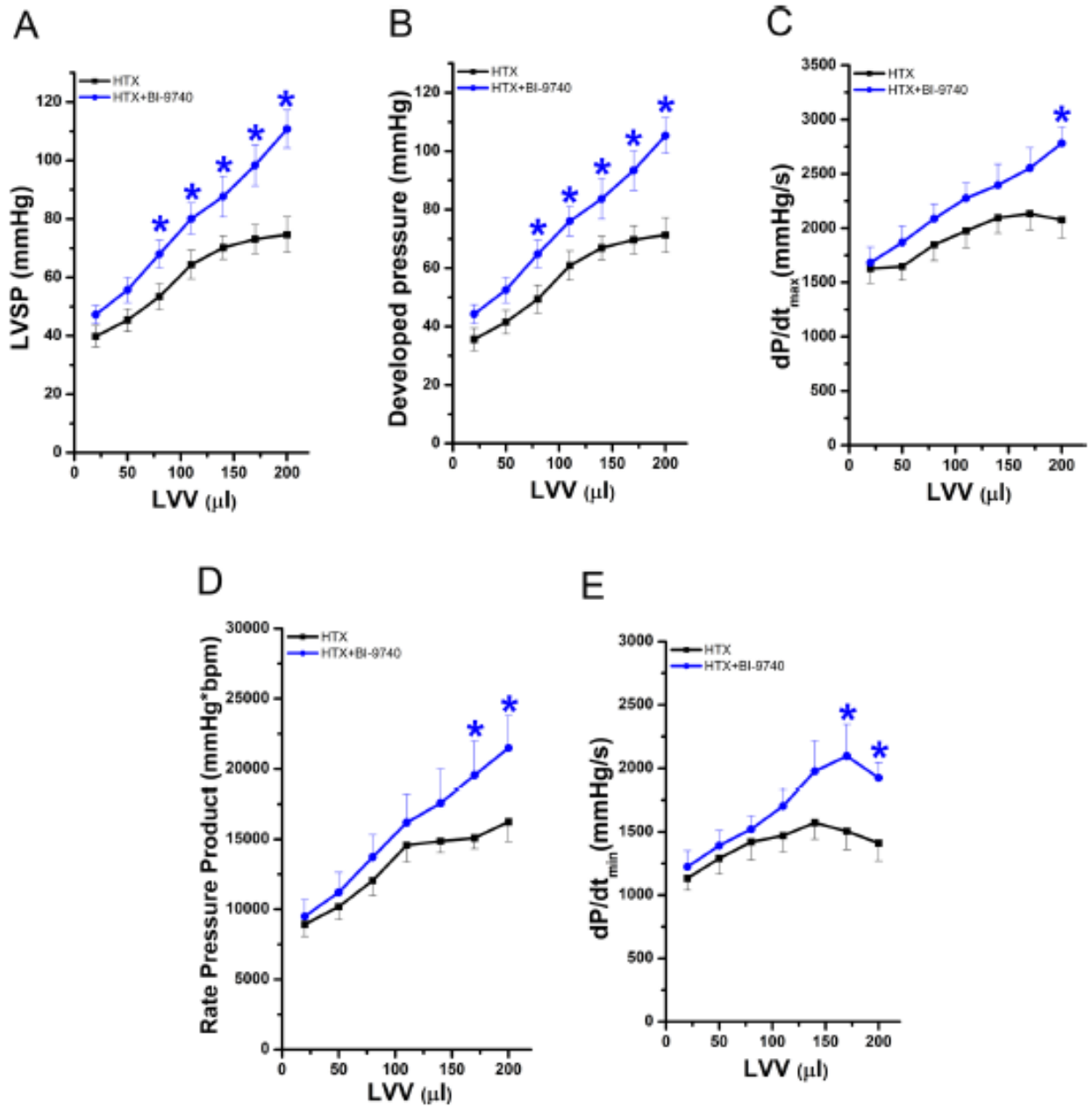


**Fig. 6** Effect of BI-9740 on left-ventricular (LV) graft function after heart transplantation (HTX). **A** Left-ventricular systolic pressure (LVSP), **B** developed pressure, **C** maximal slope of systolic pressure increment ($dP/dt_{max}$), **D** rate pressure product, and **E** maximal slope of diastolic pressure decrement ($dP/dt_{min}$) were measured at different LV volumes. Values are expressed as mean ± SEM. *$p < 0.05$ vs. HTX. n = 11–12 rats/group

indicate the benefits of CatC inhibition, opening avenues toward drug repurposing strategies. The findings of Jerke et al. using BI-9740 encourage clinical studies involving adjunctive CatC inhibitor administration in patients with proteinase 3-ANCA vasculitis [24]. Xiao et al. showed that the systemic administration of Brensocatib effectively inhibited breast cancer lung metastasis in a mouse model [16]. Chen et al. showed that the small molecule inhibitor SF38 inhibited CatC activity in the bone marrow and blood, decreased the activation of NSPs, and exhibited anti-inflammatory activity in an animal model of acute lung injury [25]. A recent study showed that the downregulation of CatC improved HUVEC viability and enhanced antiapoptotic capacity, anti-oxidative capability, invasive ability, as well as the angiogenic potential of hypoxia/reoxygenation-stimulated human umbilical vein

endothelial cells (HUVECs) [26]. This improvement was achieved by repressing the p38 mitogen activated protein kinase (MAPK)/nuclear factor-kappaB (NF-κB) pathway, suggesting a novel promising approach for preeclampsia therapies [26]. In a preclinical murine lung transplant model, the administration of CatC inhibitor to recipients alleviated early primary post-transplant graft dysfunction [27]. These findings together strongly suggest other applications of CatC inhibitors besides non-cystic fibrosis bronchiectasis and make them excellent drug candidates for organ transplantation as well. In our heterotopic transplant rat model, we showed that global IR injury leads to myofiber disorganization, which is related to a dense infiltration of inflammatory cells and interstitial edema. Treatment with BI-9740 resulted in reduced irregular fiber arrangement, decreased inflammatory infiltrates, and less edema. Additionally, the increased number of CatC positive cells in the transplanted heart was reduced by the inhibition of CatC. Administering BI-9740 for 12 days did not induce a loss of body weight, a parameter used for safety assessment, and had no effect on baseline heart rate values compared to rats treated with a placebo.

The over-activation of PARP is involved in various types of tissue injury, including systemic inflammation and IR injury [28]. During IR injury, DNA-strand breaks caused by ROS and reactive nitrogen species lead to PARP-1 activation. Excessive activation of PARP-1 can contribute to tissue injury by driving the cell into an energy crisis [29] and cell dysfunction, and by catalyzing the activation of pro-inflammatory pathways. It is recognized that CatC inhibitors have significant anti-inflammatory properties. MPO is a lysosomal enzyme mainly stored in the azurophilic granules neutrophils. It has been previously shown that pharmacological CatC inhibition does not affect MPO activity [24]. Therefore, MPO can be used as a surrogate marker for neutrophil infiltration. Our data showed that neutrophil infiltration into myocardial tissues, as evidenced by MPO-positive cells, was decreased by BI-9740 in grafts. We previously showed PARP over-activation contributes to reperfusion injury and its pharmacological inhibition prevents PARP activation, improves myocardial contractility/relaxation, coronary blood flow, and endothelial function in the transplanted heart [30]. However, this work did not yield evidence of DNA fragmentation/DNA strand breaks, nor the generation of both superoxide anions and hydrogen peroxide. The absence of ROS generation, as indicated by dihydroethidium fluorescence staining, correlates with a lack of significant protein alterations related to apoptosis, as demonstrated by western blot, and the absence of DNA damage, as evidenced by the TUNEL assay. In the present study, immunohistochemistry revealed an increased expression of nitrotyrosine, an indicator of nitrosative stress, with an increase in the number of PARP-1-positive cells in the transplanted hearts, both of which were reduced by CatC inhibition. Our functional analysis demonstrated that systolic function (evidenced by increased LVSP, developed pressure, and $dP/dt_{max}$) and myocardial relaxation (shown by increased $dP/dt_{min}$) were improved, and rate pressure product was increased by BI-9740 treatment compared to the placebo group.

From a clinical perspective, if an efficient anti-proteolytic therapy up-steam of elastase-related serine proteases by blocking their maturing enzyme CatC [10] could also be demonstrated in experimental models of myocardial global IR injury, this could open a new medical use for available drugs in treating high-risk patients categorized as high priority on the HTX waiting list. Both the 24-week Phase 2 Trial [23] and the ongoing Phase 3 Trial with Brensocatib encourage the use of CatC inhibitors in clinical practice. Importantly, it should be noted that the multiple highly redundant mechanisms of neutrophil defense responses are generally not impaired by CatC inhibitor treatment [9, 31].

In our ongoing research involving pharmacological CatC inhibition in HTX, we focused on questions that could not be addressed in the current model set-up. Firstly, the heterotopic abdominal rat HTX model was selected as appropriate for assessing global IR injury. However, the left ventricle beats in an unloaded condition, leading to a faster recovery following IR injury, making it unsuitable for studying long-term effects. Secondly, the study did not examine the structure and function of the right ventricle. Thirdly, the experiment used an isoimmune model to explore IR independently from acute rejection, so the potential adverse effects of alloimmune reactions resulting from HTX were not investigated. Fourth, only one dose of 20 mg/kg was tested. Lastly, while the measurement of graft function study did not incorporate a non-ischemic heart transplant group, such a group was, however, included in the immunohistochemistry and western blot experiments. Despite these limitations, CatC inhibitors offer great promise for the future heart surgery patients.

## Conclusion

Pharmacological inhibition of CatC decreases NE and CatG activities, ameliorates histopathological changes, reduces myocardial neutrophil infiltration and nitro-oxidative stress with a decrease in the number of PARP-1-positive cells. Consequently, it results in an improvement in the LV graft function after HTX in rats. The clinical relevance of our findings should be further carefully evaluated.

**Abbreviations**

| | |
|---|---|
| BCA | Bicinchoninic acid |
| BSA | Bovine serum albumin |
| CatC | Cathepsin C |
| CatG | Cathepsin G |
| $dP/dt_{max}$ | Maximum rate of rise of left-ventricular pressure |
| $dP/dt_{min}$ | Maximum rate of fall of left-ventricular pressure |
| DPPI | Dipeptidylpeptidase I |
| GAPDG | Glyceraldehyde-3-phosphate dehydrogenase |
| HTX | Heart transplantation |
| HUVECs | Human umbilical vein endothelial cells |
| IR | Ischemia/reperfusion injury |
| LV | Left-ventricular |
| LVSP | Left-ventricular systolic pressure |
| MAPK | Mitogen activated protein kinase |
| MPO | Myeloperoxidase |
| NE | Neutrophil elastase |
| NF-κB | Nuclear factor-kappaB |
| NSPs | Neutrophil serine proteases |
| PARP | Poly(ADP-ribose) polymerase |
| PBS | Phosphate-buffered saline |
| RIPA | Radioimmunoprecipitation assay |
| ROS | Reactive oxygen species |
| SDS | Sodium dodecyl sulfate |
| SEM | Standard error of the mean |
| TBS | Tris-buffered saline |
| TUNEL | Terminal deoxynucleotidyl transferase-mediated dUTP nick-end labeling |

## Supplementary Information

The online version contains supplementary material available at https://doi.org/10.1186/s12967-023-04659-6.

**Additional file 1: Figure S1.** Effects of BI-9740 (BI) on reactive oxygen species (ROS) generation and DNA strand breaks in grafts after transplantation (HTX). (A) Representative images of dihydroethidium fluorescence staining (×10, scale bar: 1 mm) followed by semi-quantitative analysis. Dihydroethidium is freely permeable to cell membranes and emits a red fluorescent signal when oxidized by ROS to ethidium. (1 picture from 10 rats/group). Values are expressed as mean ± SEM. (B) Representative images of myocardial tissue showing pink nuclei with fragmented DNA, visualized by terminal deoxynucleotidyl transferase-mediated dUTP nick end-labeling (TUNEL) staining. Blue nuclei represents 4',6-diamino-2-phenylindole staining (magnification × 40; scale bar: 100 µm) followed by quantification based TUNEL-positive cells expressed as a percentage over the total cell count. The evaluation of TUNEL assay was carried out on 6 randomly selected non-overlapping fields within each rat's myocardial tissue (59–60 pictures from 10 rats/group). Values are expressed as mean ± SEM and correspond to the mean of all pictures. The samples were assessed by examiners who were blinded to the experimental groups.

**Acknowledgements**

The expert technical assistance of Karin Sonnenberg and Lutz Hoffmann is gratefully acknowledged. The authors acknowledge Boehringer Ingelheim Pharma GmbH & Co KG for the donation of BI-9740.

**Author contributions**

Conception and design: BK; SKI. Analysis and interpretation: BL, BK; TM; MAG; RD; GS; SKI. Data collection: BL; BK; PK; RD; TM; SKI. Writing the manuscript: BL; BK; MAG; AAS; RD; MK; GS; SKI. Critical revision: BK; MAG; AAS; MAG; MK; GS; SKI. "All authors read and approved the final manuscript."

**Funding**

Open Access funding enabled and organized by Projekt DEAL. This study was supported by the by the "Ministere de l'Enseignement Superieur et de la Recherche et de l'Innovation" and the "Region Centre Val de Loire" (to Dr. B. Korkmaz, Project Pirana).

**Availability of data and materials**

"The datasets generated and/or analyzed during the current study are available from the corresponding author on reasonable request."

## Declarations

**Ethics approval and consent to participate**

The approval was obtained by the Ethical Committee of the Regional Council of Karlsruhe, Germany for Animal Experimentation (G257/20).

**Competing interests**

Dr. M. A. Grundl is employed by Boehringer Ingelheim Pharma GmbH & Co KG, Biberach a.d. Riss, Germany. Dr B. Korkmaz has been paid for the time spent as a committee member for advisory boards (Brensocatib Advisory Board (BRAB) INSMED, USA), other forms of consulting (Boehringer Ingelheim (Germany), Neuprozyme Therapeutics Aps (Denmark), Santhera Pharmaceuticals (Switzerland), Chiesi (Italy), Gerson Lehrman Group (GLG) (USA), symposium organisation (INSMED) and travel support, lectures or presentations, outside the submitted work. Other authors declare no competing financial interests.

**Author details**

[1]Department of Cardiac Surgery, University Hospital Heidelberg, 69120 Heidelberg, Germany. [2]Department of Cardiac Surgery, University Hospital Halle (Saale), 06120 Halle, Germany. [3]INSERM UMR-1100, "Research Center for Respiratory Diseases" and Université de Tours, 37032 Tours, France. [4]Heart and Vascular Center, Semmelweis University, Budapest 1122, Hungary. [5]Department of Medicinal Chemistry, Boehringer Ingelheim Pharma GmbH & Co KG, 88397 Biberach a.d. Riss, Germany.

Received: 23 May 2023 Accepted: 25 October 2023
Published online: 09 November 2023

**References**

1. Andrew J, Macdonald P. Latest developments in heart transplantation: a review. Clin Ther. 2015;37:10. https://doi.org/10.1016/j.clinthera.2015.08.019.
2. Gupta T, Krim SR. Cardiac transplantation: update on a road less traveled. Ochsner J. 2019;19:4. https://doi.org/10.31486/toj.19.0022.
3. Bugger H, Pfeil K. Mitochondrial ROS in myocardial ischemia reperfusion and remodeling. Biochim Biophys Acta Mol Basis Dis. 2020;1866:7. https://doi.org/10.1016/j.bbadis.2020.165768.
4. Dhalla NS, Shah AK, Adameova A, Bartekova M. Role of oxidative stress in cardiac dysfunction and subcellular defects due to ischemia-reperfusion injury. Biomedicines. 2022;10:7. https://doi.org/10.3390/biomedicines10071473.
5. Eltzschig HK, Eckle T. Ischemia and reperfusion–from mechanism to translation. Nat Med. 2011;17:11. https://doi.org/10.1038/nm.2507.
6. Heusch G. Myocardial ischaemia-reperfusion injury and cardioprotection in perspective. Nat Rev Cardiol. 2020;17:12. https://doi.org/10.1038/s41569-020-0403-y.
7. Frank A, Bonney M, Bonney S, Weitzel L, Koeppen M, Eckle T. Myocardial ischemia reperfusion injury: from basic science to clinical bedside. Semin Cardiothorac Vasc Anesth. 2012;16:3. https://doi.org/10.1177/1089253211436350.
8. Hearse DJ, Bolli R. Reperfusion induced injury: manifestations, mechanisms, and clinical relevance. Cardiovasc Res. 1992;26:2. https://doi.org/10.1093/cvr/26.2.101.
9. Korkmaz B, Caughey GH, Chapple I, Gauthier F, Hirschfeld J, Jenne DE, et al. Therapeutic targeting of cathepsin C: from pathophysiology to treatment. Pharmacol Ther. 2018. https://doi.org/10.1016/j.pharmthera.2018.05.011.
10. Korkmaz B, Horwitz MS, Jenne DE, Gauthier F. Neutrophil elastase, proteinase 3, and cathepsin G as therapeutic targets in human diseases. Pharmacol Rev. 2010;62:4. https://doi.org/10.1124/pr.110.002733.
11. Adkison AM, Raptis SZ, Kelley DG, Pham CT. Dipeptidyl peptidase I activates neutrophil-derived serine proteases and regulates the

development of acute experimental arthritis. J Clin Invest. 2002;109:3. https://doi.org/10.1172/JCI13462.
12. Perera NC, Wiesmuller KH, Larsen MT, Schacher B, Eickholz P, Borregaard N, et al. NSP4 is stored in azurophil granules and released by activated neutrophils as active endoprotease with restricted specificity. J Immunol. 2013;191:5. https://doi.org/10.4049/jimmunol.1301293.
13. Pham CT. Neutrophil serine proteases: specific regulators of inflammation. Nat Rev Immunol. 2006;6:7. https://doi.org/10.1038/nri1841.
14. Pham CT. Neutrophil serine proteases fine-tune the inflammatory response. Int J Biochem Cell Biol. 2008;40:6–7. https://doi.org/10.1016/j.biocel.2007.11.008.
15. Korkmaz B, Lamort AS, Domain R, Beauvillain C, Gieldon A, Yildirim AO, et al. Cathepsin C inhibition as a potential treatment strategy in cancer. Biochem Pharmacol. 2021. https://doi.org/10.1016/j.bcp.2021.114803.
16. Xiao Y, Cong M, Li J, He D, Wu Q, Tian P, et al. Cathepsin C promotes breast cancer lung metastasis by modulating neutrophil infiltration and neutrophil extracellular trap formation. Cancer Cell. 2021;39:3. https://doi.org/10.1016/j.ccell.2020.12.012.
17. Loganathan S, Korkmaz-Icoz S, Radovits T, Li S, Mikles B, Barnucz E, et al. Effects of soluble guanylate cyclase activation on heart transplantation in a rat model. J Heart Lung Transplant. 2015;34:10. https://doi.org/10.1016/j.healun.2015.05.006.
18. Korkmaz B, Attucci S, Juliano MA, Kalupov T, Jourdan ML, Juliano L, et al. Measuring elastase, proteinase 3 and cathepsin G activities at the surface of human neutrophils with fluorescence resonance energy transfer substrates. Nat Protoc. 2008;3:6. https://doi.org/10.1038/nprot.2008.63.
19. Olah A, Nemeth BT, Matyas C, Horvath EM, Hidi L, Birtalan E, et al. Cardiac effects of acute exhaustive exercise in a rat model. Int J Cardiol. 2015. https://doi.org/10.1016/j.ijcard.2014.12.045.
20. Li S, Loganathan S, Korkmaz S, Radovits T, Hegedus P, Zhou Y, et al. Transplantation of donor hearts after circulatory or brain death in a rat model. J Surg Res. 2014;195:1. https://doi.org/10.1016/j.jss.2014.12.038.
21. Tanaka M, Mokhtari GK, Terry RD, Gunawan F, Balsam LB, Hoyt G, et al. Prolonged cold ischemia in rat cardiac allografts promotes ischemia-reperfusion injury and the development of graft coronary artery disease in a linear fashion. J Heart Lung Transplant. 2005;24:11. https://doi.org/10.1016/j.healun.2004.06.007.
22. Iyer A, Kumarasinghe G, Hicks M, Watson A, Gao L, Doyle A, et al. Primary graft failure after heart transplantation. J Transplant. 2011. https://doi.org/10.1155/2011/175768.
23. Chalmers JD, Haworth CS, Metersky ML, Loebinger MR, Blasi F, Sibila O, et al. Phase 2 trial of the DPP-1 inhibitor brensocatib in bronchiectasis. N Engl J Med. 2020;383:22. https://doi.org/10.1056/NEJMoa2021713.
24. Jerke U, Eulenberg-Gustavus C, Rousselle A, Nicklin P, Kreideweiss S, Grundl MA, et al. Targeting cathepsin C in PR3-ANCA vasculitis. J Am Soc Nephrol. 2022;33:5. https://doi.org/10.1681/ASN.2021081112.
25. Chen X, Yan Y, Du J, Shen X, He C, Pan H, et al. Non-peptidyl non-covalent cathepsin C inhibitor bearing a unique thiophene-substituted pyridine: Design, structure-activity relationship and anti-inflammatory activity in vivo. Eur J Med Chem. 2022. https://doi.org/10.1016/j.ejmech.2022.114368.
26. Lu F, Gong H, Lei H, Li J. Downregulation of cathepsin C alleviates endothelial cell dysfunction by suppressing p38 MAPK/NF-kappaB pathway in preeclampsia. Bioengineered. 2022;13:2. https://doi.org/10.1080/21655979.2021.2023994.
27. Rehm SRT, Smirnova NF, Morrone C, Gotzfried J, Feuchtinger A, Pedersen J, et al. Premedication with a cathepsin C inhibitor alleviates early primary graft dysfunction in mouse recipients after lung transplantation. Sci Rep. 2019;9:1. https://doi.org/10.1038/s41598-019-46206-8.
28. Ba X, Garg NJ. Signaling mechanism of poly(ADP-ribose) polymerase-1 (PARP-1) in inflammatory diseases. Am J Pathol. 2011;178:3. https://doi.org/10.1016/j.ajpath.2010.12.004.
29. Pieper AA, Verma A, Zhang J, Snyder SH. Poly (ADP-ribose) polymerase, nitric oxide and cell death. Trends Pharmacol Sci. 1999;20:4. https://doi.org/10.1016/S0165-6147(99)01292-4.
30. Szabo G, Bahrle S, Stumpf N, Sonnenberg K, Szabo EE, Pacher P, et al. Poly(ADP-Ribose) polymerase inhibition reduces reperfusion injury after heart transplantation. Circ Res. 2002;90:1. https://doi.org/10.1161/hh0102.102657.
31. Korkmaz B, Lesner A, Marchand-Adam S, Moss C, Jenne DE. Lung protection by cathepsin C inhibition: a new hope for COVID-19 and ARDS? J Med Chem. 2020;63:22. https://doi.org/10.1021/acs.jmedchem.0c00776.

## Publisher's Note

Springer Nature remains neutral with regard to jurisdictional claims in published maps and institutional affiliations.

**Ready to submit your research? Choose BMC and benefit from:**

- fast, convenient online submission
- thorough peer review by experienced researchers in your field
- rapid publication on acceptance
- support for research data, including large and complex data types
- gold Open Access which fosters wider collaboration and increased citations
- maximum visibility for your research: over 100M website views per year

**At BMC, research is always in progress.**

**Learn more** biomedcentral.com/submissions

BMC

# Roxane DOMAIN

## Mécanismes protéolytiques impliqués dans la maturation de la cathepsine C et de ses protéases à serine cibles dans les cellules immunitaires


**Résumé**

La cathepsine C (CatC) est une protéase à cystéine qui catalyse la maturation des protéases à sérine pro-inflammatoires du neutrophile (PSN), telles que l'élastase, la protéinase 3 et la cathepsine G, et des granzymes (Gzms) des lymphocytes cytotoxiques (LC) impliquées dans l'activation des voies de signalisation qui déclenchent la mort cellulaire programmée des cellules cancéreuses ou infectées par un virus. La CatC représente ainsi une cible thérapeutique potentielle dans toutes les pathologies inflammatoires et/ou auto-immunes impliquant les PSN. Les inhibiteurs chimiques de la CatC sont actuellement évalués dans les essais précliniques et cliniques. Une inactivation génétique de la CatC est observée chez les patients atteints du syndrome de Papillon-Lefèvre (SPL). Dans les neutrophiles de ces patients, seules de faibles quantités de PSN actives sont détectées (<10% par rapport aux individus sains) ce qui suggère l'implication d'une protéase alternative à la CatC, que nous avons nommé la NSPs-AAP-1 (NSPs-Alternative Activating Protease-1) impliquée dans l'activation des zymogènes de PSN. La caractérisation enzymatique des Gzms dans les LC de patients atteints du SPL a également révélé une voie d'activation indépendante de la CatC impliquée dans l'activation des Gzms (~50% par rapport aux individus sains). Au cours de ce travail de thèse, nous avons étudié les processus protéolytiques non-dépendants de la CatC impliqués dans l'activation des PSN et des Gzms en bloquant la maturation de la CatC dans des modèles cellulaires. Nos résultats ont démontré l'existence de la NSPs-AAP-1 impliquée dans l'activation des PSN qui est une protéase à cystéine inhibée par les inhibiteurs de type nitrile de la CatC. La voie non-dépendante de la CatC de l'activation des Gzms dans les LC est médiée par une protéase alternative différente de la NSPs-AAP-1. Cette protéase est résistante aux inhibiteurs de protéase à cystéine. Cette étude suggère que le ciblage pharmacologique de la CatC pour bloquer les PSN dans les maladies inflammatoires ou auto-immunes ne devrait pas altérer l'activité cytotoxique des LC.



**Mots clés** : neutrophile, lymphocyte, cathepsine C, protéase à sérine du neutrophile, granzyme, inhibiteur de protéase



**Summary**

The cysteine protease cathepsin C (CatC) activates immune cells serine proteases including pro-inflammatory neutrophil serine proteases (NSPs) (elastase, proteinase 3 and cathepsin G) and cytotoxic lymphocyte (CL) granzymes (Gzms) involved in the activation of signaling pathways that trigger programmed cell death in virus-infected or cancerous cells. CatC represents a potential therapeutic target in all inflammatory and/or autoimmune diseases involving NSPs. Chemical inhibitors of CatC are currently being evaluated in preclinical and clinical trials. Genetic inactivation of CatC has been observed in patients with Papillon-Lefèvre syndrome (PLS). In neutrophils from these patients, only small amounts of active NSPs are detected (<10% compared to healthy individuals), suggesting the involvement of an alternative protease to CatC, which we have named NSPs-AAP-1 (NSPs-Alternative Activating Protease-1) involved in the activation of NSP zymogens. Enzymatic characterization of Gzms in CLs from PLS patients also revealed a CatC-independent activation pathway involved in Gzms activation (~50% compared to healthy individuals). In this thesis work, we investigated CatC-independent proteolytic processes involved in the activation of NSPs and Gzms by blocking CatC maturation in cellular models. Our results clearly demonstrated the existence of NSPs-AAP-1 involved in the activation of NSPs, which is a cysteine protease inhibited by nitrile-type CatC inhibitors. The CatC-independent pathway of Gzms activation in CLs is mediated by an alternative protease different from NSPs-AAP-1. This protease is resistant to cysteine protease inhibitors, suggesting that pharmacological targeting of CatC to block NSPs in inflammatory or autoimmune diseases would not alter the cytotoxic activity of CLs.



**Keywords** : neutrophil, lymphocyte, cathepsin C, neutrophil serine protease, granzymes, protease inhibitor